

$$\mathcal{M}^{-1} = [\mathbf{I} - \mathsf{H}\boldsymbol{\psi}\mathcal{K}]^*\mathcal{D}^{-1}[\mathbf{I} - \mathsf{H}\boldsymbol{\psi}\mathcal{K}]$$

$$\mathcal{M}^{-1} = [\mathbf{I} - \mathsf{H}\boldsymbol{\psi}\mathcal{K}]^*\mathcal{D}^{-1}[\mathbf{I} - \mathsf{H}\boldsymbol{\psi}\mathcal{K}]$$

$\mathsf{H}\boldsymbol{\psi}\mathcal{K}$

Abhinandan Jain
 $\overset{\psi}{\underset{\mathsf{H}\boldsymbol{\psi}\mathcal{K}}{\curvearrowright}}$

Robot and Multibody Dynamics

$\boldsymbol{\psi}(k+1, k)$

Analysis and Algorithms

$\tau(k)$

 Springer

Robot and Multibody Dynamics

Abhinandan Jain

Robot and Multibody Dynamics

Analysis and Algorithms



Springer

Abhinandan Jain Ph.D.
Jet Propulsion Laboratory
4800 Oak Grove Drive
Pasadena, California 91109
USA
abhi.jain@jpl.nasa.gov

ISBN 978-1-4419-7266-8 e-ISBN 978-1-4419-7267-5
DOI 10.1007/978-1-4419-7267-5
Springer New York Dordrecht Heidelberg London

Library of Congress Control Number: 2010938443

© Springer Science+Business Media, LLC 2011
All rights reserved. This work may not be translated or copied in whole or in part without the written permission of the publisher (Springer Science+Business Media, LLC, 233 Spring Street, New York, NY 10013, USA), except for brief excerpts in connection with reviews or scholarly analysis. Use in connection with any form of information storage and retrieval, electronic adaptation, computer software, or by similar or dissimilar methodology now known or hereafter developed is forbidden.
The use in this publication of trade names, trademarks, service marks, and similar terms, even if they are not identified as such, is not to be taken as an expression of opinion as to whether or not they are subject to proprietary rights.

Printed on acid-free paper

Springer is part of Springer Science+Business Media (www.springer.com)

*In memory of Guillermo Rodriguez,
an exceptional scholar and a gentleman.*

*To my parents,
and to my wife, Karen.*

Preface

“It is a profoundly erroneous truism, repeated by copybooks and by eminent people when they are making speeches, that we should cultivate the habit of thinking of what we are doing. The precise opposite is the case. Civilization advances by extending the number of important operations which we can perform without thinking about them. Operations of thought are like cavalry charges in a battle – they are strictly limited in number; they require fresh horses, and must only be made at decisive moments.”

Alfred North Whitehead

Robotics, and its need for real-time control, has expanded research in multibody dynamics beyond modeling and systematic formulations, to computational and control issues. While significant progress has been made in these areas, the mathematical complexity of the system dynamics, and the paucity of analytical concepts and mathematical tools to manage the complexity, present imposing challenges.

The body of work known as the *spatial operator algebra (SOA)* provides such analytical and mathematical techniques that address these challenges. The SOA provides *spatial operator* mathematical constructs, that concisely describe the system dynamics and enable dynamics analysis in a unified and general setting.

That the equations of multibody dynamics can be described by an algebra of spatial operators is certainly of mathematical interest. However, the SOA also provides the means to manipulate at a high level of abstraction the equations describing multi-body behavior. The significance of this goes beyond the mathematics and is useful in a practical sense. At any stage of the manipulation of equations, spatially recursive algorithms to implement the operator expressions can be readily obtained by inspection. Therefore, the transition from abstract operator mathematics to practical implementation is straightforward, and often requires only a simple mental exercise. The focus of this book is on providing a comprehensive and coherent description of the SOA methodology and techniques, and of the interplay between mathematical analysis, structural properties, and computational algorithms.

The material in this book serves as a point of departure for further exploration of topics in multibody dynamics. Thus, while the text is written in a style that is accessible to a newcomer, it would be best appreciated by practitioners and researchers in the field.

The book is organized into three parts. Part 1, consisting of Chaps. 1–7, is a study of the dynamics of rigid-link, serial-chain systems. These are the simplest examples of multi-link systems. They serve to introduce the notion of spatial operators, and to develop the concepts of mapping operator expressions into low-order computational algorithms. In Part 2, consisting of Chaps. 8–13, the operator techniques are generalized to include the broader class of multibody systems. Graph theory ideas are used to describe the structure of the operators at a level of abstraction that makes them independent of the size, the topological structure, and the detailed properties of the linkages. Part 3 is an exploration of the application of SOA techniques to advanced topics. These include methods for partitioning and sub-structuring multibody models, constraint embedding for transforming closed-chain systems into tree systems, the dynamics of under-actuated systems and free-flying systems, derivation of analytical sensitivity expressions, and diagonalized dynamics formulations.

The text is interspersed with exercises that further explore a topic or present a related idea. All solutions are provided at the end of the book. Key results are summarized in lemmas with self-contained assumptions and conclusions.

Rarely is there a single approach or solution that works for the variety of problems encountered when working with robot and multibody system dynamics. The emphasis of this book therefore is on deepening the theoretical and mathematical understanding of the operator tools, and on the rich tapestry of inter-relationships among them. A single topic is thus sometimes explored from different angles, and themes and concepts cutting across different contexts are highlighted.

Acknowledgments

My introduction to the fields of robotics and multibody dynamics began when I joined the Jet Propulsion Laboratory (JPL). Guillermo Rodriguez had recently discovered the rich parallels between the mathematical theory underlying optimal filtering and estimation theory, and the structure of the dynamical properties of robotic systems that formed the basis of the SOA. I had the good fortune of joining in this pioneering research. and, until his untimely passing, had the incredible personal experience of collaborating and working with Guillermo.

Over the years, I have benefited in no small measure from the continuous interactions and support from many exceptional colleagues at JPL. Ken Kreutz-Delgado introduced me to the early developments of the SOA methodology. Guy Man's vision helped initiate the "real-world" application of the SOA techniques to solve challenging dynamics modeling problems for NASA's space missions. I am grateful to my colleagues at JPL's DARTS Lab, including Bob Balaram, Jonathan Cameron, Christopher Lim, Marc Pomerantz, Hari Nayar, Jeff Biesiadecki and many others who have continued to advance the methodology and make possible its application to challenges in space robotics. It has also been a pleasure to work with Nagarajan Vaidehi in the non-engineering application of the SOA ideas to the molecular dynamics arena. I would like to thank John Wen and Rich Volpe for their persuasive

encouragement to work on and to publish this book. Last, but not least, I would like to thank my family, Karen, Aarti, and Nikhil, who valiantly helped with figures, proof-reading, and stylistic suggestions for the text, and for their incredible patience and forbearance through the months of its preparation.

Contents

Part I Serial-Chain Dynamics

1	Spatial Vectors	3
1.1	Homogeneous Transforms	3
1.2	Differentiation of Vectors	5
1.2.1	Vector Derivatives in Rotating Frames	5
1.2.2	Rigid Body Vector Derivatives	6
1.3	Spatial Vectors	8
1.3.1	Six-Dimensional Spatial Notation	9
1.3.2	The Cross-Product for Spatial Vectors	9
1.4	The Rigid Body Transformation Matrix $\phi(x, y)$	11
1.4.1	Spatial Velocity Transformations	12
1.4.2	Properties of $\phi(\cdot)$	12
1.5	Spatial Forces	15
2	Single Rigid Body Dynamics	17
2.1	Spatial Inertia and Momentum of a Rigid Body	17
2.1.1	The Spatial Inertia	17
2.1.2	The Parallel-Axis Theorem for Spatial Inertias	20
2.1.3	Spatial Inertia of a Composite Assemblage of Rigid Bodies	21
2.1.4	The Spatial Momentum of a Rigid Body	21
2.2	Motion Coordinates	22
2.2.1	Generalized Coordinates and Velocities	23
2.2.2	Generalized Forces	24
2.2.3	Generalized Accelerations	24
2.3	Equations of Motion with Inertial Frame Derivatives	25
2.3.1	Equations of Motion with $\beta_J = {}^I\mathcal{V}(C)$	25
2.3.2	Equations of Motion with $\beta_J = {}^I\mathcal{V}(z)$	27
2.4	Equations of Motion with Body Frame Derivatives	29
2.5	Equations of Motion with an Inertially Fixed Velocity Reference Frame	31
2.6	Comparison of the Different Dynamics Formulations	33

3	Serial-Chain Kinematics	35
3.1	Serial-Chain Model	35
3.2	Hinge Kinematics	36
3.2.1	Hinge Generalized Coordinates	37
3.2.2	Relative and Absolute Coordinates	38
3.2.3	Hinge Generalized Velocities	38
3.2.4	Examples of Hinges	40
3.3	Serial-Chain Kinematics	42
3.3.1	Serial-Chain Configuration Kinematics	42
3.3.2	Serial-Chain Differential Kinematics	43
3.3.3	Differential Kinematics with $\mathbb{B}_k \neq \mathbb{O}_k$	45
3.4	Spatial Operators	47
3.4.1	The ϕ Spatial Operator	49
3.4.2	Velocity Operator Expression	50
3.4.3	The $\tilde{\phi}$ Spatial Operator	51
3.5	Recursions Associated with the ϕ Operator	51
3.6	The Jacobian Operator	53
4	The Mass Matrix	57
4.1	Mass Matrix of a Serial-Chain System	57
4.1.1	Kinetic Energy of the Serial-Chain	57
4.1.2	Composite Rigid Body Inertias	59
4.1.3	Decomposition of $\phi M \phi^*$	61
4.1.4	$O(N^2)$ Algorithm for Computing the Mass Matrix	63
4.1.5	Relationship to the Composite Rigid Body Method	65
4.2	Lagrangian Approach to the Equations of Motion	66
4.2.1	Properties of \mathcal{M} and \mathcal{C}	67
4.2.2	Hamiltonian Form of the Equations of Motion	70
4.2.3	Transformation of Lagrangian Coordinates	70
5	Serial-Chain Dynamics	75
5.1	Equations of Motion for a Typical Link	75
5.1.1	Expression for the Spatial Acceleration $\alpha(k)$	77
5.1.2	Overall Equations of Motion	81
5.1.3	Spatial Operators with Body Frame Derivatives but $\mathbb{B}_k \neq \mathbb{O}_k$	83
5.2	Inclusion of External Forces and Gravity	85
5.2.1	Inclusion of External Forces	85
5.2.2	Compensating for External Forces	86
5.2.3	Inclusion of Gravitational Forces	87
5.3	Inverse Dynamics of Serial-Chains	88
5.3.1	Newton–Euler Inverse Dynamics Algorithm	88
5.3.2	Computing the Mass Matrix Using Inverse Dynamics	90
5.3.3	Composite Rigid Body Inertias Based Inverse Dynamics	91

5.4	Equations of Motion with an Inertially Fixed Velocity Reference Frame	93
5.4.1	Relationship Between $\phi_{\mathbb{I}}$ and ϕ	96
6	Articulated Body Model for Serial Chains	97
6.1	Alternate Models for Multibody Systems	97
6.1.1	Terminal Body Model	97
6.1.2	Composite Body Model	98
6.1.3	Articulated Body Model	99
6.2	The $\mathcal{P}(k)$ Articulated Body Inertia	100
6.2.1	Induction Argument for $\mathcal{P}(k)$	100
6.2.2	The $\mathcal{D}(k)$ and $\mathcal{G}(k)$ Matrices	101
6.2.3	The $\tau(k)$ and $\bar{\tau}(k)$ Projection Matrices	102
6.2.4	The $\mathcal{P}^+(k)$ Matrix	104
6.2.5	Conclusion of the Induction Argument for $\mathcal{P}(k)$	105
6.3	Articulated Body Model Force Decomposition	107
6.3.1	The $\epsilon(k)$ Vector	109
6.3.2	Acceleration Relationships	110
6.4	Parallels with Estimation Theory	111
6.4.1	Process Covariances	112
6.4.2	Optimal Filtering	112
6.4.3	Optimal Smoothing	113
6.4.4	Extensions	114
7	Mass Matrix Inversion and AB Forward Dynamics	115
7.1	Articulated Body Spatial Operators	115
7.1.1	Some Operator Identities	117
7.1.2	Innovations Operator Factorization of the Mass Matrix	120
7.1.3	Operator Inversion of the Mass Matrix	121
7.2	Forward Dynamics	122
7.2.1	$O(N)$ AB Forward Dynamics Algorithm	123
7.3	Extensions to the Forward Dynamics Algorithm	128
7.3.1	Computing Inter-Link f Spatial Forces	128
7.3.2	Including Gravitational Accelerations	128
7.3.3	Including External Forces	129
7.3.4	Including Implicit Constraint Forces	130

Part II General Multibody Systems

8	Graph Theory Connections	135
8.1	Directed Graphs and Trees	135
8.2	Adjacency Matrices for Digraphs	138
8.2.1	Properties of Digraph Adjacency Matrices	138
8.2.2	Properties of Tree Adjacency Matrices	140
8.2.3	Properties of Serial-Chain Adjacency Matrices	140
8.3	Block Weighted Adjacency Matrices	141

8.4	BWA Matrices for Tree Digraphs	142
8.4.1	The 1-Resolvent of Tree BWA Matrices	143
8.5	Similarity Transformations of a Tree BWA Matrix	147
8.5.1	Permutation Similarity Transformations	148
8.5.2	Similarity-Shift Transformations	149
8.6	Multibody System Digraphs	150
8.6.1	BWA Matrices and Serial-Chain, Rigid Body Systems	151
8.6.1.1	\mathcal{E}_ϕ Is a BWA Matrix	153
8.6.2	Non-Canonical Serial-Chains	154
8.7	BWA Matrices and Tree-Topology, Rigid Body Systems	154
8.7.1	Equations of Motion for Tree Topology Systems	155
9	SKO Models	159
9.1	SKO Models	160
9.1.1	Definition of SKO Models	160
9.1.2	Existence of SKO Models	161
9.1.3	Generalizations of SKO Models	161
9.2	SPO Operator/Vector Products for Trees	162
9.2.1	SKO Model $O(N)$ Newton–Euler Inverse Dynamics	165
9.3	Lyapunov Equations for SKO Models	166
9.3.1	Forward Lyapunov Recursions for SKO Models	166
9.3.2	Mass Matrix Computation for an SKO Model	168
9.3.3	Backward Lyapunov Recursions for SKO Models	170
9.4	Riccati Equations for SKO Models	174
9.4.1	The \mathcal{E}_ψ and ψ SKO and SPO Operators	175
9.4.2	Operator Identities	176
9.5	SKO Model Mass Matrix Factorization and Inversion	179
9.5.1	$O(N)$ AB Forward Dynamics	180
9.6	Generalized SKO Formulation Process	182
9.6.1	Procedure for Developing an SKO Model	183
9.6.2	Potential Non-Tree Topology Generalizations	185
10	Operational Space Dynamics	187
10.1	Operational Space Equations of Motion	187
10.1.1	Physical Interpretation	189
10.1.2	Operational Space Control	189
10.2	Structure of the Operational Space Inertia	190
10.2.1	The Ω Extended Operational Space Compliance Matrix	190
10.2.2	Decomposition of Ω	191
10.2.3	Computing Δ	193
10.2.4	The Υ Operational Space Compliance Kernel	194
10.2.5	Simplifications for Serial-Chain Systems	197
10.2.6	Explicit Computation of the Mass Matrix Inverse \mathcal{M}^{-1}	198
10.3	The Operational Space \mathcal{C}_{os} Coriolis/Centrifugal Term	199
10.3.1	The \mathfrak{U} and \mathfrak{U}_\perp Projection Operators	199

10.3.2 Computing \mathcal{C}_{os}	202
10.4 Divide and Conquer Forward Dynamics	204
11 Closed-Chain Dynamics	209
11.1 Modeling Closed-Chain Dynamics	209
11.1.1 Types of Bilateral Motion Constraints	209
11.1.2 Constrained System Forward Dynamics Strategies	211
11.2 Augmented Approach for Closed-Chain Forward Dynamics	212
11.2.1 Move/Squeeze Decompositions	214
11.2.2 Augmented Dynamics with Loop Constraints	215
11.2.3 Dual-Arm System Example	219
11.3 Projected Closed-Chain Dynamics	221
11.4 Equivalence of Augmented and Projected Dynamics	222
11.5 Unilateral Constraints	224
11.5.1 Complementarity Problems	225
11.5.2 Forward Dynamics	227
12 Systems with Geared Links	229
12.1 Equations of Motion	230
12.1.1 Reformulated Equations of Motion	232
12.1.2 Eliminating the Geared Constraint	233
12.2 SKO Model for Geared Systems	234
12.2.1 Expression for the Mass Matrix	236
12.3 Computation of the Mass Matrix	237
12.3.1 Optimized Composite Body Inertia Algorithm	238
12.4 O(N) AB Forward Dynamics	239
12.4.1 Mass Matrix Factorization and Inversion	239
12.4.2 Recursive AB Forward Dynamics Algorithm	241
12.4.3 Optimization of the Forward Dynamics Algorithm	242
13 Systems with Link Flexibility	245
13.1 Lumped Mass Model for a Single Flexible Body	245
13.1.1 Equations of Motion of the \mathbb{O}_k^j Node	246
13.1.2 Nodal Equations of Motion for the kth Flexible Body	247
13.1.3 Recursive Relationships Across the Flexible Bodies	248
13.2 Modal Formulation for Flexible Bodies	249
13.2.1 Modal Mass Matrix for a Single Body	251
13.2.2 Recursive Relationships Using Modal Coordinates	252
13.2.3 Recursive Propagation of Accelerations	253
13.2.4 Recursive Propagation of Forces	254
13.2.5 Overall Equations of Motion	255
13.3 SKO Models for Flexible Body Systems	255
13.3.1 Operator Expression for the System Mass Matrix	257
13.3.2 Illustration of the SKO Formulation Procedure	257
13.4 Inverse Dynamics Algorithm	259

13.5	Mass Matrix Computation	261
13.6	Factorization and Inversion of the Mass Matrix	262
13.7	AB Forward Dynamics Algorithm	264
13.7.1	Simplified Algorithm for the Articulated Body Quantities ..	264
13.7.2	Simplified AB Forward Dynamics Algorithm	266
Part III Advanced Topics		
14	Transforming SKO Models	273
14.1	Partitioning Digraphs	273
14.1.1	Partitioning by Path-Induced Sub-Graphs	274
14.2	Partitioning SKO Models	275
14.2.1	Partitioning SKO Model Operators	275
14.2.2	Partitioning of an SKO Model	277
14.3	SPO Operator Sparsity Structure	278
14.3.1	Decomposition into Serial-Chain Segments	278
14.3.2	Sparsity Structure of the \mathcal{E}_A SKO Matrix	280
14.3.3	Sparsity Structure of the \mathbb{A} Matrix	281
14.3.4	Sparsity Structure of the \mathcal{M} Mass Matrix	282
14.4	Aggregating Sub-Graphs	282
14.4.1	Edge and Node Contractions	283
14.4.2	Tree Preservation After Sub-Graph Aggregation	284
14.4.3	The \mathfrak{S}_A Aggregation Sub-Graph	287
14.5	Transforming SKO Models Via Aggregation	287
14.5.1	SKO Operators After Body Aggregation	287
14.5.2	SKO Model for the $\mathfrak{T}_{\mathfrak{S}}$ Aggregated Tree	290
14.6	Aggregation Relationships at the Component Level	292
14.6.1	Velocity Relationships	293
14.6.2	Acceleration Relationships	294
14.6.3	Force Relationships	295
15	Constraint Embedding	297
15.1	Constraint Embedding Strategy	297
15.1.1	Embedding Constraint Sub-Graphs	299
15.2	Examples of Constraint Embedding	303
15.2.1	Geared Links	304
15.2.2	Planar Four-Bar Linkage System (Terminal Cut)	305
15.2.3	Planar Four-Bar Linkage System (Internal Cut)	306
15.3	Recursive AB Forward Dynamics	307
15.3.1	Articulated Body Inertias for the Aggregated System	307
15.3.2	Mass Matrix Factorization and Inversion	308
15.3.3	AB Forward Dynamics Algorithm	308
15.4	Computing $X_{\mathfrak{S}}$ and $\dot{X}_{\mathfrak{S}}$	309
15.5	Generalization to Multiple Branches and Cut-Edges	311

16 Under-Actuated Systems	313
16.1 Modeling of Under-Actuated Manipulators	314
16.1.1 Decomposition into Passive and Active Systems	315
16.1.2 Partitioned Equations of Motion	316
16.1.3 Spatial Operator Expression for \mathcal{M}_{pp}^{-1}	317
16.1.4 Operator Expressions for S Blocks	319
16.2 $O(N)$ Generalized Dynamics Algorithms	320
16.2.1 Application to Prescribed Motion Dynamics	324
16.3 Jacobians for Under-Actuated Systems	324
16.3.1 The Generalized Jacobian \mathcal{J}_G	325
16.3.2 Computed-Torque for Under-Actuated Systems	326
16.3.3 The Disturbance Jacobian \mathcal{J}_D	327
16.4 Free-Flying Systems as Under-Actuated Systems	329
16.4.1 Integrals of Motion for Free-Flying Systems	329
17 Free-Flying Systems	331
17.1 Dynamics of Free-Flying Manipulators	331
17.1.1 Dynamics with Link n as Base-Body	331
17.1.2 Dynamics with Link 1 as Base-Body	332
17.1.3 Direct Computation of Link Spatial Acceleration	336
17.1.4 Dynamics with Link k as Base-Body	336
17.2 The Base-Invariant Forward Dynamics Algorithm	337
17.2.1 Parallels with Smoothing Theory	338
17.2.2 Simplifications Using Non-Minimal Coordinates	339
17.2.3 Computational Issues	340
17.2.4 Extensions to Tree-Topology Manipulators	340
17.3 SKO Model with k th Link as Base-Body	341
17.3.1 Generalized Velocities with k th Link as the Base-Body	341
17.3.2 Link Velocity Recursions with k th Link as the Base-Body	342
17.3.3 Partitioned System	343
17.3.4 Properties of a Serial-Chain SKO Operator	344
17.3.5 Reversing the SKO Operator	345
17.3.6 Transformed SKO Model	347
17.4 Base-Invariant Operational Space Inertias	348
18 Spatial Operator Sensitivities for Rigid-Body Systems	353
18.1 Preliminaries	353
18.1.1 Notation	353
18.1.2 Identities for \mathcal{V}^v	354
18.2 Operator Time Derivatives	356
18.2.1 Time Derivatives of $\phi(k+1, k)$, $H(k)$ and $M(k)$	356
18.2.2 Time Derivatives with $\mathbb{O}_k \neq \mathbb{B}_k$	358
18.2.3 Time Derivative of the Mass Matrix	360
18.3 Operator Sensitivities	361
18.3.1 The $\tilde{\mathcal{H}}_{\leq i}^\omega$, $\tilde{\mathcal{H}}_{^\omega$, and $\tilde{\mathcal{H}}_{=i}^\omega$ Operators	362

18.4	Mass Matrix Related Quantities	365
18.4.1	Sensitivity of $\phi M \phi^*$	365
18.4.2	Sensitivity of the Mass Matrix M_{θ_i}	365
18.4.3	Sensitivity of the Kinetic Energy	366
18.4.4	Equivalence of Lagrangian and Newton–Euler Dynamics	367
18.5	Time Derivatives of Articulated Body Quantities	368
18.6	Sensitivity of Articulated Body Quantities	373
18.7	Sensitivity of Innovations Factors	375
19	Diagonalized Lagrangian Dynamics	379
19.1	Globally Diagonalized Dynamics	379
19.2	Diagonalization in Velocity Space	382
19.2.1	Coriolis Force Does No Work	384
19.2.2	Rate of Change of the Kinetic Energy	384
19.3	The Innovations Factors as Diagonalizing Transformations	385
19.3.1	Transformations Between $\dot{\theta}$ and $\dot{\eta}$	386
19.4	Expression for $C(\theta, \eta)$ for Rigid-Link Systems	387
19.4.1	Closed-Form Expression for $\dot{m}\eta$	387
19.4.2	Operator Expression for $C(\theta, \eta)$	389
19.4.3	Decoupled Control	392
19.5	Un-normalized Diagonalized Equations of Motion	393
19.5.1	$O(N)$ Forward Dynamics	394
	Useful Mathematical Identities	397
A.1	3-Vector Cross-Product Identities	397
A.2	Matrix and Vector Norms	397
A.3	Schur Complement and Matrix Inverse Identities	398
A.4	Matrix Inversion Identities	400
A.5	Matrix Trace Identities	400
A.6	Derivative and Gradient Identities	401
A.6.1	Function Derivatives	401
A.6.2	Vector Gradients	401
A.6.3	Matrix Derivatives	402
	Attitude Representations	403
B.1	Euler Angles	403
B.2	Angle/Axis Parameters	404
B.3	Unit Quaternions/Euler Parameters	406
B.3.1	The $E_+(\underline{q})$ and $E_-(\underline{q})$ Matrices	408
B.3.2	Quaternion Transformations	409
B.3.3	Quaternion Differential Kinematics	410
B.4	Gibbs Vector Attitude Representations	412
	Solutions	415
	References	475

Contents	xix
List of Notation	483
Index	493

Part I

Serial-Chain Dynamics

Chapter 1

Spatial Vectors

This chapter establishes notation and several foundational concepts required for the study of multibody kinematics and dynamics. Beginning with the notion of coordinate-free representations, we introduce homogeneous transformations, spatial vectors and their properties. Spatial vectors are used to define spatial velocities, accelerations and forces for coordinate frames and bodies. Rigid body transformation matrices that transform spatial velocities and forces across frames on a rigid body are also introduced. This chapter also studies time derivatives of spatial quantities with respect to different frames.

1.1 Homogeneous Transforms

The location of coordinate frames and points are described using 3-vectors. Figure 1.1 shows a pair of frames, \mathbb{F} and \mathbb{G} , and a point \mathbb{O} . With $p(\mathbb{F}, \mathbb{O})$ de-

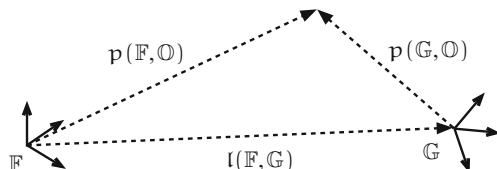


Fig. 1.1 Relationship between two coordinate frames

noting the 3-vector position of \mathbb{O} with respect to the \mathbb{F} frame, its location with respect to the \mathbb{G} frame is

$$\mathbf{p}(\mathbb{F}, \mathbb{O}) = \mathbf{l}(\mathbb{F}, \mathbb{G}) + \mathbf{p}(\mathbb{G}, \mathbb{O}) \quad (1.1)$$

$\mathbf{l}(\mathbb{F}, \mathbb{G})$ denotes the vector from \mathbb{F} to \mathbb{G} . Equation (1.1) is a **coordinate-free** description of relationship between the vectors. While coordinate-free notation is simpler, actual computations require working with **coordinate-frame representations** of vectors. For a vector \mathbf{x} , the notation ${}^{\mathbb{F}}\mathbf{x}$ denotes its representation in the \mathbb{F} frame. Thus, using it, (1.1) can be stated using coordinate-frame representations as follows:

$${}^{\mathbb{F}}\mathbf{p}(\mathbb{F}, \mathbb{O}) = {}^{\mathbb{F}}\mathbf{l}(\mathbb{F}, \mathbb{G}) + {}^{\mathbb{F}}\mathfrak{R}_{\mathbb{G}} {}^{\mathbb{G}}\mathbf{p}(\mathbb{G}, \mathbb{O}) \quad (1.2)$$

${}^{\mathbb{F}}\mathfrak{R}_{\mathbb{G}}$ denotes the rotation matrix¹ that transforms the representation of a 3-vector in frame \mathbb{G} into its representation in frame \mathbb{F} . Binary operations such as addition require that the respective vector representations be in a common coordinate-frame. Since coordinate-free representations are more general and notationally simpler, we use them by default, and resort to specific coordinate representations only when numeric evaluations are required. The distinction between coordinate-free and coordinate-dependent forms of vectors are also discussed in [69, 185].

Define the **homogeneous transform** matrix, ${}^{\mathbb{F}}\mathbb{T}_{\mathbb{G}} \in \mathcal{R}^{4 \times 4}$, as

$${}^{\mathbb{F}}\mathbb{T}_{\mathbb{G}} \triangleq \begin{pmatrix} {}^{\mathbb{F}}\mathfrak{R}_{\mathbb{G}} & {}^{\mathbb{F}}\mathbf{l}(\mathbb{F}, \mathbb{G}) \\ 0 & 1 \end{pmatrix} \quad (1.3)$$

Using it, (1.2) can be restated in the following matrix form:

$$\begin{bmatrix} {}^{\mathbb{F}}\mathbf{p}(\mathbb{F}, \mathbb{O}) \\ 1 \end{bmatrix} = {}^{\mathbb{F}}\mathbb{T}_{\mathbb{G}} \begin{bmatrix} {}^{\mathbb{G}}\mathbf{p}(\mathbb{G}, \mathbb{O}) \\ 1 \end{bmatrix} \quad (1.4)$$

Thus ${}^{\mathbb{F}}\mathbb{T}_{\mathbb{G}}$ defines the transformation relationship between the coordinate-frame representations of position vectors with respect to the \mathbb{F} and \mathbb{G} frames. It is easy to verify that

$${}^{\mathbb{F}}\mathbb{T}_{\mathbb{G}}^{-1} = {}^{\mathbb{G}}\mathbb{T}_{\mathbb{F}} \quad \text{and} \quad {}^{\mathbb{F}}\mathbb{T}_{\mathbb{G}} {}^{\mathbb{G}}\mathbb{T}_{\mathbb{H}} = {}^{\mathbb{F}}\mathbb{T}_{\mathbb{H}} \quad (1.5)$$

These imply that homogeneous transforms form a group,² with the group composition operation being matrix multiplication. The identity element is simply the 4×4 identity matrix.

¹ A rotation matrix (also known as a direction cosine matrix) is a 3×3 orthogonal matrix with determinant 1.

² The group of homogeneous transforms in fact form a Lie group. This, and other differential geometric connections, are explored more thoroughly in [128, 162].

1.2 Differentiation of Vectors

Unlike scalar functions, the derivative of a vector with respect to a scalar variable (often time) is defined with respect to a coordinate frame. Thus, given a frame, \mathbb{F} , and a vector $x(s)$ that is a function of a scalar variable “ s ”, its *derivative with respect to “ s ” as observed in frame \mathbb{F}* is defined as the derivative of the ${}^{\mathbb{F}}x(s)$ coordinate representation with respect to s , that is

$$\frac{d_{\mathbb{F}x}}{ds} \triangleq \frac{d[{}^{\mathbb{F}}x(s)]}{ds} = \begin{bmatrix} \frac{dx_1(s)}{ds} \\ \frac{dx_2(s)}{ds} \\ \frac{dx_3(s)}{ds} \end{bmatrix} \quad (1.6)$$

This vector derivative is itself a vector, and, strictly speaking, (1.6) defines the coordinate-representation of this derivative vector in frame \mathbb{F} . The coordinate-representation of the derivative vector in a different frame \mathbb{G} can be obtained as follows:

$$\frac{{}^{\mathbb{G}}d_{\mathbb{F}x}}{ds} = {}^{\mathbb{G}}\mathfrak{R}_{\mathbb{F}} \frac{{}^{\mathbb{F}}d_{\mathbb{F}x}}{ds} \quad (1.7)$$

Since the representation of vectors in different frames is different, the vector derivatives with respect to different frames can also be different. In general, when the location and orientation of the frames themselves also depend on “ s ”,

$$\frac{d_{\mathbb{F}x}}{ds} \neq \frac{d_{\mathbb{G}x}}{ds}$$

The clear identification of the frame in which a vector derivative is being carried out is essential. In the multibody dynamics context, we will encounter numerous instances where time derivatives of vectorial quantities with respect to different rotating and translating frames are used during kinematics and dynamics analysis.

1.2.1 Vector Derivatives in Rotating Frames

Let us now examine the important special case where the vector derivatives are with respect to time, “ t ”, and where frames are rotating with respect to each other. The 3-vector **angular velocity** of a frame with respect to another frame defines the rate of change of the relative attitude of the pair of frames. Specifically, with $\omega(\mathbb{F}, \mathbb{G})$ denoting the angular velocity of a frame \mathbb{G} with respect to another frame \mathbb{F} , the following differential equation governs the time evolution of the ${}^{\mathbb{F}}\mathfrak{R}_{\mathbb{G}}$ rotation matrix [69, 96]:

$$\frac{d{}^{\mathbb{F}}\mathfrak{R}_{\mathbb{G}}}{dt} = {}^{\mathbb{F}}\tilde{\omega}(\mathbb{F}, \mathbb{G}) {}^{\mathbb{F}}\mathfrak{R}_{\mathbb{G}} = {}^{\mathbb{F}}\mathfrak{R}_{\mathbb{G}} {}^{\mathbb{G}}\tilde{\omega}(\mathbb{F}, \mathbb{G}) \quad (1.8)$$

The notation, \tilde{l} , (alternatively l^\sim) for a 3-vector l denotes the following 3×3 dimensional skew-symmetric matrix:

$$\tilde{l} = l^\sim \triangleq \begin{pmatrix} 0 & -c & b \\ c & 0 & -a \\ -b & a & 0 \end{pmatrix} \quad \text{where} \quad l \triangleq \begin{bmatrix} a \\ b \\ c \end{bmatrix}, \quad (1.9)$$

The \tilde{l} matrix is closely related to the 3-vector cross-product operation $l \otimes (\cdot)$, so that for an arbitrary 3-vector x :

$$l \otimes x = \tilde{l} x \quad (1.10)$$

Unlike linear velocities which are defined for points, angular velocities are always defined for frames. The $\omega(\mathbb{F}, \mathbb{G})$ angular velocity plays an important role in relating vector time derivatives in different frames. Differentiating both sides of $\mathbb{F}x = \mathbb{F}\mathfrak{R}_{\mathbb{G}}^{\mathbb{G}}x$ with respect to time t leads to

$$\frac{d[\mathbb{F}x]}{dt} \stackrel{1.8}{=} \mathbb{F}\mathfrak{R}_{\mathbb{G}} \frac{d[\mathbb{G}x]}{dt} + \mathbb{F}\mathfrak{R}_{\mathbb{G}}^{\mathbb{G}} \tilde{\omega}(\mathbb{F}, \mathbb{G})^{\mathbb{G}}x \quad (1.11)$$

In coordinate-free notation, (1.11) can be expressed as

$$\frac{d_{\mathbb{F}}x}{dt} = \frac{d_{\mathbb{G}}x}{dt} + \tilde{\omega}(\mathbb{F}, \mathbb{G})x \quad (1.12)$$

Equation (1.12) defines the relationship between the time derivatives of a 3-vector in different rotating frames. Observe that the time derivative vectors are equal when the pair of frames are not rotating with respect to each other.

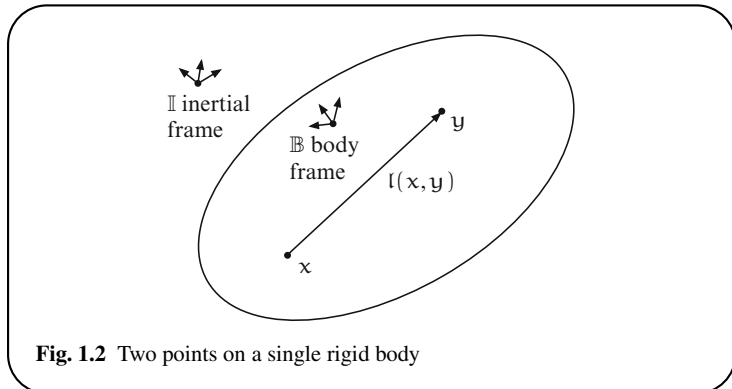
1.2.2 Rigid Body Vector Derivatives

The motion of a rigid body involves both rotation and translation with respect to the inertial frame. Due to the rigidity assumption, the relative position and attitude of frames fixed to a rigid body remain constant at all times. As illustrated in Fig. 1.2, let x and y denote a pair of points attached to a rigid body with body fixed frame \mathbb{B} . Assume that the body is rotating with angular velocity ω with respect to the inertial frame \mathbb{I} . With $l(x, y)$ denoting the 3-vector from point x to point y , we have

$$l(\mathbb{I}, y) = l(\mathbb{I}, x) + l(x, y) \quad (1.13)$$

Then differentiating (1.13) with respect to time we obtain

$$\frac{d_{\mathbb{I}}l(\mathbb{I}, y)}{dt} = \frac{d_{\mathbb{I}}l(\mathbb{I}, x)}{dt} + \frac{d_{\mathbb{I}}l(x, y)}{dt} \quad (1.14)$$



The linear velocity of a point x with respect to frame \mathbb{I} is denoted, $v(x)$, and defined as

$$v(x) \triangleq \frac{d_{\mathbb{I}}l(\mathbb{I}, x)}{dt}$$

Using this in (1.14) leads to

$$v(y) \stackrel{1.14, 1.11}{=} v(x) + \frac{d_{\mathbb{B}}l(x, y)}{dt} + \tilde{\omega} l(x, y) = v(x) + \tilde{\omega} l(x, y) \quad (1.15)$$

The last equality used the constancy of $l(x, y)$ in the body frame \mathbb{B} . Thus, physically, while all frames on a rigid body move with the same angular velocity, i.e.,

$$\omega(y) = \omega(x) \quad (1.16)$$

the points on a rigid body move with different linear velocities when observed from a frame rotating with respect to the body.

Equation (1.16) has used a notational flourish which is worth highlighting. Since x is a point, it does not really have an angular velocity. $\omega(x)$ and $\omega(y)$ represent the angular velocities of the rigid body frame \mathbb{B} rigidly translated to the points x and y , respectively. In other words, in the context of a rigid body, there is a frame implicitly located at every point on the body defined by translating the body frame to the point. Thus, $\omega(x)$ for a point on a rigid body refers to the angular velocity of this frame at x . We will by default continue to use this notational shorthand for points on a rigid body – for angular velocities as well as other types of vectorial quantities – except in cases where a frame is explicitly identified. The following exercise examines acceleration level relationships for vectors and rotating frames.

Exercise 1.1 Position and velocity vector derivatives.

Let \mathbb{I} and \mathbb{B} denote a pair of frames. Let $v(\mathbb{B})$ and $\omega(\mathbb{B})$ denote the linear and angular velocities of frame \mathbb{B} with respect to frame \mathbb{I} . Also, the linear and angular inertial frame accelerations, defined as the \mathbb{I} frame derivatives of the linear and

angular velocities, respectively are denoted as:

$$\alpha(\cdot) \triangleq \frac{d_{\mathbb{I}} v(\cdot)}{dt}, \quad \text{and} \quad \dot{\alpha}(\cdot) \triangleq \frac{d_{\mathbb{I}} \omega(\cdot)}{dt}$$

1. Show that

$$\frac{d_{\mathbb{B}} \omega(\mathbb{B})}{dt} = \alpha(\mathbb{B}), \quad \text{and} \quad \frac{d_{\mathbb{B}} v(\mathbb{B})}{dt} = a(\mathbb{B}) - \tilde{\omega}(\mathbb{B})v(\mathbb{B}) \quad (1.17)$$

2. Let \mathbb{B} denote the body-fixed frame of a rigid body that is rotating with angular velocity, ω , with respect to the inertial frame, \mathbb{I} . With x and y denoting a pair of points on the rigid body, as shown in Fig. 1.2, show that the linear acceleration of the points are related by:

$$a(y) = a(x) + \tilde{\alpha}(x)l(x,y) + \tilde{\omega}\tilde{\omega}l(x,y) \quad (1.18)$$

3. Now let P denote a particle moving on the body with velocity $\delta_v(P)$ with respect to the \mathbb{B} body frame. Let y denote the instantaneous location of P on the body. Show that the linear velocity, $v(P)$, and linear acceleration, $a(P)$, of the particle P with respect to the inertial frame \mathbb{I} are given by

$$v(P) = v(y) + \delta_v(P) \quad (1.19a)$$

$$a(P) = a(y) + \frac{d_{\mathbb{B}} \delta_v(P)}{dt} + 2\tilde{\omega}\delta_v(P) \quad (1.19b)$$

where $v(y)$ and $a(y)$ are defined by (1.15) and (1.18). ■

1.3 Spatial Vectors

In this section, we introduce two types of quantities:

- *Spatial vectors*, which combine 3-vector translational and rotational quantities (e.g., velocities, forces) into a single 6-dimensional vector.
- The *rigid body transformation matrix* $\phi(\cdot)$, which relates the spatial velocity and force at a frame on a rigid body to the spatial velocity and force at another frame on the same body.

The spatial notation used here is based upon references [51, 140, 151]. A slight variant, based on the classical concepts of screws and wrenches, was used originally in [47, 48].

1.3.1 Six-Dimensional Spatial Notation

Use of 6-dimensional **spatial notation** is a step towards simpler expressions of rigid body kinematics and dynamics equations. A **spatial vector** is defined as a 6-vector consisting of a pair of component angular and linear 3-vectors. A concrete example of a spatial vector is the 6-dimensional **spatial velocity**, $\mathcal{V}(x)$, of a frame x defined as

$$\mathcal{V}(x) \triangleq \begin{bmatrix} \omega(x) \\ v(x) \end{bmatrix} \quad (1.20)$$

$\mathcal{V}(x)$ is a 6-dimensional vector consisting of the pair of $\omega(x)$ angular velocity and the $v(x)$ linear velocity 3-vectors. Strictly speaking spatial vectors live in the $\mathcal{R}^3 \times \mathcal{R}^3$ space, but for notational simplicity we will treat them as members of the \mathcal{R}^6 space. Like angular velocities, spatial velocities are always defined for frames, and not for points. However, in the context of a rigid body, the *spatial velocity of a point x on the body* will denote by default the spatial velocity of the body frame translated to point x on the rigid body.

There will be times when we need to work with just the angular or just the linear components of a spatial vector. So for a spatial vector X , X^ω will denote the spatial vector with just the angular component of X , while X^v will denote the spatial vector with just the linear component of X . In particular for the spatial velocity vector $\mathcal{V}(x)$,

$$\mathcal{V}^\omega(x) \triangleq \begin{bmatrix} \omega(x) \\ \mathbf{0} \end{bmatrix} \quad \text{and} \quad \mathcal{V}^v(x) \triangleq \begin{bmatrix} \mathbf{0} \\ v(x) \end{bmatrix} \quad (1.21)$$

Clearly the following identity is always true:

$$X = X^\omega + X^v \quad (1.22)$$

1.3.2 The Cross-Product for Spatial Vectors

With $z \triangleq \begin{bmatrix} x \\ y \end{bmatrix}$ and $c \triangleq \begin{bmatrix} a \\ b \end{bmatrix}$ denoting a pair of spatial vectors, the **6-dimensional spatial vector cross-product** is defined as:

$$z \otimes c \triangleq \tilde{z}c = \begin{pmatrix} \tilde{x}a \\ \tilde{y}a + \tilde{x}b \end{pmatrix} \quad \text{where } \tilde{z} \triangleq \begin{pmatrix} \tilde{x} & \mathbf{0}_3 \\ \tilde{y} & \tilde{x} \end{pmatrix} \in \mathcal{R}^{6 \times 6} \quad (1.23)$$

The $(\tilde{})$ operator defined above for spatial vectors is a natural generalization of the 3-dimensional cross-product operator defined in (1.9) for 3-vectors. The following exercise establishes identities for the spatial vector cross-product that are analogous to the ones for 3-vectors in (A.1) in Appendix A.

Exercise 1.2 Spatial vector cross-product identities.

Verify the following spatial vector identities:

$$\begin{aligned}\tilde{\mathbf{A}}\mathbf{A} &= \mathbf{0} \\ \tilde{\mathbf{A}}\mathbf{B} &= -\tilde{\mathbf{B}}\mathbf{A} \quad (\text{skew-symmetry}) \\ \tilde{\mathbf{A}}\tilde{\mathbf{B}}\mathbf{C} + \tilde{\mathbf{B}}\tilde{\mathbf{C}}\mathbf{A} + \tilde{\mathbf{C}}\tilde{\mathbf{A}}\mathbf{B} &= \mathbf{0} \quad (\text{Jacobi identity}) \\ \tilde{\mathbf{A}}\tilde{\mathbf{B}} - \tilde{\mathbf{B}}\tilde{\mathbf{A}} &= \tilde{\mathbf{A}}\mathbf{B} \quad (\text{commutator})\end{aligned}\tag{1.24}$$

where \mathbf{A} , \mathbf{B} and \mathbf{C} are arbitrary spatial vectors. ■

We now define the related $\overline{(\cdot)}$ and the skew-symmetric $\widehat{(\cdot)}$ operators for a spatial vector \mathbf{z} as follows:

$$\bar{\mathbf{z}} \triangleq \begin{pmatrix} \tilde{x} & \tilde{y} \\ \mathbf{0}_3 & \tilde{x} \end{pmatrix} \quad \text{and} \quad \hat{\mathbf{z}} \triangleq \begin{pmatrix} \tilde{x} & \tilde{y} \\ \tilde{y} & \mathbf{0}_3 \end{pmatrix} \tag{1.25}$$

It is easy to verify the following relationships:

$$\bar{\mathbf{z}} = -\hat{\mathbf{z}}^*, \quad \bar{\mathbf{z}}^* \mathbf{z} = \mathbf{0} \quad \text{and} \quad \bar{\mathbf{z}}\mathbf{z} = \begin{bmatrix} \mathbf{0} \\ \tilde{x}\mathbf{y} \end{bmatrix} \tag{1.26}$$

The following exercise establishes relationships between these different spatial vector operators.

Exercise 1.3 Relationship between the $\widetilde{(\cdot)}$, $\overline{(\cdot)}$ and $\widehat{(\cdot)}$ operators.

Verify the following identities relating the $\widetilde{(\cdot)}$, $\overline{(\cdot)}$ and $\widehat{(\cdot)}$ spatial vectors operators:

$$\mathbf{A}^* \overline{\mathbf{B}} = -\mathbf{B}^* \overline{\mathbf{A}} \tag{1.27a}$$

$$\widetilde{\mathbf{A}}^* \mathbf{B} = \widehat{\mathbf{B}} \mathbf{A} = -\widehat{\mathbf{B}}^* \mathbf{A} = -\overline{\mathbf{A}} \mathbf{B} \tag{1.27b}$$

$$\mathbf{A}^* \widetilde{\mathbf{B}} \mathbf{C} = \mathbf{B}^* \overline{\mathbf{C}} \mathbf{A} = \mathbf{C}^* \widehat{\mathbf{A}} \mathbf{B} \tag{1.27c}$$

The following exercise extends the 3-vector time derivative relationship for rotating frames in (1.12) to a corresponding relationship for spatial vectors.

Exercise 1.4 Time derivative relationship for spatial vectors.

Show that the generalization of (1.12) for the time derivative of a spatial vector $\mathbf{X}(t)$ is given by

$$\frac{d_{\mathbb{F}} \mathbf{X}}{dt} = \frac{d_{\mathbb{G}} \mathbf{X}}{dt} + \tilde{\mathcal{V}}^{\omega}(\mathbb{F}, \mathbb{G}) \mathbf{X} \tag{1.28}$$

where $\mathcal{V}(\mathbb{F}, \mathbb{G})$ denotes the spatial velocity of frame \mathbb{G} with respect to frame \mathbb{F} . ■

1.4 The Rigid Body Transformation Matrix $\phi(x, y)$

The 6×6 dimensional **rigid body transformation matrix**, $\phi(x, y)$, for a pair of frames x and y is defined in coordinate-free form as

$$\phi(x, y) \triangleq \begin{pmatrix} \mathbf{I}_3 & \tilde{l}(x, y) \\ \mathbf{0}_3 & \mathbf{I}_3 \end{pmatrix} \quad (1.29)$$

where $l(x, y)$ denotes the vector between the x and y frames. The symbol \mathbf{I}_3 denotes the 3×3 identity matrix. The inertial frame coordinate-frame representation of $\phi(x, y)$ has the following form:

$$\phi(x, y) = \begin{pmatrix} \mathbf{I}_3 & \mathbb{I}\tilde{l}(x, y) \\ \mathbf{0}_3 & \mathbf{I}_3 \end{pmatrix} \quad (1.30)$$

In general there is no rotational component in a coordinate-frame representation of $\phi(x, y)$ when it transforms spatial vectors expressed in the same frame.

Clearly, other coordinate-frame representations of $\phi(x, y)$ are possible. The following coordinate-frame representation of ϕ transforms spatial vectors expressed in frame \mathbb{G} into ones expressed in a different frame, \mathbb{F} :

$$\begin{aligned} \phi(x, y) &= \begin{pmatrix} \mathbf{I}_3 & \mathbb{F}\tilde{l}(x, y) \\ \mathbf{0}_3 & \mathbf{I}_3 \end{pmatrix} \begin{pmatrix} \mathbb{F}\mathfrak{R}_{\mathbb{G}} & \mathbf{0}_3 \\ \mathbf{0}_3 & \mathbb{F}\mathfrak{R}_{\mathbb{G}} \end{pmatrix} \\ &= \begin{pmatrix} \mathbb{F}\mathfrak{R}_{\mathbb{G}} & \mathbb{F}\tilde{l}(x, y) \mathbb{F}\mathfrak{R}_{\mathbb{G}} \\ \mathbf{0}_3 & \mathbb{F}\mathfrak{R}_{\mathbb{G}} \end{pmatrix} \end{aligned} \quad (1.31)$$

This coordinate-frame representation includes rotation matrices, and is convenient when chaining together rigid-body transformations across a sequence of frames. In this context, the x and y points are normally the \mathbb{F} and \mathbb{G} frames, respectively, i.e., $\phi(x, y) \equiv \phi(\mathbb{F}, \mathbb{G})$.

The following lemma establishes important group properties of $\phi(\cdot)$.

Lemma 1.1 Group properties of $\phi(\cdot)$.

The following group properties hold for the $\phi(x, y)$ transformation matrix:

$$\begin{aligned} \phi(x, x) &= \mathbf{I}_6 \\ \phi(x, z) &= \phi(x, y)\phi(y, z) \\ \phi^{-1}(x, y) &= \phi(y, x) \end{aligned} \quad (1.32)$$

Proof: The first equation in (1.32) follows from (1.29) and uses the $l(x, x) = \mathbf{0}$ identity.

To verify the second equation, observe that $\mathbf{l}(x, z) = \mathbf{l}(x, y) + \mathbf{l}(y, z)$. Thus,

$$\begin{aligned}\phi(x, y)\phi(y, z) &= \begin{pmatrix} \mathbf{I}_3 & \tilde{\mathbf{l}}(x, y) \\ \mathbf{0}_3 & \mathbf{I}_3 \end{pmatrix} \begin{pmatrix} \mathbf{I}_3 & \tilde{\mathbf{l}}(y, z) \\ \mathbf{0}_3 & \mathbf{I}_3 \end{pmatrix} \\ &= \begin{pmatrix} \mathbf{I}_3 & \tilde{\mathbf{l}}(x, y) + \tilde{\mathbf{l}}(y, z) \\ \mathbf{0}_3 & \mathbf{I}_3 \end{pmatrix} = \begin{pmatrix} \mathbf{I}_3 & \tilde{\mathbf{l}}(x, z) \\ \mathbf{0}_3 & \mathbf{I}_3 \end{pmatrix} = \phi(x, z)\end{aligned}$$

The third equation follows by setting $z = x$ in the second identity to obtain $\phi(x, y)\phi(y, x) = \phi(x, x) = \mathbf{I}$. ■

1.4.1 Spatial Velocity Transformations

Using (1.20) and (1.29), the spatial velocity relationship in (1.15) and (1.16) for a pair of points x and y on a rigid body can be rephrased as:

$$\mathcal{V}(y) = \phi^*(x, y)\mathcal{V}(x) \quad (1.33)$$

The above uses the following fact:

$$\phi^*(x, y) = \begin{pmatrix} \mathbf{I}_3 & \tilde{\mathbf{l}}(x, y) \\ \mathbf{0}_3 & \mathbf{I}_3 \end{pmatrix}^* = \begin{pmatrix} \mathbf{I}_3 & \mathbf{0}_3 \\ \tilde{\mathbf{l}}^*(x, y) & \mathbf{I}_3 \end{pmatrix} = \begin{pmatrix} \mathbf{I}_3 & \mathbf{0}_3 \\ -\tilde{\mathbf{l}}(x, y) & \mathbf{I}_3 \end{pmatrix}$$

The more compact (1.33) encompasses the information in the (1.15) and (1.16) pair of equations. Equation (1.33) shows that $\phi^*(x, y)$ relates the spatial velocity at x to the spatial velocity at y on the body. This relationship thus, allows us to obtain the spatial velocity at any point on the rigid body from the spatial velocity of a single point on the body.

1.4.2 Properties of $\phi(\cdot)$

The following exercise establishes some basic properties of $\phi(x, y)$ and spatial vector operators.

Exercise 1.5 Identities involving $\widetilde{(\cdot)}$, $\widehat{(\cdot)}$ and $\phi(\cdot, \cdot)$.

For a spatial vector X , and a pair of frames x and y , prove the following identities:

$$\begin{aligned}[\widehat{\phi(x, y)} X] &= \phi(x, y)\widehat{X}\phi^*(x, y) \\ [\phi^*(x, y) X]^\sim &= \phi^*(x, y)\widetilde{X}\phi^{-*}(x, y) \\ [\phi^*(x, y) X]^\sim \phi^*(x, y) &= \phi^*(x, y)\widetilde{X}\end{aligned} \quad (1.34)$$

The second identity in (1.34) parallels the well known identity $\widetilde{\mathfrak{R}\mathfrak{l}(x, y)} = \widetilde{\mathfrak{R}}\widetilde{\mathfrak{l}}(x, y)\mathfrak{R}^*$, where \mathfrak{R} is a rotation matrix and \mathfrak{l} is a 3-vector.

Exercise 1.6 Rigid body transformation of $\widetilde{\mathcal{V}}(x)$.

For two points, x and y on a rigid body, show that

$$\begin{aligned}\phi^*(x, y)\widetilde{\mathcal{V}}(x) &= \widetilde{\mathcal{V}}(y)\phi^*(x, y) \\ \overline{\mathcal{V}(x)} \phi(x, y) &= \phi(x, y) \overline{\mathcal{V}(y)}\end{aligned}\quad (1.35)$$

Exercise 1.7 Relationships involving X^ω and X^v .

For spatial vectors, X and Y , show that

$$\overline{X}^v Y^\omega = \widetilde{X}^v Y^\omega = \mathbf{0} \quad (1.36a)$$

$$\widetilde{X}^v Y = \widetilde{X}^v Y^\omega \quad (1.36b)$$

$$\overline{X}^v X = \overline{X}^v X^v = \mathbf{0} \quad (1.36c)$$

$$\overline{X} X = \widetilde{X}^\omega X = \widetilde{X}^\omega X^v \quad (1.36d)$$

$$\phi(x, y)\overline{X}^v = \overline{X}^v \phi(x, y) = \overline{X}^v \quad (1.36e)$$

Exercise 1.8 The inertial frame derivative of $\phi(x, y)$.

For an arbitrary pair of frames x and y , derive the following expressions for the inertial frame derivative of $\phi(x, y)$

$$\frac{d_{\mathbb{I}}\phi(x, y)}{dt} = \overline{\mathcal{V}}^v(y) - \overline{\mathcal{V}}^v(x) \quad (1.37)$$

where $\mathcal{V}(x)$ and $\mathcal{V}(y)$ denote spatial velocities with respect to the inertial frame of x and y , respectively. Observe that this inertial derivative is independent of the angular velocity of the frames. When x and y are points on a rigid body, (1.37) can be equivalently stated as

$$\frac{d_{\mathbb{I}}\phi(x, y)}{dt} = \overline{\mathcal{V}}(y) - \overline{\mathcal{V}}(x) \quad (1.38)$$

Exercise 1.9 Local time derivative of $\phi^*(x, y)$.

This exercise examines the relationships between time derivatives with respect to frames that are translating and rotating with respect to each other.

1. Let \mathbb{F} and \mathbb{G} denote a pair of frames (not necessarily on a rigid body) with $\omega(\mathbb{F}, \mathbb{G})$ denoting the angular velocity of frame \mathbb{G} frame with respect to frame \mathbb{F} . Show that

$$\mathcal{V}_{\mathbb{F}}(\mathbb{F}, \mathbb{G}) = \phi^*(\mathbb{F}, \mathbb{G}) \mathcal{V}_{\mathbb{G}}(\mathbb{F}, \mathbb{G}) \quad (1.39)$$

where

$$\begin{aligned} \mathcal{V}_{\mathbb{F}}(\mathbb{F}, \mathbb{G}) &\triangleq \begin{bmatrix} \omega(\mathbb{F}, \mathbb{G}) \\ v_{\mathbb{F}}(\mathbb{F}, \mathbb{G}) \end{bmatrix} \quad \text{and} \quad \mathcal{V}_{\mathbb{G}}(\mathbb{F}, \mathbb{G}) \triangleq \begin{bmatrix} \omega(\mathbb{F}, \mathbb{G}) \\ v_{\mathbb{G}}(\mathbb{F}, \mathbb{G}) \end{bmatrix} \\ v_{\mathbb{F}}(\mathbb{F}, \mathbb{G}) &\triangleq \frac{d_{\mathbb{F}} \mathbf{l}(\mathbb{F}, \mathbb{G})}{dt} \quad \text{and} \quad v_{\mathbb{G}}(\mathbb{F}, \mathbb{G}) \triangleq \frac{d_{\mathbb{G}} \mathbf{l}(\mathbb{F}, \mathbb{G})}{dt} \end{aligned} \quad (1.40)$$

Observe that $\mathcal{V}_{\mathbb{F}}(\mathbb{F}, \mathbb{G})$ and $\mathcal{V}_{\mathbb{G}}(\mathbb{F}, \mathbb{G})$ are both zero when \mathbb{F} and \mathbb{G} are frames on the same rigid body.

2. With the coordinate representation of $\phi^*(\mathbb{F}, \mathbb{G})$ defined by (1.31), we have:

$$\phi^*(\mathbb{F}, \mathbb{G}) = \begin{pmatrix} {}^{\mathbb{G}}\mathfrak{R}_{\mathbb{F}} & \mathbf{0}_3 \\ \mathbf{0}_3 & {}^{\mathbb{G}}\mathfrak{R}_{\mathbb{F}} \end{pmatrix} \begin{pmatrix} \mathbf{I}_3 & \mathbf{0}_3 \\ -{}^{\mathbb{F}}\tilde{\mathbf{l}}(\mathbb{F}, \mathbb{G}) & \mathbf{I}_3 \end{pmatrix} \quad (1.41)$$

Show that the time-derivative of this coordinate representation of $\phi^*(\mathbb{F}, \mathbb{G})$ is given by:

$$\frac{d\phi^*(\mathbb{F}, \mathbb{G})}{dt} = \tilde{\mathcal{V}}_{\mathbb{F}}(\mathbb{G}, \mathbb{F}) \phi^*(\mathbb{F}, \mathbb{G}) = \phi^*(\mathbb{F}, \mathbb{G}) \tilde{\mathcal{V}}_{\mathbb{G}}(\mathbb{G}, \mathbb{F}) \quad (1.42)$$

3. Applying (1.42) to $\phi^*(\mathbb{G}, \mathbb{F})$ it follows that

$$\frac{d\phi^*(\mathbb{G}, \mathbb{F})}{dt} = \tilde{\mathcal{V}}_{\mathbb{G}}(\mathbb{F}, \mathbb{G}) \phi^*(\mathbb{G}, \mathbb{F}) = \phi^*(\mathbb{G}, \mathbb{F}) \tilde{\mathcal{V}}_{\mathbb{F}}(\mathbb{F}, \mathbb{G}) \quad (1.43)$$

On the other hand, since $\phi^*(\mathbb{G}, \mathbb{F}) = \phi^{-*}(\mathbb{F}, \mathbb{G})$, it follows from the matrix inverse derivative identity in (A.28) on page 402 that

$$\frac{d\phi^*(\mathbb{G}, \mathbb{F})}{dt} = -\phi^*(\mathbb{G}, \mathbb{F}) \frac{d\phi^*(\mathbb{F}, \mathbb{G})}{dt} \phi^*(\mathbb{G}, \mathbb{F}) \quad (1.44)$$

Verify that the expressions in (1.42) and (1.43) satisfy the identity in (1.44).

4. For frames \mathbb{F} , \mathbb{G} and \mathbb{H} , we have $\phi^*(\mathbb{F}, \mathbb{H}) = \phi^*(\mathbb{G}, \mathbb{H}) \phi^*(\mathbb{F}, \mathbb{G})$. Show that the time derivative expression in (1.42) satisfies the product rule for derivatives:

$$\frac{d\phi^*(\mathbb{F}, \mathbb{H})}{dt} = \frac{d\phi^*(\mathbb{G}, \mathbb{H})}{dt} \phi^*(\mathbb{F}, \mathbb{G}) + \phi^*(\mathbb{G}, \mathbb{H}) \frac{d\phi^*(\mathbb{F}, \mathbb{G})}{dt} \quad (1.45)$$

■

1.5 Spatial Forces

Define the **spatial force** spatial vector, $f(x)$, at a frame x as

$$f(x) \triangleq \begin{bmatrix} N(x) \\ F(x) \end{bmatrix} \quad (1.46)$$

where the $N(x)$ denotes the rotational moment component and $F(x)$ the linear force component.

We now look at the relationship between spatial forces at a pair of points x and y on a rigid body. The input power generated by a spatial force f is independent of the body reference point x or y . Thus

$$f^*(x)\mathcal{V}(x) = f^*(y)\mathcal{V}(y)$$

Using $\mathcal{V}(y) \stackrel{1.33}{=} \phi^*(x,y)\mathcal{V}(x)$ in the above we obtain:

$$f^*(x)\mathcal{V}(x) = f^*(y)\phi^*(x,y)\mathcal{V}(x)$$

Since $\mathcal{V}(x)$ can be chosen arbitrarily, it follows that the following relationship must hold:

$$f(x) = \phi(x,y)f(y) \quad (1.47)$$

This implies that the $f(y)$ spatial force at a point y on a rigid body is equivalent to a spatial force $f(x) = \phi(x,y)f(y)$ at another point x on the body. The transformation relationships in (1.47) and (1.33) are the duals of each other, and the $\phi^*(x,y)$ transformation for spatial velocities is the adjoint of the $\phi(x,y)$ transformation for spatial forces.

Chapter 2

Single Rigid Body Dynamics

This chapter develops the dynamical equations of motion for a single rigid body in multiple different ways: about the body center of mass, about an arbitrary point on the body, using body and inertial frame derivatives, and finally using an inertially fixed velocity reference point. The properties of each of these formulations are explored. These alternative formulations also help illustrate the analytical and transformation properties of spatial quantities.

2.1 Spatial Inertia and Momentum of a Rigid Body

We begin first by defining the spatial inertia and the spatial momentum of a rigid body, and their relationships for points on the rigid body.

2.1.1 The Spatial Inertia

The kinetic energy of a single rigid body can be expressed as the following volume integral:

$$\mathfrak{K}_e = \frac{1}{2} \int_{\Omega} v^*(x) \rho(x) v(x) d\vartheta(x) \quad (2.1)$$

Here $v(x)$ is the linear velocity of point x , $\rho(x)$ the mass density at x , $d\vartheta(x)$ is an infinitesimal volume element containing x , and Ω is the body volume. The linear velocity $v(x)$ and the spatial velocity $\mathcal{V}(x)$ at the same point x are related by

$$v(x) \stackrel{1.20}{=} [\mathbf{0}, \quad \mathbf{I}] \mathcal{V}(x) \quad (2.2)$$

Substitution of (2.2) in (2.1) leads to the following new expression for the kinetic energy:

$$\mathfrak{K}_e = \frac{1}{2} \int_{\Omega} \mathcal{V}^*(x) \begin{bmatrix} \mathbf{0} \\ \mathbf{I} \end{bmatrix} \rho(x) [\mathbf{0}, \quad \mathbf{I}] \mathcal{V}(x) d\vartheta(x) \quad (2.3)$$

Now pick a point k on the rigid body and let $\mathcal{V}(k)$ denote the spatial velocity at that point. The spatial velocity at any other point x on the rigid body, $\mathcal{V}(x)$, is related to $\mathcal{V}(k)$ via

$$\mathcal{V}(x) \stackrel{1.33}{=} \phi^*(k, x) \mathcal{V}(k) \quad \forall x \in \Omega \quad (2.4)$$

This equation states that the spatial velocity $\mathcal{V}(x)$ at any point x on a rigid body can be obtained from $\mathcal{V}(k)$ by making use of the $\phi^*(k, x)$ rigid body transformation matrix. Use of (2.4) in (2.3) allows us to re-express the kinetic energy of the body as

$$\begin{aligned} \mathfrak{K}_e &\stackrel{2.3, 2.4}{=} \frac{1}{2} \mathcal{V}^*(k) \left\{ \int_{\Omega} \phi(k, x) \begin{bmatrix} \mathbf{0} \\ \mathbf{I} \end{bmatrix} \rho(x) [\mathbf{0}, \quad \mathbf{I}] \phi^*(k, x) d\vartheta(x) \right\} \mathcal{V}(k) \\ &= \frac{1}{2} \mathcal{V}^*(k) M(k) \mathcal{V}(k) \end{aligned} \quad (2.5)$$

$M(k)$ is the **spatial inertia** of the body about the point k defined by the inner term in the integral as follows:

$$\begin{aligned} M(k) &\triangleq \int_{\Omega} \phi(k, x) \begin{bmatrix} \mathbf{0} \\ \mathbf{I} \end{bmatrix} \rho(x) [\mathbf{0}, \quad \mathbf{I}] \phi^*(k, x) d\vartheta(x) \\ &= \int_{\Omega} \begin{pmatrix} \mathbf{I} & \tilde{l}(k, x) \\ \mathbf{0} & \mathbf{I} \end{pmatrix} \begin{bmatrix} \mathbf{0} \\ \mathbf{I} \end{bmatrix} \rho(x) [\mathbf{0}, \quad \mathbf{I}] \begin{pmatrix} \mathbf{I} & \mathbf{0} \\ -\tilde{l}(k, x) & \mathbf{I} \end{pmatrix} d\vartheta(x) \\ &= \int_{\Omega} \begin{pmatrix} -\tilde{l}(k, x) \tilde{l}(k, x) & \tilde{l}(k, x) \\ -\tilde{l}(k, x) & \mathbf{I} \end{pmatrix} \rho(x) d\vartheta(x) \end{aligned} \quad (2.6)$$

In other words,

$$M(k) = \begin{pmatrix} \mathcal{J}(k) & \mathfrak{m} \tilde{p}(k) \\ -\mathfrak{m} \tilde{p}(k) & \mathfrak{m} I_3 \end{pmatrix} \in \mathcal{R}^{6 \times 6} \quad (2.7)$$

where

$$\begin{aligned} \mathfrak{m} &\triangleq \int_{\Omega} \rho(x) d\vartheta(x) \quad \in \mathcal{R}^1 \\ p(k) &\triangleq \frac{1}{\mathfrak{m}} \int_{\Omega} l(k, x) \rho(x) d\vartheta(x) \quad \in \mathcal{R}^3 \\ \mathcal{J}(k) &\triangleq - \int_{\Omega} \tilde{l}(k, x) \tilde{l}(k, x) \rho(x) d\vartheta(x) \quad \in \mathcal{R}^{3 \times 3} \end{aligned} \quad (2.8)$$

$\mathcal{J}(k)$ represents the **rotational inertia** of the body about the point k ; m is the **mass** of the body; and $p(k)$ is a 3-vector. Often, m , $mp(k)$ and $\mathcal{J}(k)$ are referred to as the **zeroth, first and second order moments of inertia**, respectively of the body about the point k .

Exercise 2.1 Rigid body center of mass.

For two points x and y on a rigid body, show that the first moment vectors, $p(x)$ and $p(y)$, respectively, are related by

$$p(x) = l(x, y) + p(y) \quad (2.9)$$

■

A consequence of this observation is that the point C , referred to as the **center of mass** or **centroid** of the body, and defined by the first moment vector, $p(k)$, is the same point defined by the first moment vector, $p(x)$ for the different reference point x . Thus, the location of the center of mass, is *unique* and *independent* of the choice of reference point. From the definition of the center of mass, it is clear that $p(C) = 0$, and therefore the $M(C)$ spatial inertia about the center of mass has the simpler block-diagonal form

$$M(C) = \begin{pmatrix} \mathcal{J}(C) & \mathbf{0} \\ \mathbf{0} & mI_3 \end{pmatrix} \quad (2.10)$$

Except for the mass, the first and second moments of inertia, as well as the spatial inertia itself depend on the choice of the reference point.

Exercise 2.2 Parallel-axis theorem for rotational inertias.

1. For an arbitrary point x , show that the rotational moment of inertia $\mathcal{J}(x)$ is related to $\mathcal{J}(C)$ as follows:

$$\mathcal{J}(x) = \mathcal{J}(C) - m\tilde{p}(x)\tilde{p}(x) \quad (2.11)$$

- Equation (2.11) is referred to as the **parallel-axis theorem** for computing the rotational inertia of a rigid body at point other than the center of mass from the rotational inertia at the center of mass.
2. Show that $\mathcal{J}(x)$ is symmetric and positive semi-definite for all x . Also, show that its minimum value is at the center of mass of the body. That is, $\mathcal{J}(x) \geq \mathcal{J}(C)$ for all points x .
 3. $\mathcal{J}(x)$ fails to be positive definite only for “pathological” rigid bodies. Give examples of rigid bodies for whom $\mathcal{J}(x)$ fails to be positive definite.

■

A coordinate-frame representation of $M(z)$ is a 6×6 symmetric, positive semi-definite matrix. While, in general, 21 elements are required to specify a 6×6 symmetric matrix, only ten elements are required to specify a spatial inertia matrix

because of its special structure: one for the mass scalar, three for the center of mass location 3-vector, and six for the symmetric rotational inertia matrix.

2.1.2 The Parallel-Axis Theorem for Spatial Inertias

Let us now examine the relationship between the spatial inertias, $M(x)$ and $M(y)$, about a pair of points x and y . From (2.6) we have

$$\begin{aligned} M(x) &= \int_{\Omega} \phi(x, z) \begin{bmatrix} \mathbf{0} \\ \mathbf{I} \end{bmatrix} \rho(z) [\mathbf{0}, \quad \mathbf{I}] \phi^*(x, z) d\vartheta(z) \\ &\stackrel{1.32}{=} \int_{\Omega} \phi(x, y) \left[\phi(y, z) \begin{bmatrix} \mathbf{0} \\ \mathbf{I} \end{bmatrix} \rho(z) [\mathbf{0}, \quad \mathbf{I}] \phi^*(y, z) \right] \phi^*(x, y) d\vartheta(z) \\ &= \phi(x, y) \left[\int_{\Omega} \phi(y, z) \begin{bmatrix} \mathbf{0} \\ \mathbf{I} \end{bmatrix} \rho(z) [\mathbf{0}, \quad \mathbf{I}] \phi^*(y, z) d\vartheta(z) \right] \phi^*(x, y) \\ &\stackrel{2.6}{=} \phi(x, y) M(y) \phi^*(x, y) \end{aligned}$$

Thus, the spatial inertia $M(x)$ about a point x is related to the spatial inertia $M(y)$ about another point y by the following expression:

$$M(x) = \phi(x, y) M(y) \phi^*(x, y) \quad (2.12)$$

Equation (2.12) is the **parallel axis theorem for spatial inertias** and defines the relationship between the spatial inertias about arbitrary pairs of points on a rigid body. Observe that neither of the points in (2.12) has to be the center of mass \mathbb{C} . Using (2.11) (or alternatively by expanding out both sides of (2.12)) we obtain the following expression relating the rotational inertias about the points x and y :

$$\mathcal{J}(x) = \mathcal{J}(y) - m \tilde{p}(x) \tilde{p}(x) + m \tilde{p}(y) \tilde{p}(y) \quad (2.13)$$

The parallel axis theorem for spatial inertias is more compact when compared with the parallel axis theorem for rotational inertias. It encapsulates (2.9) and (2.13) into a single equation. While the concise form of (2.12) is analytically convenient, the component level expressions in (2.9) and (2.13) are utilized for efficient computational implementation of expressions involving the spatial inertia matrix.

Exercise 2.3 Positive semi-definiteness of spatial inertias.

Show that $M(x)$ is always positive semi-definite. Show that it is positive definite if and only if $\mathcal{J}(\mathbb{C})$ is positive definite. ■

2.1.3 Spatial Inertia of a Composite Assemblage of Rigid Bodies

Equation (2.12) provides a way to compute the total spatial inertia of a body made up of several component rigid bodies. For example, if a body is composed of a rigid body with spatial inertia $M_1(x)$ about point x , rigidly attached to a second rigid body with spatial inertia $M_2(y)$ about point y , then the overall spatial inertia of the composite body $M(z)$ about another point z is given by

$$M(z) = \phi(z, x)M_1(x)\phi^*(z, x) + \phi(z, y)M_2(y)\phi^*(z, y)$$

In other words, the process of computing the overall spatial inertia of a body consists of first using the parallel-axis theorem to transform all the component spatial inertias to a common reference point, and then adding them up to obtain the overall spatial inertia. This process is necessary because the addition of spatial inertias is permissible only for spatial inertias referenced about the same point.

Exercise 2.4 Invariance of the kinetic energy.

Show that the kinetic energy of a rigid body defined by (2.5) does not depend on the reference point chosen for its computation. That is, for an arbitrary pair of points x and y on a rigid body, we have

$$\mathcal{K}_e = \frac{1}{2}\mathcal{V}^*(x)M(x)\mathcal{V}(x) = \frac{1}{2}\mathcal{V}^*(y)M(y)\mathcal{V}(y) \quad (2.14)$$

■

2.1.4 The Spatial Momentum of a Rigid Body

Let us consider a rigid body rotating with angular velocity ω , and center of mass linear velocity, $mv(\mathbb{C})$. About its center of mass, $mv(\mathbb{C})$ represents the linear momentum of the body, while $\mathcal{J}(\mathbb{C})\omega$ represents its angular momentum. We combine these to define the **spatial momentum** of the body about its center of mass, $\mathfrak{h}(\mathbb{C})$, as

$$\mathfrak{h}(\mathbb{C}) \triangleq \begin{bmatrix} \mathcal{J}(\mathbb{C})\omega(\mathbb{C}) \\ mv(\mathbb{C}) \end{bmatrix} \stackrel{2.10}{=} M(\mathbb{C})\mathcal{V}(\mathbb{C}) \quad (2.15)$$

Generalizing the expression $\mathfrak{h}(\mathbb{C}) = M(\mathbb{C})\mathcal{V}(\mathbb{C})$ to arbitrary points, the spatial momentum of a rigid body about an arbitrary point z , $\mathfrak{h}(z)$, is defined as

$$\mathfrak{h}(z) \triangleq M(z)\mathcal{V}(z) \in \mathcal{R}^6 \quad (2.16)$$

Since $M(z)$ and $\mathcal{V}(z)$ depend on the reference point z , the $\mathfrak{h}(z)$ spatial momentum does as well. The following exercise examines the relationship between the spatial momenta about points on a rigid body.

Exercise 2.5 Relationship of spatial momenta about points x and y .

Show that the $\mathfrak{h}(x)$, spatial momentum of a rigid body about a point x , is related to the $\mathfrak{h}(y)$ spatial momentum about another point y on the body, by the following expression:

$$\mathfrak{h}(x) = \phi(x, y)\mathfrak{h}(y) \quad (2.17)$$

■

Equation (2.17) states that we can obtain the spatial momentum of a rigid body about any point on the body from the knowledge of the spatial momentum about a specific point on the body.

So far we have encountered several instances of transformations that relate spatial properties of a rigid body across different points on the body. Table 2.1 summarizes some of the key relationships involving the spatial quantities for a pair of points x and y on a rigid body.

Table 2.1 Relationship between rigid body quantities for a pair of points x and y on a rigid body.

	Point y	Point x
Spatial velocities	$\mathcal{V}(y) = \phi^*(x, y)\mathcal{V}(x)$	$\mathcal{V}(x)$
Spatial forces	$\mathfrak{f}(y)$	$\mathfrak{f}(x) = \phi(x, y)\mathfrak{f}(y)$
Spatial inertias	$M(y)$	$M(x) = \phi(x, y)M(y)\phi^*(x, y)$
Spatial momenta	$\mathfrak{h}(y)$	$\mathfrak{h}(x) = \phi(x, y)\mathfrak{h}(y)$
Kinetic energy	$\frac{1}{2}\mathcal{V}^*(y)M(y)\mathcal{V}(y)$	$\frac{1}{2}\mathcal{V}^*(x)M(x)\mathcal{V}(x)$

The central role played by $\phi(x, y)$ in these transformations is the reason for referring to it as the *rigid body transformation matrix*.

2.2 Motion Coordinates

The motion state of a rigid body is completely characterized by its position and attitude *configuration* and its linear and angular *velocity* coordinates. More generally, the motion state of any mechanical system is defined by its configuration and velocity coordinates. The dynamics problem addresses the properties and mathematical analysis of the evolution of the motion state of a system with time. A key step in the development of dynamics models is the determination of the functional dependency

of the time derivative of the motion state on the motion state itself, and the external forces being applied on the system. This mathematical relationship is referred to as the **equations of motion for the system**. More precisely, the part of the equations of motion pertaining to the time derivatives of configuration coordinates are referred to as the **kinematics** part. The remaining part describing the derivatives of the velocities is referred to as the **dynamics** part. While the kinematics and dynamics differential equations are typically coupled, specific choices of coordinates can help decouple and simplify their expressions.

2.2.1 Generalized Coordinates and Velocities

The coordinates used to define the configuration state of a system are referred to as the **generalized coordinates** for the system. We use θ to denote the vector of generalized configuration coordinates for a system. The dimensionality of θ is at least as large as the number of velocity degrees of freedom in the system.

For a rigid body, the positional part of the generalized coordinates is typically just the components of the position vector of the body frame with respect to the inertial coordinate frame. The remaining generalized coordinates define the attitude of the body. Appendix B describes some of the possible attitude generalized coordinates choices for a rigid body. Options include Euler angles, angle-axis parameters and quaternion attitude representations.

The variables for parametrizing the velocity space of the system are referred to as the **generalized velocities** for the system. We use β to denote the vector of generalized velocity coordinates for a system. While the time derivatives of the generalized coordinates, $\dot{\theta}$, are typically chosen as generalized velocities, this is not required – and at times not the best choice. The generalized velocities are not even required to be integrable quantities. Non-integrable velocity coordinates are also referred to as **quasi-velocities**. The term quasi-velocities designates pseudo-derivative since the velocity coordinates are not the time derivatives of any function of the generalized coordinates.

For a rigid body, an obvious choices of generalized velocity coordinates are the components of the spatial velocity, $\mathcal{V}(x)$, of a point x on the body represented either in the body frame, \mathbb{B} , or in the \mathbb{I} inertial frame. For convenience, the point x is often chosen as the location of the body frame \mathbb{B} itself. For the \mathbb{B} frame representation, the generalized velocity coordinates are denoted $\beta_{\mathbb{B}} = {}^{\mathbb{B}}\mathcal{V}(x)$, while for the \mathbb{I} frame representation, the generalized velocities are denoted $\beta_{\mathbb{I}} = {}^{\mathbb{I}}\mathcal{V}(x)$. The angular velocity components of the generalized velocities are examples of non-integrable velocity coordinates.

2.2.2 Generalized Forces

The definition of the **generalized forces** for a system depends on the choice of generalized velocities for the system. With β and \mathcal{T} denoting the vectors of generalized velocities and forces, respectively for the system, the generalized forces must satisfy the requirement that the $\mathcal{T}^* \beta$ expression represents the input power. Since the input power is independent of the specific choice of generalized velocities, this requirement implies that, if a new set of generalized velocities γ is chosen, the definition of the generalized forces must be changed accordingly. Thus, if γ is related to β by the relationship $\gamma = A(\theta)\beta$, then it requires that $A^{-*}(\theta)\mathcal{T}$ be the corresponding generalized forces. It is important to remember that the generalized forces do not have to directly correspond to physical forces on the system, and can be a transformation of these forces.

2.2.3 Generalized Accelerations

The **generalized acceleration coordinates** are defined as the time-derivatives of the generalized velocity coordinates. Different choices for the generalized velocity coordinates lead to different generalized acceleration coordinates. The generalized accelerations corresponding to the two choices of rigid body generalized velocities we have discussed are:

$$\dot{\beta}_{\mathbb{B}}(x) \triangleq \frac{d^{\mathbb{B}}\mathcal{V}(x)}{dt} = \frac{d_{\mathbb{B}}\mathcal{V}(x)}{dt} \quad \text{and} \quad \dot{\beta}_{\mathcal{J}}(x) \triangleq \frac{d^{\mathcal{I}}\mathcal{V}(x)}{dt} = \frac{d_{\mathcal{I}}\mathcal{V}(x)}{dt} \quad (2.18)$$

The relationship between $\dot{\beta}_{\mathbb{B}}(x)$ and $\dot{\beta}_{\mathcal{J}}(x)$ is as follows:

$$\begin{aligned} \dot{\beta}_{\mathcal{J}}(x) &\stackrel{1.28, 2.18}{=} \dot{\beta}_{\mathbb{B}}(x) + \tilde{\mathcal{V}}^{\omega}(x)\mathcal{V}(x) \stackrel{1.36d}{=} \dot{\beta}_{\mathbb{B}}(x) + \bar{\mathcal{V}}(x)\mathcal{V}(x) \\ &= \dot{\beta}_{\mathbb{B}}(x) + \begin{bmatrix} 0 \\ \tilde{\omega}(x)v(x) \end{bmatrix} \end{aligned} \quad (2.19)$$

Equation (2.19) defines the relationship between the two definitions of generalized accelerations. As we will see in the following sections, different choices for the generalized velocities lead to different formulations of the equations of motion. Undoubtedly, since these different formulations refer to the same physical system, they are fundamentally equivalent descriptions of the system and can be transformed into each other.

2.3 Equations of Motion with Inertial Frame Derivatives

In this section we formulate the equations of motion of a rigid body using inertial frame derivatives for generalized velocities.

2.3.1 Equations of Motion with $\beta_J = \mathbb{I}\mathcal{V}(\mathbb{C})$

It is well known that the linear and angular equations of motion of a rigid body are decoupled from each other about the center of mass \mathbb{C} . With $N(\mathbb{C})$ and $F(\mathbb{C})$ denoting the moment and linear force at the center of mass of the body, the dynamical equations of motion for a rigid body are defined by Newton's law and Euler's equations [185] as follows:

$$N(\mathbb{C}) = \frac{d_{\mathbb{I}} \mathcal{J}(\mathbb{C}) \omega(\mathbb{C})}{dt} \quad \text{and} \quad F(\mathbb{C}) = \frac{d_{\mathbb{I}} m v(\mathbb{C})}{dt} \quad (2.20)$$

Equation (2.20) states that about the center of mass, the rate of change of the angular and linear momentum of the rigid body are equal to the applied moment and force, respectively. In other words, with the spatial force at \mathbb{C} denoted as $f(\mathbb{C}) \triangleq \begin{bmatrix} N(\mathbb{C}) \\ F(\mathbb{C}) \end{bmatrix}$, and using (2.15), (2.20) can be rephrased as

$$f(\mathbb{C}) = \frac{d_{\mathbb{I}} M(\mathbb{C}) \mathcal{V}(\mathbb{C})}{dt} = \frac{d_{\mathbb{I}} h(\mathbb{C})}{dt} \quad (2.21)$$

This more compact expression states that the rate of change of the inertial frame spatial momentum about the center of mass for the body, $h(\mathbb{C})$, is equal to the external spatial force at its center of mass.

It follows that in the absence of external spatial forces, i.e., $f(\mathbb{C}) \equiv \mathbf{0}$, the spatial momentum vector $h(\mathbb{C})$ remains constant with time in the inertial frame. This property is also known as the *conservation of spatial momentum* property for a rigid body in the absence of external forces.

The following exercise derives an expression for the inertial time derivative of the spatial inertia of a rigid body about an arbitrary point on the body. We will use this later to establish the equations of motion for the body.

Exercise 2.6 Time derivative of rigid body spatial inertia.

Let z denote an arbitrary point on a rigid body. Since the spatial inertia of a rigid body is constant, the body frame time derivative of the spatial inertia matrix $M(z)$ is zero. Show that the inertial frame time derivative, $\dot{M}(z)$, is

$$\dot{M}(z) \triangleq \frac{d_{\mathbb{I}} M(z)}{dt} = \tilde{\mathcal{V}}^{\omega}(z) M(z) - M(z) \tilde{\mathcal{V}}^{\omega}(z) \quad (2.22)$$

where $\tilde{\mathcal{V}}^\omega(z)$ contains the angular component of the spatial velocity $\mathcal{V}(z)$ as defined in (1.21) on page 9. ■

The following lemma summarizes the equations of motion for a rigid body using ${}^I\mathcal{V}(\mathbb{C})$ as the generalized velocities.

Lemma 2.1 Body equations of motion using $\beta_J = {}^I\mathcal{V}(\mathbb{C})$.

The equations of motion for a rigid body about its center of mass using inertial frame derivatives are as follows:

$$\begin{aligned}\mathfrak{f}(\mathbb{C}) &= M(\mathbb{C})\dot{\beta}_J(\mathbb{C}) + \mathfrak{b}_J(\mathbb{C}) \\ \text{where } \mathfrak{b}_J(\mathbb{C}) &\stackrel{\triangle}{=} \tilde{\mathcal{V}}^\omega(\mathbb{C})M(\mathbb{C})\mathcal{V}^\omega(\mathbb{C}) \\ &= \bar{\mathcal{V}}^\omega(\mathbb{C})M(\mathbb{C})\mathcal{V}^\omega(\mathbb{C}) = \begin{bmatrix} \tilde{\omega} \mathcal{J}(\mathbb{C})\omega \\ \mathbf{0} \end{bmatrix} \quad (2.23)\end{aligned}$$

Proof: We have

$$\begin{aligned}\mathfrak{f}(\mathbb{C}) &\stackrel{2.21}{=} M(\mathbb{C})\dot{\beta}_J(\mathbb{C}) + \frac{d_I M(\mathbb{C})}{dt} \mathcal{V}(\mathbb{C}) \\ &\stackrel{2.22}{=} M(\mathbb{C})\dot{\beta}_J(\mathbb{C}) + [\tilde{\mathcal{V}}^\omega(\mathbb{C})M(\mathbb{C}) - M(\mathbb{C})\tilde{\mathcal{V}}^\omega(\mathbb{C})] \mathcal{V}(\mathbb{C}) \\ &\stackrel{1.22}{=} M(\mathbb{C})\dot{\beta}_J(\mathbb{C}) + \tilde{\mathcal{V}}^\omega(\mathbb{C})M(\mathbb{C})\mathcal{V}^\omega(\mathbb{C}) \\ &\quad + [\tilde{\mathcal{V}}^\omega(\mathbb{C})M(\mathbb{C})\mathcal{V}^\omega(\mathbb{C}) - M(\mathbb{C})\tilde{\mathcal{V}}^\omega(\mathbb{C})\mathcal{V}^\omega(\mathbb{C})] \\ &\stackrel{2.10}{=} M(\mathbb{C})\dot{\beta}_J(\mathbb{C}) + \tilde{\mathcal{V}}^\omega(\mathbb{C})M(\mathbb{C})\mathcal{V}^\omega(\mathbb{C})\end{aligned}$$

The last step used the expression for $M(\mathbb{C})$ from 2.10 to verify that

$$[\tilde{\mathcal{V}}^\omega(\mathbb{C})M(\mathbb{C})\mathcal{V}^\omega(\mathbb{C}) - M(\mathbb{C})\tilde{\mathcal{V}}^\omega(\mathbb{C})\mathcal{V}^\omega(\mathbb{C})] = \mathbf{0}$$

The last equality in (2.23) follows from expanding out $\tilde{\mathcal{V}}^\omega(\mathbb{C})M(\mathbb{C})\mathcal{V}^\omega(\mathbb{C})$. ■

The following exercise establishes that the $\mathfrak{b}_J(\mathbb{C})$ gyroscopic spatial force is a non-working spatial force.

Exercise 2.7 $\mathfrak{b}_J(\mathbb{C})$ gyroscopic spatial force does no work.

The power generated by a spatial force at a point on a rigid body is its dot product with the spatial velocity at the point. Show that the $\mathfrak{b}_J(\mathbb{C})$ gyroscopic spatial force term does no work, i.e., $\mathcal{V}^*(\mathbb{C})\mathfrak{b}_J(\mathbb{C}) = \mathbf{0}$. ■

2.3.2 Equations of Motion with $\beta_J = \mathbb{V}(z)$

The previous section used the spatial velocity at the \mathbb{C} center of mass, $\mathbb{V}(\mathbb{C})$, as the generalized velocity coordinates for the rigid body. In this section we switch to using the spatial velocity, $\mathbb{V}(z)$, at an arbitrary point z on the body as the generalized velocity coordinates for the body. First, the following exercise establishes the relationship between the generalized accelerations $\dot{\beta}_J$ between different points on a rigid body.

Exercise 2.8 Inertial generalized accelerations at two points.

Show that the “inertial” generalized accelerations, $\dot{\beta}_J(x)$ and $\dot{\beta}_J(y)$, at a pair of points x and y on a rigid body are related to each other as follows:

$$\begin{aligned}\dot{\beta}_J(y) &\triangleq \frac{d\mathbb{V}(y)}{dt} = \phi^*(x, y)\dot{\beta}_J(x) - \tilde{\mathcal{V}}(y)\mathcal{V}(x) \\ &= \phi^*(x, y)\dot{\beta}_J(x) + \begin{bmatrix} \mathbf{0} \\ \tilde{\omega} \tilde{\omega} I(x, y) \end{bmatrix}\end{aligned}\quad (2.24)$$

■

For an arbitrary point z on the rigid body, $I(z, \mathbb{C})$ is the first moment vector $p(z)$. Thus, from (2.24) it follows that:

$$\dot{\beta}_J(z) \triangleq \frac{d\mathbb{V}(z)}{dt} = \phi^*(\mathbb{C}, z)\dot{\beta}_J(\mathbb{C}) + \begin{bmatrix} \mathbf{0} \\ -\tilde{\omega} \tilde{\omega} p(z) \end{bmatrix} \quad (2.25)$$

The equations of motion of a rigid body about an arbitrary point z using inertial frame derivatives are summarized in the following lemma.

Lemma 2.2 Body equations of motion with $\beta_J = \mathbb{V}(z)$.

The equations of motion for a rigid body about an arbitrary point, z , using inertial frame derivatives are:

$$\begin{aligned}f(z) &= M(z)\dot{\beta}_J(z) + b_J(z) \\ \text{where } b_J(z) &\triangleq \tilde{\mathcal{V}}^\omega(z)M(z)\mathcal{V}^\omega(z) = \bar{\mathcal{V}}^\omega(z)M(z)\mathcal{V}^\omega(z) \\ &= \begin{bmatrix} \tilde{\omega} \mathcal{J}(z)\omega \\ m \tilde{\omega} \tilde{\omega} p(z) \end{bmatrix}\end{aligned}\quad (2.26)$$

Proof: We have,

$$\begin{aligned}
 M(z)\dot{\beta}_J(z) &\stackrel{2.25}{=} M(z) \left(\phi^*(C, z)\dot{\beta}_J(C) + \begin{bmatrix} \mathbf{0} \\ -\tilde{\omega} \tilde{\omega} p(z) \end{bmatrix} \right) \\
 &\stackrel{2.12, 2.7}{=} \phi(z, C)M(C)\dot{\beta}_J(C) - \begin{bmatrix} m \tilde{p}(z) \tilde{\omega} \tilde{\omega} p(z) \\ m \tilde{\omega} \tilde{\omega} p(z) \end{bmatrix} \\
 &\stackrel{2.23, A.1}{=} \phi(z, C) \left(f(C) - \begin{bmatrix} \tilde{\omega} J(C)\omega \\ \mathbf{0} \end{bmatrix} \right) - \begin{bmatrix} -m \tilde{\omega} \tilde{p}(z) \tilde{p}(z) \omega \\ m \tilde{\omega} \tilde{\omega} p(z) \end{bmatrix} \\
 &\stackrel{1.47}{=} f(z) - \begin{bmatrix} \tilde{\omega} (J(C) - m \tilde{p}(z) \tilde{p}(z)) \omega \\ m \tilde{\omega} \tilde{\omega} p(z) \end{bmatrix} \\
 &\stackrel{2.11}{=} f(z) - \begin{bmatrix} \tilde{\omega} J(z)\omega \\ m \tilde{\omega} \tilde{\omega} p(z) \end{bmatrix}
 \end{aligned}$$

This establishes the latter equality in (2.26). The middle equality follows from the following:

$$\tilde{v}^\omega(z)M(z)v^\omega(z) = \begin{pmatrix} \tilde{\omega} & \mathbf{0} \\ \mathbf{0} & \tilde{\omega} \end{pmatrix} \begin{bmatrix} J(C)\omega \\ -m \tilde{p}(z) \omega \end{bmatrix} = \begin{bmatrix} \tilde{\omega} J(z)\omega \\ m \tilde{\omega} \tilde{\omega} p(z) \end{bmatrix}$$

■

The more general equations of motion in (2.24) reduce to the ones about the center of mass C when $z = C$ since $p(C) = \mathbf{0}$. Observe that the expression for the gyroscopic spatial force in (2.26) depends only on the angular velocity component and is independent of the linear velocity. Thus, the instantaneous generalized acceleration in this formulation is independent of the linear velocity of the body. This formulation is therefore, less susceptible to numeric integration errors for systems with large linear velocities (e.g. space vehicles).

Exercise 2.9 $b_J(z)$ gyroscopic spatial force does work.

Show that the $b_J(z)$ gyroscopic force term does work. On the other hand, show that as is to be expected, the kinetic energy is conserved in the absence of external forces when using the inertial derivative form of the equations of motion. ■

Exercise 2.10 Non-conservation of spatial momentum.

In (2.21) we observed that the rate of change of the spatial momentum about the center of mass is equal to the spatial force at the center of mass. In contrast, show that this equality does not hold for other reference points, z , that is

$$f(z) \neq \frac{d_{\mathbb{I}} h(z)}{dt} \quad (2.27)$$

when the point z is not the center of mass. ■

One consequence of (2.27) is that the spatial momentum $\mathfrak{h}(z)$ vector is *not constant* in the inertial frame even in the absence of external forces, i.e., even when $\mathfrak{f}(z) \equiv \mathbf{0}$ when the point z is not the center of mass of the body. In other words, the spatial momentum is not conserved in the absence of external forces at points other than the center of mass.

2.4 Equations of Motion with Body Frame Derivatives

In this section we switch gears to examine the equations of motion of a rigid body using body frame derivatives for the generalized velocities.

Lemma 2.3 **Body equations of motion with** $\beta_{\mathbb{B}} = {}^{\mathbb{B}}\mathcal{V}(z)$.

The equations of motion for a rigid body about an arbitrary point z using body frame derivatives are:

$$\begin{aligned} \mathfrak{f}(z) &= M(z)\dot{\beta}_{\mathbb{B}}(z) + \mathfrak{b}(z) \\ \text{where } \mathfrak{b}(z) &\stackrel{\triangle}{=} \bar{\mathcal{V}}(z)\mathfrak{h}(z) = \bar{\mathcal{V}}(z)M(z)\mathcal{V}(z) \end{aligned} \quad (2.28)$$

Proof: Using (2.19) we have

$$\begin{aligned} M(z)\dot{\beta}_{\mathbb{B}}(z) &\stackrel{2.19}{=} M(z)\left(\dot{\beta}_{\mathcal{J}}(z) - \begin{bmatrix} 0 \\ \tilde{\omega} v(z) \end{bmatrix}\right) \\ &\stackrel{2.26,2.7}{=} \mathfrak{f}(z) - \begin{bmatrix} \tilde{\omega} \mathcal{J}(z)\omega \\ m \tilde{\omega} \tilde{\omega} p(z) \end{bmatrix} - \begin{bmatrix} m \tilde{p}(z) \tilde{\omega} v(z) \\ m \tilde{\omega} v(z) \end{bmatrix} \\ &= \mathfrak{f}(z) - \begin{bmatrix} \tilde{\omega} \mathcal{J}(z)\omega + m \tilde{p}(z) \tilde{\omega} v(z) \\ m \tilde{\omega} \tilde{\omega} p(z) + m \tilde{\omega} v(z) \end{bmatrix} \\ &\stackrel{A.1}{=} \mathfrak{f}(z) - \begin{bmatrix} \tilde{\omega} \mathcal{J}(z)\omega - m(\tilde{\omega} \tilde{v}(z)p(z) + \tilde{v}(z)\tilde{p}(z)\omega) \\ m \tilde{\omega}(\tilde{\omega} p(z) + v(z)) \end{bmatrix} \\ &= \mathfrak{f}(z) - \begin{bmatrix} \tilde{\omega}(\mathcal{J}(z)\omega + m \tilde{p}(z)v(z)) - m \tilde{v}(z)\tilde{p}(z)\omega \\ m \tilde{\omega}(\tilde{\omega} p(z) + v(z)) \end{bmatrix} \\ &= \mathfrak{f}(z) - \bar{\mathcal{V}}(z) \begin{bmatrix} \mathcal{J}(z)\omega + m \tilde{p}(z)v(z) \\ -m \tilde{p}(z)\omega + mv(z) \end{bmatrix} \\ &\stackrel{2.7}{=} \mathfrak{f}(z) - \bar{\mathcal{V}}(z)M(z)\mathcal{V}(z) \stackrel{2.16}{=} \mathfrak{f}(z) - \bar{\mathcal{V}}(z)\mathfrak{h}(z) \end{aligned}$$

In contrast with the inertial derivative formulations, the expression for the gyroscopic spatial force in (2.28) depends on the linear velocity of the body. ■

Thus, this formulation is more susceptible to numeric errors when the linear velocities are large.

Remark 2.1 Gyroscopic force $b(z)$ does no work.

We show now that the gyroscopic spatial force $b(z)$ in the equations of motion in Lemma 2.3 does no work. The power generated by the gyroscopic force $b(z)$ is

$$\mathcal{V}^*(z)b(z) \stackrel{2.28}{=} \mathcal{V}^*(z)\bar{\mathcal{V}}(z)\mathfrak{h}(z) \stackrel{1.24}{=} 0 \quad (2.29)$$

confirming that $b(z)$ is a non-working force. ■

That the gyroscopic spatial force does no work for equations of motion about arbitrary points when body frame derivatives are used is in contrast with our observation in Exercise 2.9 that this property only holds at the center of mass when inertial frame derivatives are used.

Remark 2.2 Conservation of kinetic energy for a rigid body.

We now show that the equations of motion in Lemma 2.3 further imply that the kinetic energy of a body is conserved in the absence of external forces, i.e., $\mathfrak{f}(z) \equiv 0$. The time derivative of the kinetic energy is given by

$$\frac{1}{2} \frac{d\mathcal{V}^*(z)\mathcal{M}(z)\mathcal{V}(z)}{dt} = \mathcal{V}^*(z)\mathcal{M}(z)\dot{\beta}_{\mathbb{B}}(z) \stackrel{2.28}{=} -\mathcal{V}^*(z)b(z) \stackrel{2.29}{=} 0$$

This implies that the kinetic energy of a body is conserved when the external forces on the body are zero. ■

Exercise 2.11 Equations of motion using spatial momentum.

Using the spatial momentum derivative expression in (2.21) as a starting point, derive the equations of motion in (2.28). ■

Remark 2.3 Body dynamics invariance across Newtonian frames.

Newtonian frames are free-falling frames. A frame moving at fixed linear velocity with respect to a Newtonian frame is also a Newtonian frame. Frames that are accelerating or rotating with respect to a Newtonian frame are not Newtonian frames. In general, the dynamics of a multibody system are invariant across Newtonian frames but not across non-Newtonian ones.

We examine the implications of this invariance property for the single rigid body system that we have studied so far. We should expect that formulations using derivatives with respect to Newtonian frames (e.g. inertial frame derivatives) would have equations of motion that are independent of the linear velocity of the body. On the other hand we can expect that formulations using derivatives in the non-Newtonian frames (e.g. rotating body frames) would not necessarily retain this invariance property.

These conjectures can be verified by examining the expression for the $b_J(z)$ spatial force in (2.26) for the inertial frame derivative dynamics, and noting that it is independent of the linear velocity. On the other hand, the corresponding gyroscopic spatial force, $b(z)$ in (2.28) for body frame derivatives does depend on the linear velocity of the body.

■

2.5 Equations of Motion with an Inertially Fixed Velocity Reference Frame

In the previous sections we have used the spatial velocity of a physical point on the rigid body as the generalized velocity coordinates of a rigid body to derive its equations of motion. However, there is another interesting option that uses the effective spatial velocity of an inertially fixed reference point as the generalized velocities for

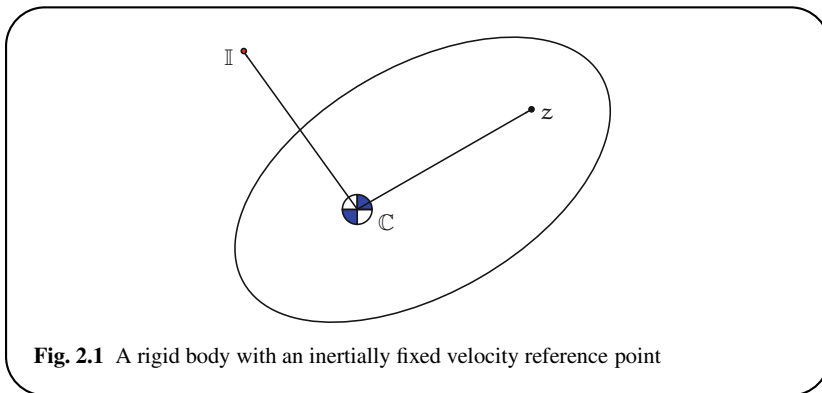


Fig. 2.1 A rigid body with an inertially fixed velocity reference point

the body. Without loss in generality, we denote the inertial frame \mathbb{I} as this **velocity reference point**. The **inertially referenced spatial velocity**, $\mathcal{V}_{\mathbb{I}}$, is defined as the spatial velocity of the velocity reference \mathbb{I} viewed as being instantaneously attached to the rigid body (see Fig. 2.1). Thus, $\mathcal{V}_{\mathbb{I}}$ is given by the expression

$$\mathcal{V}_{\mathbb{I}} \triangleq \begin{bmatrix} \omega \\ v_{\mathbb{I}} \end{bmatrix} \triangleq \phi^*(\mathbb{C}, \mathbb{I}) \mathcal{V}(\mathbb{C}) \quad (2.30)$$

with ω and $v_{\mathbb{I}}$ denoting the angular and linear velocity components, respectively. The exercise below shows that the use of the center of mass \mathbb{C} as the point of reference for defining $\mathcal{V}_{\mathbb{I}}$ in (2.30) is in fact arbitrary, in the sense that any other point on the body would yield the same value for $\mathcal{V}_{\mathbb{I}}$.

Exercise 2.12 Invariance of $\mathcal{V}_{\mathbb{I}}$ to velocity reference point.

Equation (2.30) used the spatial velocity at the center of mass to obtain the value of $\mathcal{V}_{\mathbb{I}}$. Show that the value of $\mathcal{V}_{\mathbb{I}}$ is the same if a different point on the rigid body was used instead. That is, show that for any other point x on the rigid body

$$\mathcal{V}_{\mathbb{I}} = \phi^*(x, \mathbb{I})\mathcal{V}(x) \quad (2.31)$$

■

Due to the invariance with respect to the reference point, we use the terminology $\mathcal{V}_{\mathbb{I}}$ instead of $\mathcal{V}_{\mathbb{I}}(\mathbb{C})$ for the inertially referenced spatial velocity of a body. In essence, the use of an inertially fixed spatial velocity reduces all the points on the rigid body to an equivalence class. We now use the inertial frame representation of $\mathcal{V}_{\mathbb{I}}$ as the generalized velocities to derive the equations of motion for a rigid body.

The spatial inertia, $M_{\mathbb{I}}$, of the body about the \mathbb{I} reference frame is given by

$$M_{\mathbb{I}} \triangleq \phi(\mathbb{I}, \mathbb{C})M(\mathbb{C})\phi^*(\mathbb{I}, \mathbb{C}) = \begin{pmatrix} \mathcal{J}_{\mathbb{I}} & m\tilde{\mathbf{p}}_{\mathbb{I}} \\ -m\tilde{\mathbf{p}}_{\mathbb{I}} & m\mathbf{I}_3 \end{pmatrix} \quad (2.32)$$

$\mathbf{p}_{\mathbb{I}} = \mathbf{l}(\mathbb{I}, \mathbb{C})$ denotes the 3-vector from the inertial frame to the location of the center of mass of the body.

While Exercise 2.6 on page 25 derives the expression for the time derivative of the $M(z)$ body spatial inertia with respect to the inertial frame, the next exercise derives the corresponding expression for the time derivative of $M_{\mathbb{I}}$ with respect to the inertial frame.

Exercise 2.13 Time derivative of $M_{\mathbb{I}}$.

Show that the inertial time derivative of $M_{\mathbb{I}}$ is given by

$$\dot{M}_{\mathbb{I}} \triangleq \frac{d_{\mathbb{I}} M_{\mathbb{I}}}{dt} = \bar{\mathcal{V}}_{\mathbb{I}} M_{\mathbb{I}} - M_{\mathbb{I}} \tilde{\mathcal{V}}_{\mathbb{I}} = \bar{\mathcal{V}}_{\mathbb{I}} M_{\mathbb{I}} + M_{\mathbb{I}} (\bar{\mathcal{V}}_{\mathbb{I}})^* \quad (2.33)$$

■

The inertially referenced spatial momentum, $\mathfrak{h}_{\mathbb{I}}$, is defined as

$$\mathfrak{h}_{\mathbb{I}} \triangleq M_{\mathbb{I}} \mathcal{V}_{\mathbb{I}} = \phi(\mathbb{I}, x)\mathfrak{h}(x) \quad (2.34)$$

Similarly, the inertially referenced spatial force, $f_{\mathbb{I}}$, is defined as

$$f_{\mathbb{I}} \triangleq \phi(\mathbb{I}, \mathbb{C})f(\mathbb{C}) \quad (2.35)$$

Exercise 2.14 Equations of motion about a fixed velocity reference point.

1. Show that the momentum form of the equations of motion about the inertially fixed velocity reference frame is given by:

$$\mathbf{f}_{\mathbb{I}} = \frac{d_{\mathbb{I}} \mathbf{h}_{\mathbb{I}}}{dt} \quad (2.36)$$

This expression is similar to (2.21), where the generalized velocities were the inertial frame derivative of the center of mass spatial velocity. Equation (2.36) implies that the inertially referenced spatial momentum vector $\mathbf{h}_{\mathbb{I}}$ is constant when the external spatial force $\mathbf{f}_{\mathbb{I}} \equiv \mathbf{0}$.

2. Define the generalized velocity coordinates as $\beta_{\mathbb{I}} \stackrel{\triangle}{=} {}^{\mathbb{I}}\mathcal{V}_{\mathbb{I}}$. Show that the equations of motion using $\beta_{\mathbb{I}}$ are given by

$$\mathbf{f}_{\mathbb{I}} = M_{\mathbb{I}} \dot{\beta}_{\mathbb{I}} + \mathbf{b}_{\mathbb{I}} \quad (2.37)$$

where

$$\mathbf{b}_{\mathbb{I}} \stackrel{\triangle}{=} \dot{M}_{\mathbb{I}} \mathcal{V}_{\mathbb{I}} = \bar{\mathcal{V}}_{\mathbb{I}} M_{\mathbb{I}} \mathcal{V}_{\mathbb{I}} = \bar{\mathcal{V}}_{\mathbb{I}} \mathbf{h}_{\mathbb{I}} \quad (2.38)$$

Observe that the spatial vector expression for $\mathbf{b}_{\mathbb{I}}$ in (2.38) is identical in form to the $\mathbf{b}(z)$ gyroscopic force expression for body fixed velocity reference frames in (2.28).

3. Verify that the gyroscopic term $\mathbf{b}_{\mathbb{I}}$ is non-working and that the kinetic energy of the body is indeed conserved when $\mathbf{f}_{\mathbb{I}}(t) \equiv \mathbf{0}$.

■

2.6 Comparison of the Different Dynamics Formulations

Summarized here and in Table 2.2 are some of the properties for the alternative rigid body dynamics formulations. the following conservation facts are true:

- The kinetic energy of the body is always conserved in the absence of external forces (Remark 2.2).
- In the absence of external forces,
 - The spatial momentum vector of a body about its center of mass remains constant in the inertial frame (2.21).
 - The spatial momentum vector of a body about points on the rigid body other than the center of mass does not remain constant (Exercise 2.10).
 - The spatial momentum vector about an inertially fixed velocity reference point remains constant (Exercise 2.14).
- The gyroscopic force for the body does not do any work when the generalized velocities are either body frame derivatives of the body spatial velocity (Remark 2.1) or are inertially referenced spatial velocities (Exercise 2.14). However the body gyroscopic force does do work when the generalized velocities are inertial frame derivatives of the body spatial velocity about a non- \mathbb{C} location (Exercise 2.9).

- The gyroscopic force terms are independent of the linear velocity of the body when inertial derivatives are used for the generalized velocities. This independence does not hold for body frame derivatives or for the inertially reference spatial velocity based generalized velocities.

While analytically all of the formulations are essentially equivalent, the conclusion from the above comparison is the numeric and computational superiority of formulating the dynamics of a rigid body about its center of mass using inertial frame derivatives for the generalized velocities. In practice, other considerations may drive the choice of one of the alternate formulations. More discussion on rigid body dynamics is available in [60, 69, 70, 96, 112, 124, 153, 185].

Table 2.2 A comparison of the properties of the different formulations for the dynamics of a single rigid body

Formulation	\mathbb{I} deriv, \mathbb{C}	\mathbb{I} deriv, z	\mathbb{B} deriv, z	Inertial ref, \mathbb{I}
Section	2.3.1	2.3.2	2.4	2.5
Gen. vel. β	$\mathbb{V}(\mathbb{C})$	$\mathbb{V}(z)$	$\mathbb{B}\mathcal{V}(z)$	$\mathcal{V}_{\mathbb{I}}$
Gyroscopic force b	$\bar{\mathcal{V}}^{\omega}(\mathbb{C})\mathcal{M}(\mathbb{C})\mathcal{V}^{\omega}(\mathbb{C})$	$\bar{\mathcal{V}}^{\omega}(z)\mathcal{M}(z)\mathcal{V}^{\omega}(z)$	$\bar{\mathcal{V}}(z)\mathfrak{h}(z)$	$\bar{\mathcal{V}}_{\mathbb{I}}\mathfrak{h}_{\mathbb{I}}$
Conserved spatial momentum	✓			✓
Non-working b	✓		✓	✓
Independent of linear velocity	✓	✓		

Remark 2.4 Motion invariances for a rigid body.

We have examined the conservation properties of the kinetic energy and spatial angular momentum of a body in the absence of external forces. These conservation properties are a consequence of **Noether's theorem** [11, 60] which shows that certain symmetries of the system Lagrangian of a system result in **integrals of motion**, i.e., quantities that are conserved with time.

For our rigid body example, the non-dependency of the kinetic energy of the body on time results in the conservation of kinetic energy over time. Moreover, the non-dependence of the kinetic energy on the location as well as the orientation of the rigid body results in the conservation of the linear and angular momentum properties for the body. ■

Chapter 3

Serial-Chain Kinematics

This chapter develops kinematics models for serial-chain rigid multibody systems. Although serial-chains are perhaps the simplest examples of multibody systems, many of the concepts and techniques developed for these systems apply, with only modest extensions, to general multibody systems.

3.1 Serial-Chain Model

A rigid multibody system consists of a collection of rigid bodies (also referred to as **links**) connected to each other via **hinges** (also referred to as **joints**). A hinge connecting a pair of bodies defines the allowable relative motion between the bodies, and implicitly the constraints on the relative motion between the bodies. The hinge terminology is not restricted to just physical hinges, but can be used to represent general bilateral constraints between bodies.

Topologically, a **serial-chain** multibody system contains a single base-body and a single tip-body. Each internal body has one parent and one child body. The base-body has no parent body and the tip-body has no child body. The neighboring link in the direction towards the base (tip) is referred to as the **inboard (outboard)** link. The serial-chain is assumed to have a total of n links (and thus, has n hinges). Without loss in generality, the links are assumed to be numbered from 1 through n from the tip to the base.¹ The k th hinge connects the $(k+1)$ th and the k th link, as illustrated in Fig. 3.1. Associated with the k th hinge are a pair of frames, \mathbb{O}_k and \mathbb{O}_k^+ , attached to the k th and $(k+1)$ th links, respectively. Even though for the sake of clarity Fig. 3.1 shows the \mathbb{O}_k^+ and \mathbb{O}_k hinge frames at different locations, these frames at any instant coincide with each other. The relative spatial velocity across the k th hinge is defined as the relative spatial velocity of the \mathbb{O}_k frame with respect to the \mathbb{O}_k^+ frame. Associated with each body in the serial-chain is a body-fixed

¹ Section 6.4 on page 111 studies important mathematical parallels between multibody dynamics and estimation theory. The parallels are made more evident by this link numbering scheme.

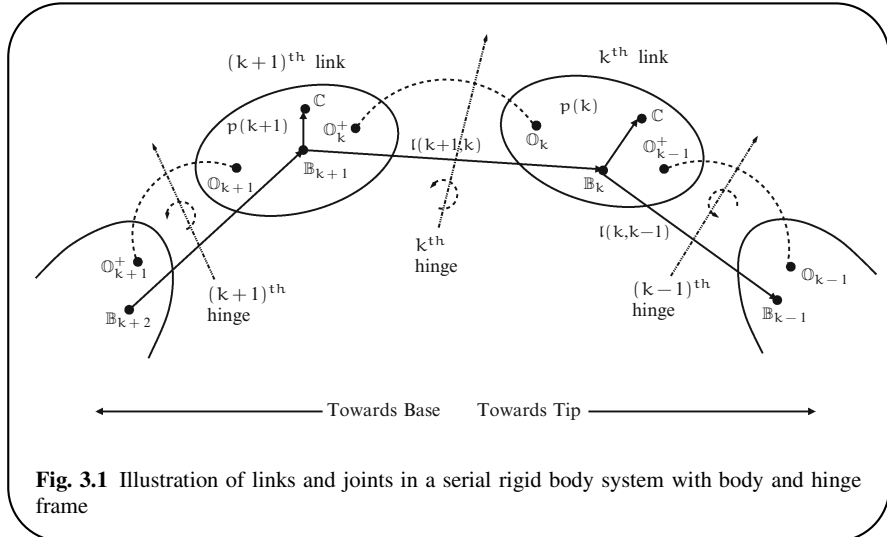


Fig. 3.1 Illustration of links and joints in a serial rigid body system with body and hinge frame

reference frame. The body frame for the k^{th} body is denoted \mathbb{B}_k . In general, \mathbb{B}_k can be located anywhere on the k^{th} body. Common location choices for \mathbb{B}_k include the center of mass of the link, the \mathbb{O}_k frame or other convenient locations on the body.

3.2 Hinge Kinematics

Hinges represent constraints between two bodies which restrict the relative configuration as well as motion between them. A noteworthy fact is that, while the constraints on the relative configuration can be complex nonlinear equations, the constraints on the relative velocity for virtually all known physical systems are in the form of linear constraints. The constraints on the relative spatial velocity may be expressed via a hinge map operator which specifies the allowable velocity range space in \mathcal{R}^6 , or alternatively, via constraint equations on the relative spatial velocity. The former is an **explicit** characterization while the latter is an **implicit** characterization of the hinge constraints. Typically, for physical hinges, the explicit characterization is easy to obtain from the description of the hinge, while for hinges that are a part of kinematic loops, the implicit characterization is often more readily available. The two characterizations are equivalent, and either one can be chosen based on convenience.

3.2.1 Hinge Generalized Coordinates

To simplify notation, we will frequently use “ k ” instead of \mathbb{B}_k in expressions pertinent to the serial-chain bodies. Thus, ${}^{k+1}\mathbb{T}_k$ will denote the ${}^{\mathbb{B}_{k+1}}\mathbb{T}_{\mathbb{B}_k}$ homogeneous transform between the body frames of the $(k+1)$ th and k th bodies. It has the general form:

$${}^{k+1}\mathbb{T}_k = {}^{k+1}\mathbb{T}_{\mathbb{O}_k} \cdot {}^{\mathbb{O}_k}\mathbb{T}_k = \left({}^{k+1}\mathbb{T}_{\mathbb{O}_k^+} \cdot {}^{\mathbb{O}_k^+}\mathbb{T}_{\mathbb{O}_k} \right) \cdot {}^{\mathbb{O}_k}\mathbb{T}_k \quad (3.1)$$

We can make the following observations:

- ${}^{k+1}\mathbb{T}_{\mathbb{O}_k^+}$ is a pure translation transformation since the \mathbb{B}_{k+1} and \mathbb{O}_k^+ frame are attached to the $(k+1)$ th body. For hinges with translational components, the translation vector between these frames will vary with the hinge motion.
- ${}^{\mathbb{O}_k}\mathbb{T}_k$ is also a pure translation transformation that is constant, since the \mathbb{O}_k and \mathbb{B}_k frames are rigidly attached to the k th body.
- ${}^{\mathbb{O}_k^+}\mathbb{T}_{\mathbb{O}_k}$ is a pure rotational transformation. For hinges with rotational components, the rotation value varies with the motion of the hinge.

The variation in ${}^{k+1}\mathbb{T}_{\mathbb{O}_k}$ with changes in the hinge configuration can be parametrized by a set of variables. If the hinge has $r_p(k)$ configuration degrees of freedom, it is natural and quite common to use an $r_p(k)$ -dimensional vector to parametrize the configuration of the hinge. The elements of this vector, denoted $\theta(k)$, are referred to as the **generalized coordinates** for the hinge. $r_p(k)$ is the minimal number of parameters that are required, and in most cases they are adequate for the required parametrization. However, there are situations where a larger number of parameters, i.e., a non-minimal parameter representation of the configuration of the hinge, is desirable, especially when dealing with the representation of orientations. It is well-known that a minimal 3-parameter representation (such as the Euler angles) cannot provide a globally singularity-free representation for general orientations, and a 4-variable parametrization (such as the Euler parameters) is needed to meet this requirement (see Wittenburg [185]). Thus, even when the physical hinge is well-behaved, the use of minimal representations may lead to undesirable numerically ill-conditioned behavior. Issues such as this may dictate the use of configuration variables of dimension larger than the number of configuration degrees of freedom.

Even though most systems have single degree of freedom hinges (i.e., $r_p(k) = 1$), there are important examples of hinges with $r_p(k) > 1$. The specification of the $\theta(k)$ hinge generalized coordinates completely determines the configuration of the k th hinge. Thus, the full set of these hinge coordinates are referred to as the generalized coordinates for the full serial-chain.

3.2.2 Relative and Absolute Coordinates

The hinge generalized coordinates are also referred to as **relative** coordinates, since they specify the relative configuration of neighboring bodies. An alternative is the use of **absolute** coordinates, which directly specify the configuration of each body with respect to the inertial frame. In contrast with relative coordinates, absolute coordinates for each body are of dimension 6 or more, as seen in the discussion of single body dynamics in Chap. 2.

Absolute coordinate formulations are popular in the dynamics simulation arena, due to the relative simplicity of such models, when compared with relative coordinate models [158]. However, relative coordinates offer distinct advantages that we believe more than compensate for the added complexity. The minimal size of relative coordinate representations, avoids over-parametrization related issues that arise from the use of absolute coordinates (e.g. drift error control, differential-algebraic equations). Moreover, the minimal size of relative coordinate representations provides a natural, dynamical state representation, for robotics control system analysis and design.

We adopt relative coordinates in our study of multibody system dynamics. The apparent added complexity of the relative coordinates system dynamics is easily overcome with the right set of mathematical tools and concepts. In the forthcoming chapters, we develop several analytical techniques, that provide insight into the structural properties of relative coordinate dynamics models. In addition, we derive significantly more efficient, and numerically superior, computational algorithms using the relative coordinates approach.

3.2.3 Hinge Generalized Velocities

Since the motion of the bodies in a serial-chain are caused by hinge motions, we now look at formalizing the differential (i.e., velocity) kinematics for hinges. Towards this, differentiating ${}^{k+1}\mathbb{T}_{\mathbb{O}_k}$ with respect to time yields:

$$\frac{d^{k+1}\mathbb{T}_{\mathbb{O}_k}}{dt} \stackrel{1.3}{=} \begin{pmatrix} \tilde{\omega}(\mathbb{O}_k^+, \mathbb{O}_k) & v(\mathbb{O}_k^+, \mathbb{O}_k) \\ \mathbf{0} & 0 \end{pmatrix} \quad (3.2)$$

where $\omega(\mathbb{O}_k^+, \mathbb{O}_k)$ and $v(\mathbb{O}_k^+, \mathbb{O}_k)$ denote the angular and linear velocities of the \mathbb{O}_k frame with respect to the \mathbb{O}_k^+ frame. Adopting the notation

$$\Delta_\omega(k) \triangleq \omega(\mathbb{O}_k^+, \mathbb{O}_k) \quad \text{and} \quad \Delta_v(k) \triangleq v(\mathbb{O}_k^+, \mathbb{O}_k) \quad (3.3)$$

allows us to re-express (3.2) as

$$\frac{d^{k+1} \mathbb{T}_{\mathbb{O}_k}}{dt} = \begin{pmatrix} \tilde{\Delta}_\omega(k) & \Delta_v(k) \\ \mathbf{0} & 0 \end{pmatrix} \quad (3.4)$$

The spatial velocity across the k th hinge, i.e., the spatial velocity of the \mathbb{O}_k frame with respect to the \mathbb{O}_k^+ frame is denoted $\Delta_v(k)$ and is defined as

$$\Delta_v(k) \triangleq \mathcal{V}(\mathbb{O}_k) - \mathcal{V}(\mathbb{O}_k^+) = \begin{bmatrix} \Delta_\omega(k) \\ \Delta_v(k) \end{bmatrix} \quad (3.5)$$

The dimensionality of the configuration dependent subspace (of \mathcal{R}^6) in which the relative spatial velocity lives defines the number of **velocity degrees of freedom**, $r_v(k)$, for the hinge. Though in most cases $r_p(k) = r_v(k)$, in general

$$r_p(k) \geq r_v(k) \quad (3.6)$$

When a hinge is simple with small number of degrees of freedom, it is a common practice to parametrize its velocity degrees of freedom using the time derivatives of the generalized coordinates. However, generalized velocity coordinates are more generally allowed to be non-integrable quasi-velocities. These can represent a more convenient choice for parametrizing the velocity degrees of freedom, and can decouple and simplify the dynamical and kinematical equations of motion. A classic example of the use of quasi-velocities is in the development of the dynamical equations of motion for a free rigid body. The use of the time derivatives of the orientation parameters (such as Euler angles, Euler parameters, etc.) as part of the 6-dimensional motion parameters leads to complicated equations of motion. However, the use of the spatial velocity vector as the set of the 6-dimensional generalized velocities leads to much simpler equations of motion [124]. The time derivatives of the generalized coordinates are related to the generalized velocities via a bi-directional, possibly configuration dependent, map.

The relationship of the generalized velocities to the relative spatial velocity across the hinge is usually quite straightforward. The configuration dependent basis vectors for the hinge relative spatial velocity subspace are used as column vectors to define the configuration-dependent, full-rank **hinge map matrix**,² denoted $H^*(k) \in \mathcal{R}^{6 \times r_v(k)}$, for the k th hinge. $H^*(k)$ defines a linear mapping of the **generalized velocity coordinates vector**, $\beta(k) \in \mathcal{R}^{r_v(k)}$, for the hinge to the relative spatial velocity $\Delta_v(k)$ across the hinge as follows:

$$\Delta_v(k) = H^*(k)\beta(k) \quad (3.7)$$

In some instances, the above equation can have an additional bias term on the right of the above equation. As discussed in more detail in Sect. 11.1 on page 209, the hinge constraint is said to be **catastatic** or **acatastatic** depending on whether this term is zero, or non-zero, respectively.

² A hinge map matrix is also at times referred to as the *joint map matrix*.

Since $H^*(k)$, can be configuration dependent, it is possible for its rank to change at certain configurations. When this happens, it is important to redefine it so that the hinge map matrix has maximal column rank again. Partitioned into the angular and linear components $h_\omega(k) \in \mathcal{R}^{3 \times r_v}$ and $h_v(k) \in \mathcal{R}^{3 \times r_v}$, $H^*(k)$ can be expressed in the form

$$H^*(k) = \begin{bmatrix} h_\omega(k) \\ h_v(k) \end{bmatrix} \text{ where } \Delta_\omega(k) = h_\omega(k)\beta(k), \quad \Delta_v(k) = h_v(k)\beta(k) \quad (3.8)$$

In general the time derivatives of the generalized coordinate vector, $\dot{\theta}(k) \in \mathcal{R}^{r_p(k)}$, and the generalized velocity coordinates vector, $\beta(k) \in \mathcal{R}^{r_v(k)}$, are related to each other by a configuration dependent linear transformation. However, in most cases $\beta(k) = \dot{\theta}(k)$, and in this case, $r_p(k) = r_v(k)$ and the transform is the identity transformation.

Collectively, the $\beta(k)$ generalized velocities for the hinges completely parametrize the velocities of all the bodies in the multibody system. Hence, the full set of these hinge generalized velocities is also referred to as the generalized velocities for the full serial-chain.

3.2.4 Examples of Hinges

Figure 3.2 shows examples of $H^*(\cdot)$ hinge map matrices for some common hinge types.

$\begin{pmatrix} 0 \\ 0 \\ 1 \\ 0 \\ 0 \\ 0 \end{pmatrix}$	$\begin{pmatrix} 0 \\ 0 \\ 0 \\ 0 \\ 0 \\ 1 \end{pmatrix}$	$\begin{pmatrix} 0 \\ 0 \\ 1 \\ 0 \\ 0 \\ p \end{pmatrix}$	$\begin{pmatrix} 0 & 0 \\ 0 & 0 \\ 1 & 0 \\ 0 & 0 \\ 0 & 0 \\ 0 & 1 \end{pmatrix}$	$\begin{pmatrix} 1 & 0 & 0 \\ 0 & 1 & 0 \\ 0 & 0 & 1 \\ 0 & 0 & 0 \\ 0 & 0 & 0 \\ 0 & 0 & 0 \end{pmatrix}$
rotary pin hinge 1 dof	prismatic hinge 1 dof	helical hinge 1 dof	cylindrical hinge 2 dof	spherical hinge 3 dof

Fig. 3.2 Examples of hinge map matrices represented in the body frame

- The *rotary pin* hinge is a single degree of freedom hinge which only allows rotational motion across the hinge. The example in Fig. 3.2 allows motion about the z-axis.
- The *prismatic* example in the figure is also a 1 degree of freedom hinge, but allows only translational motion along the z-axis.

- The *helical* hinge allows 1 degree of freedom rotational and translational motion – but where the rotational and translational motions are coupled. The p term in its hinge map matrix represents the *pitch*, and denotes the ratio of translational to rotational motion for the hinge.
- The *cylindrical* hinge is a 2 degree of freedom hinge, with independent 1 degree of freedom rotational and translational motions about and along the z -axis.
- The last example in Fig. 3.2 is a *spherical* rotational hinge, where full 3 degree of freedom rotational motion is allowed across the hinge. A popular choice for generalized coordinates for such hinges are *Euler angle* coordinates discussed in Sect. B.1 in the Appendix. While these coordinates have the virtue of being of minimal size, their representation of the hinge configuration is not singularity free. It is well known that representations of size 4 or more, such as the *unit quaternions* discussed in Sect. B.3, are required for singularity-free representations. These latter choices for coordinates are examples of cases where $r_p(k) > r_v(k)$.

One way of modeling a free-flying system is to assign a 6 degree of freedom hinge between the base-body and the inertial frame. The H^* hinge map matrix for this hinge is simply the 6×6 identity matrix.

Exercise 3.1 Hinge map matrix for a universal joint.

Derive the configuration dependent hinge map matrix H^ for a 2 degree of freedom universal joint whose two axes are parallel to the X and Y axes, respectively, in the zero configuration.*



Unlike all the constant hinge map matrix examples in Fig. 3.2, the hinge map matrix for a universal joint is configuration dependent. However, the matrix depends only upon the first hinge degree of freedom coordinate, and not the second one.

Exercise 3.2 Hinge map matrix for a sphere rolling on a surface.

Consider a spherical ball rolling without slipping on a level surface. The no slippage condition requires that the linear velocity of the point on the ball that is instantaneously in contact with the surface be zero. Let the reference frame for the ball be located at its center. It is easy to see that there are 3 velocity degrees of freedom between the ball and the surface. Determine the 6×3 hinge map H^ for the hinge defined by the contact between the ball and the surface.*



In Exercise 3.2, there is only one holonomic constraint on the hinge which constrains the center of the ball to remain a fixed distance from the floor. It precludes motions of the ball in the vertical direction, i.e., no bouncing motion is allowed. The remaining constraints are examples of non-holonomic constraints.³ The ball possesses five configuration degrees of freedom: two positional degrees of freedom which specify the location of the ball on the floor, and all three orientational degrees of freedom for the ball. However, due to the non-slippage restriction, the ball has only three velocity degrees of freedom: it can roll along the floor, and it can

³ Holonomic and non-holonomic constraints are defined more precisely in Sect. 11.1 on page 209.

twist about the vertical. It cannot move with a purely linear velocity on the floor since sliding is not possible. In fact during the roll motion, the linear and angular velocities are directly coupled together.

The point of contact between the ball and the surface changes as the ball moves. The hinge map matrix for this contact constraint is a constant matrix in the inertial frame because of the spherical nature of the ball. However, for non-symmetrical balls, the hinge map matrix will be configuration dependent. A more detailed discussion of generalized hinges and constraints can be found in Schwertassek and Senger [161].

3.3 Serial-Chain Kinematics

The **forward kinematics** problem for multibody systems deals with the mathematical mapping from the generalized coordinates and velocities of the system to the spatial location, orientation and velocities of the link frames. The **inverse kinematics** problem focuses on the converse, i.e., the mathematical mapping from link frame configuration and velocity data (usually end-effector frame in robotics) to the corresponding generalized coordinate and velocities for the system. Differential kinematics refers specifically to the velocity mappings.

3.3.1 Serial-Chain Configuration Kinematics

Let $\mathbb{I}\mathbb{T}_{\mathbb{B}_k}$ (or equivalently $\mathbb{I}\mathbb{T}_k$) denote the homogeneous transform relating frame \mathbb{B}_k to the inertial frame \mathbb{I} . The following recursive relationship relates the homogeneous transforms for the k th and $(k+1)$ th bodies:

$$\mathbb{I}\mathbb{T}_k \stackrel{1.5}{=} \mathbb{I}\mathbb{T}_{k+1} \cdot {}^{k+1}\mathbb{T}_k \quad (3.9)$$

This mathematical relationship for the configuration kinematics of the serial-chain describes how the inertial transforms for the component links are related to the inter-link transforms. Algorithm 3.1 describes a recursive algorithm for computing the $\mathbb{I}\mathbb{T}_k$ transforms for all the links.

The location and orientation of any link frame with respect to another link frame can be obtained by chaining together the component link-to-link homogeneous transformations. Thus, with the k th link being outboard of the j th link, the transformation between these frames can be obtained using the following product of link-to-link component transformations in a base-to-tip recursion:

$${}^j\mathbb{T}_k \stackrel{1.5}{=} {}^j\mathbb{T}_{j-1} \cdots {}^{k+1}\mathbb{T}_k \quad (3.10)$$

Algorithm 3.1 Recursive computation of link transformations

$$\left\{ \begin{array}{l} {}^{\mathbb{I}}\mathbb{T}_{n+1} = \mathbf{I} \\ \textbf{for } k = n \cdots 1 \\ \quad {}^{\mathbb{I}}\mathbb{T}_k = {}^{\mathbb{I}}\mathbb{T}_{k+1} \cdot {}^{k+1}\mathbb{T}_k \\ \textbf{end loop} \end{array} \right.$$

3.3.2 Serial-Chain Differential Kinematics

For a serial-chain with known $\theta(k)$ generalized coordinates and $\dot{\theta}(k)$ generalized velocities, the particular problem addressed here is the computation of the corresponding spatial velocities of the links. The spatial velocity of the k th link is defined as the spatial velocity of its body frame \mathbb{B}_k , and denoted

$$\mathcal{V}(k) \equiv \mathcal{V}(\mathbb{B}_k) \quad (3.11)$$

For the sake of simpler exposition, and without losing any generality, we assume for now that the body reference frame, \mathbb{B}_k , for the k th link is simply the outboard hinge frame, \mathbb{O}_k , for the k th hinge, i.e.,

$$\mathbb{B}_k \equiv \mathbb{O}_k \quad (3.12)$$

Figure 3.3 illustrates a serial-chain that satisfies this assumption. For these systems, ${}^{\mathbb{O}_k}\mathbb{T}_k = \mathbf{I}$ and (3.1) simplifies to

$${}^{k+1}\mathbb{T}_k = {}^{k+1}\mathbb{T}_{\mathbb{O}_k^+} \cdot {}^{\mathbb{O}_k^+}\mathbb{T}_{\mathbb{O}_k} \quad (3.13)$$

Extensions for the more general situation when $\mathbb{B}_k \neq \mathbb{O}_k$ are discussed in Sect. 3.3.3. The $\mathcal{V}(k)$ spatial velocity depends upon the spatial velocity of the inboard link frame, \mathbb{O}_{k+1} , as well as on the motion of the hinge itself. The frame \mathbb{O}_k^+ allows us to distinguish between these two contributions as follows:

$$\mathcal{V}(k) \stackrel{3.12}{=} \mathcal{V}(\mathbb{O}_k) \stackrel{3.5}{=} \mathcal{V}^+(k) + \Delta\mathcal{V}(k) \text{ where } \mathcal{V}^+(k) \triangleq \mathcal{V}(\mathbb{O}_k^+) \quad (3.14)$$

$\mathcal{V}^+(k)$ is the spatial velocity of the \mathbb{O}_k^+ frame and represents the contribution to $\mathcal{V}(k)$ purely from the motion of the inboard $(k+1)$ th link, while $\Delta\mathcal{V}(k)$ represents the contribution from the motion of the k th hinge. Since frames \mathbb{B}_{k+1} and \mathbb{O}_k^+ are both on the $(k+1)$ th body, the spatial velocity of the \mathbb{O}_k^+ frame is related to the spatial velocity of \mathbb{B}_{k+1} by the expression

$$\mathcal{V}^+(k) \stackrel{1.33}{=} \phi^*(\mathbb{B}_{k+1}, \mathbb{O}_k^+) \mathcal{V}(k+1) \quad (3.15)$$

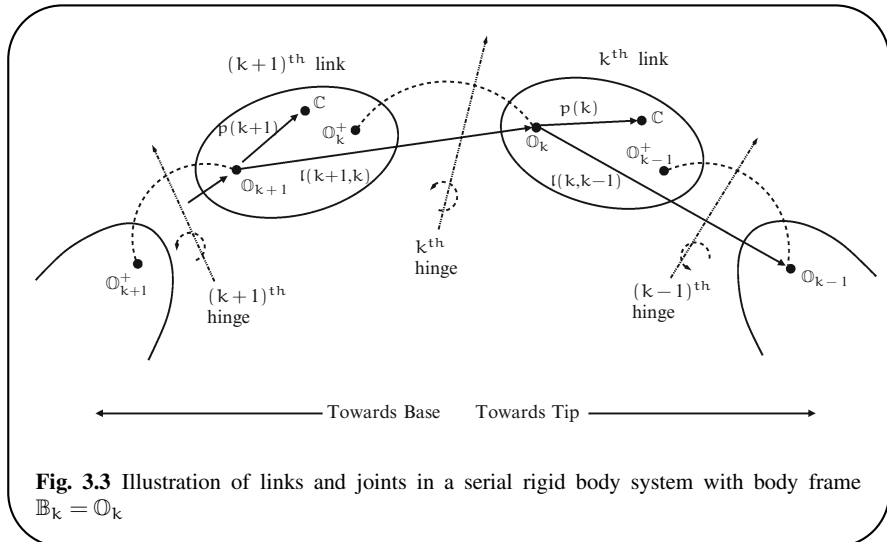


Fig. 3.3 Illustration of links and joints in a serial rigid body system with body frame $\mathbb{B}_k = \mathbb{O}_k$

The $\phi(k+1, k)$ rigid body transformation matrix associated with the k th link has the form

$$\phi(k+1, k) \triangleq \begin{pmatrix} \mathbf{I} & \tilde{l}(\mathbb{B}_{k+1}, \mathbb{B}_k) \\ \mathbf{0} & \mathbf{I} \end{pmatrix} = \begin{pmatrix} \mathbf{I} & \tilde{l}(k+1, k) \\ \mathbf{0} & \mathbf{I} \end{pmatrix} \quad (3.16)$$

where

$$l(k+1, k) \triangleq l(\mathbb{B}_{k+1}, \mathbb{B}_k) \quad (3.17)$$

Since the location of the \mathbb{O}_k^+ frame coincides with the \mathbb{O}_k frame, which in turn coincides with \mathbb{B}_k (per (3.12)), it follows that

$$\phi(k+1, k) \triangleq \phi(\mathbb{B}_{k+1}, \mathbb{B}_k) = \phi(\mathbb{B}_{k+1}, \mathbb{O}_k) = \phi(\mathbb{B}_{k+1}, \mathbb{O}_k^+) \quad (3.18)$$

If the k th hinge contains a prismatic component, then both $l(k, k-1)$ and $\phi(k, k-1)$ will depend on the configuration of the $(k-1)$ th hinge.

Combining together (3.7), (3.14), (3.15) and (3.18) we obtain

$$\mathcal{V}^+(k) \stackrel{3.15, 3.18}{=} \phi^*(k+1, k)\mathcal{V}(k+1) \quad (3.19a)$$

$$\begin{aligned} \mathcal{V}(k) &\stackrel{3.14, 3.19a}{=} \phi^*(k+1, k)\mathcal{V}(k+1) + \Delta\mathcal{V}(k) \\ &\stackrel{3.7}{=} \phi^*(k+1, k)\mathcal{V}(k+1) + H^*(k)\beta(k) \end{aligned} \quad (3.19b)$$

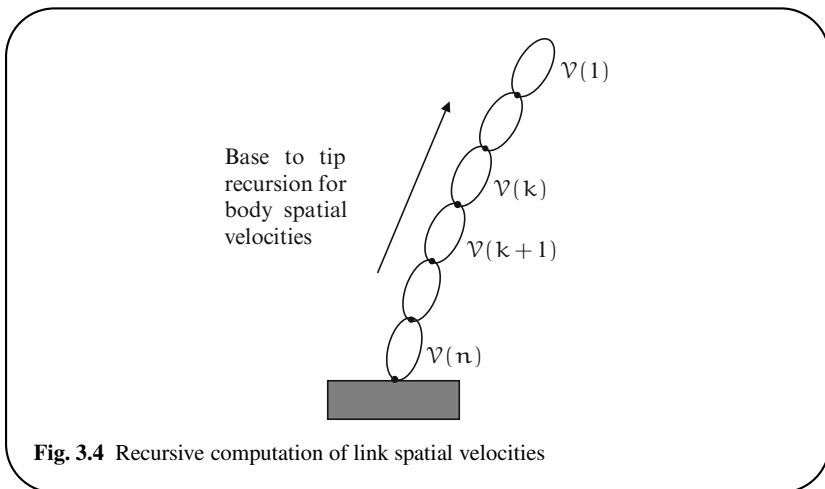
Equation (3.19b) shows how the spatial velocity of a link can be obtained from the spatial velocity of the inboard link and the relative spatial velocity across the hinge connecting the links. As illustrated in Fig. 3.4, the sequence $\mathcal{V}(1), \dots, \mathcal{V}(n)$

of spatial velocities for all the links can be obtained by means of the base-to-tip recursive sweep described in Algorithm 3.2. The sequence begins at the base with

Algorithm 3.2 Recursive computation of link spatial velocities

$$\left\{ \begin{array}{l} \mathcal{V}(n+1) = 0 \\ \textbf{for } k = n \cdots 1 \\ \quad \mathcal{V}(k) = \phi^*(k+1, k)\mathcal{V}(k+1) + H^*(k)\beta(k) \\ \textbf{end loop} \end{array} \right.$$

the initial condition $\mathcal{V}(n+1) = \mathbf{0}$ (which is equivalent to saying that the inertial frame is stationary). The computations proceed in an outward direction from base-to-tip and ends with the computation of the $\mathcal{V}(1)$ spatial velocity of the tip-body.



3.3.3 Differential Kinematics with $\mathbb{B}_k \neq \mathbb{O}_k$

The assumption in the previous section was that the \mathbb{B}_k body frame coincided with the \mathbb{O}_k hinge frame for the k th body. In general, this assumption may not hold, and the body frame may not coincide with \mathbb{O}_k . Such a system with $\mathbb{B}_k \neq \mathbb{O}_k$ is

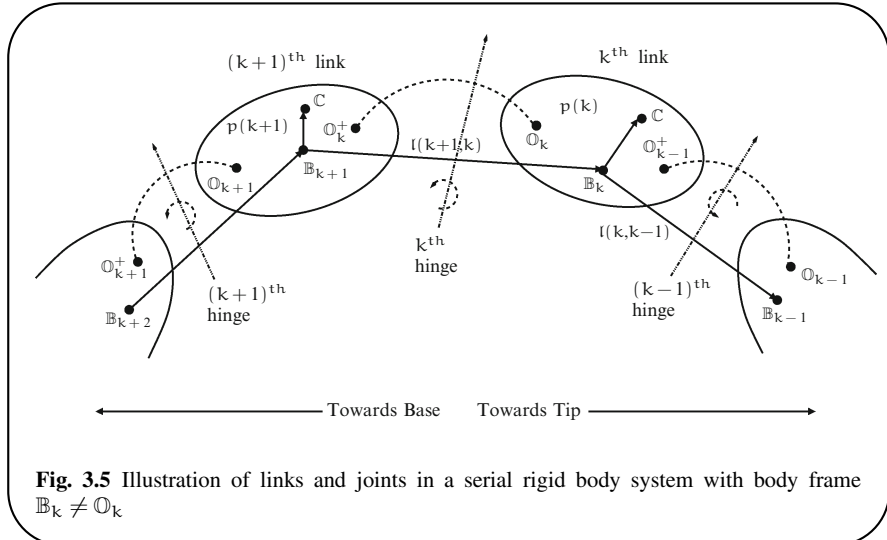


Fig. 3.5 Illustration of links and joints in a serial rigid body system with body frame $\mathbb{B}_k \neq \mathbb{O}_k$

illustrated in Fig. 3.5. For this system, the more general form of (3.14) for the body spatial velocity is given by:

$$\mathcal{V}(k) \triangleq \mathcal{V}(\mathbb{B}_k) = \phi^*(\mathbb{O}_k, \mathbb{B}_k) \mathcal{V}(\mathbb{O}_k) \quad (3.20)$$

The following exercise examines the modified velocity recursion relationships for the bodies in the system.

Exercise 3.3 Velocity recursion with $\mathbb{B}_k \neq \mathbb{O}_k$.

Show that the new version of spatial velocity of the recursion in (3.19a) has the following form:

$$\begin{aligned} \mathcal{V}(k) &= \phi^*(k+1, k) \mathcal{V}(k+1) + \Delta_{\mathcal{V}}^{\mathbb{B}}(k) \\ &= \phi^*(k+1, k) \mathcal{V}(k+1) + H_{\mathbb{B}}^*(k) \beta(k) \end{aligned} \quad (3.21)$$

where

$$\Delta_{\mathcal{V}}^{\mathbb{B}}(k) \triangleq \phi^*(\mathbb{O}_k, \mathbb{B}_k) \Delta_{\mathcal{V}}(k) \quad \text{and} \quad H_{\mathbb{B}}^*(k) \triangleq \phi^*(\mathbb{O}_k, \mathbb{B}_k) H^*(k) \quad (3.22)$$

$$\begin{aligned} \phi(k+1, k) &\triangleq \phi(\mathbb{B}_{k+1}, \mathbb{B}_k) \\ &= \phi(\mathbb{B}_{k+1}, \mathbb{O}_{k+1}) \phi(\mathbb{O}_{k+1}, \mathbb{O}_k) \phi(\mathbb{O}_k, \mathbb{B}_k) \end{aligned} \quad (3.23)$$

$\Delta_{\mathcal{V}}^{\mathbb{B}}(k)$ is the hinge relative spatial velocity referenced to the k th body frame \mathbb{B}_k . ■

The expression for $\phi(k+1, k)$ in (3.23) generalizes (3.18).

$H_{\mathbb{B}}^*(k)$ is the k th hinge's joint map matrix referenced to the \mathbb{B}_k body frame, and is a generalization of $H^*(k)$. Even when the k th hinge is a pure rotational hinge,

it follows from (3.22) that the $H_{\mathbb{B}}^*(k)$ joint map matrix will have non-zero rotational and translational components when $\mathbb{B}_k \neq \mathbb{O}_k$.

The recursive spatial velocity relationship in (3.21) represents a generalization of (3.19b). The recursive Algorithm 3.2 continues to apply with $H^*(k)$ replaced with $H_{\mathbb{B}}^*(k)$. We can thus, conclude that, apart from minor modifications when $\mathbb{B}_k \neq \mathbb{O}_k$, the relationships remain essentially the same. As a result, there is little generality lost in continuing to assume that $\mathbb{B}_k = \mathbb{O}_k$.

Exercise 3.4 Velocity recursion with inertially fixed reference point.

Exercise 2.14 introduced the notion of using an inertially fixed point \mathbb{I} as the velocity reference point for a rigid body. In fact the same point \mathbb{I} can be used as the velocity reference point for all the links in the system. We use $V_{\mathbb{I}}(k)$ to denote the inertially referenced spatial velocity for the k th link. It is defined as

$$V_{\mathbb{I}}(k) \triangleq \phi^*(\mathbb{O}_k, \mathbb{I}) V(\mathbb{O}_k) \quad (3.24)$$

With

$$H_{\mathbb{I}}^*(k) \triangleq \phi^*(\mathbb{O}_k, \mathbb{I}) H^*(k) \quad \text{and} \quad \Delta_{\mathcal{V}}^{\mathbb{I}}(k) \triangleq H_{\mathbb{I}}^*(k) \beta(k) \quad (3.25)$$

show that the inter-link spatial velocity recursive relationship is given by:

$$V_{\mathbb{I}}(k) = V_{\mathbb{I}}(k+1) + \Delta_{\mathcal{V}}^{\mathbb{I}}(k) = V_{\mathbb{I}}(k+1) + H_{\mathbb{I}}^*(k) \beta(k) \quad (3.26)$$

■

For the inertially referenced case, we observe from (3.26) that the analog of the body transformation operator $\phi(k+1, k)$, denoted $\phi_{\mathbb{I}}(k+1, k)$, is simply the identity matrix! However, this simplicity has been achieved at the cost of additional complexity of the $H_{\mathbb{I}}(k)$ hinge map matrix.

3.4 Spatial Operators

In the previous sections, we have developed component body-to-body velocity relationships. In this section, we use these to develop corresponding relationships at the system level.

In the rest of this chapter, and without losing any generality, we make the following notationally convenient assumption regarding the hinges in the serial-chain:

We assume that $\beta(\cdot) = \dot{\theta}(\cdot)$, and thus $r_p(\cdot) = r_v(\cdot)$ for all the hinges.

In the general case when these assumptions do not hold, all that is required is that, wherever $\dot{\theta}$ and $\ddot{\theta}$ appear in the dynamical and kinematical equations, they be replaced by the appropriate β generalized velocities vector and the corresponding $\dot{\beta}$ acceleration vector, respectively.

The number of overall velocity degrees of freedom for the system is denoted \mathcal{N} , and is defined as the sum of all the individual hinge velocity degrees of freedom, i.e.,

$$\mathcal{N} \triangleq \sum_{k=1}^n r_v(k) \quad (3.27)$$

Now we introduce **stacked** vectors required to define system level relationships. We begin by defining the stacked vectors \mathcal{V} and θ as

$$\mathcal{V} \triangleq \text{col} \left\{ \mathcal{V}(k) \right\}_{k=1}^n = \begin{bmatrix} \mathcal{V}(1) \\ \mathcal{V}(2) \\ \vdots \\ \mathcal{V}(n) \end{bmatrix} \in \mathcal{R}^{6n}, \text{ and } \theta \triangleq \text{col} \left\{ \theta(k) \right\}_{k=1}^n = \begin{bmatrix} \theta(1) \\ \theta(2) \\ \vdots \\ \theta(n) \end{bmatrix} \in \mathcal{R}^{\mathcal{N}}$$

The \mathcal{V} stacked vector consists of the component body-level $\mathcal{V}(k)$ spatial velocity vectors assembled into a single large vector. Correspondingly, the θ stacked vector consists of the component body-level $\theta(k)$ generalized coordinates assembled into a single large vector. Similarly define the \mathcal{V}^+ and Δ_V stacked vectors as:

$$\mathcal{V}^+ \triangleq \text{col} \left\{ \mathcal{V}^+(k) \right\}_{k=1}^n \in \mathcal{R}^{6n} \quad \text{and} \quad \Delta_V \triangleq \text{col} \left\{ \Delta_V(k) \right\}_{k=1}^n \in \mathcal{R}^{6n} \quad (3.28)$$

From these definitions, it follows that the component level (3.14) expression can be equivalently restated at the system-level as

$$\mathcal{V} = \mathcal{V}^+ + \Delta_V \quad (3.29)$$

Now define the strictly block lower-triangular **spatial operator** \mathcal{E}_ϕ as:

$$\mathcal{E}_\phi \triangleq \begin{pmatrix} \mathbf{0} & \mathbf{0} & \mathbf{0} & \mathbf{0} & \mathbf{0} \\ \phi(2,1) & \mathbf{0} & \dots & \mathbf{0} & \mathbf{0} \\ \mathbf{0} & \phi(3,2) & \dots & \mathbf{0} & \mathbf{0} \\ \vdots & \vdots & \ddots & \vdots & \vdots \\ \mathbf{0} & \mathbf{0} & \dots & \phi(n,n-1) & \mathbf{0} \end{pmatrix} \in \mathcal{R}^{6n \times 6n} \quad (3.30)$$

It is easy to verify that the component level (3.19a) relationship, $\mathcal{V}^+(k) = \phi^*(k+1,k)\mathcal{V}(k+1)$, can be equivalently re-expressed using \mathcal{E}_ϕ and the stacked vectors as:

$$\mathcal{V}^+ = \mathcal{E}_\phi^* \mathcal{V} \quad (3.31)$$

Continuing on, define the block-diagonal H spatial operator as

$$H \triangleq \text{diag}\left\{ H(k) \right\}_{k=1}^n = \begin{pmatrix} H(1) & \mathbf{0} & \dots & \mathbf{0} \\ \mathbf{0} & H(2) & \dots & \mathbf{0} \\ \vdots & \vdots & \ddots & \vdots \\ \mathbf{0} & \mathbf{0} & \dots & H(n) \end{pmatrix} \in \mathcal{R}^{N \times 6n} \quad (3.32)$$

Using the H operator, the component-level relationship in (3.7) can be re-expressed at the system level as:

$$\Delta \mathcal{V} = H^* \dot{\theta} \quad (3.33)$$

Combining (3.29), (3.31) and (3.33), we obtain the relationship

$$\mathcal{V} = \mathcal{E}_\phi^* \mathcal{V} + H^* \dot{\theta} \quad (3.34)$$

Equation (3.34) is an equivalent compact version of the link-level velocity relationship in (3.19b) for all the links in the system. Equation (3.34) is an implicit relationship because \mathcal{V} appears on both sides of the equality. Rearranging terms, (3.34) can be restated as

$$(I - \mathcal{E}_\phi^*) \mathcal{V} = H^* \dot{\theta} \quad (3.35)$$

3.4.1 The ϕ Spatial Operator

Being strictly lower-triangular, \mathcal{E}_ϕ is nilpotent,⁴ i.e., its power vanishes for some finite exponent. In fact, $\mathcal{E}_\phi^n = \mathbf{0}$. With this property, we can make use of Lemma A.1 on page 400 which discusses inverses related to nilpotent matrices and provides an explicit expression for the inverse of $(I - \mathcal{E}_\phi)$. From Lemma A.1, the inverse of $(I - \mathcal{E}_\phi)$, denoted $\phi \in \mathcal{R}^{6n \times 6n}$, exists and has the form

$$\phi \triangleq (I - \mathcal{E}_\phi)^{-1} = I + \mathcal{E}_\phi + \mathcal{E}_\phi^2 + \dots + \mathcal{E}_\phi^{n-1} \quad (3.36)$$

Exercise 3.5 Internal structure of the ϕ operator.

Show that the ϕ spatial operator has the following block lower-triangular form

$$\phi = \begin{pmatrix} I & \mathbf{0} & \dots & \mathbf{0} \\ \phi(2,1) & I & \dots & \mathbf{0} \\ \vdots & \vdots & \ddots & \vdots \\ \phi(n,1) & \phi(n,2) & \dots & I \end{pmatrix} \quad (3.37)$$

⁴ A matrix X is said to be nilpotent if there exists an integer, n , such that $X^n = \mathbf{0}$.

Verify that for $i > j$, the $\phi(i,j) \in \mathcal{R}^{6 \times 6}$ elements of ϕ are also rigid body transformation operators and are given by:

$$\phi(i,j) = \phi(i,i-1) \cdots \phi(j+1,j) = \begin{pmatrix} \mathbf{I} & \tilde{l}(i,j) \\ \mathbf{0} & \mathbf{I} \end{pmatrix} \quad (3.38)$$

$\tilde{l}(i,j)$ denotes the vector from the i th link frame \mathbb{B}_i , to the j th link frame \mathbb{B}_j . Equation (3.38) is a carry-over of the (1.32) semi-group property of the $\phi(i,j)$ elements. ■

The ϕ spatial operator is generally configuration dependent since its $\phi(k,j)$ elements are configuration dependent.

3.4.2 Velocity Operator Expression

Now that we have an expression for the inverse of $(\mathbf{I} - \mathcal{E}_\phi)$, we use it to obtain the following explicit expression for the \mathcal{V} spatial velocity stacked vector:

$$\mathcal{V} \stackrel{3.35}{=} (\mathbf{I} - \mathcal{E}_\phi^*)^{-1} \mathbf{H}^* \dot{\theta} \stackrel{3.36}{=} \phi^* \mathbf{H}^* \dot{\theta} \quad (3.39)$$

Before proceeding further, an important point to emphasize is that the system-level relationship between the stacked vectors $\dot{\theta}$ and \mathcal{V} , as defined by the spatial operator expression in (3.39), is derived from and mathematically equivalent to the component-level relationship in (3.19b).

However, the computational story is different. On the face of it, the expression $\mathcal{V} = \phi^* \mathbf{H}^* \dot{\theta}$ in (3.39) suggests that the evaluation of \mathcal{V} from $\dot{\theta}$ requires at least two matrix vector products, with the first being $\Delta\mathcal{V} = \mathbf{H}^* \dot{\theta}$ and the second being $\phi^* \Delta\mathcal{V}$. While the first product involving the block-diagonal \mathbf{H}^* matrix can be carried out at $O(N)$ cost, the latter product involves the populated, though upper-triangular, ϕ^* matrix and is of $O(N^2)$ computational cost. Hence, the overall cost of computing \mathcal{V} through this process is of $O(N^2)$ computational complexity. In contrast, Algorithm 3.2 involves a base-to-tip recursion for computing the elements of \mathcal{V} , a process that scales linearly with the number of bodies and is of just $O(N)$ computational complexity. Thus, we see here the existence of a direct recursive computational algorithm of simpler complexity than would be suggested by the brute force matrix/vector products implied by the $\mathcal{V} = \phi^* \mathbf{H}^* \dot{\theta}$ operator expression.

This is just the first of many examples we will encounter, where the special structure of the spatial operators allows us to implement computational algorithms that are far less expensive than those implied by the operator expressions. Indeed, in Sect. 3.5 we will start to examine patterns that allow us to directly generate such simpler recursive computational algorithms by direct examination of spatial operator expressions. We will see that while spatial operators provide the means to concisely represent complex multibody relationships, and the tools to carry out mathematical analysis of multibody quantities, they also provide a straightforward avenue for

converting operator relationships into low-order computational algorithms when the expressions need to be evaluated.

3.4.3 The $\tilde{\phi}$ Spatial Operator

Define the spatial operator $\tilde{\phi} \in \mathcal{R}^{6n \times 6n}$ as

$$\tilde{\phi} \triangleq \phi - \mathbf{I} \quad (3.40)$$

Observe that $\tilde{\phi}$ is strictly lower-triangular. The following exercise establishes basic properties of $\tilde{\phi}$.

Exercise 3.6 The $\tilde{\phi}$ spatial operator.

1. Show that

$$\tilde{\phi} = \mathcal{E}_\phi \phi = \phi \mathcal{E}_\phi \quad (3.41)$$

2. Show that the stacked vector of spatial velocities \mathcal{V}^+ satisfies the relationship

$$\mathcal{V}^+ = \tilde{\phi}^* \mathbf{H}^* \dot{\theta} \quad (3.42)$$

■

3.5 Recursions Associated with the ϕ Operator

We have seen how the apparent $O(N^2)$ procedure for computing the body spatial velocities, \mathcal{V} , can in fact be replaced by an $O(N)$ recursive algorithm. In this section we identify principles and structural properties of spatial operators that make this possible more generally. We begin with the following lemma which shows how an expression such as $y = \phi x$ can be evaluated using a tip-to-base $O(N)$ recursive algorithm involving only the $\phi(k+1, k)$ elements and x .

Lemma 3.1 Tip-to-base recursion to evaluate ϕx .

Given a stacked vector $x \in \mathcal{R}^{6n}$, the $y = \phi x$ operator expression can be evaluated using the following $O(N)$ **tip-to-base** recursive algorithm:

$$y = \phi x \Leftrightarrow \begin{cases} y(0) = 0 \\ \text{for } k = 1 \dots n \\ \quad y(k) = \phi(k, k-1)y(k-1) + x(k) \\ \text{end loop} \end{cases} \quad (3.43)$$

The structure of this tip-to-base computational algorithm is illustrated on the left side of Fig. 3.6.

Proof: Using the expression for ϕ in (3.37), it follows that the expression for the k th element of $y = \phi x$ is given by:

$$y(k) \stackrel{3.37}{=} \sum_{j=1}^k \phi(k,j)x(j) \quad (3.44)$$

Thus,

$$\begin{aligned} y(k) &\stackrel{3.38}{=} \phi(k,k-1) \sum_{j=1}^{k-1} \phi(k-1,j)x(j) + x(k) \\ &\stackrel{3.44}{=} \phi(k,k-1)y(k-1) + x(k) \end{aligned}$$

This establishes the result. ■

This lemma illustrates how recursive dynamical algorithms can be derived naturally by exploiting the special semi-group properties of the elements of the ϕ spatial operator. Thus given a stacked vector x , evaluating the matrix–vector product ϕx does not require an $O(N^2)$ operator–vector product computation, and not even the explicit computation of the elements of ϕ !

Similarly, the product $x = \phi^* y$ is equivalent to a base-to-tip $O(N)$ recursive computational algorithm as described in the following lemma.

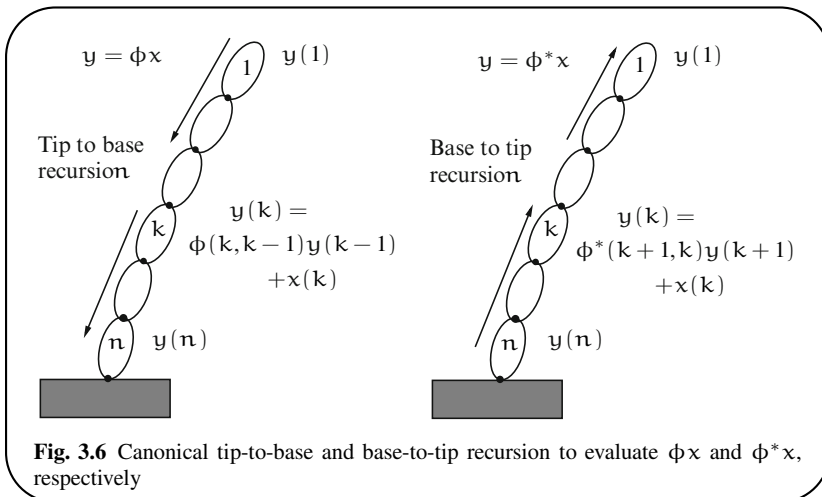


Fig. 3.6 Canonical tip-to-base and base-to-tip recursion to evaluate ϕx and $\phi^* x$, respectively

Lemma 3.2 Base-to-tip recursion to evaluate $\phi^* x$.

Given a stacked vector $x \in \mathcal{R}^{6n}$, the $y = \phi^* x$ operator relationship can be evaluated

using the following $O(N)$ **base-to-tip** recursive algorithm:

$$y = \phi^* x \Leftrightarrow \begin{cases} y(n+1) = 0 \\ \textbf{for } k = n \dots 1 \\ \quad y(k) = \phi^*(k+1, k)y(k+1) + x(k) \\ \textbf{end loop} \end{cases} \quad (3.45)$$

The structure of this base-to-tip computational algorithm is illustrated on the right side of Fig. 3.6.

Proof: Using the expression for ϕ in (3.37), we have

$$y(k) \stackrel{3.37}{=} \sum_{j=n}^k \phi^*(j, k)x(j) \quad (3.46)$$

Thus,

$$\begin{aligned} y(k) &\stackrel{3.38}{=} \phi^*(k+1, k) \sum_{j=n}^{k+1} \phi^*(j, k+1)x(j) + x(k) \\ &\stackrel{3.46}{=} \phi^*(k+1, k)y(k+1) + x(k) \end{aligned}$$

This establishes the result. ■

The equivalence described in (3.45) is precisely the correspondence between the concise operator-based $\mathcal{V} = \phi^* H^* \dot{\theta}$ velocity relationship in (3.39) and the equivalent recursive algorithm for the link spatial velocities in Algorithm 3.2 on page 45, with $x = H^* \dot{\theta}$ and $y = \mathcal{V}$.

Exercise 3.7 Recursive evaluation of $\tilde{\phi}x$ and $\tilde{\phi}^*x$.

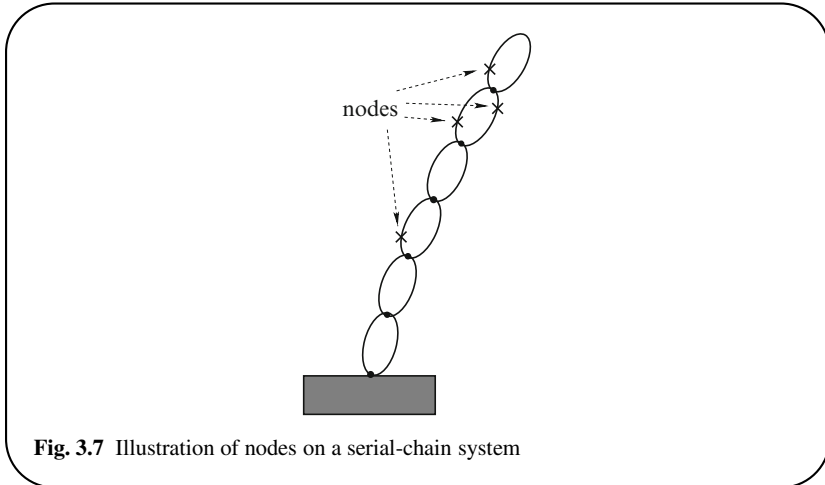
Develop $O(N)$ recursive algorithms similar to those in (3.43) and (3.45) for evaluating $\tilde{\phi}x$ and $\tilde{\phi}^*x$. ■

Section 9.2 on page 162 extends the ϕ operator and related recursions to more general multibody systems such as tree-topology systems, where the link numbering can be arbitrary and the ϕ and ϕ^* operators are not necessarily triangular.

3.6 The Jacobian Operator

Robotic multibody systems typically have distinguished *frames of interest* (also referred to as *nodes*) that need to be monitored and/or controlled. The end-effector frame is an example of such a node for robotic arms and is generally located on

the outer-most link. As illustrated in Fig. 3.7, these nodes may not coincide with the body frames or the hinge frames. Also, a body can have none to multiple such nodes. In this section, we explore the Jacobian operators that define the differential relationship between the generalized velocities of the system and the spatial velocities of such distinguished nodes.



Since individual bodies can have multiple nodes, we introduce the notation \mathbb{O}_k^i to denote the i th node on the k th link. The number of nodes on the k th body is denoted $n_{nd}(k)$. A single end-effector frame located on link 1 would be denoted \mathbb{O}_1^0 . The spatial velocity of the \mathbb{O}_k^i node frame is denoted $\mathcal{V}(\mathbb{O}_k^i)$, and is related to the $\mathcal{V}(k)$ spatial velocity of the k th link by

$$\mathcal{V}(\mathbb{O}_k^i) \stackrel{1.33}{=} \phi^*(k, \mathbb{O}_k^i) \mathcal{V}(k) \quad (3.47)$$

where $\phi(k, \mathbb{O}_k^i)$ is the rigid body transformation matrix from the k th link frame, \mathbb{B}_k , to the rigidly attached \mathbb{O}_k^i node frame. Let n_{nd} denote the total number of such nodes across all the links in the system, i.e.,

$$n_{nd} \triangleq \sum_{k=1}^n n_{nd}(k) \quad (3.48)$$

Now define the $6n_{nd}$ dimensional stacked vector, \mathcal{V}_{nd} as consisting of the spatial velocities of all the nodes on all the bodies in the system, i.e.,

$$\begin{aligned}\mathcal{V}_{nd}(k) &\triangleq \text{col} \left\{ \mathcal{V} \left(\mathbb{O}_k^i \right) \right\}_{i=1}^{n_{nd}(k)} \in \mathcal{R}^{6n_{nd}(k)} \\ \mathcal{V}_{nd} &\triangleq \text{col} \left\{ \mathcal{V}_{nd}(k) \right\}_{i=1}^n \in \mathcal{R}^{6n_{nd}}\end{aligned}\quad (3.49)$$

The component-level relationship in (3.47) implies the following system-level relationship between the \mathcal{V} and \mathcal{V}_{nd} stacked vectors

$$\mathcal{V}_{nd} \stackrel{3.47}{=} \mathcal{B}^* \mathcal{V} \quad (3.50)$$

where the $6n \times 6n_{nd}$ dimensional **pick-off spatial operator** \mathcal{B} is a block-matrix whose row indices are the bodies, and the column indices are the nodes in the system. \mathcal{B} contains one $6n \times 6$ dimensional block-column of 6×6 matrices for each \mathbb{O}_k^i node. The column for the \mathbb{O}_k^i node has $\phi(k, \mathbb{O}_k^i)$ as the only non-zero element at the k th parent link slot. While each column of \mathcal{B} has only one non-zero 6×6 matrix element, its k th row can have multiple 6×6 non-zero matrix elements, one for each node on the k th link. \mathcal{B} is referred to as a *pick off* spatial operator, since it picks off and maps the link spatial velocities into the spatial velocities of the nodes, as per (3.50). When the only node is a single end-effector node on the outermost link, \mathcal{B} has the form

$$\mathcal{B} \triangleq \begin{bmatrix} \phi(1, \mathbb{O}_1^0) \\ \mathbf{0} \\ \vdots \\ \mathbf{0} \end{bmatrix} \in \mathcal{R}^{6n \times 6} \quad (3.51)$$

Using the expression for \mathcal{V} in (3.39), (3.50) can be re-expressed as

$$\mathcal{V}_{nd} \stackrel{3.50, 3.39}{=} \mathcal{B}^* \phi^* \mathcal{H}^* \dot{\theta} \quad (3.52)$$

In other words,

$$\mathcal{V}_{nd} = \mathcal{J} \dot{\theta} \quad \text{where} \quad \mathcal{J} \triangleq \mathcal{B}^* \phi^* \mathcal{H}^* \in \mathcal{R}^{6n_{nd} \times \mathcal{N}} \quad (3.53)$$

\mathcal{J} is referred to as the **Jacobian operator** for the serial-chain. It maps the $\dot{\theta}$ generalized velocities into the \mathcal{V}_{nd} spatial velocities of the nodes for the serial-chain [41]. The Jacobian operator \mathcal{J} in (3.53) is the product of three operators \mathcal{B}^* , ϕ^* and \mathcal{H}^* . The action of the Jacobian operator on the joint angle rates $\dot{\theta}$ is as follows:

1. $\mathcal{H}^* \dot{\theta}$ results in the $\Delta \gamma$ relative spatial velocities across the hinges.
2. ϕ^* then propagates these relative velocities from the base-to-tip (Algorithm 3.2) to obtain the link spatial velocities.
3. \mathcal{B}^* then picks out the $\mathcal{V}(k)$ link spatial-velocities from \mathcal{V} and propagates them to the nodes to obtain their $\mathcal{V}(\mathbb{O}_k^i)$ spatial velocities.

The key point to note is that \mathcal{J} has a operator factorization which has immediate physical interpretation and obvious recursive algorithm equivalents. The operator factorization of the Jacobian matrix will play an important part in studying the kinematics and dynamics of systems in later chapters.

Chapter 4

The Mass Matrix

While the mass and rotational inertia of a body are the elemental quantities for studying single rigid body dynamics, the mass matrix plays the corresponding role for multibody systems. One crucial difference is that the mass matrix varies with the configuration of the system. In this chapter, we derive expressions for the mass matrix of a serial-chain multibody system, study its properties, and develop related computational algorithms.

4.1 Mass Matrix of a Serial-Chain System

4.1.1 Kinetic Energy of the Serial-Chain

For a serial-chain system, we use (2.7) to define the $M(k)$ spatial inertia of the k th link about its body frame \mathbb{B}_k as follows:

$$M(k) \triangleq \begin{pmatrix} \mathcal{J}(k) & m(k)\tilde{p}(k) \\ -m(k)\tilde{p}(k) & m(k)\mathbf{I} \end{pmatrix} \quad (4.1)$$

$\mathcal{J}(k)$ is the inertia tensor for the k th link about \mathbb{B}_k , $\tilde{p}(k)$ is the vector from \mathbb{B}_k to the center of mass of the k th link, and $m(k)$ is the mass of the k th link.

The total kinetic energy of the system, \mathfrak{K}_e , is the sum of the kinetic energies of each of the individual links:

$$\mathfrak{K}_e \stackrel{2.5}{=} \frac{1}{2} \sum_{k=1}^n \mathcal{V}^*(k) M(k) \mathcal{V}(k) \quad (4.2)$$

Equation (4.2) can be re-expressed as

$$\begin{aligned}\hat{\mathcal{K}}_e &= \frac{1}{2} [\mathcal{V}^*(1), \dots, \mathcal{V}^*(n)] \begin{pmatrix} M(1) & \mathbf{0} & \cdots & \mathbf{0} \\ \mathbf{0} & M(2) & \cdots & \mathbf{0} \\ \vdots & \vdots & \ddots & \vdots \\ \mathbf{0} & \mathbf{0} & \cdots & M(n) \end{pmatrix} \begin{pmatrix} \mathcal{V}(1) \\ \mathcal{V}(2) \\ \vdots \\ \mathcal{V}(n) \end{pmatrix} \\ &= \frac{1}{2} \mathcal{V}^* \mathbf{M} \mathcal{V}\end{aligned}\quad (4.3)$$

where \mathbf{M} is the block-diagonal, symmetric and positive semi-definite **spatial inertia spatial operator** defined as

$$\mathbf{M} \triangleq \text{diag} \left\{ M(k) \right\}_{k=1}^n \in \mathcal{R}^{6n \times 6n} \quad (4.4)$$

Equation (4.3) expresses the total system kinetic energy in terms of the spatial velocity vector \mathcal{V} . Substituting $\mathcal{V} = \phi^* H^* \dot{\theta}$ from (3.52) into (4.3) allows us to express the kinetic energy of the serial-chain in terms of the generalized velocities $\dot{\theta}$:

$$\hat{\mathcal{K}}_e \stackrel{3.39, 4.3}{=} \frac{1}{2} \dot{\theta}^* H \phi \mathbf{M} \phi^* H^* \dot{\theta} = \frac{1}{2} \dot{\theta}^* \mathcal{M}(\theta) \dot{\theta} \quad (4.5)$$

where

$$\mathcal{M}(\theta) \triangleq H \phi \mathbf{M} \phi^* H^* \in \mathcal{R}^{N \times N} \quad (4.6)$$

Equation (4.5) has the familiar quadratic form for kinetic energy. \mathcal{M} in (4.6) is referred to as the **mass matrix** of the multibody system. Since \mathbf{M} is symmetric and positive semi-definite, so is the \mathcal{M} mass matrix. However, since ϕ is configuration-dependent, the mass matrix is also configuration-dependent. The mass matrix is a natural generalization of the notion of spatial inertia of single rigid bodies for articulated multibody systems and plays a central role in their dynamics.

Equation (4.6) can also be viewed as a spatial operator factorization of the mass matrix. This factored form of the mass matrix is referred to as the **Newton–Euler Operator Factorization** of the mass matrix. We will further explore the rich internal structure of the mass matrix in Chap. 7, and develop an alternative analytical Innovations Operator Factorization for it, as well as an expression for its inverse.

We now turn to the problem of computing the configuration dependent mass matrix. Possible methods include:

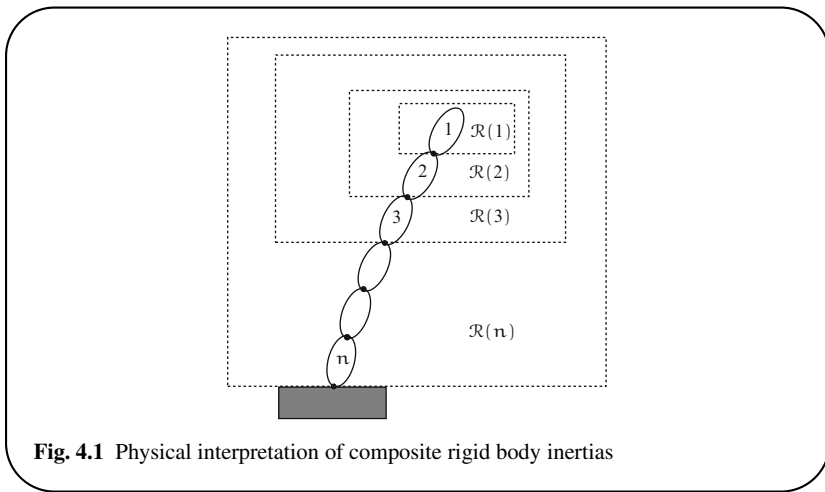
1. The Lagrangian approach which consists of forming a configuration dependent expression for the kinetic energy in (4.2), and taking its second order partial derivative with respect to the generalized velocities to obtain the mass matrix elements. This approach can become very complex for even moderately sized systems.
2. An approach based on (4.6). Here, the component operators ϕ , \mathbf{M} , and H are computed explicitly, and the mass matrix is computed by evaluating the prod-

ucts in (4.6). This approach is also computationally quite expensive with $O(N^3)$ computational complexity in the number of degrees of freedom.

3. The most efficient approach, with only $O(N^2)$ computational complexity, is based on composite body inertias. It is discussed in the next section.

4.1.2 Composite Rigid Body Inertias

The **composite body inertia** associated with a hinge is defined as the effective spatial inertia of the composite body formed by all of the bodies outboard of the hinge. This is illustrated in Fig. 4.1. Thus, the composite body inertia for the k th link,



denoted $R(k)$, is the effective spatial inertia about B_k of the $k \cdots 1$ links, assuming that they form a rigid body obtained by freezing hinges $(k-1) \cdots 1$. The value of $R(k)$ is not a constant and depends on the configuration of the 1 through $(k-1)$ hinges.

Now let us examine how we might go about computing the composite rigid body inertias for all the links. Clearly, for the outer-most link, $R(1) = M(1)$, the spatial inertia of link 1. $R(2)$ is the spatial inertia at B_2 of links 1 and 2 combined to form a composite rigid body by “freezing” hinge 1 and ignoring the inboard links. Similarly, the composite rigid body inertia, $R(k)$, at the k th link can be obtained by using the parallel axis theorem for spatial inertias to combine together the composite rigid body inertia $R(k-1)$ at link $(k-1)$, with the spatial inertia, $M(k)$, of the k th link, i.e.,

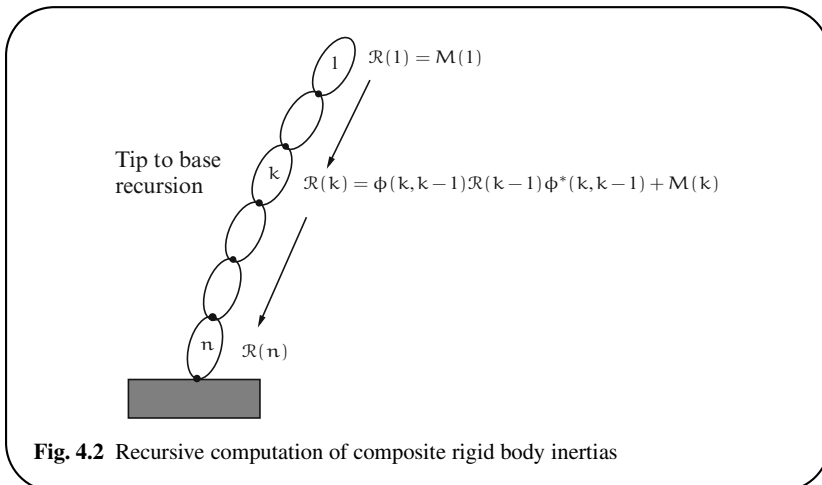
$$R(k) = \phi(k, k-1)R(k-1)\phi^*(k, k-1) + M(k) \quad (4.7)$$

We can thus, compute all the composite inertias starting from the tip body and proceeding towards the base. This $O(N)$ tip-to-base recursive computational process is described in Algorithm 4.1 and illustrated in Fig. 4.2.

Algorithm 4.1 Recursive computation of Composite Body Inertias

$$\left\{ \begin{array}{l} \mathcal{R}(0) = \mathbf{0} \\ \text{for } k = 1 \dots n \\ \quad \mathcal{R}(k) = \phi(k, k-1) \mathcal{R}(k-1) \phi^*(k, k-1) + M(k) \\ \text{end loop} \end{array} \right. \quad (4.8)$$

This recursive procedure is also known as a **Lyapunov recursion**¹ since it is closely associated with the Lyapunov equation for composite body inertias, which we will encounter in the next section. Algorithm 9.2 on page 169 describes the generalization of this composite body inertia algorithm for tree-topology systems.



Since $\mathcal{R}(k)$ is the composition of spatial inertias, it is itself a spatial inertia. Thus, it can be parameterized by just ten parameters: one for the mass, three for the mass center location, and six for the rotational inertia. This reduces the number of computations required to evaluate the composite body inertias.

¹ Section 6.4 on page 111 discusses the roots of this terminology which arise from the mathematical parallels with estimation theory.

Remark 4.1 $\mathcal{R}(k)$ does not depend upon inboard bodies.

The composite body inertia $\mathcal{R}(k)$ depends only on the outboard hinge coordinates $\theta(i)$ for $i < k$ and is independent of the hinge coordinates of the inboard links. ■

4.1.3 Decomposition of $\phi \mathbf{M} \phi^*$

Define $\mathcal{R} \triangleq \text{diag} \left\{ \mathcal{R}(k) \right\}_{k=1}^n \in \mathcal{R}^{6n \times 6n}$ to be the block-diagonal, symmetric, positive semi-definite operator with the k th block-diagonal entry being $\mathcal{R}(k)$. The following lemma shows that the $\phi \mathbf{M} \phi^*$ operator product can be decomposed into diagonal and triangular factors using the \mathcal{R} operator.

Lemma 4.1 Lyapunov decomposition using composite body inertias.
 \mathcal{R} satisfies the operator equation

$$\mathbf{M} = \mathcal{R} - \mathcal{E}_\phi \mathcal{R} \mathcal{E}_\phi^* \quad (4.9)$$

In addition, $\phi \mathbf{M} \phi^*$ can be decomposed into the following disjoint sum:

$$\phi \mathbf{M} \phi^* = \mathcal{R} + \tilde{\phi} \mathcal{R} + \mathcal{R} \tilde{\phi}^* \quad (4.10)$$

In this disjoint partitioning of $\phi \mathbf{M} \phi^*$, the first term on the right-hand side is block-diagonal, the second is strictly lower-triangular, and the last term is strictly upper-triangular as illustrated in Fig. 4.3.

Proof: It is a straightforward exercise to verify that $\mathcal{E}_\phi \mathcal{R} \mathcal{E}_\phi^*$ is block-diagonal with the k th k diagonal entry being $\phi(k, k-1) \mathcal{R}(k-1) \phi^*(k, k-1)$. Thus (4.9) is merely a restatement in stacked notation of the recursions in (4.8).

Multiplying (4.9) from the left and right by ϕ and ϕ^* , respectively then leads to

$$\begin{aligned} \phi \mathbf{M} \phi^* &\stackrel{4.9}{=} \phi \mathcal{R} \phi^* - \phi \mathcal{E}_\phi \mathcal{R} \mathcal{E}_\phi^* \phi^* \stackrel{3.41}{=} \phi \mathcal{R} \phi^* - \tilde{\phi} \mathcal{R} \tilde{\phi}^* \\ &\stackrel{3.40}{=} (\tilde{\phi} + \mathbf{I}) \mathcal{R} (\tilde{\phi} + \mathbf{I}) - \tilde{\phi} \mathcal{R} \tilde{\phi}^* \stackrel{3.40}{=} \mathcal{R} + \tilde{\phi} \mathcal{R} + \mathcal{R} \tilde{\phi}^* \end{aligned}$$

This establishes (4.10).

Since $\tilde{\phi}$ is strictly lower-triangular and \mathcal{R} is block-diagonal, it follows that $\tilde{\phi} \mathcal{R}$ is strictly lower-triangular. ■

Equation (4.9) is identical in form to the discrete **Lyapunov equations** that arise in the theory of linear discrete-time systems [5]. \mathcal{R} is block-diagonal, $\tilde{\phi} \mathcal{R}$ is strictly lower-triangular, and $\mathcal{R} \tilde{\phi}^*$ strictly upper-triangular. The three terms, \mathcal{R} , $\tilde{\phi} \mathcal{R}$, and $\mathcal{R} \tilde{\phi}^*$, on the right in (4.10) can be computed from just the knowledge of \mathcal{R} and ϕ . Due to its symmetry, computing $\phi \mathbf{M} \phi^*$, requires computing just the \mathcal{R} and $\tilde{\phi} \mathcal{R}$ terms. Furthermore, with the knowledge of \mathcal{R} , the $\tilde{\phi} \mathcal{R}$ product can be computed recursively. This is so because the block entries in the j th column of $\tilde{\phi} \mathcal{R}$ have the form:

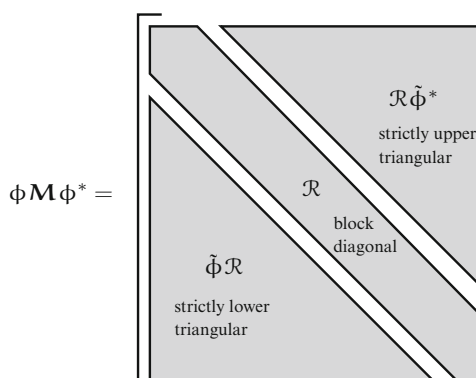


Fig. 4.3 The decomposition of $\phi \mathbf{M} \phi^*$ into diagonal and triangular components

$$[\tilde{\phi} \mathcal{R}] (k, j) = \begin{cases} \mathbf{0} & \text{for } 1 \leq k \leq j \\ \phi(k, j) \mathcal{R}(j) & \text{for } j < k \leq n \end{cases} \quad (4.11)$$

Since $\phi(k+1, j) = \phi(k+1, k) \phi(k, j)$, this implies that

$$[\tilde{\phi} \mathcal{R}] (k+1, j) \stackrel{4.11}{=} \phi(k+1, k) \cdot [\tilde{\phi} \mathcal{R}] (k, j) \quad (4.12)$$

This forms the basis for a recursion sequence, starting from the $\mathcal{R}(j)$ diagonal element, to compute the j th column elements of $\tilde{\phi} \mathcal{R}$, ending up with the (n, j) th element of $\tilde{\phi} \mathcal{R}$. We will exploit this structure in the following section when developing efficient procedures for computing the mass matrix \mathbf{M} .

Exercise 4.1 System center of mass.

This exercise explores the instantaneous properties, such as the spatial inertia, the center of mass location, and angular momentum, for the overall system.

1. Show that the overall spatial inertia of the system referenced to the \mathbb{B}_n base-body frame, \mathbf{M}_S , is the composite body inertia $\mathcal{R}(n)$, for the base-body, i.e.,

$$\mathbf{M}_S = \mathcal{R}(n) = E^* \mathcal{R} E \quad (4.13)$$

where E is the base pick-off operator (dual of the B tip pick-off operator) defined as

$$E \triangleq [\mathbf{0}_6, \dots, \mathbf{0}_6, \mathbf{I}_6] \in \mathcal{R}^{6 \times 6n} \quad (4.14)$$

The first moment vector, $\mathbf{l}(\mathbf{n}, \mathbb{C}_S)$ of $\mathcal{R}(\mathbf{n})$ specifies the instantaneous location of the center of mass of the system, \mathbb{C}_S , with respect to the reference frame \mathbb{B}_n of the base-body.

2. Show that the instantaneous spatial momentum of the system, \mathbf{h}_S , referenced about the \mathbb{B}_n base-body frame, is given by the expression

$$\mathbf{h}_S = \mathbf{E}\phi\mathcal{R}\mathbf{H}^*\dot{\theta} \quad (4.15)$$

For a free-flying system, i.e., one whose n th hinge is a full 6 degree of freedom hinge, show that (4.15) can be re-expressed as:

$$\mathbf{h}_S = \mathcal{R}(\mathbf{n})\mathcal{V}(\mathbf{n}) + \sum_{k=1}^{n-1} \phi(\mathbf{n}, k)\mathcal{R}(k)\mathbf{H}^*(k)\dot{\theta}(k) \quad (4.16)$$

3. Show that the instantaneous spatial velocity $\mathcal{V}_{\mathbb{C}}$, of the center of mass of the system, referenced to the \mathbb{B}_n frame, is given by the expression:

$$\mathcal{V}_{\mathbb{C}} = \mathbf{M}_S^{-1}\mathbf{h}_S = \mathcal{R}^{-1}(\mathbf{n}) \sum_{k=1}^{n-1} \phi(\mathbf{n}, k)\mathcal{R}(k)\mathbf{H}^*(k)\dot{\theta}(k) \quad (4.17)$$

4. For a free-flying system, show that (4.17) simplifies to:

$$\mathcal{V}_{\mathbb{C}} = \mathcal{V}(\mathbf{n}) + \mathcal{R}^{-1}(\mathbf{n}) \sum_{k=1}^{n-1} \phi(\mathbf{n}, k)\mathcal{R}(k)\mathbf{H}^*(k)\dot{\theta}(k) \quad (4.18)$$

Hence, show that an additional spatial velocity of $-\mathcal{V}_{\mathbb{C}}$ at the base-body nullifies the spatial momentum of the system, i.e., it makes $\mathbf{h}_S = \mathbf{0}$. ■

Since $\mathcal{V}_{\mathbb{C}}$ represents the spatial velocity of the center of mass of the system referenced to \mathbb{B}_n , the spatial velocity of the system center of mass with respect to the inertial frame is $\phi^*(\mathbb{B}_n, \mathbb{C}_S)\mathcal{V}_{\mathbb{C}}$.

The next section uses the decomposition in (4.10) to develop a recursive $O(N^2)$ algorithm for evaluating the configuration dependent mass matrix.

4.1.4 $O(N^2)$ Algorithm for Computing the Mass Matrix

Lemma 4.2 Decomposition of the mass matrix.

The mass matrix can be decomposed into disjoint diagonal and strictly triangular terms as follows:

$$\mathcal{M} = \mathcal{H}\mathcal{R}\mathbf{H}^* + \mathcal{H}\tilde{\Phi}\mathcal{R}\mathbf{H}^* + \mathcal{H}\tilde{\mathcal{R}}\tilde{\Phi}^*\mathcal{H}^* \quad (4.19)$$

Proof: The result follows by pre- and post-multiplying (4.10) with H and H^* , respectively, and recalling from (4.6) that $\mathcal{M} = H\phi\mathbf{M}\phi^*H^*$. Since H is block-diagonal, the disjoint property of the decomposition in (4.10) continues to hold for (4.19). \blacksquare

From this decomposition and (4.11), it follows that the elements of \mathcal{M} are given by the following expressions:

$$\mathcal{M}(i,j) = \begin{cases} H(i)\mathcal{R}(i)H^*(i) & \text{for } i=j \\ H(i)\phi(i,j)\mathcal{R}(j)H^*(j) & \text{for } i>j \\ \mathcal{M}^*(j,i) & \text{for } i<j \end{cases} \quad (4.20)$$

Thus, the $\mathcal{M}(i,j)$ element of the mass matrix depends only upon $H(i)$, $\phi(i,j)$ and $\mathcal{R}(j)$. This means that $\mathcal{M}(i,j)$ depends only upon $\theta(k)$, where k is in the range $(1 \cdots \max(i,j))$. That is, the element depends only upon the generalized coordinates of the hinges outboard of the i th and j th hinges, and is independent of the generalized coordinates of the inboard hinges!

Combining (4.8) and (4.19), we obtain the $O(N^2)$ Algorithm 4.2 for computing the mass matrix \mathcal{M} . This algorithm includes Algorithm 4.1 for computing the composite body inertias, and makes use of the recursive expression in (4.12) and (4.20) for the off-diagonal terms.

Algorithm 4.2 Recursive computation of the mass matrix

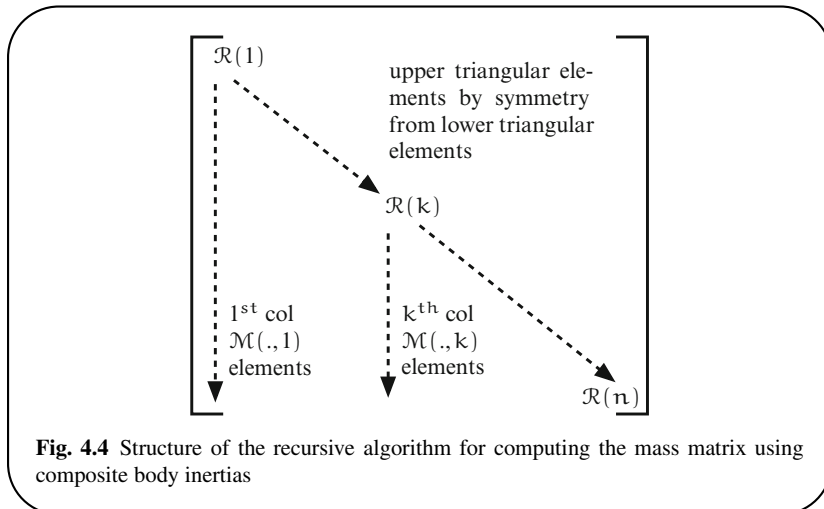
```

 $\mathcal{R}(0) = \mathbf{0}$ 
for  $k = 1 \cdots n$ 
   $\mathcal{R}(k) = \phi(k,k-1)\mathcal{R}(k-1)\phi^*(k,k-1) + M(k)$ 
   $X(k) = \mathcal{R}(k)H^*(k), \quad \mathcal{M}(k,k) = H(k)X(k)$ 
  for  $j = (k+1) \cdots n$ 
     $X(j) = \phi(j,j-1)X(j-1)$ 
     $\mathcal{M}(j,k) = \mathcal{M}^*(k,j) = H(j)X(j)$ 
  end loop
end loop

```

This algorithm evaluates the lower-triangular mass matrix elements represented by the elements of the $H\mathcal{R}H^*$ and $H\tilde{\phi}\mathcal{R}H^*$ terms in (4.19). Since the mass matrix is symmetric, this is sufficient to evaluate all of the elements of the mass matrix.

The outer loop of the algorithm computes the $\mathcal{R}(k)$ matrices recursively in a tip-to-base recursion. As illustrated in Fig. 4.4, as each $\mathcal{R}(k)$ is computed, the inner-loop recursively computes the lower-diagonal elements of the k th column of the mass matrix.



This composite body inertia algorithm for computing the mass matrix is another example of the development of computationally efficient algorithms using spatial operators. This algorithm corresponds to Option 3 in the mass matrix computation options described on page 59. It is the most efficient option.

Exercise 4.2 Trace of the mass matrix.

Derive the following expression for the trace of the mass matrix:

$$\text{Trace}\{\mathcal{M}(\theta)\} = \sum_{i=1}^n \text{Trace}\{H(k)\mathcal{R}(k)H^*(k)\} \quad (4.21)$$

For a 1 degree of freedom hinge, $\text{Trace}\{H(k)\mathcal{R}(k)H^*(k)\} = H(k)\mathcal{R}(k)H^*(k)$. This can be used to further simplify (4.21). ■

4.1.5 Relationship to the Composite Rigid Body Method

We now show that Algorithm 4.2 can be interpreted as a version of what is referred to as the **composite body method** for computing \mathcal{M} developed in Walker and Orin [179]. We show this correspondence by expressing the above recursions in terms of the changes undergone by the mass, the mass center location, and the rotational inertia of the composite body composed of the links outboard of hinge $k - 1$ as body k is added to it.

Since $\mathcal{R}(k)$ is a spatial inertia at \mathbb{B}_k , it can be expressed as

$$\mathcal{R}(k) = \begin{pmatrix} \mathfrak{J}(k) & \tilde{\mathbf{l}}(k, \mathbb{C}_k) \rho(k) \\ -\rho(k) \tilde{\mathbf{l}}(k, \mathbb{C}_k) & \rho(k) \mathbf{I} \end{pmatrix} \quad (4.22)$$

in which $\rho(k)$, \mathbb{C}_k , and $\mathfrak{J}(k)$ are the mass, the location of the center of mass, and the rotational inertia of the composite body formed by links $1, \dots, k$. $\mathbf{l}(k, \mathbb{C}_k)$ denotes the vector from \mathbb{O}_k to \mathbb{C}_k . Substitution of (4.22) for $\mathcal{R}(k-1)$ in Algorithm 4.2, and defining

$$\mathbf{l}(k, \mathbb{C}_{k-1}) \stackrel{\Delta}{=} \mathbf{l}(k, k-1) + \mathbf{l}(k-1, \mathbb{C}_{k-1})$$

leads to

$$\begin{aligned} \rho(k) &= \rho(k-1) + \mathfrak{m}(k) \\ \mathbf{l}(k, \mathbb{C}_k) \rho(k) &= \mathbf{l}(k, \mathbb{C}_{k-1}) \rho(k-1) + \mathfrak{m}(k) \rho(k) \\ \mathfrak{J}(k) &= \mathfrak{J}(k-1) + \rho(k-1) [\mathbf{l}^*(k, \mathbb{C}_{k-1}) \mathbf{l}(k, \mathbb{C}_{k-1}) \mathbf{I} - \mathbf{l}(k, \mathbb{C}_{k-1}) \mathbf{l}^*(k, \mathbb{C}_{k-1})] \\ &\quad - \rho(k-1) [\mathbf{l}^*(k-1, \mathbb{C}_{k-1}) \mathbf{l}(k-1, \mathbb{C}_{k-1}) \mathbf{I} \\ &\quad - \mathbf{l}(k-1, \mathbb{C}_{k-1}) \mathbf{l}^*(k-1, \mathbb{C}_{k-1})] + \mathcal{J}(k) \\ &\stackrel{\text{A.1}}{=} \mathfrak{J}(k-1) - \rho(k-1) \tilde{\mathbf{l}}(k, \mathbb{C}_{k-1}) \tilde{\mathbf{l}}(k, \mathbb{C}_{k-1}) \\ &\quad + \rho(k-1) \tilde{\mathbf{l}}(k-1, \mathbb{C}_{k-1}) \tilde{\mathbf{l}}(k-1, \mathbb{C}_{k-1}) + \mathcal{J}(k) \end{aligned} \quad (4.23)$$

Equation (4.23) computes the new mass $\rho(k)$ for the composite body consisting of links 1 through k , by adding the mass of body k to the old mass $\rho(k-1)$. Similarly, it computes the new mass center location vector $\mathbf{l}(k, \mathbb{C}_k)$. Comparing with (2.13), we see that the last equation computes the inertia tensor $\mathfrak{J}(k)$ for the composite body. Equation (4.23) describes the terms that are used in the *composite rigid body inertia method* described in Walker and Orin [179] for the mass matrix. Algorithm 4.2 can be viewed as the composite rigid body inertia method expressed more compactly using spatial quantities.

4.2 Lagrangian Approach to the Equations of Motion

The approach for formulating the system-level equations of motion described in this section is referred to as the **Lagrangian approach**. In this approach, the equations of motion of a system can be derived from just the system Lagrangian, which for our multibody systems is typically just the kinetic energy. This technique is very general and is independent of the multibody system topology. The key quantities characterizing the dynamics of the systems are the mass matrix $\mathcal{M}(\theta)$ and the Coriolis forces vector $\mathcal{C}(\theta, \dot{\theta})$. The Lagrangian approach requires that:

- The generalized coordinates vector θ be of minimal dimension
- The generalized velocity vector β be $\dot{\theta}$

The Lagrangian equations of motion have the following form [11, 60, 111]:

$$\frac{d}{dt} \frac{\partial \mathcal{L}}{\partial \dot{\theta}} - \frac{\partial \mathcal{L}}{\partial \theta} = \mathcal{T} \quad (4.24)$$

\mathcal{T} denotes the vector of generalized forces and \mathcal{L} the Lagrangian for the system. The notation for the derivative and gradient with respect to vectors in (4.24) is described in more detail in Sect. A.6.2 on page 401 in the appendix.

In the absence of a potential field, the Lagrangian \mathcal{L} of a system is simply its kinetic energy. As is the case for multibody systems, we assume that the kinetic energy has the following quadratic form:

$$\mathcal{L} = \mathfrak{K}_e \stackrel{4.5}{=} \frac{1}{2} \dot{\theta}^* \mathcal{M}(\theta) \dot{\theta} \quad (4.25)$$

where the configuration dependent, symmetric matrix $\mathcal{M}(\theta) \in \mathcal{R}^{N \times N}$ is referred to as the **mass matrix** of the system. Beyond borrowing the mass matrix terminology and the \mathcal{M} notation from that for serial-chain systems, we have made no specific assumptions that limit the discussion to serial-chain systems. Using (4.25) in (4.24) leads to equations of motion of the form

$$\mathcal{M}(\theta) \ddot{\theta} + \mathcal{C}(\theta, \dot{\theta}) = \mathcal{T} \quad (4.26)$$

where

$$\mathcal{C}(\theta, \dot{\theta}) \triangleq \dot{\mathcal{M}}(\theta) \dot{\theta} - \frac{1}{2} \frac{\partial [\dot{\theta}^* \mathcal{M}(\theta) \dot{\theta}]}{\partial \theta} \in \mathcal{R}^N \quad (4.27)$$

$\mathcal{C}(\theta, \dot{\theta})$ is referred to as the **Coriolis and gyroscopic forces vector**. It depends nonlinearly upon both the configuration and velocity coordinates for the system.

4.2.1 Properties of \mathcal{M} and \mathcal{C}

In this section we look at the properties of the mass matrix, \mathcal{M} , and the Coriolis forces vector, \mathcal{C} , associated with the Lagrangian form of the equations of motion in (4.26) and (4.27). First, define the **generalized momentum** of the system, \mathfrak{p} , as

$$\mathfrak{p} \triangleq \mathcal{M} \dot{\theta} \quad (4.28)$$

Exercise 4.3 The $\mathcal{M}_D(\theta, \dot{\theta})$ matrix.

Define the matrix $\mathcal{M}_D(\theta, \dot{\theta}) \in \mathcal{R}^{N \times N}$ [180] as the gradient of the generalized momentum with respect to the generalized coordinates, i.e.,

$$\mathcal{M}_D(\theta, \dot{\theta}) \triangleq \nabla_{\theta}(\mathfrak{p}) = \nabla_{\theta}(\mathcal{M} \dot{\theta}) \quad (4.29)$$

1. Show that

$$2 \frac{\partial \mathfrak{K}_e}{\partial \theta} \stackrel{4.25}{=} \frac{\partial (\dot{\theta}^* \mathcal{M} \dot{\theta})}{\partial \theta} = M_D^* \dot{\theta} \quad (4.30)$$

2. Show that for arbitrary vectors $\dot{\theta}$ and $\underline{\dot{\theta}}$:

$$\dot{\mathcal{M}}(\theta) \underline{\dot{\theta}} = M_D(\theta, \underline{\dot{\theta}}) \dot{\theta} \quad (4.31)$$

■

The $M_D(\theta, \dot{\theta})$ matrix plays an important role in energy-based controller design for robot manipulators [8, 105, 180, 182]. Remark 18.1 on page 365 derives an explicit expression for the elements of M_D . It follows from (4.27), (4.30) and (4.31) that the \mathcal{C} Coriolis vector can be expressed as:

$$\mathcal{C}(\theta, \dot{\theta}) = \left[M_D - \frac{1}{2} M_D^* \right] \dot{\theta} \quad (4.32)$$

Exercise 4.4 $\dot{\mathcal{M}}\dot{\theta} - 2\mathcal{C}$ is a non-working force.

1. Show that

$$\dot{\mathcal{M}}\dot{\theta} - 2\mathcal{C} = (M_D^* - M_D) \dot{\theta} \quad (4.33)$$

Observe that $(M_D^* - M_D)$ is a skew-symmetric matrix.

2. Show that the generalized forces vector defined by $\dot{\mathcal{M}}\dot{\theta} - 2\mathcal{C}$ does no work.
 3. Show that the \mathcal{C} Coriolis forces vector does do work, i.e., $\dot{\theta}^* \mathcal{C}(\theta, \dot{\theta}) \neq 0$.

■

Exercise 4.5 Rate of change of the kinetic energy.

For (4.25), show that the rate of change of the kinetic energy is given by

$$\frac{d\mathfrak{K}_e}{dt} = \dot{\theta}^* \mathcal{T} \quad (4.34)$$

■

An immediate consequence of this result is that, as expected, the system kinetic energy is conserved when the \mathcal{T} generalized forces vector is zero.

Exercise 4.6 Christoffel symbols of the first kind.

Christoffel symbols of the first kind are defined as²

$$\mathfrak{C}_i(j, k) \triangleq \frac{1}{2} \left[\frac{\partial \mathcal{M}(i, j)}{\partial \theta(k)} + \frac{\partial \mathcal{M}(i, k)}{\partial \theta(j)} - \frac{\partial \mathcal{M}(j, k)}{\partial \theta(i)} \right] \quad (4.35)$$

for $i, j, k = 1 \dots n$

² The notation, $[ij, k]$, is also often used for $\mathfrak{C}_k(i, j)$ in the literature for Christoffel symbols of the first kind.

1. Show that the Christoffel symbols satisfy the following properties:

$$\begin{aligned}\mathfrak{C}_i(j, k) &= \mathfrak{C}_i(k, j) \\ \frac{\partial \mathcal{M}(i, i)}{\partial \theta_k} &= 2\mathfrak{C}_i(i, k)\end{aligned}\quad (4.36)$$

If, in addition, the mass matrix $\mathcal{M}(\theta)$ is symmetric, then show that

$$\frac{\partial \mathcal{M}(k, j)}{\partial \theta_i} = \mathfrak{C}_j(i, k) + \mathfrak{C}_k(j, i) \quad (4.37)$$

2. For multibody systems, the mass matrix is always symmetric. Also, for trees, the $\mathcal{M}(j, k)$ element only depends on the configuration coordinates for bodies that are outboard of the j th or the k th body. For such systems, show that the Christoffel symbols satisfy the following additional properties:

$$\begin{aligned}\mathfrak{C}_i(j, k) &= -\mathfrak{C}_k(j, i) \quad \forall j \geq i, k \\ \mathfrak{C}_i(j, i) &= \mathfrak{C}_i(i, j) = 0 \quad \forall j \geq i\end{aligned}\quad (4.38)$$

Also, show that $\mathfrak{C}_i(j, k)$ is a function of $\theta(1) \cdots \theta(m-1)$ alone, where $m \triangleq \max(i, j, k)$.

3. Christoffel symbols provide an alternate way for obtaining the Coriolis forces vector $\mathcal{C}(\theta, \dot{\theta})$. Let \mathfrak{C}_i be the symmetric matrix whose (j, k) th element is given by the Christoffel symbol $\mathfrak{C}_i(j, k)$. Show that the i th element, $\mathcal{C}(i)$, of the Coriolis forces vector in (4.27) is given by the expression:

$$\mathcal{C}(i) = \dot{\theta}^* \mathfrak{C}_i \dot{\theta} \quad (4.39)$$

Thus it follows from (4.39) that

$$\mathcal{C}(\theta, \dot{\theta}) \stackrel{4.39}{=} \begin{bmatrix} \dot{\theta}^* \mathfrak{C}_1 \dot{\theta} \\ \vdots \\ \dot{\theta}^* \mathfrak{C}_n \dot{\theta} \end{bmatrix} \quad (4.40)$$

4. For a symmetric mass matrix \mathcal{M} show that

$$\mathcal{M}_D(i, j) = \sum_{k=1}^N \frac{\partial \mathcal{M}(i, k)}{\partial \theta(j)} \dot{\theta}(k) = \sum_{k=1}^N [\mathfrak{C}_k(i, j) + \mathfrak{C}_i(k, j)] \dot{\theta}(k) \quad (4.41)$$



4.2.2 Hamiltonian Form of the Equations of Motion

The following exercise derives the Hamiltonian form of the equations of motion. This is an alternative to the Lagrangian form in (4.24). One advantage of the Hamiltonian form is that the equations of motion are in the form of first order ordinary differential equations instead of the second order ones in Lagrangian formulations.

Exercise 4.7 Hamiltonian form of the equations of motion.

Observe that the kinetic energy in (4.5) can be expressed in terms of the generalized momentum \mathbf{p} as:

$$\mathfrak{K}_e = \frac{1}{2} \mathbf{p}^* \mathcal{M}^{-1} \mathbf{p} \quad (4.42)$$

With the system Hamiltonian defined by $\mathcal{H} \triangleq \mathfrak{K}_e$, derive the following Hamiltonian form of the equations of motion

$$\dot{\theta} = \frac{\partial \mathcal{H}}{\partial \mathbf{p}} \quad \text{and} \quad \dot{\mathbf{p}} = -\frac{\partial \mathcal{H}}{\partial \theta} + \mathcal{T} \quad (4.43)$$

from the Lagrangian form in (4.24). ■

4.2.3 Transformation of Lagrangian Coordinates

In this section, we examine the impact of transforming the system generalized coordinates on the Lagrangian equations of motion. The Lagrangian equations of motion in (4.24) require that the generalized velocity vector β be chosen as $\dot{\theta}$. However, this condition did not hold for our earlier choice of angular velocities for generalized velocities for a rigid body. The following exercise generalizes (4.24) to the case where $\beta \neq \dot{\theta}$, and where β can in fact consist of quasi-velocities.

Exercise 4.8 Lagrangian equations of motion using quasi-velocities.

Let $\beta \triangleq A(\theta)\dot{\theta}$ denote a new generalized velocity vector for the system with $A(\theta)$ being a differentiable, non-singular, coordinate dependent transformation matrix. The elements of β are quasi-velocities when they are non-integrable. The new Lagrangian is defined as $\dot{\mathcal{L}}(\theta, \beta) = \mathcal{L}(\theta, \dot{\theta})$. Show that the Lagrangian equations of motion in the (θ, β) coordinates have the following form:

$$\frac{d}{dt} \frac{\partial \dot{\mathcal{L}}}{\partial \beta} - A^{-*} \frac{\partial \dot{\mathcal{L}}}{\partial \theta} + A^{-*} \gamma^* \frac{\partial \dot{\mathcal{L}}}{\partial \beta} = A^{-*} \mathcal{T} \quad (4.44)$$

with the matrix $\gamma(\theta, \dot{\theta})$ defined as

$$\gamma \triangleq \dot{\mathbf{A}} - \nabla_{\theta}(\mathbf{A}\dot{\theta}) = \dot{\mathbf{A}} - \nabla_{\theta}\beta(\theta) \quad (4.45)$$

The $\gamma(i,j)$ matrix elements are given by

$$\gamma(i,j) \triangleq \dot{\mathbf{A}}(i,j) - \frac{\partial[\mathbf{A}\dot{\theta}](i)}{\partial\theta(j)} = \sum_k \left(\frac{\partial A(i,j)}{\partial\theta(k)} - \frac{\partial A(i,k)}{\partial\theta(j)} \right) \dot{\theta}(k) \quad (4.46)$$

The Lagrangian formulation of the equations of motion using quasi-velocities are also discussed in Duindam and Stramigioli [45]. In the language of tensor analysis, γ , as defined in (4.45), is a measure of the *non-closedness*, i.e., the *non-integrability*, of the differential form defined by A . ■

Remark 4.2 The angular velocity as quasi-velocities.

While the equations of motion in (4.44) based on quasi-velocities appear more complex than those in (4.24), the rigid body rotational equations of motion are a good example where the converse is true.

Focusing on just the rotational dynamics of a rigid body, we choose its angular velocity, ω , as the generalized velocities for the body. For this case, the Lagrangian $\mathcal{L} = \frac{1}{2}\omega^* \mathcal{J} \omega$ is independent of the θ generalized coordinates. While ω is non-integrable, there is nevertheless a smooth and invertible transformation $A(\theta)$ such that $\tilde{\omega} = A(\theta)\dot{\theta}$. Equation (B.2) on page 404 provides an explicit expression for $A(\theta)$ for one such choice of Euler angles for θ . It can be shown that $A^{-*}\gamma^* = \tilde{\omega}$. Since \mathcal{J} is constant in the body frame, (4.44) reduces to the following simpler form of the equations of motion seen in (2.20):

$$\mathcal{J}\dot{\omega} + \tilde{\omega}\mathcal{J}\omega = A^{-*}\mathfrak{f} \quad (4.47)$$

In contrast, if we choose to work with integrable generalized velocities, such as the time derivatives of Euler angle generalized coordinates, the resulting equations of motion are significantly more complex than (4.47). ■

This example is an illustration of the use of quasi-velocities to simplify the dynamical equations of motion. The price paid is that the kinematic relationship between the generalized velocities and the time derivatives of the generalized coordinates is more complex.

Observe that

$$\gamma\dot{\theta} \stackrel{4.45}{=} [\dot{\mathbf{A}} - \nabla_{\theta}(\mathbf{A}\dot{\theta})]\dot{\theta} = \dot{\mathbf{A}}\dot{\theta} - \mathbf{A}\dot{\theta} = \mathbf{0} \quad (4.48)$$

However, γ itself vanishes if and only if the form A is a *closed* differential form [119].

Exercise 4.9 Lagrangian equations of motion under coordinate transformations.

Let $\eta = h(\theta)$ denote a smooth, invertible nonlinear transformation of the generalized coordinates, and define the generalized velocities vector to be $\dot{\eta}$. The

Lagrangian is now $\dot{\mathcal{L}}(\eta, \dot{\eta}) = \mathcal{L}(\theta, \dot{\theta})$. Show that $\gamma = \mathbf{0}$ for this case, leading to the following simplified version of the Lagrangian equations of motion

$$\frac{d}{dt} \frac{\partial \dot{\mathcal{L}}}{\partial \dot{\eta}} - \frac{\partial \dot{\mathcal{L}}}{\partial \eta} = A^{-*} \mathcal{T} \quad \text{where} \quad A(\theta) \triangleq \nabla_{\theta} h(\theta) \quad (4.49)$$

■

Observe that in Exercise 4.9, $\beta = \dot{\eta} = A\dot{\theta}$ is the time-derivative of η and its elements are therefore, *not* quasi-velocities. A simple instance of a closed differential form $A(\theta)$ is when it is configuration independent and constant.

When the Lagrangian is of the form $\mathcal{L} = \frac{1}{2}\dot{\theta}^* \mathcal{M}(\theta)\dot{\theta}$ as defined in (4.25), the (4.44) equations of motion take the form:

$$\underline{\mathcal{M}}(\theta)\hat{\beta} + \underline{\mathcal{C}}(\theta, \beta) = A^{-*} \mathcal{T}$$

where $\underline{\mathcal{M}} \triangleq A^{-*} \mathcal{M} A^{-1}$ and $\underline{\mathcal{C}} \triangleq \dot{\underline{\mathcal{M}}}\beta - A^{-*} \frac{\partial \dot{\mathcal{L}}}{\partial \theta} + A^{-*} \gamma^* \frac{\partial \dot{\mathcal{L}}}{\partial \beta}$ (4.50)

The following exercise shows that the $\dot{\underline{\mathcal{M}}}\beta - 2\underline{\mathcal{C}}$ generalized force is a non-working force similar to the non-working property derived earlier in Exercise 4.4 for $\dot{\mathcal{M}} - 2\mathcal{C}$. Thus this non-working property remains unaffected by the transformation of the Lagrangian equations of motion using quasi-velocities.

Exercise 4.10 Non-working $\dot{\underline{\mathcal{M}}}\beta - 2\underline{\mathcal{C}}$ generalized force.

Show that $\dot{\underline{\mathcal{M}}}\beta - 2\underline{\mathcal{C}}$ is a non-working generalized force, i.e., $\beta^*(\dot{\underline{\mathcal{M}}}\beta - 2\underline{\mathcal{C}}) = 0$.

■

The following exercise looks at a special class of coordinate transformations that diagonalize and decouple the system equations of motion.

Exercise 4.11 Nonlinear diagonalizing coordinate transformations.

Exercise 4.8 studied the transformation of the equations of motion from a change in coordinates. Now we study special coordinate transformations that diagonalize and simplify the equations of motion in (4.50).

- Let $\eta = h(\theta) \in \mathbb{R}^N$ denote a new set of generalized coordinates defined by a globally invertible, smooth, and nonlinear coordinate transformation $h(\theta)$. Show that if the matrix $A(\theta) \triangleq \nabla_{\theta} h(\theta) \in \mathbb{R}^{N \times N}$ is such that $\mathcal{M}(\theta) = A^*(\theta)A(\theta)$, then the equations of motion are completely diagonalized in the $(\eta, \dot{\eta})$ coordinates and have the form

$$\ddot{\eta} = \zeta \quad (4.51)$$

where the new generalized forces vector $\zeta \triangleq A^{-*}(\theta)\mathcal{T} \in \mathbb{R}^N$. In effect, the mass matrix for the transformed system is the constant identity matrix, and the Coriolis term is zero! In addition, the dynamics of the component $\eta(k)$ generalized coordinates are completely decoupled and independent of each other.

2. We now relax the requirement that $A(\theta)$ is the gradient of a smooth transformation. Instead, we only require that $A(\theta)$ be such that $\mathcal{M}(\theta) = A^*(\theta)g(\theta)$. With the new velocity coordinates defined as $\beta \stackrel{\triangle}{=} A(\theta)\dot{\theta} \in \mathcal{R}^N$, show that the equations of motion in the (θ, β) coordinates have the form

$$\dot{\beta} + \mathcal{C}(\theta, \beta) = \zeta, \quad \mathcal{C}(\theta, \beta) \stackrel{\triangle}{=} -A^{-*}\gamma^*\beta \quad (4.52)$$

While the mass matrix is once again the constant identity matrix, the Coriolis term is no longer zero in this formulation. Since $A(\theta)$ is no longer required to be the gradient of a function, the β velocity coordinates are in general quasi-velocities. This is another example of the use of quasi-velocities to simplify the equations of motion.

3. Show that while non-zero, the $\mathcal{C}(\theta, \beta)$ Coriolis forces vector in (4.52) do no work. This is in contrast with the working nature of the $\mathcal{C}(\theta, \dot{\theta})$ Coriolis forces vector in (4.27).

■

The result in part (1) of this exercise is mainly of theoretical interest because the conditions on $g(\theta)$ are rarely satisfied by systems. These conditions are equivalent to requiring that the *Riemannian symbols of the first kind*, associated with the mass matrix, vanish [46] as discussed in more detail in Chap. 19. In the same chapter, spatial operator factorizations of the mass matrix are used to show that $A(\theta)$ satisfying the weaker conditions in part (2) always exists for tree-topology multibody systems. Thus, the (4.52) formulation of the diagonalized equations of motion always exists for these systems.

Chapter 5

Serial-Chain Dynamics

We now study the dynamics of serial-chain multibody systems and derive their equations of motion. The approach builds upon the single rigid body dynamics and serial-chain kinematics developments in Chaps. 2 and 3. The component link-level equations of motion are assembled into compact system-level operator versions of the equations of motion using the serial-chain mass matrix. Algorithms for the system inverse dynamics are also discussed.

5.1 Equations of Motion for a Typical Link

The first step in deriving the equations of motion for the serial-chain system is to develop the free-body dynamics of the component links. To simplify the development, we continue to assume that the k th body frame, \mathbb{B}_k , coincides with the \mathbb{O}_k hinge frame. Initially we assume that there are no external forces on the serial-chain; the only forces on the links are from their mutual interactions across the connecting hinges.

Let $f(k)$ denote the spatial force of interaction between the $(k+1)$ th and the k th links at \mathbb{O}_k . As illustrated in Fig. 5.1, $f(k)$ and $-f(k)$ are equal and opposite spatial forces felt by the k th link at the \mathbb{O}_k frame, and the $(k+1)$ th link at the \mathbb{O}_k^+ frame, respectively, from the k th hinge coupling the two bodies. Thus, the total external spatial forces on link k are the $f(k)$ spatial force at the \mathbb{O}_k frame and the $-f(k-1)$ spatial force at the \mathbb{O}_{k-1}^+ frame due to interactions across the k th and $(k-1)$ th hinges, respectively. Using (1.47), the overall external force on the k th link referenced to frame \mathbb{O}_k is therefore, $[f(k) - \phi(k, k-1)f(k-1)]$. Using the equations of motion for a single rigid body from (2.28) on page 29, it follows that the equations of motion of the k th link can be stated as:

$$f(k) - \phi(k, k-1)f(k-1) = M(k)\alpha(k) + b(k) \quad (5.1)$$

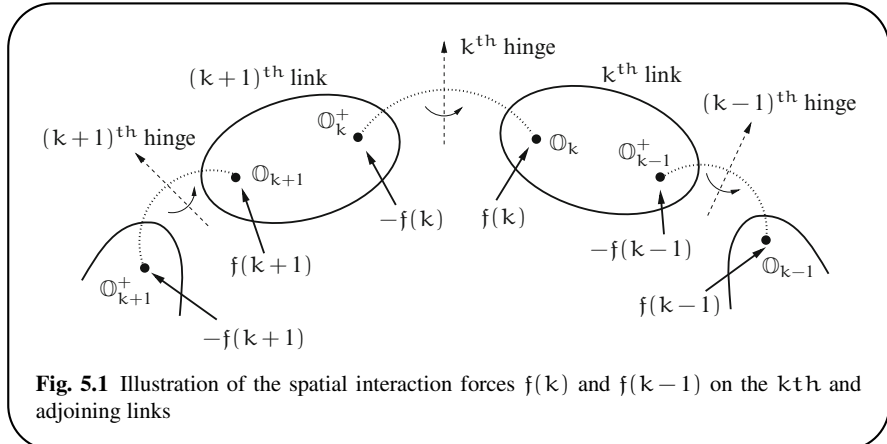


Fig. 5.1 Illustration of the spatial interaction forces $f(k)$ and $f(k-1)$ on the k^{th} and adjoining links

$\alpha(k) \in \mathcal{R}^6$ and $b(k) \in \mathcal{R}^6$ denote the **spatial acceleration** and the velocity dependent **gyroscopic force** vectors for the k^{th} link. Among the rigid body dynamics options discussed in Chap. 2, one option is to define $\alpha(k)$ as the time derivative of the spatial velocity $\mathcal{V}(k)$ in the \mathbb{B}_k frame. In this case, from Lemma 2.3 on page 29, we obtain

$$\alpha(k) \triangleq \frac{d_{\mathbb{B}_k} \mathcal{V}(k)}{dt} = \frac{d_k \mathcal{V}(k)}{dt} \quad \text{with} \quad b(k) \stackrel{2.28}{=} \bar{\mathcal{V}}(k) M(k) \mathcal{V}(k) \quad (5.2)$$

An equally valid alternate option is to use inertial frame derivatives of $\mathcal{V}(k)$, in which case from Lemma 2.2 we would obtain

$$\alpha(k) \triangleq \frac{d_{\mathbb{I}} \mathcal{V}(k)}{dt} \quad \text{with} \quad b(k) \stackrel{2.26}{=} \tilde{\mathcal{V}}^\omega(k) M(k) \mathcal{V}^\omega(k) \quad (5.3)$$

Based on either choice, (5.1) can be restated as

$$f(k) = \phi(k, k-1) f(k-1) + M(k) \alpha(k) + b(k) \quad (5.4)$$

Equation (5.4) defines a recursive relationship between the $f(k)$ and $f(k-1)$ spatial forces and the spatial acceleration of the k^{th} link. We refer to it as the *terminal-body model* for the component k^{th} links.¹

With $f(0) = \mathbf{0}$, we see that (5.4) holds for even the tip-body, which has no child body. It thus, applies to all the links in the system. Observe that (5.4) is merely establishing the relationships that the inter-link spatial forces and spatial accelerations must satisfy. At this point, these quantities are only implicitly defined. The

¹ We will study alternative *composite-body* and *articulated-body* dynamics models for the component links in Chap. 6.

generalized force $\mathcal{T}(k) \in \mathcal{R}^{r_v(k)}$ for the k th hinge is the projection of the spatial force $f(k)$ onto the hinge axis given by

$$\mathcal{T}(k) = H(k)f(k) \quad (5.5)$$

5.1.1 Expression for the Spatial Acceleration $\alpha(k)$

Equation (3.19b) established the following recursive relationship between the spatial velocities of the k th and $(k+1)$ th bodies:

$$v(k) = \phi^*(k+1, k)v(k+1) + H^*(k)\dot{\theta}(k) \quad (5.6)$$

Equation (5.2) defines the spatial accelerations $\alpha(k)$ and $\alpha(k+1)$ of the k th and $(k+1)$ th bodies as time derivatives of their spatial velocities with respect to their own body frames. For this choice, differentiating (5.6) in the link frame \mathbb{O}_k , and keeping in mind that the relative spatial velocity of \mathbb{O}_k with respect to \mathbb{O}_{k+1} is $\Delta v(k)$, we obtain

$$\begin{aligned} \alpha(k) &\stackrel{5.2}{=} \frac{d_k v(k)}{dt} \stackrel{1.12}{=} \frac{d_{k+1} v(k)}{dt} - \tilde{\Delta}_v^\omega(k)v(k) \\ &\stackrel{3.19b}{=} \frac{d_{k+1} [\phi^*(k+1, k)v(k+1) + H^*(k)\dot{\theta}(k)]}{dt} - \tilde{\Delta}_v^\omega(k)v(k) \end{aligned} \quad (5.7)$$

That is,

$$\alpha(k) = \phi^*(k+1, k)\alpha(k+1) + H^*(k)\ddot{\theta}(k) + a(k) \quad (5.8)$$

where the velocity dependent **Coriolis spatial acceleration** $a(k) \in \mathcal{R}^6$ is defined as

$$a(k) \triangleq -\tilde{\Delta}_v^\omega(k)v(k) + \frac{d_{k+1}\phi^*(k+1, k)}{dt}v(k+1) + \frac{d_{k+1}H^*(k)}{dt}\dot{\theta}(k) \quad (5.9)$$

While $H^*(k)$ is constant in the body frame for most hinge types, it can depend on the hinge generalized coordinates for more complex hinges. In this case, the time derivative of $H^*(k)$ in (5.9) is related to its gradient with respect to the generalized coordinate of the hinge as follows:

$$\frac{d_{k+1}H^*(k)}{dt} = [\nabla_{\theta(k)}(H^*(k))] \dot{\theta}(k) \quad (5.10)$$

Equation (5.8) has a recursive structure similar to that for link spatial velocities in (5.6). The explicit expression for the $a(k)$ Coriolis acceleration is derived in the following lemma.

Lemma 5.1 $a(k)$ with body frame derivatives and $\mathbb{B}_k = \mathbb{O}_k$.

For the case when body-frame derivatives in (5.2) are used, and $\mathbb{B}_k = \mathbb{O}_k$, the Coriolis acceleration, $a(k)$, is given by the expression:

$$a(k) = \tilde{v}(k)\Delta v(k) - \bar{\Delta}_v(k)\Delta v(k) + \frac{d_{k+1}H^*(k)}{dt}\dot{\theta}(k) \quad (5.11)$$

The explicit component level expression for $\alpha(k)$ is

$$\alpha(k) = - \begin{bmatrix} \tilde{\Delta}_\omega(k)\omega(k) \\ \tilde{\Delta}_\omega(k)v(k) + \tilde{\Delta}_v(k)\omega(k+1) \end{bmatrix} + \frac{d_{k+1}H^*(k)}{dt}\dot{\theta}(k) \quad (5.12)$$

Proof: When the k th hinge contains a prismatic component, the hinge to hinge vector $l(k+1, k)$ in (3.16) is not constant but instead depends on the configuration variable $\theta(k)$. The relative linear velocity across the hinge, $\Delta_v(k)$, is the time derivative of $l(k+1, k)$ in the $(k+1)$ th body frame, i.e.,

$$\Delta_v(k) = \frac{d_{k+1} l(k+1, k)}{dt} \quad (5.13)$$

As a consequence

$$\frac{d_{k+1}\phi(k+1, k)}{dt} \stackrel{3.16}{=} \begin{pmatrix} \mathbf{0} & \tilde{\Delta}_v(k) \\ \mathbf{0} & \mathbf{0} \end{pmatrix} = \bar{\Delta}_v(k) \quad (5.14)$$

Using (5.14) in (5.9), we have

$$\begin{aligned} \alpha(k) &\stackrel{5.14}{=} -\tilde{\Delta}_v^\omega(k)\mathcal{V}(k) - \tilde{\Delta}_v^v(k)\mathcal{V}(k+1) + \frac{d_{k+1}H^*(k)}{dt}\dot{\theta}(k) \\ &\stackrel{1.22}{=} -\tilde{\Delta}_v(k)\mathcal{V}(k) + \tilde{\Delta}_v^v(k)\{\mathcal{V}(k) - \mathcal{V}(k+1)\} + \frac{d_{k+1}H^*(k)}{dt}\dot{\theta}(k) \\ &= \tilde{\mathcal{V}}(k)\Delta_v(k) + \begin{bmatrix} \mathbf{0} \\ \tilde{\Delta}_v(k)\Delta_\omega(k) \end{bmatrix} + \frac{d_{k+1}H^*(k)}{dt}\dot{\theta}(k) \\ &= \tilde{\mathcal{V}}(k)\Delta_v(k) + \tilde{\Delta}_v^v(k)\Delta_v^\omega(k) + \frac{d_{k+1}H^*(k)}{dt}\dot{\theta}(k) \\ &\stackrel{1.24, 1.36d}{=} \tilde{\mathcal{V}}(k)\Delta_v(k) - \bar{\Delta}_v(k)\Delta_v(k) + \frac{d_{k+1}H^*(k)}{dt}\dot{\theta}(k) \end{aligned}$$

This establishes (5.11). ■

Equation (5.12) is obtained by evaluating the components of the expression in (5.11). ■

It is worth emphasizing that the Coriolis acceleration expression in (5.11) is based on the following assumptions:

1. The k th body spatial acceleration is defined as the time derivative of the body spatial velocity $\mathcal{V}(k)$ with respect to the k th body frame.
2. The k th body reference frame \mathbb{B}_k coincides with the hinge frame \mathbb{O}_k , i.e., the choice for the k th body spatial velocity $\mathcal{V}(k)$ is the spatial velocity of the \mathbb{O}_k frame.
3. The k th body spatial velocity $\mathcal{V}(k)$ is not an “inertially referenced” spatial velocity.

As we will see in later exercises, other choices are possible and lead to different expressions for the Coriolis acceleration.

Remark 5.1 $\alpha(k)$ for simple hinges.

While (5.11) provides the general expression for the link Coriolis acceleration spatial vector, it is usually simpler in practice. When the joint map matrix $H^*(k)$ is constant in the body frame, the last time derivative in (5.11) vanishes. Also, if the hinge is either purely prismatic or purely rotational then the second term vanishes as well. For these cases, $\alpha(k)$ simplifies to

$$\alpha(k) = \tilde{V}(k)\Delta_V(k) \quad (5.15)$$

Examples of non-simple hinges include helical hinges, which contain both rotational and prismatic components, and compound hinges, such as universal and gimbal hinges, where the direction of the axes depends on the configuration of the hinge. ■

We now look at specific examples of simple hinges such as the one degree of freedom rotary and prismatic hinges.

Example 5.1 $\alpha(k)$ for a 1 degree of freedom rotary pin hinge.

When the k th hinge is the 1 degree of freedom rotary pin hinge in Fig. 3.2, $H^*(k) = \begin{bmatrix} h_\omega(k) \\ \mathbf{0} \end{bmatrix}$, where $h_\omega(k) \in \mathbb{R}^3$ is the vector representation of the hinge axis in the link frame. In this case $\Delta_V(k) = \begin{bmatrix} \Delta_\omega(k) \\ \mathbf{0} \end{bmatrix}$. Since the joint axis is constant in the body frame, it follows from (5.15) that

$$\alpha(k) = \tilde{V}(k)\Delta_V(k) = \begin{bmatrix} \tilde{\omega}(k)\Delta_\omega(k) \\ \tilde{v}(k)\Delta_\omega(k) \end{bmatrix} \quad (5.16)$$

■

Example 5.2 $\alpha(k)$ for a 1 degree of freedom prismatic hinge.

When the k th hinge is the 1 degree of freedom prismatic hinge in Fig. 3.2, $H^*(k) = \begin{bmatrix} \mathbf{0} \\ h_v(k) \end{bmatrix}$. In this case $\Delta_V(k) = \begin{bmatrix} \mathbf{0} \\ \Delta_v(k) \end{bmatrix}$. Since the joint axis is constant in the body frame, it follows from (5.15) that:

$$\alpha(k) = \begin{bmatrix} \mathbf{0} \\ \tilde{\omega}(k)\Delta_v(k) \end{bmatrix} \quad (5.17)$$

■

Exercise 5.1 $\alpha(k)$ for helical & cylindrical hinges.

Derive the Coriolis vector $\alpha(k)$ for the helical and cylindrical hinges shown in Fig. 3.2. ■

Equation (5.11) provides an expression for the link Coriolis acceleration $\alpha(k)$, with the assumption that the \mathbb{B}_k body reference frame coincides with the \mathbb{O}_k hinge frame. However, the link reference frame does not necessarily have to coincide with \mathbb{O}_k and may be a different frame of convenience, as discussed in Exercise 3.3 on page 46. The Coriolis acceleration for such links is the subject of the next exercise.

Exercise 5.2 $\alpha_{\mathbb{B}}(k)$ with body frame derivatives but $\mathbb{B}_k \neq \mathbb{O}_k$.

For the case when body-frame derivatives in (5.2) are used, but $\mathbb{B}_k \neq \mathbb{O}_k$, show that the Coriolis acceleration, $\alpha_{\mathbb{B}}(k)$, is given by the expression:

$$\alpha_{\mathbb{B}}(k) = \phi^*(\mathbb{O}_k, \mathbb{B}_k) \alpha(k)$$

$$\stackrel{5.11}{=} \phi^*(\mathbb{O}_k, \mathbb{B}_k) \left[\tilde{\mathcal{V}}(\mathbb{O}_k) \Delta_{\mathcal{V}}(k) - \bar{\Delta}_{\mathcal{V}}(k) \Delta_{\mathcal{V}}(k) + \frac{d_{k+1} H^*(k)}{dt} \dot{\theta}(k) \right]$$

where $\alpha(k)$ is defined in (5.11). The direct expression for $\alpha_{\mathbb{B}}(k)$ is:

$$\alpha_{\mathbb{B}}(k) = \tilde{\mathcal{V}}(k) \Delta_{\mathcal{V}}^{\mathbb{B}}(k) - \bar{\Delta}_{\mathcal{V}}(k) \Delta_{\mathcal{V}}(k) + \phi^*(\mathbb{O}_k, \mathbb{B}_k) \frac{d_{k+1} H^*(k)}{dt} \dot{\theta}(k) \quad (5.18)$$

where $\Delta_{\mathcal{V}}^{\mathbb{B}}(k)$ is the hinge relative spatial velocity referenced to the k th body frame \mathbb{B}_k defined in (3.22). ■

Yet another option is to define the spatial acceleration of the link as the time derivative of the spatial velocity of the link with respect to the inertial frame. This option is the subject of the next exercise.

Exercise 5.3 $\alpha_{\mathcal{J}}(k)$ with inertial frame derivatives.

For the case when inertial-frame derivatives described in (5.3) are used for spatial accelerations, show that the Coriolis acceleration, $\alpha_{\mathcal{J}}(k)$, is given by the expression:

$$\begin{aligned} \alpha_{\mathcal{J}}(k) &= \alpha(k) + \bar{\mathcal{V}}(k) \mathcal{V}(k) - \bar{\mathcal{V}}(k+1) \mathcal{V}(k+1) \\ &= \tilde{\mathcal{V}}^{\omega}(k+1) [\mathcal{V}^v(k) - \mathcal{V}^v(k+1) + \Delta_{\mathcal{V}}(k)] + \frac{d_{k+1} H^*(k)}{dt} \dot{\theta}(k) \end{aligned} \quad (5.19)$$

where $\alpha(k)$ is as defined in (5.11). The component level expression for $\alpha_{\mathcal{J}}(k)$ is:

$$\mathbf{a}_J(k) = \mathbf{a}(k) + \begin{bmatrix} \mathbf{0} \\ \tilde{\omega}(k)v(k) - \tilde{\omega}(k+1)v(k+1) \end{bmatrix} \quad (5.20a)$$

$$= \begin{bmatrix} \tilde{\omega}(k)\Delta_{\omega}(k) \\ \tilde{\omega}(k+1)[v(k) - v(k+1) + \Delta_v(k)] \end{bmatrix} + \frac{d_{k+1}H^*(k)}{dt}\dot{\theta}(k) \quad (5.20b)$$

■

5.1.2 Overall Equations of Motion

Taken together, (5.4)–(5.6) and (5.8), define the following link-level equations of motion for the serial-chain system:

$$\begin{aligned} \mathcal{V}(k) &= \phi^*(k+1, k)\mathcal{V}(k+1) + H^*(k)\dot{\theta}(k) \\ \alpha(k) &= \phi^*(k+1, k)\alpha(k+1) + H^*(k)\ddot{\theta}(k) + \mathbf{a}(k) \\ f(k) &= \phi(k, k-1)f(k-1) + M(k)\alpha(k) + b(k) \\ \mathcal{T}(k) &= H(k)f(k) \end{aligned} \quad (5.21)$$

These equations of motion fully describe the relationship between the generalized accelerations, $\ddot{\theta}(k)$, and the corresponding generalized forces, $\mathcal{T}(k)$, given a specific $(\theta, \dot{\theta})$ state of the system.

Now that we have the component level equations of motion, we can proceed to develop system-level operator versions of the equations of motion. Analogous to the stacked vector definition of \mathcal{V} and $\dot{\theta}$ in Sect. 3.4, define the additional stacked vectors:

$$\begin{aligned} \mathcal{T} &\triangleq \text{col}\left\{\mathcal{T}(k)\right\}_{k=1}^n \in \mathcal{R}^N \\ f &\triangleq \text{col}\left\{f(k)\right\}_{k=1}^n \in \mathcal{R}^{6n} \quad \alpha \triangleq \text{col}\left\{\alpha(k)\right\}_{k=1}^n \in \mathcal{R}^{6n} \\ \mathbf{a} &\triangleq \text{col}\left\{\mathbf{a}(k)\right\}_{k=1}^n \in \mathcal{R}^{6n} \quad \mathbf{b} \triangleq \text{col}\left\{b(k)\right\}_{k=1}^n \in \mathcal{R}^{6n} \end{aligned}$$

Using these stacked vectors, the component-level expressions in (5.21) can be assembled into the following equivalent system-level operator expressions:

$$\begin{aligned} \mathcal{V} &= \mathcal{E}_\phi^* \mathcal{V} + H^* \dot{\theta} \\ \alpha &= \mathcal{E}_\phi^* \alpha + H^* \ddot{\theta} + \mathbf{a} \\ f &= \mathcal{E}_\phi f + M\alpha + \mathbf{b} \\ \mathcal{T} &= Hf \end{aligned} \quad (5.22)$$

Using $\phi = (\mathbf{I} - \mathcal{E}_\phi)^{-1}$ from (3.36), these implicit expressions can be converted into the following explicit ones:

$$\begin{aligned}\mathcal{V} &= \phi^* H^* \dot{\theta} \\ \alpha &= \phi^*(H^* \ddot{\theta} + \mathbf{a}) \\ \mathbf{f} &= \phi(\mathbf{M}\alpha + \mathbf{b}) \\ \mathcal{T} &= H\mathbf{f}\end{aligned}\tag{5.23}$$

Combining the expressions in (5.23) we obtain

$$\mathcal{T} = \mathcal{M}(\theta) \ddot{\theta} + \mathcal{C}(\theta, \dot{\theta})\tag{5.24}$$

where

$$\mathcal{M}(\theta) = H\phi M\phi^* H^* \in \mathcal{R}^{N \times N} \text{ and } \mathcal{C}(\theta, \dot{\theta}) \triangleq H\phi(M\phi^*\mathbf{a} + \mathbf{b}) \in \mathcal{R}^N\tag{5.25}$$

Recall that the above expression for the \mathcal{M} mass matrix is the same as the Newton–Euler Operator Factorization expression derived in (4.6) on page 58. \mathcal{C} consists of the velocity dependent Coriolis and gyroscopic hinge forces.

The expression for \mathcal{C} in (5.25) is different from the one derived in (4.27) using Lagrangian techniques. Exercise 18.9 on page 368 shows that the two expressions are in fact equivalent. References [94, 96, 111, 132, 138, 159, 160, 163] discuss other approaches to formulating the dynamics of multibody systems, with [9, 32, 51, 66, 166] focusing specifically on dynamics for the robotics context.

By differentiating the expression for \mathcal{V} in (5.23) and comparing it to the expression for α , we can conclude that

$$\frac{d\phi^* H^*}{dt} \dot{\theta} = \phi^* \mathbf{a}\tag{5.26}$$

The time derivative above is assumed to be consistent with the time derivative used to define α from \mathcal{V} .

Remark 5.2 Body dynamics invariance across Newtonian frames.

Remark 2.3 on page 30 discussed the invariance of the dynamics of a single body in Newtonian frames. This fact extends to multibody systems as well. The dynamics of a multibody system are invariant across Newtonian frames though not across non-Newtonian ones.

Observe that the velocity values enter into the dynamics equations of motion only through the $\mathbf{a}(k)$ and $\mathbf{b}(k)$ terms and any impact on the equations of motion has to happen through these quantities.

Switching to a different Newtonian frame can result in a δ_v change in the linear velocity of the base-body. This change results in a similar additive change to the linear velocity of each body in the system, so that $v(k)$ becomes $v(k) + \delta_v$. Focusing on the inertial frame derivatives form of the equations of motion, we see that δ_v has no effect on the expression for $\alpha_j(k)$ in (5.19) because it is eliminated from the $v(k) - v(k+1)$ sub-expression. Also, the expression for the $b_j(k)$ gyroscopic force in (2.23) does not contain the linear velocity term, and hence, δ_v has no effect

on it either. Thus, the dynamics equations of motion are independent of the linear velocity of the base-body, and hence, they are unaffected by the specific choice of a Newtonian frame.

On the other hand, both the Coriolis acceleration and gyroscopic force expressions involve the body angular velocities. Any changes in the angular velocity of the base-body – due to the use of non-Newtonian rotating frames – ripple through the angular velocities of all the bodies, changing the values of these Coriolis and gyroscopic terms and, in effect, changing the dynamics of the system. ■

5.1.3 Spatial Operators with Body Frame Derivatives but $\mathbb{B}_k \neq \mathbb{O}_k$

Equation (5.23) provides expressions for the spatial operators ϕ , H etc., with the assumption that the body reference frame \mathbb{B}_k coincides with the hinge frame \mathbb{O}_k . However, as we have seen in Sect. 3.3.3 on page 45, the link reference frames do not necessarily have to coincide with the hinge frame. The $\mathcal{E}_{\phi_{\mathbb{B}}}$ operator for this formulation contains $\phi(\mathbb{B}_{k+1}, \mathbb{B}_k)$ entries instead of $\phi(\mathbb{O}_{k+1}, \mathbb{O}_k)$ along the sub-diagonal. We now derive expressions for the $\phi_{\mathbb{B}}$, $H_{\mathbb{B}}$ and $M_{\mathbb{B}}$ operators for this alternate formulation in terms of the component level terms in (5.23).

From (3.23) and (3.22) we have

$$\begin{aligned}\phi(\mathbb{B}_{k+1}, \mathbb{B}_k) &= \phi(\mathbb{B}_{k+1}, \mathbb{O}_{k+1}) \phi(\mathbb{O}_{k+1}, \mathbb{O}_k) \phi(\mathbb{O}_k, \mathbb{B}_k) \\ H_{\mathbb{B}}^*(k) &\stackrel{3.22}{=} \phi^*(\mathbb{O}_k, \mathbb{B}_k) H^*(k) \\ M_{\mathbb{B}}(k) &\stackrel{\Delta}{=} \phi(\mathbb{B}_k, \mathbb{O}_k) M(\mathbb{O}_k) \phi^*(\mathbb{B}_k, \mathbb{O}_k)\end{aligned}\quad (5.27)$$

$M_{\mathbb{B}}(k)$ is the spatial inertia of the k th body, referenced to its \mathbb{B}_k body frame. Define the block-diagonal operator

$$\Delta_{\mathbb{B}/\mathbb{O}} \stackrel{\Delta}{=} \text{diag} \left\{ \phi(\mathbb{B}_k, \mathbb{O}_k) \right\}_{k=1}^n \in \mathcal{R}^{6n \times 6n} \quad (5.28)$$

It is easy to verify that $\mathcal{E}_{\phi_{\mathbb{B}}}$ and \mathcal{E}_{ϕ} are related via the following similarity transformation²

$$\mathcal{E}_{\phi_{\mathbb{B}}} \stackrel{5.27}{=} \Delta_{\mathbb{B}/\mathbb{O}} \mathcal{E}_{\phi} \Delta_{\mathbb{B}/\mathbb{O}}^{-1} \quad (5.29)$$

It thus, follows that

$$\begin{aligned}\phi_{\mathbb{B}} &\stackrel{\Delta}{=} (\mathbf{I} - \mathcal{E}_{\phi_{\mathbb{B}}})^{-1} = (\mathbf{I} - \Delta_{\mathbb{B}/\mathbb{O}} \mathcal{E}_{\phi} \Delta_{\mathbb{B}/\mathbb{O}}^{-1})^{-1} \\ &= \Delta_{\mathbb{B}/\mathbb{O}} (\mathbf{I} - \mathcal{E}_{\phi})^{-1} \Delta_{\mathbb{B}/\mathbb{O}}^{-1} = \Delta_{\mathbb{B}/\mathbb{O}} \phi \Delta_{\mathbb{B}/\mathbb{O}}^{-1}\end{aligned}\quad (5.30)$$

² With T being an invertible matrix and A another matrix, the TAT^{-1} matrix is referred to as a similarity transformation of A .

Thus, $\phi_{\mathbb{B}}$ is also related to \mathcal{E}_{ϕ} by the same similarity transformation. Also,

$$\begin{aligned} \mathbf{H}_{\mathbb{B}} &\triangleq \text{diag}\left\{\mathbf{H}_{\mathbb{B}}(k)\right\}_{k=1}^n = \mathbf{H}\Delta_{\mathbb{B}/\mathbb{O}}^{-1} \\ \mathbf{M}_{\mathbb{B}} &\triangleq \text{diag}\left\{\mathbf{M}_{\mathbb{B}}(k)\right\}_{k=1}^n = \Delta_{\mathbb{B}/\mathbb{O}}\mathbf{M}\Delta_{\mathbb{B}/\mathbb{O}}^* \end{aligned} \quad (5.31)$$

While we now have expressions for the new spatial operators, it is noteworthy that the mass matrix remains invariant in this new formulation. This follows from:

$$\begin{aligned} \mathbf{H}_{\mathbb{B}}\phi_{\mathbb{B}}\mathbf{M}_{\mathbb{B}}\phi_{\mathbb{B}}^*\mathbf{H}_{\mathbb{B}}^* &\stackrel{5.30, 5.31}{=} (\mathbf{H}\Delta_{\mathbb{B}/\mathbb{O}}^{-1}) \cdot (\Delta_{\mathbb{B}/\mathbb{O}}\phi_{\mathbb{B}}\Delta_{\mathbb{B}/\mathbb{O}}^{-1})(\Delta_{\mathbb{B}/\mathbb{O}}\mathbf{M}\Delta_{\mathbb{B}/\mathbb{O}}^*) \\ &\quad \cdot ((\Delta_{\mathbb{B}/\mathbb{O}}^{-1})^*\phi_{\mathbb{B}}^*\Delta_{\mathbb{B}/\mathbb{O}}) \cdot ((\Delta_{\mathbb{B}/\mathbb{O}}^{-1})^*\mathbf{H}^*) \\ &= \mathbf{H}\phi_{\mathbb{B}}\mathbf{M}\phi_{\mathbb{B}}^*\mathbf{H}^* \stackrel{5.25}{=} \mathcal{M} \end{aligned}$$

This implies that even though the internal structure and formulation of the spatial operators is different, the mass matrix remains unaffected.

The same is true for the \mathcal{C} generalized forces vector, whose value remains unaffected by the specific choices of link frame locations and derivative frames. This is true, despite the values of α , \mathfrak{a} and \mathfrak{b} etc., depending on the frame choices. The paramount requirement, for a valid definition of the equations of motion, is that the component terms be defined *consistently* for a specific selection of link frame locations (e.g. hinge or non-hinge frame) and derivative frames (e.g. body frame or inertial frame). Thus, the \mathfrak{a} definition in Lemma 5.1 applies to the frame choices in (5.2), while the definition in Exercise 5.3 applies to the frame choices in (5.3). Other factors, including computational considerations, may influence the selection of the frames. Assuming such consistency, and in the spirit of coordinate-free notation, we will henceforth refer to, and use α , \mathfrak{a} and \mathfrak{b} etc., in the equations of motion without specifying the associated frames – except in situations where it is necessary to do so. As a reference, Table 5.1 summarizes the $\mathfrak{a}(k)$ and $\mathfrak{b}(k)$ expressions for different

Table 5.1 The body Coriolis acceleration and gyroscopic force expressions for the different choices of link spatial velocities

Link spatial velocity	$\alpha(k)$ Derivative frame	Coriolis accel $\mathfrak{a}(k)$	Gyroscopic force $\mathfrak{b}(k)$
$\mathcal{V}(\mathbb{O}_k)$	\mathbb{B}_k	(5.11)	(2.28)
$\mathcal{V}(\mathbb{B}_k)$	\mathbb{B}_k	(5.18)	(2.28)
$\mathcal{V}(\mathbb{O}_k)$	\mathbb{I}	(5.19)	(2.26)
$\mathcal{V}_{\mathbb{I}}(k)$	\mathbb{I}	(5.55)	(2.38)

link spatial velocity and derivative options. Note that the last row for the inertially referenced link spatial velocity $\mathcal{V}_{\mathbb{I}}(k)$ is discussed later in Sect. 5.4.

Section 8.5 on page 147 discusses generalizations of the (5.29) and (5.30) similarity transformations of spatial operators in a broader and more general context.

5.2 Inclusion of External Forces and Gravity

We now study the effect of external spatial forces being applied at the nodes on the equations of motion.

5.2.1 Inclusion of External Forces

Our development of the equations of motion so far has assumed that the only forces on the links are from the interaction forces among the links and has not taken into account any external forces on the system. Thus, the free-body equations of motion for the k th link in (5.1) only involve the $f(k)$ and $f(k-1)$ inter-link forces. We now look at extensions to handle external forces on the system.

Let us assume that external spatial forces are being applied at nodes on the bodies in the serial-chain. Adopting the notation for nodes from Sect. 3.6 on page 53, \mathbb{O}_k^i denotes the i th such node on the k th link. Let $f_{ext}^i(k)$ denote the external spatial force being applied at the \mathbb{O}_k^i node. This spatial force is effectively $\phi(k, \mathbb{O}_k^i) f_{ext}^i(k)$ at the \mathbb{B}_k body frame. Summing up all such external spatial forces on the k th link, the free-body equations of motion for the link in (5.1) are modified as follows:

$$f(k) - \phi(k, k-1)f(k-1) + \sum_i \phi(\mathbb{B}_k, \mathbb{O}_k^i) f_{ext}^i(k) = M(k)\alpha(k) + b(k) \quad (5.32)$$

Assuming that there are n_{nd} such external forces on the system, analogous to (3.49), define the $6n_{nd}$ dimensional stacked vector, f_{ext} of all external forces as

$$f_{ext} = \text{col} \left\{ f_{ext}^i(k) \right\} \in \mathcal{R}^{6n_{nd}} \quad (5.33)$$

Using (5.32), the equivalent operator-level expression for (5.32) is

$$f = \mathcal{E}_\phi f - \mathcal{B} f_{ext} + M\alpha + b \quad (5.34)$$

where \mathcal{B} is the pick-off spatial operator for the nodes from (3.51). Equation (5.34) leads to the following non-implicit expression that replaces the version in (5.23):

$$f = \phi(M\alpha + b - \mathcal{B} f_{ext}) \quad (5.35)$$

The overall equations of motion in (5.24) take the new form:

$$\mathcal{T} = \mathcal{M}\ddot{\theta} + \mathcal{C} - H\phi B f_{ext} \stackrel{3.53}{=} \mathcal{M}\ddot{\theta} + \mathcal{C} - J^* f_{ext} \quad (5.36)$$

with $J = B^* \phi^* H^*$ being the Jacobian from (3.53) for the external force nodes. Thus, in the operator formulation, the external forces can be incorporated into the equations of motion by including the additional $J^* f_{ext}$ term. One option is to absorb the term within the Coriolis generalized forces vector as follows

$$\mathcal{C}(\theta, \dot{\theta}) = H\phi[M\phi^* a + b - B f_{ext}] \quad (5.37)$$

and continue to work with the $\mathcal{T} = \mathcal{M}\ddot{\theta} + \mathcal{C}$ expression from (5.24).

5.2.2 Compensating for External Forces

In control applications, sometimes there is a need to apply additional generalized forces at the hinge actuators to neutralize the effect of external disturbances perturbing the motion of the system. To compensate for such f_{ext} external forces, (5.36) shows that adding the additional $J^* f_{ext}$ term to the nominal \mathcal{T} generalized force neutralizes the effect of the external forces on the system dynamics. In other words, if \mathcal{T} represents the generalized forces to be applied in the absence of external forces, then $\mathcal{T} - \delta_{\mathcal{T}}$, is the required generalized forces that will result in the same motion in the presence of f_{ext} external forces, where

$$\delta_{\mathcal{T}} \triangleq J^* f_{ext} = H\phi B f_{ext} \quad (5.38)$$

A recursive tip-to-base procedure for computing $\delta_{\mathcal{T}}$ is described in Algorithm 5.1.

Algorithm 5.1 Compensating generalized forces for external spatial forces

```


$$\left\{ \begin{array}{l} x(0) = \mathbf{0} \\ \text{for } k = 1 \cdots n \\ \quad x(k) = \phi(k, k-1)x(k-1) + \sum_i \phi(B_k, O_k^i) f_{ext}^i(k) \\ \quad \delta_{\mathcal{T}}(k) = H(k)x(k) \\ \text{end loop} \end{array} \right.$$

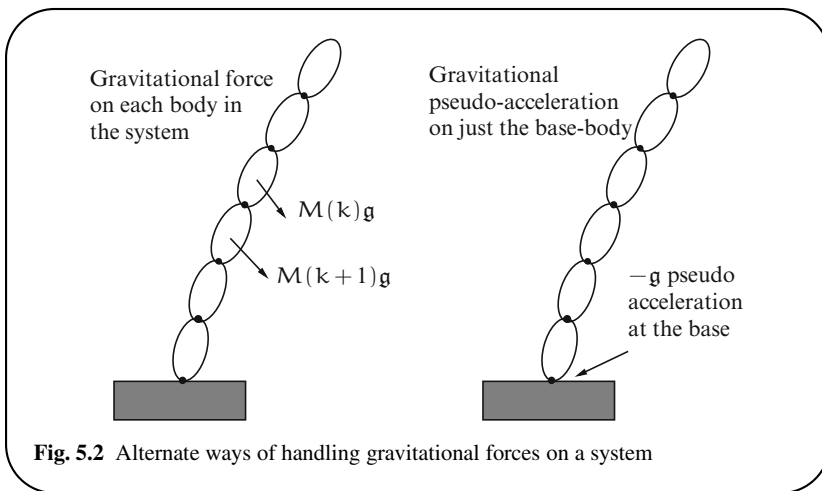

```

5.2.3 Inclusion of Gravitational Forces

Extensions to the equations of motion in (5.23) to include the effect of a uniform gravity field is the subject of the following exercise.

Exercise 5.4 Inclusion of gravitational forces.

Let $\mathbf{g} = \begin{bmatrix} 0 \\ \mathbf{g}_1 \end{bmatrix}$ denote the uniform gravitational spatial acceleration vector, with \mathbf{g}_1 denoting the linear gravitational acceleration.



1. The effect of gravity can be handled by applying a pseudo-acceleration of \mathbf{g} to the base-body. Show that this is equivalent to replacing \mathbf{a} by $\mathbf{a} + \mathbf{E}^* \mathbf{g}$ in the expression for \mathcal{C} in (5.25), so that

$$\mathcal{C}(\theta, \dot{\theta}) = \mathbf{H}\phi [\mathbf{M}\phi^*(\mathbf{a} + \mathbf{E}^* \mathbf{g}) + \mathbf{b}] \quad (5.39)$$

- \mathbf{E} is the pick-off spatial operator defined in (4.14).
2. An alternative approach is to add an additional gravitational spatial force of $-\mathbf{M}(k)\mathbf{g}$ to the right-hand side of the free-body equation in (5.1). Verify that this leads to the following expression for the Coriolis forces vector:

$$\mathcal{C}(\theta, \dot{\theta}) = \mathbf{H}\phi [\mathbf{M}(\phi^* \mathbf{a} + \bar{\mathbf{E}}^* \mathbf{g}) + \mathbf{b}], \text{ where } \bar{\mathbf{E}} \triangleq [\mathbf{I}_6, \dots, \mathbf{I}_6, \mathbf{I}_6] \in \mathbb{R}^{6 \times 6n} \quad (5.40)$$

3. Show that the two expressions for \mathcal{C} in (5.39) and (5.40) are equivalent, i.e., show that

$$\phi^* E^* g = \bar{E}^* g \quad (5.41)$$

(Hint: That g only has a non-zero linear acceleration component plays a key role in the proof.) ■

5.3 Inverse Dynamics of Serial-Chains

Two topics of considerable interest for multibody system dynamics are the inverse and forward dynamics problems.

- The **inverse dynamics** problem consists of computing the \mathcal{T} generalized forces required to obtain a desired $\ddot{\theta}$ multibody generalized acceleration for a given $(\theta, \dot{\theta})$ state of the system. Thus, it requires the evaluation of $\mathcal{T} = \mathcal{M}\ddot{\theta} + \mathcal{C}$ to obtain \mathcal{T} . The inverse dynamics problem appears in the context of multi-link robot control, where its solution is used to generate real-time actuator force commands for hinge actuators, to obtain desired system motion trajectory profiles [107]. Efficient algorithms for solving the system inverse dynamics problem are needed for use in real-time control loops. We examine computational algorithms for the inverse dynamics problem in the following section.
- The **forward dynamics** problem is the converse. It involves computing the $\ddot{\theta}$ generalized accelerations that result from the application of a specified \mathcal{T} generalized forces for a given $(\theta, \dot{\theta})$ state of the system. Thus, it requires the evaluation of $\ddot{\theta} = \mathcal{M}^{-1}(\mathcal{T} - \mathcal{C})$ for $\ddot{\theta}$. The solution to the forward dynamics problem is required for the simulation of the system dynamics. The input generalized forces are obtained from actuator commands and environmental interactions. The computed generalized accelerations are numerically integrated to predict the evolution of the state of the system. Simulation speed and accuracy is the driver for developing efficient and numerically sound algorithms for solving the forward dynamics problem. Low-cost solution techniques for the forward dynamics of serial-chain systems are discussed in Chap. 7.

5.3.1 Newton–Euler Inverse Dynamics Algorithm

It would appear that the evaluation of $\mathcal{T} = \mathcal{M}\ddot{\theta} + \mathcal{C}$ for the inverse dynamics solution requires the explicit computation of \mathcal{M} and \mathcal{C} . Such computations would be of at least $O(N^2)$ complexity since it involves the computation of a matrix of size N . We can do much better than this using ideas from Sect. 3.5. There we encountered the feature that spatial operator expressions can be evaluated using low order recursive algorithms. We take this approach to develop the $O(N)$ Newton–Euler inverse dynamics algorithm.

For the inverse dynamics problem, the hinge accelerations $\ddot{\theta}$ are assumed to be known. The spatial operator equations of motion in (5.21) map easily into Algorithm 5.2, which is referred to as the **Newton–Euler inverse dynamics algorithm** for computing the inverse dynamics of the serial-chain. The structure of this algorithm is illustrated in Fig. 5.3. This algorithm is an $O(N)$ computational procedure involving a base-to-tip recursion sequence to compute the spatial velocities and accelerations, followed by a tip-to-base recursion to compute the hinge forces.

Algorithm 5.2 Newton–Euler inverse dynamics algorithm

$$\left\{ \begin{array}{l} \mathcal{V}(n+1) = \mathbf{0}, \quad \alpha(n+1) = \mathbf{0} \\ \textbf{for } k = n \cdots 1 \\ \quad \mathcal{V}(k) = \phi^*(k+1, k)\mathcal{V}(k+1) + H^*(k)\dot{\theta}(k) \\ \quad \alpha(k) = \phi^*(k+1, k)\alpha(k+1) + H^*(k)\ddot{\theta}(k) + a(k) \\ \textbf{end loop} \\ \\ \mathbf{f}(0) = \mathbf{0} \\ \textbf{for } k = 1 \cdots n \\ \quad \mathbf{f}(k) = \phi(k, k-1)\mathbf{f}(k-1) + M(k)\alpha(k) + b(k) \\ \quad \mathcal{T}(k) = H(k)\mathbf{f}(k) \\ \textbf{end loop} \end{array} \right. \quad (5.42)$$

The first base-to-tip recursion in (5.42) is an unrolling of the operator expressions for \mathcal{V} and α in (5.23), and an application of Lemma 3.2 to convert the operator expressions into base-to-tip recursive steps. Similarly, the latter tip-to-base recursion in (5.42) follows from the operator expressions for \mathbf{f} and \mathcal{T} in (5.23), and an application of Lemma 3.1 to convert the operator expressions into tip-to-base recursive steps.

Except for the use of spatial notation, Algorithm 5.2 is essentially the inverse dynamics algorithm from Luh et al. [120]. Based on (5.32) and (5.40), the following revision to the $\mathbf{f}(k)$ expression in (5.42) allows us to include the effects of external forces and gravity into the inverse dynamics algorithms:

$$\begin{aligned} \mathbf{f}(k) &= \phi(k, k-1)\mathbf{f}(k-1) + M(k)(\alpha(k) + \mathbf{g}) + \mathbf{b}(k) \\ &\quad - \sum_i \phi(\mathbb{B}_k, \mathbb{O}_k^i) f_{ext}^i(k) \end{aligned} \quad (5.43)$$

The Newton–Euler inverse dynamics algorithm accomplishes the computation of $\mathcal{T} = M\ddot{\theta} + \mathcal{C}$ without requiring the explicit computation of M or \mathcal{C} . In fact, neither the explicit computation of the operator ϕ nor of any of the operator-operator

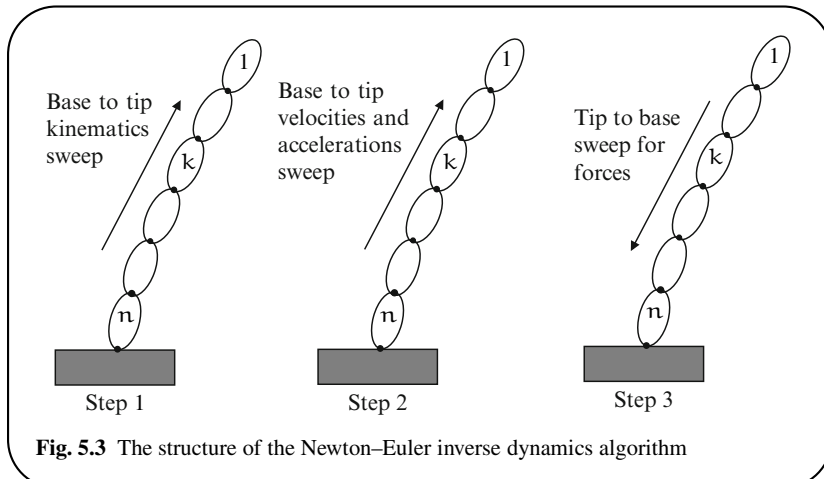


Fig. 5.3 The structure of the Newton–Euler inverse dynamics algorithm

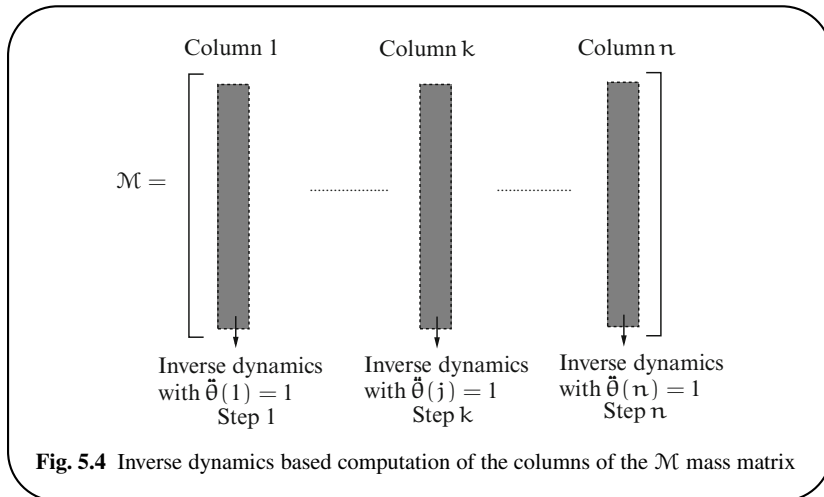
products was required. This again exemplifies the property whereby the evaluation of operator expressions rarely requires the explicit (and expensive) computation of the operators, but can typically be accomplished by recursive computations at the component level. References [19, 54–56, 114] describe other approaches, including parallel algorithms, for solving the inverse dynamics problem.

5.3.2 Computing the Mass Matrix Using Inverse Dynamics

Algorithm 4.2 on page 64 describes a procedure for computing the mass matrix using composite body inertias. We now describe an alternative algorithm for computing the mass matrix, using the $O(N)$ Newton–Euler inverse dynamics algorithm.

First the generalized velocities vector $\dot{\theta}$ is set to zero, so that the \mathcal{C} vector becomes zero. The j th column of \mathcal{M} can be computed by running the inverse dynamics algorithm with all the hinge accelerations set to zero, except the j th hinge acceleration which is set to 1. The resulting \mathcal{T} vector is the j th column of \mathcal{M} . Repeating this for all j , from 1 through n , yields all n columns of \mathcal{M} . This process is illustrated in Fig. 5.4.

We can improve upon this algorithm by realizing that, due to its symmetry, only the upper-triangular half of \mathcal{M} needs to be explicitly computed. To compute the upper part of the j th column, we can use the smaller manipulator made up of just links 1 through j , and run the inverse dynamics with the above set of accelerations (ignoring the ones for $k > j$). The resulting generalized forces vector yields the j th column elements of \mathcal{M} above the diagonal. Repeating this for all j from 1 to n yields the upper-triangular half of \mathcal{M} , and, in effect, all the elements of \mathcal{M} .



Since the $O(N)$ steps are repeated n times, the computational cost of this algorithm remains $O(N^2)$, as for the composite body inertia based Algorithm 4.2. However this procedure is decoupled in that the inverse dynamics sweeps for each of the columns can be run independently in parallel. Thus, the cost of this procedure reduces to $O(N)$ when n processors are used. However, for single processor implementations, the composite body inertia algorithm remains considerably more efficient than this inverse dynamics based procedure. Additional discussion of the computational issues can be found in Walker and Orin [179].

5.3.3 Composite Rigid Body Inertias Based Inverse Dynamics

While the discussion of composite rigid body inertias in Sect. 4.1.2 on page 59 was motivated by the goal of computing the mass matrix, in the following exercise, we look at how the composite body inertias can be used to develop an inverse dynamics problem.

Exercise 5.5 Inverse dynamics using composite body inertias.

Equation (5.23) described the spatial forces expression $\mathbf{f} = \phi(\mathbf{M}\boldsymbol{\alpha} + \mathbf{b})$. Here we will look at an alternative expression for \mathbf{f} using the $\mathcal{R}(k)$ composite body inertias.

1. Show that \mathbf{f} can be expressed in the form

$$\mathbf{f} = \mathcal{R}\boldsymbol{\alpha} + \mathbf{y} \quad \text{where} \quad \mathbf{y} \stackrel{\triangle}{=} \phi[\mathbf{b} + \mathcal{E}_\phi \mathcal{R}(\mathbf{H}^* \ddot{\boldsymbol{\theta}} + \mathbf{a})] \quad (5.44)$$

2. Show that the elements of y can be computed using the following tip-to-base recursion:

$$\left\{ \begin{array}{l} y^+(0) = \mathbf{0} \\ \textbf{for } k = 1 \cdots n \\ \quad y(k) = \phi(k, k-1)y^+(k-1) + b(k) \\ \quad y^+(k) = y(k) + R(k)[H^*(k)\ddot{\theta}(k) + a(k)] \\ \textbf{end loop} \end{array} \right. \quad (5.45)$$

■

Equation (5.44) may be thought of as a *composite-body model* that is an alternative to the terminal-body model for the serial-chain in the sense that, at the component link level, the following relationship holds:

$$f(k) = R(k)\alpha(k) + y(k) \quad (5.46)$$

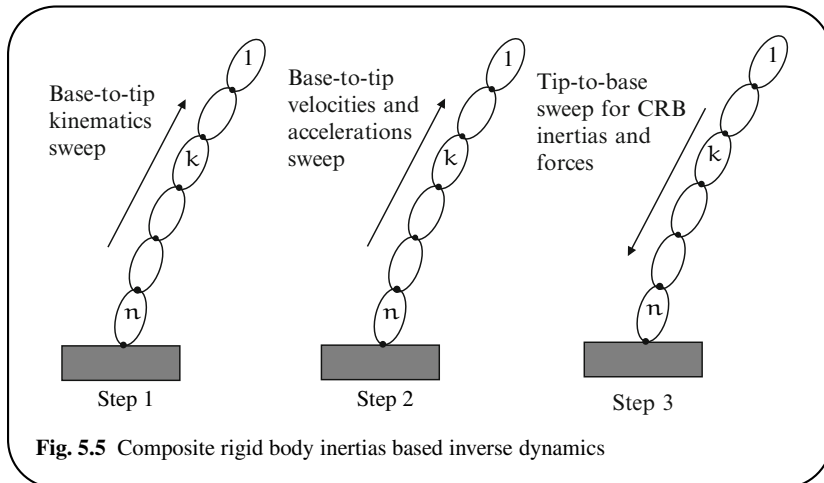
The physical interpretation of this model is as follows. $f(k)$ is the force that the $(k+1)$ th link exerts on the outboard links at \mathbb{O}_k and it produces a spatial acceleration of $\alpha(k)$ at \mathbb{O}_k . If the outboard links did indeed form a composite body, their composite spatial inertia at \mathbb{O}_k would be $R(k)$, and the $R(k)\alpha(k)$ D'Alembert force would be equal to $f(k)$. However, the links k through 1 in the serial-chain do not form a composite body, and the deviation from the composite body model at \mathbb{O}_k is because the hinge accelerations $\ddot{\theta}(j) \neq 0$ for $j \in (k-1) \cdots 1$. The extra correction force $y(k)$ compensates for this. By this argument, $y(k)$ should be a function of only the hinge accelerations $\ddot{\theta}(j)$ for $j \in (k-1) \cdots 1$. This is indeed the case. The spatial force decomposition in (5.44) also forms the basis for Algorithm 5.3 for solving the inverse dynamics of the system. The structure of this algorithm is illustrated in Fig. 5.5.

Algorithm 5.3 Composite rigid body inertias based inverse dynamics

1. Compute the kinematics of the system in a base-to-tip recursion.
2. Use the base-to-tip recursion part of Algorithm 5.2 on page 89 to compute the $\alpha(k)$ link spatial accelerations and the $a(k)$ and $b(k)$ Coriolis and gyroscopic terms. This recursion can be combined with the one in (1).
3. Use (5.45) and Algorithm 4.1 on page 60 in a combined tip-to-base recursion to compute the $R(k)$ composite body inertia and $y(k)$ terms. Compute the hinge generalized force for the k th hinge using the relationship

$$\mathcal{T}(k) \stackrel{5.21}{=} H(k)f(k) \stackrel{5.44}{=} H(k)[R(k)\alpha(k) + y(k)]$$

The (5.46) decomposition is in contrast with the terminal-body decomposition in (5.4), wherein the correction term $\phi(k, k-1)f(k-1)$ is a function of all the hinge accelerations. The notion of alternate models is useful in multibody dynamics



analysis. The composite-body model is appropriate for developing efficient algorithms for the inverse dynamics problem. As will be seen in Chap. 6, an articulated-body model, and its accompanying decomposition, form the basis for a recursive forward dynamics algorithm.

5.4 Equations of Motion with an Inertially Fixed Velocity Reference Frame

Exercise 2.14 on page 32 studied the equations of motion of a single rigid body using an inertially fixed velocity reference frame, \mathbb{I} . Exercise 3.4 on page 47 further developed the kinematics for a serial-chain using an inertially fixed velocity reference frame. We now extend this to develop the equations of motion for a inertially fixed velocity reference frame formulation.

Recall from (2.32) that the spatial inertia, $M_{\mathbb{I}}(k)$, of the k th link about frame \mathbb{I} is defined as

$$M_{\mathbb{I}}(k) = \phi(\mathbb{I}, \mathbb{O}_k) M(k) \phi^*(\mathbb{I}, \mathbb{O}_k) = \begin{pmatrix} \mathcal{J}_{\mathbb{I}}(k) & m(k) \tilde{p}_{\mathbb{I}}(k) \\ -m(k) \tilde{p}_{\mathbb{I}}(k) & m(k) I_3 \end{pmatrix} \quad (5.47)$$

Also, recall from (3.24) on page 47, that the inertially referenced spatial velocity of the k th link, $V_{\mathbb{I}}(k)$, is defined by

$$V_{\mathbb{I}}(k) = \phi^*(\mathbb{O}_k, \mathbb{I}) V(\mathbb{O}_k) = \begin{bmatrix} \omega(k) \\ v_{\mathbb{I}}(k) \end{bmatrix} \quad (5.48)$$

with $\omega(k)$ and $v_{\mathbb{I}}(k)$ denoting its angular and linear velocity components. As discussed in (3.26) on page 47, the $\mathcal{V}_{\mathbb{I}}(k)$ link spatial velocities satisfy the recursive relationship

$$\mathcal{V}_{\mathbb{I}}(k) = \mathcal{V}_{\mathbb{I}}(k+1) + \Delta_{\mathcal{V}}^{\mathbb{I}}(k) = \mathcal{V}_{\mathbb{I}}(k+1) + H_{\mathbb{I}}^*(k)\dot{\theta}(k) \quad (5.49)$$

With $f_{\mathbb{I}}(k) \triangleq \phi(\mathbb{I}, \mathcal{O}_k)f(\mathcal{O}_k)$ denoting the spatial interaction force between the $(k+1)$ th and the k th links (referred to frame \mathbb{I}), the total external spatial force on the k th link is $[f_{\mathbb{I}}(k) - f_{\mathbb{I}}(k-1)]$. From (2.37) on page 33, the equations of motion for the k th link are:

$$f_{\mathbb{I}}(k) = f_{\mathbb{I}}(k-1) + M_{\mathbb{I}}(k)\alpha_{\mathbb{I}}(k) + b_{\mathbb{I}}(k) \quad (5.50)$$

where

$$\alpha_{\mathbb{I}}(k) \triangleq \frac{d_{\mathbb{I}}\mathcal{V}_{\mathbb{I}}(k)}{dt} \quad \text{and} \quad b_{\mathbb{I}}(k) \stackrel{2.38}{=} \bar{\mathcal{V}}_{\mathbb{I}}(k)M_{\mathbb{I}}(k)\mathcal{V}_{\mathbb{I}}(k) \quad (5.51)$$

Exercise 5.6 Expression for $\dot{H}_{\mathbb{I}}^*(k)$.

Show that

$$\dot{H}_{\mathbb{I}}^*(k) \triangleq \frac{d_{\mathbb{I}}H_{\mathbb{I}}^*(k)}{dt} = \tilde{\mathcal{V}}_{\mathbb{I}}(k)H_{\mathbb{I}}^*(k) + \phi^*(\mathcal{O}_k, \mathbb{I})\frac{d_{k+1}H^*(k)}{dt} \quad (5.52)$$

In most situations, $\frac{d_{k+1}H^*(k)}{dt} \equiv 0$, and then (5.52) simplifies to

$$\dot{H}_{\mathbb{I}}(k) = \tilde{\mathcal{V}}_{\mathbb{I}}(k)H_{\mathbb{I}}^*(k) \quad (5.53)$$

■

Differentiating (5.49), it follows that the link spatial accelerations $\alpha(k)$ satisfy the recursive relationship

$$\alpha_{\mathbb{I}}(k) = \alpha_{\mathbb{I}}(k+1) + H_{\mathbb{I}}^*(k)\ddot{\theta}(k) + a_{\mathbb{I}}(k) \quad (5.54)$$

with

$$\begin{aligned} a_{\mathbb{I}}(k) &\triangleq \dot{H}_{\mathbb{I}}^*(k)\dot{\theta}(k) \stackrel{5.52}{=} \tilde{\mathcal{V}}_{\mathbb{I}}(k)H_{\mathbb{I}}^*(k)\dot{\theta}(k) + \phi^*(\mathcal{O}_k, \mathbb{I})\frac{d_{k+1}H^*(k)}{dt} \\ &\stackrel{3.25}{=} \tilde{\mathcal{V}}_{\mathbb{I}}(k)\Delta_{\mathcal{V}}^{\mathbb{I}}(k) + \phi^*(\mathcal{O}_k, \mathbb{I})\frac{d_{k+1}H^*(k)}{dt} \end{aligned} \quad (5.55)$$

The hinge torque at the k th hinge is

$$\tau(k) = H_{\mathbb{I}}(k)f_{\mathbb{I}}(k) \quad (5.56)$$

Together, the relationships in (5.49), (5.50), (5.54), and (5.56) define the following equations of motion for the serial-chain:

$$\begin{aligned}
V_{\mathbb{I}}(k) &= V_{\mathbb{I}}(k+1) + H_{\mathbb{I}}^*(k)\dot{\theta}(k) \\
\alpha_{\mathbb{I}}(k) &= \alpha_{\mathbb{I}}(k+1) + H_{\mathbb{I}}^*(k)\ddot{\theta}(k) + \dot{H}_{\mathbb{I}}^*(k)\dot{\theta}(k) \\
f_{\mathbb{I}}(k) &= f_{\mathbb{I}}(k-1) + M_{\mathbb{I}}(k)\alpha_{\mathbb{I}}(k) + b_{\mathbb{I}}(k) \\
T(k) &= H_{\mathbb{I}}(k)f_{\mathbb{I}}(k)
\end{aligned} \tag{5.57}$$

Define the block diagonal spatial operators $H_{\mathbb{I}} = \text{diag}\{H_{\mathbb{I}}(k)\}$, $M_{\mathbb{I}} = \text{diag}\{M_{\mathbb{I}}(k)\}$, with $\mathcal{E}_{\mathbb{I}}$ and $\phi_{\mathbb{I}}$ as

$$\mathcal{E}_{\mathbb{I}} = \begin{pmatrix} \mathbf{0} & \dots & \dots & \dots & \mathbf{0} \\ \mathbf{I} & \mathbf{0} & \dots & \dots & \vdots \\ \mathbf{0} & \mathbf{I} & \mathbf{0} & \dots & \vdots \\ \vdots & \ddots & \ddots & \ddots & \vdots \\ \mathbf{0} & \dots & \dots & \mathbf{I} & \mathbf{0} \end{pmatrix} \in \mathcal{R}^{6n \times 6n}, \quad \text{and} \quad \phi_{\mathbb{I}} = \begin{pmatrix} \mathbf{I} & \dots & \dots & \mathbf{0} \\ \mathbf{I} & \mathbf{I} & & \vdots \\ \vdots & & \ddots & \vdots \\ \mathbf{I} & \dots & \dots & \mathbf{I} \end{pmatrix} \in \mathcal{R}^{6n \times 6n} \tag{5.58}$$

Analogous to (3.36), we have

$$\phi_{\mathbb{I}} = [\mathbf{I} - \mathcal{E}_{\mathbb{I}}]^{-1}, \quad \text{and} \quad \mathcal{E}_{\mathbb{I}}\phi_{\mathbb{I}} = \phi_{\mathbb{I}}\mathcal{E}_{\mathbb{I}} = \phi_{\mathbb{I}} - \mathbf{I} \stackrel{\triangle}{=} \tilde{\phi}_{\mathbb{I}} \tag{5.59}$$

It is noteworthy that, for the inertially referenced case, $\phi_{\mathbb{I}}$ is independent of the system configuration, though now $H_{\mathbb{I}}^*$ and $M_{\mathbb{I}}$ are configuration dependent. Define the overall link spatial velocity vector $V_{\mathbb{I}}$ for the system as

$$V_{\mathbb{I}} \stackrel{\triangle}{=} \text{col}\{V_{\mathbb{I}}(k)\}_{k=1}^n$$

Using a similar procedure, define the $\alpha_{\mathbb{I}}$, $f_{\mathbb{I}}$ etc., stacked vectors. Using these spatial operators and the stacked vectors, (5.57) can be re-expressed in the form,

$$\begin{aligned}
V_{\mathbb{I}} &= \phi_{\mathbb{I}}^* H_{\mathbb{I}}^* \dot{\theta} \\
\alpha_{\mathbb{I}} &= \phi_{\mathbb{I}}^* [H_{\mathbb{I}}^* \ddot{\theta} + \dot{H}_{\mathbb{I}}^* \dot{\theta}] = \phi_{\mathbb{I}}^* \frac{d[H_{\mathbb{I}}^* \dot{\theta}]}{dt} \\
x &= M_{\mathbb{I}} \alpha_{\mathbb{I}} + \dot{M}_{\mathbb{I}} V_{\mathbb{I}} = \frac{d[M_{\mathbb{I}} \phi_{\mathbb{I}}^* H_{\mathbb{I}}^* \dot{\theta}]}{dt} = \frac{dM_{\mathbb{I}} V_{\mathbb{I}}}{dt} \\
f_{\mathbb{I}} &= \phi_{\mathbb{I}} x = \phi_{\mathbb{I}} \frac{d[M_{\mathbb{I}} \phi_{\mathbb{I}}^* H_{\mathbb{I}}^* \dot{\theta}]}{dt} \\
T &= H_{\mathbb{I}} f_{\mathbb{I}} = H_{\mathbb{I}} \phi_{\mathbb{I}} \frac{d[M_{\mathbb{I}} \phi_{\mathbb{I}}^* H_{\mathbb{I}}^* \dot{\theta}]}{dt} = \mathcal{M} \ddot{\theta} + \mathcal{C}
\end{aligned} \tag{5.60}$$

where

$$\begin{aligned}\mathcal{M}(\theta) &\stackrel{\Delta}{=} H_{\mathbb{I}} \phi_{\mathbb{I}} M_{\mathbb{I}} \phi_{\mathbb{I}}^* H_{\mathbb{I}}^* \\ \mathcal{C}(\theta, \dot{\theta}) &\stackrel{\Delta}{=} H_{\mathbb{I}} \phi_{\mathbb{I}} \frac{d[M_{\mathbb{I}} \phi_{\mathbb{I}}^* H_{\mathbb{I}}^*]}{dt} \dot{\theta} = H_{\mathbb{I}} \phi_{\mathbb{I}} [\dot{M}_{\mathbb{I}} \mathcal{V}_{\mathbb{I}} + M_{\mathbb{I}} \phi_{\mathbb{I}}^* H_{\mathbb{I}}^* \dot{\theta}]\end{aligned}\quad (5.61)$$

5.4.1 Relationship Between $\phi_{\mathbb{I}}$ and ϕ

Along the lines of Sect. 5.1.3, we examine the relationship between the operators for the regular and inertially referenced equations of motion. We have

$$I = \phi_{\mathbb{I}}(k+1, k) = \phi(\mathbb{I}, \mathbb{O}_{k+1})\phi(\mathbb{O}_{k+1}, \mathbb{O}_k)\phi(\mathbb{O}_k, \mathbb{I}) \quad (5.62)$$

Define the block-diagonal operator

$$\Delta_{\mathbb{I}/\mathbb{O}} \stackrel{\Delta}{=} \text{diag} \left\{ \phi(\mathbb{I}, \mathbb{O}_k) \right\}_{k=1}^n \in \mathcal{R}^{6n \times 6n} \quad (5.63)$$

Then, from (5.62), $\mathcal{E}_{\mathbb{I}}$ and \mathcal{E}_{ϕ} are related by the following similarity transformation:

$$\mathcal{E}_{\mathbb{I}} = \Delta_{\mathbb{I}/\mathbb{O}} \mathcal{E}_{\phi} \Delta_{\mathbb{I}/\mathbb{O}}^{-1} \quad (5.64)$$

Thus, $\phi_{\mathbb{I}}$ is related to ϕ as follows:

$$\begin{aligned}\phi_{\mathbb{I}} &\stackrel{5.59}{=} (I - \mathcal{E}_{\mathbb{I}})^{-1} \stackrel{5.64}{=} (I - \Delta_{\mathbb{I}/\mathbb{O}} \mathcal{E}_{\phi} \Delta_{\mathbb{I}/\mathbb{O}}^{-1})^{-1} \\ &= \Delta_{\mathbb{I}/\mathbb{O}} (I - \mathcal{E}_{\phi})^{-1} \Delta_{\mathbb{I}/\mathbb{O}}^{-1} = \Delta_{\mathbb{I}/\mathbb{O}} \phi \Delta_{\mathbb{I}/\mathbb{O}}^{-1}\end{aligned}\quad (5.65)$$

Thus, $\phi_{\mathbb{I}}$ and ϕ are also related by the same similarity transformation. It is straightforward to also see that

$$H_{\mathbb{I}} = H \Delta_{\mathbb{I}/\mathbb{O}}^{-1} \quad M_{\mathbb{I}} = \Delta_{\mathbb{I}/\mathbb{O}} M \Delta_{\mathbb{I}/\mathbb{O}}^* \quad (5.66)$$

Even though the internal structure of these spatial operators is different, the mass matrix remains unchanged in the new formulation, since

$$\begin{aligned}H_{\mathbb{I}} \phi_{\mathbb{I}} M_{\mathbb{I}} \phi_{\mathbb{I}}^* H_{\mathbb{I}}^* &\stackrel{5.65, 5.66}{=} (H \Delta_{\mathbb{I}/\mathbb{O}}^{-1}) \cdot (\Delta_{\mathbb{I}/\mathbb{O}} \phi \Delta_{\mathbb{I}/\mathbb{O}}^{-1}) \cdot (\Delta_{\mathbb{I}/\mathbb{O}} M \Delta_{\mathbb{I}/\mathbb{O}}^*) \\ &\quad \cdot (\Delta_{\mathbb{I}/\mathbb{O}} \phi \Delta_{\mathbb{I}/\mathbb{O}}^{-1})^* \cdot (H \Delta_{\mathbb{I}/\mathbb{O}}^{-1})^* \\ &= H \phi M \phi^* H^* \stackrel{5.25}{=} \mathcal{M}\end{aligned}$$

Chapter 6

Articulated Body Model for Serial Chains

This chapter introduces articulated body models for the component links in a serial-chain system. This model is an alternative to the terminal and composite body models discussed earlier. While the composite body model is appropriate for the inverse dynamics problem, the articulated body model is better suited for the forward dynamics problem.

6.1 Alternate Models for Multibody Systems

Chapter 5 discusses two alternative models for the dynamics of the component links in the serial-chain system. They are the *terminal body* and the *composite body* models. Each of these models uses different effective inertias to define the system dynamics as viewed from the k th link in the system. Since these models do not by themselves fully capture the articulated dynamics of the system, they require correction force terms to compensate for the gap between the reference model and the correct system dynamics [71].

6.1.1 Terminal Body Model

In the terminal body model, the k th link is viewed as a terminal body and the connection to its children bodies is initially ignored. For this case, the effective inertia at the k th link is the familiar spatial inertia of the k th link. Thus, for this terminal body reference model, the force/acceleration relationship at the k th link is defined as:

$$f(k) = M(k)\alpha(k) \quad (6.1)$$

The terminal body reference model is only correct for truly terminal bodies. For non-terminal bodies, the coupling to the children bodies is accounted for by the addition

of the “correction” force $\phi(k, k-1)f(k-1)$, so that the correct force/acceleration relationship for the k th link is given by

$$f(k) = M(k)\alpha(k) + \phi(k, k-1)f(k-1) \quad (6.2)$$

This expression is the same as the one in the equations of motion in (5.21). Thus, the $M(k)\alpha(k)$ inertia/acceleration part reflects the “predicted” dynamics based on the reference model, while the $\phi(k, k-1)f(k-1)$ spatial force compensates for the mismatch between the predicted and the actual dynamics. The $\phi(k, k-1)f(k-1)$ correction force is a function of the hinge forces and accelerations of the inboard, as well as the outboard, bodies in the system.

6.1.2 Composite Body Model

In the composite body model, the links 1 through k are viewed as forming a composite body by locking the 1 through $k-1$ hinges. The articulation of the outboard hinges is initially ignored. The effective inertia at the k th link, then, is the $R(k)$ composite body inertia. This reference model leads to the following force/acceleration relationship at the k th link:

$$f(k) = R(k)\alpha(k) \quad (6.3)$$

In other words, this reference model assumes that all the hinges outboard of the k th link are frozen and the sub-system can be treated as a rigid body with $R(k)$ spatial inertia. Since the outboard hinges are not frozen in reality, a correction term is needed to account for the presence of non-zero accelerations at the outboard 1 through $k-1$ hinges. As seen in (5.46) on page 92, the spatial force $y(k)$ provides the necessary correction term, so that the correct force/acceleration relationship at the k th link is given by

$$f(k) = R(k)\alpha(k) + y(k) \quad (6.4)$$

The force/acceleration relationship in (6.4) at the k th link is an alternative to the one in (6.2). The representations differ in both the spatial inertia term and the correction force term. The $R(k)$ spatial inertia term is a function of the spatial inertias of all the links 1 through k , in contrast with $M(k)$, which depends on the spatial inertia of the k th link alone. The $y(k)$ residual force term is simpler than the earlier $\phi(k, k-1)f(k-1)$ term in that it depends only on the outboard hinge accelerations $\ddot{\theta}(j)$, $j < k$, as discussed in Sect. 5.3.3. This is in contrast with the $\phi(k, k-1)f(k-1)$ correction force for the terminal body model, which is a function of all hinge accelerations. When the outboard hinge accelerations are indeed zero, $y(k) = \mathbf{0}$, and the force/acceleration relationship reduces to the one in (6.3).

6.1.3 Articulated Body Model

We now introduce another dynamics model, referred to as the **articulated body model** for serial-chain systems. In this model, it is assumed that all the outboard 1 through $k - 1$ hinges are completely free with zero hinge forces, i.e., $\mathcal{T}(j) = 0$, for $j < k$. The prevalence of non-zero generalized forces at these hinges is initially ignored. This is in contrast with the composite body model, where the outboard hinges are assumed to be locked with zero hinge accelerations. We will establish that this reference model leads to the following force/acceleration relationship at the k th link:

$$f(k) = \mathcal{P}(k)\alpha(k) \quad (6.5)$$

and that the $\mathcal{P}(k)$ inertia term in (6.5), referred to as the **articulated body inertia**, is well defined.

Since, in reality, the outboard 1 through $(k - 1)$ hinges have non-zero generalized forces, we will further show that there is a well-defined correction spatial force, $\mathfrak{z}(k)$, that compensates for these non-zero hinge forces. The correct force/acceleration relationship has the form:

$$f(k) = \mathcal{P}(k)\alpha(k) + \mathfrak{z}(k) \quad (6.6)$$

In the articulated body model, $\mathcal{P}(k)$ plays the role of the inertia, while $\mathfrak{z}(k)$ plays the role of the correction force term. We will see that the $\mathfrak{z}(k)$ spatial force depends only upon the outboard hinge forces, and is zero when all the outboard hinge forces are indeed zero. Figure 6.1 illustrates the three different reference models and their corresponding force decompositions at the k th link.

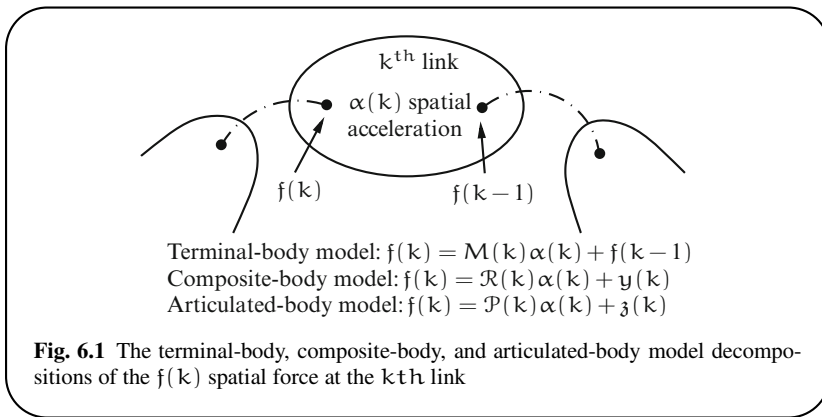


Fig. 6.1 The terminal-body, composite-body, and articulated-body model decompositions of the $f(k)$ spatial force at the k th link

The concept of articulated body inertias for a serial rigid multibody system was originally introduced in Featherstone [47], to develop the remarkable $O(N)$ AB algorithm for solving the forward dynamics problem for serial-chain systems.

Independently, Rodriguez [139] arrived at the same concept, but from a very different perspective – one inspired by the close mathematical parallels between the recursive structure of multibody system dynamics and those of optimal filtering problems for time-domain dynamical systems. These parallels are explored further in Sect. 6.4.

6.2 The $\mathcal{P}(k)$ Articulated Body Inertia

We refer to the sub-system consisting of just links k through 1 as the k th articulated body system for the serial-chain. Thus, there are n such articulated body systems associated with the system, with the first one being simply link 1 all by itself, and the n th one being the full serial-chain. We assume for now that the system is at rest so that the velocity dependent $a(k)$ Coriolis accelerations and the $b(k)$ gyroscopic force terms are zero and can be ignored.

We focus first on characterizing the $\mathcal{P}(k)$ articulated body inertia term in (6.5). In keeping with the assumptions of the articulated body reference model, all the generalized forces in the system are assumed to be zero, i.e., $\mathcal{T}(k) = 0$ for $1 \leq k \leq n$. In Sect. 6.3 we will remove this restriction when we shift attention to the $\mathcal{Z}(k)$ correction spatial force term in (6.6).

6.2.1 Induction Argument for $\mathcal{P}(k)$

We adopt an induction based argument to show that the articulated body inertia at the k th link, denoted $\mathcal{P}(k)$, is a well-defined, symmetric and positive semi-definite quantity satisfying the force/acceleration relationship in (6.5) for the k th articulated body system. We will show that the assumption that the outboard hinge forces are zero imposes a strict relationship between the spatial accelerations of neighboring bodies and their hinge generalized accelerations. This will allow us to develop an expression for the articulated body inertia.

To start the induction based argument, let us consider the first articulated body system which consists of just link 1 alone. The relationship between a spatial force $f(1)$ being applied at frame \mathcal{O}_1 on link 1 and its spatial acceleration $\alpha(1)$ is simply given by

$$f(1) = M(1)\alpha(1)$$

Thus, choosing the articulated body inertia $\mathcal{P}(1)$ as

$$\mathcal{P}(1) = M(1)$$

satisfies (6.5) for link 1. The symmetry and positive semi-definiteness of $\mathcal{P}(1)$ follows from the symmetry and positive semi-definiteness of the $M(1)$ spatial inertia.

Obtaining the expression for $\mathcal{P}(1)$ allows us to begin our induction argument. For the purposes of induction, assume that (6.5) holds for the k th articulated body system, and that its articulated body inertia $\mathcal{P}(k)$ is well-defined, symmetric and positive semi-definite, i.e.,

$$\mathbf{f}(k) = \mathcal{P}(k)\boldsymbol{\alpha}(k) \quad \text{with} \quad \mathcal{T}(j) = H(j)\mathbf{f}(j) = \mathbf{0} \quad \forall j < k \quad (6.7)$$

Our goal now is to establish (6.5) for the $(k+1)$ th link, i.e., to derive an expression for $\mathcal{P}(k+1)$ such that

$$\mathbf{f}(k+1) = \mathcal{P}(k+1)\boldsymbol{\alpha}(k+1) \quad \text{with} \quad \mathcal{T}(j) = H(j)\mathbf{f}(j) = \mathbf{0} \quad \forall j < k+1 \quad (6.8)$$

6.2.2 The $\mathcal{D}(k)$ and $\mathcal{G}(k)$ Matrices

Define $\boldsymbol{\alpha}^+(k)$ as

$$\boldsymbol{\alpha}^+(k) = \phi^*(k+1, k)\boldsymbol{\alpha}(k+1) \quad (6.9)$$

With the system at rest, $\boldsymbol{\alpha}^+(k)$ represents the spatial acceleration of the \mathbb{O}_{k+1} frame. Thus, the spatial acceleration relationship in the equations of motion in (5.21) can be restated as

$$\boldsymbol{\alpha}(k) = \boldsymbol{\alpha}^+(k) + H^*(k)\ddot{\theta}(k) \quad (6.10)$$

$\boldsymbol{\alpha}(k)$ is absent from (6.10) because we have assumed that the system is at rest. It follows from (6.7) that

$$\begin{aligned} \mathbf{0} &\stackrel{6.7}{=} \mathcal{T}(k) \stackrel{6.7}{=} H(k)\mathbf{f}(k) = H(k)\mathcal{P}(k)\boldsymbol{\alpha}(k) \\ &\stackrel{6.10}{=} H(k)\mathcal{P}(k)\boldsymbol{\alpha}^+(k) + H(k)\mathcal{P}(k)H^*(k)\ddot{\theta}(k) \end{aligned} \quad (6.11)$$

Therefore, the hinge acceleration $\ddot{\theta}(k)$ is given by the expression

$$\ddot{\theta}(k) \stackrel{6.11}{=} -\mathcal{D}^{-1}(k)H(k)\mathcal{P}(k)\boldsymbol{\alpha}^+(k) = -\mathcal{G}^*(k)\boldsymbol{\alpha}^+(k) \quad (6.12)$$

where the quantities $\mathcal{G}(k) \in \mathcal{R}^{6 \times r_v(k)}$ and $\mathcal{D}(k) \in \mathcal{R}^{r_v(k) \times r_v(k)}$ are defined as

$$\mathcal{D}(k) \triangleq H(k)\mathcal{P}(k)H^*(k) \quad \text{and} \quad \mathcal{G}(k) \triangleq \mathcal{P}(k)H^*(k)\mathcal{D}^{-1}(k) \quad (6.13)$$

The invertibility of $\mathcal{D}(k)$ would necessarily follow from (6.13) if $\mathcal{P}(k)$ were non-singular since the hinge map matrix $H^*(k)$ is full-rank. This is true in all but pathological cases. We will continue by assuming that $\mathcal{D}(k)$ is invertible. Equation (6.12) provides a well defined relationship between the spatial acceleration of frame \mathbb{O}_k^+ and the generalized acceleration of the k th hinge. $\mathcal{G}(k)$ is referred to as the **Kalman gain** at the k th hinge, and $\mathcal{D}(k)$ as the **articulated body hinge inertia** at the k th hinge.

Remark 6.1 $\mathcal{G}(k)$ is a generalized-inverse of $H(k)$.

It is easy to verify from the definitions in (6.13) that the following identity holds:

$$H(k)\mathcal{G}(k) = \mathbf{I} \quad (6.14)$$

It follows therefore, that $H(k)\mathcal{G}(k)H(k) = H(k)$ and, hence, $\mathcal{G}(k)$ is a generalized-inverse¹ of $H(k)$. ■

6.2.3 The $\tau(k)$ and $\bar{\tau}(k)$ Projection Matrices

Using (6.12) in (6.10) leads to

$$\alpha(k) \stackrel{6.10, 6.12}{=} [\mathbf{I} - H^*(k)\mathcal{G}^*(k)]\alpha^+(k) = \bar{\tau}^*(k)\alpha^+(k) \quad (6.15)$$

where the quantities $\tau(k)$ and $\bar{\tau}(k)$ in $\mathcal{R}^{6 \times 6}$ are defined as

$$\tau(k) \triangleq \mathcal{G}(k)H(k) \quad \text{and} \quad \bar{\tau}(k) \triangleq \mathbf{I} - \tau(k) = \mathbf{I} - \mathcal{G}(k)H(k) \quad (6.16)$$

Taken together, (6.12) and (6.15) show that the generalized acceleration of the k th hinge, and the spatial acceleration of the k th link, can be determined directly from the $\alpha^+(k)$ spatial acceleration of the inboard \mathbb{O}_k^+ frame. $\tau(k)$ and $\bar{\tau}(k)$ have the important property that they are **projection matrices**.² This is the subject of the following exercise.

Exercise 6.1 Properties of the $\tau(k)$ and $\bar{\tau}(k)$ projection matrices.

1. Show that $\tau(k)$, $\tau^*(k)$, $\bar{\tau}(k)$ and $\bar{\tau}^*(k)$ are all projection matrices.
2. Show that

$$\tau(k)\mathcal{G}(k) = \mathcal{G}(k) \quad \text{and} \quad \tau^*(k)H^*(k) = H^*(k) \quad (6.17)$$

Thus the range spaces of the $\tau(k)$ and $\tau^*(k)$ projection operators are in fact the range spaces of $\mathcal{G}(k)$ and $H^*(k)$, respectively. Also, it follows that the range spaces of $\mathcal{G}(k)$ and $H^*(k)$ are the null-spaces of the $\bar{\tau}(k)$ and $\bar{\tau}^*(k)$ projections, respectively, that is

$$\bar{\tau}(k)\mathcal{G}(k) = \mathbf{0} \quad \text{and} \quad \bar{\tau}^*(k)H^*(k) = \mathbf{0} \quad (6.18)$$

■

From (6.15), $\bar{\tau}^*(k)$ has the physical interpretation of projecting out the part of $\alpha^+(k)$ that is along the $H^*(k)$ hinge axis in such a way that no generalized force is generated at the hinge. This is illustrated in Fig. 6.2.

¹ A matrix X is said to be the generalized-inverse of another matrix Y if $YXY = Y$.

² A matrix U is a projection matrix if and only if it is square and $U^2 = U$.

Remark 6.2 Nulling out of hinge accelerations.

It follows from (6.15) and (6.18) that if $\alpha^+(k) = H^*(k)\ddot{\theta}(k)$, then $\alpha(k) = \mathbf{0}$! In effect, in the articulated body model, accelerations along the hinge axis are not transmitted across the freely articulated hinge. The only motion that is transmitted

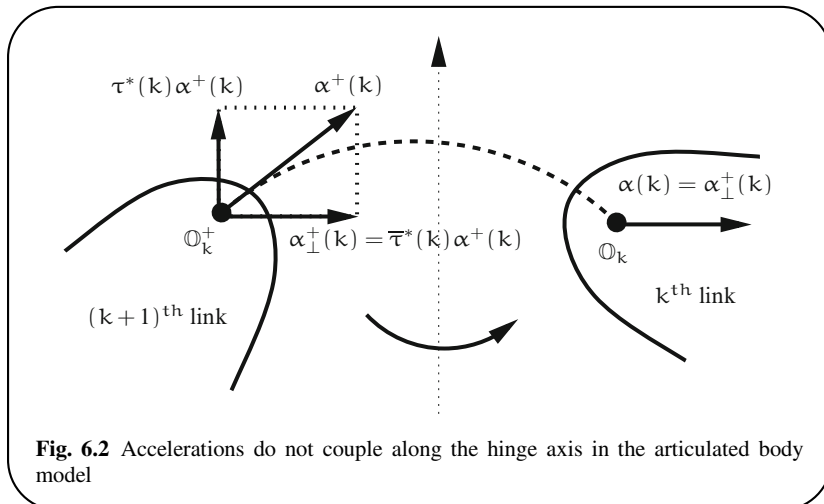


Fig. 6.2 Accelerations do not couple along the hinge axis in the articulated body model

is along the other axes where there is rigid coupling. The information about this selective coupling across the hinge is contained in the $\bar{\tau}(k)$ projection operator. ■

Remark 6.3 Alternative derivation of $\tau(k)$ expression.

An alternative reasoning leading to the derivation of the projection operator $\bar{\tau}(k)$ is described here. First we restate the following relationships established earlier:

$$\alpha(k) \stackrel{5.21, 6.9}{=} \alpha^+(k) + H^*(k)\ddot{\theta}(k) \quad \text{and} \quad H(k)\mathcal{P}(k)\alpha(k) \stackrel{6.7}{=} \mathbf{0} \quad (6.19)$$

The unknown quantity in (6.19) is the hinge acceleration $\ddot{\theta}(k)$ for the k th hinge. If the k th hinge were frozen, $\ddot{\theta}(k) = \mathbf{0}$ and $\alpha(k) = \alpha^+(k)$. However, due to the presence of a hinge, only a part of $\alpha^+(k)$ gets transmitted across the k th hinge as $\alpha(k)$. The above equations require that $\alpha(k) \in \text{Null}[H(k)\mathcal{P}(k)]$. Hence, $\alpha(k)$ is the (non-orthogonal) projection of $\alpha^+(k)$ onto $\text{Null}[H(k)\mathcal{P}(k)]$ along $\text{Range}[H^*(k)]$.³ The specification of the left and right null-spaces of a projection operator uniquely defines it. That is, if Q is a projection operator whose left null-space is specified by the

³ x is said to be a projection of z onto the subspace X along the subspace Y if we can uniquely write the decomposition $z = x + y$, where $x \in X$ and $y \in Y$. The projection is orthogonal if and only if the subspaces X and Y are orthogonal to each other.

columns of X , i.e., $X^*Q = 0$, and whose right null-space is specified by the columns of Y , i.e., $QY = 0$, then Q is uniquely defined by

$$Q = I - Y(X^*Y)^{-1}X^* \quad (6.20)$$

From the above discussion, the right and left null-spaces of $\bar{\tau}^*(k)$ are defined by:

$$\bar{\tau}^*(k) : \begin{cases} \bar{\tau}^*(k)H^*(k) = \mathbf{0} \\ H(k)\mathcal{P}(k)\bar{\tau}^*(k) = \mathbf{0} \end{cases} \quad (6.21)$$

Using (6.20), the two conditions on the right in (6.21) are thus sufficient to uniquely define the $\bar{\tau}^*(k)$ projection expression as the one defined in (6.16). ■

Exercise 6.2 The $\mathcal{G}(k)$ Kalman gain and the link spatial acceleration.
For the articulated body model, show that

$$\mathcal{G}^*(k)\alpha(k) = \mathbf{0} \quad (6.22)$$

■

6.2.4 The $\mathcal{P}^+(k)$ Matrix

Turning to the force relationships in the articulated body model, we have

$$f(k) \stackrel{6.7}{=} \mathcal{P}(k)\alpha(k) \stackrel{6.15}{=} \mathcal{P}(k)\bar{\tau}^*(k)\alpha^+(k) = \mathcal{P}^+(k)\alpha^+(k) \quad (6.23)$$

where the matrix $\mathcal{P}^+(k) \in \mathcal{R}^{6 \times 6}$ is defined as

$$\mathcal{P}^+(k) \triangleq \mathcal{P}(k)\bar{\tau}^*(k) \quad (6.24)$$

The expression $f(k) = \mathcal{P}^+(k)\alpha^+(k)$ in (6.23), parallels the earlier $f(k) = \mathcal{P}(k)\alpha(k)$ expression. While $\mathcal{P}(k)$ represents the effective articulated body inertia of the k th articulated body system at the \mathbb{O}_k frame, $\mathcal{P}^+(k)$ can be interpreted as the effective articulated body inertia of the same system at the \mathbb{O}_k^+ frame, i.e., on the inboard side of the k th hinge. As a result of crossing the hinge, the inertia $\mathcal{P}^+(k)$ is no longer non-singular, as shown in the following exercise.

Exercise 6.3 Properties of $\mathcal{P}^+(k)$.

This exercise establishes that $\mathcal{P}^+(k)$ is a symmetric, positive semi-definite matrix.

1. Show that

$$\mathcal{P}^+(k) = \bar{\tau}(k)\mathcal{P}(k) = \mathcal{P}(k)\bar{\tau}^*(k) = \bar{\tau}(k)\mathcal{P}(k)\bar{\tau}^*(k) \quad (6.25)$$

Since $\mathcal{P}(k)$ is symmetric and positive semi-definite, it follows from the last expression that $\mathcal{P}^+(k)$ is symmetric and positive semi-definite as well.

2. Show that

$$\mathbf{H}(k)\mathcal{P}^+(k) = \mathbf{0} \quad \text{and} \quad \mathcal{P}^+(k)\mathbf{H}^*(k) = \mathbf{0} \quad (6.26)$$

Thus, $\mathcal{P}^+(k)$ is singular, with null-space the same as the null-space of $\bar{\tau}^*(k)$. ■

6.2.5 Conclusion of the Induction Argument for $\mathcal{P}(k)$

The equations of motion at frame \mathbb{O}_{k+1} on the $(k+1)$ th link are given by the expression

$$\begin{aligned} \mathfrak{f}(k+1) &\stackrel{5.21}{=} \phi(k+1, k)\mathfrak{f}(k) + M(k+1)\alpha(k+1) \\ &\stackrel{6.23}{=} \phi(k+1, k)\mathcal{P}^+(k)\alpha^+(k) + M(k+1)\alpha(k+1) \\ &\stackrel{6.9}{=} [\phi(k+1, k)\mathcal{P}^+(k)\phi^*(k+1, k) + M(k+1)]\alpha(k+1) \end{aligned} \quad (6.27)$$

Comparing this expression with (6.8), we see that choosing $\mathcal{P}(k+1)$ as

$$\mathcal{P}(k+1) \stackrel{\triangle}{=} \phi(k+1, k)\mathcal{P}^+(k)\phi^*(k+1, k) + M(k+1) \quad (6.28)$$

satisfies (6.8). This expression for $\mathcal{P}(k+1)$ effectively concludes the induction based argument to establish that the articulated body inertias are well-defined for all links in the articulated body model.

Defining $\psi(k+1, k) \in \mathcal{R}^{6 \times 6}$ as

$$\psi(k+1, k) \stackrel{\triangle}{=} \phi(k+1, k)\bar{\tau}(k) \quad (6.29)$$

Equation (6.28) can be rewritten in the form

$$\mathcal{P}(k+1) \stackrel{6.29}{=} \psi(k+1, k)\mathcal{P}(k)\psi^*(k+1, k) + M(k+1) \quad (6.30)$$

Equation (6.30) is of the same form as the **discrete Riccati equations**⁴ that appear in the optimal filtering of discrete-time systems [5]. The recursion in (6.30) is similar to the recursions for the $\mathcal{R}(k)$ composite body inertias in (4.8). From (6.30), it is evident that $\mathcal{P}(k+1)$ is symmetric and positive definite due to the positive definiteness of the link spatial inertias. $\psi(k+1, k)$ is the force/velocity transformation operator for articulated bodies, analogous to the transformation matrix $\phi(k+1, k)$ for rigid bodies. While the rigid body transformation matrix $\phi(k+1, k)$ is a function

⁴ Section 6.4 on page 111 discusses the roots of this terminology in the mathematical parallels with estimation theory.

of $\mathbf{I}(k+1, k)$ alone, $\psi(k+1, k)$ depends additionally on the hinge type and spatial inertias of all the outboard links.

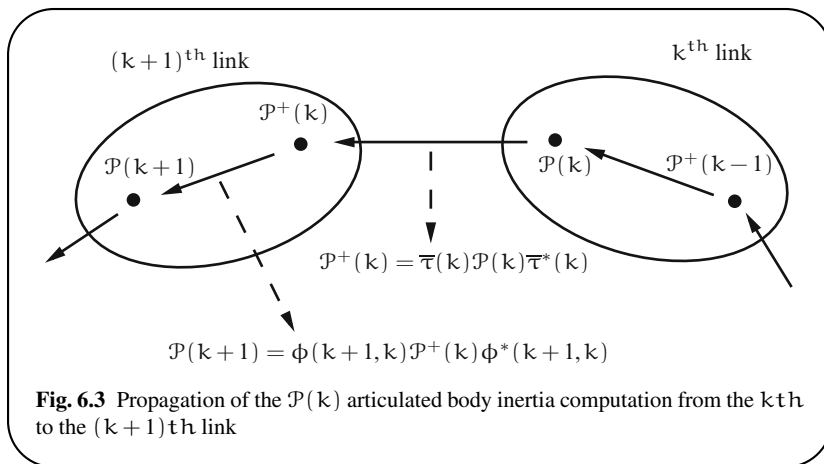


Fig. 6.3 Propagation of the $\mathcal{P}(k)$ articulated body inertia computation from the k^{th} to the $(k+1)^{\text{th}}$ link

Based on (6.28), an algorithm for the computation of the articulated body inertias is described in Algorithm 6.1 and illustrated in Fig. 6.3. The recursive $O(N)$ tip-to-base algorithm propagates the articulated body inertia from body to body and across hinges. During this process, other articulated body quantities, such as $\mathcal{D}(k)$, $\mathcal{G}(k)$, etc., are also computed.

Algorithm 6.1 Recursive algorithm for the articulated body inertias

```


$$\left\{ \begin{array}{l} \mathcal{P}^+(0) = \mathbf{0} \\ \text{for } k = 1 \cdots n \\ \quad \mathcal{P}(k) = \phi(k, k-1)\mathcal{P}^+(k-1)\phi^*(k, k-1) + \mathcal{M}(k) \\ \quad \mathcal{D}(k) = \mathcal{H}(k)\mathcal{P}(k)\mathcal{H}^*(k) \\ \quad \mathcal{G}(k) = \mathcal{P}(k)\mathcal{H}^*(k)\mathcal{D}^{-1}(k) \\ \quad \bar{\tau}(k) = \mathbf{I} - \mathcal{G}(k)\mathcal{H}(k) \\ \quad \mathcal{P}^+(k) = \bar{\tau}(k)\mathcal{P}(k) \\ \text{end loop} \end{array} \right.$$


```

Remark 6.4 $\mathcal{P}(k)$ is not a spatial inertia.

The computations for the articulated body inertias are analogous to those that determine the composite spatial inertia matrix in Sect. 4.1.2. However, there is a fundamental difference. The composite spatial inertia matrix can be parametrized

by ten parameters. These parameters corresponded to the mass, mass center, and the rotational inertia of the composite body outboard of hinge k. However, no such reduced parametrization of the articulated body inertias is possible. The main reason for this is that $\mathcal{P}(k)$, while inertia-like, is not a spatial inertia. And thus, the property of a parametrization by only ten parameters, and the resultant structure, is lost. The articulated body inertias are fully populated 6×6 symmetric matrices requiring a full parametrization by 21 parameters. ■

Exercise 6.4 Ordering of $\mathcal{R}(k)$, $\mathcal{P}(k)$ and $M(k)$.

Show that

$$\mathcal{P}(k) \geq \mathcal{P}^+(k) \quad \text{and} \quad \mathcal{R}(k) \geq \mathcal{P}(k) \geq M(k) \quad \forall k \quad (6.31)$$

■

A physical interpretation of the second expression in (6.31) is that, for a composite body, the motion of a component body couples fully into the motion of the outboard bodies. On the other hand, for an articulated body, the motion along the hinge axis is projected out, and, only a part of the motion is coupled into the motion of the outboard bodies. Hence, the $\mathcal{P}(k)$ inertia experienced in the articulated body model is smaller than $\mathcal{R}(k)$. On the other hand, $\mathcal{P}(k)$ is larger than $M(k)$ because it includes not only the spatial inertia of the kth body, but the articulated body inertias of the outboard bodies.

6.3 Articulated Body Model Force Decomposition

If the outboard hinges were truly un-actuated, i.e., there were no hinge forces at the outboard hinges, then it follows from (6.21) and (6.7) that

$$\alpha(k) = \bar{\tau}^* \alpha^+(k) \quad \text{and} \quad f(k) = \mathcal{P}(k)\alpha(k) = \mathcal{P}^+(k)\alpha^+(k)$$

We now extend the reference articulated body model to handle the general situation where the $\mathcal{T}(\cdot)$ generalized forces are non-zero. We compensate for the non-zero generalized forces by introducing an additional residual force term in (6.6), $\mathfrak{z}(k)$, such that $f(k) = \mathcal{P}(k)\alpha(k) + \mathfrak{z}(k)$. This expression will complete the spatial force decomposition for the articulated body model.

Once again, we use an induction based argument to establish the force decomposition in (6.6). For the first link, $f(1) = \mathcal{P}(1)\alpha(1)$, and thus (6.6) clearly holds for this case, with $\mathfrak{z}(1) = 0$. Let us assume that (6.6) holds for the kth link, and we wish to establish this relationship at the $(k+1)$ th link, i.e., we wish to find expressions for $\mathfrak{z}(k+1)$ such that $f(k+1) = \mathcal{P}(k+1)\alpha(k+1) + \mathfrak{z}(k+1)$. We have that

$$\begin{aligned}
f(k) &\stackrel{6.16}{=} \bar{\tau}(k)f(k) + \tau(k)f(k) \stackrel{6.16, 6.6}{=} g(k)H(k)f(k) + \bar{\tau}(k)[P(k)\alpha(k) + z(k)] \\
&\stackrel{5.21}{=} g(k)\mathcal{T}(k) + \bar{\tau}(k)P(k)\alpha(k) + \bar{\tau}(k)z(k) \\
&\stackrel{6.25, 6.10}{=} g(k)\mathcal{T}(k) + P^+(k)[\alpha^+(k) + H^*(k)\ddot{\theta}(k)] + \bar{\tau}(k)z(k) \\
&\stackrel{6.26}{=} g(k)\mathcal{T}(k) + P^+(k)\alpha^+(k) + \bar{\tau}(k)z(k)
\end{aligned}$$

That is,

$$f(k) = P^+(k)\alpha^+(k) + z^+(k) \quad (6.32)$$

where $z^+(k)$ is defined as

$$z^+(k) \triangleq \bar{\tau}(k)z(k) + g(k)\mathcal{T}(k) \quad (6.33)$$

Equation (6.32) extends (6.6) to the \mathbb{O}_k^+ frame on the inboard side of the hinge. Now, from the equations of motion, it follows that

$$\begin{aligned}
f(k+1) &\stackrel{5.21}{=} \phi(k+1, k)f(k) + M(k+1)\alpha(k+1) \\
&\stackrel{6.32}{=} \phi(k+1, k)[P^+(k)\alpha^+(k) + z^+(k)] + M(k+1)\alpha(k+1) \\
&\stackrel{6.9}{=} \phi(k+1, k)P^+(k)\phi^*(k+1, k)\alpha(k+1) + \phi(k+1, k)z^+(k) \\
&\quad + M(k+1)\alpha(k+1) \\
&\stackrel{6.28}{=} P(k+1)\alpha(k+1) + \phi(k+1, k)z^+(k)
\end{aligned}$$

Comparing the above with (6.6) at the $(k+1)$ th link, we have

$$f(k+1) = P(k+1)\alpha(k+1) + z(k+1) \quad (6.34)$$

where $z(k+1)$ is defined as

$$z(k+1) \triangleq \phi(k+1)z^+(k) \stackrel{6.33, 6.29}{=} \psi(k+1, k)z(k) + K(k+1, k)\mathcal{T}(k) \quad (6.35)$$

with $K(k+1, k) \in \mathcal{R}^6$ defined as

$$K(k+1, k) \triangleq \phi(k+1, k)g(k) \quad (6.36)$$

Equations (6.34) and (6.35) establish (6.6) for the $(k+1)$ th articulated body system. This concludes the proof by induction.

Figure 6.4 summarizes the spatial force decomposition relations at the different frame locations on the bodies. The $z(k)$ residual force is only a function of the hinge forces for the hinges outboard of the k th link, and does not depend upon the hinge forces at the inboard hinges. $z(k)$ is zero when all the outboard hinge forces are zero. Table 6.1 compares the properties of the terminal, composite, and articulated body models.

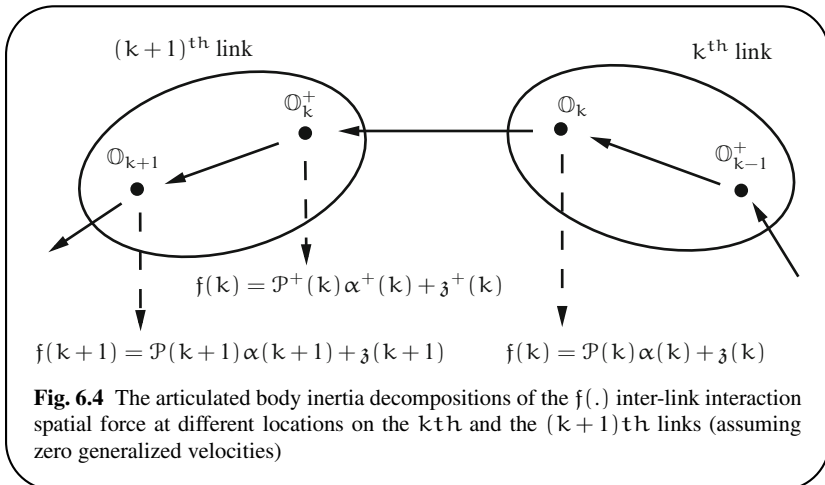


Fig. 6.4 The articulated body inertia decompositions of the $f(\cdot)$ inter-link interaction spatial force at different locations on the k^{th} and the $(k+1)^{\text{th}}$ links (assuming zero generalized velocities)

Table 6.1 A comparison of the terminal, composite, and articulated body models

Model	Terminal body	Composite body	Articulated body
Reference model	Ignore children bodies	Ignore outboard hinge accelerations	Ignore outboard hinge generalized forces
$f(k)$ force decomposition	(6.2)	(6.4)	(6.6)
Inertia recursion		(4.7)	(6.30)
Inertia dependence	Local link inertia	Outboard link inertias	Outboard link inertias and hinges
Residual force recursion	(5.42)	(5.45)	(6.35)
Residual force dependence	All link accelerations	Outboard hinge accelerations	Outboard hinge generalized forces

6.3.1 The $\epsilon(k)$ Vector

Defining $\epsilon(k)$ as

$$\epsilon(k) \triangleq \mathcal{T}(k) - H(k)\mathfrak{z}(k) \quad (6.37)$$

Equation (6.33) can be re-expressed as

$$\mathfrak{z}^{+}(k) \stackrel{6.33}{=} \mathfrak{z}(k) + G(k)(\mathcal{T}(k) - H(k)\mathfrak{z}(k)) \stackrel{6.37}{=} \mathfrak{z}(k) + G(k)\epsilon(k) \quad (6.38)$$

Algorithm 6.2 describes a recursive algorithm for computing all the $\mathfrak{z}(k)$ residual forces. The tip-to-base algorithm propagates the $\mathfrak{z}(k)$ residual forces from body to body starting at the tip and proceeding towards the base. Along the way, the related $\epsilon(k)$ terms are also computed. This recursive equation for $\mathfrak{z}(k)$ is similar in form

Algorithm 6.2 The residual spatial forces vector $\mathfrak{z}(k)$

$$\left\{ \begin{array}{l} \mathfrak{z}^+(0) = \mathbf{0} \\ \textbf{for } k = 1 \dots n \\ \quad \mathfrak{z}(k) = \phi(k, k-1) \mathfrak{z}^+(k-1) \\ \quad \epsilon(k) = \mathcal{T}(k) - \mathcal{H}(k) \mathfrak{z}(k) \\ \quad \mathfrak{z}^+(k) = \mathfrak{z}(k) + \mathcal{G}(k) \epsilon(k) \\ \textbf{end loop} \end{array} \right.$$

to the $y(k)$ composite rigid body inertia term defined in the Exercise 5.5 inverse dynamics algorithm.

6.3.2 Acceleration Relationships

We now explore the implications of the force decomposition for the articulated body model on the spatial accelerations. From (6.6) it follows that

$$\mathcal{T}(k) \stackrel{5.21}{=} \mathcal{H}(k) \mathfrak{f}(k) \stackrel{6.32}{=} \mathcal{H}(k) \mathcal{P}(k) \alpha(k) + \mathcal{H}(k) \mathfrak{z}(k) \quad (6.39)$$

Thus,

$$\begin{aligned} \epsilon(k) &\stackrel{6.39}{=} \mathcal{H}(k) \mathcal{P}(k) \alpha(k) \stackrel{5.21}{=} \mathcal{H}(k) \mathcal{P}(k) [\phi^*(k+1, k) \alpha(k+1) + \mathcal{H}^*(k) \ddot{\theta}(k)] \\ &\stackrel{6.13}{=} \mathcal{D}(k) \ddot{\theta}(k) + \mathcal{H}(k) \mathcal{P}(k) \phi^*(k+1, k) \alpha(k+1) \end{aligned} \quad (6.40)$$

Rearranging the above, and defining $\nu(k)$ as

$$\nu(k) \triangleq \mathcal{D}^{-1}(k) \epsilon(k) \quad (6.41)$$

it follows that

$$\begin{aligned} \ddot{\theta}(k) &\stackrel{6.40}{=} \mathcal{D}^{-1}(k) \{ \epsilon(k) - \mathcal{H}(k) \mathcal{P}(k) \phi^*(k+1, k) \alpha(k+1) \} \\ &\stackrel{6.41, 6.13}{=} \nu(k) - \mathcal{G}^*(k) \phi^*(k+1, k) \alpha(k+1) \\ &\stackrel{6.36}{=} \nu(k) - \mathcal{K}^*(k+1, k) \alpha(k+1) \end{aligned} \quad (6.42)$$

Moreover

$$\begin{aligned}\alpha(k) &\stackrel{5.21}{=} \phi^*(k+1, k)\alpha(k+1) + H^*(k)\ddot{\theta}(k) \\ &\stackrel{6.42}{=} \phi^*(k+1, k)\alpha(k+1) + H^*(k)[\nu(k) - K^*(k+1, k)\alpha(k+1)] \\ &\stackrel{6.29, 6.36}{=} \psi^*(k+1, k)\alpha(k+1) + H^*(k)\nu(k)\end{aligned}\quad (6.43)$$

Comparing the last expression in (6.43) with the expression for spatial accelerations in (5.21), we can interpret $\psi^*(k+1, k)$ as being the transformation matrix in the articulated body model, analogous to the transformation matrix $\phi^*(k+1, k)$ for the composite body model. Similarly, $\nu(k)$ can be thought of as the relative hinge acceleration for the articulated body model, analogous to the relative hinge acceleration $\ddot{\theta}(k)$ for the composite body model.

Exercise 6.5 Relationship of $\nu(k)$ to $\alpha(k)$.

Establish the following relationship:

$$\nu(k) = G^*(k)\alpha(k) \quad (6.44)$$

■

Unlike the $G^*(k)\alpha(k) = \mathbf{0}$ expression in (6.22), (6.44) contains the generally non-zero $\nu(k)$ term. The $\nu(k)$ term arises from the presence of non-zero generalized forces at the outboard hinges. This term is not present in (6.22) because it derivation assumes that the outboard generalized forces are zero.

6.4 Parallels with Estimation Theory

Some of the terminology we have used thus far has its roots in optimal estimation theory. We take a look at such parallels in this section because the mathematical connections run deep. Let us begin by considering a discrete-time, time-varying, linear dynamical system described by the following state-transition equations:

$$\begin{aligned}x(k) &= \phi(k, k-1)x(k-1) + w(k) \\ T(k) &= H(k)x(k)\end{aligned}\quad (6.45)$$

In the above equations, we have deliberately borrowed notation from the multibody dynamics context to this time-domain problem, to highlight the mathematical parallels across the domains. However, the meaning of the symbols are quite different and are as follows:

- k represents the time variable
- $x(k)$ is the system state vector at time k
- $w(k)$ is an input white noise process with covariance $M(k)$
- $\phi(k, k-1)$ is a time-varying state-transition matrix that propagates the state at time $(k-1)$ to the state at time k

- $\mathcal{T}(k)$ is the output observable process at time k
- $H(k)$ is the time-varying output matrix at time k that maps the $x(k)$ system state into the $\mathcal{T}(k)$ output process at time k

6.4.1 Process Covariances

In the optimal estimation literature [5], it is known that the covariance matrix for the $x(k)$ system state, $\mathcal{R}(k)$, satisfies the following equation:

$$\mathcal{R}(k) = \phi(k, k-1)\mathcal{R}(k-1)\phi^*(k, k-1) + M(k) \quad (6.46)$$

This recursive equation is referred to as a **Lyapunov equation** in the optimal estimation literature. Equation (6.46) is identical in form to the recursive relationship for composite body inertias in (4.7) on page 59. The cross-covariances of the system state at different time instants are given by the elements of the $\phi M \phi^*$ matrix, where the ϕ , H , and M matrices have structure identical to the matrix definitions in (3.32), (3.37), and (4.4), respectively. The cross-covariances of the output process, $\mathcal{T}(k)$, are the elements of the $\mathcal{M} = H\phi M \phi^* H^*$ matrix, which is identical in form to the mass matrix of the serial-chain system.

6.4.2 Optimal Filtering

The **optimal filtering** problem consists of generating an optimal estimate of the unknown internal state, $x(k)$, from just the knowledge of the current and past noisy observations, namely the $\mathcal{T}(j)$ values prior to, and including, time k . The **optimal smoothing** problem consists of using additional observations after time k to optimally improve the filtered state estimate at time k . Thus, the optimal filtering process is said to be **causal**, since it is only uses current and past observations. On the other hand, the optimal smoothing process is **anti-causal**, since it is allowed to use future observations to improve the current estimate.

Kalman and others [5, 91, 93] developed elegant solutions to the optimal filtering and smoothing problems. The optimal filter estimate of the system state at time k , denoted $\hat{x}^+(k)$, satisfies a recursive relationship with the optimal filter estimate, $\hat{x}^+(k-1)$, from the previous time step $k-1$. We sketch out this two stage filter estimate generation technique that takes place at each time step:

1. First, with no additional observations, the optimal filter estimate from the previous time $k-1$, $\hat{x}^+(k-1)$, is propagated to form a prediction $\hat{x}(k)$ of the optimal filter estimate of $x(k)$ at time k .
2. Next, the new observation $\mathcal{T}(k)$ at time k , is processed to remove the part that is predictable from the past observations, to create a residual **innovations** term, $\epsilon(k)$, containing just the new information. This innovation term is used to update

the predicted optimal filter estimate, $\mathbf{z}(k)$, to obtain the optimal filter estimate, $\mathbf{z}^+(k)$, at time k .

This 2-step recursive procedure is applied at each new time step as new observation values are obtained.

The covariance of the optimal filter estimate error, $\mathbf{x}(k) - \mathbf{z}(k)$, at time k , denoted $\mathcal{P}(k)$, satisfies the equation

$$\mathcal{P}(k) = \psi(k, k-1)\mathcal{P}(k-1)\psi^*(k, k-1) + M(k) \quad (6.47)$$

This equation is referred to as the discrete form of the **Riccati equation**. This equation is identical in form to the (6.30) for articulated body inertia quantities. The definition of $\psi(k, k-1)$ is mathematically identical to that in (6.29).

Given the optimal filtered estimate at time $(k-1)$, $\mathbf{z}^+(k-1)$, the best prediction of the system state (without any additional observations), $\mathbf{z}(k)$, is obtained by simply propagating this estimate using the state-transition matrix as follows:

$$\mathbf{z}(k) = \phi(k, k-1)\mathbf{z}^+(k-1) \quad (6.48)$$

Once the new observation at time k , $\mathcal{T}(k)$, is available, it can be used to first extract the *new information* in the observation, $\epsilon(k)$, and can then be used to update $\mathbf{z}(k)$ to obtain the new optimal filtered estimate at time k , $\mathbf{z}^+(k)$, as follows:

$$\begin{aligned} \epsilon(k) &= \mathcal{T}(k) - H^*(k)\mathbf{z}(k) \\ \mathbf{z}^+(k) &= \mathbf{z}(k) + G(k)\epsilon(k) \end{aligned} \quad (6.49)$$

$\mathcal{D}(k) = H(k)\mathcal{P}(k)H^*(k)$ is the covariance of the $\epsilon(k)$ innovations process. $G(k) = \mathcal{P}(k)H^*(k)\mathcal{D}^{-1}(k)$ is known as the **Kalman gain** in the estimation literature, and depends directly on the $\mathcal{P}(k)$ covariance obtained as a solution to the Riccati equation. Observe that the optimal filter estimate at time k only depends on the past observations and, hence, this optimal filter is said to be a causal filter.

Equations (6.48) and (6.49) are identical in form to (6.35), (6.37), and (6.38) from the multibody context. Thus, we have observed that several quantities in the articulated body model are mathematically equivalent to terms in Kalman optimal filtering for discrete-time systems.

6.4.3 Optimal Smoothing

The parallels continue. The optimal smoothed estimate, of the $\mathbf{x}(k)$ state at time k , $\mathbf{f}(k)$, is based on the knowledge of the $\mathcal{T}(j)$ observations over the full time interval 1 through n , and not on just the past observations, as for the $\mathbf{z}^+(k)$ optimal filtered estimate. The smoothed estimate, $\mathbf{f}(k)$, can be obtained by updating the filtered estimate as follows:

$$\mathbf{f}(k) = \mathbf{z}(k) + \mathcal{P}(k)\alpha(k) = \mathbf{z}^+(k) + \mathcal{P}^+(k)\alpha^+(k) \quad (6.50)$$

The α and $\alpha^+(k)$ quantities above are obtained by an anti-causal recursion that uses the future observations in a time-reversed recursion that is mathematically identical to (6.43). Equation (6.50) is precisely the form of the force decomposition from the articulated body model in (6.32) and (6.34)!

6.4.4 Extensions

The mathematical parallels between estimation theory and multibody dynamics are extensive. In the next chapter, we derive a new factorization of the mass matrix and an analytical expression for its inverse. These results mirror spectral factorization techniques from estimation theory [20, 92]. These parallels were first identified by Rodriguez and discussed in [139–143, 145].

However, it is also appropriate to point out areas where the parallels start to breakdown and the domains diverge. Unlike the strict sequential order imposed by time for discrete-time systems, no such ordering is required for the links in multi-body systems. The link numbering is not restricted to the parent/child sequence. Moreover, when we explore non-serial-chain multibody systems with branched topologies, the sequential parallels with time are again less obvious. However, as we will see in later chapters, it is remarkable that, with modest extensions, several of the insights developed by exploiting the mathematical parallels between time-domain and serial-chain system domains continue to hold for more general multi-body systems.

Chapter 7

Mass Matrix Inversion and AB Forward Dynamics

This chapter uses the articulated body model to derive a new Innovations Operator Factorization of the serial-chain mass matrix, \mathcal{M} . This factorization has square factors, in contrast to the non-square Newton–Euler factorization of $\mathcal{M} = \mathbf{H}\phi\mathbf{M}\phi^*\mathbf{H}^*$ in (5.23). The Innovations factorization is subsequently used to obtain an explicit analytical operator expression for the inverse of the mass matrix. These factorizations have many important uses, which will be explored in subsequent chapters.

At this stage, we continue to focus on serial-chain rigid multibody systems. However, we will see later that these operator factorization and inversion results and identities continue to hold for a very broad class of multibody systems.

7.1 Articulated Body Spatial Operators

First, we summarize the recursive relationships for articulated body quantities defined in Algorithm 6.1 on page 106 in the previous chapter:

$$\left\{ \begin{array}{l} \mathcal{P}^+(0) = \mathbf{0}, \quad \bar{\tau}(0) = \mathbf{0} \\ \textbf{for } k = 1 \cdots n \\ \quad \psi(k, k-1) = \phi(k, k-1)\bar{\tau}(k-1) \\ \quad \mathcal{P}(k) = \phi(k, k-1)\mathcal{P}^+(k-1)\phi^*(k, k-1) + \mathcal{M}(k) \\ \quad \mathcal{D}(k) = \mathbf{H}(k)\mathcal{P}(k)\mathbf{H}^*(k) \\ \quad \mathcal{G}(k) = \mathcal{P}(k)\mathbf{H}^*(k)\mathcal{D}^{-1}(k) \\ \quad \mathcal{K}(k+1, k) = \phi(k+1, k)\mathcal{G}(k) \\ \quad \bar{\tau}(k) = \mathbf{I} - \mathcal{G}(k)\mathbf{H}(k) \\ \quad \mathcal{P}^+(k) = \bar{\tau}(k)\mathcal{P}(k) \\ \textbf{end loop} \end{array} \right. \quad (7.1)$$

$\psi(k+1, k)$ is the force/velocity transformation matrix for the articulated body model analogous to the $\phi(k+1, k)$ transformation matrix for the composite body model. While $\phi(k+1, k)$ is a function of kinematical quantities alone, $\psi(k+1, k)$ depends additionally on the hinge types and spatial inertias of all the outboard links. Also, unlike $\phi(k+1, k)$, $\psi(k+1, k)$ is not invertible.

Now define the block diagonal operator \mathcal{P} as

$$\mathcal{P} \triangleq \text{diag} \left\{ \mathcal{P}(k) \right\}_{k=1}^n \in \mathcal{R}^{6n \times 6n} \quad (7.2)$$

and the following additional spatial operators:

$$\begin{aligned} \mathcal{D} &\triangleq \text{diag} \left\{ \mathcal{D}(k) \right\}_{k=1}^n = \mathcal{H} \mathcal{P} \mathcal{H}^* && \in \mathcal{R}^{N \times N} \\ \mathcal{G} &\triangleq \text{diag} \left\{ \mathcal{G}(k) \right\}_{k=1}^n = \mathcal{P} \mathcal{H}^* \mathcal{D}^{-1} && \in \mathcal{R}^{6n \times N} \\ \mathcal{K} &\triangleq \mathcal{E}_\phi \mathcal{G} && \in \mathcal{R}^{6n \times N} \\ \tau &\triangleq \text{diag} \left\{ \tau(k) \right\}_{k=1}^n = \mathcal{G} \mathcal{H} && \in \mathcal{R}^{6n \times 6n} \\ \bar{\tau} &\triangleq \text{diag} \left\{ \bar{\tau}(k) \right\}_{k=1}^n = \mathbf{I} - \tau && \in \mathcal{R}^{6n \times 6n} \\ \mathcal{P}^+ &\triangleq \text{diag} \left\{ \mathcal{P}^+(k) \right\}_{k=1}^n = \bar{\tau} \mathcal{P} \bar{\tau}^* = \bar{\tau} \mathcal{P} = \mathcal{P} \bar{\tau}^* && \in \mathcal{R}^{6n \times 6n} \\ \mathcal{E}_\psi &\triangleq \mathcal{E}_\phi \bar{\tau} && \in \mathcal{R}^{6n \times 6n} \end{aligned} \quad (7.3)$$

The operators \mathcal{D} , \mathcal{G} , τ , $\bar{\tau}$, and \mathcal{P}^+ are all block diagonal, with the k th diagonal entry being defined by the recursions in (7.1). On the other hand, \mathcal{K} has non-zero elements only along its first sub-diagonal and has the form:

$$\mathcal{K} = \begin{pmatrix} \mathbf{0} & \mathbf{0} & \mathbf{0} & \mathbf{0} & \mathbf{0} \\ \mathcal{K}(2,1) & \mathbf{0} & \dots & \mathbf{0} & \mathbf{0} \\ \mathbf{0} & \mathcal{K}(3,2) & \dots & \mathbf{0} & \mathbf{0} \\ \vdots & \vdots & \ddots & \vdots & \vdots \\ \mathbf{0} & \mathbf{0} & \dots & \mathcal{K}(n,n-1) & \mathbf{0} \end{pmatrix} \quad (7.4)$$

\mathcal{E}_ψ has the following similar structure:

$$\mathcal{E}_\psi = \begin{pmatrix} \mathbf{0} & \mathbf{0} & \mathbf{0} & \mathbf{0} & \mathbf{0} \\ \psi(2,1) & \mathbf{0} & \dots & \mathbf{0} & \mathbf{0} \\ \mathbf{0} & \psi(3,2) & \dots & \mathbf{0} & \mathbf{0} \\ \vdots & \vdots & \ddots & \vdots & \vdots \\ \mathbf{0} & \mathbf{0} & \dots & \psi(n,n-1) & \mathbf{0} \end{pmatrix} \quad (7.5)$$

The structure of \mathcal{E}_ψ is the same as that of \mathcal{E}_ϕ and, like it, \mathcal{E}_ψ is nilpotent ($\mathcal{E}_\psi^n = \mathbf{0}$). Analogous to ϕ in (3.36), we use Lemma A.1 on page 400 to define $\psi \in \mathcal{R}^{6n \times 6n}$

$$\begin{aligned}\psi &\stackrel{\triangle}{=} (\mathbf{I} - \mathcal{E}_\psi)^{-1} = \mathbf{I} + \mathcal{E}_\psi + \mathcal{E}_\psi^2 + \cdots + \mathcal{E}_\psi^{n-1} \\ &= \begin{pmatrix} \mathbf{I} & \mathbf{0} & \cdots & \mathbf{0} \\ \psi(2,1) & \mathbf{I} & \cdots & \mathbf{0} \\ \vdots & \vdots & \ddots & \vdots \\ \psi(n,1) & \psi(n,2) & \cdots & \mathbf{I} \end{pmatrix} \quad (7.6)\end{aligned}$$

where

$$\psi(i,j) \stackrel{\triangle}{=} \psi(i,i-1) \cdots \psi(j+1,j) \quad \text{for } i > j$$

The structure of ψ is very similar to that of ϕ , and its elements have semi-group properties that can be used in the development of recursive relationships and algorithms using the lemmas from Sect. 3.5. ϕ may be viewed as the transformation operator for the composite body model (i.e., as if all the hinges are locked), and ψ as the transformation operator for the articulated body model (i.e., as if all the hinges are free).

Table 7.1 summarizes the differences and similarities between the composite rigid body model and the articulated body model for serial-chains using the above articulated body inertia operators and component level expressions from Chap. 6.

7.1.1 Some Operator Identities

Lemma 7.1 Riccati equation for articulated body inertias.

\mathcal{P} satisfies the following Riccati equation

$$\mathbf{M} = \mathcal{P} - \mathcal{E}_\psi \mathcal{P} \mathcal{E}_\psi^* = \mathcal{P} - \mathcal{E}_\psi \mathcal{P} \mathcal{E}_\phi^* \quad (7.7)$$

Proof: The first equality in (7.7) is merely a restatement in stacked notation of the following recursive component-wise definition of the $\mathcal{P}(k)$ matrices from (6.30)

$$\mathcal{P}(k+1) \stackrel{6.29}{=} \psi(k+1,k) \mathcal{P}(k) \psi^*(k+1,k) + \mathbf{M}(k+1)$$

Moreover,

$$\mathcal{E}_\psi \mathcal{P} \mathcal{E}_\psi^* \stackrel{7.3}{=} \mathcal{E}_\psi \mathcal{P} \bar{\tau}^* \mathcal{E}_\phi^* \stackrel{7.3}{=} \mathcal{E}_\psi \bar{\tau} \mathcal{P} \mathcal{E}_\phi^* \stackrel{7.3}{=} \mathcal{E}_\phi \bar{\tau} \bar{\tau} \mathcal{P} \mathcal{E}_\phi^* = \mathcal{E}_\psi \mathcal{P} \mathcal{E}_\phi^*$$

Using this in the first equality in (7.7) leads to the second equality. ■

Table 7.1 Comparison between composite and articulated body models, while ignoring the Coriolis and gyroscopic terms

Variable	Composite body	Articulated body
Relative hinge acceleration α	$\ddot{\theta}$ $\phi^* H^* \ddot{\theta}$	γ $\psi^* H^* \gamma$
$\alpha(k)$ α with respect to α^+	$\phi^*(k+1, k) \alpha(k+1) + H^*(k) \ddot{\theta}(k)$ $\alpha^+ + H^* \ddot{\theta}$	$\psi^*(k+1, k) \alpha(k+1) + H^*(k) \gamma(k)$ $\bar{\tau}^* \alpha^+ + H^* \gamma$ ($\bar{\tau}^* \alpha = \bar{\tau}^* \alpha^+$)
γ	$\mathcal{G}^* \alpha^+ + \ddot{\theta}$	$\mathcal{G}^* \alpha$
Effective inertia Relationship to M	\mathcal{R} $\mathcal{R} - \mathcal{E}_\phi \mathcal{R} \mathcal{E}_\phi^*$	\mathcal{P} $\mathcal{P} - \mathcal{E}_\psi \mathcal{P} \mathcal{E}_\psi^*$
Inertia recursions	$\mathcal{R}^+(k) = \mathcal{R}(k)$ $\mathcal{R}(k+1) = \phi(k+1, k) \mathcal{R}^+(k) \phi^*(k+1, k) + M(k)$	$\mathcal{P}^+(k+1) = \bar{\tau}(k) \mathcal{P}(k) \bar{\tau}^*(k)$ $\mathcal{P}(k+1) = \phi(k+1, k) \mathcal{P}^+(k) \phi^*(k+1, k) + M(k)$
f on (- side) Correction force (- side)	$\mathcal{R} \alpha + y$ $y = \tilde{\phi} \mathcal{R} H^* \ddot{\theta}$	$\mathcal{P} \alpha + \delta$ $\delta = \tilde{\phi} \mathcal{P} H^* \gamma$
f on + side Correction force (+ side)	$\mathcal{R}^+ \alpha^+ + y^+$ $y^+ = y + \mathcal{R} H^* \ddot{\theta}$	$\mathcal{P}^+ \alpha^+ + \delta^+$ $\delta^+ = \delta + \mathcal{P} H^* \gamma$

Extensions of the Riccati equation in Lemma 7.1, and the operator identities in Lemma 7.2 for general multibody systems, are discussed in Sect. 9.4. Now, we establish several operator identities that will be needed later in this chapter.

Lemma 7.2 Useful spatial operator identities.

1.

$$\tilde{\psi} \stackrel{\triangle}{=} \psi \mathcal{E}_\psi = \mathcal{E}_\psi \psi = \psi - \mathbf{I} \quad (7.8)$$

2.

$$\psi \mathbf{M} \psi^* = \mathcal{P} + \tilde{\psi} \mathcal{P} + \mathcal{P} \tilde{\psi}^* \quad (7.9)$$

3.

$$\psi^{-1} - \phi^{-1} = \mathcal{K} \mathcal{H} \quad (7.10)$$

4.

$$\begin{aligned} \psi^{-1} \phi &= \mathbf{I} + \mathcal{K} \mathcal{H} \phi \\ \phi \psi^{-1} &= \mathbf{I} + \phi \mathcal{K} \mathcal{H} \\ \phi^{-1} \psi &= \mathbf{I} - \mathcal{K} \mathcal{H} \psi \\ \psi \phi^{-1} &= \mathbf{I} - \psi \mathcal{K} \mathcal{H} \end{aligned} \quad (7.11)$$

5.

$$\begin{aligned} [\mathbf{I} - \mathcal{H} \psi \mathcal{K}] \mathcal{H} \phi &= \mathcal{H} \psi \\ \phi \mathcal{K} [\mathbf{I} - \mathcal{H} \psi \mathcal{K}] &= \psi \mathcal{K} \\ [\mathbf{I} + \mathcal{H} \phi \mathcal{K}] \mathcal{H} \psi &= \mathcal{H} \phi \\ \psi \mathcal{K} [\mathbf{I} + \mathcal{H} \phi \mathcal{K}] &= \phi \mathcal{K} \end{aligned} \quad (7.12)$$

6.

$$\mathcal{H} \psi \mathbf{M} \psi^* \mathcal{H}^* = \mathcal{D} \quad (7.13)$$

Proof:

1. The proof is identical to that of (3.41) in Exercise 3.6 except that we now work with ψ and \mathcal{E}_ψ instead of ϕ and \mathcal{E}_ϕ .
2. Pre- and post-multiplying (7.7) by ψ and ψ^* we have

$$\begin{aligned} \psi \mathbf{M} \psi^* &= \psi \mathcal{P} \psi^* - \psi \mathcal{E}_\psi \mathcal{P} \mathcal{E}_\psi^* \psi^* \stackrel{7.8}{=} (\tilde{\psi} + \mathbf{I}) \mathcal{P} (\tilde{\psi} + \mathbf{I})^* - \tilde{\psi} \mathcal{P} \tilde{\psi}^* \\ &= \mathcal{P} + \tilde{\psi} \mathcal{P} + \mathcal{P} \tilde{\psi}^* \end{aligned}$$

3. From (7.6),

$$\begin{aligned} \psi^{-1} &= \mathbf{I} - \mathcal{E}_\psi \stackrel{7.3}{=} \mathbf{I} - \mathcal{E}_\phi \bar{\tau} \stackrel{7.3}{=} (\mathbf{I} - \mathcal{E}_\phi) + \mathcal{E}_\phi \tau \\ &\stackrel{3.36, 7.3}{=} \phi^{-1} + \mathcal{E}_\phi \mathcal{G} \mathcal{H} \stackrel{7.3}{=} \phi^{-1} + \mathcal{K} \mathcal{H} \end{aligned}$$

4. Pre- and post-multiplying (7.10) by ϕ leads to the first pair of identities. Repeating the process, using ψ , leads to the latter pair.

5. We have

$$[\mathbf{I} - \mathbf{H}\psi\mathcal{K}]\mathbf{H}\phi = \mathbf{H}[\mathbf{I} - \psi\mathcal{K}\mathbf{H}]\phi \stackrel{7.11}{=} \mathbf{H}(\psi\phi^{-1})\phi = \mathbf{H}\psi$$

Similar use of the other identities in (7.11) leads to the remaining ones in (7.12).

6. We have

$$\begin{aligned} \mathbf{H}\psi\mathbf{M}\psi^*\mathbf{H}^* &\stackrel{7.7}{=} \mathbf{H}(\mathcal{P} + \tilde{\psi}\mathcal{P} + \mathcal{P}\tilde{\psi}^*)\mathbf{H}^* \stackrel{7.3}{=} \mathcal{D} + \mathbf{H}\tilde{\psi}\mathcal{P}\mathbf{H}^* + \mathbf{H}\mathcal{P}\tilde{\psi}^*\mathbf{H}^* \\ &\stackrel{7.8}{=} \mathcal{D} + \mathbf{H}\psi\mathcal{E}_\psi\mathcal{P}\mathbf{H}^* + \mathbf{H}\mathcal{P}\mathcal{E}_\psi^*\psi^*\mathbf{H}^* \\ &\stackrel{7.3}{=} \mathcal{D} + \mathbf{H}\psi\mathcal{E}_\phi\bar{\tau}\mathcal{P}\mathbf{H}^* + \mathbf{H}\bar{\tau}^*\mathcal{E}_\phi^*\psi^*\mathbf{H}^* \\ &\stackrel{7.3}{=} \mathcal{D} + \mathbf{H}\psi\mathcal{E}_\phi\mathcal{P}^+\mathbf{H}^* + \mathbf{H}\mathcal{P}^+\mathcal{E}_\phi^*\psi^*\mathbf{H}^* \\ &\stackrel{6.26}{=} \mathcal{D} \end{aligned}$$

■

7.1.2 Innovations Operator Factorization of the Mass Matrix

The following lemma establishes a new operator factorization, referred to as the **Innovations Operator Factorization** of the serial-chain mass matrix, \mathcal{M} .

Lemma 7.3 Innovations operator factorization of the mass matrix.

The mass matrix, \mathcal{M} , has the following square factorization, referred to as the Innovations Operator Factorization:

$$\mathcal{M} = [\mathbf{I} + \mathbf{H}\phi\mathcal{K}]\mathcal{D}[\mathbf{I} + \mathbf{H}\phi\mathcal{K}]^* \quad (7.14)$$

Proof: We have that

$$\begin{aligned} \mathcal{M} &\stackrel{5.25}{=} \mathbf{H}\phi\mathbf{M}\phi^*\mathbf{H}^* = \mathbf{H}(\phi\phi^{-1})\psi\mathbf{M}\psi^*(\phi\phi^{-1})^*\mathbf{H}^* \\ &\stackrel{7.11}{=} \mathbf{H}[\mathbf{I} + \phi\mathcal{K}\mathbf{H}]\psi\mathbf{M}\psi^*[\mathbf{I} + \phi\mathcal{K}\mathbf{H}]^*\mathbf{H}^* \\ &= [\mathbf{I} + \mathbf{H}\phi\mathcal{K}](\mathbf{H}\psi\mathbf{M}\psi^*\mathbf{H}^*)[\mathbf{I} + \mathbf{H}\phi\mathcal{K}]^* \stackrel{7.13}{=} [\mathbf{I} + \mathbf{H}\phi\mathcal{K}]\mathcal{D}[\mathbf{I} + \mathbf{H}\phi\mathcal{K}]^* \end{aligned}$$

■

The factor $[\mathbf{I} + \mathbf{H}\phi\mathcal{K}] \in \mathcal{R}^{N \times N}$ is square and block lower-triangular, while \mathcal{D} is block diagonal. Thus, the factorization in (7.14) may be thought of as an analytical block LDL* factorization of the mass matrix. This factorization is known as the Innovations Operator Factorization because of its relationship to factorization results in the innovations approach to filtering and prediction theory discussed in

Sect. 6.4 on page 111. In contrast to the Innovations Factorization, the factors in the Newton–Euler Operator Factorization of the mass matrix (5.23) are not square.

In (4.10) on page 61, we encountered the following decomposition of $\phi\mathbf{M}\phi^*$ using the composite body inertias \mathcal{R}

$$\phi\mathbf{M}\phi^* = \mathcal{R} + \tilde{\phi}\mathcal{R} + \mathcal{R}\tilde{\phi}^*$$

and in (7.9), the following decomposition of $\psi\mathbf{M}\psi^*$ using \mathcal{P}

$$\psi\mathbf{M}\psi^* = \mathcal{P} + \tilde{\psi}\mathcal{P} + \mathcal{P}\tilde{\psi}^*$$

Exercise 7.1 develops decompositions of $\phi\mathbf{M}\phi^*$ and $\phi\mathbf{M}\psi^*$ using \mathcal{P} .

Exercise 7.1 Decomposition of $\phi\mathbf{M}\phi^*$ using \mathcal{P} .

- Derive the following disjoint decomposition of $\phi\mathbf{M}\psi^*$ using the articulated body inertias:

$$\phi\mathbf{M}\psi^* = \mathcal{P} + \tilde{\phi}\mathcal{P} + \mathcal{P}\tilde{\psi}^* \quad (7.15)$$

- Also, derive the following decomposition of $\phi\mathbf{M}\phi^*$:

$$\phi\mathbf{M}\phi^* = \mathcal{P} + \tilde{\phi}\mathcal{P} + \mathcal{P}\tilde{\phi}^* + \phi\mathcal{K}\mathcal{D}\mathcal{K}^*\phi^* \quad (7.16)$$

- Use (7.16) to show that $\mathcal{R} \geq \mathcal{P}$.

■

7.1.3 Operator Inversion of the Mass Matrix

The following lemma derives an analytical expression for the inverse of $[\mathbf{I} + \mathbf{H}\phi\mathcal{K}]$.

Lemma 7.4 The operator inverse of $[\mathbf{I} + \mathbf{H}\phi\mathcal{K}]$.
 $[\mathbf{I} + \mathbf{H}\phi\mathcal{K}]$ has an operator inverse given by

$$[\mathbf{I} + \mathbf{H}\phi\mathcal{K}]^{-1} = [\mathbf{I} - \mathbf{H}\psi\mathcal{K}] \quad (7.17)$$

Proof: From the standard matrix identity $(\mathbf{I} + \mathbf{AB})^{-1} = \mathbf{I} - \mathbf{A}(\mathbf{I} + \mathbf{BA})^{-1}\mathbf{B}$ from (A.18) on page 400, we have (with $A = \mathbf{H}$ and $B = \phi\mathcal{K}$):

$$\begin{aligned} [\mathbf{I} + \mathbf{H}\phi\mathcal{K}]^{-1} &= \mathbf{I} - \mathbf{H}[\mathbf{I} + \phi\mathcal{K}\mathbf{H}]^{-1}\phi\mathcal{K} \stackrel{7.11}{=} \mathbf{I} - \mathbf{H}(\phi\psi^{-1})^{-1}\phi\mathcal{K} \\ &= \mathbf{I} - \mathbf{H}\psi\mathcal{K} \end{aligned}$$

■

Since $[\mathbf{I} + \mathbf{H}\Phi\mathcal{K}]$ is lower-triangular, it follows that so is its inverse $[\mathbf{I} - \mathbf{H}\Psi\mathcal{K}]$. By combining Lemmas 7.3 and 7.4, we obtain the following operator expression for the inverse of the mass matrix.

Lemma 7.5 Operator factorization of \mathcal{M}^{-1} .

The inverse of the mass matrix is given by the expression:

$$\mathcal{M}^{-1} = [\mathbf{I} - \mathbf{H}\Psi\mathcal{K}]^* \mathcal{D}^{-1} [\mathbf{I} - \mathbf{H}\Phi\mathcal{K}] \quad (7.18)$$

Proof: We have

$$\begin{aligned} \mathcal{M}^{-1} &\stackrel{7.14}{=} \{[\mathbf{I} + \mathbf{H}\Phi\mathcal{K}] \mathcal{D} [\mathbf{I} + \mathbf{H}\Phi\mathcal{K}]^*\}^{-1} = [\mathbf{I} + \mathbf{H}\Phi\mathcal{K}]^{-*} \mathcal{D}^{-1} [\mathbf{I} + \mathbf{H}\Phi\mathcal{K}]^{-1} \\ &\stackrel{7.4}{=} [\mathbf{I} - \mathbf{H}\Psi\mathcal{K}]^* \mathcal{D}^{-1} [\mathbf{I} - \mathbf{H}\Psi\mathcal{K}]^{-1} \end{aligned}$$

■

This result is remarkable in that it provides an explicit, analytical expression for \mathcal{M}^{-1} . The factor $[\mathbf{I} - \mathbf{H}\Psi\mathcal{K}]$ is square and block lower-triangular, while \mathcal{D}^{-1} is block diagonal. Thus, the factorization in (7.17) may be thought of as an analytical block L*DL factorization of the mass matrix inverse. The following section applies these analytical operator expressions to develop an efficient solution to the forward dynamics problem for serial-chain systems. The mass matrix operator factorization and inversion expressions described in this section are based on [71, 140, 149, 151].

7.2 Forward Dynamics

In the forward dynamics problem, the known quantities are the \mathcal{T} hinge forces and the $(\theta, \dot{\theta})$ current state, and the quantities to be computed are the $\ddot{\theta}$ hinge accelerations. Thus, this problem requires solving for the $\ddot{\theta}$ accelerations vector from the following equations of motion:

$$\mathcal{M}(\theta)\ddot{\theta} + \mathcal{C}(\theta, \dot{\theta}) = \mathcal{T} \quad (7.19)$$

given the state $(\theta, \dot{\theta})$ and the vector of generalized forces, \mathcal{T} . This is only a conceptual statement of the problem, since, typically, neither the mass matrix \mathcal{M} nor the Coriolis forces vector \mathcal{C} are available. We describe below possible approaches for solving this problem [71]:

1. The direct approach is to compute $\mathcal{M}(\theta)$ using the $O(N^2)$ composite body inertia algorithm, and the Coriolis vector $\mathcal{C}(\theta, \dot{\theta})$ using the $O(N)$ inverse dynamics procedure, and to subsequently solve the linear matrix equation in (7.19). Since solving an N -size linear matrix equation is an $O(N^3)$ procedure, this leads to a forward dynamics algorithm of overall $O(N^3)$ cost. The cubic computational cost makes this algorithm very expensive for even moderately sized systems.

2. An alternative is to take advantage of the Innovations factorization of the mass matrix

$$\mathcal{M} = [\mathbf{I} + \mathbf{H}\phi\mathcal{K}] \mathcal{D} [\mathbf{I} + \mathbf{H}\phi\mathcal{K}]^*$$

in (7.14) to develop an $O(N^2)$ forward dynamics algorithm. This is possible because, while solving a general $N \times N$ linear matrix equation is an $O(N^3)$ procedure, it is of only $O(N^2)$ complexity when the coefficient matrix happens to be triangular. Once again, assuming that \mathcal{C} has already been computed and is available, the $O(N^2)$ forward dynamics procedure involves the successive solution of two triangular systems of equations outlined in the following steps [155]:

- Compute the $[\mathbf{I} + \mathbf{H}\phi\mathcal{K}]$ matrix.
- Solve $[\mathbf{I} + \mathbf{H}\phi\mathcal{K}]x = \mathcal{T} - \mathcal{C}$ for x .
- Solve $[\mathbf{I} + \mathbf{H}\phi\mathcal{K}]^* \ddot{\theta} = \mathcal{D}^{-1}x$ for $\ddot{\theta}$.

In contrast with the $O(N^3)$ methods discussed above, this method requires the explicit computation of the articulated body inertia quantities and the $[\mathbf{I} + \mathbf{H}\phi\mathcal{K}]$ factor, but does not require the explicit computation of the mass matrix itself. Thus, the development of the Innovations Operator Factorization has paid off in reducing the computational cost of the forward dynamics problem from $O(N^3)$ to $O(N^2)$ computational cost.

3. The following section describes an even lower order algorithm for solving the forward dynamics problem, that takes advantage of the analytical expression for the mass matrix inverse in Lemma 7.5.

7.2.1 $O(N)$ AB Forward Dynamics Algorithm

We now develop an optimal $O(N)$ forward dynamics algorithm based on the expression for the mass matrix inverse derived in Lemma 7.5. Using this lemma in (7.19) leads to the following operator expression for $\ddot{\theta}$:

$$\ddot{\theta} = \mathcal{M}^{-1}(\mathcal{T} - \mathcal{C}) = [\mathbf{I} - \mathbf{H}\psi\mathcal{K}]^* \mathcal{D}^{-1} [\mathbf{I} - \mathbf{H}\psi\mathcal{K}] (\mathcal{T} - \mathcal{C}) \quad (7.20)$$

The following lemma derives a simpler form of (7.20).

Lemma 7.6 Operator expression for the generalized accelerations $\ddot{\theta}$.
The operator expression for $\ddot{\theta}$ is given by

$$\ddot{\theta} = [\mathbf{I} - \mathbf{H}\psi\mathcal{K}]^* \mathcal{D}^{-1} [\mathcal{T} - \mathbf{H}\psi(\mathcal{K}\mathcal{T} + \mathcal{P}\mathbf{a} + \mathbf{b})] - \mathcal{K}^* \psi^* \mathbf{a} \quad (7.21)$$

Proof: We have

$$\begin{aligned} \ddot{\theta} &\stackrel{7.20}{=} [\mathbf{I} - \mathbf{H}\psi\mathcal{K}]^* \mathcal{D}^{-1} [\mathbf{I} - \mathbf{H}\psi\mathcal{K}] (\mathcal{T} - \mathcal{C}) \\ &\stackrel{5.25}{=} [\mathbf{I} - \mathbf{H}\psi\mathcal{K}]^* \mathcal{D}^{-1} [\mathbf{I} - \mathbf{H}\psi\mathcal{K}] \{ \mathcal{T} - \mathbf{H}\phi(\mathbf{M}\phi^* \mathbf{a} + \mathbf{b}) \} \\ &= [\mathbf{I} - \mathbf{H}\psi\mathcal{K}]^* \mathcal{D}^{-1} [\mathbf{I} - \mathbf{H}\psi\mathcal{K}] \mathcal{T} \\ &\quad - [\mathbf{I} - \mathbf{H}\psi\mathcal{K}]^* \mathcal{D}^{-1} [\mathbf{I} - \mathbf{H}\psi\mathcal{K}] \mathbf{H}\phi(\mathbf{M}\phi^* \mathbf{a} + \mathbf{b}) \end{aligned} \quad (7.22)$$

Now,

$$\begin{aligned} & [\mathbf{I} - \mathbf{H}\psi\mathcal{K}] \mathbf{H}\phi(\mathbf{M}\phi^*\mathbf{a} + \mathbf{b}) \\ & \stackrel{7.12}{=} \mathbf{H}\psi(\mathbf{M}\phi^*\mathbf{a} + \mathbf{b}) \stackrel{7.15}{=} \mathbf{H}(\{\psi\mathcal{P} + \mathcal{P}\tilde{\phi}^*\}\mathbf{a} + \psi\mathbf{b}) \\ & \stackrel{7.3}{=} (\mathbf{H}\psi\mathcal{P} + \mathcal{D}\mathcal{K}^*\phi^*)\mathbf{a} + \mathbf{H}\psi\mathbf{b} = \mathbf{H}\psi(\mathcal{P}\mathbf{a} + \mathbf{b}) + \mathcal{D}\mathcal{K}^*\phi^*\mathbf{a} \end{aligned} \quad (7.23)$$

Using this in the second half of (7.22), it follows that

$$\begin{aligned} & [\mathbf{I} - \mathbf{H}\psi\mathcal{K}]^*\mathcal{D}^{-1}[\mathbf{I} - \mathbf{H}\psi\mathcal{K}] \mathbf{H}\phi(\mathbf{M}\phi^*\mathbf{a} + \mathbf{b}) \\ & \stackrel{7.23}{=} [\mathbf{I} - \mathbf{H}\psi\mathcal{K}]^*\mathcal{D}^{-1}[\mathbf{H}\psi(\mathcal{P}\mathbf{a} + \mathbf{b}) + \mathcal{D}\mathcal{K}^*\phi^*\mathbf{a}] \\ & \stackrel{7.11}{=} [\mathbf{I} - \mathbf{H}\psi\mathcal{K}]^*\mathcal{D}^{-1}\mathbf{H}\psi(\mathcal{P}\mathbf{a} + \mathbf{b}) + \mathcal{K}^*\psi^*\mathbf{a} \end{aligned} \quad (7.24)$$

Using this in (7.22) leads to (7.21). ■

Now group together sub-expressions in (7.21) to define intermediate quantities as shown below:

$$\begin{aligned} \ddot{\theta} &= [\mathbf{I} - \mathbf{H}\psi\mathcal{K}]^*\mathcal{D}^{-1}[\mathcal{T} - \underbrace{\mathbf{H}\psi(\mathcal{K}\mathcal{T} + \mathcal{P}\mathbf{a} + \mathbf{b})}_{\mathfrak{z}}] - \mathcal{K}^*\psi^*\mathbf{a} \\ &\quad \underbrace{\mathcal{E}}_{\mathfrak{v}} \end{aligned}$$

Using these intermediate quantities, (7.21) can be re-expressed as

$$\mathfrak{z} \triangleq \psi(\mathcal{K}\mathcal{T} + \mathcal{P}\mathbf{a} + \mathbf{b}) \quad (7.25a)$$

$$\epsilon \triangleq \mathcal{T} - \mathbf{H}\mathfrak{z} \stackrel{7.25a}{=} \mathcal{T} - \mathbf{H}\psi(\mathcal{K}\mathcal{T} + \mathcal{P}\mathbf{a} + \mathbf{b}) \quad (7.25b)$$

$$\mathfrak{v} \triangleq \mathcal{D}^{-1}\epsilon \stackrel{7.25b}{=} \mathcal{D}^{-1}[\mathcal{T} - \mathbf{H}\psi(\mathcal{K}\mathcal{T} + \mathcal{P}\mathbf{a} + \mathbf{b})] \quad (7.25c)$$

$$\ddot{\theta} \stackrel{7.21, 7.25c}{=} [\mathbf{I} - \mathbf{H}\psi\mathcal{K}]^*\mathfrak{v} - \mathcal{K}^*\psi^*\mathbf{a} \quad (7.25d)$$

The following exercise introduces the new \mathfrak{z}^+ term to further simplify the expression for \mathfrak{z} .

Exercise 7.2 Expression relating \mathfrak{z} and \mathfrak{z}^+ .

1. Derive the following operator expressions for \mathfrak{z} that are an alternative to (7.25a):

$$\mathfrak{z} = \phi[\mathcal{K}\epsilon + \mathcal{P}\mathbf{a} + \mathbf{b}] \quad (7.26)$$

2. With \mathfrak{z}^+ defined as

$$\mathfrak{z}^+ \triangleq \mathfrak{z} + \mathcal{G}\epsilon \quad (7.27)$$

show that

$$\mathfrak{z} = \mathcal{E}_\phi \mathfrak{z}^+ + \mathcal{P}\mathbf{a} + \mathbf{b} \quad (7.28)$$

3. Show that

$$\mathfrak{z}^+ \triangleq \phi[\mathcal{G}\epsilon + \mathcal{P}\alpha + \mathfrak{b}] \quad (7.29)$$

■

Exercise 7.3 Expression for α in terms of ν .

We have from (5.23) that $\alpha = \phi^*(H^*\ddot{\theta} + \mathfrak{a})$. Derive the following alternative expression for α :

$$\alpha = \psi(H^*\nu + \mathfrak{a}) \quad (7.30)$$

Furthermore, show that the generalized and innovations accelerations are related to each other by the following expressions:

$$\ddot{\theta} = \nu - \mathcal{K}^* \alpha = \nu - \mathcal{G}^* \alpha^+ \text{ where } \alpha^+ \triangleq \text{col} \left\{ \alpha^+(k) \right\}_{k=1}^n \stackrel{6.9}{=} \mathcal{E}_\phi^* \alpha \quad (7.31)$$

■

Observe that the (ψ^*, ν) pair play a very similar role to $(\phi^*, \ddot{\theta})$ in the expression for the α spatial accelerations. We can think of the former pair as corresponding to the articulated body inertia model while the latter pair corresponds to the composite body model. Due to these parallels, we refer to ν as the **innovations accelerations** for the system.

The operator expressions in (7.25) can be simplified using Exercises 7.2 and 7.3 as follows:

$$\mathfrak{z} \stackrel{7.28}{=} \mathcal{E}_\phi \mathfrak{z}^+ + \mathcal{P}\alpha + \mathfrak{b} \quad (7.32a)$$

$$\mathfrak{z}^+ \stackrel{7.27}{=} \mathfrak{z} + \mathcal{G}\epsilon \quad (7.32b)$$

$$\epsilon \stackrel{7.25b}{=} \mathcal{T} - H\mathfrak{z} \quad (7.32c)$$

$$\nu \stackrel{7.25c}{=} \mathcal{D}^{-1}\epsilon \quad (7.32d)$$

$$\alpha^+ = \mathcal{E}_\phi^* \alpha \quad (7.32e)$$

$$\ddot{\theta} \stackrel{7.31}{=} \nu - \mathcal{G}^* \alpha^+ \quad (7.32f)$$

$$\alpha = \alpha^+ + H^* \ddot{\theta} + \mathfrak{a} \quad (7.32g)$$

These expressions are essentially stacked vector representations of the corresponding component link terms (e.g. $\mathfrak{z}(k)$, $\epsilon(k)$) introduced in the discussion of the articulated body model in Chap. 6. The equivalence is complete except that the above expressions are more general; they allow non-zero velocities and include the \mathfrak{a} and \mathfrak{b} terms.

The operator expressions in (7.32) can be converted into recursive computational algorithms without requiring the explicit computation of the component operators using lemmas from Sect. 3.5 on page 51. The resulting $O(N)$ articulated body (AB) forward dynamics procedure is described in Algorithm 7.1 [47, 139].

Algorithm 7.1 The $O(N)$ AB forward dynamics algorithm

```

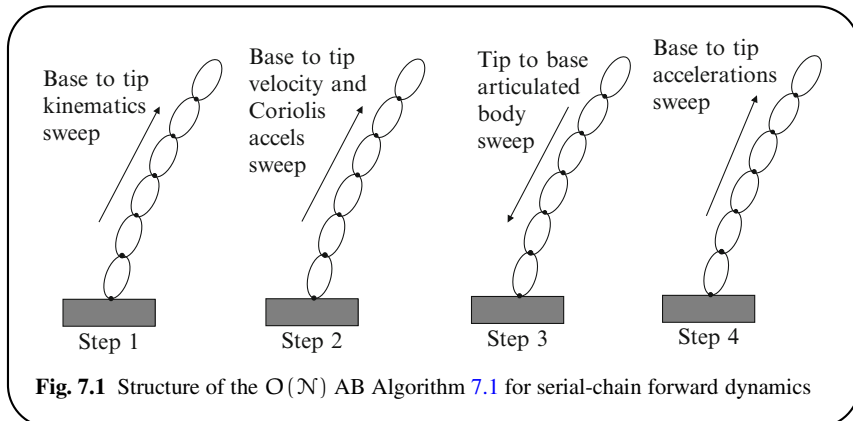
 $\mathcal{P}^+(0) = \mathbf{0}, \quad \mathfrak{z}^+(0) = \mathbf{0}, \quad \mathcal{T}(0) = \mathbf{0}, \quad \bar{\tau}(0) = \mathbf{0}$ 
for  $k = 1 \dots n$ 
   $\mathcal{P}(k) = \phi(k, k-1)\mathcal{P}^+(k-1)\phi^*(k, k-1) + M(k)$ 
   $\mathcal{D}(k) = H(k)\mathcal{P}(k)H^*(k)$ 
   $\mathcal{G}(k) = \mathcal{P}(k)H^*(k)\mathcal{D}^{-1}(k)$ 
   $\bar{\tau}(k) = I - \mathcal{G}(k)H(k)$ 
   $\mathcal{P}^+(k) = \bar{\tau}(k)\mathcal{P}(k)$ 
   $\mathfrak{z}(k) = \phi(k, k-1)\mathfrak{z}^+(k-1) + \mathcal{P}(k)a(k) + b(k)$ 
   $\epsilon(k) = \mathcal{T}(k) - H(k)\mathfrak{z}(k)$ 
   $v(k) = \mathcal{D}^{-1}(k)\epsilon(k)$ 
   $\mathfrak{z}^+(k) = \mathfrak{z}(k) + \mathcal{G}(k)\epsilon(k)$ 
end loop

 $\alpha(n+1) = \mathbf{0}$ 
for  $k = n \dots 1$ 
   $\alpha^+(k) = \phi^*(k+1, k)\alpha(k+1)$ 
   $\ddot{\theta}(k) = v(k) - \mathcal{G}^*(k)\alpha^+(k)$ 
   $\alpha(k) = \alpha^+(k) + H^*(k)\ddot{\theta}(k) + a(k)$ 
end loop

```

The first tip-to-base recursive sweep contains steps for computing the $\mathcal{P}(.)$ s and $\mathfrak{z}(.)$ s articulated body inertia quantities discussed in Chap. 6. One difference here is in the computation of the $\mathfrak{z}(.)$ terms, since we no longer assume that the system is at rest. These steps now include contributions from the $a(k)$ Coriolis acceleration and $b(k)$ gyroscopic force terms. The second sweep is a base-to-tip recursion that uses the $v(k)$, and other terms computed in the first sweep, to compute the hinge and spatial accelerations for all the links. Referring back to the parallels with time-domain, optimal filtering discussed in Sect. 6.4, the steps in the tip-to-base recursion are analogous to the steps in an optimal filter recursion for computing state estimates. Similarly, the steps in the base-to-tip Step 4 recursion are analogous to the steps in an optimal smoother recursion for computing smoothed state estimates.

The Steps 1 and 2 sweeps shown in the illustration of the forward dynamics algorithm in Fig. 7.1 compute the kinematic velocity dependent Coriolis and gyroscopic terms for all the bodies in base-to-tip recursions. This pair of sweeps can be combined into a single base-to-tip sweep. The AB algorithm recursions are shown as Steps 3 and 4 in the figure.



The AB algorithm has $O(N)$ computational cost because the cost of each of the steps in the above algorithm is fixed, and the steps are carried out n times during the course of the algorithm. The AB algorithm the fastest forward dynamics algorithm for systems with greater than 6–8 bodies. A detailed discussion of the computational costs and issues for the AB algorithm can be found in Featherstone [51]. In addition, the AB algorithm is also numerically more robust compared with alternatives [13], a well known feature of Kalman filtering techniques as well.

This forward dynamics algorithm does not require the explicit computation of either \mathcal{M} or \mathcal{C} . Indeed, it does not require the explicit computation of any of the spatial operators. This is another illustration of the ease with which operator-level manipulations can be used to establish key identities and results. At a later stage, when the time for computations arises, these results can be mapped into highly efficient computational algorithms.

The general version of the AB algorithm was originally derived from first principles in Featherstone [47]. Rodriguez [139] derived the same algorithm using spatial operator methods exploiting the mathematical parallels from optimal estimation theory. Several other notable variations of the AB forward dynamics algorithm have been published in the literature [6, 10, 16, 28, 154, 156, 178]. A comparison of several of these techniques is described in Jain [71]. Other approaches to solving the forward dynamics algorithm are described in [23, 56, 89, 113, 115].

Exercise 7.4 Relationship between ν , α and a .

Establish the following relationships:

$$\begin{aligned}\alpha &= \bar{\tau}^* \alpha^+ + H^* \nu + a \\ \nu &= G^* [\alpha - a]\end{aligned}\tag{7.33}$$

Observe that the latter expression is similar to the one in Exercise 6.5 on page 111. ■

An interesting application of the mass matrix operator factorization and inversion technique, together with the AB algorithm, to the problem of computing the inverse of manipulator Jacobian matrix, \mathcal{J} is discussed in Rodriguez and Scheid [150].

7.3 Extensions to the Forward Dynamics Algorithm

Having developed the basic AB forward dynamics algorithm, we now look at some related issues and extensions to the algorithm.

7.3.1 Computing Inter-Link \mathfrak{f} Spatial Forces

The AB forward dynamics algorithm described in the previous section does not explicitly compute the $f(k)$ body interaction spatial forces. These forces may be required in certain situations. One option is to use the body spatial acceleration computed in the forward dynamics algorithm to run the second tip-to-base recursion in the Newton–Euler inverse dynamics algorithm (Algorithm 5.2) to compute these spatial forces. The following exercise describes a better alternative based on the articulated body model that avoids the additional recursion and allows us to directly compute $f(k)$ for any link, as needed.

Exercise 7.5 Computing inter-link spatial force $f(k)$.

Show that the inter-link spatial forces f are given by:

$$f = \mathcal{P}(\alpha - a) + z = \mathcal{P}^+ \alpha^+ + z^+ \quad (7.34)$$

■

These expressions are generalizations of the force decompositions discussed in Sect. 6.3 for the articulated body model that assumed zero generalized velocities. They provide a direct way to compute the inter-link spatial forces, without the need for additional recursions, once α and z from the forward dynamics solution are available.

7.3.2 Including Gravitational Accelerations

Exercise 5.4 on page 87 shows that a uniform gravitational field represented by a $g = \begin{bmatrix} 0 \\ g_1 \end{bmatrix}$ linear gravitational spatial acceleration vector can be included in the equations of motion as a pseudo spatial acceleration at the base-body. The more general expression for $C(\theta, \dot{\theta})$ that includes the gravity term (see (5.39) on page 87) is:

$$\mathcal{C}(\theta, \dot{\theta}) = H\phi [M\phi^*(a + E^*g) + b] \quad (7.35)$$

with E defined by (4.14). The following exercise derives the generalizations of the AB forward dynamics algorithm to accommodate gravitational accelerations.

Exercise 7.6 Including gravitational accelerations.

Assume that the system is under the influence of a uniform, linear gravitational acceleration field g .

1. Show that the updated expression for (7.21) with gravity included is as follows:

$$\ddot{\theta} = [I - H\psi K]^* \{ D^{-1} [T - H\psi(KT + Pa + b)] - G^* \bar{E}^* g \} - K^* \psi^* a \quad (7.36)$$

where \bar{E} is defined by (5.40).

2. Define \bar{v} as

$$\bar{v} \triangleq v - G^* \bar{E}^* g \quad (7.37)$$

Show that the altered forms of (7.30) and (7.31) are as follows:

$$\alpha = \psi^* (H^* \bar{v} + a) \quad (7.38a)$$

$$\ddot{\theta} = [I - H\psi K]^* \bar{v} - K^* \psi^* a \quad (7.38b)$$

$$= \bar{v} - G^* \alpha^+ \quad (7.38c)$$

3. Derive the following new version of (7.33):

$$\begin{aligned} \alpha &= \bar{T}^* \alpha^+ + H^* \bar{v} + a \\ \bar{v} &= G^* [\alpha - a] \end{aligned} \quad (7.39)$$

4. Derive the following new version of the force decomposition relationships in (7.34):

$$f = P(\alpha + \bar{E}^* g - a) + z = P^+(\alpha^+ + \bar{E}^* g) + z^+ \quad (7.40)$$

5. Show that the forward dynamics step for $\ddot{\theta}(k)$ in Algorithm 7.1 needs to be modified as follows to handle the gravitational acceleration:

$$\ddot{\theta}(k) = \bar{v}(k) - G^*(k) \alpha^+(k) \quad (7.41)$$



7.3.3 Including External Forces

External forces at nodes on the bodies can be incorporated directly into the forward dynamics algorithm as well. Using (5.32), one approach is to absorb the external forces on the k th link into the $z(k)$ term. Thus, the external forces can be incorporated into the $z(k)$ expression in Algorithm 7.1 by altering it as follows:

$$\begin{aligned}\mathfrak{z}(k) = & \phi(k, k-1)\mathfrak{z}^+(k-1) + \mathcal{P}(k)\mathfrak{a}(k) + \mathfrak{b}(k) \\ & - \sum_i \phi(\mathbb{B}_k, \mathbb{O}_k^i) f_{ext}^i(k)\end{aligned}\quad (7.42)$$

The general version of Algorithm 7.1, extended to handle gravity and external forces, is shown in Algorithm 7.2.

Algorithm 7.2 The generalized $O(N)$ AB forward dynamics algorithm

```

 $\mathcal{P}^+(0) = \mathbf{0}, \quad \mathfrak{z}^+(0) = \mathbf{0}, \quad \mathcal{T}(0) = \mathbf{0}, \quad \bar{\tau}(0) = \mathbf{0}$ 
for  $k = 1 \dots n$ 
   $\mathcal{P}(k) = \phi(k, k-1)\mathcal{P}^+(k-1)\phi^*(k, k-1) + M(k)$ 
   $\mathcal{D}(k) = H(k)\mathcal{P}(k)H^*(k)$ 
   $\mathcal{G}(k) = \mathcal{P}(k)H^*(k)\mathcal{D}^{-1}(k)$ 
   $\bar{\tau}(k) = I - \mathcal{G}(k)H(k)$ 
   $\mathcal{P}^+(k) = \bar{\tau}(k)\mathcal{P}(k)$ 
   $\mathfrak{z}(k) = \phi(k, k-1)\mathfrak{z}^+(k-1) + \mathcal{P}(k)\mathfrak{a}(k) + \mathfrak{b}(k) - \sum_i \phi(\mathbb{B}_k, \mathbb{O}_k^i) f_{ext}^i(k)$ 
   $\epsilon(k) = \mathcal{T}(k) - H(k)\mathfrak{z}(k)$ 
   $\nu(k) = \mathcal{D}^{-1}(k)\epsilon(k)$ 
   $\mathfrak{z}^+(k) = \mathfrak{z}(k) + \mathcal{G}(k)\epsilon(k)$ 
end loop

 $\alpha(n+1) = \mathbf{0}$ 
for  $k = n \dots 1$ 
   $\alpha^+(k) = \phi^*(k+1, k)\alpha(k+1)$ 
   $\bar{v}(k) = \nu(k) - \mathcal{G}^*(k)\mathfrak{g}$ 
   $\ddot{\theta}(k) = \bar{v}(k) - \mathcal{G}^*(k)\alpha^+(k)$ 
   $\alpha(k) = \alpha^+(k) + H^*(k)\ddot{\theta}(k) + \mathfrak{a}(k)$ 
end loop
```

7.3.4 Including Implicit Constraint Forces

For constrained system dynamics (discussed in Chap. 11), the system is subject to constraint forces at constrained nodes on the bodies. These constraint forces are

implicitly defined, and their value is determined based on the “free” generalized acceleration values, $\ddot{\theta}_f$, obtained by using the forward dynamics algorithm on the unconstrained system. Once the constraint forces are known, it is necessary to determine the “correction” generalized accelerations, $\ddot{\theta}_\delta$, resulting from the constraint forces. The full constrained dynamics solution for the $\ddot{\theta}$ generalized accelerations is given by

$$\ddot{\theta} = \ddot{\theta}_f + \ddot{\theta}_\delta$$

with

$$\ddot{\theta}_f = \mathcal{M}^{-1}(\mathcal{T} - \mathcal{C}) \quad \text{and} \quad \ddot{\theta}_\delta = -\mathcal{M}^{-1}\mathcal{J}^*\mathbf{f}_c \quad (7.43)$$

Here \mathbf{f}_c denotes the implicit constraint forces at nodes on the bodies. The discussion of the methods to compute \mathbf{f}_c are deferred until Chap. 11. It is assumed here that it has been computed and is available. The objective here is to derive a relationship between the constraint forces and the $\ddot{\theta}_\delta$ correction generalized accelerations resulting from them. Now,

$$\begin{aligned} \ddot{\theta}_\delta &\stackrel{7.43}{=} -(\mathbf{I} - \mathbf{H}\psi\mathcal{K})^*\mathcal{D}^{-1}(\mathbf{I} - \mathbf{H}\psi\mathcal{K})\mathbf{H}\phi\mathcal{B}\mathbf{f}_c \\ &\stackrel{7.12}{=} -(\mathbf{I} - \mathbf{H}\psi\mathcal{K})^*\mathcal{D}^{-1}\mathbf{H}\psi\mathcal{B}\mathbf{f}_c \end{aligned} \quad (7.44)$$

Equation (7.44) provides an expression for $\ddot{\theta}_\delta$ in terms of the constraint forces. Based on this expression, an $O(N)$ procedure for computing $\ddot{\theta}_\delta$ is shown in Algorithm 7.3. The algorithm begins with a tip-to-base recursion, followed by a base-to-tip recursion, to compute the correction generalized accelerations.

Algorithm 7.3 Correction $\ddot{\theta}^\delta$ accelerations for constraint forces

```


$$\left\{ \begin{array}{l} \mathbf{z}_\delta(0) = \mathbf{0} \\ \mathbf{for} \ k = 1 \cdots n \\ \quad \mathbf{z}_\delta(k) = \psi(k, k-1)\mathbf{z}_\delta(k-1) - \sum_i \phi(\mathbb{B}_k, \mathbb{O}_k^i)\mathbf{f}_c^i(k) \\ \quad \mathbf{v}(k) = -\mathcal{D}^{-1}(k)\mathbf{H}(k)\mathbf{z}_\delta(k) \\ \mathbf{end loop} \\ \mathbf{lambda}(n+1) = \mathbf{0} \\ \mathbf{for} \ k = n \cdots 1 \\ \quad \lambda(k) = \psi^*(k+1, k)\lambda(k+1) + \mathbf{H}^*(k)\mathbf{v}(k) \\ \quad \ddot{\theta}_\delta(k) = \mathbf{v}(k) - \mathcal{K}^*(k+1, k)\lambda(k+1) \\ \mathbf{end loop} \end{array} \right.$$


```

Part II

General Multibody Systems

Chapter 8

Graph Theory Connections

So far, we have studied the kinematics and dynamics of serial-chain multibody systems. Key developments have included the introduction of stacked vectors and spatial operators, such as ϕ , to provide succinct descriptions of the system level relationships. The spatial operators led to analytical developments, such as the Innovations Factorization of the mass matrix, and analytical expressions for the mass matrix inverse. These results also formed the basis for efficient computational algorithms for the system mass matrix, and for solving the inverse and forward dynamics problems.

Associated with multibody systems are directed graphs that describe the topology of the system and play an important role in formulating their dynamics. In this chapter, we begin exploring concepts from graph theory that allow us to generalize the spatial operator formulation to the broader class of multibody systems.

8.1 Directed Graphs and Trees

We begin with an overview of terminology and concepts from graph theory. A **graph** is a collection of **nodes**, and **edges** connecting pairs of nodes. A **directed graph** (also known as a **digraph**) is a graph where the edges have direction, i.e., an edge from one node to another is not the same as an edge in the reverse direction [183]. Each edge in a digraph defines a parent/child relationship between the node pair of that edge. Nodes defining an edge are said to be **adjacent** nodes. The node from which the edge emanates is referred to as the **parent node**, and the destination node is said to be the **child node**. The set of parent nodes of the k^{th} node is denoted $\mathcal{P}(k)$, and the set of its children nodes is $\mathcal{C}(k)$. Nodes without parent nodes are referred to as **root nodes**. Digraphs can have zero, one, or multiple root nodes. We assume that there is at most a single edge in the same direction between any pair of nodes, i.e., parallel edges between a pair of nodes are not allowed.

A node, j , is said to be the **ancestor** of another node, i , if there is a directed path from the node j to the node i . We use the notation $i \prec j$ (or equivalently $j \succ i$) to

indicate that node j is an ancestor of node i . The notation $i \not\prec j$ implies that node j is not an ancestor of node i . Node i is said to be the **descendant** of node j if j is an ancestor of node i . A pair of nodes, i and j , are said to be **related** if one of them is the ancestor of the other; otherwise they are said to be **unrelated**.

Figure 8.1 shows a taxonomy for graphs and digraphs adapted from Ramoni [137]. We briefly describe the left branch of this classification hierarchy in increasing order of specialization [38, 184]:

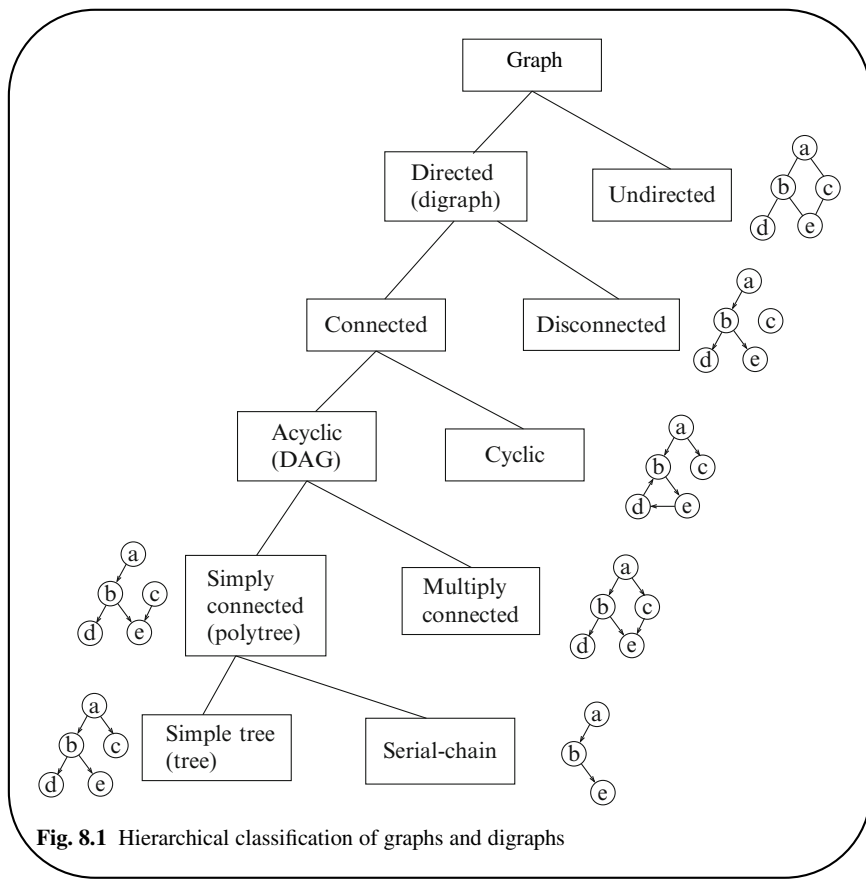


Fig. 8.1 Hierarchical classification of graphs and digraphs

1. A **connected digraph** is a digraph such that there is an undirected path connecting any pair of nodes, i.e., it is a digraph without disjoint components.
2. A **rooted digraph** is a connected digraph with a single root node that is the ancestor of every other node in the digraph. All edges connected to the root node are directed away from the root node. Thus, with r denoting the root node, we have $r \succeq k$ for all nodes k in a rooted digraph.
3. A **directed acyclic graph (DAG)** is a connected digraph without any directed cycles, i.e., there is no directed path from any node back to itself. Thus, a node

cannot be its own ancestor in a DAG, i.e., $k \not\prec k$ for any node k in the digraph. The first figure in Fig. 8.2 illustrates a DAG.

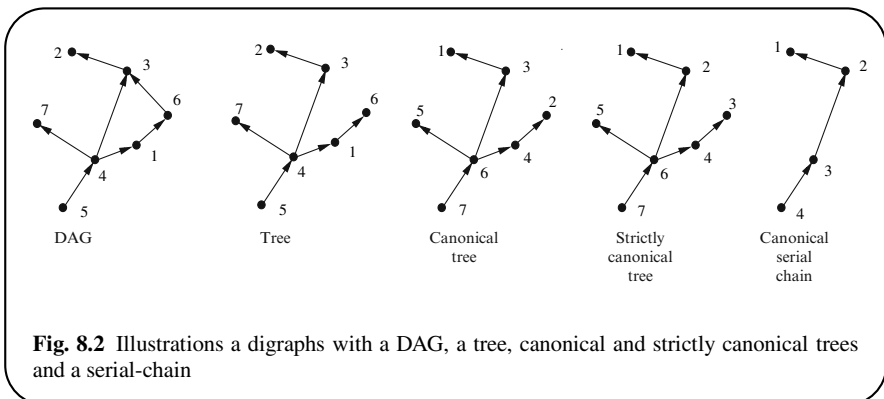


Fig. 8.2 Illustrations a digraphs with a DAG, a tree, canonical and strictly canonical trees and a serial-chain

4. A **simply connected graph**, or a **polytree** (also known as *singly connected networks*), is a DAG in which there is at most one directed path between any pair of nodes. For such digraphs, if nodes i and j are both ancestors of node k , then one of the i and j nodes must be an ancestor of the other. Notationally, this condition states that if $k \prec i$ and $k \prec j$, then either $i \preceq j$ or $j \preceq i$. Removing an edge decomposes a polytree into a pair of polytrees. A node in a polytree can have multiple parent nodes.
5. A **simple tree**, or **tree**, illustrated in the second figure in Fig. 8.2, is a polytree where a node has at most one parent node, i.e., $\varphi(k)$ contains at most one node for any node k . All trees have a *unique root node*. A tree is a rooted digraph, and is also referred to as a **rooted tree** or an **arborescence**. Removing an edge decomposes a tree into a pair of trees.
While a node in a tree can have at most one parent, there is no restriction on the number of children nodes. The branching structure implies that it is possible for nodes to be on different branches with no directed path connecting them. Thus, trees can have *unrelated* nodes, i.e., nodes that have no directed paths connecting them. Another noteworthy fact is that, for a pair of nodes, i and j , while $j \succ i \implies i \not\prec j$, the converse is not true in general. For a tree, we use the notation $\varphi(i, j)$ for the closest ancestor node of a pair of nodes i and j .
6. A **serial-chain** is a tree where each node has at most one child. The last graph in Fig. 8.2 illustrates a serial-chain. Unlike trees, serial-chains have the stronger property that all node pairs are *related*, i.e., for any pair of nodes in the serial-chain, one of the nodes is necessarily an ancestor of the other.
7. An **arborescence forest**, or **forest**, is a collection of disjoint trees. Removing an edge from a tree converts it into a forest. Adding a common root node to the independent trees in a forest converts them into a single tree. Conversely, removing the root node from a tree converts it into a forest.

A tree is said to be **canonical** if the index of a parent node is always greater than the index of its child node, i.e., $\rho(k) > k$ for any node k . The third digraph in Fig. 8.2 illustrates a canonical tree. Any tree can be converted into a canonical tree with a suitable renumbering of the nodes. The node numbering for a canonical tree is not unique since the canonical tree requirement imposes only a partial ordering on the node indices. The canonical numbering is, however, unique for a serial-chain.

A **strictly canonical tree** is a canonical tree such that each of the serial-chain segments within it is canonical. The fourth digraph in Fig. 8.2 illustrates a strictly canonical tree. Once again, any rooted tree can be converted into a strictly canonical tree with a suitable renumbering of the nodes.

Every rooted digraph has a **spanning tree**, i.e., a tree that contains all the nodes in the digraph and whose edges belong to the digraph. The edges removed to convert a rooted digraph into its spanning tree are referred to as **cut-edges**.

8.2 Adjacency Matrices for Digraphs

One way of representing the node/edge connectivity of a digraph is through an **adjacency matrix** for the digraph. For a digraph with n nodes, the adjacency matrix is an $n \times n$ square matrix. The only non-zero elements of an adjacency matrix are for adjacent node pairs. Thus, the $(i, j)^{th}$ element of an adjacency matrix is 1 if and only if the j^{th} node is a child of the i^{th} node, and is 0 otherwise. With the “.” entries indicating 0 entries, adjacency matrices for the digraphs in Fig. 8.2 are shown in Fig. 8.3.

8.2.1 Properties of Digraph Adjacency Matrices

The adjacency matrix, \mathbb{S} , of a digraph can be expressed as

$$\mathbb{S} = \sum_{j=1}^n \sum_{k \in \rho(j)} e_k e_j^* \quad (8.1)$$

where e_i denotes a vector of length n , containing all zeros except for the i^{th} element which has value 1, i.e.,

$$e_i(r) = \begin{cases} 1 & \text{for } i = r \\ 0 & \text{otherwise} \end{cases} = \mathbb{1}_{[i=r]} \quad (8.2)$$

$\mathbb{1}_{[<\text{cond}>]}$ denotes the **indicator function**, whose value is 1 when the condition specified in its subscript is true, and whose value is 0 otherwise. Observe that

$$e_j^* \cdot e_k = \mathbb{1}_{[j=k]} \quad (8.3)$$

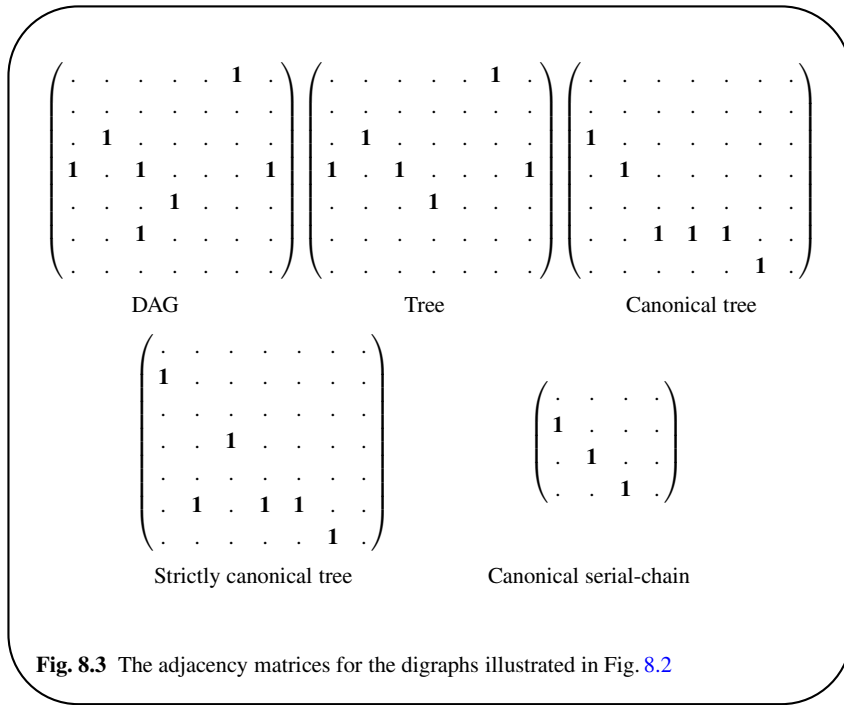


Fig. 8.3 The adjacency matrices for the digraphs illustrated in Fig. 8.2

The number of $e_k e_j^*$ terms in (8.1) is precisely the number of edges in the digraph. Each $e_k e_j^*$ edge term is an $n \times n$ matrix, with a single non-zero element of value 1 for the associated (k, j) edge. Key structural properties of an adjacency matrix, \mathbb{S} , for a digraph are summarized below:

1. The non-zero entries in the j th column of \mathbb{S} are for the $\wp(j)$ parent nodes of the j th node. Thus, the product of \mathbb{S} with the i th unit vector e_i is a vector whose non-zero entries are the parent nodes of the i th node. In particular, a node p is a root node if and only if

$$\mathbb{S} \cdot e_p = \mathbf{0} \quad (8.4)$$

In other words, root node columns of \mathbb{S} have all zero elements.

2. The non-zero entries in the i th row of \mathbb{S} are for the $\wp(i)$ child nodes of the i th node. Thus, the product of \mathbb{S}^* with the i th unit vector, e_i , is a vector whose non-zero entries are the child nodes of the i th node. In particular, a node t is a *tip* node, i.e., it has no children, if and only if

$$e_t^* \cdot \mathbb{S} = \mathbf{0} \quad (8.5)$$

In other words, tip node rows of \mathbb{S} have all zero elements.

3. Permutation matrices can be used to re-index the nodes in a digraph. Permutation matrices are orthogonal, i.e., the transpose of a permutation matrix is its inverse.

With T denoting such a permutation matrix, and \mathbb{S} the adjacency matrix of the original digraph, the adjacency matrix of the digraph after re-indexing is $T\mathbb{S}T^*$.

8.2.2 Properties of Tree Adjacency Matrices

Since nodes in a tree can have at most one parent node, the adjacency matrix of a tree digraph in (8.1) can be expressed in the following simpler form:

$$\mathbb{S} = \sum_{k=1}^n e_{\varphi(k)} e_k^* \quad (8.6)$$

We now examine the properties of an adjacency matrix, \mathbb{S} , for a tree digraph.

1. Since a node can have at most one parent in a tree, there can be at most one non-zero entry in any column of \mathbb{S} .
2. Only a single column, corresponding to the root node, is all zero in \mathbb{S} .
3. A row can have multiple non-zero elements.
4. For *canonical* trees, \mathbb{S} is always strictly *lower-triangular*.
5. Reversing the direction of the edges in a tree typically destroys the tree character; leaving only a polytree. The reversal process converts multiple children nodes into multiple parent nodes. \mathbb{S}^* is the adjacency matrix for the polytree.
6. For *strictly canonical trees*, \mathbb{S} has the structure shown in Fig. 8.4. It consists of the adjacency matrix for canonical serial-chain branch segments, \mathbb{S}_i , along the diagonal, along with off-diagonal $\mathbb{S}_{i,j}$, connector elements for the edges connecting the serial-chain branch segments.
7. The k th power of the adjacency matrix, \mathbb{S}^k , contains non-zero elements only for paths of length k connecting the nodes. That is, the (i,j) element of \mathbb{S}^k is non-zero if and only if there is a directed path of length k from node i to node j .
8. With n denoting the number of nodes in the tree, the n^{th} power of the adjacency matrix, \mathbb{S}^n , is zero. This is because the length of any path in a tree with n nodes is less than n . Thus \mathbb{S} is a nilpotent matrix. In other words, the adjacency matrix for a tree digraph is always nilpotent.

8.2.3 Properties of Serial-Chain Adjacency Matrices

We now review the properties of an adjacency matrix, \mathbb{S} , for a serial-chain digraph.

1. Since a node can have at most one child in a serial-chain, its adjacency matrix can have at most one non-zero element per row.
2. For a canonical serial-chain, only the first sub-diagonal of \mathbb{S} is non-zero.
3. For a canonical serial-chain, only the k th sub-diagonal of \mathbb{S}^k contains non-zero elements. Each additional power shifts the sub-diagonal one level lower.

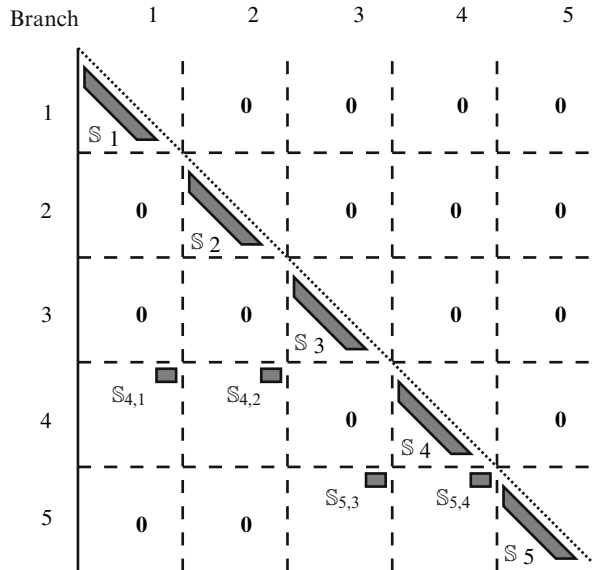


Fig. 8.4 Structure of the \mathbb{S} adjacency matrix for a strictly canonical tree topology system

4. A reversed serial chain is once again a serial-chain.

8.3 Block Weighted Adjacency Matrices

Adjacency matrices have 1 or 0 scalar entries for the node pair of each edge in a digraph. We now generalize these adjacency matrices to define **block-weighted adjacency (BWA)** matrices. Instead of scalars, BWA matrices contain weight matrix elements for the node pair of each edge. First, each tree node, j , is assigned a *weight dimension*, m_j , and its parent edge is assigned a non-zero *weight matrix* of dimension $m_{\varphi(j)} \times m_j$, denoted $w(\varphi(j), j)$. The $(k, j)^{\text{th}}$ block-matrix element of a BWA matrix, \mathbb{S}_W , is thus defined as

$$\mathbb{S}_W(k, j) = \begin{cases} w(k, j) & \text{if } k = \varphi(j) \\ \mathbf{0} & \text{otherwise} \end{cases} \in \mathcal{R}^{m_k \times m_j} \quad (8.7)$$

The standard adjacency matrix, \mathbb{S} , in (8.1) is a special case of a BWA matrix, where all the node dimensions are 1, and the edge weights are the scalar 1. \mathbb{S}_W has non-zero block-entries only for node pairs corresponding to edges in the digraph. It is easy to verify from the definition of the block-elements in (8.7) that \mathbb{S}_W is a well-

defined *square matrix* of dimension

$$N \triangleq \sum_{k=1}^n m_k \quad (8.8)$$

We extend the notion of the e_k unit vectors in (8.2), to the BWA context by assigning them block matrix entries as follows:

$$e_k(i) = \begin{cases} I_{m_k} & \text{if } i = k \\ \mathbf{0}_{m_i \times m_k} & \text{otherwise} \end{cases} \quad (8.9)$$

Thus, the e_k unit “vector” is a matrix of dimension $N \times m_k$, with n block matrix elements. The new version of (8.3) is

$$e_j^* \cdot e_k = \begin{cases} I_{m_j} & \text{if } j = k \\ \mathbf{0}_{m_j \times m_k} & \text{otherwise} \end{cases} \quad (8.10)$$

Using the unit vectors, and the component definitions in (8.7), \mathbb{S}_W can be expressed as:

$$\mathbb{S}_W = \sum_{j=1}^n \sum_{k \in \wp(j)} e_k w(k, j) e_j^* \quad (8.11)$$

Equation (8.11) is a generalization of (8.1) for BWA matrices.

8.4 BWA Matrices for Tree Digraphs

Analogous to (8.6), the BWA matrix expression in (8.11) has the following simpler form for tree digraphs:

$$\mathbb{S}_W = \sum_{k=1}^n e_{\wp(k)} w(\wp(k), k) e_k^* \quad (8.12)$$

The following lemma provides an expression for the block elements of \mathbb{S}_W^k for tree digraphs.

Lemma 8.1 Elements of \mathbb{S}_W^k for a tree digraph.

For a tree digraph, \mathbb{S}_W^k , the k th power of the \mathbb{S}_W BWA matrix, contains non-zero block-elements only for node pairs connected by directed paths of length k . The value of its block-element is the product of the k weights for the edges along the path, i.e., the non-zero elements are of the form

$$\mathbb{S}_W^k(\wp^k(i), i) = w(\wp^k(i), \wp^{k-1}(i)) * \dots * w(\wp(i), i) \in \mathcal{R}^{m_{\wp^k(i)} \times m_i} \quad (8.13)$$

Here, $\wp^k(i)$ denotes the k th ancestor of the i th node.

Proof: Let us illustrate the proof for $k = 2$. \mathbb{S}_W^2 is given by

$$\begin{aligned}\mathbb{S}_W^2 &\stackrel{8.12}{=} \left(\sum_{j=1}^n e_{\wp(j)} w(\wp(j), j) e_j^* \right) * \left(\sum_{i=1}^n e_{\wp(i)} w(\wp(i), i) e_i^* \right) \\ &\stackrel{8.3}{=} \sum_{j=1}^n \sum_{i=1}^n e_{\wp(j)} w(\wp(j), j) \mathbb{1}_{[j=\wp(i)]} w(\wp(i), i) e_i^* \\ &= \sum_{i=1}^n e_{\wp^2(i)} w(\wp^2(i), \wp(i)) * w(\wp(i), i) e_i^*\end{aligned}$$

The $(\wp^2(i), i)$ block-element of \mathbb{S}_W^2 is thus,

$$\mathbb{S}_W^2(\wp^2(i), i) = w(\wp^2(i), \wp(i)) * w(\wp(i), i)$$

which establishes (8.13) for \mathbb{S}_W^2 . Continuing in a similar vein, (8.13) can be established for arbitrary k . ■

8.4.1 The 1-Resolvent of Tree BWA Matrices

The following lemma establishes the nilpotency of \mathbb{S}_W for tree digraphs.

Lemma 8.2 Nilpotency of tree BWA matrices.

The n^{th} power of a tree BWA matrix, \mathbb{S}_W^n , is zero, where n denotes the number of nodes in the system. Hence, the BWA matrix for a tree digraph is a nilpotent matrix.

Proof: Lemma 8.1 states that the non-zero entries of \mathbb{S}_W^n correspond to node pairs connected by paths of length n . Since paths can be of length at most $n - 1$ in a tree with n nodes, it follows that \mathbb{S}_W^n is the zero matrix. ■

In matrix theory, the resolvent of a matrix A , is defined as the $(\lambda I - A)^{-1}$ matrix for a scalar λ . We use the term, **1-resolvent**, to denote the specific resolvent with $\lambda = 1$. The following lemma derives an explicit expression for the 1-resolvent of a tree BWA matrix.

Lemma 8.3 The 1-resolvent of a tree BWA matrix.

The 1-resolvent, $(I - \mathbb{S}_W)^{-1}$, of a tree BWA matrix exists and can be expressed as the following disjoint sum of its powers:

$$(I - \mathbb{S}_W)^{-1} = I + \mathbb{S}_W + \mathbb{S}_W^2 + \cdots + \mathbb{S}_W^{n-1} \quad (8.14)$$

Proof: Lemma 8.2 states that the adjacency matrix of a tree, \mathbb{S}_W , is nilpotent. (8.14) follows by applying the expression from Lemma A.1 for the 1-resolvent of a nilpotent matrix to \mathbb{S}_W . ■

Lemma 8.3 is an important result. It provides an explicit expression for the 1-resolvent of the \mathbb{S}_W BWA matrix for tree systems. For cyclic digraphs, i.e., ones with *directed loops*, the 1-resolvent is not defined because \mathbb{S}_W is not nilpotent and $(\mathbf{I} - \mathbb{S}_W)$ is non-invertible. This topological difference has significant implications for the dynamics properties of tree versus cyclic digraph multibody systems. This is discussed in more detail in Sect. 9.6.2.

Now we introduce new notation that better reflects the intimate relationship between a BWA matrix and its 1-resolvent matrix for a tree digraph. With \mathbb{A} denoting the 1-resolvent matrix for a tree, we will use the notation $\mathcal{E}_{\mathbb{A}}$ to denote its associated BWA matrix. Thus, the relationship between the earlier notation and the new notation is as follows:

$$\mathbb{A} \equiv (\mathbf{I} - \mathbb{S}_W)^{-1} \quad \text{and} \quad \mathcal{E}_{\mathbb{A}} \equiv \mathbb{S}_W = \mathbf{I} - \mathbb{A}^{-1} \quad (8.15)$$

The following lemma describes the expression for the block elements of a 1-resolvent matrix.

Lemma 8.4 Elements of a 1-resolvent matrix \mathbb{A} .

The (k, j) element of the 1-resolvent matrix of a tree, $\mathbb{A} = (\mathbf{I} - \mathcal{E}_{\mathbb{A}})^{-1}$, is given by

$$\mathbb{A}(i, j) = \begin{cases} \mathbf{0}_{m_i \times m_j} & \text{for } i \not\sim j \\ \mathbf{I}_{m_i} & \text{for } i = j \\ w(i, j) & \text{for } i = \varphi(j) \\ w(\varphi^k(j), \varphi^{k-1}(j)) * \dots * w(\varphi(j), j) & \text{for } i = \varphi^k(j) \end{cases} \quad (8.16)$$

Proof: Equation (8.16) follows from the expression for $(\mathbf{I} - \mathcal{E}_{\mathbb{A}})^{-1}$ in (8.14), together with Lemma 8.1 which describes the elements of the powers of $\mathcal{E}_{\mathbb{A}}$. ■

Thus, \mathbb{A} has identity matrices along the diagonal. The non-zero block elements correspond to (i, j) node pairs where node i is an ancestor of node j . For such cases, the block element is the product of the weight matrices associated with each of the edges in the path from i to j . From (8.16), it is clear that the \mathbb{A} 1-resolvent is sparse, with its sparsity structure directly reflecting the topological structure of the associated tree.

Remark 8.1 Structure of canonical serial-chain $\mathcal{E}_{\mathbb{A}}$ and \mathbb{A} matrices.

Let us now examine the structure of the 1-resolvent matrix \mathbb{A} for a canonical serial-chain digraph. We assume for this example that the serial-chain has four nodes, and thus $\mathcal{E}_{\mathbb{A}}^4 = \mathbf{0}$. Using (8.14), \mathbb{A} is given by the following disjoint sum:

$$\mathbb{A} = \mathbf{I} + \mathcal{E}_{\mathbb{A}} + \mathcal{E}_{\mathbb{A}}^2 + \mathcal{E}_{\mathbb{A}}^3$$

The non-zero elements of the above matrices are as shown below (with “.” entries indicating zero blocks and the X entries the non-zero ones):

$$\mathcal{E}_{\mathbb{A}} = \begin{pmatrix} \cdot & \cdot & \cdot & \cdot \\ X & \cdot & \cdot & \cdot \\ \cdot & X & \cdot & \cdot \\ \cdot & \cdot & X & \cdot \end{pmatrix}, \quad \mathcal{E}_{\mathbb{A}}^2 = \begin{pmatrix} \cdot & \cdot & \cdot & \cdot \\ \cdot & \cdot & \cdot & \cdot \\ X & \cdot & \cdot & \cdot \\ \cdot & X & \cdot & \cdot \end{pmatrix}, \quad \mathcal{E}_{\mathbb{A}}^3 = \begin{pmatrix} \cdot & \cdot & \cdot & \cdot \\ \cdot & \cdot & \cdot & \cdot \\ \cdot & \cdot & \cdot & \cdot \\ X & \cdot & \cdot & \cdot \end{pmatrix}$$

$\mathcal{E}_{\mathbb{A}}$ has non-zero block entries only along its first sub-diagonal. Each subsequent power of $\mathcal{E}_{\mathbb{A}}$ shifts the non-zero sub-diagonal lower, until it vanishes entirely for the n^{th} power. Thus, \mathbb{A} has the following structure:

$$\mathbb{A} = \begin{pmatrix} I & \cdot & \cdot & \cdot \\ X & I & \cdot & \cdot \\ X & X & I & \cdot \\ X & X & X & I \end{pmatrix}$$

\mathbb{A} is lower-triangular, with all of the diagonal and lower-triangular block-elements being non-zero. All of these terms are non-zero because all nodes in serial-chains are related, i.e., there is a directed path between all node pairs.

■

This example shows that, for a canonical serial-chain, all of the lower-triangular elements of \mathbb{A} are non-zero. The following example looks at the structure of a 1-resolvent matrix for a canonical tree.

Remark 8.2 Structure of canonical tree $\mathcal{E}_{\mathbb{A}}$ and \mathbb{A} matrices.

The sparsity structure of the $\mathcal{E}_{\mathbb{A}}$ and \mathbb{A} matrices for the canonical tree in Fig. 8.2 is shown below. The “.” entries indicate zero block-elements.

$$\mathcal{E}_{\mathbb{A}} = \begin{pmatrix} \cdot & \cdot \\ \cdot & \cdot \\ X & \cdot \\ \cdot & X & \cdot & \cdot & \cdot & \cdot & \cdot & \cdot \\ \cdot & \cdot \\ \cdot & \cdot & X & X & X & \cdot & \cdot & \cdot \\ \cdot & \cdot & \cdot & \cdot & \cdot & X & \cdot & \cdot \end{pmatrix} \quad \text{and} \quad \mathbb{A} = \begin{pmatrix} I & \cdot \\ \cdot & I & \cdot & \cdot & \cdot & \cdot & \cdot & \cdot \\ X & \cdot & I & \cdot & \cdot & \cdot & \cdot & \cdot \\ \cdot & X & \cdot & I & \cdot & \cdot & \cdot & \cdot \\ \cdot & \cdot & \cdot & \cdot & I & \cdot & \cdot & \cdot \\ X & X & X & X & X & I & \cdot & \cdot \\ X & X & X & X & X & X & I & \cdot \end{pmatrix}$$

These matrices illustrate that, for canonical trees, the $\mathcal{E}_{\mathbb{A}}$ matrix is strictly lower-triangular, and \mathbb{A} is lower-triangular. However, some of the lower-triangular blocks of \mathbb{A} are zero, in contrast with the all non-zero case for canonical serial-chains. The zero terms correspond to the unrelated nodes in the tree, i.e., node pairs that

are not connected by a path. Section 14.3 takes a more detailed look at the sparsity structures of the $\mathcal{E}_\mathbb{A}$ and \mathbb{A} matrices. ■

This example shows that there is significant sparsity in the lower-triangular blocks of \mathbb{A} for a tree. The sparsity is a function of the branching topological structure of the tree. Serial-chain systems represent the most dense topological structure since all of their nodes are related. Trees, on the other hand, can have unrelated nodes, i.e., nodes with no directed paths connecting them. This decreased connectivity of the nodes is reflected in the sparsity of \mathbb{A} .

The following lemma highlights the semi-group properties of the block elements of \mathbb{A} .

Lemma 8.5 Semi-group property of $\mathbb{A}(i,j)$ elements.

For a tree, let i , j , and k denote nodes, where the i th node is an ancestor of the j th node, and the k th node is on the path connecting them. Then, the block-elements of the \mathbb{A} 1-resolvent satisfy the following relationship:

$$\mathbb{A}(i,j) = \mathbb{A}(i,k)\mathbb{A}(k,j) \quad \forall k : i \succeq k \succeq j \quad (8.17)$$

This property is also known as the **semi-group** property for the elements of a 1-resolvent matrix.

Proof: Let $i = \varphi^m(j)$ for some m , and $k = \varphi^r(j)$ for some $r < m$. Let l denote the child node of k that is on the path to node j . From the (8.16) expression for the block elements of \mathbb{A} , we have

$$\begin{aligned} \mathbb{A}(i,j) &\stackrel{8.16}{=} w(\varphi^m(j), \varphi^{m-1}(j)) * \dots * w(\varphi(j), j) \\ &= [w(\varphi^m(j), \varphi^{m-1}(j)) * \dots * w(\varphi(k), k)] * [w(k, l) * \dots * w(\varphi(j), j)] \\ &\stackrel{8.16}{=} \mathbb{A}(\varphi^m(j), k) * \mathbb{A}(k, j) = \mathbb{A}(i, k) * \mathbb{A}(k, j) \end{aligned}$$

Define the $\tilde{\mathbb{A}}$ matrix derived from the \mathbb{A} 1-resolvent matrix as follows:

$$\tilde{\mathbb{A}} \triangleq \mathbb{A} - \mathbf{I} \quad (8.18)$$

$\tilde{\mathbb{A}}$ is strictly lower-triangular for canonical trees. The following lemma establishes some basic properties of $\tilde{\mathbb{A}}$.

Lemma 8.6 The $\tilde{\mathbb{A}}$ spatial operator.

For a 1-resolvent \mathbb{A} , the following identities hold:

$$\tilde{\mathbb{A}} = \mathbb{A} - \mathbf{I} = \mathcal{E}_\mathbb{A}\mathbb{A} = \mathbb{A}\mathcal{E}_\mathbb{A} \quad (8.19)$$

Proof: For any matrix X , such that $(\mathbf{I} - X)$ is invertible, the following matrix identity holds:

$$X(\mathbf{I} - X)^{-1} = (\mathbf{I} - X)^{-1}X = (\mathbf{I} - X)^{-1} - \mathbf{I}$$

With $X = \mathcal{E}_{\mathbb{A}}$, the above equation, together with (8.18), directly lead to (8.19). ■

The following exercise extends the adjacency matrix properties in (8.4) and (8.5) to BWA matrices and their 1-resolvents.

Exercise 8.1 Root/tip nodes and BWA matrices.

1. A node r is a root node of the tree if and only if

$$\mathcal{E}_{\mathbb{A}} \cdot e_r = \mathbf{0}, \quad \mathbb{A} \cdot e_r = e_r \quad (8.20)$$

2. A node t is a tip node of the tree, i.e., it has no children nodes, if and only if

$$\mathcal{E}_{\mathbb{A}}^* \cdot e_t = \mathbf{0}, \quad \mathbb{A}^* \cdot e_t = e_t \quad (8.21)$$

The following remark describes properties of the product of a general matrix, and a diagonal matrix, that we will use in the forthcoming sections. ■

Remark 8.3 Matrix products.

Recall that any block-matrix, Y , can be expressed as

$$Y = \sum_{j=1}^n \sum_{k=1}^n e_j Y(j, k) e_k^*$$

Let $X \triangleq \text{diag}\left\{X(i)\right\}_{i=1}^n$ and $Z \triangleq \text{diag}\left\{Z(i)\right\}_{i=1}^n$ denote compatible block-diagonal matrices. Then it is easy to verify that

$$\begin{aligned} XY &= \sum_{j=1}^n \sum_{k=1}^n e_j X(j) Y(j, k) e_k^* \\ \text{and } YZ &= \sum_{j=1}^n \sum_{k=1}^n e_j Y(j, k) Z(k) e_k^* \end{aligned} \quad (8.22)$$

While the discussion in this section has been devoted to BWA matrices and 1-resolvents for tree digraphs, all of the properties and results extend directly to forests, i.e., to digraphs consisting of a set of disjoint trees. ■

8.5 Similarity Transformations of a Tree BWA Matrix

We now examine the effect of applying similarity transformations to a BWA matrix.

Lemma 8.7 Similarity transformation of a BWA matrix.

Let T denote an invertible matrix and \mathcal{E}_A a tree BWA matrix. Let $Y \triangleq T\mathcal{E}_A T^{-1}$ denote a similarity transformation of \mathcal{E}_A by the T matrix. Then Y is nilpotent, and its 1-resolvent is given by the following similarity transformation:

$$(I - Y)^{-1} = T\mathbb{A}T^{-1} \quad (8.23)$$

Proof: Since \mathcal{E}_A is nilpotent, we have

$$Y^n = (T\mathcal{E}_A T^{-1})^n = T(\mathcal{E}_A)^n T^{-1} = \mathbf{0}$$

Hence, Y is nilpotent. Also,

$$(I - Y)^{-1} = (I - T\mathcal{E}_A T^{-1})^{-1} = T(I - \mathcal{E}_A)^{-1}T^{-1} = T\mathbb{A}T^{-1}$$

This establishes (8.23). ■

The above lemma provides an expression for the 1-resolvent of the matrix obtained by applying a similarity transformation to a BWA matrix. However, there is no guarantee that the transformed matrix, Y , retains the block partitioned structure of the original BWA matrix. Generally, the transformed Y matrix will not be a BWA matrix for the tree.

8.5.1 Permutation Similarity Transformations

A special case, where the BWA property is preserved under similarity transformations, occurs when the transformation matrix is a **permutation matrix** used to re-index the nodes in the tree. For such a permutation matrix, denoted T , we know that $T^{-1} = T^*$. The transformed matrix, $\mathcal{E}_B \triangleq T\mathcal{E}_A T^{-1}$ is indeed a BWA matrix for the tree, and its 1-resolvent B is given by:

$$\mathcal{E}_B = T\mathcal{E}_A T^* \quad \text{and} \quad B \triangleq (I - \mathcal{E}_B)^{-1} \stackrel{8.23}{=} T\mathbb{A}T^* \quad (8.24)$$

In the multibody context, such permutation transformations relate the equations of motion obtained using different body numbering schemes. In particular, any tree can be converted into a canonical tree with an appropriate re-labeling of the nodes. This implies that the \mathcal{E}_A and \mathbb{A} matrices for any tree are related to the lower-triangular versions for the corresponding canonical tree via permutation matrices.

8.5.2 Similarity-Shift Transformations

Another type of similarity transformation, referred to as a **similarity-shift transformation**, that preserves the BWA property is discussed next. Let $\Delta_{\mathbb{C}}$ be an invertible, block-diagonal matrix defined as follows:

$$\Delta_{\mathbb{C}} \triangleq \text{diag} \left\{ \Delta_{\mathbb{C}}(k) \right\}_{k=1}^n \quad \text{where} \quad \Delta_{\mathbb{C}}(k) \in \mathcal{R}^{m_k \times m_k} \quad (8.25)$$

Let $\mathbb{B}(\varphi(k), k)$ denote new weight matrices defined from the original $\mathbb{A}(\varphi(k), k)$ weight matrices as follows:

$$\mathbb{B}(\varphi(k), k) = \Delta_{\mathbb{C}}(\varphi(k)) \mathbb{A}(\varphi(k), k) \Delta_{\mathbb{C}}^{-1}(k) \quad (8.26)$$

Let $\mathcal{E}_{\mathbb{B}}$ denote the BWA matrix with the $\mathbb{B}(\varphi(k), k)$ weight matrices. The following lemma establishes the relationship between the $\mathcal{E}_{\mathbb{A}}$ and $\mathcal{E}_{\mathbb{B}}$ BWA matrices and their 1-resolvents.

Lemma 8.8 Similarity-shift transformation of a BWA matrix.

Let $\mathcal{E}_{\mathbb{A}}$ and $\mathcal{E}_{\mathbb{B}}$ be BWA matrices whose weight matrices satisfy (8.26). Then the BWA matrices $\mathcal{E}_{\mathbb{B}}$ and $\mathcal{E}_{\mathbb{A}}$ are related by the following similarity transformation:

$$\mathcal{E}_{\mathbb{B}} = \Delta_{\mathbb{C}} \mathcal{E}_{\mathbb{A}} \Delta_{\mathbb{C}}^{-1} \quad (8.27)$$

Also, the 1-resolvent matrices, $\mathbb{A} = (\mathbf{I} - \mathcal{E}_{\mathbb{A}})^{-1}$ and $\mathbb{B} = (\mathbf{I} - \mathcal{E}_{\mathbb{B}})^{-1}$, are related by the same similarity transformation:

$$\mathbb{B} = \Delta_{\mathbb{C}} \mathbb{A} \Delta_{\mathbb{C}}^{-1} \quad (8.28)$$

Proof: Now

$$\begin{aligned} \mathcal{E}_{\mathbb{B}} &\stackrel{8.26}{=} \sum_{k=1}^n e_{\varphi(k)} \Delta_{\mathbb{C}}(\varphi(k)) \mathbb{A}(\varphi(k), k) \Delta_{\mathbb{C}}^{-1}(k) e_k^* \\ &\stackrel{8.22}{=} \sum_{k=1}^n \Delta_{\mathbb{C}} e_{\varphi(k)} \mathbb{A}(\varphi(k), k) e_k^* \Delta_{\mathbb{C}}^{-1} \\ &= \Delta_{\mathbb{C}} \sum_{k=1}^n e_{\varphi(k)} \mathbb{A}(\varphi(k), k) e_k^* \Delta_{\mathbb{C}}^{-1} = \Delta_{\mathbb{C}} \mathcal{E}_{\mathbb{A}} \Delta_{\mathbb{C}}^{-1} \end{aligned}$$

This establishes (8.27). Further application of Lemma 8.7 leads to (8.28). ■

In the multibody context, similarity-shift transformations define the relationship between equations of motion associated with different choices of body frames. ■

8.6 Multibody System Digraphs

Digraphs provide natural mathematical constructs for describing the topology and connectivity of bodies in a multibody system. They have been used for the systematic formulation of the equations of motion [123, 164, 185], as well as for kinematical analysis [189].

We define the **standard** digraph associated with a multibody system as one with the inertial frame as the root node, and all the links in the system as the remaining nodes in the digraph. Thus, an n -link multibody system has a digraph with $n + 1$ nodes.

The edges in the digraph are defined by the motion constraints among the bodies, and between the bodies and the inertial frame. Thus, each hinge is represented by an edge, with the edges orientated from the inboard to the outboard body. Additional edges are assigned to other non-hinge motion constraints in the system. All motion constraints with respect to the inertial frame are defined so that edges from the inertial frame node to the link nodes are directed away from the inertial frame root node. These assignments result in a *rooted digraph* representation for the multibody system. Figure 8.5 illustrates the correspondence between the bodies and hinges in a serial-chain multibody system and the standard, serial-chain digraph for the system. The convention is to depict the inertial frame node as unfilled, and the edges from the node as dashed lines. Multibody systems are classified as follows, based on the

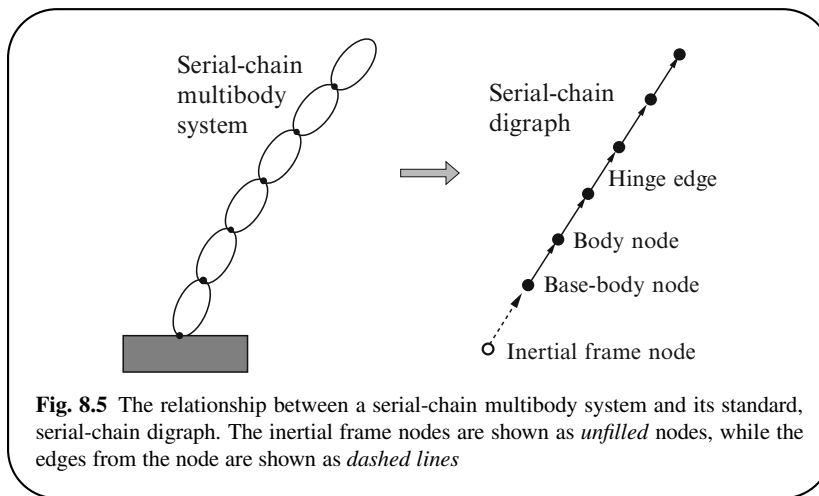


Fig. 8.5 The relationship between a serial-chain multibody system and its standard, serial-chain digraph. The inertial frame nodes are shown as *unfilled* nodes, while the edges from the node are shown as *dashed lines*

topology of their standard digraph:

- Systems with tree standard digraphs are referred to as **tree-topology systems**.

- Systems with serial-chain standard digraphs are referred to as the familiar **serial-chain systems**. They are special cases of tree-topology systems.
- Systems with non-tree standard digraphs are referred to as **closed-chain** or **constrained systems**. These digraphs can have directed cycles and/or multiply-connected nodes. Recall that every rooted digraph can be decomposed (non-uniquely) into a spanning tree together with a set of cut-edges. A decomposition into a spanning tree with $n + 1$ nodes and a set of cut-edges is often used when working with closed-chain systems.

Removing the inertial root node converts the spanning tree into a forest. We will refer to this forest as the **SKO-forest** for the system. The SKO-forest has just n nodes, matching the number of bodies in the system. Nodes corresponding to base-bodies in the multibody system are root nodes in the SKO-forest. We will make extensive use of n -node SKO-forests since they allow us to work with adjacency matrices of dimension n instead of dimension $n + 1$. There is no information loss because the spanning tree can be fully recovered by adding the inertial frame root node and its edges to the root nodes in the SKO-forest. The inertial frame node is, in reality, redundant in the spanning tree of a multibody system since it is always present as the root node.

Figure 8.6 illustrates several examples of multibody systems and their associated standard digraph representations, as described below:

1. A serial-chain system with a serial-chain digraph.
2. A tree-topology system consisting of a pair of independent serial manipulators.
The resulting digraph is a tree.
3. A tree-topology system with branching reflected in its tree digraph.
4. A closed-chain four-bar linkage with an internal loop constraint. Based on the directionality of the constraint hinge, the digraph contains a directed cycle or is multiply-connected.
5. A closed-chain pair of serial-manipulators whose end-effectors are constrained.
The digraph for this system is a multiply-connected.
6. A closed-chain serial manipulator with constrained end-effector. The digraph is multiply-connected.

In later chapters, we will encounter non-standard digraphs for multibody systems where the bodies and digraph nodes are not in one-to-one correspondence with each other.

8.6.1 BWA Matrices and Serial-Chain, Rigid Body Systems

In this section, we use a canonical serial-chain multibody system to help establish ties between BWA matrices and their 1-resolvents, and multibody dynamics formulations. Consider an n -link rigid body canonical serial-chain system, with links numbered so that the tip link is link 1, and the base-body is the n th link.

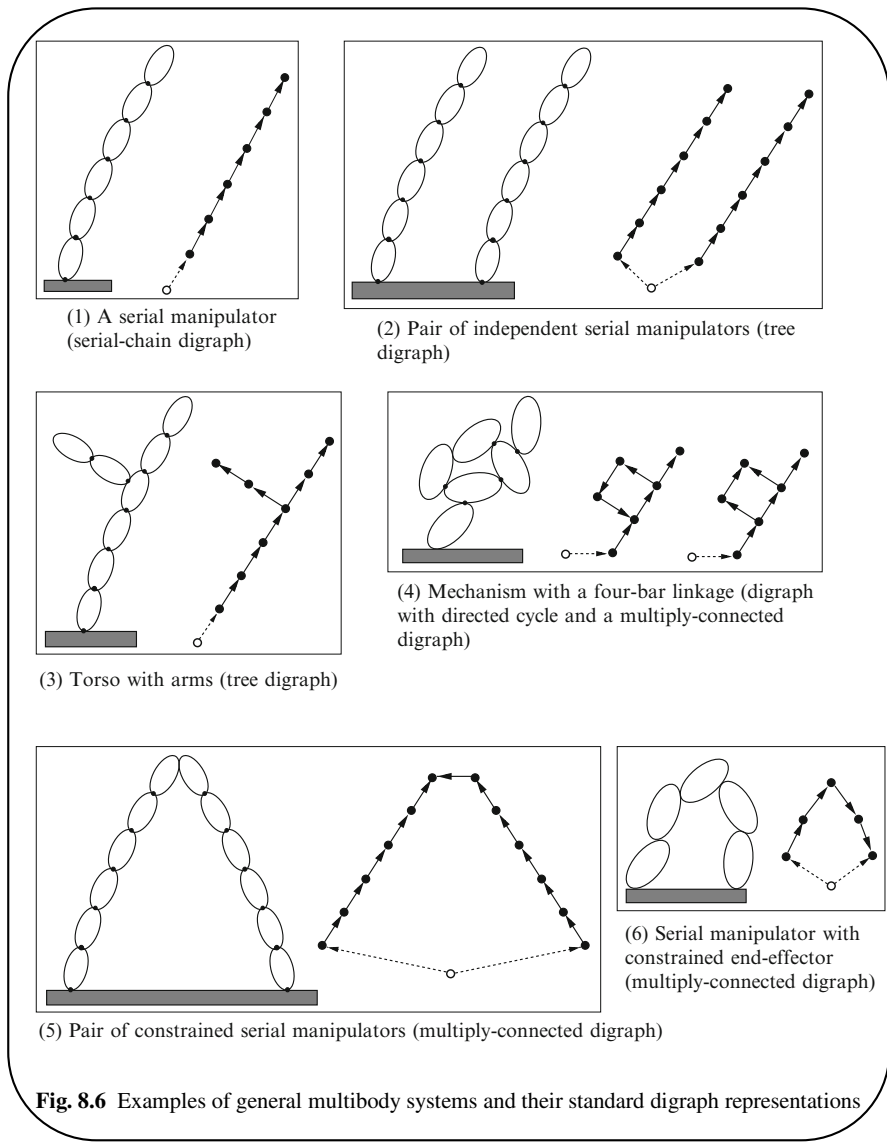


Fig. 8.6 Examples of general multibody systems and their standard digraph representations

Its digraph is a strictly canonical serial-chain with the parent/child relationship defined by $\wp(k) = k + 1$.

Recall the following expression for the link spatial velocities from (3.34):

$$\mathcal{V} = \mathcal{E}_\phi^* \mathcal{V} + \mathbf{H}^* \dot{\theta} \quad (8.29)$$

with the spatial operator \mathcal{E}_ϕ in (3.30) defined as

$$\mathcal{E}_\phi = \begin{pmatrix} \mathbf{0} & \mathbf{0} & \mathbf{0} & \mathbf{0} & \mathbf{0} \\ \phi(2,1) & \mathbf{0} & \dots & \mathbf{0} & \mathbf{0} \\ \mathbf{0} & \phi(3,2) & \dots & \mathbf{0} & \mathbf{0} \\ \vdots & \vdots & \ddots & \vdots & \vdots \\ \mathbf{0} & \mathbf{0} & \dots & \phi(n,n-1) & \mathbf{0} \end{pmatrix} \quad (8.30)$$

8.6.1.1 \mathcal{E}_ϕ Is a BWA Matrix

Equation (8.30) can restated as

$$\mathcal{E}_\phi = \sum_{k=1}^n e_{k+1}\phi(k+1,k)e_k^* = \sum_{k=1}^n e_{\varphi(k)}\phi(\varphi(k),k)e_k^* \quad (8.31)$$

Comparing with (8.12), we see that \mathcal{E}_ϕ in (8.31) has the structure of a BWA matrix for a tree digraph with n nodes. *In fact, \mathcal{E}_ϕ is a BWA matrix for the SKO-forest associated with the canonical serial-chain system.* The weight dimensions for the BWA matrix are uniformly of size 6, and the edge weight matrices are 6×6 matrices defined as

$$w(\varphi(k), k) = w(k+1, k) \stackrel{\triangle}{=} \phi(k+1, k) = \phi(\varphi(k), k) \quad (8.32)$$

Since \mathcal{E}_ϕ is a BWA matrix, by Lemma 8.3, its 1-resolvent, $\phi = (\mathbf{I} - \mathcal{E}_\phi)^{-1}$, is well-defined, and is given by

$$\phi = \begin{pmatrix} \mathbf{I} & \mathbf{0} & \dots & \mathbf{0} \\ \phi(2,1) & \mathbf{I} & \dots & \mathbf{0} \\ \vdots & \vdots & \ddots & \vdots \\ \phi(n,1) & \phi(n,2) & \dots & \mathbf{I} \end{pmatrix} \in \mathcal{R}^{6n \times 6n} \quad (8.33)$$

This expression is identical to the one for ϕ in (3.36). Thus, we have established that the \mathcal{E}_ϕ and ϕ spatial operators for canonical serial-chain multibody systems are in fact BWA and 1-resolvent matrices, respectively, for the SKO-forest associated with the system. The strictly lower-triangular and lower-triangular structures of the \mathcal{E}_ϕ and ϕ matrices, respectively, are consistent with their association with canonical serial-chain digraphs.

8.6.2 Non-Canonical Serial-Chains

For non-canonical serial-chains, the $(k+1)$ th link is not necessarily the parent body of the k th link. So a natural question is whether the \mathcal{E}_ϕ and ϕ spatial operators for non-canonical serial-chains continue to be BWA and 1-resolvent matrices? The answer is in the affirmative. We simply need to discard the implicit assumption that the parent body of the k th link is the $(k+1)$ th link, and switch to the more general $\wp(k)$ notation for the parent link. The generalization of (3.19b) for non-canonical serial-chain systems is:

$$\mathcal{V}(k) = \phi^*(\wp(k), k)\mathcal{V}(\wp(k)) + H^*(k)\dot{\theta}(k) \quad (8.34)$$

The velocity relationship in (8.29) continues to hold, with \mathcal{E}_ϕ defined by the more general second half of (8.31). Thus, \mathcal{E}_ϕ is once again a BWA matrix. Indeed, the rest of the development in Sect. 5.1 on page 75, leading to the equations of motion in (5.23) and (5.24), continues to apply. However, since the system is non-canonical, neither \mathcal{E}_ϕ nor ϕ in (8.30) and (8.33), respectively, are lower-triangular. Thus, even though the component-level equations and the operator structure depend on the body indexing scheme, the BWA and 1-resolvent properties of the \mathcal{E}_ϕ and ϕ spatial operators, and the operator forms of the equations of motion, remain intact! In the next section, we will encounter this theme again for tree-topology systems.

8.7 BWA Matrices and Tree-Topology, Rigid Body Systems

The key difference between serial-chain and tree-topology multibody systems is that, in a tree system, bodies can have multiple children bodies. The standard digraph for an n -links tree-topology multibody system is a tree with $(n+1)$ nodes, as illustrated in Fig. 8.7. We make no specific assumptions about the indexing scheme for the bodies. However, as usual, structural properties are easier to visualize when canonical indexing schemes are used.

Examining the kinematic velocity relationships across the links, the inter-link velocity relationship shown in (8.34) continues to apply to bodies in a tree-topology system:

$$\mathcal{V}(k) = \phi^*(\wp(k), k)\mathcal{V}(\wp(k)) + H^*(k)\dot{\theta}(k) \quad (8.35)$$

That is, the spatial velocity of the k th link can be expressed as the sum of the rigidly propagated spatial velocity of the parent body and the relative spatial velocity, $H^*(k)\dot{\theta}(k)$, across the k th hinge. Defining the \mathcal{V} and $\dot{\theta}$ stacked vectors and the H spatial operator in the same way as in Sect. 3.4, it is easy to verify that the following operator expression is a system-level rearrangement of the component-level velocity relationship in (8.35):

$$\mathcal{V} = \mathcal{E}_\phi^* \mathcal{V} + H^* \dot{\theta} \quad (8.36)$$

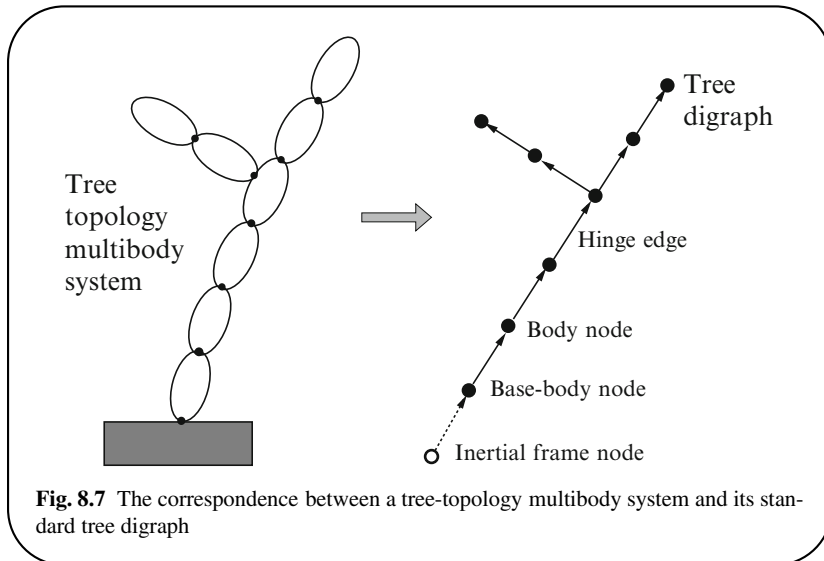


Fig. 8.7 The correspondence between a tree-topology multibody system and its standard tree digraph

with \mathcal{E}_ϕ defined as

$$\mathcal{E}_\phi = \sum_{k=1}^n e_{\phi(k)} \phi(\varrho(k), k) e_k^* \quad (8.37)$$

The \mathcal{E}_ϕ spatial operator has the (8.12) form of a BWA matrix for the SKO-forest associated with the system. The $\phi(\varrho(k), k)$ matrices are the 6×6 weight matrices. Since the SKO-forest is a forest, \mathcal{E}_ϕ is nilpotent and, from Lemma 8.3, it has a well defined 1-resolvent, $\phi = (\mathbf{I} - \mathcal{E}_\phi)^{-1}$. Hence, (8.36) can be transformed into

$$(\mathbf{I} - \mathcal{E}_\phi^*) \mathcal{V} = \mathbf{H}^* \dot{\theta} \quad \text{and} \quad \mathcal{V} = \phi^* \mathbf{H}^* \dot{\theta} \quad (8.38)$$

This operator expression is identical to the one in (8.29) for serial-chain systems.

8.7.1 Equations of Motion for Tree Topology Systems

To develop the equations of motion for the tree system, we once again start with the free-body equations of motion of the k th link, as was done in (5.1) for serial-chain systems. The key difference is that we need to take into consideration the $f(\cdot)$ spatial interaction forces from all the children bodies, instead of from just a single child body, as is the case for serial-chain systems. The following is the generalization of the force balance expression from (5.1) extended to tree-topology systems:

$$\mathfrak{f}(k) - \sum_{\forall j \in C(k)} \phi(k, j) f(j) = M(k) \alpha(k) + b(k) \quad (8.39)$$

Rearranging the above leads to the following analog of (5.4):

$$\mathfrak{f}(k) = \sum_{\forall j \in C(k)} \phi(k, j) f(j) + M(k) \alpha(k) + b(k) \quad (8.40)$$

Switching to the system-level stacked vector form of (8.40), we obtain

$$\mathfrak{f} = \mathcal{E}_\phi \mathfrak{f} + M \alpha + b \quad (8.41)$$

Continuing in this mode, the following expressions summarize the operator expressions for tree-topology systems:

$$\begin{aligned} \mathcal{V} &\stackrel{8.36}{=} \mathcal{E}_\phi^* \mathcal{V} + H^* \dot{\theta} \\ \alpha &= \mathcal{E}_\phi^* \alpha + H^* \ddot{\theta} + a \\ \mathfrak{f} &\stackrel{8.41}{=} \mathcal{E}_\phi \mathfrak{f} + M \alpha + b \\ \mathcal{T} &= H \mathfrak{f} \end{aligned} \quad (8.42)$$

These expressions are identical to the corresponding expressions in (5.22) for serial-chain systems. Using $\phi = (I - \mathcal{E}_\phi)^{-1}$, these expressions can be transformed from implicit ones into the following explicit operator expressions:

$$\begin{aligned} \mathcal{V} &= \phi^* H^* \dot{\theta} \\ \alpha &= \phi^* (H^* \ddot{\theta} + a) \\ \mathfrak{f} &= \phi(M \alpha + b) \\ \mathcal{T} &= H \mathfrak{f} \end{aligned} \quad (8.43)$$

These expressions are identical to the corresponding expressions in (5.23) for serial-chain systems. Combining the expressions in (8.43) leads to

$$\mathcal{T} = \mathcal{M}(\theta) \ddot{\theta} + \mathcal{C}(\theta, \dot{\theta}) \quad (8.44)$$

where

$$\mathcal{M}(\theta) = H \phi M \phi^* H^* \in \mathcal{R}^{N \times N} \text{ and } \mathcal{C}(\theta, \dot{\theta}) \triangleq H \phi (M \phi^* a + b) \in \mathcal{R}^N \quad (8.45)$$

$\mathcal{M} \in \mathcal{R}^{N \times N}$ denotes the mass matrix for the tree-topology system, and $\mathcal{C} \in \mathcal{R}^N$ is the vector of velocity dependent nonlinear Coriolis and gyroscopic velocity dependent terms. These operator expressions are identical to the ones in (5.25) for serial-chain systems. Adopting the terminology from the serial-chain case, we refer to the expression for \mathcal{M} in (8.45) as the Newton–Euler Factorization of the mass matrix.

We thus conclude that, even though the component-level relationships and the respective operator structures are quite different between canonical and non-canonical serial-chain systems and tree-topology systems, the BWA and 1-resolvent matrix properties of the \mathcal{E}_ϕ and ϕ spatial operators persist, and the operator level form of the equations of motion and the mass matrix, remarkably, remain unchanged! The connection between BWA matrices and multibody spatial operators was originally described in [75, 76].

Chapter 9

SKO Models

For canonical serial-chain systems, spatial operator techniques have been used to establish important analytical results, such as decompositions and factorizations of the mass matrix, and an operator expression for its inverse. This analytical groundwork led to low-order computational algorithms, such as for inverse dynamics, forward dynamics, and for computing the mass matrix.

Chapter 8 revealed that the \mathcal{E}_ϕ and ϕ spatial operators are BWA and 1-resolvent matrices for serial-chain, rigid-link multibody systems. We also found that very similar spatial operator level formulations, along with the associated BWA and 1-resolvent matrix properties, extended virtually unchanged to non-canonical serial-chains and to tree-topology rigid body systems. This remarkable consistency persists despite significant differences in the component structure of the corresponding \mathcal{E}_ϕ and ϕ spatial operators for these different systems. BWA matrices and 1-resolvent matrices will start to play a central role in our study of the dynamics of multibody systems. We will henceforth refer to multibody system spatial operators that are BWA matrices (such as \mathcal{E}_ϕ) as **spatial kernel operators (SKO)**, and to their associated 1-resolvent matrices (such as ϕ) as **spatial propagation operators (SPO)**.

A natural question that arises is whether the spatial operator analytical and algorithmic techniques developed for canonical serial-chain rigid body systems carry-over to tree-topology rigid body systems as well? Indeed, they do, and with very modest changes. In fact, these extensions are not limited to rigid-body tree-topology systems either, but are more broadly applicable.

To establish their generality, we use the SKO formulation as a point of departure. We will see that the spatial operator analytical techniques and algorithms developed for serial-chain systems originate from the SKO nature of the dynamics formulation, rather than from the specific, canonical, serial-chain, or rigid-body nature of the system. This motivates the use of SKO techniques as a general approach for formulating the dynamics of multibody systems, with the assurance that the powerful results from SKO formulations will automatically be available for further analysis and algorithm development.

9.1 SKO Models

Central to SKO formulations are the development of SKO models for multibody systems. These models are formally defined in the following section, and their properties are explored in the rest of the chapter.

9.1.1 Definition of SKO Models

An **SKO model** for an n -links tree-topology multibody system consists of the following:

1. A tree digraph reflecting the bodies and their connectivity in the system.
2. An $\mathcal{E}_\mathbb{A}$ SKO operator and associated SPO operator, \mathbb{A} .
3. A full-rank block-diagonal, joint map matrix operator, H .
4. A block-diagonal and positive-definite spatial inertia operator, M .
5. Stacked vectors: $\dot{\theta}$ denoting independent generalized velocities, \mathcal{T} the generalized forces, \mathcal{V} the node velocities, α the node accelerations, f the inter-node forces, a the node Coriolis accelerations, b the node gyroscopic forces the system, N the number of degrees of freedom, and the equations of motion defined as:

$$\begin{aligned}\mathcal{V} &= \mathbb{A}^* H^* \dot{\theta} \\ \alpha &= \mathbb{A}^* (H^* \ddot{\theta} + a) \\ f &= \mathbb{A}(M\alpha + b) \\ \mathcal{T} &= Hf\end{aligned}\tag{9.1}$$

Thus,

$$\mathcal{T} = \mathcal{M}(\theta) \ddot{\theta} + \mathcal{C}(\theta, \dot{\theta})\tag{9.2}$$

where

$$\mathcal{M}(\theta) \triangleq H\mathbb{A}M\mathbb{A}^*H^* \in \mathcal{R}^{N \times N} \text{ and } \mathcal{C}(\theta, \dot{\theta}) \triangleq H\mathbb{A}(M\mathbb{A}^*a + b) \in \mathcal{R}^N\tag{9.3}$$

\mathcal{M} is the symmetric and positive-definite mass matrix for the tree system and \mathcal{C} is the vector of nonlinear Coriolis and gyroscopic velocity dependent terms. (9.3) is the *Newton–Euler operator factorization* of the mass matrix.

To maximize generality, no assumptions have been made about the specific nature of the weight matrices in the SKO operators, about the component elements of H and M , or that the tree digraph is the *standard digraph* in an SKO model.

9.1.2 Existence of SKO Models

The SKO formulations derived in Chap. 8 for rigid-body, serial-chain and tree-topology, multibody systems are examples of SKO models with \mathcal{E}_ϕ and ϕ as the respective $\mathcal{E}_{\mathbb{A}}$ SKO and \mathbb{A} SPO operators. The existence of an SKO model does not depend on any exceptional or unusual features of tree-topology multibody systems. Indeed, SKO models can be viewed as a refinement of the models obtained from the classic, and widely used, *Kane's method* for developing multibody dynamics models [95, 96]. Central to Kane's method is the identification of *partial velocities* that define the mapping from generalized velocities to body velocities. The elements of the $\mathbb{A}^* \mathbb{H}^*$ matrix product of an SKO model are *precisely* Kane's partial velocities. This is an important connection between these modeling techniques.

While the partial velocity elements are adequate for formulating dynamics models using Kane's method, the important SPO property is unfortunately lost once the $\mathbb{A}^* \mathbb{H}^*$ partial velocities product is formed. The SPO nature of the operator \mathbb{A} plays a crucial role in analysis and algorithm development. Therefore, SKO models retain the more fundamental $(\mathbb{H}, \mathbb{A}, \mathbb{M})$ family of operators to not only define the (9.2) dynamics model, but also to derive important analytical and algorithmic techniques. We will, at times refer to an SKO model by its $(\mathbb{H}, \mathbb{A}, \mathbb{M})$ triplet of operators.

Section 9.6 describes a systematic process for developing SKO models for multi-body systems; in later chapters, we will apply this process to develop SKO models for a variety of systems.

9.1.3 Generalizations of SKO Models

To highlight the possible areas of generalization of SKO models, we contrast, below, the properties of BWA matrices with those of the familiar SKO operators for serial and tree-topology rigid body systems.

- BWA weight matrices are not limited to $6 \times 6 \phi(\varphi(k), k)$ rigid-body transformation matrices.
- BWA weight matrices can be non-square.
- BWA weight matrices can be of non-uniform size across edges.
- BWA weight matrices can be singular.

In general, SKO weight matrices can, and will, deviate in all of these respects from those for rigid body systems. We will see that the wide variability of the multibody systems is embodied in the definitions of their SKO model digraphs and, in the specific definitions of the weight matrices and operator component values.

We now mention two cautionary points concerning SKO models.

Definition of body nodes: The *standard* digraph for a multibody system assigns a node to each physical body in the system. This one-to-one correspondence between physical bodies and digraph nodes has been used to develop the SKO

models for tree-topology systems. However, this one-to-one correspondence is not a requirement for an SKO model. We will encounter cases where multiple physical bodies are associated with a single node in the digraph, as well as the converse, where multiple nodes are assigned to a single body! Since the majority of models will indeed be using the standard digraphs, we will use the *nodes* and *bodies* terminology interchangeably, and will highlight the exceptional cases when we encounter them.

Spatial operator compatibility: By construction, spatial operators have block structure derived from a combination of the underlying model digraph and the node weight dimensions. However, SKO models for a system are not unique, and may differ in the choices of digraph nodes, edges and weight dimensions.

Spatial operators and stacked vectors are said to be **compatible** when they are associated with the same SKO model. Expressions composing spatial operators and stacked vectors are only meaningful when all the component terms are *compatible*. Therefore, care is needed to avoid mixing spatial operators associated with different SKO models. The compatibility requirement, however, does not preclude the definition of transformations that relate operators across different SKO models.

In this section, and the following ones, we develop analytical results and algorithms for SKO models with no assumptions beyond those listed for the definition of these models. Therefore, the results can be used for any system for which an SKO model is available. We will also apply these results to important dynamics problems. Several of the spatial operator techniques and algorithms for serial-chain, rigid body systems will be generalized to the broader class of SKO models. SKO models will also be used to study the dynamics of closed-chain multibody systems in later chapters.

9.2 SPO Operator/Vector Products for Trees

In addition to the mathematical analysis supported by spatial operators, there is an intimate relationship between operator expressions and efficient recursive computational algorithms. We begin by studying this relationship in detail in the following lemma.

Lemma 9.1 Tips-to-base gather recursion to evaluate $\mathbb{A}x$.

Given an SPO operator, \mathbb{A} , and a compatible stacked vector, x , for a tree-topology system, the $y(k)$ elements of $y = \mathbb{A}x$, satisfy the following parent/child recursive relationship:

$$y(k) = \sum_{\forall i \in C(k)} \mathbb{A}(k,i)y(i) + x(k) \quad (9.4)$$

Based on this relationship, the elements of y can be computed using the following $O(N)$ **tips-to-base gather** recursive procedure:

$$\left\{ \begin{array}{l} \text{for all nodes } k \text{ (tips-to-base gather)} \\ y(k) = \sum_{\forall i \in \mathcal{C}(k)} \mathbb{A}(k, i)y(i) + x(k) \\ \text{end loop} \end{array} \right. \quad (9.5)$$

As will be customary, the steps in such gather recursions only apply to the body nodes and not the inertial node in the digraph.

Proof: The $y = \mathbb{A}x$ expression implies that

$$y(k) = \sum_{j=1}^n \mathbb{A}(k, j)x(j) \stackrel{8.16}{=} \sum_{\forall j \leq k} \mathbb{A}(k, j)x(j) \quad (9.6)$$

Therefore,

$$y(k) \stackrel{9.6, 8.17}{=} \sum_{\forall i \in \mathcal{C}(k)} \mathbb{A}(k, i) \sum_{\forall j \leq i} \mathbb{A}(i, j)x(j) + x(k) \stackrel{9.6}{=} \sum_{\forall i \in \mathcal{C}(k)} \mathbb{A}(k, i)y(i) + x(k)$$

This establishes (9.4). The procedure in (9.5) follows directly from this recursive expression. ■

The left side of Fig. 9.1 illustrates the flow of the recursive procedure in (9.5) for computing the $y(k)$ elements. It starts at the tip bodies of the tree and proceeds towards the base-body, while gathering together values converging at the branches. The computational cost of this tips-to-base gather procedure is just of $O(N)$ complexity, instead of the $O(N^2)$ complexity of a direct $\mathbb{A}x$ matrix/vector product. We will encounter several applications later that use this lemma to efficiently evaluate operator expressions involving products of SPO operators and stacked vectors. For a canonical serial-chain system, this gather algorithm simplifies to the one in Lemma 3.1 on page 51.

Similarly, the $x = \mathbb{A}^*y$ product can be evaluated using a base-to-tips, $O(N)$ scatter computational algorithm described in the following lemma.

Lemma 9.2 Base-to-tips scatter recursion to evaluate \mathbb{A}^*x .

Given an SPO operator, \mathbb{A} , and a compatible stacked vector x , for a tree-topology system, the $y(k)$ elements of $y = \mathbb{A}^*x$, satisfy the following parent/child recursive relationship:

$$y(k) = \mathbb{A}^*(\varrho(k), k)y(\varrho(k)) + x(k) \quad (9.7)$$

Based on this relationship, the elements of y can be computed using the following $O(N)$ **base-to-tips scatter** recursive procedure:

$$\left\{ \begin{array}{l} \text{for all nodes } k \text{ (base-to-tips scatter)} \\ y(k) = \mathbb{A}^*(\varrho(k), k)y(\varrho(k)) + x(k) \\ \text{end loop} \end{array} \right. \quad (9.8)$$

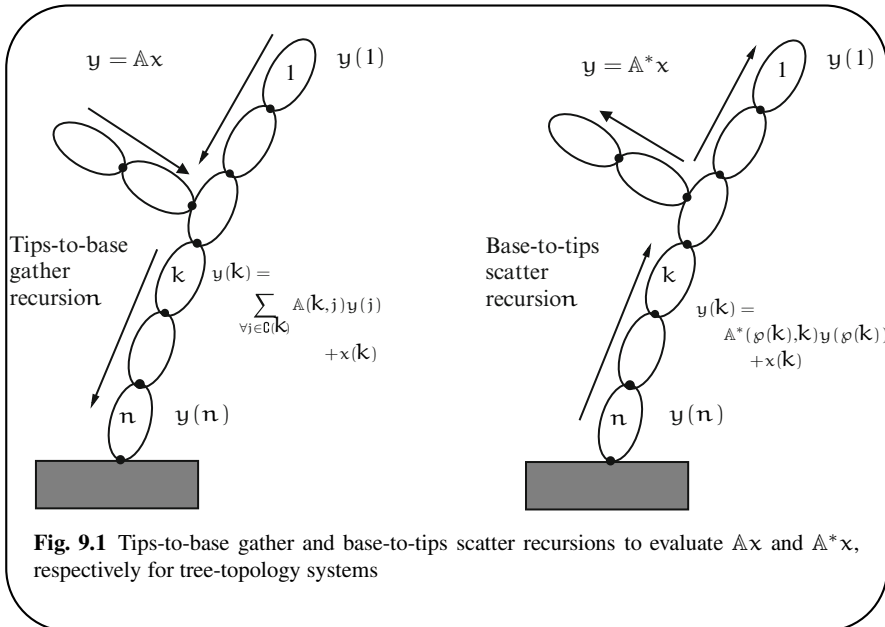


Fig. 9.1 Tips-to-base gather and base-to-tips scatter recursions to evaluate $\mathbb{A}x$ and \mathbb{A}^*x , respectively for tree-topology systems

As will be customary, the steps in such scatter recursions only apply to the body nodes and not the inertial nodes in the digraph. The quantities for the inertial node required in the initial step for the base-bodies in the scatter recursion are always assumed to be zero.

Proof: The $y = \mathbb{A}^*x$ expression implies that

$$y(k) = \sum_{j=1}^n \mathbb{A}^*(j, k)x(j) \stackrel{8.16}{=} \sum_{\forall j \succeq k} \mathbb{A}^*(j, k)x(j) \quad (9.9)$$

Therefore,

$$\begin{aligned} y(k) &\stackrel{9.9, 8.17}{=} \mathbb{A}^*(\varphi(k), k) \sum_{\forall i \succeq \varphi(k)} \mathbb{A}^*(i, \varphi(k))x(i) + x(k) \\ &\stackrel{9.9}{=} \mathbb{A}^*(\varphi(k), k)y(\varphi(k)) + x(k) \end{aligned}$$

This establishes (9.7). The recursion in (9.8) is a direct consequence of this relationship. ■

The right side of Fig. 9.1 illustrates the flow of the recursive procedure in (9.8) for computing the $y(k)$ elements. It starts at the base-body of the tree and proceeds towards the tips, while scattering the values onto diverging branches. The computational cost of this procedure is again just of $O(N)$ complexity, instead of the $O(N^2)$ complexity of a direct \mathbb{A}^*x matrix/vector product. We will encounter

several applications that use this lemma to efficiently evaluate products involving the transpose of an SPO operator and a stacked vector. For a serial-chain system, this scatter algorithm simplifies to the one derived in Lemma 3.2 on page 52.

Exercise 9.1 Recursive evaluation of $\tilde{A}x$ and \tilde{A}^*x .

Similar to (9.5) and (9.8), show that the elements of $y = \tilde{A}x$ satisfy the following recursive gather relationship:

$$y(k) = \sum_{\forall j \in C(k)} A(k, j)[y(j) + x(j)]$$

Additionally, show that the elements of $y = \tilde{A}^*x$ satisfy the following recursive scatter relationship:

$$y(k) = A^*(\varphi(k), k)[y(\varphi(k)) + x(\varphi(k))] \quad \blacksquare$$

Exercise 9.1 is a generalization of the serial-chain system algorithm described previously in Exercise 3.7 on page 53 for the $\tilde{\Phi}x$ and $\tilde{\Phi}^*x$ products.

Based on the results in this section, we can make the important observation that the *serial-chain recursive algorithms for operator expressions can be easily generalized to tree-topology systems by simply replacing tip-to-base recursions with tips-to-base gather recursions, and base-to-tip recursions with base-to-tips scatter recursions.*

9.2.1 SKO Model $O(N)$ Newton–Euler Inverse Dynamics

We now apply the mapping of SPO and stacked vector products to develop an efficient $O(N)$ recursive algorithm for the inverse dynamics problem for a system with an SKO model. For the inverse dynamics problem, the $\ddot{\Theta}$ generalized accelerations are assumed to be known, and the corresponding \mathcal{T} generalized forces need to be computed. (9.1) and (9.2) define the operator expressions for this mapping for the system. These operator expressions are precisely in the form of SPO and stacked vector products. Thus Lemmas 9.1 and 9.2 can be used to evaluate them using recursive scatter and gather algorithms. Algorithm 9.1 describes such an implementation. The algorithm begins with a base-to-tips scatter recursion that implement the operator expressions for \mathcal{V} and α in (9.1). This is followed by a recursive tips-to-base gather recursion to evaluate the expressions for f and \mathcal{T} in (9.1). This algorithm is a generalization of the serial-chain inverse dynamics algorithm described previously in Algorithm 5.2 on page 89. The primary changes are the switch to scatter/gather recursions required for tree systems, and the use of the generic component weight matrices for the SKO model.

Algorithm 9.1 Newton–Euler inverse dynamics algorithm for an SKO model

$$\left\{ \begin{array}{l} \textbf{for all nodes } k \text{ (base-to-tips scatter)} \\ \quad \mathcal{V}(k) = \mathbb{A}^*(\varphi(k), k)\mathcal{V}(\varphi(k)) + H^*(k)\dot{\theta}(k) \\ \quad \alpha(k) = \mathbb{A}^*(\varphi(k), k)\alpha(\varphi(k)) + H^*(k)\ddot{\theta}(k) + \alpha(k) \\ \textbf{end loop} \\ \\ \textbf{for all nodes } k \text{ (tips-to-base gather)} \\ \quad f(k) = \sum_{\forall j \in \mathcal{C}(k)} \mathbb{A}(k, j)f(j) + M(k)\alpha(k) + b(k) \\ \quad T(k) = H(k)f(k) \\ \textbf{end loop} \end{array} \right. \quad (9.10)$$

9.3 Lyapunov Equations for SKO Models

This section studies SPO operator quadratic expressions that are related to forward and backward Lyapunov equations for an SKO model.

9.3.1 Forward Lyapunov Recursions for SKO Models

Lemma 9.3 Structure of $\mathbb{A}\mathbb{X}\mathbb{B}^*$.

Let \mathbb{A} and \mathbb{B} denote compatible SPO operators and \mathbb{X} be a compatible block-diagonal operator. Then the $Z \stackrel{\triangle}{=} \mathbb{A}\mathbb{X}\mathbb{B}^*$ product can be decomposed into the following disjoint sum

$$Z = Y + \tilde{\mathbb{A}}Y + Y\tilde{\mathbb{B}}^* \quad (9.11)$$

where Y is a block-diagonal operator satisfying the **forward Lyapunov equation**:

$$X = Y - \mathcal{E}_{\mathbb{A}}Y\mathcal{E}_{\mathbb{B}}^* \quad (9.12)$$

The $Y(k)$ diagonal elements satisfy the recursive parent/child relationship:

$$Y(k) = \sum_{\forall j \in \mathcal{C}(k)} \mathbb{A}(k, j)Y(j)\mathbb{B}^*(k, j) + X(k) \quad (9.13)$$

Based on this relationship, the $Y(k)$ terms can be computed via the $O(N)$ tips-to-base, forward Lyapunov gather recursion:

$$\left\{ \begin{array}{l} \textbf{for all nodes } k \text{ (tips-to-base gather)} \\ Y(k) = \sum_{\forall j \in C(k)} A(k,j)Y(j)B^*(k,j) + X(k) \\ \textbf{end loop} \end{array} \right. \quad (9.14)$$

While Y defines the block-diagonal elements of Z , the following recursive expressions describe all the $Z(i,j)$ terms, including the off-diagonal ones:

$$Z(i,j) = \begin{cases} Y(i) & \text{for } i=j \\ A(i,k)Z(k,j) & \text{for } i \succ k \succeq j, \quad k \in C(i) \\ Z(i,k)B^*(j,k) & \text{for } i \preceq k \prec j, \quad k \in C(j) \\ \mathbf{0} & \text{otherwise} \end{cases} \quad (9.15)$$

Proof: First let us verify that (9.12) is well-posed, i.e., that $\mathcal{E}_A Y \mathcal{E}_B^*$ is block-diagonal when Y is block diagonal. This follows from:

$$\begin{aligned} \mathcal{E}_A Y \mathcal{E}_B^* &\stackrel{8.37}{=} \left\{ \sum_{j=1}^n e_{\varphi(j)} A(\varphi(j), j) e_j^* \right\} Y \left\{ \sum_{k=1}^n e_k B^*(\varphi(k), k) e_{\varphi(k)}^* \right\} \\ &\stackrel{8.3}{=} \sum_{j=1}^n e_{\varphi(j)} A(\varphi(j), j) Y(j) B^*(\varphi(j), j) e_{\varphi(j)}^* \end{aligned} \quad (9.16)$$

This has the form of a block-diagonal matrix with the k th diagonal element being $\sum_{j \in C(k)} A(k,j)Y(j)B^*(k,j)$. This implies that, at the component level, (9.12) is equivalent to

$$X(k) \stackrel{9.12, 9.16}{=} Y(k) - \sum_{\forall j \in C(k)} A(k,j)Y(j)B^*(k,j)$$

from which (9.13) follows.

Pre and post multiply (9.12) by A and B^* to get:

$$AXB^* \stackrel{8.19}{=} (\tilde{A} + I)Y(\tilde{B}^* + I) - \tilde{A}Y\tilde{B}^* = \tilde{A}Y + Y\tilde{B}^* + Y$$

This establishes (9.11).

The middle pair of expressions in (9.15) follow directly from the structure of $\tilde{A}Y$ and $Y\tilde{B}^*$. ■

The disjoint terms in (9.11) represent the following:

- The non-zero block-elements of the block-diagonal Y are the block-diagonal elements of AXB^* .
- The non-zero block-elements of $\tilde{A}Y$ and $Y\tilde{B}^*$ correspond to *related* node pairs in the system, i.e., nodes connected by a directed path.

- The remaining terms are zero, and correspond to *unrelated* node pairs, i.e., nodes with no directed path connecting them.

Since entries corresponding to node pairs that do not have an ancestor/child relationship are zero, \mathbf{AXB}^* is in general sparse. The sparsity structure reflects the topological connectivity of the nodes. Based on (9.15), the strategy for computing \mathbf{AXB}^* consists of:

1. First, compute the non-zero block-diagonal terms in \mathbf{Y} using the tips-to-base gather algorithm in (9.14).
2. Now consider the case of computing $Z(j, k)$, where j is an ancestor of k . Assume that node i is the child of j on the path to k . Use (9.15) to compute $Z(j, k) = \mathbb{A}(j, i)Z(i, k)$. This expression implies a recursion that starts with the $Z(k, k) = \mathbf{Y}(k)$ diagonal element, and computes the $Z(i, k)$ elements recursively along the path to node j .
3. Now consider the converse case of computing $Z(j, k)$, where j is a descendant of k . Assume that node i is the child of k on the path to j . Use (9.15) to compute $Z(j, k) = Z(j, i)\mathbb{B}^*(k, i)$. This expression implies a recursion that starts with the $Z(j, j) = \mathbf{Y}(j)$ diagonal element, and computes the $Z(j, i)$ elements recursively along the path to node k .

In the special case where $\mathbb{A} = \mathbb{B}$, case (3) above is unneeded because Z is symmetric, and $Z(j, k) = Z^*(k, j)$.

9.3.2 Mass Matrix Computation for an SKO Model

As seen in (9.2), the mass matrix in the SKO model has the operator expression $\mathcal{M} = \mathbf{H}\mathbf{A}\mathbf{A}^*\mathbf{H}^*$. The following lemma uses Lemma 9.3 to derive a decomposition of, and computational procedure for, the mass matrix.

Lemma 9.4 SKO model mass matrix decomposition.

The SKO model mass matrix can be decomposed into a sum of disjoint terms as follows:

$$\mathcal{M} = \mathbf{H}\mathcal{R}\mathbf{H}^* + \tilde{\mathbf{H}}\tilde{\mathcal{R}}\mathbf{H}^* + \mathbf{H}\tilde{\mathcal{R}}\tilde{\mathbf{A}}^*\mathbf{H}^* \quad (9.17)$$

where the block-diagonal composite body inertia operator, \mathcal{R} , satisfies the following forward Lyapunov equation:

$$\mathbf{M} = \mathcal{R} - \mathcal{E}_{\mathbb{A}}\mathcal{R}\mathcal{E}_{\mathbb{A}}^* \quad (9.18)$$

Proof: The results here are a direct consequence of Lemma 9.3, once we identify $\mathbb{B} = \mathbb{A}$, and $\mathbf{X} = \mathbf{M}$. From the lemma, we have the following disjoint decomposition of $\mathbf{A}\mathbf{M}\mathbf{A}^*$:

$$\mathbf{A}\mathbf{M}\mathbf{A}^* = \mathcal{R} + \tilde{\mathbf{A}}\mathcal{R} + \mathcal{R}\tilde{\mathbf{A}}^* \quad (9.19)$$

Equation (9.17) follows by pre and post multiplying the above expression with the block-diagonal H and H^* , respectively. ■

The tips-to-base gather Algorithm 9.2 describes the general composite body inertia algorithm for an SKO model. This algorithm is a generalization of the serial-chain composite body inertia Algorithm 4.1 on page 60.

Algorithm 9.2 Recursive computation of composite body inertias for an SKO model

$$\left\{ \begin{array}{l} \textbf{for all nodes } k \text{ (tips-to-base gather)} \\ \quad \mathcal{R}(k) = \sum_{\forall i \in \mathcal{C}(k)} \mathbb{A}(k,i)\mathcal{R}(i)\mathbb{A}^*(k,i) + M(k) \\ \textbf{end loop} \end{array} \right. \quad (9.20)$$

Remark 8.2 on page 145 discussed the sparsity structure of the $\mathcal{E}_{\mathbb{A}}$ and \mathbb{A} matrices for the canonical tree in Fig. 8.2. Based on (9.17), the following matrix illustrates the sparsity structure of the mass matrix for the same system:

$$\mathcal{M} = \begin{pmatrix} X & . & X & . & . & X & X \\ . & X & . & X & . & X & X \\ X & . & X & . & . & X & X \\ . & X & . & X & . & X & X \\ . & . & . & . & X & X & X \\ X & X & X & X & X & X & X \\ X & X & X & X & X & X & X \end{pmatrix}$$

The above matrix shows that, for trees, the \mathcal{M} mass matrix contains block-elements that are zero, because, unlike serial-chains, trees can have *unrelated* nodes. For serial-chain systems, the mass matrix is dense and fully populated because all nodes in a serial-chain system are *related*.

The sparsity of the mass matrix depends on the underlying branching structure of the system. As discussed in Sect. 14.3, the sparsity structure of the mass matrix is determined by the connectivity of its serial-chain segments; blocks corresponding to the segments are dense, while those corresponding to unrelated segments are zero. Section 14.3 also examines the sparsity structure of the mass matrix for the more complex tree system in Fig. 14.3.

Based on the decomposition in (9.17), Algorithm 9.3 describes a recursive procedure for computing the mass matrix of a tree-topology system. The outer loop includes the tips-to-base gather computation of the composite body inertias. The inner loop computes the mass matrix cross-terms for all the ancestors of a body. This algorithm for computing the mass matrix for SKO models is a generalization of the corresponding serial-chain Algorithm 4.2 on page 64.

Algorithm 9.3 Recursive computation of the SKO model mass matrix

```

    / for all nodes k (tips-to-base gather)
    R(k) = sum_{i in C(k)} A(k,i)R(i)A^*(k,i) + M(k)

    {
        j = k, X(k) = R(k)H^*(k), M(k,k) = H(k)X(k)
        while j
            l = g(j)
            X(l) = phi(l,j)X(j)
            M(l,k) = M^*(k,l) = H(l)X(l)
            j = l
        end loop
    end loop

```

9.3.3 Backward Lyapunov Recursions for SKO Models

Complementing the discussion on forward Lyapunov equations is the following lemma regarding backward Lyapunov equations for SKO models.

Lemma 9.5 Structure of $A^*X\mathbb{B}$.

Let \mathbb{A} and \mathbb{B} denote compatible SPO operators and X be a compatible block-diagonal operator. Then the $Z = A^*X\mathbb{B}$ product can be expressed as the following sum of disjoint terms:

$$Z = Y + \tilde{A}^*Y + Y\tilde{\mathbb{B}} + R$$

$$\text{where } R \triangleq \sum_{\substack{\forall i,j: i \neq j \\ k=g(i,j)}} e_i A^*(k,i) Y(k) \mathbb{B}(k,j) e_j^*$$
(9.21)

Y is a block-diagonal operator satisfying the following backward Lyapunov equation:

$$X = Y - \text{diagOf}\left\{ \mathcal{E}_{\mathbb{A}}^* Y \mathcal{E}_{\mathbb{B}} \right\}$$
(9.22)

The $\text{diagOf}\left\{ \mathcal{E}_{\mathbb{A}}^* Y \mathcal{E}_{\mathbb{B}} \right\}$ term represents just the diagonal block elements of the (generally non block-diagonal) $\mathcal{E}_{\mathbb{A}}^* Y \mathcal{E}_{\mathbb{B}}$ matrix. The $Y(k)$ diagonal elements satisfy the following parent/child recursive relationship:

$$Y(k) = A^*(g(k),k)Y(g(k))\mathbb{B}(g(k),k) + X(k)$$
(9.23)

Based on this relationship, the $Y(k)$ diagonal elements can be computed via the following $O(N)$ base-to-tips scatter recursion:

$$\begin{cases} \text{for all nodes } k \text{ (base-to-tips scatter)} \\ \quad Y(k) = A^*(\varphi(k), k)Y(\varphi(k))B(\varphi(k), k) + X(k) \\ \text{end loop} \end{cases} \quad (9.24)$$

While Y defines the block-diagonal elements of Z , the following recursive expressions describe all the $Z(i, j)$ terms, including the off-diagonal ones:

$$Z(i, j) = \begin{cases} Y(i) & \text{for } i = j \\ A^*(k, i)Z(k, j) & \text{for } i \prec k \preceq j, \quad k = \varphi(i) \\ Z(i, k)B(k, j) & \text{for } i \succeq k \succ j, \quad k = \varphi(j) \\ A^*(k, i)Y(k)B(k, j) & \text{for } i \not\simeq j, \quad j \not\simeq i, \quad k = \varphi(i, j) \end{cases} \quad (9.25)$$

Proof: We have

$$\begin{aligned} E_A^*YE_B &= \left\{ \sum_{j=1}^n e_j A^*(\varphi(j), j) e_{\varphi(j)}^* \right\} Y \left\{ \sum_{k=1}^n e_{\varphi(k)} B(\varphi(k), k) e_k^* \right\} \\ &\stackrel{8.3}{=} \sum_{\forall j, k: \varphi(j) = \varphi(k)} e_j A^*(\varphi(j), j) Y(\varphi(j)) B(\varphi(k), k) e_k^* \end{aligned}$$

Therefore,

$$\text{diagOf}\left\{ E_A^*YE_B \right\} = \sum_{j=1}^n e_j A^*(\varphi(j), j) Y(\varphi(j)) B(\varphi(j), j) e_j^* \quad (9.26)$$

This implies that, at the component level, (9.22) is equivalent to

$$X(k) \stackrel{9.22, 9.26}{=} Y(k) - A^*(\varphi(j), j) Y(\varphi(j)) B(\varphi(j), j)$$

from which (9.23) follows.

Now let us examine the elements of $Z = A^*XB$ in (9.21).

$$\begin{aligned} Z &= \left\{ \sum_{i=1}^n \sum_{\forall m \succeq i} e_i A^*(m, i) e_m^* \right\} X \left\{ \sum_{j=1}^n \sum_{\forall l \succeq j} e_l B(l, j) e_l^* \right\} \\ &= \sum_{i=1}^n \sum_{j=1}^n \sum_{\forall m \succeq i, j} e_i A^*(m, i) X(m) B(m, j) e_j^* \end{aligned}$$

Hence,

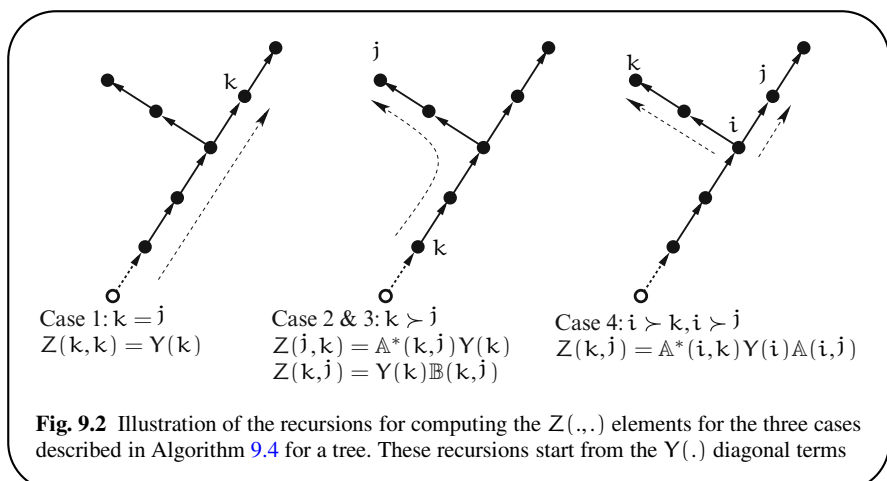
$$Z(i, j) = \sum_{\forall m \succeq i, j} A^*(m, i) X(m) B(m, j)$$

The expressions in (9.25) are a direct consequence of the above expression for $Z(i,j)$. ■

Unlike $\mathbb{A}X\mathbb{B}^*$, $\mathbb{A}^*X\mathbb{B}$ is a fully populated matrix. The disjoint partitioned terms in (9.21) have the following properties:

- The block-diagonal Y contains the diagonal block elements terms of $\mathbb{A}^*X\mathbb{B}$.
- The non-zero block-elements of $\tilde{\mathbb{A}}^*Y$ and $Y\tilde{\mathbb{B}}$ correspond to all *related* nodes.
- The non-zero block-elements of R on the other hand are for the remaining *unrelated* node pairs, i.e., ones that have no directed path connecting them.

As is evident from (9.25), all the block-elements of $\mathbb{A}^*X\mathbb{B}$ intimately dependent on the elements of the Y block-diagonal matrix. An important application of this lemma is to operational space inertias, as discussed in Chap. 10. The recursive computational strategy for the elements of $\mathbb{A}^*X\mathbb{B}$ is described in Algorithm 9.4. For the special case where $\mathbb{A} = \mathbb{B}$, Z is symmetric, and Step (3) in the algorithm can be skipped since these elements can be obtained from the transposes of the corresponding elements in Step (2).



The following Lemma describes simplifications of the backwards Lyapunov equation for serial-chain systems.

Lemma 9.6 $\mathbb{A}^*X\mathbb{B}$ structure for a serial-chain SKO model.

For a serial-chain system, $Z = \mathbb{A}^*X\mathbb{B}$ can be decomposed into disjoint diagonal, strictly upper triangular, and strictly lower triangular terms as follows:

$$Z = Y + \tilde{\mathbb{A}}^*Y + Y\tilde{\mathbb{B}} \quad (9.27)$$

Algorithm 9.4 Computation of $Z = A^* X B$

We have four situations to consider when computing a $Z(k,j)$ element. The respective recursive steps are described below and illustrated in Fig. 9.2.

1. To obtain a block-diagonal element, $Z(k,k)$, compute the $Y(k)$ element using the base-to-tips scatter $O(N)$ algorithm described in (9.24) as illustrated in the diagram on the left in Fig. 9.2.
2. If the k th body is an ancestor of the j th body, $Z(j,k)$ can be computed recursively, starting with the $Z(k,k) \equiv Y(k)$ diagonal element, which, in turn, is computed using the process described in case (1). The recursion for $Z(j,k)$, illustrated by the middle diagram of Fig. 9.2, starts with this $Y(k)$ diagonal entry, and propagates it along the path from the k th to the j th body, using the second expression in (9.25) to compute the $Z(k-1,k), Z(k-2,k)$, etc., terms.
3. If, on the other hand, the k th body is an ancestor of the j th body, then $Z(k,j)$ can be computed recursively, starting with the $Z(k,k) \equiv Y(k)$ diagonal element, which, in turn, is computed using the process described in case (1). The recursion for $Z(k,j)$, illustrated in the middle diagram of Fig. 9.2, starts with this $Y(k)$ diagonal entry, and propagates it along the path from the k th to the j th body, using the third expression in (9.25) to compute the $Z(k,k-1), Z(k,k-2)$, etc., terms.
4. Now consider the remaining case where the (k,j) node pair are *unrelated*. In this case, identify the body that is the closest ancestor for this pair of bodies. If the bodies do not have a common ancestor, then $Z(k,j)$ is zero since the bodies belong to independent, decoupled multibody trees.

If, on the other hand, there is a common ancestor, denoted the i th body, then the first step is to compute $Z(k,i)$, using the recursive procedure described in case (2). This value is then recursively propagated along the path from the i th body to the j th body, using the procedure in case (3) to compute the $Z(k,i-1), Z(k,i-2)$, etc., terms. This process is illustrated in the diagram on the right in Fig. 9.2.

where $Y \in \mathcal{R}^{6n \times 6n}$ is a block-diagonal operator satisfying the following backward Lyapunov equation:

$$X = Y - \mathcal{E}_A^* Y \mathcal{E}_B \quad (9.28)$$

Assuming that the serial-chain is canonical, the symmetric positive semi-definite $Y(k)$ diagonal matrices can be computed via the following $O(N)$ base-to-tip scatter recursion:

$$\left\{ \begin{array}{l} Y(n+1) = \mathbf{0} \\ \text{for } k = 1 \dots n \\ \quad Y(k) = A^*(k+1,k)Y(k+1)B(k+1,k) + X(k) \\ \text{end loop} \end{array} \right. \quad (9.29)$$

While Y defines the block-diagonal elements of Z , the following recursive expressions describe all the terms, including the off-diagonal ones:

$$Z(i,j) = \begin{cases} Y(i) & \text{for } i=j \\ A^*(i+1,i)Z(i+1,j) & \text{for } i < j \\ Z(i,j+1)B(j+1,j) & \text{for } i > j \end{cases} \quad (9.30)$$

Proof: Unlike trees, all nodes in a serial-chain systems are related, i.e., every pair of nodes is connected by a directed path. Hence, $R = \mathbf{0}$ in (9.21) for these systems. Substituting this in (9.21), and remembering that $\mathcal{E}_A^* Y \mathcal{E}_B$ in (9.22) is block-diagonal for serial-chains leads to this result. ■

Observe that Step (4) in Algorithm 9.4 is not needed for serial-chain systems.

9.4 Riccati Equations for SKO Models

This section studies another type of SPO quadratic equation, known as a Riccati equation, for SKO models.

Lemma 9.7 The Riccati equation for SKO models.

Let (H, A, M) denote spatial operators for an SKO model. The following Riccati equation has a block-diagonal, symmetric and positive-definite operator solution, P :

$$M = P - \mathcal{E}_A [P - PH^*(HPH^*)^{-1}HP] \mathcal{E}_A^* \quad (9.31)$$

The expression in (9.31) can be broken down into simpler sub-expressions as follows:

$$M = P - \mathcal{E}_A \left[P - \underbrace{P H^* (\underbrace{H P H^*}_{\mathcal{D}})^{-1} H P}_{\mathcal{G}} \right] \mathcal{E}_A^*$$

$$\mathcal{D}$$

$$\mathcal{G}$$

$$\tau$$

$$\mathcal{P}^+$$

The above sub-expressions define the block-diagonal spatial operators:

$$\begin{aligned} \mathcal{D} &\triangleq HPH^*, & \mathcal{G} &\triangleq PH^*\mathcal{D}^{-1}, & \tau &\triangleq \mathcal{G}H \\ \bar{\tau} &\triangleq I - \tau, & \mathcal{P}^+ &\triangleq \bar{\tau}P = \bar{\tau}\mathcal{P}\bar{\tau}^* \end{aligned} \quad (9.32)$$

The $\mathcal{P}(k)$ and other diagonal elements can be computed by the following $O(N)$ tips-to-base gather recursion:

$$\left\{ \begin{array}{l} \textbf{for all nodes } k \text{ (tips-to-base gather)} \\ \quad \mathcal{P}(k) = \sum_{\forall j \in \mathbb{C}(k)} \mathbb{A}(k,j) \mathcal{P}^+(j) \mathbb{A}^*(k,j) + \mathbf{M}(k) \\ \quad \mathcal{D}(k) = \mathbb{H}(k) \mathcal{P}(k) \mathbb{H}^*(k) \\ \quad \mathcal{G}(k) = \mathcal{P}(k) \mathbb{H}^*(k) \mathcal{D}^{-1}(k) \\ \quad \tau(k) = \mathcal{G}(k) \mathbb{H}(k) \\ \quad \bar{\tau}(k) = \mathbf{I} - \tau(k) \\ \quad \mathcal{P}^+(k) = \bar{\tau}(k) \mathcal{P}(k) \\ \textbf{end loop} \end{array} \right. \quad (9.33)$$

Proof: Equation (9.33) is essentially a component level restatement of (9.31). The positive definiteness of \mathbf{M} and full row-rankness of \mathbb{H} ensures that $\mathcal{D}^{-1}(k)$ exists and is well defined. \blacksquare

This lemma is a generalization of the corresponding Riccati equation in Lemma 7.1 on page 117 for serial-chain rigid body systems.

9.4.1 The \mathcal{E}_ψ and ψ SKO and SPO Operators

Lemma 9.8 The \mathcal{E}_ψ SKO operator.

Let $\mathcal{E}_\mathbb{A}$ be an SKO operator, and \mathbb{H}, \mathbf{M} , be compatible operators satisfying the conditions in Lemma 9.7. Let \mathcal{P} denote the block-diagonal solution to the (9.31) Riccati equation. Define

$$\mathcal{E}_\psi \stackrel{\triangle}{=} \mathcal{E}_\mathbb{A} \bar{\tau} \quad (9.34)$$

Then \mathcal{E}_ψ is an SKO operator, with weights and SPO operator ψ , defined by

$$\psi(\varphi(k), k) \stackrel{\triangle}{=} \mathbb{A}(\varphi(k), k) \bar{\tau}(k), \quad \text{and} \quad \psi \stackrel{\triangle}{=} (\mathbf{I} - \mathcal{E}_\psi)^{-1} \quad (9.35)$$

Moreover, the (9.31) Riccati equation can be re-expressed as:

$$\mathbf{M} = \mathcal{P} - \mathcal{E}_\psi \mathcal{P} \mathcal{E}_\psi^* = \mathcal{P} - \mathcal{E}_\mathbb{A} \mathcal{P} \mathcal{E}_\psi^* \quad (9.36)$$

Proof: Since $\mathcal{E}_\mathbb{A}$ is an SKO operator, we have

$$\begin{aligned} \mathcal{E}_\psi &\stackrel{9.34}{=} \left(\sum_{k=1}^n e_{\varphi(k)} \mathbb{A}(\varphi(k), k) e_k^* \right) \bar{\tau} \stackrel{8.22}{=} \sum_{k=1}^n e_{\varphi(k)} \mathbb{A}(\varphi(k), k) \bar{\tau}(k) e_k^* \\ &\stackrel{9.35}{=} \sum_{k=1}^n e_{\varphi(k)} \psi(\varphi(k), k) e_k^* \end{aligned}$$

This implies that \mathcal{E}_ψ is indeed an SKO operator, with weights defined by $\psi(\varphi(k), k)$. Thus, its 1-resolvent, ψ , defined by (9.35) exists.

The first part of the Riccati equation expression in (9.36). This is equivalent to (9.31) follows from the direct use of the expressions in (9.32) to observe that:

$$\mathcal{P} - \mathcal{P}H^*(H\mathcal{P}H^*)^{-1}H\mathcal{P} = \bar{\tau}\mathcal{P} = \mathcal{P}\bar{\tau}^* = \bar{\tau}\mathcal{P}\bar{\tau}^* = \mathcal{P}^+$$

■

Unlike the \mathcal{E}_A SKO operators, which are defined during the SKO model formulation process, the \mathcal{E}_ψ SKO operators are derived operators obtained from the solution to the Riccati equation. Likewise, the ψ SPO operator is also a derived by-product of the solution of the Riccati equation. Observe that the $\psi(\varphi(k), k)$ matrices are singular even when $A(\varphi(k), k)$ is non-singular.

9.4.2 Operator Identities

Define the \mathcal{K} spatial operator as follows:

$$\mathcal{K} = \mathcal{E}_A \mathcal{G} \quad (9.37)$$

\mathcal{K} is *not* block-diagonal, but has structure similar to that of \mathcal{E}_A . The following lemma establishes operator identities that will be needed later.

Lemma 9.9 Useful spatial operator identities.

1.

$$\begin{aligned} H\mathcal{G} &= I, & H\tau &= H, & H\bar{\tau} &= 0 \\ I + H\mathcal{A}\mathcal{K} &= H\mathcal{A}\mathcal{G} \end{aligned} \quad (9.38)$$

2.

$$H\mathcal{A}\bar{\tau} = H\mathcal{A}\mathcal{E}_\psi \quad (9.39)$$

3.

$$H\mathcal{A}\tau = H\mathcal{A}(I - \mathcal{E}_\psi) = H\mathcal{A}\psi^{-1} \quad (9.40)$$

4. $\mathcal{A}\mathbf{M}\psi^*$ has the following disjoint decomposition:

$$\mathcal{A}\mathbf{M}\psi^* = \mathcal{P} + \tilde{\mathcal{A}}\mathcal{P} + \mathcal{P}\tilde{\psi}^* \quad (9.41)$$

Proof:

1. The expressions in (9.38) follow from (9.32) and (9.37).
2. We have

$$H\mathcal{A}\bar{\tau} \stackrel{8.19}{=} H(\tilde{\mathcal{A}} + I)\bar{\tau} \stackrel{8.19}{=} H\mathcal{A}\mathcal{E}_A\bar{\tau} + H\bar{\tau} \stackrel{9.34, 9.32}{=} H\mathcal{A}\mathcal{E}_\psi$$

3. We have

$$\mathbb{H}\mathbb{A}\tau \stackrel{9.32}{=} \mathbb{H}\mathbb{A}(\mathbf{I} - \bar{\tau}) \stackrel{9.39}{=} \mathbb{H}\mathbb{A}(\mathbf{I} - \mathcal{E}_\psi) \stackrel{9.35}{=} \mathbb{H}\mathbb{A}\psi^{-1}$$

4. Pre and post multiplying (9.36) by \mathbb{A} and ψ^* , then simplifying, leads to (9.41). ■

The following lemma derives additional operator identities. Several of these identities (and their proofs) are similar to those in Lemma 7.2 on page 119 for serial-chain systems, but, for completeness, they are repeated here in the more general SKO model context.

Lemma 9.10 Additional spatial operator identities.

1.

$$\psi \mathbf{M} \psi^* = \mathcal{P} + \tilde{\psi} \mathcal{P} + \mathcal{P} \tilde{\psi}^* \quad (9.42)$$

2.

$$\psi^{-1} - \mathbb{A}^{-1} = \mathcal{K}\mathcal{H} \quad (9.43)$$

3.

$$\begin{aligned} \psi^{-1}\mathbb{A} &= \mathbf{I} + \mathcal{K}\mathcal{H}\mathbb{A} \\ \mathbb{A}\psi^{-1} &= \mathbf{I} + \mathbb{A}\mathcal{K}\mathcal{H} \\ \mathbb{A}^{-1}\psi &= \mathbf{I} - \mathcal{K}\mathcal{H}\psi \\ \psi\mathbb{A}^{-1} &= \mathbf{I} - \psi\mathcal{K}\mathcal{H} \end{aligned} \quad (9.44)$$

4.

$$\begin{aligned} [\mathbf{I} - \mathcal{H}\psi\mathcal{K}]\mathcal{H}\mathbb{A} &= \mathcal{H}\psi \\ \mathbb{A}\mathcal{K}[\mathbf{I} - \mathcal{H}\psi\mathcal{K}] &= \psi\mathcal{K} \\ [\mathbf{I} + \mathcal{H}\mathbb{A}\mathcal{K}]\mathcal{H}\psi &= \mathcal{H}\mathbb{A} \\ \psi\mathcal{K}[\mathbf{I} + \mathcal{H}\mathbb{A}\mathcal{K}] &= \mathbb{A}\mathcal{K} \end{aligned} \quad (9.45)$$

5.

$$\mathcal{H}\psi \mathbf{M} \psi^* \mathcal{H}^* = \mathcal{D} \quad (9.46)$$

6.

$$\mathbb{A}\mathbf{M}\mathbb{A}^* = \mathcal{P} + \tilde{\mathbb{A}}\mathcal{P} + \mathcal{P}\tilde{\mathbb{A}}^* + \mathbb{A}\mathcal{K}\mathcal{D}\mathcal{K}^*\mathbb{A}^* \quad (9.47)$$

7.

$$\mathbb{A}\mathbf{M}\mathbb{A}^* \mathcal{H}^* = [\mathbf{I} + \mathbb{A}\mathcal{K}\mathcal{H}]\mathcal{P}\mathbb{A}^* \mathcal{H}^* \quad (9.48)$$

Proof:

1. Pre- and post-multiplying (9.36) by ψ and ψ^* , we obtain

$$\begin{aligned} \psi \mathbf{M} \psi^* &= \psi \mathcal{P} \psi^* - \psi \mathcal{E}_\psi \mathcal{P} \mathcal{E}_\psi^* \psi^* \stackrel{8.19}{=} (\tilde{\psi} + \mathbf{I}) \mathcal{P} (\tilde{\psi} + \mathbf{I})^* - \tilde{\psi} \mathcal{P} \tilde{\psi}^* \\ &= \mathcal{P} + \tilde{\psi} \mathcal{P} + \mathcal{P} \tilde{\psi}^* \end{aligned}$$

2. From (8.15)

$$\begin{aligned}\Psi^{-1} &= \mathbf{I} - \mathcal{E}_\Psi \stackrel{9.32}{=} \mathbf{I} - \mathcal{E}_\mathbb{A} \bar{\tau} \stackrel{9.32}{=} (\mathbf{I} - \mathcal{E}_\mathbb{A}) + \mathcal{E}_\mathbb{A} \tau \\ &\stackrel{8.15, 9.32}{=} \mathbb{A}^{-1} + \mathcal{E}_\mathbb{A} \mathcal{G} \mathcal{H} \stackrel{9.32}{=} \mathbb{A}^{-1} + \mathcal{K} \mathcal{H}\end{aligned}$$

3. Pre- and post-multiplying (9.43) by \mathbb{A} leads to the first pair of identities in (9.44).

Repeating the process using ψ leads to the latter pair.

4. We have

$$[\mathbf{I} - \mathcal{H}\psi\mathcal{K}] \mathcal{H}\mathbb{A} = \mathcal{H}[\mathbf{I} - \psi\mathcal{K}\mathcal{H}] \mathbb{A} \stackrel{9.44}{=} \mathcal{H}(\psi\mathbb{A}^{-1})\mathbb{A} = \mathcal{H}\psi$$

Similar use of the other identities in (9.44) leads to the remaining identities in (9.45).

5. We have

$$\begin{aligned}\mathcal{H}\psi \mathbf{M} \psi^* \mathcal{H}^* &\stackrel{9.36}{=} \mathcal{H}(\mathcal{P} + \tilde{\psi}\mathcal{P} + \mathcal{P}\tilde{\psi}^*) \mathcal{H}^* \\ &\stackrel{9.32}{=} \mathcal{D} + \mathcal{H}\tilde{\psi}\mathcal{P}\mathcal{H}^* + \mathcal{H}\mathcal{P}\tilde{\psi}^*\mathcal{H}^* \\ &\stackrel{8.19}{=} \mathcal{D} + \mathcal{H}\psi\mathcal{E}_\Psi\mathcal{P}\mathcal{H}^* + \mathcal{H}\mathcal{P}\mathcal{E}_\Psi^*\psi^*\mathcal{H}^* \\ &\stackrel{9.32}{=} \mathcal{D} + \mathcal{H}\psi\mathcal{E}_\mathbb{A}\bar{\tau}\mathcal{P}\mathcal{H}^* + \mathcal{H}\mathcal{P}\bar{\tau}^*\mathcal{E}_\mathbb{A}^*\psi^*\mathcal{H}^* \\ &\stackrel{9.32}{=} \mathcal{D} + \mathcal{H}\psi\mathcal{E}_\mathbb{A}\mathcal{P}^+\mathcal{H}^* + \mathcal{H}\mathcal{P}^+\mathcal{E}_\mathbb{A}^*\psi^*\mathcal{H}^* \\ &\stackrel{9.38, 9.32}{=} \mathcal{D}\end{aligned}$$

6. Now

$$\begin{aligned}\mathbb{A} \mathbf{M} \mathbb{A}^* &= (\mathbb{A}\psi^{-1})\psi \mathbf{M} \mathbb{A}^* \stackrel{9.41}{=} (\mathbb{A}\psi^{-1})(\psi\mathcal{P} + \mathcal{P}\tilde{\mathbb{A}}^*) \\ &\stackrel{9.43}{=} \mathbb{A}\mathcal{P} + (\mathbf{I} + \mathbb{A}\mathcal{K}\mathcal{H})\mathcal{P}\tilde{\mathbb{A}}^* = \mathbb{A}\mathcal{P} + \mathcal{P}\tilde{\mathbb{A}}^* + \mathbb{A}\mathcal{K}\mathcal{H}\mathcal{P}\tilde{\mathbb{A}}^* \\ &\stackrel{9.32, 9.37, 8.19}{=} \mathcal{P} + \tilde{\mathbb{A}}\mathcal{P} + \mathcal{P}\tilde{\mathbb{A}}^* + \mathbb{A}\mathcal{K}\mathcal{D}\mathcal{K}^*\mathbb{A}^*\end{aligned}$$

7. We have

$$\begin{aligned}\mathbb{A} \mathbf{M} \mathbb{A}^* \mathcal{H}^* &= (\mathbb{A}\psi^{-1})(\psi \mathbf{M} \mathbb{A}^*) \mathcal{H}^* \stackrel{9.41}{=} (\mathbb{A}\psi^{-1})(\tilde{\psi}\mathcal{P} + \mathcal{P}\mathbb{A}^*) \mathcal{H}^* \\ &\stackrel{8.19}{=} \mathbb{A}\mathcal{E}_\Psi\mathcal{P}\mathcal{H}^* + (\mathbb{A}\psi^{-1})\mathcal{P}\mathbb{A}^*\mathcal{H}^* \\ &\stackrel{9.32}{=} \mathbb{A}\mathcal{E}_\Psi\mathcal{P}^+\mathcal{H}^* + (\mathbf{I} + \mathbb{A}\mathcal{K}\mathcal{H})\mathcal{P}\mathbb{A}^*\mathcal{H}^* \\ &\stackrel{9.38}{=} (\mathbf{I} + \mathbb{A}\mathcal{K}\mathcal{H})\mathcal{P}\mathbb{A}^*\mathcal{H}^*\end{aligned}$$

■

It is noteworthy that the $\mathcal{H}\psi \mathbf{M} \psi^* \mathcal{H}^*$ expression in (9.46) is block-diagonal, in contrast to the similar expression, $\mathcal{M} = \mathcal{H} \mathbf{M} \mathbf{A}^* \mathcal{H}^*$, for the non-diagonal mass matrix.

9.5 SKO Model Mass Matrix Factorization and Inversion

The following lemma derives the mass matrix factorization and inversion properties for SKO models.

Lemma 9.11 SKO mass matrix factorization and inversion.

Let (H, A, M) denote spatial operators for an SKO model. Recall that its mass-matrix is defined as $\mathcal{M} = HAM^*A^*H^*$.

1. The \mathcal{M} mass matrix has an alternative Innovations Operator factorization defined by

$$\mathcal{M} = [I + HAK] \mathcal{D} [I + HAK]^* \quad (9.49)$$

In this equation, \mathcal{D} and \mathcal{K} are operators obtained from the solution of the discrete Riccati equation from Lemma 9.8. for the SKO model.

2. $[I + HAK]$ is invertible, with inverse given by:

$$[I + HAK]^{-1} = [I - H\psi K] \quad (9.50)$$

3. The mass matrix \mathcal{M} is invertible, and the expression for its inverse is

$$\mathcal{M}^{-1} = [I - H\psi K]^* \mathcal{D}^{-1} [I - H\psi K] \quad (9.51)$$

Proof:

1. We have

$$\begin{aligned} \mathcal{M} &= HAM^*A^*H^* = H(A\psi^{-1})\psi M\psi^*(A\psi^{-1})^*\psi^*H^* \\ &\stackrel{9.44}{=} H[I + A\mathcal{K}H]\psi M\psi^*[I + A\mathcal{K}H]^*\psi^*H^* \\ &= [I + HAK](H\psi M\psi^*H^*)[I + HAK]^* \\ &\stackrel{9.46}{=} [I + HAK]\mathcal{D}[I + HAK]^* \end{aligned}$$

2. From the standard matrix identity $(I + AB)^{-1} = I - A(I + BA)^{-1}B$, we have:

$$\begin{aligned} [I + HAK]^{-1} &= I - H[I + A\mathcal{K}H]^{-1}A\mathcal{K} \stackrel{9.44}{=} I - H(A\psi^{-1})^{-1}A\mathcal{K} \\ &= I - H\psi K \end{aligned}$$

3. We have

$$\begin{aligned} \mathcal{M}^{-1} &\stackrel{9.49}{=} \{[I + HAK]\mathcal{D}[I + HAK]^*\}^{-1} = [I + HAK]^{-*}\mathcal{D}^{-1}[I + HAK]^{-1} \\ &\stackrel{9.50}{=} [I - H\psi K]^*\mathcal{D}^{-1}[I - H\psi K]^{-1} \end{aligned}$$

■

This lemma is a generalization of the serial-chain, rigid multibody system mass matrix factorization and inversion results from Chap. 7.

Exercise 9.2 Determinant of the mass matrix.

1. Show that $[\mathbf{I} + \mathbf{H}\mathbf{A}\mathcal{K}]$ and $[\mathbf{I} - \mathbf{H}\psi\mathcal{K}]$ are strictly lower triangular for canonical trees, and that they have identity block matrices along the diagonal.
2. Show that the determinant of the Newton–Euler operator factor $[\mathbf{I} + \mathbf{H}\mathbf{A}\mathcal{K}]$ is

$$\det\{\mathbf{I} + \mathbf{H}\mathbf{A}\mathcal{K}\} = 1 \quad (9.52)$$

3. Furthermore, show that the determinant of the mass matrix is given by

$$\det\{\mathcal{M}\} = \prod_{k=1}^n \det\{\mathcal{D}(k)\} \quad (9.53)$$

■

9.5.1 $O(N)$ AB Forward Dynamics

The forward dynamics problem consists of computing the $\ddot{\theta}$ generalized accelerations, given the \mathcal{T} generalized forces for the system. The following lemma derives an explicit operator expression for $\ddot{\theta}$. This lemma is a generalization of the corresponding Lemma 7.6 for canonical serial-chain systems.

Lemma 9.12 Expression for $\ddot{\theta} = \mathcal{M}^{-1}(\mathcal{T} - \mathcal{C})$.

The explicit expression for $\ddot{\theta}$ is

$$\ddot{\theta} = \mathcal{M}^{-1}(\mathcal{T} - \mathcal{C}) = [\mathbf{I} - \mathbf{H}\psi\mathcal{K}]^* \mathcal{D}^{-1} [\mathcal{T} - \mathbf{H}\psi(\mathcal{K}\mathcal{T} + \mathcal{P}\mathbf{a} + \mathbf{b})] - \mathcal{K}^* \psi^* \mathbf{a} \quad (9.54)$$

Proof: We have

$$\begin{aligned} \ddot{\theta} &\stackrel{9.51}{=} [\mathbf{I} - \mathbf{H}\psi\mathcal{K}]^* \mathcal{D}^{-1} [\mathbf{I} - \mathbf{H}\psi\mathcal{K}] (\mathcal{T} - \mathcal{C}) \\ &\stackrel{9.2}{=} [\mathbf{I} - \mathbf{H}\psi\mathcal{K}]^* \mathcal{D}^{-1} [\mathbf{I} - \mathbf{H}\psi\mathcal{K}] (\mathcal{T} - \mathbf{H}\mathbf{A}(\mathbf{M}\mathbf{A}^* \mathbf{a} + \mathbf{b})) \\ &= [\mathbf{I} - \mathbf{H}\psi\mathcal{K}]^* \mathcal{D}^{-1} [\mathbf{I} - \mathbf{H}\psi\mathcal{K}] \mathcal{T} \\ &\quad - [\mathbf{I} - \mathbf{H}\psi\mathcal{K}]^* \mathcal{D}^{-1} [\mathbf{I} - \mathbf{H}\psi\mathcal{K}] \mathbf{H}\mathbf{A}(\mathbf{M}\mathbf{A}^* \mathbf{a} + \mathbf{b}) \end{aligned} \quad (9.55)$$

Now,

$$\begin{aligned}
 [\mathbf{I} - \mathsf{H}\psi\mathcal{K}] \mathsf{H}\mathbb{A}(\mathbf{M}\mathbb{A}^*\mathfrak{a} + \mathfrak{b}) &= \mathsf{H}[\mathbf{I} - \mathsf{H}\mathcal{K}\mathsf{H}]\mathbb{A}(\mathbf{M}\mathbb{A}^*\mathfrak{a} + \mathfrak{b}) \\
 &\stackrel{9.44}{=} \mathsf{H}(\psi\mathbb{A}^{-1})\mathbb{A}(\mathbf{M}\mathbb{A}^*\mathfrak{a} + \mathfrak{b}) \\
 &= \mathsf{H}\psi(\mathbf{M}\mathbb{A}^*\mathfrak{a} + \mathfrak{b}) \\
 &\stackrel{9.41}{=} \mathsf{H}((\mathsf{P}\mathcal{P} + \mathcal{P}\tilde{\mathbb{A}}^*)\mathfrak{a} + \psi\mathfrak{b}) \\
 &\stackrel{9.32}{=} (\mathsf{H}\psi\mathcal{P} + \mathcal{D}\mathcal{K}^*\mathbb{A}^*)\mathfrak{a} + \mathsf{H}\psi\mathfrak{b}
 \end{aligned} \tag{9.56}$$

Substituting this expression into the second half of (9.55), it follows that

$$\begin{aligned}
& [\mathbf{I} - \mathsf{H}\Psi\mathcal{K}]^*\mathcal{D}^{-1}[\mathbf{I} - \mathsf{H}\Psi\mathcal{K}] \mathsf{H}\mathbb{A}(\mathbf{M}\mathbb{A}^*\mathfrak{a} + \mathfrak{b})) \\
&= [\mathbf{I} - \mathsf{H}\Psi\mathcal{K}]^*\mathcal{D}^{-1}[(\mathsf{H}\Psi\mathcal{P} + \mathcal{D}\mathcal{K}^*\mathbb{A}^*)\mathfrak{a} + \mathsf{H}\Psi\mathfrak{b}] \\
&\stackrel{9.44}{=} [\mathbf{I} - \mathsf{H}\Psi\mathcal{K}]^*\mathcal{D}^{-1}[\mathsf{H}\Psi\mathcal{P}\mathfrak{a} + \mathsf{H}\Psi\mathfrak{b}] + \mathcal{K}^*(\mathbb{A}^{-1}\Psi)^*\mathbb{A}^*\mathfrak{a} \quad (9.57) \\
&\stackrel{9.44}{=} [\mathbf{I} - \mathsf{H}\Psi\mathcal{K}]^*\mathcal{D}^{-1}\mathsf{H}\Psi(\mathcal{P}\mathfrak{a} + \mathfrak{b}) + \mathcal{K}^*\Psi^*\mathfrak{a}
\end{aligned}$$

Substituting this expression in (9.55) leads to (9.54).

Using similar steps to those in Sect. 7.2.1 on page 123, we group together sub-expressions in (9.54) to define intermediate quantities as shown below:

$$\ddot{\theta} = [\mathbf{I} - \mathbf{H}\psi\mathcal{K}]^* \mathcal{D}^{-1} [\mathcal{T} - \mathbf{H} \underbrace{\Psi(\mathcal{K}\mathcal{T} + \mathcal{P}\alpha + \mathfrak{b})}_{\mathfrak{z}}] - \mathcal{K}^* \psi^* \alpha$$

$$\underbrace{\qquad\qquad\qquad}_{\epsilon}$$

$$\underbrace{\qquad\qquad\qquad}_{\gamma}$$

Using these intermediate quantities, and simplifications similar to those in Sect. 7.2.1, (9.54) can be re-expressed as

$$\mathfrak{z} = \mathcal{E}_\phi \mathfrak{z}^+ + \mathcal{P}\mathfrak{a} + \mathfrak{b} \quad (9.58a)$$

$$\mathfrak{z}^+ = \mathfrak{z} + \mathcal{G}\epsilon \quad (9.58b)$$

$$\epsilon = \mathcal{T} - \mathsf{H}\mathfrak{z} \quad (9.58c)$$

$$\nu = \mathcal{D}^{-1} \epsilon \quad (9.58d)$$

$$\alpha^+ = \mathcal{E}_\phi^* \alpha \quad (9.58e)$$

$$\ddot{\theta} = \nu - \mathcal{G}^* \alpha^+ \quad (9.58f)$$

$$\alpha = \alpha^+ + H^* \ddot{\theta} + \alpha \quad (9.58g)$$

Recall that ψ is an SPO operator. We can thus use Lemmas 9.1 and 9.2 to develop a recursive algorithm for evaluating $\ddot{\theta}$ from the expressions in (9.58). The resulting $O(N)$ AB forward dynamics algorithm for SKO models is described in Algorithm 9.5. It is a generalization of Algorithm 7.1 on page 126 for the AB forward dynamics of serial-chain rigid body systems. The algorithm consists of a tips-to-base gather sweep to compute the residual terms, followed by a base-to-tips scatter sweep for the generalized accelerations.

Algorithm 9.5 $O(N)$ AB forward dynamics for SKO models

-
1. Compute the articulated body inertia \mathcal{P} , \mathcal{D} , etc., quantities using the gather algorithm in (9.33).
 2. Use the following gather and scatter recursions to compute $\ddot{\theta}$:

$$\left\{ \begin{array}{l} \text{for all nodes } k \text{ (tips-to-base gather)} \\ \quad \mathfrak{z}(k) = \sum_{\forall j \in \mathcal{C}(k)} \mathbb{A}(k, j) \mathfrak{z}^+(j) + \mathcal{P}(k) \mathfrak{a}(k) + \mathfrak{b}(k) \\ \quad \epsilon(k) = \mathcal{T}(k) - H(k) \mathfrak{z}(k) \\ \quad \nu(k) = \mathcal{D}^{-1}(k) \epsilon(k) \\ \quad \mathfrak{z}^+(k) = \mathfrak{z}(k) + \mathcal{G}(k) \epsilon(k) \\ \text{end loop} \\ \\ \text{for all nodes } k \text{ (base-to-tips scatter)} \\ \quad \alpha^+(k) = \mathbb{A}^*(\varphi(k), k) \alpha(\varphi(k)) \\ \quad \ddot{\theta}(k) = \nu(k) - \mathcal{G}^*(k) \alpha^+(k) \\ \quad \alpha(k) = \alpha^+(k) + H^*(k) \ddot{\theta}(k) + \mathfrak{a}(k) \\ \text{end loop} \end{array} \right.$$

9.6 Generalized SKO Formulation Process

In this chapter, we have derived analytical techniques and efficient algorithms for SKO models of multibody systems. These have included

- Recursive $O(N)$ procedures for computing SPO operator and stacked vector products.
- General $O(N)$ Newton–Euler inverse dynamics algorithms.
- Solutions for the forward Lyapunov equations and decomposition of $\mathbb{A}X\mathbb{B}^*$ operator product.
- General $O(N^2)$ algorithm for computing the mass matrix.
- Solution for the backward Lyapunov equations and decomposition of $\mathbb{A}^*X\mathbb{B}$ operator product.
- Recursive algorithms for computing the $\mathbb{A}^*X\mathbb{B}$ operator product.
- The general $O(N)$ articulated body inertia solution of the Riccati equation.
- Several operator identities.
- The alternative Innovations Operator Factorization of the mass matrix.
- An analytical expression for the inverse of the mass matrix.
- The analytical expression for the determinant of the mass matrix.
- The general $O(N)$ AB forward dynamics algorithm.

The above results required no assumptions on the SKO model regarding the SKO weight matrices, the components of the other spatial operators, or the structure of the tree digraph. Thus, any multibody system formulation satisfying the requirements of the SKO model has available to it the full spectrum of these techniques and efficient algorithms. With this as motivation, we outline the general steps in the development of an SKO multibody dynamics formulation:

Develop an SKO model: The key starting point of an SKO formulation is the development of an SKO model for the system. A systematic procedure for this is deferred till Sect. 9.6.1.

Apply SKO techniques: Once the SKO model has been developed, the analytical results and efficient algorithms for spatial operators described above can be applied to the system.

Optimize algorithms: Finally, optimizations that take advantage of the specific features of the SKO model can be further applied to the SKO algorithms. Though the SKO algorithms are already highly efficient, there are usually several opportunities for further optimizations based on the specific structure, sparsity, and redundancies of the SKO weight matrices, joint map matrices, etc. Even though such system specific optimization are applied only in this last step, they can significantly transform the structure of the eventual algorithms.

9.6.1 Procedure for Developing an SKO Model

Outlined below is a procedure for developing an SKO model for general multibody systems. It provides guidelines for identifying the SKO weight matrices and the components of the H and M operators. Figure 9.3 illustrates the key steps in the procedure.

1. Identify system tree digraph: First, identify a tree digraph for the SKO model. For tree-topology multibody systems, this is usually straightforward, with the standard tree digraph for the system being a good candidate.

However, there is no requirement that the nodes in the tree digraph be in one-to-one correspondence with the physical bodies in the system, as is the case for the standard tree digraph. Chapter 14 describes partitioning and aggregation techniques for tree digraphs that allow the assignment of multiple bodies to single nodes in the SKO model tree.

For non-tree systems, Chap. 15 discusses techniques to transform the non-tree digraph into a tree digraph using *constraint embedding* techniques. Also, Chap. 11 describes the classical *augmented constrained dynamics*, which uses the spanning tree as the tree digraph for the critical parts of the forward dynamics solution procedure.

2. Node equations of motion: Establish the equations of motion of the component nodes in the system. To accomplish this, identify the $\mathcal{V}(k)$ velocities for the component nodes. The size of the velocity vector for a node determines the m_k

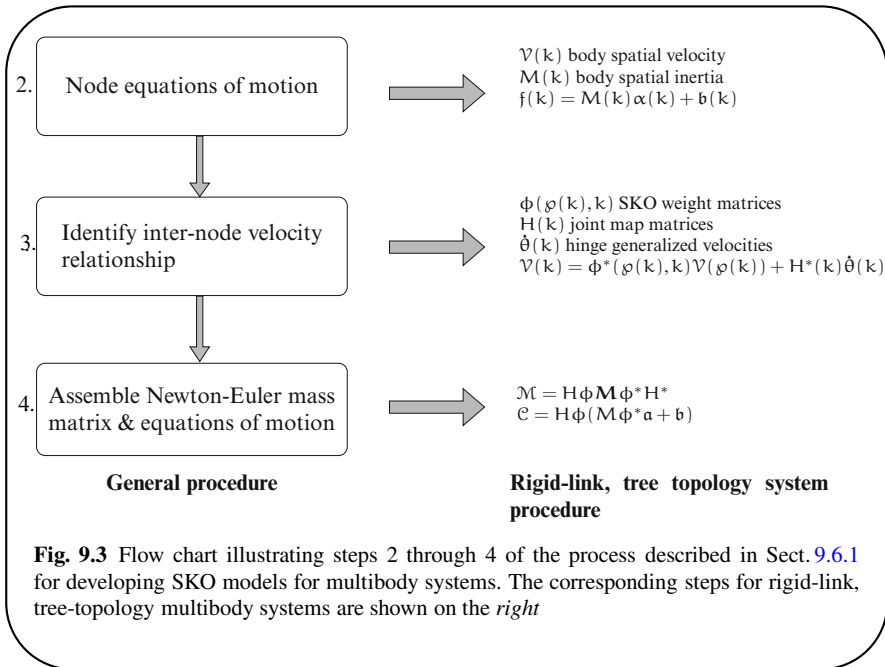


Fig. 9.3 Flow chart illustrating steps 2 through 4 of the process described in Sect. 9.6.1 for developing SKO models for multibody systems. The corresponding steps for rigid-link, tree-topology multibody systems are shown on the right

BWA weight dimension for the node. Also, identify the appropriate $m_k \times m_k$ dimensional $M(k)$ *inertia* matrix for each node. Together with the node velocity, the $\frac{1}{2}\mathcal{V}^*(k)M(k)\mathcal{V}(k)$ expression should define the kinetic energy contribution of the node.

3. Identify inter-node velocity relationships: Identify the recursive relationship between the $\mathcal{V}(k)$ velocity of a node and that of its parent node, and the $\dot{\theta}(k)$ *generalized velocities* of the hinge connecting them. This will help identify the parent/child *SKO weight matrix*, $\mathbb{A}(\varphi(k), k)$, and the component *joint map matrices* associated with the connecting hinge. The $\mathbb{A}^*(\varphi(k), k)$ term defines the contribution of the $\mathcal{V}(\varphi(k))$ parent node's velocity to $\mathcal{V}(k)$ while $H^*(k)$ defines the contribution from the $\dot{\theta}(k)$ generalized velocities.

The hinges connecting adjacent nodes are not required to be physical hinges. This is especially true in cases where multiple bodies are assigned to nodes in the digraph.

4. Assemble Newton–Euler mass matrix expression: Assemble the system-level stacked vectors for the hinge generalized velocities, the node velocities, etc., and the various SKO, SPO, etc., spatial operators leading to the system-level equations of motion, the Newton–Euler factorization of the \mathcal{M} mass matrix and the \mathcal{C} nonlinear Coriolis and velocity terms vector in (9.1) through (9.3).

In later chapters we will see several examples illustrating the use of this procedure. In particular, Sect. 13.3.2 on page 257 discusses, in detail, its application to multi-body systems with deformable links.

9.6.2 Potential Non-Tree Topology Generalizations

The digraph in an SKO model is required to be a directed tree. We address here the potential extension of an SKO model to work with non-tree digraphs. First, we recall key steps in the SKO model development:

1. Set up of the implicit (8.36) relationship $\mathcal{V} = \mathcal{E}_{\mathbb{A}}^* \mathcal{V} + \mathbf{H}^* \dot{\theta}$ for the \mathcal{V} node velocities using independent generalized hinge velocity coordinates.
2. Use the nilpotency of the $\mathcal{E}_{\mathbb{A}}$ BWA matrix to derive its \mathbb{A} 1-resolvent to convert this implicit expression into the $\mathcal{V} = \mathbb{A}^* \mathbf{H}^* \dot{\theta}$ explicit form in (8.38).

Non-tree digraphs can contain directed cycles as well as multiply-connected nodes. We now examine specific issues in developing SKO models for such non-tree digraph systems.

Digraphs with directed cycles: For digraphs with directed cycles, the BWA matrices are *not* nilpotent, and their 1-resolvents do not exist. Intuitively, the presence of cycles implies that there are paths of arbitrary lengths connecting nodes that are part of such cycles, since paths that loop around the cycle multiple times are legal. Thus, by Lemma 8.1, none of the powers of the BWA matrix, with directed cycles, are non-zero. Hence, their 1-resolvent SPO operators do not exist. This means that step (2) above breaks down, and the implicit relationship for \mathcal{V} in (8.36) cannot be transformed into the explicit (8.38) form.

Multiply-connected DAGs: Multiply-connected DAGs are digraphs containing a node with more than one parent. For these systems, the BWA matrix is still nilpotent and, hence, its 1-resolvent is well defined. The catch for such systems is the inability to identify *independent* generalized hinge velocity coordinates for the edges. Such relationships are unique and well-defined when bodies have single parents. However, when a body has multiple parents, the parent/child node velocity relationship must hold simultaneously for each parent. For them to hold simultaneously, the pair of generalized hinge velocity coordinates must be mutually consistent and, hence, they are not independent. Step (1) above therefore breaks down.

Thus, we see that the use of non-tree digraphs with SKO models has potential problems. This complicates the formulation of the dynamics of closed-chain systems. Later chapters discuss avenues for overcoming these hurdles in order to develop and use SKO models for closed-chain systems.

Chapter 10

Operational Space Dynamics

Robotic platforms are typically designed to interact with the environment at specific task space nodes on the system. For a manipulator, the set of task space nodes may consist of a single end-effector node. For a humanoid system, the arm end-effectors are task space nodes, while the feet are such nodes for legged systems. The set of task space nodes define the operational space of the system. The control problem requires managing the motion state as well as the force interactions with the environment for the task space nodes. Operational space control (OSC) is an approach to robot system control that focuses on the dynamical behavior of a system from the task (or operational) space perspective [100–103]. It is especially useful for applications involving contact between the end-effector and the environment, such as occurs in hybrid force/position control, or for artificial potential field approaches to collision avoidance and path planning. The advantage of the OSC approach over joint space control is that the control problem is posed directly in terms of task space variables. One issue is the added analytical and computational complexity of operational space dynamics. As will be seen in later chapters, the importance of operational space dynamics quantities extends to the dynamics of systems subject to closure constraints, as well as to the dynamics of under-actuated and free-flying systems. In this chapter, we study and analyze operational space dynamics and associated efficient computational algorithms for a robotic system.

While the only fundamental requirement is that the multibody system have an SKO model, for the sake of exposition, we will use the operator notation for tree-topology, rigid multi-link systems in this chapter. There is no loss in generality since the ideas developed here easily extend to general SKO models using the approach from Chap. 9.

10.1 Operational Space Equations of Motion

The operational (or task) space of a system is defined by the configuration of a set of distinguished nodes on the system. We adopt the notation from Sect. 3.6 on page 53

and denote the number of task space nodes by n_{nd} . $\mathcal{V}_{nd} \in \mathcal{R}^{6n_{nd}}$ is the stacked vector of spatial velocities of all the n_{nd} task space nodes. The relationship between \mathcal{V}_{nd} and the $\dot{\theta}$ joint velocities is given by

$$\mathcal{V}_{nd} \stackrel{3.50}{=} \mathcal{B}^* \mathcal{V} \stackrel{3.52}{=} \mathcal{B}^* \phi^* H^* \dot{\theta} \stackrel{3.53}{=} \mathcal{J} \dot{\theta} \quad (10.1)$$

\mathcal{J} denotes the Jacobian for the task space nodes defined in (3.53). The task space spatial acceleration $\alpha_{nd} \in \mathcal{R}^{6n_{nd}}$ is defined as the time derivative of \mathcal{V}_{nd} and, from (10.1), its expression is given by

$$\alpha_{nd} \triangleq \frac{d\mathcal{V}_{nd}}{dt} \stackrel{10.1}{=} \mathcal{B}^* \alpha + \dot{\mathcal{B}}^* \mathcal{V} \stackrel{9.1}{=} \mathcal{B}^* \phi^* H^* \ddot{\theta} + \mathbf{a}_{os} \stackrel{3.53}{=} \mathcal{J} \ddot{\theta} + \mathbf{a}_{os} \quad (10.2)$$

where

$$\mathbf{a}_{os} \triangleq \dot{\mathcal{J}} \dot{\theta} \stackrel{5.26}{=} \mathcal{B}^* \phi^* \mathbf{a} + \dot{\mathcal{B}}^* \mathcal{V} \quad (10.3)$$

We have left unspecified the time derivative frame in (10.2). As discussed in Sect. 5.1.3 on page 83, while specific choice of derivative frames can vary, the essential requirement is that the choice be *consistent* with the derivative frames used in the definition of α , \mathbf{a} etc. For the sake of generality, we will continue to avoid specifying such derivative frames.

In the operational space perspective, the system experiences the f_{nd} spatial forces at the operational space nodes. Recall from Remark 5.2.1 on page 85 that the joint space equations of motion for the system have the form

$$\mathcal{M} \ddot{\theta} + \mathcal{C} - \mathcal{J}^* f_{nd} \stackrel{5.36}{=} \mathcal{T} \Rightarrow \ddot{\theta} = \mathcal{M}^{-1} [\mathcal{T} - \mathcal{C} + \mathcal{J}^* f_{nd}] \quad (10.4)$$

Pre-multiplying (10.4) by \mathcal{J} and using (10.2) yields:

$$\begin{aligned} \alpha_{nd} &\stackrel{10.2, 10.4}{=} \mathcal{J} \mathcal{M}^{-1} [\mathcal{T} - \mathcal{C} + \mathcal{J}^* f_{nd}] + \mathbf{a}_{os} \\ &= \underline{\Lambda} f_{nd} + \{\mathcal{J} \mathcal{M}^{-1} (\mathcal{T} - \mathcal{C}) + \mathbf{a}_{os}\} \end{aligned} \quad (10.5)$$

where

$$\underline{\Lambda} \triangleq \mathcal{J} \mathcal{M}^{-1} \mathcal{J}^* \in \mathcal{R}^{6n_{nd} \times 6n_{nd}} \quad (10.6)$$

When $\underline{\Lambda}$ is invertible, (10.5) can be re-expressed as

$$\Lambda \alpha_{nd} + \mathcal{C}_{os} = f_{nd} \quad \text{where} \quad \Lambda \triangleq \underline{\Lambda}^{-1} \in \mathcal{R}^{6n_{nd} \times 6n_{nd}} \quad (10.7)$$

with

$$\mathcal{C}_{os} \triangleq -\Lambda \{\mathcal{J} \mathcal{M}^{-1} (\mathcal{T} - \mathcal{C}) + \mathbf{a}_{os}\} \quad (10.8)$$

Equation (10.7) defines the operational space equations of motion. It establishes the relationship between the f_{nd} operational space spatial forces and the α_{nd} spatial acceleration of the nodes. The quantity, Λ , defined in (10.7) is referred to as the **operational space inertia** of the system for its task space nodes, while its inverse

$\underline{\Lambda}$ is referred to as the **operational space compliance matrix**. The invertibility of $\underline{\Lambda}$ does not depend on \mathcal{J} being invertible – only that it be full-rank.

Observe that the $\mathcal{V}_{nd} = \mathcal{J}\dot{\theta}$ relationship from (10.1) represents a, potentially non-invertible, transformation of the generalized velocity coordinates for the operational space formulation. When \mathcal{J} is indeed square and invertible, from (10.6) and (10.7) we have $\Lambda = \mathcal{J}^{-*}\mathcal{M}\mathcal{J}^{-1}$ which agrees with the mass matrix expression in (4.50) on page 72 for invertible transformations of generalized velocity coordinates.

10.1.1 Physical Interpretation

The operational space inertia, Λ , represents the system mass matrix reflected to the operational space nodes. \mathcal{C}_{os} contains the corresponding velocity dependent Coriolis and gyroscopic terms. Though our primary interest is in Λ , we will spend much of our attention studying the $\underline{\Lambda}$ compliance matrix because the latter is always well-defined and the path to obtaining Λ typically requires computing $\underline{\Lambda}$. It is readily obvious that, while $\underline{\Lambda}$ is always well defined, its inverse, Λ , is undefined when the \mathcal{J} Jacobian matrix is singular, i.e., when the system is in a kinematically singular configuration. In this respect, the Λ operational space inertia differs from the \mathcal{M} joint space mass matrix that is always well-defined and invertible for tree systems.

Physically, the $6 \times 6 \Lambda(\mathbb{O}_k^i, \mathbb{O}_k^i)$ block-diagonal elements of Λ define the effective “inertia” of the system at the \mathbb{O}_k^i node, i.e., the mapping between an external spatial force applied at the node and the induced spatial acceleration at the node. An off-diagonal $\times 6 \Lambda(\mathbb{O}_k^i, \mathbb{O}_j^l)$ block element is a measure of the cross-coupling between the \mathbb{O}_k^i and \mathbb{O}_j^l nodes. It represents the effective “inertia” coupling between an external spatial force applied at the \mathbb{O}_k^i node and the spatial acceleration induced at the \mathbb{O}_j^l node. For a manipulator with a single end-effector task space node, the operational space inertia is a measure of the effective system inertia as seen at the end-effector node.

10.1.2 Operational Space Control

In the OSC approach to control, the feedback linearization strategy is to choose f_{nd} to be

$$f_{nd} = \Lambda u + \mathcal{C}_{os} \quad (10.9)$$

where u defines the desired spatial acceleration of the task space nodes. Assuming that Λ is non-singular, this transforms (10.7) into the following form:

$$\alpha_{nd} = u \quad (10.10)$$

The decoupled and linear transformed dynamics represent a much simpler control problem. When the dimension of the operational space generalized coordinates, \mathcal{V}_{nd} , is less than the dimension of joint space coordinates, N , we have redundant degrees of freedom in the system that can be used to meet additional task objectives.

One challenge of the OSC approach is the need for the explicit evaluation of the Λ operational space inertia and the C_{os} Coriolis/centrifugal term needed by (10.9). With $\Lambda = (\mathcal{J}\mathcal{M}^{-1}\mathcal{J}^*)^{-1}$, its computation ostensibly requires the explicit computation of Jacobian and the mass matrix inverse, a computation of their products, and the eventual inversion of the resulting matrix. These operations are of $O(N^3)$ cost, and are computationally expensive for real-time control applications.

10.2 Structure of the Operational Space Inertia

We now begin examining the structural properties of the operational space inertia and related quantities and the development of efficient algorithms for their computation.

10.2.1 The Ω Extended Operational Space Compliance Matrix

Recalling the $\mathcal{J} = \mathcal{B}^* \phi^* \mathcal{H}^*$ Jacobian matrix expression from (3.53), leads to the following expression for $\underline{\Lambda}$:

$$\underline{\Lambda} \stackrel{10.6}{=} \mathcal{J}\mathcal{M}^{-1}\mathcal{J}^* \stackrel{3.53}{=} \mathcal{B}^* \phi^* \mathcal{H}^* (\mathbf{I} - \mathcal{H}\psi\mathcal{K})^* \mathcal{D}^{-1} (\mathbf{I} - \mathcal{H}\psi\mathcal{K}) \mathcal{H}\phi\mathcal{B} \quad (10.11)$$

The use of the $(\mathbf{I} - \mathcal{H}\psi\mathcal{K})\mathcal{H}\phi = \mathcal{H}\psi$ identity from (9.45) on page 177 results in the following simpler expression:

$$\underline{\Lambda} = \mathcal{B}^* \Omega \mathcal{B}, \quad \text{where} \quad \Omega \triangleq \psi^* \mathcal{H}^* \mathcal{D}^{-1} \mathcal{H}\psi \in \mathbb{R}^{6n \times 6n} \quad (10.12)$$

We refer to Ω as the **extended operational space compliance matrix**. This terminology comes from (10.12) which shows that the operational space compliance matrix, $\underline{\Lambda}$ is obtained by a reducing transformation of the full, all body Ω matrix by the \mathcal{B} pick-off operator to just the task space nodes. From its definition, it is clear that Ω is a symmetric, positive semi-definite matrix, since \mathcal{D}^{-1} is a symmetric positive-definite matrix. From the expressions for $\underline{\Lambda}$ and Ω in (10.12), it follows that the explicit computation of \mathcal{M}^{-1} or \mathcal{J} is not needed to obtain $\underline{\Lambda}$. While this reduces the computational cost, the direct evaluation of (10.12) still remains $O(N^3)$ due to the need for carrying out the matrix products.

Physically, each diagonal $\Omega(k, k)$ block element of Ω defines the effective “compliance” at the k th body, i.e., the mapping between an external spatial force applied at the B_k body frame of the k th body and the induced spatial acceleration at the frame. On the other hand, an off-diagonal $\Omega(k, j)$ block element is a measure of the cross-coupling between the k th and j th bodies and represents the effective “compliance” mapping between an external spatial force applied at the B_j body frame of the j th body and the spatial acceleration induced at the B_k frame of the k th body.

10.2.2 Decomposition of Ω

Since $H^*D^{-1}H$ is block-diagonal, and ψ is an SPO operator, the $\psi^*H^*D^{-1}H\psi$ expression for Ω meets the conditions for the backwards Lyapunov recursion based decomposition in Lemma 9.5 on page 170. The following lemma uses it to derive a decomposition of Ω into simpler component terms and an expression for its block elements.

Lemma 10.1 Decomposition of Ω .

Ω can be decomposed into the following disjoint sum of component terms:

$$\Omega = \Upsilon + \tilde{\psi}^* \Upsilon + \Upsilon \tilde{\psi} + R$$

where $R \triangleq \sum_{\substack{\forall i,j: i \neq j \\ k=\wp(i,j)}} e_i \psi^*(k, i) \Upsilon(k) \psi(k, j) e_j^*$ (10.13)

$\Upsilon \in \mathcal{R}^{6n \times 6n}$ is a block-diagonal operator, referred to as the **operational space compliance kernel**, satisfying the following backward Lyapunov equation:

$$H^* D^{-1} H = \Upsilon - \text{diagOf}\left\{ \mathcal{E}_\psi^* \Upsilon \mathcal{E}_\psi \right\} \quad (10.14)$$

$\text{diagOf}\left\{ \mathcal{E}_\psi^* \Upsilon \mathcal{E}_\psi \right\}$ represents just the block-diagonal part of the (generally non block-diagonal) $\mathcal{E}_\psi^* \Upsilon \mathcal{E}_\psi$ matrix. The 6×6 dimensional, symmetric, positive semi-definite $\Upsilon(k)$ diagonal matrices satisfy the following parent/child recursive relationship:

$$\Upsilon(k) = \psi^*(\wp(k), k) \Upsilon(\wp(k)) \psi(\wp(k), k) + H^*(k) D^{-1}(k) H(k) \quad (10.15)$$

This relationship forms the basis for the following $O(N)$ base-to-tips scatter recursion for computing the $\Upsilon(k)$ diagonal elements:

$$\left\{ \begin{array}{l} \textbf{for all nodes } k \text{ (base-to-tips scatter)} \\ \quad \Upsilon(k) = \psi^*(\wp(k), k) \Upsilon(\wp(k)) \psi(\wp(k), k) + H^*(k) D^{-1}(k) H(k) \\ \textbf{end loop} \end{array} \right. \quad (10.16)$$

Algorithm 10.1 Computation of the $\Omega(k, j)$ elements

This algorithm is based on Algorithm 9.4 on page 173, with simplifications arising because $\mathbb{A} = \mathbb{B} = \psi$, and the symmetry of Ω . This algorithm drops case (2) from Algorithm 9.4 and uses the transposes of the elements computed from case (3) instead. Thus, we have three different situations to consider when computing a $\Omega(k, j)$ element. The respective recursive steps are described below and illustrated in Fig. 10.1.

1. To obtain a block-diagonal element, $\Omega(k, k)$, the procedure is to compute the $\Upsilon(k)$ operational space compliance kernel element using the base-to-tips scatter $O(N)$ procedure in (10.16) or the more optimized algorithm in Algorithm 10.3 described later.
 2. If the k th body is an ancestor of the j th body, then $\Omega(k, j)$ can be computed recursively starting with the $\Omega(k, k) \equiv \Upsilon(k)$ diagonal element, which in turn is computed using the process described in case (1). The recursion for $\Omega(k, j)$ starts with this diagonal entry, and propagates it along the path from the k th to the j th body. The second expression in (10.17) is used to compute the $\Omega(k, k-1)$, $\Omega(k, k-2)$, etc., terms.
If, on the other hand, the j th body happens to be the ancestor of the k th body, then compute $\Omega(j, k)$ using the above process, and take its transpose to obtain $\Omega(k, j)$.
 3. Now consider the remaining case where the (k, j) pair of bodies are unrelated, i.e., neither is the ancestor of the other. In this case, identify the body that is the closest ancestor for this pair of bodies. If the bodies do not have a common ancestor, then $\Omega(k, j)$ is zero since the bodies belong to independent, decoupled multibody trees.
If, on the other hand, there is a common ancestor, denoted the i th body, then the first step is to compute $\Omega(k, i)$ using the recursive procedure described in case (2). This value is then recursively propagated along the path from the i th body to the j th body, using the last expression in (10.17) to compute the $\Omega(k, i-1)$, $\Omega(k, i-2)$, etc., terms.
-

While Υ defines the block-diagonal elements of Ω , the following recursive expressions describe the off-diagonal terms as well:

$$\Omega(i, j) = \begin{cases} \Upsilon(i) & \text{for } i = j \\ \Omega(i, k)\psi(k, j) & \text{for } i \succeq k \succ j, \quad k = \wp(j) \\ \Omega^*(j, i) & \text{for } i \prec j \\ \Omega(i, k)\psi(k, j) & \text{for } i \not\succ j, \quad j \not\prec i, \quad k = \wp(i, j) \end{cases} \quad (10.17)$$

Proof: This lemma is a direct application of Lemma 9.5 on page 170 with $\mathcal{E}_{\mathbb{A}} = \mathcal{E}_{\mathbb{B}} = \mathcal{E}_{\psi}$, and $\mathbb{A} = \mathbb{B} = \psi$, and the block-diagonal $X = H^*D^{-1}H$. ■

This lemma shows that Ω can be decomposed into the sum of simpler terms. Furthermore, (10.17) reveals that all of the block-elements of $\Omega(i, j)$ can be obtained

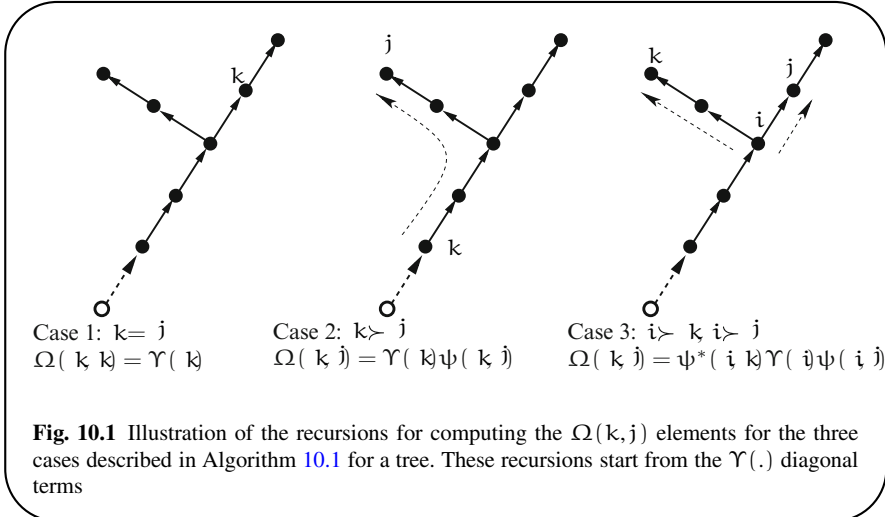


Fig. 10.1 Illustration of the recursions for computing the $\Omega(k, j)$ elements for the three cases described in Algorithm 10.1 for a tree. These recursions start from the $\Upsilon(\cdot)$ diagonal terms

from the $\Upsilon(i)$ elements of the Υ block-diagonal operational space compliance kernel. Since only a small subset of the elements of Ω are needed for computing Λ , Sect. 10.2.3 exploits this to avoid the expensive computation of the full Ω matrix.

As pointed out in the discussion following Lemma 9.5, Ω is fully populated and has no non-zero entries for a tree-system. This is because non-zero spatial forces applied at a body induce non-zero accelerations in every other body in the system. Zero entries arise only for body pairs where the bodies are on independent, disjoint trees within the multibody system.

Algorithm 10.1 uses the decomposition in (10.13) to derive a procedure for computing the required $\Omega(k, j)$ elements. The cost of computing any such element is at most $O(N)$, and many of the intermediate values can be reused when additional elements are needed.

10.2.3 Computing $\underline{\Lambda}$

From the $\underline{\Lambda} = \mathcal{B}^*\Omega\mathcal{B}$ expression, and the sparse structure of \mathcal{B} , it is clear that only a subset of the elements of Ω are needed to compute $\underline{\Lambda}$. As discussed in Sect. 3.6, the \mathcal{B} pick-off operator has one column for each of the \mathbb{O}_k^i task space nodes, with each such column having only a single non-zero 6×6 matrix entry at the k th parent link slot. From this structure of \mathcal{B} and (10.12), the 6×6 block matrix elements of the $\underline{\Lambda}$ operational space compliance matrix are given by the following expression:

$$\underline{\Lambda}(\mathbb{O}_k^i, \mathbb{O}_j^l) = \phi^*(k, \mathbb{O}_k^i)\Omega(k, j)\phi(j, \mathbb{O}_j^l) \quad (10.18)$$

Here, \mathbb{O}_k^i and \mathbb{O}_j^l denote a pair of task space nodes on the k th and j th links, respectively. It is therefore evident that only as many elements of Ω as there are elements in $\underline{\Lambda}$ are needed. Thus, just $n_{nd} \times n_{nd} 6 \times 6$ block-entries of Ω are required. In view of the symmetry of the matrices, even this reduces to needing just $n_{nd}(n_{nd} + 1)/2$ entries. The complete algorithm for the computation of the Λ operational space inertia is summarized by Algorithm 10.2.

Algorithm 10.2 Computation of the Λ operational space inertia

1. Use (10.18), together with Algorithm 10.1, to compute all the $\underline{\Lambda}(i, j)$ block elements of $\underline{\Lambda}$.
 2. Compute $\Lambda = \underline{\Lambda}^{-1}$ by numerical matrix inversion.
-

As observed in the previous section, the Ω extended operational space compliance matrix depends greatly on the Υ operational space compliance kernel operator. The next section looks at the properties of Υ and develops an efficient $O(N)$ algorithm for computing its elements. This algorithm is a generalization of the one in [73, 152] and is the lowest order algorithm available. Other algorithms for computing Λ are described in [34, 52].

10.2.4 The Υ Operational Space Compliance Kernel

Using $\psi(\varphi(k)) = \phi(\varphi(k))\bar{\tau}(k)$ from (9.35), (10.16) can be rearranged as follows:

$$\begin{aligned} \Upsilon^+(k) &\stackrel{\Delta}{=} \phi^*(\varphi(k), k)\Upsilon(\varphi(k))\phi(\varphi(k), k) \\ \Upsilon(k) &\stackrel{\Delta}{=} \bar{\tau}^*(k)\Upsilon^+(k)\bar{\tau}(k) + H^*(k)\mathcal{D}^{-1}(k)H(k) \\ \text{and } \Upsilon^+ &\stackrel{\Delta}{=} \text{diag}\left\{\Upsilon^+(k)\right\}_{k=1}^n \in \mathcal{R}^{6n \times 6n} \end{aligned} \quad (10.19)$$

The block-diagonal Υ^+ represents just the block-diagonal part of (the generally non block-diagonal) $\mathcal{E}_\phi^* \Upsilon \mathcal{E}_\phi$, i.e.,

$$\Upsilon^+ = \text{diagOf}\left\{\mathcal{E}_\phi^* \Upsilon \mathcal{E}_\phi\right\} \quad (10.20)$$

Recalling that $\bar{\tau}(k) = I - \tau(k) = I - G(k)H(k)$, from (9.33), the expression for $\Upsilon(k)$ in (10.19) can be simplified as follows:

$$\begin{aligned} \Upsilon(k) &\stackrel{10.19}{=} \bar{\tau}^*(k)\Upsilon^+(k)\bar{\tau}(k) + H^*(k)\mathcal{D}^{-1}(k)H(k) \\ &\stackrel{9.32}{=} \Upsilon^+(k) - \Upsilon^+(k)\tau(k) - \tau^*(k)\Upsilon^+(k) + \tau^*(k)\Upsilon^+(k)\tau(k) \\ &\quad + H^*(k)\mathcal{D}^{-1}(k)H(k) \end{aligned}$$

$$\begin{aligned} & \stackrel{9.32}{=} \Upsilon^+(k) - \underbrace{\mathcal{G}(k) \mathcal{H}(k)}_{Z(k)} - \mathcal{H}^*(k) \mathcal{G}^*(k) \Upsilon^+(k) \\ & + \mathcal{H}^*(k) [\mathcal{D}^{-1}(k) + \mathcal{G}^*(k) \Upsilon^+(k) \mathcal{G}(k)] \mathcal{H}(k) \\ & = \Upsilon^+(k) - Z(k) \mathcal{H}(k) + \mathcal{H}^*(k) \underbrace{[\{\mathcal{D}^{-1}(k) + \mathcal{G}^*(k) Z(k)\} \mathcal{H}(k) - Z^*(k)]}_{\mathcal{L}(k)} \\ & \qquad \qquad \qquad \underbrace{\qquad \qquad \qquad}_{\mathcal{U}(k)} \end{aligned}$$

In other words, defining the intermediate terms $Z(k)$, $L(k)$ and $U(k)$ based on the above grouping, we have:

$$\begin{aligned} Z(k) &\stackrel{\triangle}{=} \Upsilon^+(k)\mathcal{G}(k) \\ L(k) &\stackrel{\triangle}{=} \mathcal{D}^{-1}(k) + \mathcal{G}^*(k)Z(k) = \mathcal{D}^{-1}(k) + \mathcal{G}^*(k)\Upsilon^+(k)\mathcal{G}(k) \\ U(k) &\stackrel{\triangle}{=} L(k)\mathcal{H}(k) - Z^*(k) \\ \Upsilon(k) &= \Upsilon^+(k) + \mathcal{H}^*(k)U(k) - Z(k)\mathcal{H}(k) \end{aligned} \quad (10.21)$$

The restructured computations in (10.21) are computationally less expensive compared with computing the $\bar{\tau}^*(k)\Upsilon^+(k)\bar{\tau}(k)$ product directly. (10.19) and (10.21), lead to the $O(N)$ base-to-tips scatter recursive Algorithm 10.3 for computing the $\Upsilon(i)$ block-diagonal elements. This algorithm requires the $\mathcal{D}(k)$ articulated body

Algorithm 10.3 Computation of the $\Upsilon(k)$ elements

First compute the $\mathcal{D}(k)$ articulated body inertia elements using the tips-to-base gather recursion in Lemma 9.7. Then carry out the following base-to-tips scatter recursion for the $\Upsilon(k)$ elements:

for all nodes k (*base-to-tips scatter*)
 $\Upsilon^+(k) = \phi^*(\varphi(k), k)\Upsilon(\varphi(k))\phi(\varphi(k), k)$
 $Z(k) = \Upsilon^+(k)\mathcal{S}(k)$
 $L(k) = \mathcal{D}^{-1}(k) + \mathcal{G}^*(k)Z(k)$ (10.22)
 $U(k) = L(k)\mathcal{H}(k) - Z^*(k)$
 $\Upsilon(k) = \Upsilon^+(k) + \mathcal{H}^*(k)U(k) - Z(k)\mathcal{H}(k)$
end loop

hinge inertia for all the links. Two recursions are thus needed to compute Υ since \mathcal{P} , \mathcal{D} , and \mathcal{E}_ψ must be first computed using the tips-to-base gather recursion from Lemma 9.7.

Remark 10.1 Singularity of $\Upsilon(k)$ matrices.

A point worth highlighting is that the $\Upsilon(k)$ operational space compliance kernel matrices, while symmetric and positive semi-definite, may be singular. To illustrate this, let us assume that the system has single degree of freedom hinges. In this case, the $H(k)$ matrices have rank 1 and, consequently, so do the $H^*(k)D^{-1}(k)H(k)$ terms in (10.22). At the base, the $\Upsilon(n) = H^*(n)D^{-1}(n)H(n)$, and this 6×6 matrix has a rank of just 1 and is, thus, singular. As the recursion proceeds towards the tips, the $H^*(k)D^{-1}(k)H(k)$ contribution of each link can increase the rank of $\Upsilon(k)$ by at most 1. At least 6 links need to be traversed before $\Upsilon(k)$ can be expected to become non-singular.

Physically, this means that the n th body has only 1 degree of freedom and can move in only one direction. The body has zero compliance (or infinite stiffness) for motions along the constrained directions. In general, the null space of the $\Upsilon(k)$ matrix defines the directions along which the k th body cannot move. Each new outboard body acquires additional mobility, as reflected in the increasing rank of its $\Upsilon(k)$ matrix. It takes an accumulation of at least 6 degrees of freedom from the ancestor bodies to allow a body to be movable in arbitrary directions and for its $\Upsilon(\cdot)$ matrix to become non-singular. Even after 6 links, at singular configurations, mobility in some directions can be lost and the $\Upsilon(k)$ matrix then becomes singular.

■

Remark 10.2 $\mathcal{P}^{-1}(n) = \Upsilon(n)$ for a free-flying system.

For a free-flying system, the base-body hinge is a full 6 degree of freedom hinge with $H(n) = I$. It follows from (10.16) that

$$\begin{aligned}\Upsilon(n) &= H^*(n)D^{-1}(n)H(n) = D^{-1}(n) \\ &= [H(n)\mathcal{P}(n)H^*(n)]^{-1} = \mathcal{P}^{-1}(n)\end{aligned}$$

At the base-body, $\Upsilon(n)$ is simply the inverse of the $\mathcal{P}^{-1}(n)$ articulated body inertia of the link!

Section 17.4 on page 348 contains a more extended discussion of the special properties of the $\Upsilon(k)$ matrices for free-flying systems. It shows that the Ω and Υ matrices are invariant with respect to the choice of base-body. It also derives the alternative Algorithm 17.5 for computing the Υ elements by combining values from multiple articulated body inertia sweeps. One implication is that all of the $\Upsilon(k)$ matrices are always invertible for free-flying systems.

■

The following exercise looks at a scenario where one tree-topology system is attached to a body on another system. Examples of such systems are micro/macro manipulator systems [27], where a lightweight (micro) manipulator is mounted on the end-effector of a macro manipulator to create a system capable of large scale motions as well as agile, fine-manipulation tasks. This exercise explores the operational space properties of such coupled systems.

Exercise 10.1 $\Upsilon(k)$ for a micro/macro manipulator system.

We now study a system consisting of a \mathfrak{S} “micro” manipulator mounted on the end-effector body of a \mathfrak{P} “macro” manipulator. Denote the end-effector body of the macro system as the $\varphi(\mathfrak{S})$ body. Show that the $\Upsilon(1)$ end-effector operational space compliance kernel matrix for the combined system is related to $\Upsilon(\varphi(\mathfrak{S}))$ as follows:

$$\Upsilon(1) = \Upsilon_{\mathfrak{S}}(1) + \Psi^*(\mathcal{P}(\varphi(\mathfrak{S}), 1))\Upsilon(\varphi(\mathfrak{S}))\Psi(\mathcal{P}(\varphi(\mathfrak{S}), 1)) \quad (10.23)$$

In the above, $\Upsilon(1)$ is associated with the combined system, $\Upsilon_{\mathfrak{S}}(1)$ denotes the corresponding matrix for the micro manipulator by itself. $\Upsilon(\varphi(\mathfrak{S}))$, on the other hand, is the operational space compliance kernel for the combined system at the $\varphi(\mathfrak{S})$ body, i.e., at the end-effector of the macro system. In particular, (10.23) implies that

$$\Upsilon(1) \geq \Upsilon_{\mathfrak{S}}(1) \quad (10.24)$$

Physically, this implies that the end-effector of the combined system is always more compliant than the end-effector of the micro system alone regardless of the stiffness of the macro system. From the OSC control perspective, this suggests a strategy of mounting a fine motion micro-manipulator at the end-effector of a large-motion macro-manipulator. The overall system will have the large workspace of the macro-manipulator while retaining the fine-motion control and dexterity of the micro-manipulator.

■

10.2.5 Simplifications for Serial-Chain Systems

Now, we examine simplifications of Ω that arise for serial-chain systems. The key characteristic that distinguishes serial-chain systems from tree-topology systems is that all bodies are *related*. Thus, for any pair of distinct bodies in the system, one of the bodies is always an ancestor of the other. This leads to the following version of Lemma 10.1, using the simplifications in Lemma 9.6 on page 172 for serial-chain systems. One of the key simplifications is that $\mathcal{E}_{\Psi}^* \Upsilon \mathcal{E}_{\Psi}$ contains no off-diagonal terms for serial-chain systems. Without loss in any generality, the serial-chain is assumed to be canonical.

Lemma 10.2 Decomposition of Ω for serial-chains.

For a serial-chain system, Ω can be decomposed into disjoint diagonal, strictly upper triangular and strictly lower triangular parts, as follows:

$$\Omega = \Upsilon + \tilde{\Psi}^* \Upsilon + \Upsilon \tilde{\Psi} \quad (10.25)$$

where $\Upsilon \in \mathcal{R}^{6n \times 6n}$ is a block-diagonal operator satisfying the following backward Lyapunov equation:

$$H^* \mathcal{D}^{-1} H = \Upsilon - \mathcal{E}_{\Psi}^* \Upsilon \mathcal{E}_{\Psi} \quad (10.26)$$

The 6×6 dimensional, symmetric positive semi-definite $\Upsilon(k)$ diagonal matrices satisfy the parent/child recursive relationship in (10.15), and can be computed via the following $O(N)$ base-to-tips scatter recursion:

$$\left\{ \begin{array}{l} \Upsilon(n+1) = \mathbf{0} \\ \text{for } k = 1 \cdots n \\ \quad \Upsilon(k) = \psi^*(k+1, k)\Upsilon(k+1)\psi(\varphi(k), k) + H^*(k)\mathcal{D}^{-1}(k)H(k) \\ \text{end loop} \end{array} \right. \quad (10.27)$$

While Υ defines the block-diagonal elements of Ω , the following recursive expressions describe all the terms, including the off-diagonal ones:

$$\Omega(i, j) = \begin{cases} \Upsilon(i) & \text{for } i = j \\ \Omega(i, j+1)\psi(j+1, j) & \text{for } i > j \\ \Omega^*(j, i) & \text{for } i < j \end{cases} \quad (10.28)$$

Proof: This lemma follows from applying the serial-chain simplifications from Lemma 9.6 on page 172 to Lemma 10.1. ■

10.2.6 Explicit Computation of the Mass Matrix Inverse \mathcal{M}^{-1}

We have the following options for explicitly computing the mass matrix inverse of a serial-chain system:

1. Explicitly compute the \mathcal{M} mass matrix and invert this matrix numerically ($O(N^3)$ cost).
2. Compute the mass matrix factors of \mathcal{M}^{-1} in (9.51) and evaluate their products ($O(N^3)$ cost).

The following exercise uses the decomposition of Ω in Lemma 10.2 to develop a simpler $O(N^2)$ algorithm for computing the mass matrix inverse for a canonical serial-chain system.

Exercise 10.2 Computation of the mass matrix inverse.

1. Derive the following operator decomposition of the mass matrix inverse for a tree-topology system:

$$\mathcal{M}^{-1} = L - K^* \psi^* U^* - U \psi K + K^* R K \quad (10.29)$$

where L and U are defined as

$$\underline{\Upsilon} \triangleq \mathcal{E}_\Phi^* \Upsilon \mathcal{E}_\Phi, \quad L \triangleq \mathcal{D}^{-1} + \underline{G}^* \underline{\Upsilon} \underline{G} \quad \text{and} \quad U \triangleq L H - \underline{G}^* \underline{\Upsilon} \quad (10.30)$$

2. Show that, for a serial-chain system, (10.29) simplifies to the following disjoint decomposition into block-diagonal, strictly upper-triangular and strictly lower-triangular terms:

$$\mathcal{M}^{-1} = L - \mathcal{K}^* \psi^* U^* - U \psi \mathcal{K} \quad \text{and} \quad \underline{\Upsilon} = \Upsilon^+ \quad (10.31)$$

Since $\underline{\Upsilon} = \mathcal{E}_\phi^* \Upsilon \mathcal{E}_\phi$ is block-diagonal for serial-chain systems, so are L and U . Indeed, the block-diagonal elements of L and U are the $L(k)$ and $U(k)$ elements defined in (10.21). A closer examination shows that the elements of \mathcal{M}^{-1} are given by:

$$\mathcal{M}^{-1}(k,j) = \begin{cases} -U(k)\psi(k,j+1)\mathcal{K}(j+1,j) & \text{for } k > j \\ L(k) & \text{for } k = j \\ \mathcal{M}^{-1}(j,k) & \text{for } k < j \end{cases} \quad (10.32)$$

Use this to derive the $O(N^2)$ Algorithm 10.4 for explicitly computing the mass matrix inverse of a serial-chain system. ■

The use of the operational space compliance kernel elements for the computation of the mass matrix inverse is an example of its use for a non-OSC application.

10.3 The Operational Space \mathcal{C}_{os} Coriolis/Centrifugal Term

In this section we derive simpler expressions for the \mathcal{C}_{os} Coriolis terms in (10.8) [110]. First, we begin by introducing the \mathfrak{U} and \mathfrak{U}_\perp projection operators.

10.3.1 The \mathfrak{U} and \mathfrak{U}_\perp Projection Operators

Define the pair of operators, \mathfrak{U} and \mathfrak{U}_\perp , as follows:

$$\mathfrak{U} \triangleq \Omega M \quad \text{and} \quad \mathfrak{U}_\perp \triangleq I - \mathfrak{U} = I - \Omega M \quad (10.34)$$

The following lemma shows that \mathfrak{U} and \mathfrak{U}_\perp are in fact projection operators.

Lemma 10.3 The \mathfrak{U} and \mathfrak{U}_\perp projection operators.

The operators \mathfrak{U} and \mathfrak{U}_\perp are projection operators, i.e.,

$$\mathfrak{U}^2 = \mathfrak{U}, \quad \text{and} \quad \mathfrak{U}_\perp^2 = \mathfrak{U}_\perp \quad (10.35)$$

Algorithm 10.4 $O(N^2)$ Computation of the mass matrix inverse for a serial-chain

This algorithm assumes that the serial-chain is canonical for simpler notation. Thus, $\varrho(k) = k + 1$. It also assumes that the tips-to-base gather algorithm for the articulated body inertia quantities has been completed. The following recursive procedure computes all the operational space compliance kernel terms and the elements of the mass matrix inverse:

$$\left\{ \begin{array}{l} \Upsilon(n+1) = \mathbf{0} \\ \text{for } k = n \cdots 1 \\ \quad \Upsilon^+(k) = \phi^*(k+1, k)\Upsilon(k+1)\phi(k+1, k) \\ \quad Z(k) = \Upsilon^+(k)\varrho(k) \\ \quad \mathcal{M}^{-1}(k, k) = L(k) = \mathcal{D}^{-1}(k) + \varrho^*(k)Z(k) \\ \quad U(k) = L(k)H(k) - Z^*(k) \\ \quad \Upsilon(k) = \Upsilon^+(k) + H^*(k)U(k) - Z(k)H(k) \\ \quad \quad \quad X(k-1) = U(k)\phi(k, k-1) \\ \quad \text{for } j = k-1 \cdots 1 \\ \quad \quad \quad \mathcal{M}^{-1}(k, j) = [\mathcal{M}^{-1}(j, k)]^* = -X(j)\varrho(j) \\ \quad \quad \quad X(j-1) = X(j)\bar{\tau}(j)\phi(j, j-1) \\ \quad \quad \quad = [X(j) + \mathcal{M}^{-1}(k, j)H(j)]\phi(j, j-1) \\ \quad \text{end loop} \\ \text{end loop} \end{array} \right. \quad (10.33)$$

Also,

$$\begin{aligned} \mathfrak{U}\Omega &= \Omega \quad \text{and} \quad \mathfrak{U}_\perp\Omega = \mathbf{0} \\ \mathfrak{U}_\perp^*\mathbf{M}\mathfrak{U} &= \mathbf{0}, \quad \mathfrak{U}^*\mathbf{M}\mathfrak{U} = \mathbf{M}\mathfrak{U}, \quad \mathfrak{U}_\perp^*\mathbf{M}\mathfrak{U}_\perp = \mathbf{M}\mathfrak{U}_\perp \end{aligned} \quad (10.36)$$

Proof: We have

$$\Omega\mathbf{M}\Omega \stackrel{10.12}{=} \psi^*H^*\mathcal{D}^{-1}[H\psi\mathbf{M}\psi^*H^*]\mathcal{D}^{-1}H\psi \stackrel{9.46}{=} \Omega \quad (10.37)$$

Therefore,

$$\mathfrak{U}^2 \stackrel{10.34}{=} \Omega\mathbf{M}\Omega\mathbf{M} \stackrel{10.37}{=} \Omega\mathbf{M} \stackrel{10.34}{=} \mathfrak{U}$$

This implies that \mathfrak{U} is a projection operator. Since \mathfrak{U} is a projection operator, so is $\mathfrak{U}_\perp = \mathbf{I} - \mathfrak{U}$.

$\mathfrak{U}\Omega = \Omega$ follows from (10.37), and this, in turn, directly implies that $\mathfrak{U}_\perp\Omega = \mathbf{0}$.

Moreover,

$$\mathfrak{U}^*\mathbf{M}\mathfrak{U} = \mathbf{M}\Omega\mathbf{M}\Omega\mathbf{M} \stackrel{10.37}{=} \mathbf{M}\Omega\mathbf{M} = \mathbf{M}\mathfrak{U}$$

The remaining identities in (10.36) follow directly from the above result. ■

Lemma 10.4 Useful identities for \mathfrak{U} and \mathfrak{U}_\perp .

1.

$$\begin{aligned}\mathfrak{U}\phi^* &= \Omega\mathbf{M}\phi^* = \phi^* - (\psi^* - \Omega\mathcal{P}) \\ &= \phi^*\mathcal{H}^* [\mathcal{K}^*(\psi^* - \Omega\mathcal{P}) + \mathcal{D}^{-1}\mathcal{H}\psi\mathcal{P}]\end{aligned}\quad (10.38a)$$

$$\mathfrak{U}\psi^* = \Omega\mathbf{M}\psi^* = \Omega\mathcal{P} \quad (10.38b)$$

$$(\psi - \mathcal{P}\Omega)\mathbf{M}\phi^* = (\psi - \mathcal{P}\Omega)\mathcal{P} + \mathcal{P}\tilde{\psi}^* = \psi\mathbf{M}\psi^* - \mathcal{P}\Omega\mathcal{P} \quad (10.38c)$$

2.

$$\mathfrak{U}_\perp\phi^* = \mathfrak{U}_\perp\psi^* = \psi^* - \Omega\mathcal{P} \quad (10.39a)$$

$$\mathfrak{U}_\perp\phi^*\mathcal{H}^* = \mathfrak{U}_\perp\psi^*\mathcal{H}^* = \mathbf{0} \quad (10.39b)$$

Proof:

1. We have

$$\begin{aligned}\mathfrak{U}\phi^* &\stackrel{10.34}{=} \Omega\mathbf{M}\phi^* \stackrel{10.12}{=} \psi^*\mathcal{H}^*\mathcal{D}^{-1}\mathcal{H}\psi\mathbf{M}\phi^* \stackrel{9.41}{=} \psi^*\mathcal{H}^*\mathcal{D}^{-1}\mathcal{H}[\psi\mathcal{P} + \mathcal{P}\tilde{\phi}^*] \\ &\stackrel{9.32, 9.37, 10.12}{=} \Omega\mathcal{P} + \psi^*\mathcal{H}^*\mathcal{K}^*\phi^* \stackrel{9.43}{=} \phi^* - (\psi^* - \Omega\mathcal{P})\end{aligned}$$

This establishes the first equality in (10.38a).

Also,

$$\begin{aligned}\phi^*\mathcal{H}^*\mathcal{K}^*(\psi^* - \Omega\mathcal{P}) &\stackrel{10.12}{=} \phi^*\mathcal{H}^*\mathcal{K}^*\psi^*[\mathbf{I} - \mathcal{H}^*\mathcal{D}^{-1}\mathcal{H}\psi\mathcal{P}] \\ &\stackrel{9.43}{=} (\phi^* - \psi^*)[\mathbf{I} - \mathcal{H}^*\mathcal{D}^{-1}\mathcal{H}\psi\mathcal{P}] \\ &\stackrel{10.12}{=} \phi^* - (\psi^* - \Omega\mathcal{P}) - \phi^*\mathcal{H}^*\mathcal{D}^{-1}\mathcal{H}\psi\mathcal{P} \\ &\stackrel{10.38a}{=} \mathfrak{U}\phi^* - \phi^*\mathcal{H}^*\mathcal{D}^{-1}\mathcal{H}\psi\mathcal{P}\end{aligned}$$

This establishes the second equality in (10.38a).

Now,

$$\begin{aligned}\mathfrak{U}\psi^* &\stackrel{10.34}{=} \Omega\mathbf{M}\psi^* \stackrel{10.12}{=} \psi^*\mathcal{H}^*\mathcal{D}^{-1}\mathcal{H}\psi\mathbf{M}\psi^* \stackrel{9.42}{=} \psi^*\mathcal{H}^*\mathcal{D}^{-1}\mathcal{H}(\psi\mathcal{P} + \mathcal{P}\tilde{\psi}^*) \\ &\stackrel{9.32, 8.19}{=} \Omega\mathcal{P} + \psi^*\tau^*\mathcal{E}_\psi^*\psi^* \stackrel{9.34}{=} \Omega\mathcal{P} + \psi^*\tau^*\bar{\tau}^*\mathcal{E}_\phi^*\psi^* \stackrel{9.32}{=} \Omega\mathcal{P}\end{aligned}$$

establishing (10.38b).

Additionally

$$\begin{aligned} (\psi - \mathcal{P}\Omega)\mathbf{M}\phi^* &\stackrel{9.41, 10.38a}{=} \tilde{\psi}\mathcal{P} + \mathcal{P}\phi^* - \mathcal{P}[\phi^* - \psi^* + \Omega\mathcal{P}] \\ &= \tilde{\psi}\mathcal{P} + \mathcal{P}\psi^* - \mathcal{P}\Omega\mathcal{P} \stackrel{9.42}{=} \psi\mathbf{M}\psi^* - \mathcal{P}\Omega\mathcal{P} \end{aligned}$$

This establishes (10.38c).

2. The equalities in (10.39a) follow directly from (10.38a) and (10.38b).

For (10.39b),

$$\begin{aligned} (\psi - \mathbf{I})\mathcal{P}\mathbf{H}^* &\stackrel{8.19}{=} \psi\mathcal{E}_\psi\mathcal{P}\mathbf{H}^* \stackrel{9.34}{=} \psi\mathcal{E}_\phi\bar{\tau}\mathcal{P}\mathbf{H}^* \\ &\stackrel{9.32}{=} \psi\mathcal{E}_\phi(\mathbf{I} - \mathcal{G}\mathbf{H})\mathcal{P}\mathbf{H}^* \stackrel{9.32}{=} \mathbf{0} \quad \Rightarrow \quad \psi\mathcal{P}\mathbf{H}^* = \mathcal{P}\mathbf{H}^* \end{aligned} \quad (10.40)$$

Hence,

$$\Omega\mathcal{P}\mathbf{H}^* \stackrel{10.12}{=} \psi^*\mathbf{H}^*\mathcal{D}^{-1}\mathbf{H}\psi\mathcal{P}\mathbf{H}^* \stackrel{10.40}{=} \psi^*\mathbf{H}^*\mathcal{D}^{-1}\mathbf{H}\mathcal{P}\mathbf{H}^* \stackrel{9.32}{=} \psi^*\mathbf{H}^*$$

Post-multiplying (10.39a) by \mathbf{H}^* , and using the above, establishes (10.39b). ■

10.3.2 Computing \mathcal{C}_{os}

Before proceeding to the problem of computing \mathcal{C}_{os} observe that the general form of the \mathcal{C} generalized force vector in (10.8), to include external forces and gravity, is given by the following expression from (5.37) and (5.39):

$$\mathcal{C}(\theta, \dot{\theta}) = \mathbf{H}\phi[\mathbf{M}\phi^*(\mathbf{a} + \mathbf{E}^*\mathbf{g}) + \mathbf{b}] \quad (10.41)$$

Lemma 10.5 Operator expression for \mathcal{C}_{os} .

Assuming Λ exists, the \mathcal{C}_{os} operational space inertia Coriolis term is given by the following expression:

$$\begin{aligned} \mathcal{C}_{os} = \Lambda &\left(\mathcal{B}^* [\psi^* \{ \mathbf{H}^* \mathcal{D}^{-1} \mathbf{H} \psi (\mathcal{P} \mathbf{a}_{gr} + \mathbf{b} + \mathcal{K} \mathcal{T}) \right. \\ &\quad \left. - (\mathbf{a}_{gr} + \mathbf{H}^* \mathcal{D}^{-1} \mathcal{T}) \} + \bar{\mathbf{E}}^* \mathbf{g}] - \dot{\mathcal{B}}^* \mathcal{V} \right) \end{aligned} \quad (10.42)$$

with

$$\mathbf{a}_{gr} \triangleq \mathbf{a} + \mathbf{E}^* \mathbf{g} \quad (10.43)$$

Proof:

From (10.8),

$$\begin{aligned}
 \mathcal{C}_{os} &\stackrel{10.8}{=} \Lambda(\mathcal{J}\mathcal{M}^{-1}(\mathcal{C} - \mathcal{T}) - \mathbf{a}_{os}) \\
 &\stackrel{3.53, 10.41, 9.51}{=} \Lambda \left(\mathcal{B}^* \phi^* \mathcal{H}^* [\mathbf{I} - \mathcal{H}\psi\mathcal{K}]^* \mathcal{D}^{-1} [\mathbf{I} - \mathcal{H}\psi\mathcal{K}] \right. \\
 &\quad \left. * \left(\mathcal{H}\phi [\mathbf{M}\phi^* \mathbf{a}_{gr} + \mathbf{b}] - \mathcal{T} \right) - \mathbf{a}_{os} \right) \\
 &\stackrel{9.45, 10.12, 10.3}{=} \Lambda \left(\mathcal{B}^* \Omega [\mathbf{M}\phi^* \mathbf{a}_{gr} + \mathbf{b} + \mathcal{K}\mathcal{T}] - \mathbf{a}_{os} - \mathcal{B}^* \psi^* \mathcal{H}^* \mathcal{D}^{-1} \mathcal{T} \right) \\
 &\stackrel{10.38a, 10.3}{=} \Lambda \left(\mathcal{B}^* [(\phi^* - \psi^* + \Omega\mathcal{P})\mathbf{a}_{gr} + \Omega(\mathbf{b} + \mathcal{K}\mathcal{T})] \right. \\
 &\quad \left. - [\mathcal{B}^* \phi^* \mathbf{a} + \dot{\mathcal{B}}^* \mathcal{V}] - \mathcal{B}^* \psi^* \mathcal{H}^* \mathcal{D}^{-1} \mathcal{T} \right) \\
 &\stackrel{10.43}{=} \Lambda \left(\mathcal{B}^* [(-\psi^* + \Omega\mathcal{P})\mathbf{a} + (\phi^* - \psi^* + \Omega\mathcal{P})\mathbf{E}^* \mathbf{g} + \Omega(\mathbf{b} + \mathcal{K}\mathcal{T})] \right. \\
 &\quad \left. - \dot{\mathcal{B}}^* \mathcal{V} - \mathcal{B}^* \psi^* \mathcal{H}^* \mathcal{D}^{-1} \mathcal{T} \right) \\
 &\stackrel{10.43}{=} \Lambda \left(\mathcal{B}^* [\Omega(\mathcal{P}\mathbf{a}_{gr} + \mathbf{b} + \mathcal{K}\mathcal{T}) - \psi^*(\mathbf{a}_{gr} + \mathcal{H}^* \mathcal{D}^{-1} \mathcal{T}) + \phi^* \mathbf{E}^* \mathbf{g}] - \dot{\mathcal{B}}^* \mathcal{V} \right) \\
 &\stackrel{5.41, 10.12}{=} \Lambda \left(\mathcal{B}^* [\psi^* \{ \mathcal{H}^* \mathcal{D}^{-1} \mathcal{H}\psi(\mathcal{P}\mathbf{a}_{gr} + \mathbf{b} + \mathcal{K}\mathcal{T}) \right. \\
 &\quad \left. - (\mathbf{a}_{gr} + \mathcal{H}^* \mathcal{D}^{-1} \mathcal{T}) \} + \bar{\mathbf{E}}^* \mathbf{g}] - \dot{\mathcal{B}}^* \mathcal{V} \right)
 \end{aligned}$$

■

The expression in (10.42) can be broken down into the following intermediate set of expressions:

$$\begin{aligned}
 \vartheta &\triangleq \psi(\mathcal{P}\mathbf{a}_{gr} + \mathbf{b} + \mathcal{K}\mathcal{T}) \\
 \eta &\triangleq \psi^* (\mathcal{H}^* \mathcal{D}^{-1} (\mathcal{H}\vartheta - \mathcal{T}) - \mathbf{a}_{gr}) \\
 \zeta &\triangleq \eta + \bar{\mathbf{E}}^* \mathbf{g} \\
 \mathcal{C}_{os} &= \Lambda \left(\mathcal{B}^* \zeta - \dot{\mathcal{B}}^* \mathcal{V} \right)
 \end{aligned} \tag{10.44}$$

The recursive algorithm implied by (10.44) is shown in Algorithm 10.5.

This $O(N)$ algorithm consists of tips-to-base gather sweep followed by a base-to-tips scatter sweep, followed by the solution of a linear matrix equation. This algorithm requires the articulated body inertia quantities, as well as $\underline{\Lambda}$. If these quantities are not available, then the tips-to-base gather sweep can be modified to also compute the articulated body inertia quantities, while the subsequent base-to-tips scatter sweep can be modified to compute the components of $\underline{\Lambda}$.

Algorithm 10.5 The operational space Coriolis/centrifugal force term

```


$$\left\{ \begin{array}{l} \textbf{for all nodes } k \text{ (tips-to-base gather)} \\ \quad \vartheta(k) = \sum_{\forall j \in \mathcal{C}(k)} (\psi(k,j)\vartheta(j) + \mathcal{K}(k,j)\mathcal{T}(j)) + \mathcal{P}(k)\mathfrak{a}_{gr}(k) + \mathfrak{b}(k) \\ \textbf{end loop} \\ \textbf{for all nodes } k \text{ (base-to-tips scatter)} \\ \quad \eta(k) = \psi^*(\varphi(k),k)\eta(\varphi(k)) + H^*(k)\mathcal{D}^{-1}(k)[H(k)\vartheta(k) - \mathcal{T}] - \mathfrak{a}_{gr}(k) \\ \quad \zeta(k) = \eta(k) + \mathfrak{g} \\ \textbf{end loop} \\ \mathcal{C}_{os} = \Lambda \left( \mathcal{B}^* \zeta - \dot{\mathcal{B}}^* \mathcal{V} \right) \end{array} \right.$$


```

10.4 Divide and Conquer Forward Dynamics

The Divide and Conquer Algorithm (DCA) [49] is a parallelizable procedure for solving the forward dynamics problem. The algorithm is based on the idea that the equations of motion of a system can be assembled from the equations of motion of component sub-systems. In this context, hinges are viewed as constraints between independent component systems. Lemma 10.6, below, describes the procedure for combining the operational space dynamics of a pair of independent sub-systems into one where the systems are coupled by a hinge. This result forms the basis for the DCA forward dynamics algorithm, which is outlined subsequently.

To begin, let us assume that we have a pair of independent systems A and B whose equations of motion are given by¹:

$$\underline{\Lambda}^A f_{nd}^A + \bar{\mathcal{C}}_{os}^A = \dot{\beta}^A \quad \text{and} \quad \underline{\Lambda}^B f_{nd}^B + \bar{\mathcal{C}}_{os}^B = \dot{\beta}^B \quad (10.45)$$

Initially, A and B systems are assumed to be uncoupled, and the f_{nd}^A and f_{nd}^B are stacked vectors of external forces at a pair of *handles*, 1 and 2, on each of the systems, as illustrated in Fig. 10.2. $\dot{\beta}^A$ and $\dot{\beta}^B$ denote the stacked spatial acceleration vectors of the handles, and $\underline{\Lambda}^A$ and $\underline{\Lambda}^B$ denote the operational space compliance matrix for the pair of systems. The handles are used to partition these equations of motion as follows:

¹ The form of these equations are similar, but not identical, to the operational space inertia form in (10.7) on page 188. We adopt this alternate form since it is closer to that in Featherstone [49].

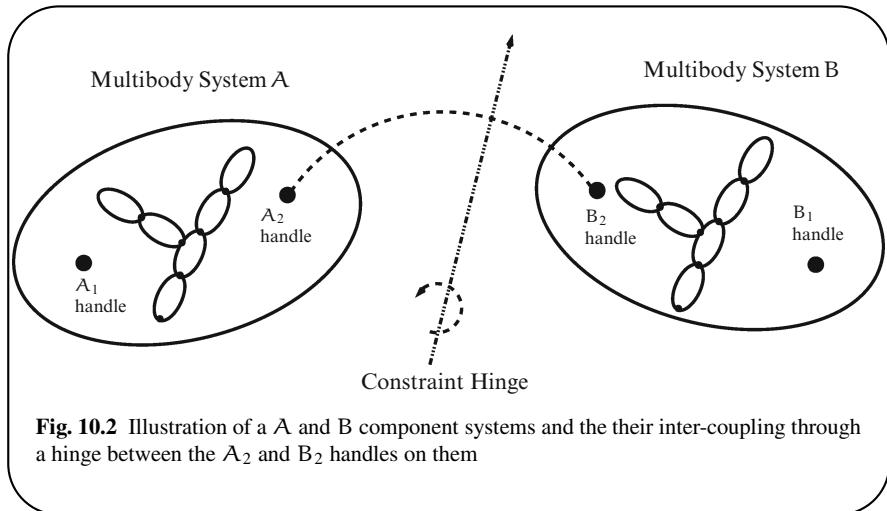


Fig. 10.2 Illustration of a A and B component systems and the their inter-coupling through a hinge between the A₂ and B₂ handles on them

$$\begin{aligned} \begin{pmatrix} \underline{\Delta}_{11}^A & \underline{\Delta}_{12}^A \\ \underline{\Delta}_{21}^A & \underline{\Delta}_{22}^A \end{pmatrix} \begin{bmatrix} f_{nd1}^A \\ f_{nd2}^A \end{bmatrix} + \begin{bmatrix} \bar{C}_{os1}^A \\ \bar{C}_{os2}^A \end{bmatrix} &= \begin{bmatrix} \dot{\beta}_1^A \\ \dot{\beta}_2^A \end{bmatrix} \\ \text{and } \begin{pmatrix} \underline{\Delta}_{11}^B & \underline{\Delta}_{12}^B \\ \underline{\Delta}_{21}^B & \underline{\Delta}_{22}^B \end{pmatrix} \begin{bmatrix} f_{nd1}^B \\ f_{nd2}^B \end{bmatrix} + \begin{bmatrix} \bar{C}_{os1}^B \\ \bar{C}_{os2}^B \end{bmatrix} &= \begin{bmatrix} \dot{\beta}_1^B \\ \dot{\beta}_2^B \end{bmatrix} \end{aligned} \quad (10.46)$$

The following lemma describes the overall equations of motion resulting from connecting the two systems via a hinge constraint between one handle each on the A and B systems.

Lemma 10.6 Combined operational space equations of motion.

Let A and B be systems with operational space equations of motion defined by (10.46). Let the systems be connected via a constraint in the form of a hinge between the A₂ and B₂ pair of handles – one on each of the A and B systems. Assume that R is the joint map matrix for the hinge, with orthogonal complement matrix P (i.e., PR = 0). Thus,

$$(\dot{\beta}_2^A - \dot{\beta}_2^B) = R\ddot{\theta} \quad \text{and} \quad P(\dot{\beta}_2^A - \dot{\beta}_2^B) = 0 \quad (10.47)$$

$\ddot{\theta}$ denotes the generalized acceleration of the constraint hinge. The equations of motion of the combined system are given by the following expressions:

$$\begin{aligned} \underline{\Delta}^C \begin{bmatrix} f_{nd1}^A \\ f_{nd2}^B \end{bmatrix} + \bar{C}_C^C &= \begin{bmatrix} \dot{\beta}_1^A \\ \dot{\beta}_2^B \end{bmatrix} \text{ where } W \triangleq P^* \left[P(\underline{\Delta}_{22}^A + \underline{\Delta}_{22}^B)P^* \right]^{-1} P \\ \text{and } \underline{\Delta}^C &= \begin{pmatrix} \underline{\Delta}_{11}^A & \mathbf{0} \\ \mathbf{0} & \underline{\Delta}_{11}^B \end{pmatrix} - \begin{bmatrix} \underline{\Delta}_{12}^A \\ -\underline{\Delta}_{12}^B \end{bmatrix} W \begin{bmatrix} \underline{\Delta}_{21}^A & -\underline{\Delta}_{21}^B \end{bmatrix} \end{aligned}$$

$$\text{and } \bar{\mathcal{C}}_{os}^C = \begin{bmatrix} \bar{\mathcal{C}}_{os1}^A \\ \bar{\mathcal{C}}_{os1}^B \end{bmatrix} - \begin{bmatrix} \underline{\Delta}_{12}^A \\ -\underline{\Delta}_{12}^B \end{bmatrix} \left(W \begin{bmatrix} \bar{\mathcal{C}}_{os2}^A - \bar{\mathcal{C}}_{os2}^B \\ \underline{\Delta}_{22}^A + \underline{\Delta}_{22}^B \end{bmatrix} - [\mathbf{I} - W(\underline{\Delta}_{22}^A + \underline{\Delta}_{22}^B)] R \mathcal{T} \right) \quad (10.48)$$

with \mathcal{T} denoting the generalized force at the hinge.

Proof: The constraint in (10.47) can be expressed as:

$$P[\mathbf{I}, -\mathbf{I}] \begin{bmatrix} \dot{\beta}_2^A \\ \dot{\beta}_2^B \end{bmatrix} = \mathbf{0} \quad (10.49)$$

The dual version of this equation applies to the forces between the pair of systems and takes the form:

$$\begin{bmatrix} f_{nd2}^A \\ f_{nd2}^B \end{bmatrix} = \begin{bmatrix} \mathbf{I} \\ -\mathbf{I} \end{bmatrix} (P^* \lambda + R \mathcal{T}) \quad (10.50)$$

for some λ Lagrange multiplier vector. Combining the component equations in (10.46) leads to:

$$\begin{pmatrix} \underline{\Delta}_{11}^A & \underline{\Delta}_{12}^A & \mathbf{0} & \mathbf{0} \\ \underline{\Delta}_{21}^A & \underline{\Delta}_{22}^A & \mathbf{0} & \mathbf{0} \\ \mathbf{0} & \mathbf{0} & \underline{\Delta}_{11}^B & \underline{\Delta}_{12}^B \\ \mathbf{0} & \mathbf{0} & \underline{\Delta}_{21}^B & \underline{\Delta}_{22}^B \end{pmatrix} \begin{bmatrix} f_{nd1}^A \\ f_{nd2}^A \\ f_{nd1}^B \\ f_{nd2}^B \end{bmatrix} + \begin{bmatrix} \bar{\mathcal{C}}_{os1}^A \\ \bar{\mathcal{C}}_{os2}^A \\ \bar{\mathcal{C}}_{os1}^B \\ \bar{\mathcal{C}}_{os2}^B \end{bmatrix} = \begin{bmatrix} \dot{\beta}_1^A \\ \dot{\beta}_2^A \\ \dot{\beta}_1^B \\ \dot{\beta}_2^B \end{bmatrix} \quad (10.51)$$

Rearranging the rows and columns of (10.51) so as to gather the constrained rows and columns yields:

$$\begin{pmatrix} \underline{\Delta}_{11}^A & \mathbf{0} & \underline{\Delta}_{12}^A & \mathbf{0} \\ \mathbf{0} & \underline{\Delta}_{11}^B & \mathbf{0} & \underline{\Delta}_{12}^B \\ \underline{\Delta}_{21}^A & \mathbf{0} & \underline{\Delta}_{22}^A & \mathbf{0} \\ \mathbf{0} & \underline{\Delta}_{21}^B & \mathbf{0} & \underline{\Delta}_{22}^B \end{pmatrix} \begin{bmatrix} f_{nd1}^A \\ f_{nd1}^B \\ f_{nd2}^A \\ f_{nd2}^B \end{bmatrix} + \begin{bmatrix} \bar{\mathcal{C}}_{os1}^A \\ \bar{\mathcal{C}}_{os1}^B \\ \bar{\mathcal{C}}_{os2}^A \\ \bar{\mathcal{C}}_{os2}^B \end{bmatrix} = \begin{bmatrix} \dot{\beta}_1^A \\ \dot{\beta}_1^B \\ \dot{\beta}_2^A \\ \dot{\beta}_2^B \end{bmatrix} \quad (10.52)$$

Taken together, (10.49), (10.50), and (10.52) are in a form matching (A.16) on page 400 with the following identifications:

$$\begin{aligned} A &= \begin{pmatrix} \underline{\Delta}_{11}^A & \mathbf{0} \\ \mathbf{0} & \underline{\Delta}_{11}^B \end{pmatrix}, & B &= \begin{pmatrix} \underline{\Delta}_{12}^A & \mathbf{0} \\ \mathbf{0} & \underline{\Delta}_{12}^B \end{pmatrix}, & c_1 &= \begin{bmatrix} \bar{\mathcal{C}}_{os1}^A \\ \bar{\mathcal{C}}_{os1}^B \end{bmatrix}, & c_2 &= \begin{bmatrix} \bar{\mathcal{C}}_{os2}^A \\ \bar{\mathcal{C}}_{os2}^B \end{bmatrix} \\ C &= \begin{pmatrix} \underline{\Delta}_{21}^A & \mathbf{0} \\ \mathbf{0} & \underline{\Delta}_{21}^B \end{pmatrix}, & D &= \begin{pmatrix} \underline{\Delta}_{22}^A & \mathbf{0} \\ \mathbf{0} & \underline{\Delta}_{22}^B \end{pmatrix}, & b_1 &= \begin{bmatrix} \dot{\beta}_1^A \\ \dot{\beta}_1^B \end{bmatrix}, & b_2 &= \begin{bmatrix} \dot{\beta}_2^A \\ \dot{\beta}_2^B \end{bmatrix} \\ Q &= P[\mathbf{I}, -\mathbf{I}], & \gamma &= \begin{bmatrix} \mathbf{I} \\ -\mathbf{I} \end{bmatrix} R \mathcal{T} \end{aligned}$$

Thus,

$$QDQ^* = P \left[\underline{\Lambda}_{22}^A + \underline{\Lambda}_{22}^B \right] P^*, \quad \text{and} \quad Z = \begin{bmatrix} \underline{\Lambda}_{12}^A \\ -\underline{\Lambda}_{12}^B \end{bmatrix} W [I, -I]$$

With the above identifications, we can directly apply the solution for (A.16) to this problem to obtain the following solution for (10.52):

$$\underline{\Lambda}^C \begin{bmatrix} f_{nd1}^A \\ f_{nd1}^B \end{bmatrix} + \bar{C}_{os}^C = \begin{bmatrix} \dot{\beta}_1^A \\ \dot{\beta}_1^B \end{bmatrix}$$

where the expressions for $\underline{\Lambda}^C$ and \bar{C}_{os}^C are as follows:

$$\begin{aligned} \underline{\Lambda}^C &\triangleq A - ZC = \begin{pmatrix} \underline{\Lambda}_{11}^A & \mathbf{0} \\ \mathbf{0} & \underline{\Lambda}_{11}^B \end{pmatrix} - \begin{bmatrix} \underline{\Lambda}_{12}^A \\ -\underline{\Lambda}_{12}^B \end{bmatrix} W \begin{bmatrix} \underline{\Lambda}_{21}^A & -\underline{\Lambda}_{21}^B \end{bmatrix} \\ \bar{C}_{os}^C &\triangleq c_1 + B\gamma - Z(c_1 + D\gamma)c_1 \\ &= c_1 + B \begin{bmatrix} I \\ -I \end{bmatrix} (R\mathcal{T} - W \begin{bmatrix} \bar{C}_{os2}^A - \bar{C}_{os2}^B \\ -W(\underline{\Lambda}_{22}^A + \underline{\Lambda}_{22}^B) R\mathcal{T} \end{bmatrix}) \\ &= \begin{bmatrix} \bar{C}_{os1}^A \\ \bar{C}_{os1}^B \end{bmatrix} - \begin{bmatrix} \underline{\Lambda}_{12}^A \\ -\underline{\Lambda}_{12}^B \end{bmatrix} \left(W \begin{bmatrix} \bar{C}_{os2}^A - \bar{C}_{os2}^B \\ -W(\underline{\Lambda}_{22}^A + \underline{\Lambda}_{22}^B) R\mathcal{T} \end{bmatrix} \right. \\ &\quad \left. - [I - W(\underline{\Lambda}_{22}^A + \underline{\Lambda}_{22}^B)] R\mathcal{T} \right) \end{aligned}$$

This establishes the result. ■

$\underline{\Lambda}^C$ represents the operational space compliance matrix of the combined system, and (10.48) expresses it in terms of the operational space compliance matrices of the individual systems and the hinge constraint between them.

Exercise 10.3 Ground connected equations of motion.

Use Lemma 10.6 to show that, if the A_2 handle for system A is connected to the inertial frame through the hinge (instead of to system B), then the resulting equations of motion are given by the following expressions:

$$\begin{aligned} \underline{\Lambda}^C f_{nd1}^A + \bar{C}_{os}^C &= \dot{\beta}_1^A \quad \text{where} \quad W \triangleq P^* \left[P \underline{\Lambda}_{22}^A P^* \right]^{-1} P \\ \text{and} \quad \underline{\Lambda}^C &= \underline{\Lambda}_{11}^A - \underline{\Lambda}_{12}^A W \underline{\Lambda}_{21}^A \\ \text{with} \quad \bar{C}_{os}^C &= \bar{C}_{os1}^A - \underline{\Lambda}_{12}^A \left(W \bar{C}_{os2}^A - [I - W \underline{\Lambda}_{22}^A] R\mathcal{T} \right) \end{aligned} \tag{10.53}$$
■

We have seen how the operational space dynamics of a pair of independent systems can be used to obtain the operational space dynamics when the systems are

coupled by a hinge. The expression for Δ^C was first derived in Featherstone [49] as a step towards the development of the parallelizable DCA forward dynamics algorithm. The DCA begins by treating each individual body in the system as an independent system with handles defined by the hinge connection nodes. The Δ matrix for each of these single body systems is simply the inverse of their individual spatial inertias. Neighboring bodies can then be combined using Lemma 10.6 to develop the operational space dynamics of the pairs of bodies. This assembly procedure is continued, combining pairs of these systems, until the operational space compliance matrix of the complete system is assembled. If the system is connected to the ground, then (10.53) can be used to attach this final hinge. The resulting DCA is outlined in Algorithm 10.6.

Algorithm 10.6 The DCA forward dynamics algorithm

The following describes the Divide and Conquer algorithm for tree systems:

1. Carry out a binary tree assembly sweep that begins with the formation of the operational space compliance matrix of individual bodies and uses Lemma 10.6 to couple them in each subsequent pass to build larger and larger assemblies. The assembly sweep terminates when the operational space compliance matrix for the whole system has been obtained.
 2. This sweep is a back-substitution pass that proceeds in the reverse direction by solving for, and propagating, the interaction spatial forces and generalized accelerations across the connecting hinges of the component sub-assemblies.
-

Since the assembly and the back-substitution passes across the component sub-assemblies can be carried out independently, the DCA procedure can be parallelized. While a serial implementation of this algorithm is more expensive than the AB forward dynamics algorithm, its computational cost is just $O(\log(n))$ for a parallel implementation on $O(n)$ processors. Numerical accuracy and other issues of the DCA technique are discussed in [49, 50].

Chapter 11

Closed-Chain Dynamics

The subject of this chapter is the dynamics of closed-chain multibody systems. These are systems whose underlying digraphs are not trees, but may be multiply-connected and include directed cycles, as illustrated in Fig. 8.6 on page 152. Section 9.6.2 on page 185 discussed some of the hurdles in extending SKO models to closed-chain systems. The issues identified included the fact that the SKO operator is not nilpotent when the digraph has directed cycles, and that the hinge generalized coordinates are not independent when there are multiply-connected nodes in the system digraph.

A common approach for handling such digraph systems is to decompose them into a spanning tree and a set of cut-edges representing motion constraints on the *free* dynamics of the spanning tree.

11.1 Modeling Closed-Chain Dynamics

Since the spanning tree for the digraph of the closed-chain system is a tree, an SKO model for it can be defined using the techniques from Chap. 9, with equations of motion expressed as

$$\mathcal{M}(\theta)\ddot{\theta} + \mathcal{C}(\theta, \dot{\theta}) = \mathcal{T} \quad (11.1)$$

This spanning tree SKO model has \mathcal{N} dimensional configuration, and \mathcal{N} dimensional velocity, degrees of freedom. The effect of the cut-edge motion constraints is to reduce the degrees of freedom in the system to less than \mathcal{N} .

We will focus on the handling of bilateral constraints, and discuss the extensions needed for unilateral constraints in Sect. 11.5.

11.1.1 Types of Bilateral Motion Constraints

We will consider bilateral holonomic and non-holonomic motion constraints.

Holonomic constraints: When the motion constraints can be expressed purely as a function of the generalized coordinates, the constraints are referred to as **holonomic** constraints. These constraints are defined by constraint equations of the following form:

$$\mathfrak{d}(\theta, t) = \mathbf{0} \quad (11.2)$$

where $\mathfrak{d}(., t)$ is an n_c -dimensional constraint function. Observe that the holonomic constraint equation *does not depend* upon the generalized velocities, but can depend on the generalized coordinates, and can be time varying. If the holonomic constraint function $\mathfrak{d}(., .)$ is time-invariant, then the holonomic constraints are said to be **scleronomic**. When this is not the case, the constraints are said to be **rheonomic**.

Differentiating (11.2) with respect to time leads to the following constraint equation in the velocity domain:

$$\dot{\mathfrak{d}}(\theta, t) = G_c(\theta, t)\dot{\theta} - \mathfrak{U}(t) = \mathbf{0} \quad (11.3)$$

where

$$G_c(\theta, t) \triangleq \nabla_{\theta}\mathfrak{d}(\theta, t) \in \mathcal{R}^{n_c \times N} \text{ and } \mathfrak{U}(t) \triangleq -\frac{\partial \mathfrak{d}(\theta, t)}{\partial t} \in \mathcal{R}^{n_c} \quad (11.4)$$

This differential form of constraints are also referred to as a **Pfaffian form**. When $\mathfrak{U} = \mathbf{0}$, the differential form of the constraints is said to be **catastatic**. When this is not the case, the constraints are said to be **acatastatic**. Clearly, scleronomic holonomic constraints lead to catastrophic differential constraints, while rheonomic ones lead to acatastatic ones.

We assume that $G_c(\theta, t)$ is a full-rank matrix. Some notable points about (11.3) are that it is integrable, n_c -dimensional, and equivalent (modulo a constant) to (11.2). Also, it is *linear* in the generalized velocity coordinates. These constraints effectively reduce the generalized coordinates and velocities for the system from N to $(N - n_c)$ dimensional manifolds and vector spaces, respectively.

Non-holonomic constraints: When the definition of the constraints involves non-integrable constraints on the generalized velocities, then the constraints are said to be **non-holonomic**. For such constraints, the motion constraints are expressed directly in the (11.3) Pfaffian form without the additional configuration-level constraints in (11.2) and (11.4). In the case of non-holonomic constraints, the dimension of the configuration space remains unchanged at N [153], and only the dimension of the generalized velocity subspace is reduced to $N - n_c$. We will be restricting our attention here to only non-holonomic constraints arising from equality constraints on the permissible velocities, even though more generally, inequality constraints (e.g., unilateral constraints) on the configuration of a system are also classified as non-holonomic constraints on the system.

Thus, holonomic constraints lead to a reduction in the number of configuration degrees of freedom and the motion degrees of freedom by equal amounts. On the other

hand, non-holonomic constraints only lead to a reduction in the number of motion degrees of freedom, and leave the number of configuration degrees of freedom unchanged. In other words, holonomic constraints reflect the global behavior of the hinge, while non-holonomic constraints reflect only the local behavior. A detailed discussion on holonomic and non-holonomic constraints can be found in Rosenberg [153].

We deal with both holonomic and non-holonomic motion constraints in this chapter, using the velocity domain characterization of (11.3) as the common point of departure.

11.1.2 Constrained System Forward Dynamics Strategies

The effect of the cut-edge constraints can be incorporated into the SKO model for the spanning tree via **Lagrange multipliers**, denoted $\lambda \in \mathcal{R}^{n_c}$. Augmenting (11.1) with the Lagrange multipliers results in the following overall equations of motion for the closed-chain system:

$$\begin{aligned} \mathcal{M}(\theta)\ddot{\theta} + \mathcal{C}(\theta, \dot{\theta}) - G_c^*(\theta, t)\lambda &= \mathcal{T} \\ G_c(\theta, t)\dot{\theta} &= \mathfrak{U}(t) \end{aligned} \quad (11.5)$$

The $-G_c^*(\theta, t)\lambda$ term in the first equation above represents the internal generalized constraint forces from the motion constraints.

By differentiating the constraint equation, (11.5) can be rearranged into the following matrix form:

$$\begin{pmatrix} \mathcal{M} & G_c^* \\ G_c & \mathbf{0} \end{pmatrix} \begin{bmatrix} \ddot{\theta} \\ -\lambda \end{bmatrix} = \begin{bmatrix} \mathcal{T} - \mathcal{C} \\ \mathfrak{U} \end{bmatrix} \quad \text{where } \dot{\mathfrak{U}} \triangleq \dot{\mathfrak{U}}(t) - \dot{G}_c\dot{\theta} \in \mathcal{R}^{n_c} \quad (11.6)$$

Observe that

$$\ddot{\vartheta}(\theta, t) \stackrel{11.3, 11.6}{=} G_c\ddot{\theta} - \dot{\mathfrak{U}} \quad (11.7)$$

The following options are available for solving the forward dynamics of systems with closure constraints:

Augmented approach: The *augmented* approach treats the cut-edge motion constraints as a correction to be applied to the dynamics of the spanning tree system. The SKO techniques and algorithms can be applied to efficiently solve the dynamics of the SKO model for the spanning tree. Additional steps are required to account for the motion constraints described by the cut-edges. This technique works with the larger N -dimensional set of generalized velocity coordinates rather than with the $N - n_c$ truly independent ones for the system. The use of non-minimal coordinates requires the use of differential-algebraic equation (DAE) integrators, along with error-control techniques for mitigating the solution's drift away from the constraint manifold. More precisely, (11.6) is

referred to as an index-3 DAE formulation of the equations of motion [13]. The augmented dynamics approach is described in Sect. 11.2.

Direct approach: The *direct* approach solves (11.6) for the unknown $(\ddot{\theta}, \lambda)$ using matrix solvers. Since we have assumed that G_c is full-rank, the matrix on the left is non-singular and the equation has a unique solution. This solution technique is typically used with *absolute* instead of *relative* coordinate formulations. In the absolute coordinates formulation, the mass matrix block becomes a simple block-diagonal constant matrix, while λ grows to include the closure, as well as the inter-link hinge constraints [132]. While the system dimensionality is much larger, and the solution complexity is ostensibly of $O(N^3)$ complexity, solvers exploiting the sparsity of the coefficient matrix can reduce the computational cost. Like the augmented approach, this technique uses non-minimal generalized coordinates, and is subject to similar DAE integration and error-control issues. Schwerin [158] contains an in-depth discussion of this closed-chain system dynamics approach.

Projected approach: The *projected* approach uses numerical techniques to eliminate the constraints from the equations of motion [121, 158]. This approach works with minimal coordinates that automatically satisfy the cut-edge constraints. There is no attempt to preserve the topological structure of the system during the constraint elimination process and, consequently, the resulting equations of motion do not satisfy the requirements for an SKO model. Thus, the SKO analytical and low-order algorithmic techniques are not available to this approach. This procedure is described in Sect. 11.3. Section 11.4 discusses the equivalence of the augmented and projected dynamics formulations.

Constraint embedding approach: The *constraint embedding* approach transforms the original digraph into a tree graph by aggregating the “non-tree” subgraphs in the system into nodes. Similar to the projected technique, this approach also works with minimal coordinates. One notable feature is that multiple physical bodies are assigned to individual nodes in the transformed tree. This is a departure from the standard digraphs, where there is a one-to-one correspondence between the physical bodies and the nodes in the digraph. All the SKO techniques, including low-order forward dynamics, are applicable to the SKO model for the transformed tree. Another benefit of this approach is that the minimal velocity coordinate model is more suitable for control applications. The constraint embedding technique is described in Chap. 15.

11.2 Augmented Approach for Closed-Chain Forward Dynamics

Lemma 11.1 Augmented closed-chain forward dynamics solution.

The closed-chain dynamics generalized accelerations in (11.6) can be expressed as

$$\ddot{\theta} = \ddot{\theta}_f + \ddot{\theta}_\delta \quad (11.8)$$

where, the free generalized accelerations, $\ddot{\theta}_f$, the correction generalized accelerations, $\ddot{\theta}_\delta$, and the Lagrange multipliers, λ , are given by

$$\ddot{\theta}_f \triangleq \mathcal{M}^{-1}(\mathcal{T} - \mathcal{C}) \quad (11.9a)$$

$$\lambda = -[G_c \mathcal{M}^{-1} G_c^*]^{-1} \ddot{\delta}_f \quad \text{where} \quad \ddot{\delta}_f \triangleq G_c \ddot{\theta}_f - \mathcal{U} \quad (11.9b)$$

$$\ddot{\theta}_\delta \triangleq \mathcal{M}^{-1} G_c^* \lambda \quad (11.9c)$$

Proof: Since \mathcal{M} is invertible, (11.6) satisfies the requirements of the (A.9) matrix equation on page 398. The result follows by using its solution in (A.10) to obtain (11.9). ■

The $\ddot{\theta}_f = \mathcal{M}^{-1}(\mathcal{T} - \mathcal{C})$ term represents the generalized accelerations solution for the dynamics of the spanning tree SKO model while ignoring the closure constraints and, is therefore referred to as the free generalized accelerations. $\ddot{\delta}_f$ represents the acceleration-level constraint violation resulting from just the free dynamics of the system. The solution to the closed-chain forward dynamics conceptually involves the steps described in Algorithm 11.1. It is noteworthy that the solution for the $\ddot{\theta}_f$

Algorithm 11.1 Augmented forward dynamics algorithm

1. Solve (11.9a) for the $\ddot{\theta}_f$ free generalized accelerations for the SKO model for the spanning tree.
 2. Use $\ddot{\theta}_f$ in (11.9b) to solve for the λ Lagrange multipliers.
 3. Use λ to solve (11.9c) for the $\ddot{\theta}_\delta$ correction accelerations,
 4. Compute the generalized accelerations using (11.8).
-

free accelerations requires the solution of the forward dynamics of the SKO model for the spanning tree, for which the efficient $O(N)$ AB procedure in Algorithm 9.5 on page 182 is available. The augmented formulation solves for the full N dimensional $\ddot{\theta}$ generalized accelerations vector even though only $N - n_c$ of the elements are in fact truly independent. One numerical consequence of this over-parametrization is that DAE integrators, instead of the ODE integrators for tree systems, are required for the numerical integration of the accelerations and velocities [14, 158, 173]. Furthermore, constraint error control techniques are needed to manage the inevitable numerical errors that cause the system state to drift off of the constraint manifold [24, 33, 158].

A direct relationship between the \mathcal{T} applied torques and the $\ddot{\theta}$ generalized accelerations is the subject of the following exercise.

Exercise 11.1 Mapping between \mathcal{T} and $\ddot{\theta}$ for closed-chain systems.
Show that the relationship between \mathcal{T} and $\ddot{\theta}$ for closed-chain systems is given by

$$\ddot{\theta} = \mathcal{Y}_C [\mathcal{T} - \mathcal{C}] + \mathcal{M}^{-1} G_c^* [G_c \mathcal{M}^{-1} G_c^*]^{-1} \mathcal{U} \quad (11.10)$$

where

$$\mathcal{Y}_C \triangleq \mathcal{M}^{-1} - \mathcal{M}^{-1} G_c^* [G_c \mathcal{M}^{-1} G_c^*]^{-1} G_c \mathcal{M}^{-1} \in \mathcal{R}^{N \times N} \quad (11.11)$$

■

Observe that $[G_c \mathcal{M}^{-1} G_c^*]^{-1} G_c \mathcal{M}^{-1}$ is a generalized inverse of G_c^* . Since \mathcal{Y}_C defines a symmetric and positive semi-definite mapping between \mathcal{T} and $\ddot{\theta}$, it is tempting to think of it as being the mass matrix inverse for the constrained system. However, \mathcal{Y}_C is singular and not invertible. This can be seen by noting that

$$\mathcal{Y}_C G_c^* = \mathbf{0} \quad (11.12)$$

Since \mathcal{Y}_C is singular, there is no well-defined mass matrix for the constrained system. The singularity of \mathcal{Y}_C results from the fewer than N velocity degrees of freedom in the system.

11.2.1 Move/Squeeze Decompositions

For tree-topology systems, any non-zero generalized force results in non-zero accelerations in the system. This is not the case for constrained systems; these can have generalized forces that induce no accelerations in the system at all! The motion degrees of freedom that are lost in the presence of constraints are recovered in the force domain. In other words, the generalized forces can be used to manage an n_c -dimensional sub-space of non-motion inducing internal forces within the system. This is useful during robotics manipulation and control tasks, where it is required to manage the motion, as well as the forces, in the system. Examples include tasks with manipulator end-effectors in contact with the environment, multi-arm systems manipulating objects, and locomotion involving legged systems.

From (11.10) and (11.12), it follows that any \mathcal{T} in the column space of G_c^* will result in $\ddot{\theta} = \mathbf{0}$, i.e., it will not induce any motion in the system. We refer to such generalized forces as **squeeze** generalized forces since their presence effects internal forces within the system but induces no motion. We use the \mathcal{T}_{sq} notation to denote **squeeze** generalized forces.

The complement of the subspace of squeeze forces is referred to as the subspace of **move** generalized forces. **move** forces always result in non-zero motion in the system. We use the \mathcal{T}_{mv} notation for **move** forces. We can decompose any generalized force vector, \mathcal{T} , into **move** and **squeeze** components as follows:

$$\mathcal{T} = \mathcal{T}_{mv} + \mathcal{T}_{sq} \quad (11.13)$$

This decomposition is not unique. The component forces on the right can be obtained by defining a move/squeeze projection matrix, \mathcal{P}_{ms} , as

$$\mathcal{P}_{ms} \triangleq G_c^* (X G_c^*)^{-1} X \in \mathcal{R}^{N \times N} \quad (11.14)$$

where X is an $n_c \times N$ matrix such that (XG_c^*) is invertible. Possible choices for X include $G_c W$, with W being a symmetric positive-definite matrix such as $W = I$, or an appropriate constant weight matrix.

Using the \mathcal{P}_{ms} projection, any generalized forces vector \mathcal{T} can be expressed in the form

$$\mathcal{T} = \mathcal{T}_{mv} + \mathcal{T}_{sq} \quad \text{where} \quad \mathcal{T}_{sq} \triangleq \mathcal{P}_{ms}\mathcal{T}, \quad \mathcal{T}_{mv} \triangleq (I - \mathcal{P}_{ms})\mathcal{T} \quad (11.15)$$

The move/squeeze decomposition has useful implications for coordinated motion and force control [108, 109, 181]. The control system can be decomposed into two loops. The inner loop is responsible for applying generalized forces that accomplish the motion objectives. The outer force control loop is responsible for managing the task space and internal forces within the system. The outer force control loop adds on only **squeeze** generalized forces to those generated by the inner loop. Thus, the outer loop has no effect on the motion performance of the inner loop. The force control loop can be used to load-balance the forces to avoid saturating actuators, to ensure that sufficient forces are being applied in the task space needed for tool operation, or to maintain contact or grasp. Thus, the inner loop is responsible for controlling the motion degrees of freedom while the outer loop is responsible for controlling the force degrees of freedom in the system. The following exercise investigates the use of the X matrix for load balancing of actuator torques.

Exercise 11.2 Torque minimization using squeeze forces.

Let W denote the weight matrix for a weighted vector 2-norm. Define X in (11.14) as $X = G_c W$. For a generalized force \mathcal{T} , show that $(I - \mathcal{P}_{ms})\mathcal{T}$ is the generalized force that has minimum W -norm and the same move force component as \mathcal{T} . ■

In other words, the above exercise shows that the \mathcal{T}_{mv} move component of a generalized force, \mathcal{T} , is the generalized force with minimal W -norm that accomplishes the same motion as \mathcal{T} . Minimizing such norms can be desirable, since weighted norms are often measures of actuator power and stress loads. Thus, from a control perspective, the motion control loop can generate a candidate generalized force command \mathcal{T} , which is then modified by the squeeze control loop by the amount $-\mathcal{P}_{ms}\mathcal{T}$, to derive the minimum-norm command for the actuators.

11.2.2 Augmented Dynamics with Loop Constraints

So far, we have not made any particular assumptions on the nature of, or the physical origin of, the closure constraints. In this section, we look at the important case where the constraints are due to motion constraints between nodes in a tree-topology system [152]. Such constraints are referred to as *loop* constraints. An example is illustrated in Fig. 11.1. Rigid inter-node constraints require the relative spatial velocity of the constrained nodes to be zero. More generally, these inter-node

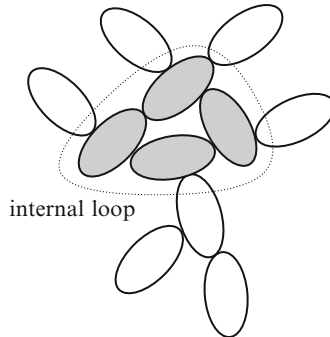


Fig. 11.1 Example of a system topology with an internal loop

constraints are defined by hinges that allow non-zero relative spatial velocities, but constrain them to lie in a subspace defined by the hinge joint map matrices. Examples of such constraints are:

1. A closure constraint between a node and the inertial frame. This constraint is characterized by an equation of the form

$$\mathcal{Q}_x^{\text{rel}} \mathcal{V}_x = \mathbf{0}$$

where $\mathcal{V}_x \in \mathcal{R}^6$ is the spatial velocity at the node x while $\mathcal{Q}_x^{\text{rel}} \in \mathcal{R}^{a \times 6}$ (with $a \leq 6$), is the constraint matrix. A rigid constraint, where the node x is not allowed to move, corresponds to an identity $\mathcal{Q}_x^{\text{rel}}$ matrix.

2. A constraint on the relative spatial velocity of a pair of nodes, x and y , can be stated as

$$\mathcal{Q}^{\text{rel}} [\mathcal{V}_x - \mathcal{V}_y] = \mathbf{0}$$

The above can be restated as

$$\mathcal{Q} \mathcal{V}_{nd} = \mathbf{0} \quad \text{where} \quad \mathcal{Q} \triangleq \begin{bmatrix} \mathcal{Q}_x^{\text{rel}} & -\mathcal{Q}_y^{\text{rel}} \end{bmatrix}, \quad \mathcal{V}_{nd} \triangleq \begin{bmatrix} \mathcal{V}_x \\ \mathcal{V}_y \end{bmatrix} \quad (11.16)$$

When the x and y nodes are constrained to rigidly follow each other, the \mathcal{Q}^{rel} matrix is the identity matrix.

More generally, let us assume that there are a set of *closure* nodes on the system, and the closed-chain constraints are constraints on the spatial velocities of these nodes. Let \mathcal{V}_{nd} denote the spatial velocities of these constrained nodes. Then for some matrix \mathcal{Q} , the closure constraints (holonomic or non-holonomic) can be expressed as

$$\dot{\mathbf{d}}(\theta, t) = \mathcal{Q} \mathcal{V}_{nd} - \mathfrak{U} = \mathcal{Q} \mathcal{J} \dot{\theta} - \mathfrak{U} = \mathbf{0} \quad (11.17)$$

with $\mathcal{J} = \mathcal{B}^* \phi^* \mathcal{H}^*$ (from (3.53)) denoting the velocity Jacobian matrix for these constraint nodes on the system. Using (11.3) we can identify G_c as

$$G_c = \mathcal{Q}\mathcal{J} = \mathcal{Q}\mathcal{B}^* \phi^* \mathcal{H}^* \quad (11.18)$$

While the only fundamental requirement is that the spanning tree multibody system have an SKO model, for the sake of exposition, we have adopted the specific rigid multi-link operator notation in the operator expression for the Jacobian matrix. There is no loss in generality since the ideas developed here easily extend to general SKO models using the approach from Chap. 9. This specific form for G_c allows us to simplify the expressions in Lemma 11.1, as described in the following lemma. For loop constraints, $\ddot{\delta}$ in (11.7) can be expressed as

$$\ddot{\delta}(\theta, t) \stackrel{11.18, 11.4}{=} \mathcal{Q}\alpha_{nd}^f + \dot{\mathcal{Q}}\mathcal{V}_{nd} - \dot{\mathcal{U}}(t) \quad (11.19)$$

Lemma 11.2 Forward dynamics with loop constraints.

The generalized accelerations for a closed-chain system with loop constraints, given by (11.18), is

$$\ddot{\theta} = \ddot{\theta}_f + \ddot{\theta}_\delta \quad (11.20)$$

where, the free generalized accelerations, $\ddot{\theta}_f$, the correction generalized accelerations, $\ddot{\theta}_\delta$, and the Lagrange multipliers, λ , are given by

$$\ddot{\theta}_f \triangleq [\mathbf{I} - \mathcal{H}\psi\mathcal{K}]^*\mathcal{D}^{-1}\{\mathcal{T} - \mathcal{H}\psi[\mathcal{K}\mathcal{T} + \mathcal{P}\mathbf{a} + \mathbf{b}]\} - \mathcal{K}^*\psi^*\mathbf{a} \quad (11.21a)$$

$$\lambda = -[\mathcal{Q}\underline{\Lambda}\mathcal{Q}^*]^{-1}\ddot{\delta} \quad (11.21b)$$

$$\ddot{\theta}_\delta \triangleq [\mathbf{I} - \mathcal{H}\psi\mathcal{K}]^*\mathcal{D}^{-1}\mathcal{H}\psi\mathcal{B}\mathcal{Q}^*\lambda \quad (11.21c)$$

with α_{nd}^f denotes the spatial accelerations of the constraint nodes for the free-dynamics solution of (11.21a), $\underline{\Lambda} = \mathcal{B}^*\Omega\mathcal{B}$ is the operational space compliance matrix, and $\Omega = \psi^*\mathcal{H}^*\mathcal{D}^{-1}\psi\mathcal{H}$ is the extended operational space compliance matrix, defined in (10.12).

Proof: The derivation of the expressions in (11.21) begins with the expressions in (11.9). Firstly, (11.21a) follows directly from the expression for tree-topology generalized accelerations in (9.54).

Equation (11.21b) follows from

$$\begin{aligned} G_c \mathcal{M}^{-1} G_c^* &\stackrel{11.18, 9.51}{=} \mathcal{Q}\mathcal{B}^* \phi^* \mathcal{H}^* [\mathbf{I} - \mathcal{H}\psi\mathcal{K}]^* \mathcal{D}^{-1} [\mathbf{I} - \mathcal{H}\psi\mathcal{K}] \mathcal{H}\phi\mathcal{B}\mathcal{Q}^* \\ &\stackrel{9.45}{=} \mathcal{Q}\mathcal{B}^* \psi^* \mathcal{H}^* \mathcal{D}^{-1} \mathcal{H}\psi\mathcal{B}\mathcal{Q}^* = \mathcal{Q}\mathcal{B}^* \Omega \mathcal{B}\mathcal{Q}^* \stackrel{10.12}{=} \mathcal{Q}\underline{\Lambda}\mathcal{Q}^* \end{aligned}$$

Using this in (11.9b) establishes (11.21b).

For (11.21c), we have

$$\begin{aligned}\mathcal{M}^{-1}G_c^* &\stackrel{11.18,9.51}{=} [\mathbf{I} - \mathbf{H}\Psi\mathcal{K}]^* \mathcal{D}^{-1} [\mathbf{I} - \mathbf{H}\Psi\mathcal{K}] \mathbf{H}\Phi\mathcal{B}\Omega^* \\ &\stackrel{9.45}{=} [\mathbf{I} - \mathbf{H}\Psi\mathcal{K}]^* \mathcal{D}^{-1} \mathbf{H}\Psi\mathcal{B}\Omega^*\end{aligned}$$

■

This lemma provides explicit operator expressions for the constraint forces and the generalized accelerations. The $\underline{\Delta}$ operational space compliance matrix appearing in (11.21b), and the Ω extended operational space compliance matrix, were originally encountered in the context of operational space dynamics in Chapter 10. The $(\underline{\mathcal{U}} - \Omega\alpha_{nd}^f)$ term in (11.21b) is a measure of the constraint violation from the free system dynamics solution in (11.21a). Indeed, with the correct node spatial accelerations, α_{nd} , the $(\underline{\mathcal{U}} - \Omega\alpha_{nd})$ vanishes. We can establish this by differentiating (11.17) to obtain:

$$\dot{\Omega}\mathcal{V}_{nd} + \Omega\alpha_{nd} = \dot{\mathcal{U}}(t) \Rightarrow \underline{\mathcal{U}} - \Omega\alpha_{nd} = \mathbf{0}$$

Thus, an intuitive interpretation of (11.21b) is that the constraint error spatial accelerations from the free-dynamics solution are used to derive the constraint forces necessary to nullify the errors. Once the constraint forces are available, (11.21c) uses them to correct the dynamics solution for the free system.

The spatial operator expressions in (11.21) can be implemented, and evaluated recursively, leading to substantial savings in computational cost over Algorithm 11.1. Algorithm 11.2 describes a complete solution to the constrained forward dynamics algorithm with loop constraints. The procedure is $O(N)$, except for the step involving the solution of the (11.21b) matrix equation. The computational complexity of this step can be cubic in the number of constraints.

References [17, 29] describe alternative recursive procedures for solving the forward dynamics of closed-chain systems. Featherstone [50] describes extensions of the tree DCA algorithm to systems with loop constraints. Other relevant references for this topic are [23, 53, 89, 132, 187].

Exercise 11.3 Expression for \mathcal{Y}_C with loop constraints.

For systems with loop constraints, show that the operator form of \mathcal{Y}_C in (11.11) is given by

$$\mathcal{Y}_C = [\mathbf{I} - \mathbf{H}\Psi\mathcal{K}]^* \mathcal{D}^{-\frac{1}{2}} [\mathbf{I} - \mathbf{H}\Psi\mathcal{B}\Omega^*(\Omega\underline{\Delta}\Omega^*)^{-1} \Omega\mathcal{B}^*\Psi^*\mathbf{H}^*] \mathcal{D}^{-\frac{1}{2}} [\mathbf{I} - \mathbf{H}\Psi\mathcal{K}]$$

That is,

$$\mathcal{Y}_C = [\mathbf{I} - \mathbf{H}\Psi\mathcal{K}]^* \mathcal{D}^{-\frac{1}{2}} [\mathbf{I} - b(b^*\mathcal{D}^{-1}b)^{-1}b^*] \mathcal{D}^{-\frac{1}{2}} [\mathbf{I} - \mathbf{H}\Psi\mathcal{K}] \quad (11.22)$$

where $b \triangleq \mathbf{H}\Psi\mathcal{B}\Omega^*$.

■

Algorithm 11.2 Forward dynamics with loop constraints

The steps for the solution of the augmented closed-chain dynamics with loop constraints in Lemma 11.2 are listed below:

1. Solve for $\ddot{\theta}_f$ in (11.21a) using the $O(N)$ AB forward dynamics Algorithm 9.5 on page 182. This also results in the computation of the articulated body inertia quantities and the α_{nd}^f node spatial accelerations required by (11.21b).
2. Use Algorithm 10.2 on page 194 to compute $\underline{\Delta}$. Then solve the (11.21b) matrix equation for the λ Lagrange multipliers.
3. Use Algorithm 7.3 on page 131 for an $O(N)$ gather/scatter recursive implementation of $\ddot{\theta}_\delta = [\mathbf{I} - \mathbf{H}\psi\mathcal{K}]^*\mathcal{D}^{-1}\mathbf{H}\psi\mathcal{B}\mathcal{Q}^*\lambda$ to compute $\ddot{\theta}_\delta$ with $f_c = -\mathcal{Q}^*\lambda$.
4. Use (11.20) to compute $\ddot{\theta}$.

When there are no closed loops in the overall system, $\mathcal{Q} = 0$, and so $b = 0$. Consequently, the middle term in (11.22) reduces to \mathbf{I} , and the expression for \mathcal{Y}_C reduces to the expression for \mathcal{M}^{-1} in (9.51) for tree-topology systems.

11.2.3 Dual-Arm System Example

Now we consider a constrained dynamics example consisting of two manipulators whose end-effectors are rigidly attached to each other (for instance when holding a rigid task object), as illustrated in Fig. 11.2. In this section, we explicitly

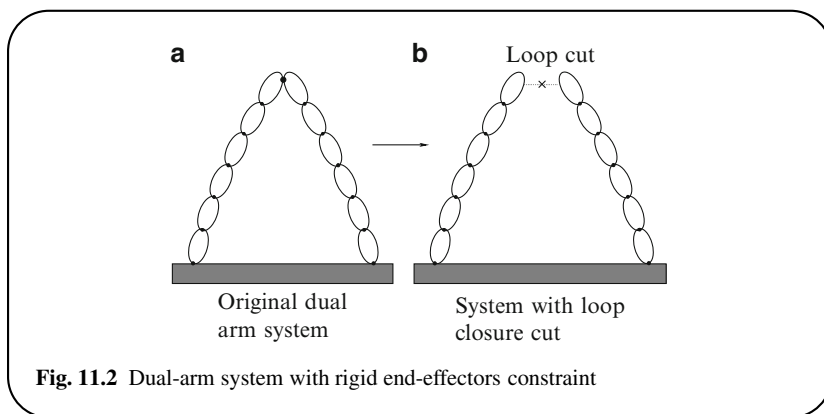


Fig. 11.2 Dual-arm system with rigid end-effectors constraint

work through the forward dynamics solution for this system using the augmented approach.

Imagine that the closed-chain is cut as shown on the right side of the figure, decomposing the system into a pair of serial-chains, and a single cut-edge constraint. Cutting the chain results in arms 1 and 2 with n_1 and n_2 links, respectively. The rigid constraint between the tips of arms 1 and 2 leads to the following constraint equations:

$$\begin{aligned} \mathcal{V}_1(0) = \mathcal{V}_2(0) &\implies \mathcal{J}_1 \dot{\theta}_1 = \mathcal{J}_2 \dot{\theta}_2 \quad \text{or} \quad \mathcal{Q} \begin{bmatrix} \mathcal{V}_1(0) \\ \mathcal{V}_2(0) \end{bmatrix} = \mathbf{0} \\ \alpha_1(0) = \alpha_2(0) &\quad \text{or} \quad \mathcal{Q} \begin{bmatrix} \alpha_1(0) \\ \alpha_2(0) \end{bmatrix} = \mathbf{0} \quad \text{with} \quad \mathcal{Q} \triangleq [\mathbf{I}_6, -\mathbf{I}_6] \end{aligned} \quad (11.23)$$

With (11.23), the dynamical behavior of arms 1 and 2 is given by

$$\mathcal{M}_1 \ddot{\theta}_1 + \mathcal{C}_1 = \mathcal{T}_1 + \mathcal{J}_1^* \mathfrak{f}_1, \quad \mathcal{M}_2 \ddot{\theta}_2 + \mathcal{C}_2 = \mathcal{T}_2 + \mathcal{J}_2^* \mathfrak{f}_2 \quad \text{where} \quad \begin{bmatrix} \mathfrak{f}_1 \\ \mathfrak{f}_2 \end{bmatrix} \triangleq \mathcal{Q}^* \mathfrak{f}(0) \quad (11.24)$$

For arm 1,

$$\ddot{\theta}_1 = \mathcal{M}_1^{-1} (\mathcal{T}_1 - \mathcal{C}_1) + \mathcal{M}_1^{-1} \mathcal{J}_1^* \mathfrak{f}_1 = \ddot{\theta}_{1f} + \ddot{\theta}_\delta^1 \quad (11.25)$$

where

$$\begin{aligned} \ddot{\theta}_{1f} &\triangleq \mathcal{M}_1^{-1} (\mathcal{T}_1 - \mathcal{C}_1) = [\mathbf{I} - \mathbf{H}\psi\mathcal{K}]^* \mathcal{D}^{-1} [\mathbf{I} - \mathbf{H}\psi\mathcal{K}] (\mathcal{T} - \mathcal{C}) \\ \text{and} \quad \ddot{\theta}_\delta^1 &\triangleq \mathcal{M}_1^{-1} \mathcal{J}_1^* \mathfrak{f}_1 = [\mathbf{I} - \mathbf{H}\psi\mathcal{K}]^* \mathcal{D}^{-1} \mathbf{H}\psi\mathcal{B}\mathfrak{f}_1 \end{aligned} \quad (11.26)$$

$\ddot{\theta}_{1f}$ represents the “free” generalized acceleration, i.e., the generalized acceleration that would exist if the tip of arm 1 were unconstrained, while $\ddot{\theta}_\delta^1$ is the correction joint acceleration for arm 1 due to the presence of the tip constraint force \mathfrak{f}_1 . $\ddot{\theta}_{1f}$ can be obtained using the recursive $O(n_1)$ AB forward dynamics algorithm, as can $\ddot{\theta}_\delta^1$, once $\mathfrak{f}(0)$ is determined. A similar story holds for arm 2.

Since $\mathcal{V}_1(0) = \mathcal{J}_1 \dot{\theta}_1$,

$$\alpha_1(0) = \dot{\mathcal{V}}_1(0) = \mathcal{J}_1 \ddot{\theta}_1 + \dot{\mathcal{J}}_1 \dot{\theta}_1 \stackrel{11.25}{=} \mathcal{J}_1 (\ddot{\theta}_{1f} + \ddot{\theta}_\delta^1) + \dot{\mathcal{J}}_1 \dot{\theta}_1 \quad (11.27)$$

It then follows from (11.26) and (11.27) that

$$\begin{aligned} \alpha_1(0) &\stackrel{11.27}{=} \alpha_{1f}(0) + \mathcal{J}_1 \ddot{\theta}_\delta^1, \quad \text{where} \quad \alpha_{1f}(0) \triangleq \mathcal{J}_1 \ddot{\theta}_{1f} + \dot{\mathcal{J}}_1 \dot{\theta}_1 \\ &\stackrel{11.26}{=} \alpha_{1f}(0) + \underline{\Delta}_1 \mathfrak{f}_1, \quad \text{where} \quad \underline{\Delta}_1 \triangleq \mathcal{J}_1 \mathcal{M}_1^{-1} \mathcal{J}_1^* \end{aligned} \quad (11.28)$$

Similarly,

$$\alpha_2(0) = \alpha_{2f}(0) + \underline{\Delta}_2 \mathfrak{f}_2 \quad \text{where} \quad \underline{\Delta}_2 \triangleq \mathcal{J}_2 \mathcal{M}_2^{-1} \mathcal{J}_2^* \quad (11.29)$$

Then, from the constraint condition in (11.23), we have

$$\begin{aligned} \mathbf{f}(0) &\stackrel{11.28,11.29}{=} -\underline{\Delta}_c^{-1} \mathcal{Q} \begin{bmatrix} \alpha_{2f}(0) \\ \alpha_{1f}(0) \end{bmatrix} \\ \text{where } \underline{\Delta}_c &\triangleq \mathcal{Q} \begin{pmatrix} \underline{\Delta}_1 & \mathbf{0} \\ \mathbf{0} & \underline{\Delta}_2 \end{pmatrix} \mathcal{Q}^* = \underline{\Delta}_1 + \underline{\Delta}_2 \end{aligned} \quad (11.30)$$

$\underline{\Delta}_c$ is the inverse of the effective inertia of the closed chain system reflected to the end-effectors point of contact. As discussed in Chap. 10, $\underline{\Delta}_1$ and $\underline{\Delta}_2$ can be obtained via $O(n_1)$ and $O(n_2)$ recursive algorithms, respectively. Noting that the inversion of $\underline{\Delta}_c \in \mathcal{R}^{6 \times 6}$ involves a flat cost independent of n_1 and n_2 , we see that this is an $O(n_1 + n_2)$ recursive algorithm for solving the forward dynamics of the dual-arm system of Fig. 11.2. Extensions of the dual-arm formulation to the multi-arm case, and to one where the task object being manipulated has internal degrees of freedom, is discussed in [86, 87, 144].

11.3 Projected Closed-Chain Dynamics

In this section, we look at the alternative projected formulation of closed-chain dynamics. In this formulation, the system dynamics is defined in terms of the actual $(N - n_c)$ velocity degrees of freedom in the constrained system. Using the minimal subset of generalized velocities ensures that the resulting motions of the system are always consistent with the constraints and do not drift off the constraint manifold. We begin by restating (11.6):

$$\begin{pmatrix} \mathcal{M} & G_c^* \\ G_c & \mathbf{0} \end{pmatrix} \begin{bmatrix} \ddot{\theta} \\ -\lambda \end{bmatrix} = \begin{bmatrix} \mathcal{T} - \mathcal{C} \\ \mathfrak{U} \end{bmatrix} \quad (11.31)$$

Since G_c has full row-rank n_c , there exists a full column rank matrix $X_c \in \mathcal{R}^{N \times N - n_c}$, whose columns span the $N - n_c$ -dimensional null-space of G_c , i.e.,

$$G_c X_c = \mathbf{0} \quad (11.32)$$

This implies that any generalized velocity vector, $\dot{\theta}$, satisfying the constraints can be expressed as:

$$\dot{\theta} = \dot{\theta}_p + X_c \dot{\theta}_r \quad (11.33)$$

where $\dot{\theta}_p$ is a particular solution to the $G_c \dot{\theta} = \mathfrak{U}$ equation, and $\dot{\theta}_r \in \mathcal{R}^{N - n_c}$ is an arbitrary vector. In other words, the $(N - n_c)$ dimensional $\dot{\theta}_r$ vector in (11.33) parametrizes the $N - n_c$ dimensional subspace of generalized velocities that is consistent with the constraints. Thus, we can think of $\dot{\theta}_r$ as the minimal, independent generalized velocity coordinates for the system. Equation (11.33) provides a way to obtain the full $\dot{\theta}$ generalized velocity coordinates from $\dot{\theta}_p$. $\dot{\theta}_p = \mathbf{0}$ for systems for

catastatic systems, i.e., for systems with $\mathfrak{U} = \mathbf{0}$. Differentiating (11.33) with respect to time we have

$$\ddot{\theta} = \ddot{\theta}_p + X_c \dot{\theta}_r + \dot{X}_c \hat{\theta}_r = \underline{\ddot{\theta}}_p + X_c \ddot{\theta}_r, \quad \text{where } \underline{\ddot{\theta}}_p \triangleq \ddot{\theta}_p + \dot{X}_c \hat{\theta}_r \quad (11.34)$$

Thus,

$$\mathfrak{U} \stackrel{11.6}{=} G_c \ddot{\theta} \stackrel{11.34}{=} G_c (\underline{\ddot{\theta}}_p + X_c \ddot{\theta}_r) \stackrel{11.32}{=} G_c \underline{\ddot{\theta}}_p \quad (11.35)$$

The top half of (11.31) is given by

$$\mathcal{T} - \mathcal{C} = \mathcal{M} \ddot{\theta} - G_c^* \lambda \stackrel{11.34}{=} \mathcal{M} (\underline{\ddot{\theta}}_p + X_c \ddot{\theta}_r) - G_c^* \lambda$$

Pre-multiplying this by X_c^* , and using (11.32), leads to

$$\mathcal{M}_r \ddot{\theta}_r = X_c^* (\mathcal{T} - \mathcal{C} - \mathcal{M} \underline{\ddot{\theta}}_p) \quad \text{where } \mathcal{M}_r \triangleq X_c^* \mathcal{M} X_c \in \mathcal{R}^{N-n_c \times N-n_c} \quad (11.36)$$

Equation (11.36) represents the equations of motion projected onto the constrained velocity subspace. \mathcal{M}_r represents the mass matrix in the projected dynamics formulation. It is symmetric, and also positive definite, because X_c is full-rank. The smaller dimension of \mathcal{M}_r matches the true $(N-n_c)$ degrees of freedom in the system. The new $\dot{\theta}_r$ generalized velocities are also of minimal $(N-n_c)$ dimension.

Observe that the λ constraint force Lagrange multipliers have been eliminated from the equations of motion. Thus the projected dynamics formulation does not require the explicit computation of the λ Lagrange multipliers needed in the augmented dynamics formulation. Moreover, the projected equations of motion in (11.36) are in the form of an ordinary differential equations (ODE) instead of the more complex differential-algebraic equations for the augmented formulation. Mariti et al. [122] discusses the performance of several proposed methods for determining the minimal independent coordinates for projected dynamics.

Algorithm 11.3 describes the $O(N^3)$ forward dynamics solution procedure for the projected formulation. It requires the computation of the projected mass matrix, \mathcal{M}_r , which can be expensive, since we need to solve for X_c . We also need to carry out the matrix products in (11.36). However, since the projected equations of motion do not correspond to an SKO model, the techniques for factorizing and inverting the mass matrix and algorithms such as the $O(N)$ AB forward dynamics algorithm for SKO models cannot be used with the projected dynamics formulation.

11.4 Equivalence of Augmented and Projected Dynamics

We now show that the augmented and projected forms of the equations of motion developed in Sects. 11.2.2 and 11.3, respectively, are indeed mathematically equivalent (even though the forward dynamics solution algorithms are very different). The derivation here is an adaptation of that in Schwerin [158].

Algorithm 11.3 Forward dynamics for projected closed-chain dynamics

The forward dynamics for the projected formulation of the equations of motion consist of the following steps:

1. Decompose the closed-chain system into a spanning tree with cut-edge constraints, and define G_c for the system.
 2. Solve (11.32) for X_c and (11.33) for $\dot{\theta}_p$.
 3. Compute the \mathcal{M} mass matrix for the tree system using Algorithm 9.3.
 4. Compute \mathcal{M}_r using (11.36).
 5. Solve (11.36) for $\ddot{\theta}_r$.
 6. Integrate these accelerations to obtain $\dot{\theta}_r$.
 7. Use $\dot{\theta}_r$ in (11.33) to obtain the $\dot{\theta}$ generalized velocities for the system.
-

Since G_c has full row-rank, there exists an invertible transformation $\underline{P} \in \mathcal{R}^{\mathcal{N} \times \mathcal{N}}$ such that

$$\underline{G} \triangleq G_c \underline{P} = [G_r, \quad \mathbf{0}] \quad \in \mathcal{R}^{n_c \times \mathcal{N}} \quad (11.37)$$

where $G_r \in \mathcal{R}^{n_c \times n_c}$ is square and non-singular. With

$$\underline{X}_c \triangleq \begin{bmatrix} \mathbf{0} \\ \mathbf{I} \end{bmatrix} \in \mathcal{R}^{\mathcal{N} \times \mathcal{N}-n_c}, \quad \underline{G} \underline{X}_c \stackrel{11.37}{=} \mathbf{0} \quad \Rightarrow \quad G_c \underline{P} \underline{X}_c \stackrel{11.37}{=} \mathbf{0} \quad (11.38)$$

It follows that

$$X_c \stackrel{11.38}{=} \underline{P} \underline{X}_c \quad (11.39)$$

satisfies the $G_c X_c = \mathbf{0}$ condition in (11.32).

Exercise 11.4 Explicit expression for \underline{P} .

Assuming that $G_{c1} \in \mathcal{R}^{n_c \times n_c}$ is non-singular in the block-partitioned expression $G_c = [G_{c1}, G_{c2}]$, show that an example of \underline{P} in (11.37) is

$$\underline{P} = \begin{pmatrix} \mathbf{I} & -G_{c1}^{-1} G_{c2} \\ \mathbf{0} & \mathbf{I} \end{pmatrix}, \quad \text{with} \quad G_r = G_{c1} \quad \text{and} \quad X_c = \begin{bmatrix} -G_{c1}^{-1} G_{c2} \\ \mathbf{I} \end{bmatrix} \quad (11.40)$$

■

The following exercise shows that the augmented dynamics can be partitioned using the \underline{P} transformation matrix from (11.41).

Exercise 11.5 Transformed and partitioned augmented dynamics.

Use the \underline{P} transform to define a new transformed generalized accelerations vector, $\ddot{\underline{\theta}}$, a generalized forces vector, $\underline{\mathcal{T}}$, and a mass matrix, $\underline{\mathcal{M}}$, as

$$\ddot{\underline{\theta}} \triangleq \underline{P}^{-1} \ddot{\theta} \in \mathcal{R}^{\mathcal{N}}, \quad \underline{\mathcal{T}} \triangleq \underline{P}^* (\mathcal{T} - \mathcal{C}) \in \mathcal{R}^{\mathcal{N}}, \quad \underline{\mathcal{M}} \triangleq \underline{P}^* \mathcal{M} \underline{P} \in \mathcal{R}^{\mathcal{N} \times \mathcal{N}} \quad (11.41)$$

Show that the (11.6) augmented equations of motion, in the transformed coordinates, can be expressed in the following equivalent block-partitioned form:

$$\begin{pmatrix} \underline{\mathcal{M}}_{11} & \underline{\mathcal{M}}_{12} & G_r^* \\ \underline{\mathcal{M}}_{21} & \underline{\mathcal{M}}_{22} & \mathbf{0} \\ G_r & \mathbf{0} & \mathbf{0} \end{pmatrix} \begin{bmatrix} \ddot{\theta}_1 \\ \ddot{\theta}_2 \\ -\lambda \end{bmatrix} = \begin{bmatrix} \mathcal{T}_1 \\ \mathcal{T}_2 \\ \mathcal{U} \end{bmatrix} \quad (11.42)$$

where the sub-blocks size is $\underline{\mathcal{M}}_{11} \in \mathcal{R}^{n_c \times n_c}$, $\underline{\mathcal{M}}_{22} \in \mathcal{R}^{N-n_c \times N-n_c}$, $\ddot{\theta}_1 \in \mathcal{R}^{n_c}$, $\ddot{\theta}_2 \in \mathcal{R}^{N-n_c}$, etc. ■

The following exercise uses the partitioned structure of the transformed equations of motion in Exercise 11.5 to develop an equivalent, reduced version of the equations of motion.

Exercise 11.6 Reduction of augmented dynamics.

Show that the augmented closed-chain dynamics equation in (11.6) is equivalent to the following reduced equations of motion:

$$\underline{\mathcal{M}}_{22} \ddot{\theta}_2 = (\mathcal{T}_2 - \underline{\mathcal{M}}_{21} G_r^{-1} \mathcal{U}) \quad (11.43)$$

The following exercise shows that the projected equations of motion in (11.36) are equivalent to the reduced version of the augmented equations of motion in (11.43). ■

Exercise 11.7 Transformed projected dynamics.

Show that the projected equations of motion in (11.36) are equivalent to the reduced, augmented equations of motion in (11.43). ■

Together, Exercises 11.6 and 11.7 establish the equivalency of the augmented and projected formulations of closed-chain system dynamics.

11.5 Unilateral Constraints

Rigid body-to-body contact and joint limits are examples of unilateral constraints. The traditional approaches for handling such constraints treat them as *soft* constraints and make use of *penalty* methods [51]. In the case of body-to-body contact, penalty methods permit the inter-penetration of bodies, and generate resisting forces that are a function of the penetration distance, using non-linear spring/damper models. While penalty methods provide continuous detail of the impact and contact processes, they can require small integration time step sizes during the contact events

due to the stiffness of the contact models. In this section, we briefly describe alternative methods for handling unilateral constraints that are known as *complementarity methods*. Unlike penalty methods, these methods do not attempt to continuously track the state of the unilateral constraints.

Instead of the equality relationship in (11.2) for bilateral constraints, unilateral constraints are defined by an inequality relationship such as:

$$\delta(\theta, t) \geq \mathbf{0} \quad (11.44)$$

For example, the non-penetration condition for rigid bodies translates into such as inequality relationship on the distance between the bodies. This constraint requires that the distance between the surfaces of rigid bodies be non-negative. $\delta(\theta, t)$ is thus commonly referred to as the *distance* or *gap* function for unilateral constraints.

Contact occurs at the constraint boundary, i.e., when $\delta(\theta, t) = \mathbf{0}$. For bodies in contact, the surface normals at the contact point are parallel. The existence of contact is often determined by geometric analysis, such as collision detection techniques. During contact, the relative linear velocity along the normals at the point of contact is zero as well. A unilateral constraint is said to be in an *active* state when

$$\delta(\theta, t) = \dot{\delta}(\theta, t) = \ddot{\delta}(\theta, t) = \mathbf{0} \quad (11.45)$$

Thus, a unilateral constraint is active when there is contact, and the contact persists. Only active constraints generate constraint forces on the system.

The constraint that is not active is said to be *inactive*. Clearly, constraints not in contact, are inactive. Contact *separation* occurs when the relative linear velocity of the contact points along the normals becomes positive and the contact points drift apart. A separating constraint is in the process of losing contact and marks the beginning of its inactive state. At the start of a separation event, we have

$$\delta(\theta, t) = \dot{\delta}(\theta, t) = \mathbf{0} \quad \text{and} \quad \ddot{\delta}(\theta, t) > \mathbf{0} \quad (11.46)$$

11.5.1 Complementarity Problems

From (11.5) it follows that

$$\ddot{\delta} = \mathcal{M}^{-1} [\mathcal{T} - \mathcal{C} + G_c^* \lambda] \stackrel{11.9a}{=} \ddot{\delta}_f + \mathcal{M}^{-1} G_c^* \lambda \quad (11.47)$$

Thus

$$\ddot{\delta} \stackrel{11.7, 11.47}{=} G_c \ddot{\delta}_f - \dot{\mathcal{U}} + G_c \mathcal{M}^{-1} G_c^* \lambda \stackrel{11.9b}{=} \ddot{\delta}_f + G_c \mathcal{M}^{-1} G_c^* \lambda \quad (11.48)$$

This provides an expression for the $\ddot{\delta}$ gap accelerations in terms of the $\ddot{\delta}_f$ gap accelerations that arise in the absence of unilateral constraints, and the unknown constraint forces λ that result from the active unilateral constraints.

When *all* the unilateral constraints are active, $\ddot{\delta} = \mathbf{0}$, and (11.48) can be solved to obtain the λ constraint forces, and subsequently used in (11.47) to obtain the generalized accelerations for the system. For this case, the forward dynamics solution for the system is precisely that given by the augmented dynamics solution in (11.9) for bilateral constraints. The same story applies in the other extreme when *all* the unilateral constraints are inactive. Since inactive constraints generate no constraint forces, the augmented forward dynamics solution applies with these constraints removed. In general, however, some unilateral constraints are active and some are inactive. If the states of the constraints are known, then the forward dynamics procedure for bilateral constraints can be directly applied with only the active unilateral constraints included. The primary challenge with unilateral constraints is the determination and tracking of the changing active and inactive states of the constraints as the dynamics of the system evolves.

To illustrate this procedure, consider the example of friction-less contact between rigid bodies. When the k th such constraint is active, $\ddot{\delta}(k) = 0$, and the $\lambda(k)$ constraint force is non-zero and positive. On the other hand, when the constraint is separating, $\ddot{\delta}(k) > 0$, and the constraint force $\lambda(k) = 0$. These dual relationships can be formally stated as

$$\mathbf{0} \leqslant \ddot{\delta} \perp \lambda \geqslant \mathbf{0} \quad (11.49)$$

The above relationship is referred to as a *complementarity* condition. The \perp in (11.49) implies that only one of the acceleration or force values can be non-zero for any component of the λ and $\ddot{\delta}$ vectors, depending on whether the corresponding constraint is active or not. This condition is equivalent to

$$\ddot{\delta} \geqslant \mathbf{0}, \quad \lambda \geqslant \mathbf{0}, \quad \text{and} \quad \lambda^* \ddot{\delta} = \mathbf{0}$$

Thus, for unilateral constraints, (11.48) needs to be solved subject to the complementarity condition in (11.49). Problems involving such complementarity conditions are referred to as *nonlinear complementarity problems (NCP)*. In general, an NCP problem requires solving for unknown vectors w and z that are subject to complementarity conditions such as:

$$\mathbf{0} \leqslant w(z) \perp z \geqslant \mathbf{0} \quad (11.50)$$

The solution of the complementarity problem identifies the active contact constraints, as well as the λ constraint forces for the active ones. The λ constraint forces can be used in (11.47) to obtain the full generalized accelerations for the system. Observe that the $G_c M^{-1} G_c^*$ matrix in (11.46) is invertible only if $G_c(\theta, t)$ is full rank, i.e., if the unilateral constraints are independent. Such independence can be lost in the case of multiple contact constraints. Other types of unilateral constraints can also be cast into appropriate complementarity conditions on the system [31, 136, 174, 175].

A *linear complementarity problems (LCP)* [40] is a special type of NCP, where a matrix F and vector f are known, and a solution for the unknown vectors w and z satisfying the following is required:

$$w = Fz + f \quad \text{where} \quad \mathbf{0} \leq w \perp z \geq \mathbf{0} \quad (11.51)$$

Since an LCP is easier to solve compared to an NCP, it is advantageous to formulate a unilateral constraint problem as an LCP. While this occurs naturally for some types of unilateral constraints, techniques such as, polyhedral approximations of the friction cone for contacts with friction, are often used to transform an underlying NCP into an LCP [175].

11.5.2 Forward Dynamics

A common variation of the complementarity formulation is to directly incorporate time-stepping into the formulation, to facilitate the solution process [131, 188]. In this formulation, the complementarity problem solves for the system state at the end of the time step and works with impulses instead of forces over the time step interval.

In addition, it is common to see formulations that cast bilateral constraints in the form of complementarity conditions. This is not recommended, since it increases the dimensionality and cost of the LCP solution, and leads to drift issues that arise from the over parametrization of bilateral constraints. The formulation described here, on the other hand, allows the normal handling of bilateral constraints so that the complementarity techniques are limited to the unilateral constraints.

Since the LCP solution can be computationally expensive, reducing the need for its solution is desirable. Featherstone [51] suggests a forward dynamics strategy based on the observation that the LCP solution is not required if the active and inactive states of the constraints are already known, since the standard augmented dynamics equations can be solved with just the active constraints included. The strategy consists of solving the forward dynamics problem assuming that there is no change in the active and inactive states of the unilateral constraints. The solution is checked to verify that it does not violate the (11.49) complementarity conditions. A violation implies that the state of a constraint is changing. In this case, the solution is discarded, and the LCP is solved to reevaluate the set of active constraints before proceeding with the solution.

Chapter 12

Systems with Geared Links

So far, we have studied the dynamics modeling of systems with non-geared, direct-drive hinge actuators. However, many systems have geared joints. When the gear ratios are large, the motor inertias have significant effect on the system dynamics, since the equations of motion contain motor inertia terms that are magnified by the square of the gear ratio. For such systems, it is important that gear and actuator dynamics be included in the dynamics model of the manipulator. Reliance on simplified and approximate models can lead to errors in control design, with consequent degradation in system stability and performance.

A useful approximation [12, 135] for handling geared actuators adds the projection of the amplified rotational inertias of the actuator motors to the diagonal elements of the manipulator mass matrix (formed by ignoring the actuators). This model ignores gyroscopic effects arising from the high spin rates of the motor. To handle geared actuator effects, various assumptions have been used to simplify and decouple the actuator dynamics from the dynamics of the manipulator [170]. These approximations, while useful in many cases, have the following disadvantages:

1. The modified mass matrix must still be inverted (or, alternatively, a linear system of equations must be solved) to solve the forward dynamics problem.
2. The powerful direct-drive computational algorithms [120, 179], cannot be used.
3. Coupling terms in the mass matrix, gyroscopic forces arising from the spinning of the motors, that significantly alter the behavior of the system are not fully accounted for [36, 37, 77, 126, 127].

In this chapter, we develop an SKO dynamics formulation for geared systems that models the geared effects correctly, and derive efficient SKO algorithms for the system.

12.1 Equations of Motion

One degree-of-freedom rotary joints are assumed, with the joint motors mounted on the inboard link. A typical link, with a motor driving the outboard link through a set of gears, is shown in Fig. 12.1. We assume that the system is a canonical serial-chain

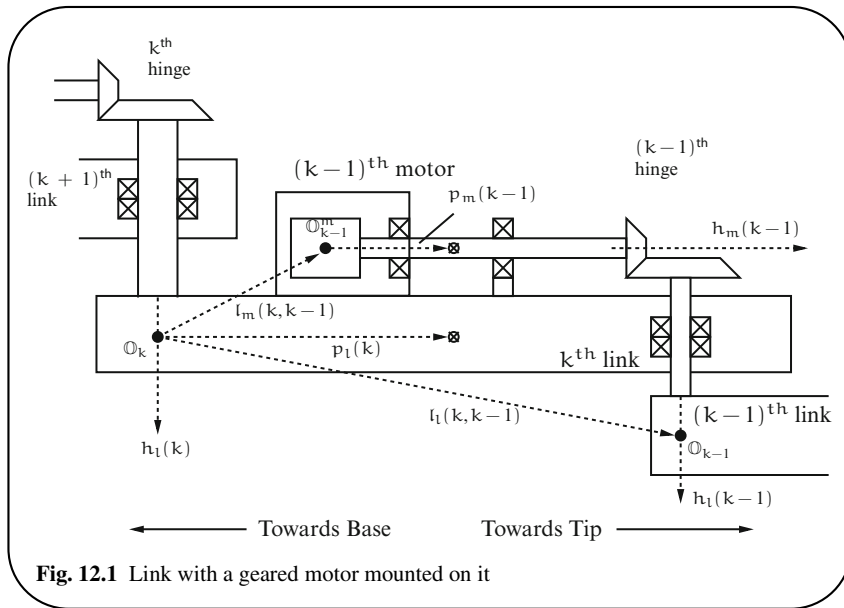
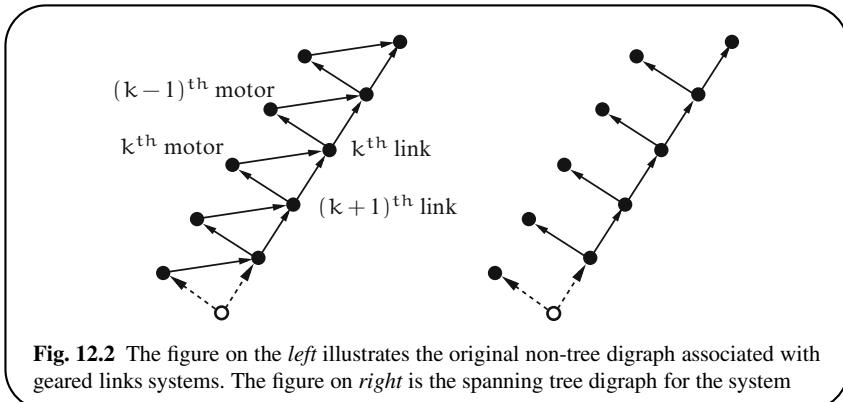


Fig. 12.1 Link with a geared motor mounted on it

system with n geared rigid-body links. Each driven link has associated with it a motor body. Thus, there are $2n$ bodies in the system. For each such link/motor pair of bodies, we refer to the driven body with the “ l ” subscript, and the motor body with the “ m ” subscript. We number the link/motor pairs with indices proceeding from tip-to-base in increasing order from 1 to n .

A key difference between geared and non-geared dynamics is the presence of a kinematic closed-loop at each of the hinges. Thus, the underlying digraph for the system, illustrated on the left in Fig. 12.2, is not a tree. Instead of using the constrained dynamics techniques from Chap. 11, we capitalize on the simple nature of the loops to develop a projected formulation, i.e., one with minimal generalized velocity coordinates that retain the SKO structure of the equations of motion. The development in this chapter also sets the stage for the more general constraint embedding technique described in Chap. 15 for non-tree-topology multibody systems.

While the only fundamental requirement is that the spanning tree for the geared system have an SKO model, for the sake of simpler exposition, we have focused here instead on a serial-chain, rigid-link geared system. There is no loss in generality



since the ideas developed here easily extend to general spanning tree SKO models using the approach from Chap. 9.

We begin by ignoring the gearing constraints, and describe the equations of motion for the spanning tree system illustrated on the right in Fig. 12.2.

$$\left\{ \begin{array}{l} \mathcal{V}(n+1) = \alpha(n+1) = \mathbf{0} \\ \text{for } k = n \cdots 1 \\ \quad \mathcal{V}_m(k) = \phi_m^*(k+1, k)\mathcal{V}_l(k+1) + H_m^*(k)\dot{\theta}_m(k) \\ \quad \mathcal{V}_l(k) = \phi_l^*(k+1, k)\mathcal{V}_l(k+1) + H_l^*(k)\dot{\theta}_l(k) \\ \quad \alpha_m(k) = \phi_m^*(k+1, k)\alpha_l(k+1) + H_m^*(k)\ddot{\theta}_m(k) + a_m(k) \\ \quad \alpha_l(k) = \phi_l^*(k+1, k)\alpha_l(k+1) + H_l^*(k)\ddot{\theta}_l(k) + a_l(k) \\ \text{end loop} \end{array} \right. \quad (12.1)$$

$$\left\{ \begin{array}{l} f_m(0) = \mathbf{0}, f_l(0) = \mathbf{0} \\ \text{for } k = 1 \cdots n \\ \quad f_m(k) = M_m(k)\alpha_m(k) + b_m(k) \\ \quad f_l(k) = \phi_l(k, k-1)f_l(k-1) + M_l(k)\alpha_l(k) \\ \quad \quad + \phi_m(k, k-1)f_m(k-1) + b_l(k) \\ \quad T_m(k) = H_m(k)f_m(k) \\ \quad T_l(k) = H_l(k)f_l(k) \\ \text{end loop} \end{array} \right.$$

The equations of motion in (12.1) are identical to the SKO versions for tree systems described in (9.10) on page 166. The only difference in form is that we have explicitly listed the pair of equations for the two bodies in each link/motor pair. The spatial velocity $\mathcal{V}_l(k)$ of the k th link at the \mathbb{O}_k frame is obtained by propagating

the spatial velocity $\mathcal{V}_l(k+1)$ of the inboard link to \mathbb{O}_k , and then adding the relative spatial velocity at the k th joint. The spatial velocity $\mathcal{V}_m(k)$ of the \mathbb{O}_k^m frame on the k th motor is obtained similarly. Acceleration equations for $\alpha_l(k)$ and $\alpha_m(k)$, obtained by differentiating velocity equations, contain the $a_l(k)$ and $a_m(k)$ Coriolis acceleration terms. There are two force balance equations. The first involves the spatial force $f_m(k)$ due to motor motion. The second involves the forces $f_l(k)$ and $f_{l-1}(k-1)$ due to the outboard and inboard links, the force $f_m(k-1)$ due to motor motion, the D'Alembert force $M_l(k)\alpha_l(k)$ due to the k th link itself, and the gyroscopic force $b_l(k)$.

12.1.1 Reformulated Equations of Motion

Define the following quantities:

$$\begin{aligned}\theta(k) &\triangleq \begin{bmatrix} \theta_m(k) \\ \theta_l(k) \end{bmatrix}, \quad a(k) \triangleq \begin{bmatrix} a_m(k) \\ a_l(k) \end{bmatrix}, \quad b(k) \triangleq \begin{bmatrix} b_m(k) \\ b_l(k) \end{bmatrix} \\ \Phi_G(k+1, k) &\triangleq \begin{pmatrix} \mathbf{0} & \mathbf{0} \\ \phi_m(k+1, k) & \phi_l(k+1, k) \end{pmatrix} \in \mathcal{R}^{12 \times 12} \\ H(k) &\triangleq \begin{pmatrix} H_m(k) & \mathbf{0} \\ \mathbf{0} & H_l(k) \end{pmatrix} \in \mathcal{R}^{2 \times 12} \\ M(k) &\triangleq \begin{pmatrix} M_m(k) & \mathbf{0}_6 \\ \mathbf{0}_6 & M_l(k) \end{pmatrix} \in \mathcal{R}^{12 \times 12}\end{aligned}\tag{12.2}$$

Using these, (12.1) can be rewritten in the following more compact form

$$\left\{ \begin{array}{l} \mathcal{V}(n+1) = \alpha(n+1) = \mathbf{0} \\ \text{for } k = n \cdots 1 \\ \mathcal{V}(k) \triangleq \begin{bmatrix} \mathcal{V}_m(k) \\ \mathcal{V}_l(k) \end{bmatrix} = \Phi_G^*(k+1, k)\mathcal{V}(k+1) + H^*(k)\dot{\theta}(k) \\ \alpha(k) \triangleq \begin{bmatrix} \alpha_m(k) \\ \alpha_l(k) \end{bmatrix} = \Phi_G^*(k+1, k)\alpha(k+1) + H^*(k)\ddot{\theta}(k) + a(k) \\ \text{end loop} \end{array} \right.$$

$$\left\{ \begin{array}{l} f(0) = \mathbf{0} \\ \text{for } k = 1 \dots n \\ \quad f(k) \triangleq \begin{bmatrix} f_m(k) \\ f_l(k) \end{bmatrix} = \Phi_G(k, k-1)f(k-1) + M(k)\alpha(k) + b(k) \\ \quad T(k) \triangleq \begin{bmatrix} T_m(k) \\ T_l(k) \end{bmatrix} = H(k)f(k) \\ \text{end loop} \end{array} \right. \quad (12.3)$$

Observe that $\Phi_G(k+1, k)$ can be factored as follows:

$$\Phi_G(k+1, k) \triangleq \mathcal{B}_G \mathcal{A}_G(k+1, k) \quad (12.4)$$

$$\text{where } \mathcal{A}_G(k+1, k) \triangleq [\phi_m(k+1, k), \phi_l(k+1, k)] \in \mathcal{R}^{6 \times 12}$$

$$\text{and } \mathcal{B}_G \triangleq \begin{bmatrix} \mathbf{0}_6 \\ \mathbf{I}_6 \end{bmatrix} \in \mathcal{R}^{12 \times 6} \quad (12.5)$$

At this stage, the equations of motion are in an SKO model form for the system spanning tree with the $\Phi_G(k+1, k)$ terms defining the SKO weight matrices. This form of the SKO model is suitable for modeling systems with flexible joints, i.e., systems whose hinge actuators have internal dynamics and states [77, 127]. The native tree-topology of these systems allows the use of SKO model techniques for further analysis and algorithm development.

On the other hand, geared actuators impose an additional holonomic constraint between the hinge and the driven link generalized coordinates. The following section discusses steps that can be taken to eliminate these constraints to obtain an SKO model for the geared system.

12.1.2 Eliminating the Geared Constraint

The holonomic geared constraint enforces the condition that the link hinge generalized coordinate is related to the motor generalized coordinate at the k th hinge by its gear ratio as follows:

$$\theta_m(k) = \mu_G(k)\theta_l(k), \quad \text{i.e.,} \quad \theta(k) = \begin{bmatrix} \mu_G(k) \\ \mathbf{I} \end{bmatrix} \theta_l(k) \quad (12.6)$$

where $\mu_G(k)$ is the gear ratio for the k th hinge. Due to this constraint, $\theta_l(k)$ and $\theta_m(k)$ are not independent. Either one can be chosen as generalized coordinates for the k th hinge. Choosing $\theta_l(k)$ as the independent generalized coordinate, the principle of virtual work states that the corresponding generalized forces are $[\mu_G(k), \mathbf{I}]T(k) = \mu_G(k)T_m(k) + T_l(k)$.

The geared constraint can be eliminated by simply redefining $\mathcal{T}(k)$, and defining $H_G(k)$ as follows:

$$\begin{aligned}\mathcal{T} &= \mu_G(k)\mathcal{T}_m(k) + \mathcal{T}_l(k) \\ H_G(k) &= [\mu_G(k), I]H(k) \stackrel{12.2}{=} [\mu_G(k)H_m(k), H_l(k)]\end{aligned}\quad (12.7)$$

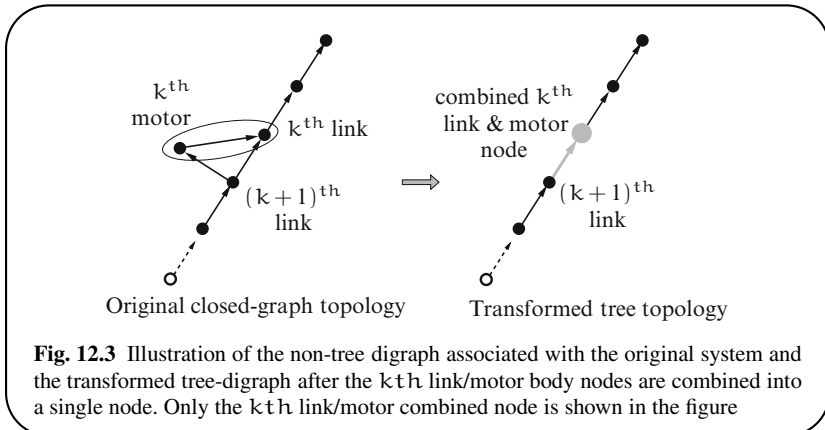
With these definitions, and replacing $H(k)$ with $H_G(k)$, (12.3) is transformed into the following equations of motion for the system:

$$\left\{ \begin{array}{l} \mathcal{V}(n+1) = \alpha(n+1) = \mathbf{0} \\ \textbf{for } k = n \cdots 1 \\ \quad \mathcal{V}(k) = \Phi_G^*(k+1, k)\mathcal{V}(k+1) + H_G^*(k)\dot{\theta}_l(k) \\ \quad \alpha(k) = \Phi_G^*(k+1, k)\alpha(k+1) + H_G^*(k)\ddot{\theta}_l(k) + \mathbf{a}(k) \\ \textbf{end loop} \\ \mathbf{f}(0) = \mathbf{0} \\ \textbf{for } k = 1 \cdots n \\ \quad \mathbf{f}(k) = \Phi_G(k, k-1)\mathbf{f}(k-1) + M(k)\alpha(k) + \mathbf{b}(k) \\ \quad \mathcal{T}(k) = H_G(k)\mathbf{f}(k) \\ \textbf{end loop} \end{array} \right. \quad (12.8)$$

Now $\theta_l(k) \in \mathcal{R}^1$ and $\mathcal{T}(k) = H_G(k)\mathbf{f}(k) \in \mathcal{R}^1$ are the generalized coordinates and forces, respectively, for the k th hinge. They automatically enforce the geared constraints, and, as a consequence, the explicit geared constraints have been eliminated! Thus, we have in effect transformed the original non-tree digraph with $2n$ nodes into a tree digraph with just n nodes as illustrated in Fig. 12.3.

12.2 SKO Model for Geared Systems

While the (12.8) formulation has only n independent $\dot{\theta}_l$ and $\ddot{\theta}_l$ generalized velocities and accelerations instead of the $2n$ values in (12.1), it also has a form identical to the SKO formulation for tree systems. This allows us to proceed with an SKO formulation of the system dynamics together with the definitions of the associated operators. One difference is that $\mathcal{V}(k)$, $\alpha(k)$, $\mathbf{f}(k)$, $\mathbf{a}(k)$ and $\mathbf{b}(k)$ are all 12-dimensional vectors, as opposed to the 6-dimensional vectors that we have encountered previously.



Define the stacked vectors

$$\mathcal{V} = \begin{bmatrix} \mathcal{V}(1) \\ \vdots \\ \mathcal{V}(n) \end{bmatrix}, \quad \alpha = \begin{bmatrix} \alpha(1) \\ \vdots \\ \alpha(n) \end{bmatrix}, \quad \mathbf{f} = \begin{bmatrix} \mathbf{f}(1) \\ \vdots \\ \mathbf{f}(n) \end{bmatrix}, \quad \mathcal{T} = \begin{bmatrix} \mathcal{T}(1) \\ \vdots \\ \mathcal{T}(n) \end{bmatrix}$$

and, similarly, the stacked vectors \mathbf{a} and \mathbf{b} . Then, (12.2) can be restated as:

$$\begin{aligned} \mathcal{V} &= \Phi_G^* H_G^* \dot{\theta}_l \\ \alpha &= \Phi_G^* [H_G^* \ddot{\theta}_l + \mathbf{a}] \\ \mathbf{f} &= \Phi_G [\mathbf{M}\alpha + \mathbf{b}] \\ \mathcal{T} &= H_G \mathbf{f} \end{aligned} \tag{12.9}$$

where $H_G \triangleq \text{diag} \left\{ H_G(1), \dots, H_G(n) \right\}_{k=1}^n$, $\mathbf{M} \triangleq \text{diag} \left\{ M(1), \dots, M(n) \right\}_{k=1}^n$, and the \mathcal{E}_{Φ_G} and Φ_G SKO and SPO operators, respectively, for the system are defined as:

$$\mathcal{E}_{\Phi_G} \triangleq \sum_{k=1}^{n-1} e_{\varphi(k)} \Phi_G(\varphi(k), k) e_k^* \quad \text{and} \quad \Phi_G \triangleq (\mathbf{I} - \mathcal{E}_{\Phi_G})^{-1} \tag{12.10}$$

Based on the velocity relationships in (12.8), $\Phi_G(j, k)$ is the (j, k) weight matrix for the \mathcal{E}_{Φ_G} SKO operator. The weights satisfy the usual semi-group property:

$$\Phi_G(k, j) \triangleq \Phi_G(k, k-1) \cdots \Phi_G(j+1, j) \text{ for } k > j$$

It is noteworthy that the $\Phi_G(k, j)$ weight matrices are neither invertible nor are they 6×6 matrices, as has been the case for rigid-link systems with non/geared hinges.

Moreover, the weight matrices are of non-uniform size for systems that have a mix of links with geared and non-geared hinges.

With our canonical serial-chain assumption for the system, \mathcal{E}_{Φ_G} and Φ_G have the following form:

$$\mathcal{E}_{\Phi_G} = \begin{pmatrix} \mathbf{0} & \mathbf{0} & \mathbf{0} & \mathbf{0} & \mathbf{0} \\ \Phi_G(2,1) & \mathbf{0} & \dots & \mathbf{0} & \mathbf{0} \\ \mathbf{0} & \Phi_G(3,2) & \dots & \mathbf{0} & \mathbf{0} \\ \vdots & \vdots & \ddots & \vdots & \vdots \\ \mathbf{0} & \mathbf{0} & \dots & \Phi_G(n,n-1) & \mathbf{0} \end{pmatrix}$$

$$\Phi_G = \begin{pmatrix} \mathbf{I} & \mathbf{0} & \dots & \mathbf{0} \\ \Phi_G(2,1) & \mathbf{I} & \dots & \mathbf{0} \\ \vdots & \vdots & \ddots & \vdots \\ \Phi_G(n,1) & \Phi_G(n,2) & \dots & \mathbf{I} \end{pmatrix}.$$

12.2.1 Expression for the Mass Matrix

Together, the expressions in (12.9) lead to the following equations of motion:

$$\mathcal{T} = \mathcal{M}_G \ddot{\theta}_l + \mathcal{C}_G \quad (12.11)$$

where the mass matrix \mathcal{M}_G is

$$\mathcal{M}_G \triangleq H_G \Phi_G M \Phi_G^* H_G^* \quad (12.12)$$

and the vector of Coriolis and gyroscopic generalized forces \mathcal{C}_G is

$$\mathcal{C}_G \triangleq H_G \Phi_G [\mathbf{b} + M \Phi_G^* \mathbf{a}] \quad (12.13)$$

From (12.12), it is clear that the mass matrix \mathcal{M}_G is symmetric. It is positive definite because M is positive definite. The expression in (12.12) is the Newton–Euler Operator Factorization of the mass matrix.

The (H_G, Φ_G, M) operators satisfy the conditions in Sect. 9.1.1 for an SKO model. Hence, we can directly apply the SKO techniques developed in Chap. 9 for decomposing, factoring and inverting the mass matrix for the geared systems. However, there are differences in the internal structure of the operators which result in differences in the component steps, and also allow for further optimization of the SKO algorithms.

12.3 Computation of the Mass Matrix

We now discuss the algorithm for computing the exact mass matrix for geared systems based on the SKO procedures from Sect. 9.3.2. First, we adapt Algorithm 9.2 on page 169 to derive the recursive Algorithm 12.1 for the $\mathcal{R}_G(k) \in \mathcal{R}^{12 \times 12}$ composite body inertias.

Algorithm 12.1 Composite rigid body inertias

$$\left\{ \begin{array}{l} \mathcal{R}_G(0) = \mathbf{0} \\ \text{for } k = 1 \cdots n \\ \quad \mathcal{R}_G(k) = \Phi_G(k+1, k)\mathcal{R}_G(k-1)\Phi_G^*(k+1, k) + M(k) \\ \text{end loop} \end{array} \right. \quad (12.14)$$

With the block-diagonal operator $\mathcal{R}_G \triangleq \text{diag}\left\{\mathcal{R}_G(k)\right\}_{k=1}^n$ we can now define the operator decomposition in the following lemma.

Lemma 12.1 Decomposition of $\Phi_G M \Phi_G^*$.

$$\Phi_G M \Phi_G^* = \mathcal{R}_G + \tilde{\Phi}_G \mathcal{R}_G + \mathcal{R}_G \tilde{\Phi}_G^* \quad (12.15)$$

where $\tilde{\Phi}_G \triangleq \Phi_G - I$.

Proof: See Lemma 9.4. ■

Substituting (12.15) in (12.12), the mass matrix M_G can be decomposed as follows:

$$M_G = H_G [\mathcal{R}_G + \tilde{\Phi}_G \mathcal{R}_G + \mathcal{R}_G \tilde{\Phi}_G^*] H_G^* \quad (12.16)$$

As seen in Lemma 9.4, the first term is block diagonal; the second is strictly upper-triangular, and the last is strictly lower-triangular. Paralleling Algorithm 9.3, this decomposition leads to the following recursive algorithm for computing the mass matrix.

$$\left\{ \begin{array}{l} \mathcal{R}_G(0) = \mathbf{0} \\ \text{for } k = 1 \cdots n \\ \quad \mathcal{R}_G(k) = \Phi_G(k, k-1)\mathcal{R}_G(k-1)\Phi_G^*(k, k-1) + M(k) \\ \quad M_G(k, k) = H_G(k)\mathcal{R}_G(k)H_G^*(k) \\ \quad \left\{ \begin{array}{l} X(k+1) = \Phi_G(k+1, k)\mathcal{R}_G(k)H_G^*(k) \\ \text{for } j = k+1 \cdots n \\ \quad M_G(j, k) = M_G^*(k, j) = H_G(j)X(j) \\ \quad X(j+1) = \Phi_G(j+1, j)X(j) \\ \text{end loop} \end{array} \right. \\ \text{end loop} \end{array} \right. \quad (12.17)$$

12.3.1 Optimized Composite Body Inertia Algorithm

Due to the sparse structure of $\Phi_G(k+1, k)$, further simplifications are possible. These are discussed in the following exercise.

Exercise 12.1 Simplification of $\mathcal{R}_G(k)$.

Show that $\mathcal{R}_G(k)$ and $X(j)$ in (12.17) have the following partitioned structure

$$\mathcal{R}_G(k) = \begin{pmatrix} M_m(k) & \mathbf{0} \\ \mathbf{0} & \mathcal{R}_{G1}(k) \end{pmatrix}, \quad X(j) = \begin{bmatrix} 0 \\ X_1(j) \end{bmatrix} \quad (12.18)$$

where $\mathcal{R}_{G1}(k) \in \mathbb{R}^{6 \times 6}$ and $X_1(k)$ are defined recursively as:

$$\begin{aligned} \mathcal{R}_{G1}(k) &= \phi_l(k, k-1)\mathcal{R}_{G1}(k-1)\phi_l^*(k, k-1) + \check{M}(k) \\ X_1(k+1) &= \mathcal{L}_m(k+1) + \phi_l(k+1, k)\mathcal{R}_{G1}(k)H_l^*(k) \\ X_1(j+1) &= \phi_l(j+1, j)X_1(j) \\ M_G(k, k) &= \mathcal{D}_m(k) + H_l(k)X_1(k) \end{aligned} \quad (12.19)$$

and

$$\begin{aligned} \check{M}(k) &\triangleq \phi_m(k, k-1)M_m(k-1)\phi_m^*(k, k-1) + M_l(k) \\ \mathcal{D}_m(k) &\triangleq \mu_G^2 H_m(k)M_m(k)H_m^*(k) \\ \mathcal{L}_m(k) &\triangleq \mu_G\phi_m(k+1, k)M_m(k)H_m(k) \end{aligned} \quad (12.20)$$

Physically, $\check{M}(k)$ is the spatial inertia about \mathbb{O}_k of a composite rigid body consisting of the k th link and the $(k-1)$ th motor. Using (12.18)–(12.20), the algorithm in (12.17) can be simplified into Algorithm 12.2. Because the quantities $\check{M}(k)$, $\mathcal{D}_m(k)$ and $\mathcal{L}_m(k)$ are all constant in the local link frame, they need to be computed just once. ■

The transformation of (12.17) into the improved Algorithm 12.2 is an example of the optimization step in the SKO formulation step described in Sect. 9.6 on page 182, where the system specific structure of the SKO and other operators is used to further optimize and improve upon the standard SKO algorithm.

An approximate way of handling gears [12, 135] is to add the projection of the motor rotational inertia to the diagonal elements of the manipulator mass matrix (without the motors), and to ignore the additional gyroscopic terms from the spinning of the motors. In particular, this approximate model ignores off-diagonal cross-coupling terms in the mass matrix. Setting $\phi_m(k, k-1) = 0$ in (12.17) leads to this approximate mass matrix. However, this approximation is unnecessary, since the exact mass matrix can be obtained with little additional overhead using Algorithm 12.2.

Algorithm 12.2 The mass matrix for geared hinge systems

```

 $\mathcal{R}_G(0) = \mathbf{0}$ 
for  $k = 1 \dots n$ 
   $\mathcal{R}_{G1}(k) = \phi_1(k, k-1)\mathcal{R}_{G1}(k-1)\phi_1^*(k, k-1) + \check{\mathcal{M}}(k)$ 
   $X_1(k) = \mathcal{R}_{G1}(k)H_1^*(k)$ 
   $\mathcal{M}_G(k, k) = \mathcal{D}_m(k) + H_1(k)X_1(k)$ 
  {
     $X_1(k+1) = \mathcal{L}_m(k+1) + \phi_1(k+1, k)\mathcal{R}_{G1}(k)H_1^*(k)$ 
    for  $j = k+1 \dots n$ 
       $\mathcal{M}_G(j, k) = \mathcal{M}_G^*(k, j) = H_1(j)X_1(j)$ 
       $X_1(j+1) = \phi_1(j+1, j)X_1(j)$ 
    end loop
  }
end loop

```

12.4 $O(N)$ AB Forward Dynamics

We now proceed to apply the SKO formulation based $O(N)$ AB forward dynamics algorithms from Sect. 9.5.1 on page 180 to the geared system.

12.4.1 Mass Matrix Factorization and Inversion

First, define the quantities $\mathcal{P}_G(k)$, $\mathcal{D}_G(k)$, $\mathcal{G}_G(k)$, $\mathcal{K}_G(k+1, k)$ and $\Psi_G(k+1, k)$ via the recursive Algorithm 12.3 which is derived from (9.33).

Define the block-diagonal operators

$$\mathcal{P}_G \triangleq \text{diag} \left\{ \mathcal{P}_G(k) \right\}_{k=1}^n, \mathcal{D}_G \triangleq \text{diag} \left\{ \mathcal{D}_G(k) \right\}_{k=1}^n, \text{ and } \mathcal{G}_G \triangleq \text{diag} \left\{ \mathcal{G}_G(k) \right\}_{k=1}^n$$

along the lines of (9.32). The operators \mathcal{E}_{Ψ_G} and \mathcal{K} are defined in the same manner as \mathcal{E}_{Φ_G} in (12.10) except that the entries are $\Psi_G(k+1, k)$ s and $\mathcal{K}(k+1, k)$ rather than the $\Phi_G(k+1, k)$ terms. As is the case for \mathcal{E}_{Φ_G} , \mathcal{E}_{Ψ_G} is also nilpotent, so the operator Ψ_G can be defined as:

$$\Psi_G \triangleq (\mathbf{I} - \mathcal{E}_{\Psi_G})^{-1} = \begin{pmatrix} I & 0 & \dots & 0 \\ \Psi_G(2, 1) & I & \dots & 0 \\ \vdots & \vdots & \ddots & \vdots \\ \Psi_G(n, 1) & \Psi_G(n, 2) & \dots & I \end{pmatrix} \quad (12.22)$$

Algorithm 12.3 Standard articulated body inertia algorithm for geared hinge systems

$$\left\{ \begin{array}{l} \mathcal{P}_G(0) = 0, \mathcal{D}_G(0) = \mathbf{0} \\ \text{for } k = 1 \cdots n \\ \quad \mathcal{P}_G(k) = \Phi_G(k, k-1) \mathcal{P}_G(k-1) \Phi_G^*(k, k-1) - \\ \quad \quad \quad \mathcal{K}_G(k, k-1) \mathcal{D}_G(k-1) \mathcal{K}_G^*(k, k-1) + \mathbf{M}(k) \\ \quad \mathcal{D}_G(k) = H_G(k) \mathcal{P}_G(k) H_G^*(k) \\ \quad \mathcal{G}_G(k) = \mathcal{P}_G(k) H_G^*(k) \mathcal{D}_G^{-1}(k) \\ \quad \mathcal{K}_G(k+1, k) = \Phi_G(k+1, k) \mathcal{G}_G(k) \\ \quad \Psi_G(k+1, k) = \Phi_G(k+1, k) - \mathcal{K}_G(k+1, k) H_G(k) \\ \text{end loop} \end{array} \right. \quad (12.21)$$

where

$$\Psi_G(k, j) \triangleq \Psi_G(k, k-1) \cdots \Psi_G(j+1, j) \text{ for } k > j$$

Using these spatial operators, we can rewrite (12.21) in stacked notation as

$$\begin{aligned} \mathcal{P}_G &= \mathcal{E}_{\Phi_G} \mathcal{P}_G \mathcal{E}_{\Phi_G}^* - \mathcal{K}_G \mathcal{D}_G \mathcal{K}_G^* + \mathbf{M} \\ \mathcal{D}_G &= H_G \mathcal{P}_G H_G^* \\ \mathcal{G}_G &= \mathcal{P}_G H_G^* \mathcal{D}_G^{-1} \\ \mathcal{K}_G &= \mathcal{E}_{\Phi_G} \mathcal{G}_G \\ \mathcal{E}_{\Psi_G} &= \mathcal{E}_{\Phi_G} - \mathcal{K}_G H_G \end{aligned} \quad (12.23)$$

The next lemma describes the familiar Innovations Operator Factorization and inversion of the mass matrix, and the operator expression for the $\ddot{\theta}_l$ generalized accelerations in terms of the \mathcal{T} generalized forces.

Lemma 12.2 Mass matrix factorization and inversion for geared systems.

$$\begin{aligned} \mathcal{M}_G &= [\mathbf{I} + H_G \Phi_G \mathcal{K}_G] \mathcal{D}_G [\mathbf{I} + H_G \Phi_G \mathcal{K}_G]^* \\ [\mathbf{I} + H_G \Phi_G \mathcal{K}_G]^{-1} &= [\mathbf{I} - H_G \Psi_G \mathcal{K}_G] \\ \mathcal{M}_G^{-1} &= [\mathbf{I} - H_G \Psi_G \mathcal{K}_G]^* \mathcal{D}_G^{-1} [\mathbf{I} - H_G \Psi_G \mathcal{K}_G] \quad (12.24) \\ \ddot{\theta}_l &= [\mathbf{I} - H_G \Psi_G \mathcal{K}_G]^* \mathcal{D}_G^{-1} \{ \mathcal{T} - H_G \Psi_G \\ &\quad * [\mathcal{K}_G \mathcal{T} + \mathbf{b} + \mathcal{P}_G \mathbf{a}] \} - \mathcal{K}_G^* \Psi_G^* \mathbf{a} \end{aligned}$$

Proof: See Lemmas 9.11 and 9.12. ■

12.4.2 Recursive AB Forward Dynamics Algorithm

Along the lines of Algorithm 9.5 on page 182, we use (12.24) to obtain the recursive AB forward dynamics Algorithm 12.4 for computing $\ddot{\theta}_l$.

Algorithm 12.4 Forward dynamics for systems with hinge flexibility

$$\left\{ \begin{array}{l} \mathbf{z}(0) = \mathbf{0}, \mathcal{T}(0) = \mathbf{0} \\ \text{for } k = 1 \cdots n \\ \quad \mathbf{z}(k) = \Phi_G(k, k-1)\mathbf{z}^+(k-1) + \mathbf{b}(k) + \mathcal{P}_G(k)\mathbf{a}(k) \\ \quad \boldsymbol{\epsilon}(k) = \mathcal{T}(k) - H_G(k)\mathbf{z}(k) \\ \quad \boldsymbol{\nu}(k) = \mathcal{D}_G^{-1}(k)\boldsymbol{\epsilon}(k) \\ \quad \mathbf{z}^+(k) = \mathbf{z}(k) + \mathcal{G}_G(k)\boldsymbol{\epsilon}(k) \\ \text{end loop} \\ \\ \mathbf{a}(n+1) = \mathbf{0} \\ \text{for } k = n \cdots 1 \\ \quad \mathbf{a}^+(k) = \Phi_G^*(k+1, k)\mathbf{a}(k+1) \\ \quad \ddot{\theta}_l(k) = \boldsymbol{\nu}(k) - \mathcal{G}_G^*(k)\mathbf{a}^+(k+1) \\ \quad \mathbf{a}(k) = \mathbf{a}^+(k) + H_G^*(k)\ddot{\theta}_l(k) + \mathbf{a}(k) \\ \text{end loop} \end{array} \right. \quad (12.25)$$

The steps in the algorithm can be summarized as follows:

1. Carry out the base-to-tip recursion sweep in (12.1) to compute the spatial velocities $\mathcal{V}_m(k)$ and $\mathcal{V}_l(k)$ for all links. The $\mathbf{a}(k)$ Coriolis spatial accelerations and $\mathbf{b}(k)$ gyroscopic spatial forces are also computed.
2. Carry out the tip-to-base sweep in (12.21) to compute the $\mathcal{P}_G(k)$, $\mathcal{D}_G(k)$, $\mathcal{G}_G(k)$ and $\mathcal{K}_G(k)$ articulated body inertia terms for all the links.
3. Carry out the tip-to-base recursion followed by the base-to-tip recursion in (12.25) to compute the generalized accelerations $\ddot{\theta}_l(k)$.

The tip-to-base recursion in step 2 can be combined with the first tip-to-base recursion in step 3.

12.4.3 Optimization of the Forward Dynamics Algorithm

The forward dynamics algorithm described in Sect. 12.4.2 can be further optimized using the sparsity of several of the quantities involved, and is the subject of the following exercise.

Exercise 12.2 Structure of $\mathcal{P}_G(k)$ and related quantities.

Use the sparsity of $\Phi_G(k+1, k)$ and the partitioning of $H_G(k)$ in (12.20) to show that the quantities in (12.21) have the following form:

$$\begin{aligned}\mathcal{P}_G(k) &= \begin{pmatrix} M_m(k) & \mathbf{0} \\ \mathbf{0} & \mathcal{P}_l(k) \end{pmatrix} \\ \mathcal{D}_G(k) &= \mathcal{D}_m(k) + H_l(k)\mathcal{P}_l(k)H_l^*(k) \\ \mathcal{G}_G(k) &= \begin{bmatrix} \mu_G M_m(k) H_m(k) \mathcal{D}_G^{-1}(k) \\ \mathcal{G}_l(k) \end{bmatrix} \\ \mathcal{K}_G(k+1, k) &= \begin{bmatrix} 0 \\ \mathcal{K}(k+1, k) \end{bmatrix}\end{aligned}\quad (12.26)$$

where the terms $\mathcal{P}_l(k) \in \mathcal{R}^{6 \times 6}$, $\mathcal{G}_l(k)$ and $\mathcal{K}(k+1, k)$ satisfy the following recursive relationships:

$$\begin{aligned}\mathcal{P}_l(k) &\stackrel{\triangle}{=} \phi_l(k, k-1)\mathcal{P}_l(k-1)\phi_l^*(k, k-1) \\ &\quad - \mathcal{K}(k, k-1)\mathcal{D}_G(k-1)\mathcal{K}^*(k, k-1) + \check{M}(k) \\ \mathcal{G}_l(k) &\stackrel{\triangle}{=} \mathcal{P}_l(k)H_l(k)\mathcal{D}_G^{-1}(k) \\ \mathcal{K}(k+1, k) &\stackrel{\triangle}{=} \mathcal{L}_m(k+1)\mathcal{D}_G^{-1}(k) + \phi_l(k+1, k)\mathcal{G}_l(k)\end{aligned}$$

Furthermore, show that the steps in (12.25) for computing $\mathfrak{z}(k)$ and $\alpha^+(k)$ can be restated as

$$\begin{aligned}\mathfrak{z}(k) &= \begin{bmatrix} M_m(k)\mathfrak{a}_m(k) + \mathfrak{b}_m(k) \\ \mathcal{A}_G(k, k-1)\mathfrak{z}^+(k-1) + \mathcal{P}_l(k)\mathfrak{a}_l(k) + \mathfrak{b}_l(k) \end{bmatrix} \\ \alpha^+(k) &= \mathcal{A}_G^*(k+1, k)\alpha_l(k+1)\end{aligned}$$

Observe that the $\mathcal{P}_l(k)$ matrices are obtained recursively as a solution to a Riccati equation, similar to the one for direct-drive manipulators. These new expressions can be used to simplify the $O(N)$ AB forward dynamics Algorithm 12.4 to obtain the optimized Algorithm 12.5. This algorithmic optimization is an additional example of the SKO formulation optimization step described in Sect. 9.6. The com-

putational cost of this $O(N)$ forward dynamics algorithm for geared systems is only slightly more than that for the $O(N)$ AB forward dynamics algorithm for non-geared systems.

Algorithm 12.5 Simplified forward dynamics for systems with hinge flexibility

$$\left\{ \begin{array}{l} \mathcal{P}_l(0) = 0, \mathcal{D}_G(0) = \mathbf{0} \\ \text{for } k = 1 \dots n \\ \quad \mathcal{P}_l(k) \stackrel{\triangle}{=} \phi_l(k, k-1) \mathcal{P}_l(k-1) \phi_l^*(k, k-1) \\ \quad \quad - \mathcal{K}(k, k-1) \mathcal{D}_G(k-1) \mathcal{K}^*(k, k-1) + \check{\mathcal{M}}(k) \\ \quad \mathcal{D}_G(k) = \mathcal{D}_m(k) + H_l(k) \mathcal{P}_l(k) H_l^*(k) \\ \quad \mathcal{G}_l(k) = \mathcal{P}_l(k) H_l(k) \mathcal{D}_G^{-1}(k) \\ \quad \mathcal{K}(k+1, k) = \mathcal{L}_m(k+1) \mathcal{D}_G^{-1}(k) + \phi_l(k+1, k) \mathcal{G}_l(k) \\ \quad \mathcal{G}_G(k) = \begin{bmatrix} \mu_G M_m(k) H_m(k) \mathcal{D}_G^{-1}(k) \\ \mathcal{G}_l(k) \end{bmatrix} \\ \\ \quad \mathfrak{z}(k) = \begin{bmatrix} M_m(k) \mathfrak{a}_m(k) + \mathfrak{b}_m(k) \\ \mathcal{A}_G(k, k-1) \mathfrak{z}^+(k-1) + \mathcal{P}_l(k) \mathfrak{a}_l(k) + \mathfrak{b}_l(k) \end{bmatrix} \\ \quad \epsilon(k) = \mathcal{T}(k) - H_G(k) \mathfrak{z}(k) \\ \quad \nu(k) = \mathcal{D}_G^{-1}(k) \epsilon(k) \\ \quad \mathfrak{z}^+(k) = \mathfrak{z}(k) + \mathcal{G}_G(k) \epsilon(k) \\ \text{end loop} \end{array} \right. \quad (12.27)$$

$$\left\{ \begin{array}{l} \alpha_l(n+1) = \mathbf{0} \\ \text{for } k = n \dots 1 \\ \quad \alpha^+(k) = \mathcal{A}_G^*(k+1, k) \alpha_l(k+1) \\ \quad \ddot{\theta}_l(k) = \nu(k) - \mathcal{G}_G^*(k) \alpha^+(k+1) \\ \quad \alpha(k) = \alpha^+(k) + H_G^*(k) \ddot{\theta}_l(k) + \mathfrak{a}(k) \\ \text{end loop} \end{array} \right.$$

Chapter 13

Systems with Link Flexibility

This chapter uses spatial operators to formulate the SKO dynamics and develop efficient recursive algorithms for systems with non-rigid links. Spacecraft and other lightweight structures are important examples of flexible multibody systems. References [22, 26, 35, 64, 65, 118, 169] describe approaches to modeling the dynamics of flexible multibody systems with Banerjee [21] providing a historical survey of the field. For the sake of simpler exposition, we will focus on a canonical serial-chain system, though generalizations to more general topologies systems along the lines discussed in Chap. 9 are straightforward.

13.1 Lumped Mass Model for a Single Flexible Body

In this section, we begin the development of the equations of motion for a canonical serial-chain flexible multibody system with n flexible bodies. The formulation assumes that the body deformations are small, but allows large articulation at the hinges.

Each flexible body is assumed to have a **lumped mass** model consisting of a collection of nodal rigid bodies. Such models are typically developed using standard finite element structural analysis techniques. Adopting the notation from Sect. 3.6 on page 53, the number of nodes for the k th body is denoted $n_{n,d}(k)$, and the j th node on the k th body is referred to as the \mathbb{O}_k^j node. Each body has associated with it a body reference frame denoted \mathbb{B}_k for the k th body. The deformations of the nodes on the body are described with respect to the \mathbb{B}_k body reference frame, while the rigid body motion of the k th body is characterized by the motion of the \mathbb{B}_k frame itself.

13.1.1 Equations of Motion of the \mathbb{O}_k^j Node

Each \mathbb{O}_k^j node frame undergoes translation and deformation with respect to the \mathbb{B}_k body frame. Assuming small deformation, the small linear and rotational deformations can be expressed as a spatial vector. The 6-dimensional **spatial deformation** (slope plus translational) of node \mathbb{O}_k^j (with respect to frame \mathbb{B}_k) is denoted $u_{nd}(\mathbb{O}_k^j) \in \mathcal{R}^6$, and has the form:

$$u_{nd}(\mathbb{O}_k^j) = \begin{bmatrix} \delta_q(\mathbb{O}_k^j) \\ \delta_l(\mathbb{O}_k^j) \end{bmatrix} \quad (13.1)$$

$\delta_q(\mathbb{O}_k^j)$ and $\delta_l(\mathbb{O}_k^j)$ denote the rotational and linear 3-vector deformation components, respectively. The translational vector from \mathbb{B}_k to the \mathbb{O}_k^j node reference frame is denoted $\mathbf{l}(k, \mathbb{O}_k^j) \in \mathcal{R}^3$, as illustrated in Fig. 13.1. $\mathbf{l}(k, \mathbb{O}_k^j)$, is deformation dependent and is given by:

$$\mathbf{l}(k, \mathbb{O}_k^j) = \mathbf{l}_0(k, \mathbb{O}_k^j) + \delta_l(\mathbb{O}_k^j) \quad (13.2)$$

where $\mathbf{l}_0(k, \mathbb{O}_k^j)$ denotes the undeformed vector. The spatial velocity of the \mathbb{O}_k^j

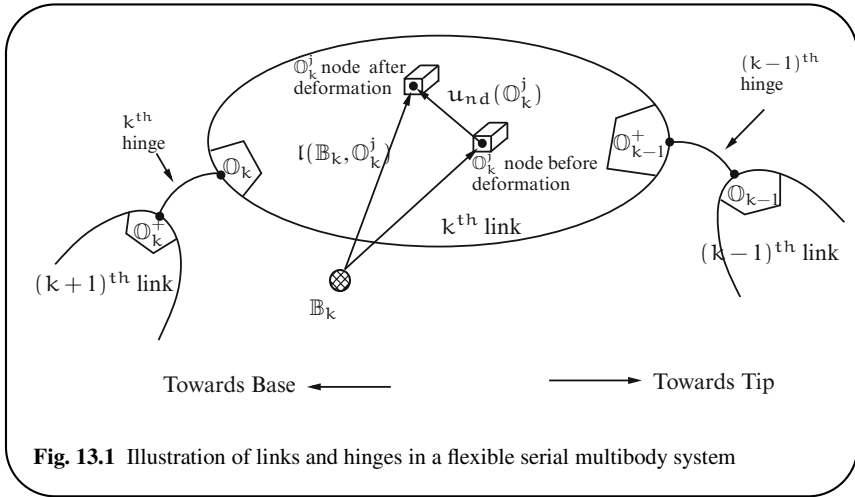


Fig. 13.1 Illustration of links and hinges in a flexible serial multibody system

node with respect to the inertial frame is denoted $\mathcal{V}(\mathbb{O}_k^j)$, and is related to the spatial velocity $\mathcal{V}(k)$ of the \mathbb{B}_k body frame as follows:

$$\mathcal{V}(\mathbb{O}_k^j) = \phi^*(k, \mathbb{O}_k^j) \mathcal{V}(k) + \dot{u}_{nd}(\mathbb{O}_k^j) \in \mathcal{R}^6 \quad (13.3)$$

$\dot{u}_{nd}(\mathbb{O}_k^j)$ denotes the spatial velocity of the \mathbb{O}_k^j with respect to the \mathbb{B}_k body frame. Since $\phi^*(k, \mathbb{O}_k^j)$ depends on $\mathbf{l}(k, \mathbb{O}_k^j)$, its value is deformation dependent. The spatial acceleration of the \mathbb{O}_k^j node, $\alpha_{nd}(\mathbb{O}_k^j)$, is defined as

$$\alpha_{nd}(\mathbb{O}_k^j) \triangleq \frac{d\mathcal{V}(\mathbb{O}_k^j)}{dt} \in \mathcal{R}^6 \quad (13.4)$$

Following the discussion in Sect. 5.1.3 on page 83, we have refrained from specifying the derivative frame in (13.4), since the choice is non-unique. The key requirement however, is that, Coriolis and gyroscopic terms, that are consistent with the derivative frame choice, be used.

For the moment, we ignore forces from interactions with other bodies in the system. With this assumption, the equations of motion of each nodal body is that of a standard rigid body – except for additional structural elastic strain forces on the node. With $M_{nd}(\mathbb{O}_k^j) \in \mathcal{R}^{6 \times 6}$ denoting the spatial inertia of the \mathbb{O}_k^j node, the equations of motion of the \mathbb{O}_k^j node are those for a rigid body described in Chap. 2:

$$f_{nd}(\mathbb{O}_k^j) = M_{nd}(\mathbb{O}_k^j) \alpha_{nd}(\mathbb{O}_k^j) + b(\mathbb{O}_k^j) + f_{nd}^{st}(\mathbb{O}_k^j) \quad (13.5)$$

In (13.5), $f_{nd}^{st}(\mathbb{O}_k^j) \in \mathcal{R}^6$ is the spatial elastic strain force at \mathbb{O}_k^j , while $b(\mathbb{O}_k^j) \in \mathcal{R}^6$ denotes the (rigid body) gyroscopic spatial force for node \mathbb{O}_k^j . The expression for $b(\mathbb{O}_k^j)$ is depends on the specific derivative frame choice for $\alpha_{nd}(\mathbb{O}_k^j)$ in (13.4).

13.1.2 Nodal Equations of Motion for the kth Flexible Body

Defining the overall deformation field, $u_{nd}(k)$, and nodal spatial velocity, $v_{nd}(k)$, stacked vectors for the kth body as

$$\begin{aligned} u_{nd}(k) &\triangleq \text{col} \left\{ u_{nd}(\mathbb{O}_k^j) \right\}_{j=1}^{n_{nd}(k)} \in \mathcal{R}^{6n_{nd}(k)} \\ v_{nd}(k) &\triangleq \text{col} \left\{ v(\mathbb{O}_k^j) \right\}_{j=1}^{n_{nd}(k)} \in \mathcal{R}^{6n_{nd}(k)} \end{aligned} \quad (13.6)$$

it follows from (13.3) that

$$v_{nd}(k) = \mathcal{B}^*(k)v(k) + \dot{u}_{nd}(k) \quad (13.7)$$

where

$$\mathcal{B}(k) \triangleq \left[\phi(k, \mathbb{O}_k^1), \phi(k, \mathbb{O}_k^2), \dots, \phi(k, \mathbb{O}_k^{n_{nd}(k)}) \right] \in \mathcal{R}^{6 \times 6n_{nd}(k)} \quad (13.8)$$

Gathering together the equations of motion for the individual \mathbb{O}_k^j nodal bodies on the k th body, we can express the equations of motion for the k th flexible body in the form:

$$\mathbf{f}_{nd}(k) = M_{nd}(k)\alpha_{nd}(k) + b_{nd}(k) + \mathcal{K}_{st}(k)u_{nd}(k) \quad (13.9)$$

where

$$\begin{aligned} \alpha_{nd}(k) &\triangleq \text{col} \left\{ \alpha_{nd}(\mathbb{O}_k^j) \right\}_{j=1}^{n_{nd}(k)} \in \mathcal{R}^{6n_{nd}(k)} \\ \mathbf{f}_{nd}(k) &\triangleq \text{col} \left\{ \mathbf{f}_{nd}(\mathbb{O}_k^j) \right\}_{j=1}^{n_{nd}(k)} \in \mathcal{R}^{6n_{nd}(k)} \\ b_{nd}(k) &\triangleq \text{col} \left\{ b(\mathbb{O}_k^j) \right\}_{j=1}^{n_{nd}(k)} \in \mathcal{R}^{6n_{nd}(k)} \end{aligned} \quad (13.10)$$

The $M_{nd}(k)$ **structural mass matrix** for the k th body is the block diagonal matrix defined as

$$M_{nd}(k) \triangleq \text{diag} \left\{ M_{nd}(\mathbb{O}_k^j) \right\}_{j=1}^{n_{nd}(k)} \in \mathcal{R}^{6n_{nd}(k) \times 6n_{nd}(k)} \quad (13.11)$$

while $\mathcal{K}_{st}(k) \in \mathcal{R}^{6n_{nd}(k) \times 6n_{nd}(k)}$ denotes the block-diagonal **structural stiffness matrix** for all the nodes on the k th flexible body. Both $M_{nd}(k)$ and $\mathcal{K}_{st}(k)$ are typically generated using finite element structural analysis.

The equations of motion above have focused on independent bodies, and have ignored interactions with the adjoining bodies. We remedy this in the following section.

13.1.3 Recursive Relationships Across the Flexible Bodies

The spatial velocity $\mathcal{V}_{nd}(\mathbb{O}_k^+) \in \mathcal{R}^6$ of node \mathbb{O}_k^+ (on the inboard of the k th hinge) is related to the spatial velocity, $\mathcal{V}(k+1)$, of the $(k+1)$ th body reference frame \mathbb{B}_{k+1} , as follows:

$$\mathcal{V}_{nd}(\mathbb{O}_k^+) = \phi^*(k+1, \mathbb{O}_k^+) \mathcal{V}(k+1) + \dot{\mathbf{u}}_{nd}(\mathbb{O}_k^+) \quad (13.12)$$

Since the $\Delta\gamma(k)$ relative spatial velocity across the k th hinge is $H^*(k)\dot{\theta}(k)$, the $\mathcal{V}(\mathbb{O}_k)$ spatial velocity of frame \mathbb{O}_k on the outboard side of the k th hinge is

$$\mathcal{V}_{nd}(\mathbb{O}_k) = \mathcal{V}_{nd}(\mathbb{O}_k^+) + H^*(k)\dot{\theta}(k) \quad (13.13)$$

The $\mathcal{V}(k)$ spatial velocity of the k th body reference frame is given by

$$\mathcal{V}(k) = \phi^*(\mathbb{O}_k, k) [\mathcal{V}_{nd}(\mathbb{O}_k) - \dot{\mathbf{u}}_{nd}(\mathbb{O}_k)] \quad (13.14)$$

Putting together (13.12), (13.13) and (13.14), it follows that

$$\begin{aligned}\mathcal{V}(k) = & \phi^*(k+1, k)\mathcal{V}(k+1) + \phi^*(\mathbb{O}_k^+, k)\dot{u}_{nd}(\mathbb{O}_k^+) \\ & + \phi^*(\mathbb{O}_k, k) [H^*(k)\dot{\theta}(k) - \dot{u}_{nd}(\mathbb{O}_k)]\end{aligned}\quad (13.15)$$

Equation (13.15) provides a recursive relationship that relates the spatial velocity of the k th body frame to the spatial velocity of the $(k+1)$ th body frame.

The equations of motion of the nodal bodies on the k th flexible body are as given by (13.5), except for the \mathbb{O}_{k-1}^+ node, which is subject to inter-body interaction force across the $(k-1)$ th hinge. The equations of motion of this particular node are as follows:

$$\begin{aligned}f_{nd}(\mathbb{O}_{k-1}^+) = & \phi(\mathbb{O}_{k-1}^+, k-1)f_{fl}^r(k-1) + M_{nd}(\mathbb{O}_{k-1}^+)\alpha_{nd}(\mathbb{O}_{k-1}^+) \\ & + b(\mathbb{O}_{k-1}^+) + f_{nd}^{st}(\mathbb{O}_{k-1}^+)\end{aligned}\quad (13.16)$$

where

$$f_{fl}^r(k) \triangleq \mathcal{B}(k)f_{nd}(k) \quad (13.17)$$

$f_{fl}^r(k) \in \mathcal{R}^6$ denotes the effective spatial force of interaction, referenced to frame \mathbb{B}_k , between the $(k+1)$ th and k th bodies across the k th hinge. It thus follows that the nodal equations of motion for the k th flexible body in (13.9) need to be altered to include this interaction force across the $(k-1)$ th hinge. The modified form is as follows:

$$\begin{aligned}f_{nd}(k) = & C_{fl}(k, k-1)f_{fl}^r(k-1) + M_{nd}(k)\alpha_{nd}(k) \\ & + b_{nd}(k) + \kappa_{st}(k)u_{nd}(k)\end{aligned}\quad (13.18)$$

where

$$C_{fl}(k, k-1) \triangleq \begin{bmatrix} \mathbf{0} \\ \vdots \\ \phi(\mathbb{O}_{k-1}^+, k-1) \\ \vdots \\ \mathbf{0} \end{bmatrix} \in \mathcal{R}^{6n_{nd}(k) \times 6} \quad (13.19)$$

13.2 Modal Formulation for Flexible Bodies

Assumed modes provide a series expansion representation of the deformation field and are often used to represent the deformation of flexible bodies. A subset of the modes can be used for reduced order models for control system design. Lumped mass models described in the previous sections are the starting point for developing assumed mode models.

There is a close relationship between the choice of a body reference frame and the type of assumed modes. The complete motion of the flexible body is defined by the motion of the body reference frame and the deformation of the body with respect to the body frame. In the multibody context, it is often convenient to choose the location of the k th body reference frame \mathbb{B}_k as a material point on the body fixed to node \mathbb{O}_k at the inboard hinge. For this choice, the assumed modes are cantilever modes, and node \mathbb{O}_k exhibits zero deformation ($u_{nd}(\mathbb{O}_k) = \mathbf{0}$). Free-free modes are also used for representing body deformation, and are often preferred for control analysis and design. For these modes, the reference frame \mathbb{B}_k is not fixed to any node, but is rather assumed to be fixed to the undeformed body, and, as a result, all nodes exhibit non-zero deformation. The dynamics models and algorithms developed here handle both types of modes. See Likins [118] for a discussion on the choice of reference frame and modal representations for a flexible body.

Assume that a set of $n_{md}(k)$ assumed modes has been chosen for the k th body. Let $\Pi_r(\mathbb{O}_k^j) \in \mathcal{R}^6$ denote the **modal spatial displacement vector** at the \mathbb{O}_k^j node for the r th mode, and $\eta(k) \in \mathcal{R}^{n_{md}(k)}$ denote the vector of modal deformation coordinates for the k th body. The $\Pi_r(\mathbb{O}_k^j) \in \mathcal{R}^6$ modal spatial displacement vectors are assumed to be constant and independent of the deformation of the body. The spatial deformation of node \mathbb{O}_k^j is represented using modal coordinates as follows:

$$u_{nd}(\mathbb{O}_k^j) = \sum_{r=1}^{n_{md}(k)} \Pi_r(\mathbb{O}_k^j) \eta_r(k) \quad (13.20)$$

$\eta_r(k)$ denotes the r th element of $\eta(k)$. Equation (13.20) defines a linear relationship between the modal coordinates and the deformation spatial displacements at the nodes. For cantilever modes,

$$\Pi_r(\mathbb{O}_k) = \mathbf{0} \quad \text{for } r = 1 \dots n_{md}(k) \quad (13.21)$$

Equation (13.20) can be re-expressed as

$$u_{nd}(\mathbb{O}_k^j) = \Pi(\mathbb{O}_k^j) \eta(k) \quad (13.22)$$

where the **modal spatial displacement influence vector** $\Pi(\mathbb{O}_k^j)$ for the \mathbb{O}_k^j node is defined as:

$$\Pi(\mathbb{O}_k^j) \triangleq \left[\Pi_1(\mathbb{O}_k^j), \dots, \Pi_{n_{md}(k)}(\mathbb{O}_k^j) \right]_{r=1}^{n_{md}(k)} \in \mathcal{R}^{6 \times n_{md}(k)}$$

The $\Pi(k)$ **modal matrix** for the k th body is defined as follows:

$$\Pi(k) \triangleq \text{col} \left\{ \Pi(\mathbb{O}_k^j) \right\}_{j=1}^{n_{nd}(k)} \in \mathcal{R}^{6n_{nd}(k) \times n_{md}(k)}$$

and relates the modal coordinates to the deformation field for the k th body as follows:

$$u_{nd}(k) \stackrel{13.22}{=} \Pi(k)\eta(k) \quad (13.23)$$

The r th column of $\Pi(k)$ is denoted $\Pi_r(k) \in \mathcal{R}^{6n_{nd}(k)}$, and is the **mode shape** for the r th assumed mode for the k th body.

The modal generalized coordinates parametrize the deformation of a body, while the hinge generalized coordinates parametrize the large angle articulation motion of the body. Taken together, they completely characterize the motion of a flexible body. Therefore, define the $\vartheta(k)$ generalized coordinates and $\dot{\vartheta}(k)$ generalized velocities vectors for the k th body as

$$\vartheta(k) \triangleq \begin{bmatrix} \eta(k) \\ \theta(k) \end{bmatrix} \in \mathcal{R}^{\bar{N}(k)} \quad \text{and} \quad \dot{\vartheta}(k) \triangleq \begin{bmatrix} \dot{\eta}(k) \\ \dot{\theta}(k) \end{bmatrix} \in \mathcal{R}^{\bar{N}(k)} \quad (13.24)$$

where $\bar{N}(k) \triangleq n_{md}(k) + r_v(k)$ represents the overall number of velocity degrees of freedom associated with the k th body.

13.2.1 Modal Mass Matrix for a Single Body

The kinetic energy of the k th body is the sum of the kinetic energies of the nodal elements and is given by

$$\begin{aligned} \mathfrak{K}_e(k) &= \frac{1}{2} \sum_{j=1}^{n_{nd}(k)} \mathcal{V}^*(\mathbb{O}_j^j) M_{nd}(\mathbb{O}_k^j) \mathcal{V}(\mathbb{O}_j^j) \stackrel{13.6, 13.11}{=} \frac{1}{2} \mathcal{V}_{nd}^*(k) M_{nd}(k) \mathcal{V}_{nd}(k) \\ &= \frac{1}{2} \mathcal{V}_{fl}^*(k) \begin{bmatrix} \Pi^*(k) \\ \mathcal{B}(k) \end{bmatrix} M_{nd}(k) [\Pi(k), \mathcal{B}^*(k)] \mathcal{V}_{fl}(k) \end{aligned}$$

where

$$\mathcal{V}_{nd}(k) \stackrel{13.7, 13.23}{=} [\Pi(k), \mathcal{B}^*(k)] \mathcal{V}_{fl}(k) \quad \text{with} \quad \mathcal{V}_{fl}(k) \triangleq \begin{bmatrix} \dot{\eta}(k) \\ \mathcal{V}(k) \end{bmatrix} \in \mathcal{R}^{\check{N}(k)} \quad (13.25)$$

and $\check{N}(k) \triangleq n_{md}(k) + 6$. We refer to $\mathcal{V}_{fl}(k)$ as the **modal spatial velocity** for the k th body. Thus, the kinetic energy of the k th body can be expressed as

$$\mathfrak{K}_e(k) = \frac{1}{2} \mathcal{V}_{fl}^*(k) M_{fl}(k) \mathcal{V}_{fl}(k) \quad (13.26)$$

where

$$\begin{aligned}
 M_{fl}(k) &\triangleq \begin{bmatrix} \Pi^*(k) \\ \mathcal{B}(k) \end{bmatrix} M_{nd}(k) [\Pi(k), \mathcal{B}^*(k)] \\
 &= \begin{pmatrix} \Pi^*(k)M_{nd}(k)\Pi(k) & \Pi^*(k)M_{nd}(k)\mathcal{B}^*(k) \\ \mathcal{B}(k)M_{nd}(k)\Pi(k) & \mathcal{B}(k)M_{nd}(k)\mathcal{B}^*(k) \end{pmatrix} \\
 &= \begin{pmatrix} M_{fl}^{ff}(k) & M_{fl}^{fr}(k) \\ M_{fl}^{rf}(k) & M_{fl}^{rr}(k) \end{pmatrix} \in \mathcal{R}^{\mathcal{N}(k) \times \mathcal{N}(k)}
 \end{aligned} \tag{13.27}$$

Corresponding to the generalized velocities vector $\dot{\vartheta}(k)$, $M_{fl}(k)$ as defined above is the **modal mass matrix** of the k th body. In the block partitioning in (13.27), the superscripts f and r denote the **flexible** and **rigid** blocks, respectively, corresponding to the flex/rigid partitioning of the ϑ flexible generalized coordinates vector in (13.24). Thus, $M_{fl}^{ff}(k)$ represents the flex/flex coupling block, while $M_{fl}^{fr}(k)$ represents the flex/rigid coupling block of $M_{fl}(k)$. We will use this notational convention throughout this chapter. $M_{fl}^{rr}(k)$ is precisely the rigid body spatial inertia of the k th body. Indeed, $M_{fl}(k)$ reduces to the rigid body spatial inertia when the body is rigid, since in this case $n_{nd}(k) = 0$ (and $\Pi(k)$ is null).

Since the vector $\mathbf{l}(k, \mathbb{O}_k^j)$ from \mathbb{B}_k to node \mathbb{O}_k^j depends on the deformation of the node, the operator $\mathcal{B}(k)$ is also deformation dependent. From (13.27) it follows that, while the block $M_{fl}^{ff}(k)$ is deformation independent, both the blocks $M_{fl}^{fr}(k)$ and $M_{fl}^{rr}(k)$ are deformation dependent. The detailed expression for the modal mass matrix can be defined using **modal integrals** which are computed as a part of the finite-element structural analysis of the flexible bodies [169]. These expressions for the modal mass matrix of the k th body were initially derived in [79]. Often the deformation dependent parts of the modal mass matrix are ignored, and free-free eigen-modes are used for the $\Pi(k)$ assumed modes. When this is the case, $M_{fl}^{fr}(k)$ is zero and $M_{fl}^{ff}(k)$ is diagonal.

13.2.2 Recursive Relationships Using Modal Coordinates

Using modal coordinates, (13.15) can be re-expressed as:

$$\begin{aligned}
 \mathcal{V}(k) &= \phi^*(k+1, k)\mathcal{V}(k+1) + \phi^*(\mathbb{O}_k^+, k)\Pi(\mathbb{O}_{k+1}^+)\dot{\eta}(k+1) \\
 &\quad + \phi^*(\mathbb{O}_k, k) [\mathcal{H}^*(k)\dot{\theta}(k) - \Pi(\mathbb{O}_k)\dot{\eta}(k)]
 \end{aligned} \tag{13.28}$$

Thus, the $m\mathcal{V}_{fl}(k)$ nodal spatial velocity for the k th body can be expressed as

$$\mathcal{V}_{fl}(k) \stackrel{13.28, 13.25}{=} \Phi_{fl}^*(k+1, k)\mathcal{V}_{fl}(k+1) + H_{fl}^*(k)\ddot{\vartheta}(k) \quad (13.29)$$

where the **inter-body transformation matrix** $\Phi_{fl}(k+1, k) \in \mathcal{R}^{\check{N}(k+1) \times \check{N}(k)}$ and the **modal joint map matrix** $H_{fl}(k) \in \mathcal{R}^{\bar{N}(k) \times \check{N}(k)}$ are defined as

$$\Phi_{fl}(k+1, k) \triangleq \begin{pmatrix} \mathbf{0} & \Pi^*(\mathbb{O}_{k+1}^+) \phi(\mathbb{O}_k^+, k) \\ \mathbf{0} & \phi(k+1, k) \end{pmatrix} \quad (13.30)$$

$$H_{fl}(k) \triangleq \begin{pmatrix} \mathbf{I} & -\Pi_B^*(\mathbb{O}_k) \\ \mathbf{0} & H_B(k) \end{pmatrix} \quad (13.31)$$

with

$$H_B(k) \triangleq H(k)\phi(\mathbb{O}_k, k) \in \mathcal{R}^{r_v(k) \times 6}$$

$$\text{and } \Pi_B(\mathbb{O}_k) \triangleq \phi^*(\mathbb{O}_k, k)\Pi(\mathbb{O}_k) \in \mathcal{R}^{6 \times \bar{N}(k)}$$

13.2.3 Recursive Propagation of Accelerations

Differentiating the velocity recursion equation (13.29), we obtain the following recursive expression for the **modal spatial acceleration** $\alpha_{fl}(k) \in \mathcal{R}^{\check{N}(k)}$ for the k th body:

$$\begin{aligned} \alpha_{fl}(k) &\triangleq \frac{d\mathcal{V}_{fl}(k)}{dt} = \begin{bmatrix} \ddot{\vartheta}(k) \\ \alpha(k) \end{bmatrix} \\ &= \Phi_{fl}^*(k+1, k)\alpha_{fl}(k+1) + H_{fl}^*(k)\ddot{\vartheta}(k) + a_{fl}(k) \end{aligned} \quad (13.32)$$

where $\alpha(k) \triangleq \dot{\mathcal{V}}(k)$, and the Coriolis acceleration term $a_{fl}(k) \in \mathcal{R}^{\check{N}(k)}$ is given by

$$a_{fl}(k) = \frac{d\Phi_{fl}^*(k+1, k)}{dt}\mathcal{V}_{fl}(k+1) + \frac{dH_{fl}^*(k)}{dt}\dot{\vartheta}(k) \quad (13.33)$$

The relationship of the $\alpha_{nd}(k)$ vector of spatial accelerations of all the nodes for the k th body to the $\alpha_{fl}(k)$ vector is obtained by differentiating (13.7):

$$\alpha_{nd}(k) = \frac{d\mathcal{V}_{nd}(k)}{dt} = [\Pi(k), \mathcal{B}^*(k)]\alpha_{fl}(k) + a_{nd}(k) \quad (13.34)$$

where

$$a_{nd}(k) \triangleq \text{col}\left\{a(\mathbb{O}_k^j)\right\} = \frac{d[\Pi(k), \mathcal{B}^*(k)]}{dt}\mathcal{V}_{fl}(k) \in \mathcal{R}^{6n_{nd}(k)} \quad (13.35)$$

The time derivative frames used in (13.32) and (13.35) are assumed to be consistent with the derivative frame choice in (13.4).

13.2.4 Recursive Propagation of Forces

Using the principle of virtual work, it follows from (13.25) that the **modal spatial forces**, $f_{fl}(k) \in \mathcal{R}^{\mathcal{N}(k)}$, for the k th body is given by

$$f_{fl}(k) \triangleq \begin{bmatrix} \Pi^*(k) \\ \mathcal{B}(k) \end{bmatrix} f_{nd}(k) \stackrel{13.17}{=} \begin{bmatrix} \Pi^*(k) f_{nd}(k) \\ f_{fl}(k) \end{bmatrix} \quad (13.36)$$

Pre-multiplying (13.18) by $\begin{bmatrix} \Pi^*(k) \\ \mathcal{B}(k) \end{bmatrix}$, and using (13.27), (13.34), and (13.36), leads to the following recursive relationship for the modal spatial forces:

$$\begin{aligned} f_{fl}(k) &= \begin{bmatrix} \Pi^*(k) C_{fl}(k, k-1) \\ \mathcal{B}(k) C_{fl}(k, k-1) \end{bmatrix} f_{fl}^r(k-1) + M_{fl}(k) \alpha_{fl}(k) \\ &\quad + b_{fl}(k) + \mathfrak{K}(k) \vartheta(k) \\ &= \begin{bmatrix} \Pi^*(\mathbb{O}_k^+) \\ \phi(k, \mathbb{O}_{k-1}^+) \end{bmatrix} \phi(\mathbb{O}_{k-1}^+, k-1) f_{fl}^r(k-1) + M_{fl}(k) \alpha_{fl}(k) \\ &\quad + b_{fl}(k) + \mathfrak{K}(k) \vartheta(k) \\ &= \Phi_{fl}(k, k-1) f_{fl}(k-1) + M_{fl}(k) \alpha_{fl}(k) + b_{fl}(k) + \mathfrak{K}(k) \vartheta(k) \quad (13.37) \end{aligned}$$

Here, we have defined

$$b_{fl}(k) \triangleq \begin{bmatrix} \Pi^*(k) \\ \mathcal{B}(k) \end{bmatrix} [b_{nd}(k) + M_{nd}(k) a_{nd}(k)] \in \mathcal{R}^{\mathcal{N}(k)} \quad (13.38)$$

and the **modal stiffness matrix**

$$\mathfrak{K}(k) \triangleq \begin{pmatrix} \Pi^*(k) \mathfrak{K}_{st}(k) \Pi(k) & \mathbf{0} \\ \mathbf{0} & \mathbf{0} \end{pmatrix} \in \mathcal{R}^{\mathcal{N}(k) \times \mathcal{N}(k)} \quad (13.39)$$

Equation (13.37) establishes a recursive relationship between the modal spatial forces across adjoining bodies. Since the columns of $\mathcal{B}^*(k)$ are indeed the *deformation dependent* rigid body modes for the k th body, they do not contribute to its elastic strain energy and lead to the expression for $\mathfrak{K}(k)$ in (13.39). Indeed, when a deformation dependent structural stiffness matrix $\mathfrak{K}_{st}(k)$ is used

$$\mathfrak{K}_{st}(k) \mathcal{B}^*(k) = \mathbf{0} \quad (13.40)$$

However, the common practice (also followed here) of using a constant, deformation-independent structural stiffness matrix leads to a situation wherein (13.40) does not hold exactly. We neglect these non-zero terms on the left-hand side of (13.40). The velocity-dependent bias term $b_{fl}(k)$ is formed using modal integrals generated using structural analysis programs.

13.2.5 Overall Equations of Motion

Gathering together the recursive equations in (13.29), (13.32) and (13.37), we obtain the following overall equations of motion for the system:

$$\left\{ \begin{array}{l} \mathcal{V}_{fl}(n+1) = 0, \quad \alpha_{fl}(n+1) = \mathbf{0} \\ \text{for } k = n \cdots 1 \\ \quad \mathcal{V}_{fl}(k) = \Phi_{fl}^*(k+1, k)\mathcal{V}_{fl}(k+1) + H_{fl}^*(k)\dot{\vartheta}(k) \\ \quad \alpha_{fl}(k) = \Phi_{fl}^*(k+1, k)\alpha_{fl}(k+1) + H_{fl}^*(k)\ddot{\vartheta}(k) + a_{fl}(k) \\ \text{end loop} \end{array} \right. \quad (13.41)$$

$$\left\{ \begin{array}{l} f_{fl}(0) = \mathbf{0} \\ \text{for } k = 1 \cdots n \\ \quad f_{fl}(k) = \Phi_{fl}(k, k-1)f_{fl}(k-1) + M_{fl}(k)\alpha_{fl}(k) + b_{fl}(k) + R(k)\vartheta(k) \\ \quad T_{fl}(k) = H_{fl}(k)f_{fl}(k) \\ \text{end loop} \end{array} \right.$$

As discussed in Remark 5.2.1 on page 85, external forces on the k th body can be handled by absorbing them into the $b_{fl}(k)$ gyroscopic force term.

13.3 SKO Models for Flexible Body Systems

The overall vectors of generalized configuration coordinates, ϑ , and generalized velocities, $\dot{\vartheta}$, for the serial multibody system are defined as

$$\vartheta \triangleq \text{col} \left\{ \vartheta(k) \right\}_{k=1}^n \in \mathcal{R}^{\mathcal{N}_{fl}} \quad \text{and} \quad \dot{\vartheta} \triangleq \text{col} \left\{ \dot{\vartheta}(k) \right\}_{k=1}^n \in \mathcal{R}^{\mathcal{N}_{fl}} \quad (13.42)$$

where $\mathcal{N}_{fl} \triangleq \sum_{k=1}^n \bar{N}(k)$ denotes the overall number of degrees of freedom for the multibody system. The state of the multibody system is defined by the pair of vectors $\{\vartheta, \dot{\vartheta}\}$. For a given system state $\{\vartheta, \dot{\vartheta}\}$, the equations of motion defining the relationship between the vector of generalized accelerations $\ddot{\vartheta}$ and the vector of generalized forces $T_{fl} \in \mathcal{R}^{\mathcal{N}_{fl}}$ are developed in this section.

With $\check{N} = \sum_{k=1}^n \check{N}(k)$, we use recursive velocity relationship in (13.29) to define the $\mathcal{E}_{\Phi_{fl}}$ and Φ_{fl} SKO and SPO operators, respectively, for the system as:

$$\mathcal{E}_{\Phi_{fl}} \triangleq \sum_k e_{\varphi(k)} \Phi_{fl}(\varphi(k), k) e_k^* \quad \text{and} \quad \Phi_{fl} \triangleq (I - \mathcal{E}_{\Phi_{fl}})^{-1} \quad (13.43)$$

The $(k, k-1)$ weight matrix for the $\mathcal{E}_{\Phi_{fl}}$ SKO operator is $\Phi_{fl}(k, k-1)$ based on the velocity relationships in (12.3), the weights satisfy the usual semi-group property:

$$\Phi_{fl}(k, j) \triangleq \Phi_{fl}(k, k-1) \cdots \Phi_{fl}(j+1, j) \text{ for } k > j$$

It is also noteworthy that the weight matrices are neither invertible nor 6×6 matrices, as is the case for systems with rigid links. Moreover, the weight matrices are of non-uniform size for systems with a mix of rigid and flexible-links, and when the number of modes varies from body to body.

With our assumption of a canonical serial-chain system, $\mathcal{E}_{\Phi_{fl}}$ and Φ_{fl} have the form:

$$\mathcal{E}_{\Phi_{fl}} = \begin{pmatrix} \mathbf{0} & \mathbf{0} & \mathbf{0} & \mathbf{0} & \mathbf{0} \\ \Phi_{fl}(2, 1) & \mathbf{0} & \dots & \mathbf{0} & \mathbf{0} \\ \mathbf{0} & \Phi_{fl}(3, 2) & \dots & \mathbf{0} & \mathbf{0} \\ \vdots & \vdots & \ddots & \vdots & \vdots \\ \mathbf{0} & \mathbf{0} & \dots & \Phi_{fl}(n, n-1) & \mathbf{0} \end{pmatrix} \quad (13.44)$$

$$\Phi_{fl} = \begin{pmatrix} I & \mathbf{0} & \dots & \mathbf{0} \\ \Phi_{fl}(2, 1) & I & \dots & \mathbf{0} \\ \vdots & \vdots & \ddots & \vdots \\ \Phi_{fl}(n, 1) & \Phi_{fl}(n, 2) & \dots & I \end{pmatrix}$$

Also, define the spatial operator $H_{fl} \triangleq \text{diag} \left\{ H_{fl}(k) \right\}_{k=1}^n \in \mathcal{R}^{N_{fl} \times \check{N}}$. Using these spatial operators, and defining $V_{fl} \triangleq \text{col} \left\{ V_{fl}(k) \right\}_{k=1}^n \in \mathcal{R}^{\check{N}}$ from (13.29), it follows that the spatial operator expression for V_{fl} is given by

$$V_{fl} = \Phi_{fl}^* H_{fl}^* \dot{\vartheta} \quad (13.45)$$

Defining $a_{fl} = \text{col} \left\{ a_{fl}(k) \right\}_{k=1}^n \in \mathcal{R}^{\check{N}}$ and $\alpha_{fl} = \text{col} \left\{ \alpha_{fl}(k) \right\}_{k=1}^n \in \mathcal{R}^{\check{N}}$, and using spatial operators, we can re-express (13.32) in the form

$$\alpha_{fl} = \Phi_{fl}^* (H_{fl}^* \ddot{\vartheta} + a_{fl}) \quad (13.46)$$

From (13.37), the operator expression for the modal spatial forces $\mathbf{f}_{fl} \triangleq \text{col}\left\{\mathbf{f}_{fl}(k)\right\}_{k=1}^n \in \mathcal{R}^{\check{N}}$ for all the bodies in the chain is given by

$$\mathbf{f}_{fl} = \Phi_{fl}(M_{fl}\alpha_{fl} + b_{fl} + \mathcal{K}\dot{\vartheta}) \quad (13.47)$$

where

$$\begin{aligned} M_{fl} &\triangleq \text{diag}\left\{M_{fl}(k)\right\}_{k=1}^n \in \mathcal{R}^{\check{N} \times \check{N}} \\ \mathcal{K} &\triangleq \text{diag}\left\{\mathcal{K}(k)\right\}_{k=1}^n \in \mathcal{R}^{\check{N} \times \check{N}} \\ \text{and } b_{fl} &\triangleq \text{col}\left\{b_{fl}(k)\right\}_{k=1}^n \in \mathcal{R}^{\check{N}} \end{aligned}$$

From the principle of virtual work, the generalized forces vector $\mathcal{T}_{fl} \in \mathcal{R}^{N_{fl}}$ for the multibody system is given by the expression

$$\mathcal{T}_{fl} = H_{fl}\mathbf{f}_{fl} \quad (13.48)$$

13.3.1 Operator Expression for the System Mass Matrix

Collecting together the operator expressions in (13.45)–(13.48), we have:

$$\begin{aligned} \mathcal{V}_{fl} &= \Phi_{fl}^* H_{fl}^* \dot{\vartheta} \\ \alpha_{fl} &= \Phi_{fl}^*(H_{fl}^* \ddot{\vartheta} + \mathbf{a}_{fl}) \\ \mathbf{f}_{fl} &= \Phi_{fl}(M_{fl}\alpha_{fl} + b_{fl} + \mathcal{K}\dot{\vartheta}) \\ \mathcal{T}_{fl} &= H_{fl}\mathbf{f}_{fl} = M_{fl}\ddot{\vartheta} + \mathcal{C}_{fl} \end{aligned} \quad (13.49)$$

where

$$\begin{aligned} M_{fl} &\triangleq H_{fl}\Phi_{fl}M_{fl}\Phi_{fl}^*H_{fl}^* \\ \text{and } \mathcal{C}_{fl} &\triangleq H_{fl}\Phi_{fl}(M_{fl}\Phi_{fl}^*\mathbf{a}_{fl} + b_{fl} + \mathcal{K}\dot{\vartheta}) \end{aligned} \quad (13.50)$$

Here, $M_{fl} \in \mathcal{R}^{N_{fl} \times N_{fl}}$ is the system mass matrix for the serial-chain, and the expression $H_{fl}\Phi_{fl}M_{fl}\Phi_{fl}^*H_{fl}^*$ is the Newton–Euler Operator Factorization of the mass matrix. $\mathcal{C}_{fl} \in \mathcal{R}^{N_{fl}}$ is the vector of Coriolis, gyroscopic, and elastic forces for the system. The above define an SKO model for the system.

13.3.2 Illustration of the SKO Formulation Procedure

Let us recap the development so far to highlight its parallels with the SKO formulation steps described in Sect. 9.6 on page 182.

- In addition to the 6-dimensional $\mathcal{V}(k)$ spatial velocity of its body frame, the velocity state of a body is defined by its $n_{md}(k)$ dimensional $\dot{\eta}(k)$ deformation rate coordinates. Thus, the $\check{\mathcal{N}}(k) = n_{md}(k) + 6$ dimensional free-body generalized velocities vector $\mathcal{V}_{fl}(k)$ for the k th body is defined as:

$$\mathcal{V}_{fl}(k) \stackrel{13.25}{=} \begin{bmatrix} \dot{\eta}(k) \\ \mathcal{V}(k) \end{bmatrix} \in \mathcal{R}^{\check{\mathcal{N}}(k)}$$

- The appropriate inertia term for the k th flexible body is defined by the following partitioned matrix:

$$M_{fl}(k) \stackrel{13.27}{=} \begin{pmatrix} M_{fl}^{ff}(k) & M_{fl}^{fr}(k) \\ M_{fl}^{rf}(k) & M_{fl}^{rr}(k) \end{pmatrix} \in \mathcal{R}^{\check{\mathcal{N}}(k) \times \check{\mathcal{N}}(k)}$$

The kinetic energy of the k th body, including both the rigid and deformation contributions, is given by:

$$\mathcal{K}_e(k) = \frac{1}{2} \mathcal{V}_{fl}^*(k) M_{fl}(k) \mathcal{V}_{fl}(k)$$

- The velocity recursion relating the $M_{fl}(k)$ velocity of the k th body to that of its parent is expressed as

$$\mathcal{V}_{fl}(k) \stackrel{13.25}{=} \Phi_{fl}^*(k+1, k) \mathcal{V}_{fl}(k+1) + H_{fl}^*(k) \dot{\vartheta}(k)$$

The inter-body transformation operator $\Phi_{fl}(k+1, k)$, the modal joint map matrix $H_{fl}(k)$, and the independent $\dot{\vartheta}(k)$ generalized coordinates, for the k th body are defined by (13.30), (13.31) and (13.24), respectively. The $n_{md}(k) \times 6$ dimensional $\Pi^*(\mathbb{O}_{k+1}^+)$ and $\Pi_{\mathbb{B}}^*(\mathbb{O}_k)$ modal influence matrices are obtained from the structural analysis of the body and define the mapping to the deformation of the nodes on either side of the k th hinge. From this, the SKO weight matrices are identified to be the $\Phi_{fl}(k+1, k)$ terms.

- The \mathcal{V}_{fl} and $\dot{\vartheta}$ stacked vectors are assembled as usual. The $\mathcal{E}_{\Phi_{fl}}$ SKO operator is defined with the $\Phi_{fl}(k+1, k)$ weight matrices. The SPO operator is defined by $\Phi_{fl} = (\mathbf{I} - \mathcal{E}_{\Phi_{fl}})^{-1}$ in (13.44). The block-diagonal H_{fl} and M_{fl} operators are defined using the $H_{fl}(k)$ and $M_{fl}(k)$ component matrices. These lead to the operator-level equations of motion in (13.49) and the definition of the SKO formulation mass matrix and its Newton–Euler Factorization in (13.50):

$$M_{fl} \triangleq H_{fl} \Phi_{fl} M_{fl} \Phi_{fl}^* H_{fl}^*$$

This defines an SKO model for the system.

5. The analytical techniques and algorithms for the SKO formulation developed in Sect. 9.2 are now directly applicable to the current formulation.
6. While it is premature to discuss specific algorithmic optimization issues, it is nevertheless worthwhile highlighting the sparsity of $\Phi_{fl}(k+1, k)$ and $H_{fl}(k)$ in (13.30). A closer look at (13.29) reveals that the computational evaluation of $\mathcal{V}_{fl}(k)$ requires only the evaluation of the lower part of $\mathcal{V}(k)$, since the upper part is a simple pass through. Thus, an obvious optimization of (13.29) is to use the partitioned sub-blocks of the $\Phi_{fl}(k+1, k)$ and $H_{fl}(k)$ matrices, instead of the full matrices, for improving algorithmic efficiency. Such optimization can be readily applied to other algorithms, e.g., for computing the mass matrix, solving the forward dynamics problem, as will be seen in later sections.

13.4 Inverse Dynamics Algorithm

The inverse dynamics problem consists of computing the vector of generalized forces \mathcal{T}_{fl} for a prescribed set of generalized accelerations $\ddot{\vartheta}$. The forward dynamics problem is the converse one, and requires the computation of the set of generalized accelerations $\ddot{\vartheta}$ resulting from a set of generalized forces \mathcal{T}_{fl} .

The equations of motion in (13.41) are written in the form of a recursive Newton–Euler inverse dynamics algorithm. As expected, the structure of this algorithm closely resembles the recursive Newton–Euler inverse dynamics algorithm for rigid multibody systems seen in Chap. 9. This section describes simplifications of the inverse dynamics algorithm obtained by exploiting the structure of the component matrices and vectors. Observe that

$$\Phi_{fl}(k+1, k) = \mathcal{A}_{fl}(k+1) \mathfrak{B}_{fl}(k+1, k) \quad (13.51)$$

where

$$\mathcal{A}_{fl}(k) \triangleq \begin{bmatrix} \Pi^*(\mathbb{O}_k^+) \\ \Phi(k, \mathbb{O}_{k-1}^+) \end{bmatrix} \in \mathcal{R}^{\check{N}(k) \times 6} \quad (13.52)$$

$$\mathfrak{B}_{fl}(k+1, k) \triangleq [\mathbf{0}, \quad \phi(\mathbb{O}_k^+, k)] \in \mathcal{R}^{6 \times \check{N}(k)}$$

Also, the modal joint map matrix $H_{fl}(k)$ can be partitioned as

$$H_{fl}(k) = \begin{bmatrix} H_{Mfl}(k) \\ H_{Rfl}(k) \end{bmatrix} \in \mathcal{R}^{\overline{N}(k) \times \check{N}(k)} \quad (13.53)$$

where

$$H_{Mfl}(k) \triangleq [\mathbf{I}, \quad -\Pi_{\mathbb{B}}^*(\mathbb{O}_k)] \in \mathcal{R}^{n_{md}(k) \times \check{N}(k)}$$

and $H_{Rfl}(k) \triangleq [\mathbf{0}, \quad H_{\mathbb{B}}(k)] \in \mathcal{R}^{r_v(k) \times \check{N}(k)}$

$$(13.54)$$

Using block partitioning and the superscripts f and r that denote the flexible and rigid components, we have

$$\begin{aligned}\mathcal{V}_{fl}(k) &= \begin{bmatrix} \mathcal{V}_{fl}^f(k) \\ \mathcal{V}_{fl}^r(k) \end{bmatrix} & \alpha_{fl}(k) &= \begin{bmatrix} \alpha_{fl}^f(k) \\ \alpha_{fl}^r(k) \end{bmatrix} \\ f_{fl}(k) &= \begin{bmatrix} f_{fl}^f(k) \\ f_{fl}^r(k) \end{bmatrix}, \quad \text{and} \quad \mathcal{T}_{fl}(k) &= \begin{bmatrix} \mathcal{T}_{fl}^f(k) \\ \mathcal{T}_{fl}^r(k) \end{bmatrix}\end{aligned}$$

By taking advantage of the special structure of $\Phi_{fl}(k+1, k)$ and $H_{fl}(k)$ in (13.52) and (13.53), the Newton–Euler inverse dynamics recursions in (13.41) can be simplified to obtain Algorithm 13.1 for flexible-link system inverse dynamics.

Algorithm 13.1 Inverse dynamics for flexible-link systems

$$\left\{ \begin{array}{l} \mathcal{V}_{fl}(n+1) = 0, \quad \alpha_{fl}(n+1) = \mathbf{0} \\ \textbf{for } k = n \cdots 1 \\ \quad \mathcal{V}_{fl}^f(k) = \dot{\eta}(k) \\ \quad \mathcal{V}_{fl}^r(k) = \phi^*(\mathbb{O}_k^+, k) \mathcal{A}_{fl}^*(k+1) \mathcal{V}_{fl}(k+1) \\ \quad \quad \quad + H_B^*(k) \dot{\theta}(k) - \Pi_B(\mathbb{O}_k) \dot{\eta}(k) \\ \quad \alpha_{fl}^f(k) = \ddot{\eta}(k) \\ \quad \alpha_{fl}^r(k) = \phi^*(\mathbb{O}_k^+, k) \mathcal{A}_{fl}^*(k+1) \alpha_{fl}(k+1) \\ \quad \quad \quad + H_B^*(k) \ddot{\theta}(k) - \Pi_B(\mathbb{O}_k) \ddot{\eta}(k) + \alpha_{fl}^r(k) \\ \textbf{end loop} \end{array} \right. \quad (13.55)$$

$$\left\{ \begin{array}{l} f_{fl}(0) = \mathbf{0} \\ \textbf{for } k = 1 \cdots n \\ \quad f_{fl}(k) = \mathcal{A}_{fl}(k) \phi(\mathbb{O}_{k-1}^+, k-1) f_{fl}^r(k-1) + M_{fl}(k) \alpha_{fl}(k) \\ \quad \quad \quad + b_{fl}(k) + \mathcal{K}(k) \vartheta(k) \\ \quad \mathcal{T}_{fl}(k) = \begin{bmatrix} \mathcal{T}_{fl}^f(k) \\ \mathcal{T}_{fl}^r(k) \end{bmatrix} = \begin{bmatrix} f_{fl}^f(k) - \Pi_B^*(\mathbb{O}_k) f_{fl}^r(k) \\ H_B(k) f_{fl}^r(k) \end{bmatrix} \\ \textbf{end loop} \end{array} \right.$$

Flexible multibody systems typically have actuators only at the hinges. Thus, for the k th body, only the subset of the $\mathcal{T}_{fl}(k)$ generalized forces vector corresponding to the $\mathcal{T}_{fl}^r(k)$ hinge actuator forces can be set, while the remaining $\mathcal{T}_{fl}^f(k)$ generalized forces are zero. Thus, in contrast with rigid multibody

systems, flexible multibody systems are under-actuated systems, since the number of available actuators is less than the number of motion degrees of freedom in the system. For such under-actuated systems, the inverse dynamics computations for the \mathcal{T}_{fl} generalized force are meaningful only when the input $\ddot{\vartheta}$ generalized accelerations form a consistent data set.

13.5 Mass Matrix Computation

Now we describe a composite-body-based recursive algorithm for the computation of the mass matrix \mathcal{M}_{fl} . This algorithm is based upon the following lemma which contains a decomposition of the mass matrix into block diagonal, block upper-triangular and block lower-triangular components.

Lemma 13.1 Decomposition of $\Phi_{fl} M_{fl} \Phi_{fl}^*$ for flexible-link systems.

Define the **composite body inertias** $\mathcal{R}_{fl}(k) \in \mathcal{R}^{\check{N}(k) \times \check{N}(k)}$ recursively for all the bodies in the serial-chain as follows:

$$\begin{cases} \mathcal{R}_{fl}(0) = \mathbf{0} \\ \text{for } k = 1 \dots n \\ \quad \mathcal{R}_{fl}(k) = \Phi_{fl}(k, k-1) \mathcal{R}_{fl}(k-1) \Phi_{fl}^*(k, k-1) + M_{fl}(k) \\ \text{end loop} \end{cases} \quad (13.56)$$

Also, define $\mathcal{R}_{fl} \triangleq \text{diag}\{\mathcal{R}_{fl}(k)\} \in \mathcal{R}^{\check{N} \times \check{N}}$. Then we have the following spatial operator decomposition

$$\Phi_{fl} M_{fl} \Phi_{fl}^* = \mathcal{R}_{fl} + \tilde{\Phi}_{fl} \mathcal{R}_{fl} + \mathcal{R}_{fl} \tilde{\Phi}_{fl}^* \quad (13.57)$$

where $\tilde{\Phi}_{fl} \triangleq \Phi_{fl} - \mathbf{I}$:

Proof: See Lemma 9.3 on page 166. ■

Physically, $\mathcal{R}_{fl}(k)$ is the modal mass matrix of the composite body formed from all the bodies outboard of the k th hinge by freezing all their (deformation plus hinge) degrees of freedom. It follows from (13.50) and Lemma 13.1 that

$$\begin{aligned} \mathcal{M}_{fl} &= H_{fl} \Phi_{fl} M_{fl} \Phi_{fl}^* H_{fl}^* \\ &= H_{fl} \mathcal{R} H_{fl}^* + H_{fl} \tilde{\Phi}_{fl} \mathcal{R} H_{fl}^* + H_{fl} \mathcal{R} \tilde{\Phi}_{fl}^* H_{fl}^* \end{aligned} \quad (13.58)$$

The three terms on the right of (13.58) are block diagonal, block lower-triangular and block upper-triangular, respectively. Algorithm 13.2 for computing the mass matrix \mathcal{M}_{fl} computes the elements of these terms recursively.

Algorithm 13.2 The mass matrix for flexible-link systems

```

 $\mathcal{R}(0) = \mathbf{0}$ 
for  $k = 1 \cdots n$ 
   $\mathcal{R}(k) = \Phi_{fl}(k, k-1)\mathcal{R}(k-1)\Phi_{fl}^*(k, k-1) + M_{fl}(k)$ 
   $= \mathcal{A}_{fl}(k)\phi(\mathbb{O}_{k-1}^+, k-1)\mathcal{R}^{rr}(k-1)\phi^*(\mathbb{O}_{k-1}^+, k-1)\mathcal{A}_{fl}^*(k)$ 
   $+ M_{fl}(k)$ 
   $X(k) = \mathcal{R}(k)H_{fl}^*(k)$ 
   $M_{fl}(k, k) = H_{fl}(k)X(k)$ 
  {
    for  $j = (k+1) \cdots n$ 
       $X(j) = \Phi_{fl}(j, j-1)X(j-1)$ 
       $= \mathcal{A}_{fl}(j)\phi(\mathbb{O}_{j-1}^+, j-1)X^r(j-1)$ 
       $M_{fl}(j, k) = M_{fl}^*(k, j) = H_{fl}(j)X(j)$ 
    end loop
  }
end loop

```

The main recursion proceeds from tip to base, and computes the blocks along the diagonal of M_{fl} . As each such diagonal element is computed, a recursion to compute the off-diagonal elements is spawned. The structure of this algorithm closely parallels the composite rigid body Algorithm 9.3 for computing the mass matrix for SKO models. Some computational simplifications of the algorithm arising from the sparsity of $H_{Mfl}(k)$ and $H_{Rfl}(k)$ have been included in the steps in the algorithm.

13.6 Factorization and Inversion of the Mass Matrix

We now follow the process defined in Sects. 9.4 and 9.5 for an SKO model to develop the Innovations Operator Factorization of the mass matrix. Algorithm 13.3 describes the recursive algorithm for the required articulated body quantities. The operator $\mathcal{P}_{fl} \in \mathcal{R}^{\tilde{N} \times \tilde{N}}$ is defined as a block diagonal matrix with the k th diagonal element being $\mathcal{P}_{fl}(k)$. The quantities defined in (13.59) form the component elements of the following spatial operators:

Algorithm 13.3 Standard AB algorithm for flexible-link systems

$$\left\{
 \begin{array}{l}
 \mathcal{P}_{fl}^+(0) = 0 \\
 \textbf{for } k = 1 \cdots n \\
 \quad \mathcal{P}_{fl}(k) = \Phi_{fl}(k, k-1) \mathcal{P}_{fl}^+(k-1) \Phi_{fl}^*(k, k-1) + M_{fl}(k) \\
 \quad \mathcal{D}_{fl}(k) = H_{fl}(k) \mathcal{P}_{fl}(k) H_{fl}^*(k) \\
 \quad \mathcal{G}_{fl}(k) = \mathcal{P}_{fl}(k) H_{fl}^*(k) \mathcal{D}_{fl}^{-1}(k) \\
 \quad \mathcal{K}_{fl}(k+1, k) = \Phi_{fl}(k+1, k) \mathcal{G}_{fl}(k) \\
 \quad \bar{\tau}(k) = I - \mathcal{G}_{fl}(k) H_{fl}(k) \\
 \quad \mathcal{P}_{fl}^+(k) = \bar{\tau}(k) \mathcal{P}_{fl}(k) \\
 \quad \Psi_{fl}(k+1, k) = \Phi_{fl}(k+1, k) \bar{\tau}(k) \\
 \textbf{end loop}
 \end{array}
 \right. \quad (13.59)$$

$$\begin{aligned}
 \mathcal{D}_{fl} &\triangleq H_{fl} \mathcal{P}_{fl} H_{fl}^* = \text{diag} \left\{ \mathcal{D}_{fl}(k) \right\}_{k=1}^n \in \mathcal{R}^{N_{fl} \times N_{fl}} \\
 \mathcal{G}_{fl} &\triangleq \mathcal{P}_{fl} H_{fl}^* \mathcal{D}_{fl}^{-1} = \text{diag} \left\{ \mathcal{G}_{fl}(k) \right\}_{k=1}^n \in \mathcal{R}^{N_{fl} \times N_{fl}} \\
 \mathcal{K}_{fl} &\triangleq \mathcal{E}_{\Phi_{fl}} \mathcal{G}_{fl} \in \mathcal{R}^{N_{fl} \times N_{fl}} \\
 \bar{\tau} &\triangleq I - \mathcal{G}_{fl} H_{fl} = \text{diag} \left\{ \bar{\tau}(k) \right\}_{k=1}^n \in \mathcal{R}^{N_{fl} \times N_{fl}} \\
 \mathcal{E}_{\Psi_{fl}} &\triangleq \mathcal{E}_{\Phi_{fl}} \bar{\tau} \in \mathcal{R}^{N_{fl} \times N_{fl}}
 \end{aligned} \quad (13.60)$$

The only non-zero block elements of \mathcal{K}_{fl} and $\mathcal{E}_{\Psi_{fl}}$ are $\mathcal{K}_{fl}(k+1, k)$ and $\Psi_{fl}(k+1, k)$ elements, respectively, along the first sub-diagonal.

As in the case for $\mathcal{E}_{\Phi_{fl}}$, $\mathcal{E}_{\Psi_{fl}}$ is an SKO operator and thus its corresponding SPO operator, Ψ_{fl} , is as follows:

$$\Psi_{fl} \triangleq (I - \mathcal{E}_{\Psi_{fl}})^{-1} = \begin{pmatrix} I & \mathbf{0} & \dots & \mathbf{0} \\ \Psi_{fl}(2, 1) & I & \dots & \mathbf{0} \\ \vdots & \vdots & \ddots & \vdots \\ \Psi_{fl}(n, 1) & \Psi_{fl}(n, 2) & \dots & I \end{pmatrix} \in \mathcal{R}^{N_{fl} \times N_{fl}} \quad (13.61)$$

where

$$\Psi_{fl}(i, j) \triangleq \Psi_{fl}(i, i-1) \dots \Psi_{fl}(j+1, j) \text{ for } i > j$$

The structure of the $\mathcal{E}_{\Psi_{fl}}$ and Ψ_{fl} operators is identical to that of the $\mathcal{E}_{\Phi_{fl}}$ and Φ_{fl} operators. The Innovations Operator Factorization of the mass matrix is defined in the following lemma.

Lemma 13.2 Mass matrix factorization and inversion for flexible link systems.

$$\begin{aligned}
 \mathcal{M}_{fl} &= [\mathbf{I} + H_{fl}\Phi_{fl}\mathcal{K}_{fl}]\mathcal{D}_{fl}[\mathbf{I} + H_{fl}\Phi_{fl}\mathcal{K}_{fl}]^* \\
 [\mathbf{I} + H_{fl}\Phi_{fl}\mathcal{K}_{fl}]^{-1} &= [\mathbf{I} - H_{fl}\Psi_{fl}\mathcal{K}_{fl}] \\
 \mathcal{M}^{-1} &= [\mathbf{I} - H_{fl}\Psi_{fl}\mathcal{K}_{fl}]^*\mathcal{D}_{fl}^{-1}[\mathbf{I} - H_{fl}\Psi_{fl}\mathcal{K}_{fl}] \\
 \ddot{\vartheta} &= [\mathbf{I} - H_{fl}\Psi_{fl}\mathcal{K}_{fl}]^*\mathcal{D}_{fl}^{-1} \left[\mathcal{T}_{fl} - H_{fl}\Psi_{fl}\{\mathcal{K}_{fl}\mathcal{T}_{fl} \right. \\
 &\quad \left. + \mathcal{P}_{fl}\alpha_{fl} + b_{fl} + \kappa\vartheta\} \right] - \mathcal{K}_{fl}^*\Psi_{fl}^*\alpha_{fl}
 \end{aligned} \tag{13.62}$$

Proof: See Lemmas 9.11 and 9.12. ■

Once again, the factor $[\mathbf{I} - H_{fl}\Psi_{fl}\mathcal{K}_{fl}]$ is square, block lower-triangular and non-singular, and so Lemma 13.2 provides an analytical closed-form expression for the block LDL^* decomposition of \mathcal{M}^{-1} .

13.7 AB Forward Dynamics Algorithm

Equation (13.62) provides an expression for the $\ddot{\vartheta}$ generalized accelerations. This expression directly leads to the recursive Algorithm 13.4 for the forward dynamics of the system. The structure of this algorithm is identical in form to the AB articulated body Algorithm 9.5 on page 182.

In accordance with the optimization step in SKO formulation process in Sect. 9.6 on page 182, we now look into exploiting the sparsity and special structure of the component matrices in (13.52)–(13.54) to further optimize the forward dynamics algorithm.

13.7.1 Simplified Algorithm for the Articulated Body Quantities

Instead of a detailed derivation, we describe here the conceptual basis for a separation of the modal and hinge degrees of freedom for each body, used in the optimization process. First, we recall the velocity recursion equation in (13.29)

$$\dot{v}_{fl}(k) = \Phi_{fl}^*(k+1, k)v_{fl}(k+1) + H_{fl}^*(k)\dot{\vartheta}(k) \tag{13.64}$$

and the partitioned form of $H_{fl}(k)$ in (13.31)

$$H_{fl}(k) = \begin{bmatrix} H_{Mfl}(k) \\ H_{Rfl}(k) \end{bmatrix} \tag{13.65}$$

Algorithm 13.4 Standard AB forward dynamics algorithm for flexible-link systems

$$\left\{ \begin{array}{l} \mathbf{z}^+(0) = \mathbf{0} \\ \textbf{for } k = 1 \dots n \\ \quad \mathbf{z}(k) = \Phi_{fl}(k, k-1)\mathbf{z}^+(k-1) + \mathcal{P}_{fl}(k)\mathbf{a}_{fl}(k) + \mathbf{b}_{fl}(k) + \mathbf{\tilde{a}}(k)\dot{\vartheta}(k) \\ \quad \boldsymbol{\epsilon}(k) = \mathcal{T}_{fl}(k) - \mathcal{H}_{fl}(k)\mathbf{z}(k) \\ \quad \boldsymbol{\nu}(k) = \mathcal{D}_{fl}^{-1}(k)\boldsymbol{\epsilon}(k) \\ \quad \mathbf{z}^+(k) = \mathbf{z}(k) + \mathcal{G}_{fl}(k)\boldsymbol{\epsilon}(k) \\ \textbf{end loop} \end{array} \right. \quad (13.63)$$

$$\left\{ \begin{array}{l} \boldsymbol{\alpha}_{fl}(n+1) = \mathbf{0} \\ \textbf{for } k = n \dots 1 \\ \quad \boldsymbol{\alpha}_{fl}^+(k) = \Phi_{fl}^*(k+1, k)\boldsymbol{\alpha}_{fl}(k+1) \\ \quad \ddot{\vartheta}(k) = \boldsymbol{\nu}(k) - \mathcal{G}_{fl}^*(k)\boldsymbol{\alpha}_{fl}^+(k) \\ \quad \boldsymbol{\alpha}_{fl}(k) = \boldsymbol{\alpha}_{fl}^+(k) + \mathcal{H}_{fl}^*(k)\ddot{\vartheta}(k) + \mathbf{a}_{fl}(k) \\ \textbf{end loop} \end{array} \right.$$

Introducing a dummy variable k' , we can rewrite (13.64) as

$$\begin{aligned} \mathcal{V}_{fl}(k') &= \Phi_{fl}^*(k+1, k')\mathcal{V}_{fl}(k+1) + \mathcal{H}_{Mfl}^*(k)\dot{\mathbf{h}}(k) \\ \mathcal{V}_{fl}(k) &= \Phi_{fl}^*(k', k)\mathcal{V}_{fl}(k') + \mathcal{H}_{Rfl}^*(k)\dot{\boldsymbol{\theta}}(k) \end{aligned} \quad (13.66)$$

where

$$\Phi_{fl}(k+1, k') \stackrel{\triangle}{=} \Phi_{fl}(k+1, k) \quad \text{and} \quad \Phi_{fl}(k', k) \stackrel{\triangle}{=} \mathbf{I}_6$$

Conceptually, each flexible body is replaced by two new bodies. The first body is assigned the kinematical and mass/inertia properties of the flexible body and also its deformation generalized coordinates. The second virtual body is mass-less, and has zero extent. It is assigned the hinge generalized coordinates. The serial-chain now contains twice the number of bodies as the original one, with half the new bodies being fictitious ones. The tree digraph associated with the new system contains twice as many nodes. The new \mathcal{H}_{fl}^* operator now has the same number of columns, but twice the number of rows, as the original \mathcal{H}_{fl}^* operator. The new Φ_{fl} operator has twice as many rows and columns as the original one. Repeating the analysis described in the previous sections, we once again obtain the SKO operator expression as (13.62). This expression also leads to a recursive forward dynamics algorithm in Algorithm 13.5. However, each sweep in the algorithm now contains twice as many steps as the original algorithm. However, since each step now processes only

Algorithm 13.5 Two stage AB algorithm for flexible-link systems

$$\left\{
 \begin{array}{l}
 \mathcal{P}_{fl}^+(0) = \mathbf{0} \\
 \text{for } k = 1 \dots n \\
 \quad \Gamma_{fl}(k) = \mathfrak{B}_{fl}(k, k-1) \mathcal{P}_{fl}^+(k-1) \mathfrak{B}_{fl}^*(k, k-1) \in \mathcal{R}^{6 \times 6} \\
 \quad \mathcal{P}_{fl}(k) = \mathcal{A}_{fl}(k) \Gamma_{fl}(k) \mathcal{A}_{fl}^*(k) + \mathcal{M}_{fl}(k) \in \mathcal{R}^{\check{N}(k) \times \check{N}(k)} \\
 \quad \mathcal{D}_m(k) = H_{Mfl}(k) \mathcal{P}_{fl}(k) H_{Mfl}^*(k) \in \mathcal{R}^{n_{md}(k) \times n_{md}(k)} \\
 \quad \mathcal{G}_m(k) = \mathcal{P}_{fl}(k) H_{Mfl}^*(k) \mathcal{D}_m^{-1}(k) \in \mathcal{R}^{\check{N}(k) \times n_{md}(k)} \\
 \quad \bar{\tau}_m(k) = \mathbf{I} - \mathcal{G}_m(k) H_{Mfl}(k) \in \mathcal{R}^{\check{N}(k) \times \check{N}(k)} \\
 \quad \mathcal{P}_{cr}(k) = \bar{\tau}_m(k) \mathcal{P}_{fl}(k) \in \mathcal{R}^{\check{N}(k) \times \check{N}(k)} \\
 \\
 \quad \mathcal{D}_{cr}(k) = H_{Rfl}(k) \mathcal{P}_{cr}(k) H_{Rfl}^*(k) \in \mathcal{R}^{r_v(k) \times r_v(k)} \\
 \quad \mathcal{G}_{cr}(k) = \mathcal{P}_{cr}(k) H_{Rfl}^*(k) \mathcal{D}_{cr}^{-1}(k) \in \mathcal{R}^{\check{N}(k) \times r_v(k)} \\
 \quad \bar{\tau}_{cr}(k) = \mathbf{I} - \mathcal{G}_{cr}(k) H_{Rfl}(k) \in \mathcal{R}^{\check{N}(k) \times \check{N}(k)} \\
 \quad \mathcal{P}_{fl}^+(k) = \bar{\tau}_{cr}(k) \mathcal{P}_{cr}(k) \in \mathcal{R}^{\check{N}(k) \times \check{N}(k)} \\
 \quad \Psi_{fl}(k+1, k) = \Phi_{fl}(k+1, k) \bar{\tau}(k) \in \mathcal{R}^{\check{N}(k) \times \check{N}(k)} \\
 \text{end loop}
 \end{array}
 \right. \quad (13.67)$$

a smaller number of degrees of freedom, this leads to a reduction in the overall cost. The new algorithm (replacing Algorithm 13.3) for computing the articulated body quantities is described in Algorithm 13.5.

We now use the sparsity of $\mathfrak{B}_{fl}(k+1, k)$, $H_{Mfl}(k)$ and $H_{Rfl}(k)$ to further simplify the above algorithm. Using the symbol “ \times ” to indicate “don’t care” blocks, the structure in block partitioned form of some of the quantities in Algorithm 13.5 is shown in Fig. 13.2. Using the structure described above, the simplified algorithm for computing the articulated body quantities is described in Algorithm 13.6.

13.7.2 Simplified AB Forward Dynamics Algorithm

Analogous to Algorithm 9.5, the complete recursive articulated body forward dynamics Algorithm 13.7 for a serial flexible multibody system follows directly from the recursive implementation of the expression in (13.62). The algorithm consists of the following steps:

1. A base-to-tip recursion as in (13.55) for computing the modal spatial velocities $\mathcal{V}_{fl}(k)$ and the Coriolis and gyroscopic terms $\mathfrak{a}_{fl}(k)$ and $\mathfrak{b}_{fl}(k)$ for all the bodies.

$$\begin{aligned}
\Gamma_{fl}(k) &= \phi(\mathbb{O}_{k-1}^+, k-1) \mathcal{P}_{pr}^+(k-1) \phi^*(\mathbb{O}_{k-1}^+, k-1), (\mathcal{P}_{pr}^+(k) \text{ is defined below}) \\
\mathcal{G}_m(k) &= \begin{bmatrix} \times \\ \mathbf{g}_{fl}(k) \end{bmatrix} \text{ where } \mathbf{g}_{fl}(k) \triangleq \mu_{fl}(k) \mathcal{D}_m^{-1}(k) \in \mathcal{R}^{6 \times n_{md}(k)} \\
&\text{and } \mu_{fl}(k) \triangleq [\mathcal{P}_{fl}^{rf}(k), \mathcal{P}_{fl}^{rr}(k)] \mathcal{H}_{Mfl}^*(k) \in \mathcal{R}^{6 \times n_{md}(k)} \\
\mathcal{P}_{cr}(k) &= \begin{pmatrix} \times & \times \\ \times & \mathcal{P}_{pr}(k) \end{pmatrix}, \text{ where } \mathcal{P}_{pr}(k) \triangleq \mathcal{P}_{fl}^{rr}(k) - \mathbf{g}_{fl}(k) \mu_{fl}^*(k) \in \mathcal{R}^{6 \times 6} \\
\mathcal{D}_{cr}(k) &= \mathcal{H}_B(k) \mathcal{P}_{pr}(k) \mathcal{H}_B^*(k) \in \mathcal{R}^{r_v(k) \times r_v(k)} \\
\mathcal{G}_{cr}(k) &= \begin{bmatrix} \times \\ \mathcal{G}_{pr}(k) \end{bmatrix}, \text{ where } \mathcal{G}_{pr}(k) \triangleq \mathcal{P}_{pr}(k) \mathcal{H}_B^*(k) \mathcal{D}_{cr}^{-1}(k) \in \mathcal{R}^{6 \times r_v(k)} \\
\bar{\tau}_{cr}(k) &= \begin{pmatrix} \mathbf{I} & \times \\ \mathbf{0} & \bar{\tau}_{pr}(k) \end{pmatrix} \text{ where } \bar{\tau}_{pr}(k) \triangleq \mathbf{I} - \mathcal{G}_{pr}(k) \mathcal{H}_B(k) \in \mathcal{R}^{6 \times 6} \\
\mathcal{P}_{fl}^+(k) &= \begin{pmatrix} \times & \times \\ \times & \mathcal{P}_{pr}^+(k) \end{pmatrix}, \text{ where } \mathcal{P}_{pr}^+(k) = \bar{\tau}_{pr}(k) \mathcal{P}_{pr}(k) \in \mathcal{R}^{6 \times 6}
\end{aligned} \tag{13.68}$$

Fig. 13.2 The partitioned structure of the articulated body inertia quantities for flexible-link systems

2. Computation of the articulated body quantities using Algorithm 13.6.
3. A tip-to-base recursion followed by a base-to-tip recursion for the joint accelerations $\ddot{\vartheta}$ as described in Algorithm 13.7.

The recursion in Algorithm 13.7 is obtained by simplifying the recursions in (13.63) in the same manner as described in the previous section for the articulated body quantities. The recursive forward dynamics algorithm described here is based on references [146, 147]. Other alternate recursive forward dynamics approaches for flexible-link systems are described in [99, 104].

It has been pointed out in the literature [98, 133] that the use of modes for modeling body flexibility leads to “premature linearization” of the dynamics, in the sense that while the dynamics model contains deformation dependent terms, the geometric stiffening terms are missing. These missing geometric stiffening terms are the dominant terms among the first order (deformation) dependent terms. In general, it is necessary to take additional steps to recover the missing geometric stiffness terms to obtain a “consistently” linearized model with the proper degree of fidelity. However, for systems with low spin rate, there is typically little loss in model fidelity when the deformation and deformation rate dependent terms are dropped altogether from the terms in the dynamical equations of motion [133]. These linearized models are considerably less complex, and do not require most of the modal integrals data for each individual flexible body. One such approximation is to ignore the depen-

Algorithm 13.6 Simplified computation of the articulated body inertias for flexible-link systems

$$\left\{ \begin{array}{l} \mathcal{P}_{pr}^+(0) = \mathbf{0} \\ \textbf{for } k = 1 \dots n \\ \quad \Gamma_{fl}(k) = \phi(\mathbb{O}_{k-1}^+, k-1) \mathcal{P}_{pr}^+(k-1) \phi^*(\mathbb{O}_{k-1}^+, k-1) \\ \quad \mathcal{P}_{fl}(k) = \mathcal{A}_{fl}(k) \Gamma_{fl}(k) \mathcal{A}_{fl}^*(k) + \mathcal{M}_{fl}(k) \\ \quad \mathcal{D}_m(k) = H_{Mfl}(k) \mathcal{P}_{fl}(k) H_{Mfl}^*(k) \\ \quad \mu_{fl}(k) = [\mathcal{P}_{fl}^{rf}(k), \mathcal{P}_{fl}^{rr}(k)] H_{Mfl}^*(k) \\ \quad \mathfrak{g}_{fl}(k) = \mu_{fl}(k) \mathcal{D}_m^{-1}(k) \\ \quad \mathcal{P}_{pr}(k) = \mathcal{P}_{fl}^{rr}(k) - \mathfrak{g}_{fl}(k) \mu_{fl}^*(k) \\ \quad \mathcal{D}_{pr}(k) = H_B(k) \mathcal{P}_{pr}(k) H_B^*(k) \\ \quad \mathcal{G}_{pr}(k) = \mathcal{P}_{pr}(k) H_B^*(k) \mathcal{D}_{pr}^{-1}(k) \\ \quad \bar{\tau}_{pr}(k) = \mathbf{I} - \mathcal{G}_{pr}(k) H_B(k) \\ \quad \mathcal{P}_{pr}^+(k) = \bar{\tau}_{pr}(k) \mathcal{P}_{pr}(k) \\ \textbf{end loop} \end{array} \right. \quad (13.69)$$

dency of $\mathcal{M}_{fl}(k)$ on the body deformation and treat it as being constant in the body frame. Simplifications arising from this are discussed in the following exercise.

Exercise 13.1 Additional forward dynamics simplifications.

With the assumption that $\mathcal{M}_{fl}(k)$ is independent of the body deformation, show that the formation of \mathcal{D}_m^{-1} in (13.69) can be simplified as follows:

$$\mathcal{D}_m^{-1}(k) = \mathfrak{L}_{fl}(k) - \mathfrak{U}_{fl}(k) [\Gamma_{fl}^{-1}(k) + \mathfrak{O}_{fl}(k)]^{-1} \mathfrak{U}_{fl}^*(k) \quad (13.70)$$

The matrices $\mathfrak{L}_{fl}(k)$, $\mathfrak{O}_{fl}(k)$, and $\mathfrak{U}_{fl}(k)$ are configuration independent and need to be computed just once as follows:

$$\left\{ \begin{array}{l} \textbf{for } k = 1 \dots n \\ \quad \mathfrak{L}_{fl}(k) = [H_{Mfl}(k) \mathcal{M}_{fl}(k) H_{Mfl}^*(k)]^{-1} \in \mathcal{R}^{\mathcal{N}_{fl} \times \mathcal{N}_{fl}} \\ \quad \zeta(k) = H_{Mfl}(k) \mathcal{A}_{fl}(k) \in \mathcal{R}^{\mathcal{N}_{fl} \times 6} \\ \quad \mathfrak{U}_{fl}(k) = \mathfrak{L}_{fl}(k) \zeta(k) \in \mathcal{R}^{\mathcal{N}_{fl} \times 6} \\ \quad \mathfrak{O}_{fl}(k) = \zeta^*(k) \mathfrak{U}_{fl}(k) \in \mathcal{R}^{6 \times 6} \\ \textbf{end loop} \end{array} \right. \quad (13.71)$$

Algorithm 13.7 Simplified AB forward dynamics for flexible-link systems

```

 $\mathbf{\dot{z}}_{pr}^+(0) = \mathbf{0}$ 
for  $k = 1 \dots n$ 
   $\mathbf{\dot{z}}(k) = \begin{bmatrix} \mathbf{\dot{z}}_m(k) \\ \mathbf{\dot{z}}_{cr}(k) \end{bmatrix} = \mathcal{A}_{fl}(k)\phi(\mathbb{O}_{k-1}^+, k-1)\mathbf{\dot{z}}_{pr}^+(k-1)$ 
     $+ \mathbf{b}_{fl}(k) + \mathbf{\tilde{K}}(k)\vartheta(k) \in \mathcal{R}^{\tilde{N}(k)}$ 
   $\epsilon_m(k) = \mathcal{T}_m(k) - \mathbf{\dot{z}}_m(k) + \Pi_B^*(\mathbb{O}_k)\mathbf{\dot{z}}_{cr}(k) \in \mathcal{R}^{n_{md}(k)}$ 
   $\nu_m(k) = \mathcal{D}_m^{-1}(k)\epsilon_m(k) \in \mathcal{R}^{n_{md}(k)}$ 

   $\mathbf{\dot{z}}_{pr}(k) = \mathbf{\dot{z}}_{cr}(k) + \mathbf{g}_{fl}(k)\epsilon_m(k) + \mathcal{P}_{pr}(k)\mathbf{a}_{mR}(k) \in \mathcal{R}^6$ 
   $\epsilon_{pr}(k) = \mathcal{T}_{pr}(k) - H_B(k)\mathbf{\dot{z}}_{pr}(k) \in \mathcal{R}^{r_v(k)}$ 
   $\nu_{pr}(k) = \mathcal{D}_{pr}^{-1}(k)\epsilon_{pr}(k) \in \mathcal{R}^{r_v(k)}$ 
   $\mathbf{\dot{z}}_{pr}^+(k) = \mathbf{\dot{z}}_{pr}(k) + \mathbf{g}_{pr}(k)\epsilon_{pr}(k) \in \mathcal{R}^6$ 
end loop

 $\alpha_{fl}(n+1) = \mathbf{0}$ 
for  $k = n \dots 1$ 
   $\alpha_{pr}^+(k) = \phi^*(\mathbb{O}_k^+, k)\mathcal{A}_{fl}^*(k+1)\alpha_{fl}(k+1) \in \mathcal{R}^6$ 
   $\ddot{\theta}(k) = \nu_{pr}(k) - \mathbf{g}_{pr}^*(k)\alpha_{pr}^+(k) \in \mathcal{R}^{r_v(k)}$ 
   $\alpha_{pr}(k) = \alpha_{pr}^+(k) + H_B^*(k)\ddot{\theta}(k) + \mathbf{a}_{mR}(k) \in \mathcal{R}^6$ 
   $\ddot{\eta}(k) = \nu_m(k) - \mathbf{g}_{fl}^*(k)\alpha_{pr}(k) \in \mathcal{R}^{n_{md}(k)}$ 
   $\alpha_{fl}(k) = \begin{bmatrix} \ddot{\eta}(k) \\ \alpha_{pr}(k) - \Pi_B(\mathbb{O}_k)\ddot{\eta}(k) \end{bmatrix} \in \mathcal{R}^{\tilde{N}(k)}$ 
end loop

```

Using (13.70) reduces the computational cost for computing the articulated body inertias to a quadratic rather than a cubic function of the number of modes.



Part III

Advanced Topics

Chapter 14

Transforming SKO Models

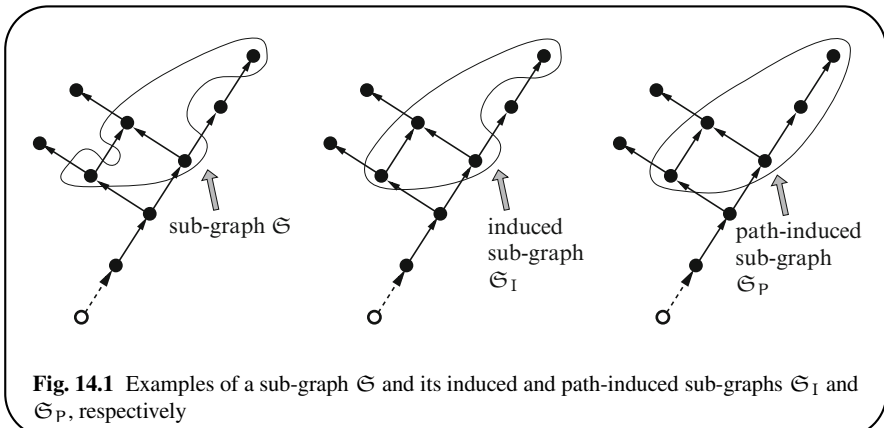
In this chapter we explore techniques for partitioning SKO models. These are subsequently used to develop methods for *aggregating* sub-graphs to transform SKO models into new ones. In Chap. 15, sub-graph aggregation forms the basis of constrained embedding techniques to develop SKO models for closed-chain multibody systems.

14.1 Partitioning Digraphs

A **sub-graph** \mathcal{S} of a digraph, \mathcal{T} , is defined as a digraph containing a subset of the nodes and edges in \mathcal{T} . \mathcal{S} is said to be **induced** if all edges in \mathcal{T} connecting node pairs in \mathcal{S} are also in \mathcal{S} [38, 183]. In other words, \mathcal{S} is induced if all node pairs in \mathcal{S} that are adjacent in \mathcal{T} are also adjacent in \mathcal{S} . Thus induced sub-graphs preserve the adjacency property for node pairs, so that a pair of nodes in an induced sub-graph are adjacent if and only if they are adjacent in the parent digraph. The **induced sub-graph** \mathcal{S}_I for a sub-graph \mathcal{S} is the minimal sub-graph containing \mathcal{S} that is also an induced sub-graph. A sub-graph, and its induced sub-graph, contain the same nodes, and differ only in the edges they contain.

A sub-graph \mathcal{S} of \mathcal{T} is said to be **path-induced** if it contains all the paths (nodes and edges) in \mathcal{T} that connect node pairs in \mathcal{S} . A path-induced sub-graph has no missing nodes or edges for paths in \mathcal{T} that connect the nodes in \mathcal{S} . Thus path-induced sub-graphs preserve the relatedness property for node pairs, so that a pair of nodes in a path-induced sub-graph are *related* if and only if they are related in the parent digraph. The **path-induced sub-graph** \mathcal{S}_P for a sub-graph \mathcal{S} is the minimal sub-graph of \mathcal{T} containing \mathcal{S} that is path-induced. Figure 14.1 illustrates a sub-graph, and its induced and path-induced sub-graphs. The path-induced property applies even to disconnected sub-graphs. A path-induced sub-graph, will generally contain more nodes and edges than the original sub-graph or its induced sub-graph. That is,

$$\mathcal{S} \subseteq \mathcal{S}_I \subseteq \mathcal{S}_P \quad (14.1)$$



Exercise 14.1 Non-tree path-induced sub-graphs.

Let \mathfrak{S} be a path-induced sub-graph of a digraph \mathfrak{T} . Show that:

1. If \mathfrak{S} contains an edge that is a part of a directed cycle in \mathfrak{T} , then the full cycle must also be in \mathfrak{S} .
2. If \mathfrak{S} contains a pair of multiply-connected nodes (i.e., nodes connected by more than one path), then all the paths connecting them must also be in \mathfrak{S} .

■

14.1.1 Partitioning by Path-Induced Sub-Graphs

We now turn our attention to partitions generated by path-induced sub-graphs.

Lemma 14.1 Induced partitions of digraphs.

Assume that \mathfrak{S} is a path-induced sub-graph of a digraph \mathfrak{T} . Define the \mathcal{C} and \mathcal{P} sub-graphs as follows:

- **\mathcal{C} child sub-graph** is the induced sub-graph for the set of nodes that are not in \mathfrak{S} , but are descendants of the nodes in \mathfrak{S} , and
- **\mathcal{P} parent sub-graph** is the induced sub-graph for the remaining nodes that are neither in \mathfrak{S} nor in \mathcal{C} .

The \mathfrak{S} , \mathcal{C} and \mathcal{P} sub-graphs represent a disjoint partitioning of the nodes in \mathfrak{T} . The following properties hold for the \mathcal{C} and \mathcal{P} sub-graphs:

1. \mathcal{C} is path-induced.
2. \mathcal{P} is path-induced.

Proof:

1. Assume that there are nodes $i \succ j \succ k$ where $i, k \in \mathcal{C}$. Since j is a descendant of i , it must belong to either \mathcal{S} or \mathcal{C} . We will show that node j must necessarily belong to \mathcal{C} . First, since $i \in \mathcal{C}$, by definition there is a node $l \in \mathcal{S}$ which is an ancestor of node i , i.e., $l \succ i \succ j$. If node $j \in \mathcal{S}$, we would have $l \succ i \succ j$. Since $i \notin \mathcal{S}$, this would contradict the assumption that \mathcal{S} is path-induced. Hence, $j \notin \mathcal{S}$ and $j \in \mathcal{C}$. Therefore, \mathcal{C} is path-induced.
2. Assume that there are nodes $i \succ j \succ k$, where $i, k \in \mathcal{P}$. We will show that node j must necessarily be in \mathcal{P} . If $j \in \mathcal{S}$, then, since node k is its child, k must be either in \mathcal{S} or \mathcal{C} , which would contradict our assumption that $k \in \mathcal{P}$. Thus $j \notin \mathcal{S}$. If instead $j \in \mathcal{C}$, then there must a node $l \in \mathcal{S}$ that is the ancestor of j , i.e., $l \succ j$. This would imply that $l \succ k$ as well, since $j \succ k$. Since k will then be a descendant of $l \in \mathcal{S}$, it must belong to either \mathcal{S} or \mathcal{C} . This would contradict our assumption that $k \in \mathcal{P}$. Hence, node j must be in \mathcal{P} . This establishes that \mathcal{P} is path-induced. ■

\mathcal{P} contains nodes that are ancestors of the nodes in \mathcal{S} but are not themselves in \mathcal{S} , together with all nodes that are *unrelated* with any of the nodes in \mathcal{S} . While all nodes in \mathcal{T} belong to one of the \mathcal{S} , \mathcal{C} and \mathcal{P} sub-graphs, connecting edges between these sub-graphs do not belong to any of the sub-graphs.

14.2 Partitioning SKO Models

When \mathcal{T} is a tree digraph, a path-induced sub-graph of \mathcal{T} is in fact a *path-induced sub-forest*, i.e., it is a collection of one or more disjoint path-induced sub-trees. Thus, in the partitioning described in Lemma 14.1, \mathcal{S} , \mathcal{C} , and \mathcal{P} are all path-induced sub-forests. This is illustrated in Fig. 14.2. The partitioning process can be continued on the component sub-forests to further sub-divide them into finer-grain path-induced sub-forests, if desired.

14.2.1 Partitioning SKO Model Operators

When \mathcal{T} is the tree digraph for an SKO model, the disjoint partitioning induced by a path-induced sub-graph \mathcal{S} also partitions the bodies in the multibody system into disjoint component multibody systems, corresponding to the \mathcal{S} , \mathcal{C} , and \mathcal{P} path-induced sub-forests. Since these are sub-forests, each of the component systems have well-defined SKO spatial operators, denoted $\mathcal{E}_{\mathbb{A}_{\mathcal{S}}}$, $\mathcal{E}_{\mathbb{A}_{\mathcal{C}}}$, and $\mathcal{E}_{\mathbb{A}_{\mathcal{P}}}$, respectively.

For ease of exposition, we assume that \mathcal{T} is a *canonical* tree. The \mathcal{S} , \mathcal{C} and \mathcal{P} sub-graphs are then also canonical. Therefore, the $\mathcal{E}_{\mathbb{A}}$, $\mathcal{E}_{\mathbb{A}_{\mathcal{S}}}$, $\mathcal{E}_{\mathbb{A}_{\mathcal{C}}}$, and $\mathcal{E}_{\mathbb{A}_{\mathcal{P}}}$ SKO

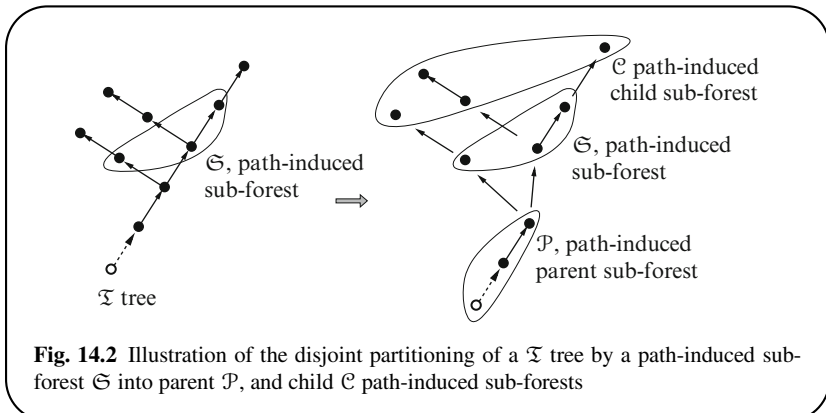


Fig. 14.2 Illustration of the disjoint partitioning of a Σ tree by a path-induced sub-forest S into parent P , and child C path-induced sub-forests

operators are all strictly lower-triangular. The system-level \mathcal{E}_A SKO operator can then be expressed in the following block-partitioned form:

$$\mathcal{E}_A = \begin{pmatrix} \mathcal{E}_{A_C} & \mathbf{0} & \mathbf{0} \\ \mathcal{B}_S & \mathcal{E}_{A_S} & \mathbf{0} \\ \mathbf{0} & \mathcal{E}_S & \mathcal{E}_{A_P} \end{pmatrix} \quad (14.2)$$

The SKO operators of the individual sub-forests form the block-diagonal elements of \mathcal{E}_A , with:

1. The \mathcal{E}_{A_C} SKO operator for C – with the smallest indices – being in the upper-left corner.
2. The \mathcal{E}_{A_P} SKO operator for P – with the largest indices – being in the lower-right corner.
3. The \mathcal{E}_{A_S} SKO operator for S being in the middle.
4. \mathcal{B}_S is a *connector* block, whose non-zero elements are for the parent/child edges between the nodes in S and their children in C .
5. \mathcal{E}_S is also a *connector* block, whose non-zero elements are for the parent/child edges between the nodes in P and their children in S .
6. The lower-left block is zero because none of the nodes in C are the children of the nodes in P .

It is worth pointing out that the block lower-triangular structure of \mathcal{E}_A in (14.2) continues to hold even under the more relaxed condition where the component systems are not necessarily canonical systems themselves, but are only canonical with respect to each other. In this situation, the index of a node in C whose parent is in S is required to be less than that of its parent. Similarly, the index of a node in S whose parent is in P is required to be less than that of its parent.

Since the component systems are sub-forests, their corresponding SPO operators are well-defined, and given by:

$$\mathbb{A}_{\mathcal{C}} \stackrel{\Delta}{=} (\mathbf{I} - \mathcal{E}_{\mathbb{A}_{\mathcal{C}}})^{-1}, \quad \mathbb{A}_{\mathfrak{S}} \stackrel{\Delta}{=} (\mathbf{I} - \mathcal{E}_{\mathbb{A}_{\mathfrak{S}}})^{-1}, \quad \mathbb{A}_{\mathcal{P}} \stackrel{\Delta}{=} (\mathbf{I} - \mathcal{E}_{\mathbb{A}_{\mathcal{P}}})^{-1} \quad (14.3)$$

The following lemma describes the corresponding partitioned structure of the system level SPO operator \mathbb{A} in terms of the SPO operators of the component systems.

Lemma 14.2 Partitioning of the \mathbb{A} SPO operator.

The \mathbb{A} SPO operator has the following partitioned structure corresponding to the partitioned structure of $\mathcal{E}_{\mathbb{A}}$ in (14.2):

$$\mathbb{A} = \begin{pmatrix} \mathbb{A}_{\mathcal{C}} & \mathbf{0} & \mathbf{0} \\ \mathbb{A}_{\mathfrak{S}} \mathcal{B}_{\mathfrak{S}} \mathbb{A}_{\mathcal{C}} & \mathbb{A}_{\mathfrak{S}} & \mathbf{0} \\ \mathbb{A}_{\mathcal{P}} (\mathcal{E}_{\mathfrak{S}} \mathbb{A}_{\mathfrak{S}} \mathcal{B}_{\mathfrak{S}}) \mathbb{A}_{\mathcal{C}} & \mathbb{A}_{\mathcal{P}} \mathcal{E}_{\mathfrak{S}} \mathbb{A}_{\mathfrak{S}} & \mathbb{A}_{\mathcal{P}} \end{pmatrix} \quad (14.4)$$

Observe that the SPO operators for the component sub-graphs are the block-diagonal elements of \mathbb{A} .

Proof: Start with the partitioned expression for $\mathcal{E}_{\mathbb{A}}$ in (14.2), and observe that

$$\begin{aligned} \mathbb{A}^{-1} &\stackrel{8.15}{=} (\mathbf{I} - \mathcal{E}_{\mathbb{A}}) \stackrel{14.2}{=} \begin{pmatrix} \mathbf{I} - \mathcal{E}_{\mathbb{A}_{\mathcal{C}}} & \mathbf{0} & \mathbf{0} \\ -\mathcal{B}_{\mathfrak{S}} & \mathbf{I} - \mathcal{E}_{\mathbb{A}_{\mathfrak{S}}} & \mathbf{0} \\ \mathbf{0} & -\mathcal{E}_{\mathfrak{S}} & \mathbf{I} - \mathcal{E}_{\mathbb{A}_{\mathcal{P}}} \end{pmatrix} \\ &\stackrel{14.3}{=} \begin{pmatrix} \mathbb{A}_{\mathcal{C}}^{-1} & \mathbf{0} & \mathbf{0} \\ -\mathcal{B}_{\mathfrak{S}} & \mathbb{A}_{\mathfrak{S}}^{-1} & \mathbf{0} \\ \mathbf{0} & -\mathcal{E}_{\mathfrak{S}} & \mathbb{A}_{\mathcal{P}}^{-1} \end{pmatrix} \end{aligned}$$

The result follows by verifying that the product of this expression for \mathbb{A}^{-1} , with \mathbb{A} in (14.4), is indeed the identity matrix. ■

If the \mathcal{P} sub-graph is empty, then the rows and columns for the parent sub-graph do not exist in the partitioned structure. Similarly, if \mathcal{C} is empty, then the corresponding columns and rows for the child sub-graph do not exist in the partitioned structure.

14.2.2 Partitioning of an SKO Model

The partitioning of the tree digraph for an SKO model also induces the following corresponding partitioning of the system-level block-diagonal H and M operators:

$$H = \begin{pmatrix} H_{\mathcal{C}} & \mathbf{0} & \mathbf{0} \\ \mathbf{0} & H_{\mathfrak{S}} & \mathbf{0} \\ \mathbf{0} & \mathbf{0} & H_{\mathcal{P}} \end{pmatrix} \quad \text{and} \quad M = \begin{pmatrix} M_{\mathcal{C}} & \mathbf{0} & \mathbf{0} \\ \mathbf{0} & M_{\mathfrak{S}} & \mathbf{0} \\ \mathbf{0} & \mathbf{0} & M_{\mathcal{P}} \end{pmatrix} \quad (14.5)$$

Observe that (H_C, A_C, M_C) , (H_S, A_S, M_S) , and (H_P, A_P, M_P) define SKO models for the component tree-topology multibody systems associated with the C , S , and P sub-graphs, respectively.

Exercise 14.2 Mass matrix invariance of the outer sub-system.

Consider an SKO model partitioned as in (14.2), but with empty C . That is, the system is partitioned into inner, P , and outer, S , SKO models. Show that the overall SKO model mass matrix has the following partitioned structure:

$$\mathcal{M} = \begin{pmatrix} \mathcal{M}_S & X \\ X^* & \mathcal{M}_P + Y \end{pmatrix} \quad (14.6)$$

where

$$\begin{aligned} \mathcal{M}_S &\triangleq H_S A_S M_S A_S^* H_S^*, \quad \mathcal{M}_P \triangleq H_P A_P M_P A_P^* H_P^* \\ X &\triangleq H_S A_S M_S A_S^* E_S A_P^* H_P^*, \quad Y \triangleq H_P A_P E_S A_S M_S A_S^* E_S A_P^* H_P^* \end{aligned} \quad (14.7)$$

■

Observe that \mathcal{M}_S and \mathcal{M}_P are the respective mass matrices for the S and P SKO models. Also, observe that the upper-right sub-block \mathcal{M}_S of \mathcal{M} is independent of quantities associated with the P sub-graph. This is consistent with a similar observation in Sect. 4.1.4 on page 63 that the elements of the mass matrix do not depend upon the properties or generalized coordinates of inboard bodies.

14.3 SPO Operator Sparsity Structure

Researchers have used system-level matrices and operators to analyze and exploit the sparsity structure of the mass matrix to develop efficient computational algorithms for the inverse and forward dynamics problems [23, 51, 132, 157]. In this section, we apply the partitioning techniques developed in Sect. 14.1 to study the sparsity structure of the SKO and SPO operators and the mass matrix for tree-topology systems.

14.3.1 Decomposition into Serial-Chain Segments

Topologically, serial-chain systems represent the simplest examples of tree systems, and serve as useful elemental units for studying the sparsity structure of matrices for tree-topology systems. Unlike trees, all bodies in a serial-chain are *related*, so that, for any pair of bodies, one is necessarily an ancestor of the other.

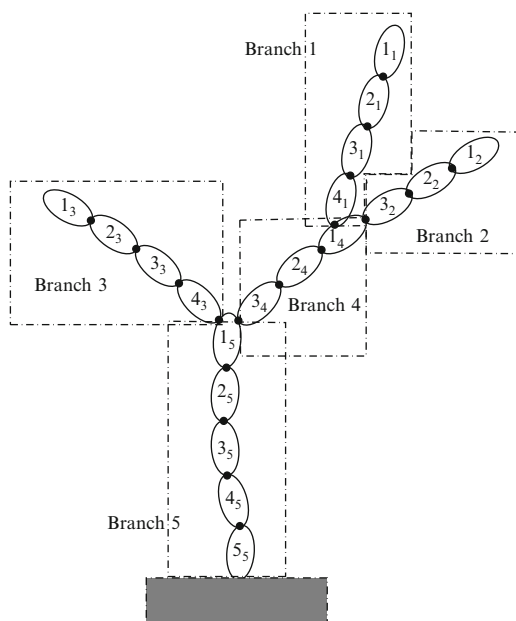
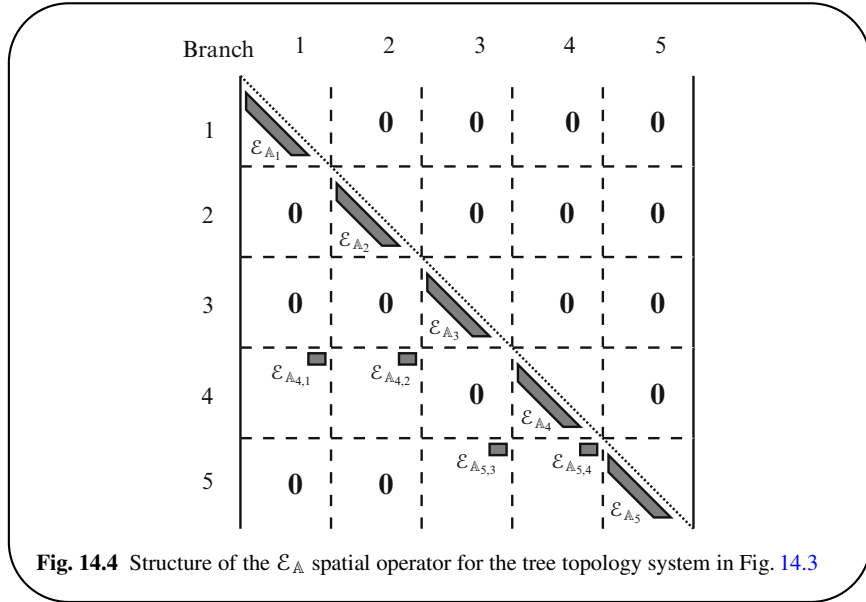


Fig. 14.3 Illustration of the decomposition of a tree-topology system into a tree of serial-chain branch segments

Since serial-chain segments are also path-induced sub-graphs, the partitioning technique from Sect. 14.1 can be used to successively decompose a tree system into disjoint serial-chain branch segments. Figure 14.3 illustrates the decomposition of a tree into branches 1 through 5, where each of the branches is a serial-chain segment. With such a decomposition, the tree system can be regarded as a new tree, with one node for each of the serial-chain branch segments. Thus, the new tree of branches is homeomorphic to the original tree.¹ The sparsity structure of the spatial operators (e.g., SPO, mass matrix) can be inferred directly from the structure of the tree of branches. Due to their serial-chain structure, the blocks associated with individual serial-chain branches are dense, with sparsity arising for branch pairs that are *unrelated*, i.e., are not connected by a directed path in the tree of branches.

¹ A pair of digraphs are said to be **homeomorphic** if they can both be obtained from a common digraph by a sequence of adding and removing nodes (also known as subdivisions) along serial segments [38, 183].



14.3.2 Sparsity Structure of the $\mathcal{E}_\mathbb{A}$ SKO Matrix

Assuming that the original tree is a canonical tree, Fig. 14.4 and (14.8) illustrate the decomposition of the system-level $\mathcal{E}_\mathbb{A}$ SKO operator in terms of the SKO operators for each of the serial-chain branch segments.

$$\mathcal{E}_\mathbb{A} = \begin{pmatrix} \mathcal{E}_{\mathbb{A}_1} & \mathbf{0} & \mathbf{0} & \mathbf{0} & \mathbf{0} \\ \mathbf{0} & \mathcal{E}_{\mathbb{A}_2} & \mathbf{0} & \mathbf{0} & \mathbf{0} \\ \mathbf{0} & \mathbf{0} & \mathcal{E}_{\mathbb{A}_3} & \mathbf{0} & \mathbf{0} \\ \mathcal{E}_{\mathbb{A}_{4,1}} & \mathcal{E}_{\mathbb{A}_{4,2}} & \mathbf{0} & \mathcal{E}_{\mathbb{A}_4} & \mathbf{0} \\ \mathbf{0} & \mathbf{0} & \mathcal{E}_{\mathbb{A}_{5,3}} & \mathcal{E}_{\mathbb{A}_{5,4}} & \mathcal{E}_{\mathbb{A}_5} \end{pmatrix} \quad (14.8)$$

\mathcal{E}_{ϕ_j} denotes the SKO operator for the j th branch segment. Also, when the k th branch is a child of the j th branch, the $\mathcal{E}_{\mathbb{A}_{j,k}}$ block denotes the non-zero connector block between them. All other blocks are zero. The structure of $\mathcal{E}_{\mathbb{A}_{j,k}}$ is as follows:

$$\mathcal{E}_{\mathbb{A}_{j,k}} \stackrel{\triangle}{=} \begin{pmatrix} \mathbf{0} & \cdots & \mathbf{0} & \mathbb{A}(1_j, n_k) \\ \mathbf{0} & \cdots & \mathbf{0} & \mathbf{0} \\ \vdots & \cdots & \vdots & \vdots \\ \mathbf{0} & \cdots & \mathbf{0} & \mathbf{0} \end{pmatrix} \quad (14.9)$$

where 1_j denotes the tip body on the j th branch that is the parent of the n_k base-body of the k th branch. This partitioned structure of $\mathcal{E}_{\mathbb{A}}$ is a generalization of the partitioned structure in (14.2).

14.3.3 Sparsity Structure of the \mathbb{A} Matrix

With $\phi_j \triangleq (\mathbf{I} - \mathcal{E}_{\phi_j})^{-1}$ denoting the SPO operator for the j th branch, the overall structure of the system level \mathbb{A} SPO operator for the Fig. 14.3 tree is illustrated in Fig. 14.5 and (14.10):

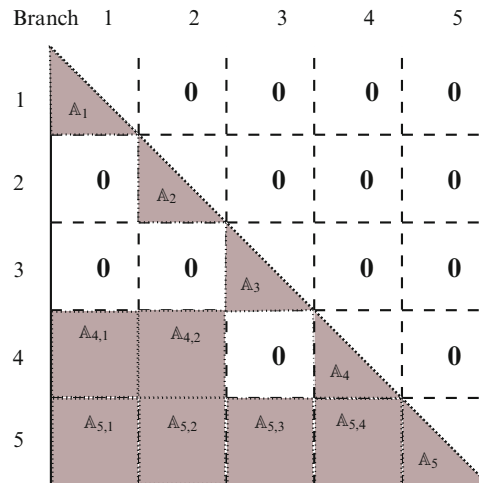


Fig. 14.5 Structure of the \mathbb{A} spatial operator for the tree-topology system in Fig. 14.3

$$\mathbb{A} = \begin{pmatrix} A_1 & 0 & 0 & 0 & 0 \\ 0 & A_2 & 0 & 0 & 0 \\ 0 & 0 & A_3 & 0 & 0 \\ A_{4,1} & A_{4,2} & 0 & A_4 & 0 \\ A_{5,1} & A_{5,2} & A_{5,3} & A_{5,4} & A_5 \end{pmatrix} \quad (14.10)$$

The $A_{j,k}$ blocks denote the non-zero connector block between *related* serial-chain segments. All other blocks are zero. This partitioned structure of $\mathcal{E}_{\mathbb{A}}$ is a generalization of the partitioned structure in (14.4). The general expression for the $A_{j,k}$ elements is:

$$\mathbb{A}_{j,k} = \mathbb{A}_j \mathcal{E}_{\mathbb{A}_{j,i}} \mathbb{A}_{i,k} \quad \text{with } i \in C(j), i \succeq k$$

In the above, $\mathbb{A}_{k,k} \equiv \mathbb{A}_k$.

14.3.4 Sparsity Structure of the \mathcal{M} Mass Matrix

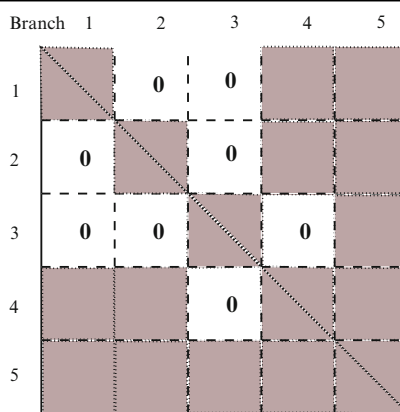


Fig. 14.6 Structure of the mass matrix \mathcal{M} for the tree topology system in Fig. 14.3

Based on the mass matrix decomposition discussed in Sect. 9.3.2, Fig. 14.6 illustrates the sparsity structure of the mass matrix for the tree-topology system in Fig. 14.3, partitioned according to its branch segments. As expected, the sparsity structure of the mass matrix mirrors the sparsity of the \mathbb{A} SPO operator in Fig. 14.5 and that of its transpose. The block-diagonal of the mass matrix contains dense blocks, one for each of the branch segments in the tree. The off-diagonal blocks are zero for *unrelated* segment pairs, i.e., ones where neither is the ancestor of the other. The remaining non-zero off-diagonal elements are for segment pairs that are related. This structure of the mass matrix is a generalization of the discussion on this subject in Sect. 9.3.2. The topology dependency of the mass matrix's sparsity structure was initially described in Rodriguez et al. [152]. Additional discussion on this topic can be found in Featherstone [51].

14.4 Aggregating Sub-Graphs

In this section we study transformations of a digraph by the process of aggregating sub-graphs into aggregated nodes.

14.4.1 Edge and Node Contractions

In graph theory, **edge-contraction** is referred to as the process of collapsing the node pair for an edge, into a single node [183]. The node and edge neighbors of the original pair of nodes become neighbors of the new *aggregated* node. Thus, the parent and children nodes of either of the original nodes (not including the node pair themselves) are the parent and children nodes of the aggregated node in the transformed digraph.

For a tree, the result of each such edge-contraction is once again a tree, with one fewer node. The edge-contraction process can be repeated to aggregate multiple edges in a tree. Thus, aggregating a sub-tree of a tree, using edge-contraction, results in a digraph that is also a tree. The process of creating a tree of branches digraph from a tree digraph in Sect. 14.3 is an example of aggregating serial-chain segments within the tree using edge-contraction.

Node-contraction is a more general concept that applies to pairs of nodes that are not necessarily connected by an edge. The node-contraction of a pair of nodes replaces the pair of nodes with a single aggregated node, where all the neighboring nodes and edges of the original pair become neighbors of the new aggregated node. Thus, edge-contraction is equivalent to node-contracting the node pair for an edge. Unlike edge-contracts, node-contracts generally do not preserve the tree property of a digraph. Node-contracts can be applied repeatedly to aggregate multiple nodes in a sub-graph. Formally, **aggregation** of a sub-graph is defined as the process of transforming a digraph by applying node-contraction to all the nodes in the sub-graph. This is illustrated in Fig. 14.7. It shows examples of trees transformed into multiply-connected and cyclic digraphs, following sub-graph aggregation. Later, we will examine the conditions under which the tree property is preserved following sub-graph aggregation.

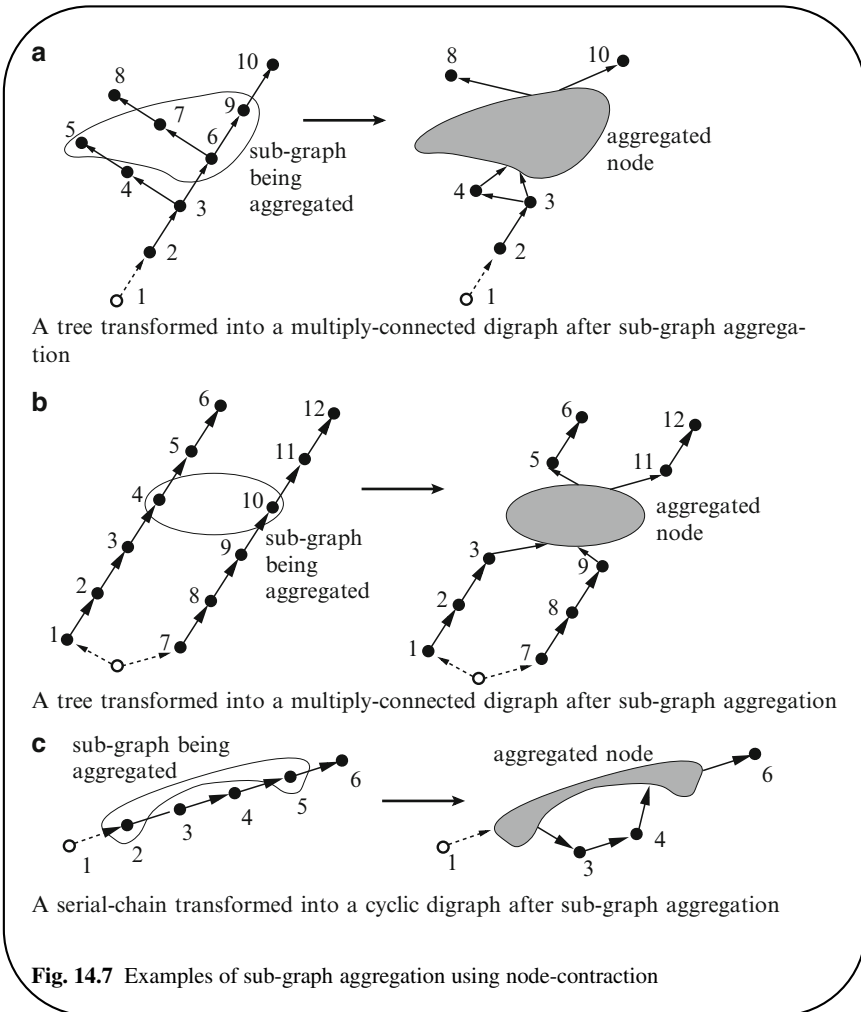
The following lemma shows that aggregating a sub-graph or its induced sub-graph result in the same transformed digraph.

Lemma 14.3 Aggregation of a sub-graph and its induced sub-graph.

Let \mathcal{S} denote the sub-graph of a digraph \mathfrak{T} . Then, the new digraph, $\mathfrak{T}_{\mathcal{S}}$, created by aggregating \mathcal{S} , is the same as the one obtained by aggregating the induced sub-graph, \mathcal{S}_I , i.e., $\mathfrak{T}_{\mathcal{S}} \equiv \mathfrak{T}_{\mathcal{S}_I}$.

Proof: \mathcal{S} and \mathcal{S}_I contain the same nodes, while the latter contains all the edges connecting the nodes as well. Node-contraction of a pair of nodes removes all edges connecting the node-pair. Thus, aggregating \mathcal{S} by node-contraction removes all edges connecting the nodes in \mathcal{S} , whether or not the edges are in \mathcal{S} itself. This implies that the aggregation of \mathcal{S} or \mathcal{S}_I results in the same transformed digraph. ■

One implication of this lemma is that the nodes and edges deleted from the transformed tree, after aggregating \mathcal{S} , are precisely the nodes and edges in the \mathcal{S}_I induced sub-graph of \mathcal{S} .



14.4.2 Tree Preservation After Sub-Graph Aggregation

Let \mathfrak{S} denote a sub-graph of a tree digraph, \mathfrak{T} . The aggregation of \mathfrak{S} results in a new $\mathfrak{T}_{\mathfrak{S}}$ digraph, where all the nodes associated with the nodes in \mathfrak{S} are replaced by a single node. We will henceforth refer to this aggregated node, as node \mathfrak{S} . Topologically, all the parent nodes of the \mathfrak{S} sub-graph, denoted $\wp(\mathfrak{S})$, are now the parents of node \mathfrak{S} , and all the children nodes of the \mathfrak{S} sub-graph, denoted $\mathcal{C}(\mathfrak{S})$, are now the children of node \mathfrak{S} . In general, $\mathfrak{T}_{\mathfrak{S}}$ obtained by this topological transformation will not be a tree.

The following defines the **aggregation condition** for sub-graphs.

Assumption 14.1 (Aggregation Condition). A sub-graph \mathfrak{S} , of a tree digraph \mathfrak{T} , is said to satisfy the aggregation condition if:

1. \mathfrak{S} is an induced sub-graph, i.e., $\mathfrak{S} \equiv \mathfrak{S}_I$.
2. $\wp(\mathfrak{S})$ contains exactly one node – one that is necessarily the ancestor of all the nodes in \mathfrak{S} .

The induced requirement for a \mathfrak{S} satisfying the aggregation condition is a mild one since Lemma 14.3 states that aggregating a sub-graph, or its induced sub-graph, lead to the same transformed digraph. Some examples of a tree sub-graph \mathfrak{S} , satisfying the aggregation condition, are:

- A single node
- A serial-chain segment
- A sub-tree

The following lemma shows that any sub-graph of a tree satisfying the aggregation condition is a path-induced sub-graph.

Lemma 14.4 Aggregation condition and path-induced sub-graphs.

If a sub-graph \mathfrak{S} of a \mathfrak{T} tree satisfies the aggregation condition, then it is path-induced, i.e., $\mathfrak{S} \equiv \mathfrak{S}_P$.

Proof: Since \mathfrak{S} satisfies the aggregation condition, it is an induced sub-graph. An induced sub-graph of a tree can differ from its path-induced sub-graph in the nodes and edges that lie on the paths connecting nodes in \mathfrak{S} .

First, let us consider the case where the node sets are the same. Since \mathfrak{S} is induced, there are no missing edges in \mathfrak{S} , and, therefore, even the set of edges are exactly the ones in the path-induced sub-graph. Hence, \mathfrak{S} and its path-induced sub-graph are the same.

Let us now consider the case when the node sets are *not* the same. Then, there exists a node k in the path-induced sub-graph \mathfrak{S}_P that is not in \mathfrak{S} . Node k must lie on a path connecting a pair of nodes in \mathfrak{S} . This implies that there is a node l on this path that belongs to $\wp(\mathfrak{S})$. However, since k is in the interior of the path, node l is not the ancestor of all the nodes in \mathfrak{S} . This contradicts the assumption that \mathfrak{S} satisfies the aggregation condition, which allows for only a single ancestor node for \mathfrak{S} . Hence, \mathfrak{S} must be a path-induced sub-graph. ■

The converse is not true, i.e., not all path-induced sub-graphs satisfy the aggregation condition. Figure 14.8 illustrates cases of path-induced sub-graphs that do, and do not, satisfy the aggregation condition.

The following lemma shows that the aggregation condition is a necessary and sufficient condition for the $\mathfrak{T}_{\mathfrak{S}}$ transformed digraph to be a tree.

Lemma 14.5 Tree property after sub-graph aggregation.

Let \mathfrak{S} denote an induced sub-graph of a tree digraph \mathfrak{T} . Let us assume that \mathfrak{S} is aggregated to create a new $\mathfrak{T}_{\mathfrak{S}}$ digraph with aggregated node \mathfrak{S} . Then, the aggregated $\mathfrak{T}_{\mathfrak{S}}$ digraph is a tree if and only if \mathfrak{S} satisfies the aggregation condition.

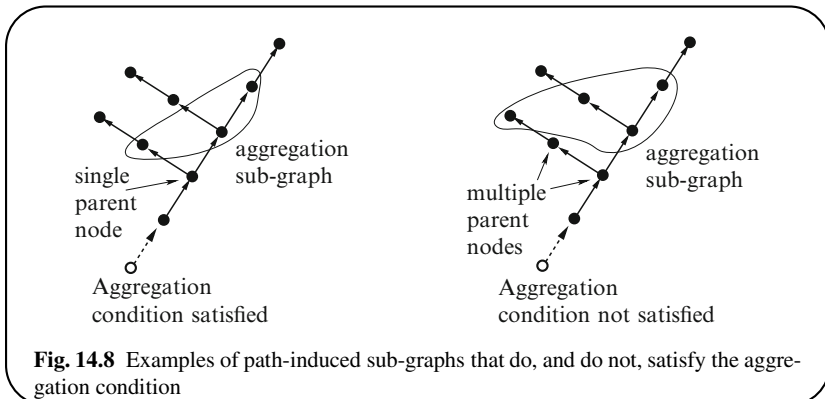


Fig. 14.8 Examples of path-induced sub-graphs that do, and do not, satisfy the aggregation condition

Proof:

1. First, let us assume the \mathcal{T}_S is indeed a tree, and we will show that $\varphi(S)$ must contain a single node. Since \mathcal{T}_S is a tree, all of its nodes, including node S , can have at most one parent. Thus, $\varphi(S)$ can have at most one node. The S sub-graph therefore satisfies the aggregation condition.
2. Now, let us consider the converse case, i.e., assume that $\varphi(S)$ contains a single node that is the ancestor for all the nodes in S . We will prove that \mathcal{T}_S must then be a tree. We need to show that \mathcal{T}_S is not a polytree, is not multiply-connected, and does not have directed cycles.
 - a. To show that \mathcal{T}_S is not a polytree, we need to focus only on node S and show that it cannot have multiple parents. This follows directly from the assumption that $\varphi(S)$ contains only one node.
 - b. To show that \mathcal{T}_S is not multiply-connected, we need to focus only on the node S and show that there is no node in \mathcal{T}_S from which there is more than one directed path to the node S . Since \mathcal{T} is a tree, it has no multiply-connected nodes. Thus, the only way for node S to be multiply-connected is for multiple paths to end at node S . This would mean that the node S has multiple parents – one from each of the paths that end on it. This would contradict the assumption that $\varphi(S)$ contains a single node.
 - c. Now, we show that \mathcal{T}_S cannot have directed cycles. Again, we need to focus on node S , and show that it cannot be part of a directed cycle. Assume that such a cycle exists. This implies that there are nodes $k, j \in S$, and a node $i \notin S$ such that $k \succ i \succ j$. In other words, there is a path from k to j containing node i . This would imply that there is a node, l , on the path from i to j that is a parent node for S . Since $\varphi(S)$ contains only one node, l must be this ancestor node. This would imply that node l , and hence node i , is an ancestor of k . However we know that k is an ancestor of i . Hence, node S is not part of any directed cycles.

■

Lemma 14.5 shows that preservation of the tree property after sub-graph aggregation requires that the sub-graph satisfy the aggregation condition. This result is not surprising, once we recall that edge-contractions preserve the tree property, and that the aggregation of a path-induced sub-graph is equivalent to applying edge-contraction to all the edges in the sub-graph,

14.4.3 The \mathfrak{S}_A Aggregation Sub-Graph

The **aggregation sub-graph**, for a sub-graph \mathfrak{S} of a tree, is defined as the minimal sub-graph containing \mathfrak{S} that also satisfies the aggregation condition. The aggregation sub-graph of a sub-graph \mathfrak{S} is denoted \mathfrak{S}_A .

Lemma 14.6 Properties of \mathfrak{S}_A .

1. \mathfrak{S}_A is a path-induced sub-graph.
2. The following containment relation holds

$$\mathfrak{S} \subseteq \mathfrak{S}_I \subseteq \mathfrak{S}_P \subseteq \mathfrak{S}_A \quad (14.11)$$

3. \mathfrak{S}_A is the sub-forest obtained by deleting the root node from the smallest sub-tree containing \mathfrak{S} .

Proof:

1. By definition, \mathfrak{S}_A satisfies the aggregation condition and, hence, by Lemma 14.4, it is path-induced.
2. By definition, $\mathfrak{S} \subseteq \mathfrak{S}_A$. Hence, the path-induced sub-graph of \mathfrak{S} , \mathfrak{S}_P , is contained in the path-induced sub-graph of \mathfrak{S}_A , which is \mathfrak{S}_A itself. This establishes the last containment in (14.11). The rest are restatements of (14.1).
3. Since \mathfrak{S}_A satisfies the aggregation condition, it has a single parent node. Thus, with the parent node added in, the new sub-graph is a sub-tree. The minimality of the sub-tree follows from the definition of a aggregation sub-graph, which is required to be minimal.

■

While aggregation of a sub-graph \mathfrak{S} will generally not preserve the tree property, aggregating \mathfrak{S}_A instead ensures that the aggregated digraph is a tree.

14.5 Transforming SKO Models Via Aggregation

14.5.1 SKO Operators After Body Aggregation

Let \mathfrak{T} be a tree digraph associated with a multibody system. We assume without loss in generality that it is canonical. Let \mathfrak{S} denote a sub-graph satisfying the aggregation

condition. By Lemma 14.5, the aggregated $\mathfrak{T}_{\mathfrak{S}}$ digraph, with aggregated node \mathfrak{S} , is also a tree. Let us now develop an SKO model for the system with the $\mathfrak{T}_{\mathfrak{S}}$ aggregated tree.

To define SKO operators for $\mathfrak{T}_{\mathfrak{S}}$, we first need to assign weight dimensions to the nodes in $\mathfrak{T}_{\mathfrak{S}}$. All nodes unaffected by the aggregation process inherit the weight dimensions from the nodes in \mathfrak{T} . The weight dimension for node \mathfrak{S} is defined as the sum of the weight dimensions of all the nodes in the \mathfrak{S} sub-graph, i.e.,

$$m_{\mathfrak{S}} \triangleq \sum_{k \in \mathfrak{S}} m_k \quad (14.12)$$

Since the \mathfrak{S} sub-graph satisfies the aggregation condition it is path-induced, as shown in Lemma 14.4. From Lemma 14.1, \mathfrak{S} induces a disjoint partitioning of \mathfrak{T} into path-induced parent \mathcal{P} and child \mathcal{C} sub-graphs respectively. These partitioned sub-graphs allow us to express the \mathcal{E}_{ϕ} SKO operator for \mathfrak{T} in the partitioned form shown in (14.2):

$$\mathcal{E}_{\mathbb{A}} = \begin{pmatrix} \mathcal{E}_{\mathbb{A}_{\mathcal{C}}} & \mathbf{0} & \mathbf{0} \\ \mathcal{B}_{\mathfrak{S}} & \mathcal{E}_{\mathbb{A}_{\mathfrak{S}}} & \mathbf{0} \\ \mathbf{0} & E_{\mathfrak{S}} & \mathcal{E}_{\mathbb{A}_{\mathcal{P}}} \end{pmatrix} \quad (14.13)$$

Lemma 14.7 SKO operator for $\mathfrak{T}_{\mathfrak{S}}$ tree.

With \mathfrak{S} satisfying the aggregation condition, define the $\mathcal{E}_{\mathbb{A}_a}$ matrix using the partitioned sub-blocks of (14.13) as follows:

$$\mathcal{E}_{\mathbb{A}_a} \triangleq \begin{pmatrix} \mathcal{E}_{\mathbb{A}_{\mathcal{C}}} & \mathbf{0} & \mathbf{0} \\ \mathcal{B}_{\mathfrak{S}} & \mathbf{0} & \mathbf{0} \\ \mathbf{0} & E_{\mathfrak{S}} A_{\mathfrak{S}} & \mathcal{E}_{\mathbb{A}_{\mathcal{P}}} \end{pmatrix} \quad (14.14)$$

The following facts hold for $\mathcal{E}_{\mathbb{A}_a}$:

1. $\mathcal{E}_{\mathbb{A}_a}$ is an SKO operator for the original tree, \mathfrak{T} .
2. $\mathcal{E}_{\mathbb{A}_a}$ is an SKO operator for the aggregated tree, $\mathfrak{T}_{\mathfrak{S}}$.

Proof:

1. Since \mathfrak{S} satisfies the aggregation condition, $\wp(\mathfrak{S})$ contains a single node. Let us denote this node as node j . Comparing the expression for $\mathcal{E}_{\mathbb{A}_a}$ in (14.14) with that of $\mathcal{E}_{\mathbb{A}}$ in (14.13), the only term that needs further examination to establish the SKO property is the $E_{\mathfrak{S}} A_{\mathfrak{S}}$ block, which differs from the $E_{\mathfrak{S}}$ block. Recall that the $E_{\mathfrak{S}}$ connector block contains non-zero entries for the edges connecting nodes in \mathcal{P} to nodes in \mathfrak{S} sub-graphs. Therefore, $E_{\mathfrak{S}}$ has the form

$$E_{\mathfrak{S}} = \sum_{l \in \wp(\mathfrak{S})} e_l \sum_{\substack{k \in \mathfrak{S} \\ \wp(k)=l}} A(l, k) e_k^* = e_j \sum_{\substack{k \in \mathfrak{S} \\ \wp(k)=j}} A(j, k) e_k^* \quad (14.15)$$

In the above equations, we have taken some notational liberties; the e_x vectors represent appropriate size vectors for the \mathcal{S} and \mathcal{P} sub-graphs, instead of the full-sized ones for the \mathfrak{T} tree.

It follows that

$$E_{\mathcal{S}} \mathbb{A}_{\mathcal{S}} \stackrel{14.15}{=} e_j \sum_{\substack{k, i \in \mathcal{S} \\ \varphi(k)=j}} \mathbb{A}(j, k) e_k^* \mathbb{A}_{\mathcal{S}} \quad (14.16)$$

The $e_k^* \mathbb{A}_{\mathcal{S}}$ product is the k th row of $\mathbb{A}_{\mathcal{S}}$. Since $\mathbb{A}_{\mathcal{S}}$ is an SPO operator, its k th row $\mathbb{A}(k, i)$ entry is non-zero only when node i is a descendant of the k th node. Hence, (14.16) can be re-expressed as

$$E_{\mathcal{S}} \mathbb{A}_{\mathcal{S}} \stackrel{14.16}{=} e_j \sum_{\substack{k \in \mathcal{S} \\ \varphi(k)=j, k \succ i}} \mathbb{A}(j, k) \mathbb{A}(k, i) e_i = e_j \sum_{\substack{i \in \mathcal{S} \\ j \succ i}} \mathbb{A}(j, i) e_i^* \quad (14.17)$$

In the last expression, $j \succ i$, denotes the condition that the j th node is an ancestor

of the i th node. From (14.17), it is clear that only the j th row of $E_{\mathcal{S}} \mathbb{A}_{\mathcal{S}}$ is non-zero. The only non-zero entries in this row are for nodes in \mathcal{S} that are descendants of the j th node.² Thus, each column of $E_{\mathcal{S}} \mathbb{A}_{\mathcal{S}}$, has at most a single non-zero element, and since the central block of $\mathcal{E}_{\mathbb{A}_a}$ is zero, this implies that the same column has only a single non-zero entry in the full $\mathcal{E}_{\mathbb{A}_a}$ matrix as well. Thus, the single non-zero entry per column requirement for an SKO operator for \mathfrak{T} is satisfied. Hence, $\mathcal{E}_{\mathbb{A}_a}$ is an SKO operator for \mathfrak{T} .

2. We have seen that $\mathcal{E}_{\mathbb{A}_a}$ is an SKO operator for \mathfrak{T} . For $\mathfrak{T}_{\mathcal{S}}$, the central rows and columns of $\mathcal{E}_{\mathbb{A}_a}$ correspond to the single \mathcal{S} node in the $\mathfrak{T}_{\mathcal{S}}$ tree. For $\mathcal{E}_{\mathbb{A}_a}$ to be an SKO operator for $\mathfrak{T}_{\mathcal{S}}$, we need to show that it satisfies the SKO operator structural requirements, as represented by (8.12). That is, $E_{\mathcal{S}} \mathbb{A}_{\mathcal{S}}$ must be of the form $e_j X$ for some X . Equation (14.17) satisfies this requirement, and, thus, $\mathcal{E}_{\mathbb{A}_a}$ is an SKO operator for $\mathfrak{T}_{\mathcal{S}}$. ■

Having derived the expression for an $\mathcal{E}_{\mathbb{A}_a}$ SKO operator for $\mathfrak{T}_{\mathcal{S}}$, the following lemma derives the expression for the corresponding SPO operator for $\mathfrak{T}_{\mathcal{S}}$.

Lemma 14.8 The \mathbb{A}_a SPO operator for the $\mathfrak{T}_{\mathcal{S}}$ tree.

Using the same assumptions and notation from Lemma 14.7, the SPO operator, \mathbb{A}_a , for $\mathfrak{T}_{\mathcal{S}}$ is given by the following expression:

² In fact all nodes in \mathcal{S} are descendants of j and therefore the row is fully populated.

$$\mathbb{A}_a \triangleq \mathfrak{J}_a \mathbb{A} \stackrel{14.4}{=} \begin{pmatrix} \mathbb{A}_{\mathcal{C}} & \mathbf{0} & \mathbf{0} \\ \mathcal{B}_{\mathfrak{S}} \mathbb{A}_{\mathcal{C}} & \mathbf{I} & \mathbf{0} \\ \mathbb{A}_{\mathcal{P}} (\mathcal{E}_{\mathfrak{S}} \mathbb{A}_{\mathfrak{S}} \mathcal{B}_{\mathfrak{S}}) \mathbb{A}_{\mathcal{C}} & \mathbb{A}_{\mathcal{P}} \mathcal{E}_{\mathfrak{S}} \mathbb{A}_{\mathfrak{S}} & \mathbb{A}_{\mathcal{P}} \end{pmatrix} \quad (14.18)$$

where $\mathfrak{J}_a \triangleq \begin{pmatrix} \mathbf{I} & \mathbf{0} & \mathbf{0} \\ \mathbf{0} & \mathbb{A}_{\mathfrak{S}}^{-1} & \mathbf{0} \\ \mathbf{0} & \mathbf{0} & \mathbf{I} \end{pmatrix}$

Proof: Since Lemma 14.8 established $\mathcal{E}_{\mathbb{A}_a}$ as an SKO operator for the $\mathfrak{T}_{\mathfrak{S}}$ tree, we need to show that $\mathbb{A}_a = (\mathbf{I} - \mathcal{E}_{\mathbb{A}_a})^{-1}$ for it to be an SPO operator for $\mathfrak{T}_{\mathfrak{S}}$. Now

$$\begin{aligned} (\mathbf{I} - \mathcal{E}_{\mathbb{A}_a}) &\stackrel{14.2}{=} \begin{pmatrix} \mathbf{I} - \mathcal{E}_{\mathbb{A}_{\mathcal{C}}} & \mathbf{0} & \mathbf{0} \\ -\mathcal{B}_{\mathfrak{S}} & \mathbf{I} & \mathbf{0} \\ \mathbf{0} & -\mathcal{E}_{\mathfrak{S}} \mathbb{A}_{\mathfrak{S}} & \mathbf{I} - \mathcal{E}_{\mathbb{A}_{\mathcal{P}}} \end{pmatrix} \\ &\stackrel{14.3}{=} \begin{pmatrix} \mathbb{A}_{\mathcal{C}}^{-1} & \mathbf{0} & \mathbf{0} \\ -\mathcal{B}_{\mathfrak{S}} & \mathbf{I} & \mathbf{0} \\ \mathbf{0} & -\mathcal{E}_{\mathfrak{S}} \mathbb{A}_{\mathfrak{S}} & \mathbb{A}_{\mathcal{P}}^{-1} \end{pmatrix} \end{aligned}$$

The result follows by verifying that the product of the above, with \mathbb{A}_a in (14.18), is the identity matrix. ■

Node \mathfrak{S} in $\mathfrak{T}_{\mathfrak{S}}$ contains all the bodies associated with the nodes in \mathfrak{S} . Unlike regular rigid links, the geometry of node \mathfrak{S} is variable, and depends on the hinge coordinates of the component links within the sub-graph \mathfrak{S} . Such variable geometry bodies have been used in other dynamics modeling contexts [42, 68, 186]. The transformation of a tree digraph into a tree of serial-chain branch segments, discussed in Sect. 14.3 on page 278, is an example of transforming one tree digraph into another by aggregating the serial-chain segment sub-graphs.

14.5.2 SKO Model for the $\mathfrak{T}_{\mathfrak{S}}$ Aggregated Tree

The key difference between the aggregated and the original tree is that the former treats the set of bodies in \mathfrak{S} as a single body. The aggregation process provides a way of transforming and *sub-structuring* SKO models for tree-topology multibody systems into coarser SKO models. The aggregation process induces the following partitioning of the $\dot{\theta}$, \mathcal{V} , \mathfrak{f} and \mathcal{T} stacked vectors:

$$\dot{\theta} = \begin{bmatrix} \dot{\theta}_{\mathcal{C}} \\ \dot{\theta}_{\mathfrak{S}} \\ \dot{\theta}_{\mathcal{P}} \end{bmatrix}, \quad \mathcal{V} = \begin{bmatrix} \mathcal{V}_{\mathcal{C}} \\ \mathcal{V}_{\mathfrak{S}} \\ \mathcal{V}_{\mathcal{P}} \end{bmatrix}, \quad \mathfrak{f} = \begin{bmatrix} \mathfrak{f}_{\mathcal{C}} \\ \mathfrak{f}_{\mathfrak{S}} \\ \mathfrak{f}_{\mathcal{P}} \end{bmatrix}, \quad \mathcal{T} = \begin{bmatrix} \mathcal{T}_{\mathcal{C}} \\ \mathcal{T}_{\mathfrak{S}} \\ \mathcal{T}_{\mathcal{P}} \end{bmatrix} \quad (14.19)$$

For the $\mathfrak{T}_{\mathfrak{S}}$ aggregated tree, the $\mathcal{V}_{\mathfrak{S}}$, $\dot{\theta}_{\mathfrak{S}}$, etc., sub-vectors of the \mathcal{V} and $\dot{\theta}$ stacked vectors correspond to the single \mathfrak{S} aggregate link. This partitioning of the

system-level $\dot{\theta}$ and \mathcal{V} stacked vectors extends to other stacked vectors such as the Coriolis spatial accelerations vector α , the gyroscopic spatial forces vector b , and to the other spatial operators.

Lemma 14.9 shows that the transformed system with the aggregated tree possesses a well-defined SKO model, and defines the equations of motion for the model.

Lemma 14.9 SKO model for an aggregated tree.

Let (H, \mathbb{A}, M) denote an SKO model with tree digraph \mathfrak{T} . Let \mathfrak{S} be a sub-graph of \mathfrak{T} satisfying the aggregation condition. Then the (H_a, \mathbb{A}_a, M) spatial operators define an SKO model for the $\mathfrak{T}_{\mathfrak{S}}$ aggregated tree, where

$$H_a \triangleq H \mathfrak{J}_a^{-1} \stackrel{14.18}{=} \begin{pmatrix} H_C & \mathbf{0} & \mathbf{0} \\ \mathbf{0} & H_{\mathfrak{S}} & \mathbf{0} \\ \mathbf{0} & \mathbf{0} & H_P \end{pmatrix} \quad \text{and} \quad \underline{H}_{\mathfrak{S}} \triangleq H_{\mathfrak{S}} \mathbb{A}_{\mathfrak{S}} \quad (14.20)$$

H_a defines the new joint map matrix for the $\mathfrak{T}_{\mathfrak{S}}$ aggregated tree, with H_C , $H_{\mathfrak{S}}$, and H_P denoting the component joint map matrices as defined in (14.5). The transformed version of the equations of motion from (9.1) are given by:

$$\begin{aligned} \mathcal{V} &= \mathbb{A}_a^* H_a^* \dot{\theta} \\ \alpha &= \mathbb{A}_a^* (H_a^* \ddot{\theta} + \underline{\alpha}), \quad \text{where} \quad \underline{\alpha} \triangleq \mathfrak{J}_a^{-*} \alpha = \begin{bmatrix} \alpha_C \\ \alpha_{\mathfrak{S}} \\ \alpha_P \end{bmatrix}, \quad \alpha_{\mathfrak{S}} \triangleq \mathbb{A}_{\mathfrak{S}}^* \alpha_{\mathfrak{S}} \\ f &= \mathbb{A}_a (M \alpha + b), \quad \text{where} \quad \underline{f} \triangleq \mathfrak{J}_a f = \begin{bmatrix} f_C \\ f'_{\mathfrak{S}} \\ f_P \end{bmatrix}, \quad f'_{\mathfrak{S}} \triangleq \mathbb{A}_{\mathfrak{S}}^{-1} f_{\mathfrak{S}} \\ \mathcal{T} &= H_a \underline{f} \end{aligned} \quad (14.21)$$

Thus,

$$\mathcal{T} = \mathcal{M} \ddot{\theta} + \mathcal{C} \quad (14.22)$$

with

$$\mathcal{M} = H_a \mathbb{A}_a M \mathbb{A}_a^* H_a^* \in \mathcal{R}^{N \times N} \quad \text{and} \quad \mathcal{C} \triangleq H_a \mathbb{A}_a (M \mathbb{A}_a^* \underline{\alpha} + b) \in \mathcal{R}^N \quad (14.23)$$

The mass matrix expression above represents the Newton–Euler operator factorization of the mass matrix for the SKO model of the aggregated system.

Proof: Lemma 14.8 established that \mathbb{A}_a is the SPO operator for $\mathfrak{T}_{\mathfrak{S}}$. With the central row and column of H_a corresponding to node \mathfrak{S} in $\mathfrak{T}_{\mathfrak{S}}$, H_a is block-diagonal for $\mathfrak{T}_{\mathfrak{S}}$. Lastly, M has remained unchanged in going from \mathfrak{T} to $\mathfrak{T}_{\mathfrak{S}}$. Thus, the structural requirements 1 through 4 for an SKO model in Sect. 9.1.1 on page 160, are satisfied for the $\mathfrak{T}_{\mathfrak{S}}$ tree, by the (H_a, \mathbb{A}_a, M) operators.

The equations of motion in (14.21) follow by substituting the expressions for H_a and \mathbb{A}_a from (14.18) and (14.20) in the original equations of motion in 9.1 on page 160. ■

Observe that, while $H_{\mathfrak{S}}$ is block-diagonal, $H_{\mathfrak{S}} = H_{\mathfrak{S}} \mathbb{A}_{\mathfrak{S}}$ is no longer block-diagonal. Consequently, H_a is not block-diagonal for \mathfrak{T} and the (H_a, \mathbb{A}_a, M) operators do *not* satisfy the structural requirements for an SKO model for the original \mathfrak{T} . Nevertheless, the above lemma shows that these operators do satisfy the SKO model structural requirements for the $\mathfrak{T}_{\mathfrak{S}}$ tree. This allows all of the SKO formulation techniques and algorithms from Chap. 9, including mass matrix factorization and inversion, to be applied to the SKO model of the aggregated tree.

Exercise 14.3 Mass matrix invariance with aggregation.

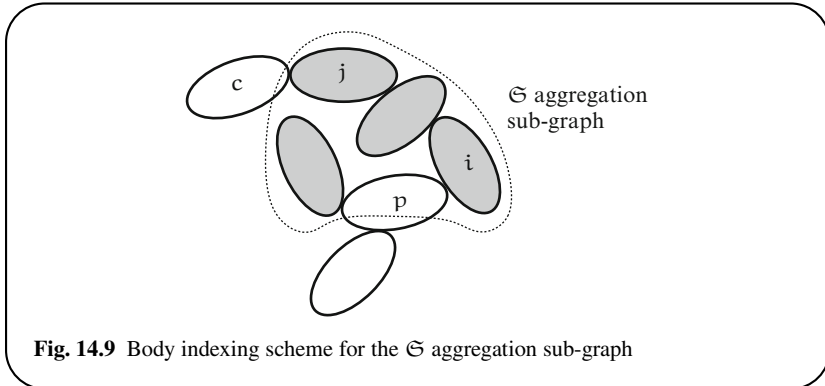
Show that the mass matrix, M , and the Coriolis vector, C , of a tree-topology system remain unchanged after sub-graph aggregation. In other words, show that the expressions for M and C in (14.23) agree with the quantities defined in (9.3), i.e.,

$$\begin{aligned} M &= H \mathbb{A} M \mathbb{A}^* H^* = H_a \mathbb{A}_a M \mathbb{A}_a^* H_a^* \\ C &= H \mathbb{A} (M \mathbb{A}^* \mathfrak{a} + \mathfrak{b}) = H_a \mathbb{A}_a (M \mathbb{A}_a^* \mathfrak{a} + \mathfrak{b}) \end{aligned} \quad (14.24)$$

The aggregation process provides a way to develop alternative SKO models for a system. As observed earlier, the tree of serial-chain branches used in Sect. 14.3 to study the sparsity structure of the SPO operator and the mass matrix of a standard SKO model, is a tree obtained by aggregating all the serial branch segments. The discussion in this section shows how to develop the sub-structured SKO model for this aggregated tree. ■

14.6 Aggregation Relationships at the Component Level

In this section, we take a closer look at the component level recursive relationships for the aggregated SKO model. The parent link for the \mathfrak{S} aggregate link is denoted p , while c denotes a child body of \mathfrak{S} . Also, i denotes a body in the \mathfrak{S} sub-graph that is a child of p , i.e., a base-body in the \mathfrak{S} sub-graph. Body j in the \mathfrak{S} sub-graph denotes the parent of body c . This notation is illustrated in Fig. 14.9. We focus on the component-level relationships involving the aggregated body and its adjacent bodies since these relationships are the only ones effected by the aggregation process. The relationships involving non-aggregated links alone remain unchanged.



14.6.1 Velocity Relationships

Recall the following link-to-link spatial velocity recursive relationship from (9.10) for bodies in the \mathfrak{T} tree:

$$\mathcal{V}(k) = \mathbb{A}^*(\varphi(k), k)\mathcal{V}(\varphi(k)) + H^*(k)\dot{\theta}(k) \quad (14.25)$$

We will use this relationship to derive velocity relationships for the \mathfrak{S} aggregated body and its adjacent bodies in the $\mathfrak{T}_{\mathfrak{S}}$ tree. First, let us develop a recursive relationship for $\mathcal{V}_{\mathfrak{S}}$. Assembling (14.25) for all the links in \mathfrak{S} , we obtain the following relationship for $\mathcal{V}_{\mathfrak{S}}$

$$\mathcal{V}_{\mathfrak{S}} = \mathcal{E}_{\mathbb{A}_{\mathfrak{S}}}^* \mathcal{V}_{\mathfrak{S}} + E_{\mathfrak{S}}^* \mathcal{V}(p) + H_{\mathfrak{S}}^* \dot{\theta}_{\mathfrak{S}} \quad \text{where } E_{\mathfrak{S}} \triangleq [\mathbf{0}, \mathbf{0}, \dots, \mathbb{A}(p, i)] \quad (14.26)$$

This implicit relationship for $\mathcal{V}_{\mathfrak{S}}$ involves quantities associated with nodes in the $\mathfrak{T}_{\mathfrak{S}}$ aggregated tree instead of nodes in the \mathfrak{T} spanning tree. $E_{\mathfrak{S}}$ is the connector block matrix for the coupling between the \mathfrak{S} aggregated body and its p parent body. While the (14.26) expression for $E_{\mathfrak{S}}$ shows only a single $\mathbb{A}(p, i)$ non-zero entry, more generally, it will have a non-zero entry for each base-body in \mathfrak{S} at locations corresponding to the indices for the base-bodies. Since $\mathcal{E}_{\mathbb{A}_{\mathfrak{S}}}$ is an SKO operator, we can use the $\mathbb{A}_{\mathfrak{S}} \triangleq (I - \mathcal{E}_{\mathbb{A}_{\mathfrak{S}}})^{-1}$ expression from (14.3) to convert the implicit form of (14.26) into the following explicit expression:

$$\mathcal{V}_{\mathfrak{S}} \stackrel{14.3}{=} \mathbb{A}_{\mathfrak{S}}^* E_{\mathfrak{S}}^* \mathcal{V}(p) + \mathbb{A}_{\mathfrak{S}}^* H_{\mathfrak{S}}^* \dot{\theta}_{\mathfrak{S}} \stackrel{14.20}{=} \mathbb{A}_{\mathfrak{S}}^* E_{\mathfrak{S}}^* \mathcal{V}(p) + \underline{H}_{\mathfrak{S}}^* \dot{\theta}_{\mathfrak{S}} \quad (14.27)$$

The form of (14.27) is similar to (14.25). It defines how the spatial velocity of the parent body p couples into the aggregated body \mathfrak{S} . From this expression, we infer that $E_{\mathfrak{S}} \mathbb{A}_{\mathfrak{S}}$ is the $\mathbb{A}(p, \mathfrak{S})$ SKO weight matrix associated with the \mathfrak{S} and p adjacent body pair in $\mathfrak{T}_{\mathfrak{S}}$, i.e.,

$$\mathbb{A}(p, \mathfrak{S}) \equiv E_{\mathfrak{S}} \mathbb{A}_{\mathfrak{S}} \quad (14.28)$$

Observe that the $E_{\mathfrak{S}} A_{\mathfrak{S}}$ weight matrix also appears in the partitioned expression for the $\mathcal{E}_{\mathbb{A}}$ aggregated SKO operator in (14.14).

The $\mathcal{V}(c)$ spatial velocity of the child link c depends on the spatial velocity of its parent link j in the \mathfrak{S} sub-graph. The (14.25) relationship for link c can be restated as:

$$\mathcal{V}(c) = \mathcal{B}_c^* \mathcal{V}_{\mathfrak{S}} + H^*(c) \dot{\theta}(c) \quad \text{where} \quad \mathcal{B}_c \triangleq \begin{bmatrix} A(j, c) \\ \mathbf{0} \\ \vdots \\ \mathbf{0} \end{bmatrix} \quad (14.29)$$

The form of this new relationship is similar to (14.25) and defines how the velocities of the \mathfrak{S} parent body couple into the child body c . Equation (14.29) involves quantities associated with nodes in the $\mathfrak{T}_{\mathfrak{S}}$ aggregated tree instead of quantities associated with nodes in the \mathfrak{T} spanning tree. \mathcal{B}_c is the connector block matrix for the coupling between the c body and its parent body \mathfrak{S} . From this expression, we infer that \mathcal{B}_c is the $A(\mathfrak{S}, c)$ SKO weight matrix associated with the c and \mathfrak{S} adjacent pair of bodies, i.e.,

$$A(\mathfrak{S}, c) \equiv \mathcal{B}_c \quad (14.30)$$

There is one \mathcal{B}_c matrix for each child body c in $C(\mathfrak{S})$. The \mathcal{B}_c matrices for all the children bodies make up the columns of the $\mathcal{B}_{\mathfrak{S}}$ matrix in the partitioned expression for $\mathcal{E}_{\mathbb{A}}$ in (14.14).

Gathering together the expressions in (14.27) and (14.29), the spatial velocity relationship between the \mathfrak{S} aggregate link and its adjacent links p and c are as follows:

$$\begin{aligned} \mathcal{V}_{\mathfrak{S}} &\stackrel{14.27, 14.28}{=} A^*(p, \mathfrak{S}) \mathcal{V}(p) + H_{\mathfrak{S}}^* \dot{\theta}_{\mathfrak{S}} \\ \mathcal{V}(c) &\stackrel{14.29, 14.30}{=} A^*(\mathfrak{S}, c) \mathcal{V}_{\mathfrak{S}} + H^*(c) \dot{\theta}(c) \end{aligned} \quad (14.31)$$

14.6.2 Acceleration Relationships

Now recall the following link-to-link spatial acceleration relationship from (9.10) for bodies in the \mathfrak{T} tree:

$$\alpha(k) = A^*(\varphi(k), k) \alpha(\varphi(k)) + H^*(k) \ddot{\theta}(k) + a(k) \quad (14.32)$$

Assembling (14.32) for all the links in \mathfrak{S} , we obtain the following implicit relationship for $\alpha_{\mathfrak{S}}$:

$$\alpha_{\mathfrak{S}} = \mathcal{E}_{\mathbb{A}_{\mathfrak{S}}}^* \alpha_{\mathfrak{S}} + E_{\mathfrak{S}}^* \alpha(p) + H_{\mathfrak{S}}^* \ddot{\theta}_{\mathfrak{S}} + a_{\mathfrak{S}}$$

Once again using the $A_{\mathfrak{S}} \triangleq (I - \mathcal{E}_{\mathbb{A}_{\mathfrak{S}}})^{-1}$ expression from (14.3), we can convert the implicit form above into the following explicit expression:

$$\begin{aligned}\alpha_{\mathfrak{S}} &\stackrel{14.3}{=} \mathbb{A}_{\mathfrak{S}}^* E_{\mathfrak{S}}^* \alpha(p) + \mathbb{A}_{\mathfrak{S}}^* H_{\mathfrak{S}}^* \ddot{\theta}_{\mathfrak{S}} + \mathbb{A}_{\mathfrak{S}}^* a_{\mathfrak{S}} \\ &\stackrel{14.21, 14.20, 14.28}{=} A^*(p, \mathfrak{S}) \alpha(p) + H_{\mathfrak{S}}^* \ddot{\theta}_{\mathfrak{S}} + a_{\mathfrak{S}}\end{aligned}\quad (14.33)$$

Similarly, the spatial acceleration relationship between body \mathfrak{S} and its child body c takes the form:

$$\begin{aligned}\alpha(c) &= \mathcal{B}_c^* \alpha(\mathfrak{S}) + H^*(c) \ddot{\theta}(c) + a(c) \\ &\stackrel{14.30}{=} A^*(\mathfrak{S}, c) \alpha(\mathfrak{S}) + H^*(c) \ddot{\theta}(c) + a(c)\end{aligned}\quad (14.34)$$

Both (14.33) and (14.34) have the familiar recursive form of (14.32), except that they are for the $\mathfrak{T}_{\mathfrak{S}}$ aggregated tree instead of the original \mathfrak{T} tree.

14.6.3 Force Relationships

We now examine the transformed spatial force expressions for the aggregated body. For this, we need the spatial inertia term, $M_{\mathfrak{S}}$, for the aggregate link. $M_{\mathfrak{S}}$ is simply the partitioned sub-block of the block-diagonal \mathbf{M} corresponding to the \mathfrak{S} aggregated body in $\mathfrak{T}_{\mathfrak{S}}$. The link-to-link spatial force relationships for bodies in the \mathfrak{T} tree from (9.10) are as follows:

$$\begin{aligned}f(k) &= \sum_{\forall j \in \mathcal{C}(k)} \mathbb{A}(k, j) f(j) + M(k) \alpha(k) + b(k) \\ T(k) &= H(k) f(k)\end{aligned}\quad (14.35)$$

Assembling these expressions for all the links in \mathfrak{S} , we obtain the following relationships for $f_{\mathfrak{S}}$:

$$\begin{aligned}f_{\mathfrak{S}} &\stackrel{14.35}{=} \mathcal{E}_{\mathbb{A}_{\mathfrak{S}}} f_{\mathfrak{S}} + \sum_{\forall c \in \mathcal{C}(\mathfrak{S})} \mathcal{B}_c f(c) + M_{\mathfrak{S}} \alpha_{\mathfrak{S}} + b_{\mathfrak{S}} \\ &\stackrel{14.30}{=} \mathcal{E}_{\mathbb{A}_{\mathfrak{S}}} f_{\mathfrak{S}} + \sum_{\forall c \in \mathcal{C}(\mathfrak{S})} A(\mathfrak{S}, c) f(c) + M_{\mathfrak{S}} \alpha_{\mathfrak{S}} + b_{\mathfrak{S}} \\ T_{\mathfrak{S}} &= H_{\mathfrak{S}} f_{\mathfrak{S}}\end{aligned}$$

Using $\mathbb{A}_{\mathfrak{S}} \triangleq (\mathbf{I} - \mathcal{E}_{\mathbb{A}_{\mathfrak{S}}})^{-1}$ leads to the following explicit form:

$$\begin{aligned}
 (\mathbf{I} - \mathcal{E}_{\mathbb{A}_{\mathfrak{S}}})\mathfrak{f}_{\mathfrak{S}} &= \sum_{\forall c \in \mathbb{C}(\mathfrak{S})} \mathbb{A}(\mathfrak{S}, c)\mathfrak{f}(c) + M_{\mathfrak{S}}\alpha_{\mathfrak{S}} + b_{\mathfrak{S}} \\
 \Rightarrow \mathfrak{f}'_{\mathfrak{S}} &\stackrel{14.21}{=} \sum_{\forall c \in \mathbb{C}(\mathfrak{S})} \mathbb{A}(\mathfrak{S}, c)\mathfrak{f}(c) + M_{\mathfrak{S}}\alpha_{\mathfrak{S}} + b_{\mathfrak{S}} \quad (14.36) \\
 \mathcal{T}_{\mathfrak{S}} &\stackrel{14.21}{=} H_{\mathfrak{S}} \mathbb{A}_{\mathfrak{S}} \mathfrak{f}'_{\mathfrak{S}} \stackrel{14.20}{=} H_{\mathfrak{S}} \mathfrak{f}'_{\mathfrak{S}}
 \end{aligned}$$

Similarly, the spatial force relationship between the \mathfrak{S} and p bodies can be expressed as:

$$\begin{aligned}
 \mathfrak{f}(p) &\stackrel{14.35}{=} E_{\mathfrak{S}} \mathfrak{f}_{\mathfrak{S}} + M(p)\alpha(p) + b(p) \\
 &\stackrel{14.36, 14.21}{=} E_{\mathfrak{S}} \mathbb{A}_{\mathfrak{S}} \mathfrak{f}'_{\mathfrak{S}} + M(p)\alpha(p) + b(p) \quad (14.37) \\
 &\stackrel{14.28}{=} \mathbb{A}(p, \mathfrak{S}) \mathfrak{f}'_{\mathfrak{S}} + M(p)\alpha(p) + b(p) \\
 \mathcal{T}(p) &= H(p) \mathfrak{f}(p)
 \end{aligned}$$

Taken together, (14.36) and (14.37) define the spatial force relationships involving the aggregated body and its adjacent links. These expressions have the recursive structure of (14.35). They are component-level versions of the equivalent operator expressions for the SKO model in (14.21). They define the altered steps for aggregated bodies in the computational algorithms derived from the SKO model formulation in Chap. 9.

Chapter 15

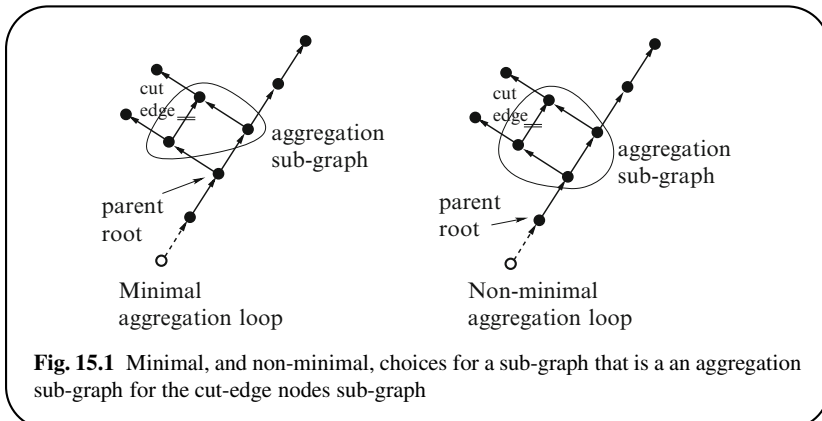
Constraint Embedding

In this chapter, we study a constraint embedding approach [74] that allows the development of SKO models for closed-chain multibody systems. Chapter 11 discussed the dynamics of closed-chain multibody systems and described the augmented dynamics approach, where the system is decomposed into a spanning tree SKO model subject to cut-edge constraints. Although this approach is able to exploit the SKO techniques to a degree, it suffers from the use of non-minimal generalized coordinates. While the alternate projected dynamics formulation uses minimal generalized coordinates, it no longer satisfies the requirements for an SKO model. The constraint embedding process uses the sub-graph aggregation process to work around these limitations to develop SKO models for closed-chain systems.

15.1 Constraint Embedding Strategy

The constraint embedding strategy is to transform the non-tree closed-chain system into an SKO model. The approach is to isolate non-tree sub-graphs and excise them using aggregation to transform the system digraph into a tree. Once the transformation is complete, an SKO model is developed for the transformed tree. The constraint embedding strategy involves the following steps:

1. Decompose the non-tree digraph for the system into a spanning tree, \mathfrak{T} , and a collection of cut-edges for the constraints. The set of cut-edges is usually not unique. Develop an SKO model for the system associated with the spanning tree, \mathfrak{T} .
2. For each cut-edge, identify the aggregation sub-graph, \mathfrak{S} , for the sub-graph consisting of the node pair for the cut-edge. Figure 15.1 illustrates minimal and non-minimal choices for an aggregation sub-graph for a system with a loop constraint. Based on Lemma 14.6, a procedure for creating this \mathfrak{S} aggregation sub-graph is as follows:
 - a. Identify the smallest sub-tree that contains the nodes in the cut-edge.
 - b. Remove the root node from this sub-tree to obtain the aggregation sub-graph \mathfrak{S} .



3. Aggregate \mathfrak{S} , and use Lemma 14.9 to derive an SKO model for the $\mathfrak{T}_{\mathfrak{S}}$ aggregated tree.
4. By construction, the nodes for each cut-edge belong to the internal \mathfrak{S} sub-graph of the aggregated body. Moreover, by Exercise 14.1, any directed cycles and multiply-connected paths associated with the cut-edge belong to \mathfrak{S} , since the sub-graph satisfies the aggregation condition and is therefore path-induced. Consequently, the cut-edge constraints can be defined purely in terms of the state of the nodes within the \mathfrak{S} sub-graph, independent of the rest of the nodes in the system! Once all the cut-edges have been processed, we are left with an aggregated tree containing a set of aggregated nodes, where the sub-graph of each aggregated node has one or more cut-edge constraints internal to it. Figure 15.2 illustrates the transformation of the original system digraph into a tree with aggregate nodes having internal cut-edge constraints. The next step is to eliminate the constraint from the sub-graph of each aggregated node. This process is described in detail in Sect. 15.1.1.

At the conclusion of the constrained embedding process, all of the constraints are absorbed into the aggregated links and subsequently eliminated from the multibody digraph. An SKO model, with minimal coordinates (satisfying the constraints), can now be developed as shown in Lemma 15.2. Being an SKO model, all SKO formulation techniques and algorithms can be applied.

Figure 15.3 illustrates the following additional examples of aggregation sub-graphs for non-tree digraphs:

1. This example contains a pair of cut-edges. Two possible choices of aggregation sub-graphs are shown. One option contains a single aggregation sub-graph with both cut-edges, while the second shows a pair of sub-graphs, each with a single cut-edge. Even though the latter option results in an aggregated tree with an extra node, it is the slightly more preferable option since the aggregation sub-graphs are smaller.

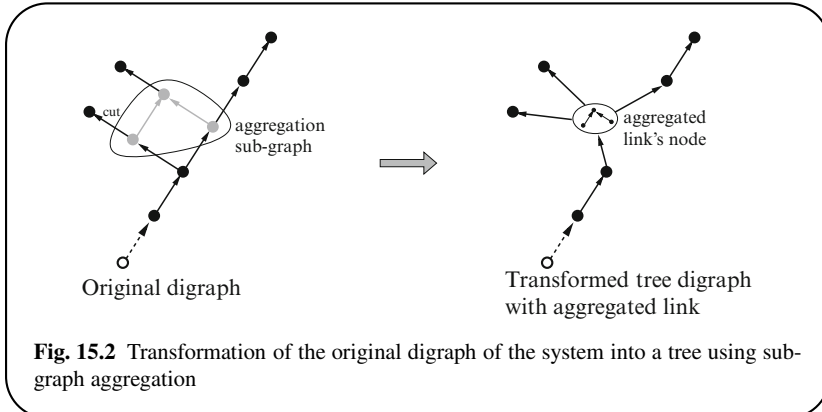


Fig. 15.2 Transformation of the original digraph of the system into a tree using sub-graph aggregation

2. In this example, the cut-edge is between nodes on disconnected systems. In this case, the aggregation sub-graph contains all the ancestor nodes of the cut-edge nodes. The aggregated node is a root node for the SKO-forest of the aggregated tree.
3. This example shows a digraph in which a pair of cut-edges share a node. In this case, the aggregated sub-graph includes the nodes from both cut-edges, and, unlike example (1), there is no split option possibility for the aggregation sub-graph.

15.1.1 Embedding Constraint Sub-Graphs

In this section, we describe the process for eliminating the constraints from the aggregation sub-graphs required in step 4 of the constraint embedding strategy in the previous section. We focus our attention on a single constraint cut-edge in the system. The process can be applied repeatedly when there are multiple cut-edge constraints. Let us assume that steps 1–3 in Sect. 15.1 have been completed to obtain an aggregated body, with sub-graph \mathfrak{S} satisfying the aggregation condition. The \mathfrak{S} aggregation sub-graph has the cut-edge constraints. One consequence of the cut-edge constraints is that the effective degrees of freedom in \mathfrak{S} is less than the total hinge degrees of freedom in \mathfrak{S} .

We adopt the body indexing scheme from Sect. 14.6 on page 292 for sub-graph aggregation. The parent link for the \mathfrak{S} aggregated link is denoted p , while c denotes a child body of \mathfrak{S} . Also, i denotes a body in the \mathfrak{S} sub-graph that is a child of p , i.e., a base-body in the \mathfrak{S} sub-graph. Body j in \mathfrak{S} sub-graph denotes the parent of body c . This indexing scheme for \mathfrak{S} is illustrated in Fig. 15.4.

Due to the cut-edge internal constraints on the \mathfrak{S} , the elements of $\dot{\theta}_{\mathfrak{S}}$ are not independent, but are instead coupled by the constraint. At the coordinate level, the constraint often takes the form of a nonlinear algebraic relationship. However, at the

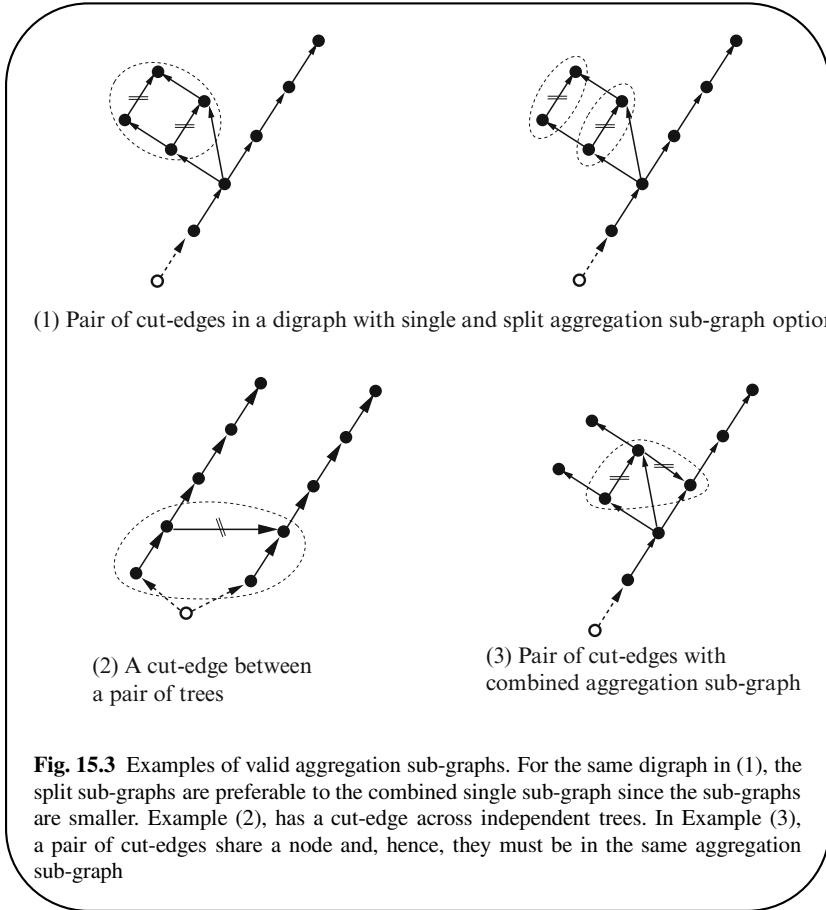
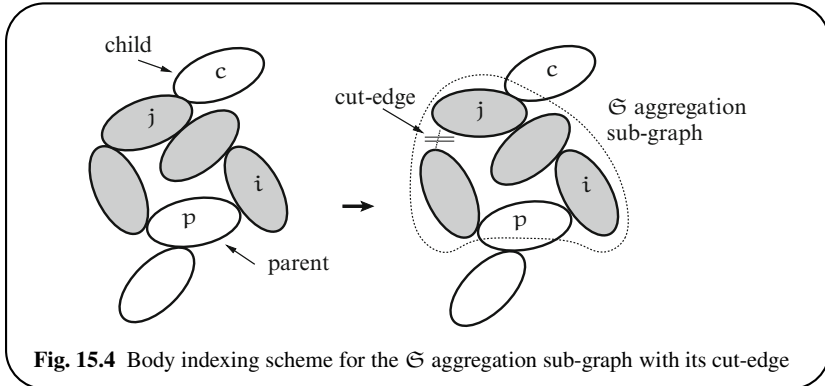


Fig. 15.3 Examples of valid aggregation sub-graphs. For the same digraph in (1), the split sub-graphs are preferable to the combined single sub-graph since the sub-graphs are smaller. Example (2), has a cut-edge across independent trees. In Example (3), a pair of cut-edges share a node and, hence, they must be in the same aggregation sub-graph

velocity level, the generalized velocities in the system are subject to a linear, configuration dependent constraint. Per our projected dynamics discussion in Sect. 11.3, it is possible to partition the $\dot{\theta}_{\mathfrak{S}}$ generalized velocities of the sub-graph into disjoint sets of independent and dependent generalized velocities. The independent set is denoted $\dot{\theta}_{R\mathfrak{S}}$. They can be used to obtain the dependent generalized velocities satisfying the cut-edge constraints on the sub-graph. In other words, there exists a (configuration dependent) mapping $X_{\mathfrak{S}}$ such that

$$\dot{\theta}_{\mathfrak{S}} = X_{\mathfrak{S}} \dot{\theta}_{R\mathfrak{S}} \quad (15.1)$$

In deriving (15.1) we have assumed for simplicity that the constraint is catastatic so that the particular solution of (11.33) is zero. When the constraint sub-graphs are isolated and of moderate size, the constraint elimination process is especially straightforward and computationally inexpensive. Examples of such local loops in-



clude constraints associated with geared motors, 4-bar linkages, wishbone suspensions, and differentials, etc.

Using the partitioned structure induced by the \mathfrak{S} sub-graph, as discussed in Sect. 14.6, define

$$\mathbf{H}_{R\alpha} \triangleq \begin{pmatrix} \mathbf{I} & \mathbf{0} & \mathbf{0} \\ \mathbf{0} & X_{\mathfrak{S}}^* & \mathbf{0} \\ \mathbf{0} & \mathbf{0} & \mathbf{I} \end{pmatrix} \mathbf{H}_\alpha \stackrel{14.20}{=} \begin{pmatrix} \mathbf{H}_C & \mathbf{0} & \mathbf{0} \\ \mathbf{0} & \underline{\mathbf{H}}_{R\mathfrak{S}} & \mathbf{0} \\ \mathbf{0} & \mathbf{0} & \mathbf{H}_P \end{pmatrix} \quad (15.2)$$

with

$$\underline{\mathbf{H}}_{R\mathfrak{S}} \triangleq X_{\mathfrak{S}}^* \mathbf{H}_{\mathfrak{S}} \stackrel{14.20}{=} X_{\mathfrak{S}}^* \mathbf{H}_{\mathfrak{S}} \mathbb{A}_{\mathfrak{S}} \quad \text{and} \quad \dot{\theta}_R \triangleq \begin{bmatrix} \dot{\theta}_C \\ \dot{\theta}_{R\mathfrak{S}} \\ \dot{\theta}_P \end{bmatrix} \quad (15.3)$$

$\dot{\theta}_R$ denotes the minimal size, system-level, generalized velocity stacked vector containing the independent generalized velocities for the constrained system. Observe from (15.1) and (15.2) that

$$\mathbf{H}_{R\alpha}^* \dot{\theta}_R = \mathbf{H}_\alpha^* \dot{\theta} \quad (15.4)$$

The following lemma establishes a relationship between the sequence of spatial operators we have introduced during the constraint embedding process.

Lemma 15.1 Velocity relationships with constraint embedding.

We have the following identities for \mathcal{V} :

$$\mathcal{V} = \mathbb{A}^* \mathbf{H}^* \dot{\theta} = \mathbb{A}_\alpha^* \mathbf{H}_\alpha^* \dot{\theta} = \mathbb{A}_\alpha^* \mathbf{H}_{R\alpha}^* \dot{\theta}_R \quad (15.5)$$

Proof: The definitions of \mathbb{A}_α and \mathbf{H}_α in (14.18) and (14.20) lead to the $\mathbb{A}^* \mathbf{H}^* = \mathbb{A}_\alpha^* \mathbf{H}_\alpha^*$ identity and the first equality in (15.5). The latter part follows from the use of (15.4). ■

The last equality in (15.5) depends on only the independent generalized velocities $\dot{\theta}_R$ for the system. It effectively eliminates the cut-edge constraints on the sub-graph, since independent generalized velocities are minimal and always satisfy the constraint.

The following lemma develops an SKO model for the closed-chain system based on the constraint embedding approach.

Lemma 15.2 Constraint embedding SKO model.

With $\dot{\theta}_R$ serving as the minimal size generalized velocities, and the $\mathfrak{T}_{\mathfrak{S}}$ aggregated tree as the system digraph, the spatial operators $(H_{Ra}, \mathbb{A}_a, M)$ define an SKO model for the closed-chain system. The equations of motion are as follows:

$$\begin{aligned} \mathcal{V} &= \mathbb{A}_a^* H_{Ra}^* \dot{\theta}_R \\ \alpha &= \mathbb{A}_a^* (H_{Ra}^* \ddot{\theta}_R + \underline{\alpha}'), \text{ where } \underline{\alpha}' \triangleq \begin{bmatrix} \underline{\alpha}_{\mathfrak{C}} \\ \underline{\alpha}'_{\mathfrak{S}} \\ \underline{\alpha}_{\mathcal{P}} \end{bmatrix}, \quad \underline{\alpha}'_{\mathfrak{S}} \triangleq \underline{\alpha}_{\mathfrak{S}} + \underline{H}_{\mathfrak{S}}^* \dot{X}_{\mathfrak{S}} \dot{\theta}_{R\mathfrak{S}} \quad (15.6) \\ \underline{f} &= \mathbb{A}_a(M\alpha + \underline{b}) \\ \mathcal{T}_R &= H_{Ra}\underline{f} \end{aligned}$$

Thus,

$$\mathcal{T}_R = \mathcal{M}_r \ddot{\theta}_R + \mathcal{C}_r \quad (15.7)$$

where

$$\mathcal{M}_r = H_{Ra} \mathbb{A}_a M \mathbb{A}_a^* H_{Ra}^* \quad \text{and} \quad \mathcal{C}_r \triangleq H_{Ra} \mathbb{A}_a (M \mathbb{A}_a^* \underline{\alpha}' + \underline{b}) \quad (15.8)$$

The mass matrix expression above represents the Newton–Euler operator expression for the SKO model mass matrix for the constrained system.

Proof: By construction, the \mathfrak{S} sub-graph satisfies the aggregation condition. Lemma 14.9 defines an SKO model for the $\mathfrak{T}_{\mathfrak{S}}$ aggregated tree with equations of motion defined as follows in (14.21):

$$\begin{aligned} \mathcal{V} &= \mathbb{A}_a^* H_a^* \dot{\theta} & \alpha &= \mathbb{A}_a^* (H_a^* \ddot{\theta} + \underline{\alpha}) \\ \underline{f} &= \mathbb{A}_a(M\alpha + \underline{b}) & \mathcal{T} &= H_a \underline{f} \quad (15.9) \end{aligned}$$

In addition, the $\dot{\theta}_R$ generalized coordinates are independent and eliminate the cut-edge constraint within \mathfrak{S} . Since the (H_a, \mathbb{A}_a, M) spatial operators satisfy the requirements for an SKO model for the $\mathfrak{T}_{\mathfrak{S}}$ tree digraph, replacing H_a by H_{Ra} leaves the required block-diagonal property intact, implying that $(H_{Ra}, \mathbb{A}_a, M)$ also satisfy the SKO model structural requirements.

The first equation in (15.6) follows directly from the use of (15.5) in the first equation in (15.9).

Differentiating (15.1) we have

$$\ddot{\theta}_{\mathfrak{S}} = X_{\mathfrak{S}} \ddot{\theta}_{R\mathfrak{S}} + \dot{X}_{\mathfrak{S}} \dot{\theta}_{R\mathfrak{S}} \quad (15.10)$$

Using this in (14.33) leads to

$$\begin{aligned} \alpha_{\mathfrak{S}} &\stackrel{14.33}{=} \mathbb{A}^*(p, \mathfrak{S})\alpha(p) + \underline{H}_{\mathfrak{S}}^* \ddot{\theta}_{\mathfrak{S}} + \underline{a}_{\mathfrak{S}} \\ &\stackrel{15.10}{=} \mathbb{A}^*(p, \mathfrak{S})\alpha(p) + \underline{H}_{R\mathfrak{S}}^* \ddot{\theta}_{R\mathfrak{S}} + \underline{a}_{\mathfrak{S}} + \underline{H}_{\mathfrak{S}}^* \dot{X}_{\mathfrak{S}} \dot{\theta}_{R\mathfrak{S}} \\ &\stackrel{15.6}{=} \mathbb{A}^*(p, \mathfrak{S})\alpha(p) + \underline{H}_{R\mathfrak{S}}^* \ddot{\theta}_{R\mathfrak{S}} + \underline{a}'_{\mathfrak{S}} \end{aligned} \quad (15.11)$$

Using this the expression for α in (15.9) leads to the corresponding expression in (15.6).

The generalized forces vector for the aggregated link with the reduced generalized velocity coordinates, $\mathcal{T}_{R\mathfrak{S}}$, is defined as

$$\mathcal{T}_{R\mathfrak{S}} \triangleq X_{\mathfrak{S}}^* \mathcal{T}_{\mathfrak{S}} \stackrel{15.3}{=} \underline{H}_{R\mathfrak{S}} \underline{f}'_{\mathfrak{S}} \quad (15.12)$$

Together these establish all the expressions in (15.6). Equation (15.8) is a simple assembly of these component relationships. ■

\mathcal{T}_R denotes the minimal size, system-level generalized force stacked vector with structure similar to that of $\dot{\theta}_R$. Similarly, the \underline{a}' stacked vector is a modified version of the \underline{a} Coriolis acceleration stacked vector with the $\underline{a}'_{\mathfrak{S}}$ term for body \mathfrak{S} .

This lemma completes the conversion of the original constrained graph multi-body model into an unconstrained tree-topology model through constraint embedding. Not only have the constraints been eliminated, but we also have an SKO model for the system and all the SKO techniques and algorithms can be applied.

The \mathcal{M}_r expression in (15.8) corresponds to the reduced mass matrix derived in Sect. 11.3 on page 221 using the projected approach for constrained dynamics. In contrast to the projected dynamics approach, the (15.8) expression is an Newton–Euler operator factorization for an SKO model for the system.

15.2 Examples of Constraint Embedding

There are two important classes of constraints to consider:

1. **Direct joint-level constraints:** In this case, the constraints are expressed as a direct (often constant) algebraic relationship between joint angles (e.g., gear-box, differential suspensions).
2. **Loop constraints:** In this case, configuration dependent, loop constraints involve nodes on different bodies in the system (e.g., four-bar linkages).

The following sections describe examples for these constraint types. Section 15.2.1 describes the direct joint-level constraint for a geared link. Sections 15.2.2 and 15.2.3 examine loop constraints for a planar four-bar linkage with different cut-edge choices. We assume that the bodies in these systems are rigid links, and

therefore we switch to the \mathcal{E}_ϕ and ϕ notation in place of the abstract $\mathcal{E}_{\mathbb{A}}$ and \mathbb{A} notation.

15.2.1 Geared Links

As discussed in Chap. 12, the motor is mounted on an inboard link driving the outer link for a geared link as shown in Fig. 15.5. This creates a closure constraint between the three bodies. The \mathfrak{S} aggregation sub-graph consists of the $(k-1)$ th motor and its driven $(k-1)$ th link body, with the k th driven link serving as the parent body for the sub-graph. Using the notation from Chap. 12, the constraint embedding terms for geared joints are given by:

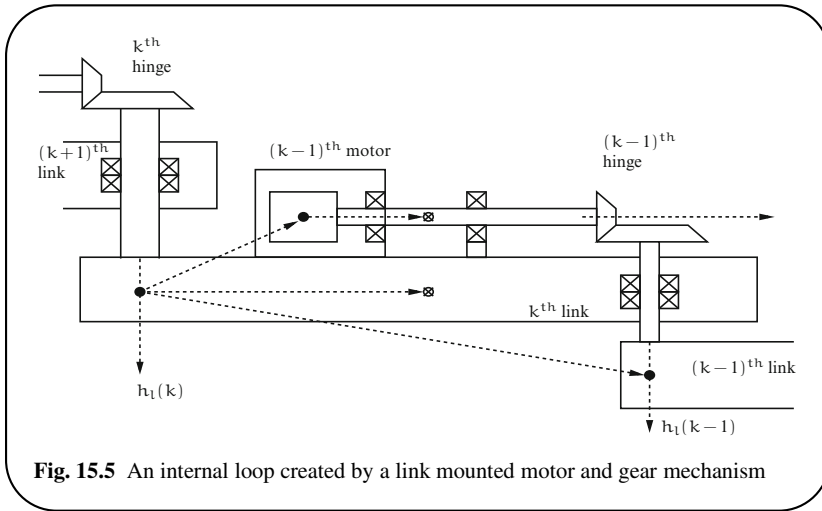


Fig. 15.5 An internal loop created by a link mounted motor and gear mechanism

$$\begin{aligned} \dot{\theta}_{\mathfrak{S}} &= \begin{bmatrix} \theta_m(k-1) \\ \theta_l(k-1) \end{bmatrix} \in \mathcal{R}^2, & \dot{\theta}_{R\mathfrak{S}} = \theta_l(k-1) \in \mathcal{R}^1 \\ X_{\mathfrak{S}} &= \begin{bmatrix} \mu_G(k-1) \\ 1 \end{bmatrix} \in \mathcal{R}^{2 \times 1} \\ \dot{X}_{\mathfrak{S}} &= \mathbf{0}, \quad \mathcal{E}_{\phi_{\mathfrak{S}}} = \mathbf{0} \in \mathcal{R}^{12 \times 12}, \quad \phi_{\mathfrak{S}} = \mathbf{I} \in \mathcal{R}^{12 \times 12} \end{aligned} \quad (15.13)$$

Observe that $X_{\mathfrak{S}}$ is constant and configuration independent. The constraint embedding approach for geared systems provides an alternative to the one described in Chap. 12. At the component level, the resulting equations of motion

have identical form. Thus, the Chap. 12 formulation can be regarded as a special case of constraint embedding.

15.2.2 Planar Four-Bar Linkage System (Terminal Cut)

Now consider a four-bar linkage within a system, as illustrated in Fig. 15.6. The aggregation sub-graph consists of links j, k, and l, with the root link being link p. We make a *terminal cut* at the hinge joining links p and l, to convert the sub-graph into a tree-topology system. The child link c is connected via a hinge to link j.

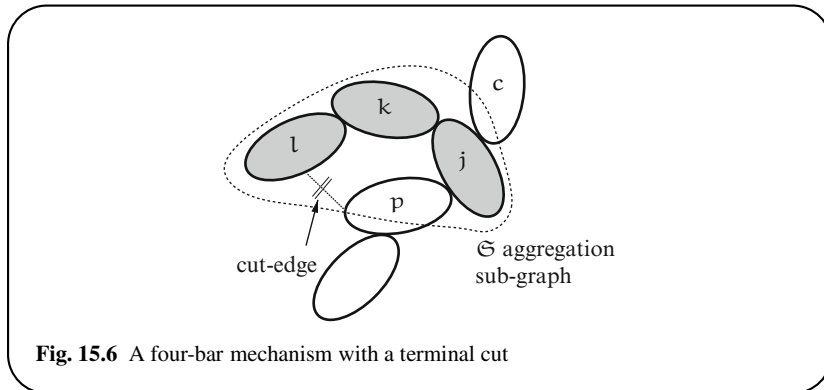


Fig. 15.6 A four-bar mechanism with a terminal cut

The constraint embedding terms for the four-bar linkage with the terminal cut are as follows:

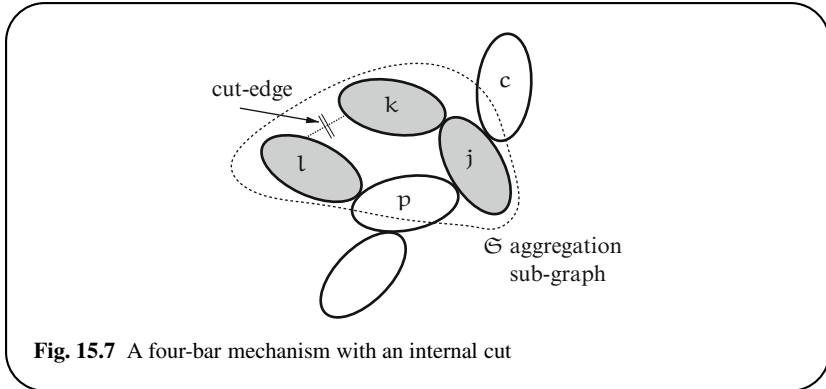
$$\begin{aligned} E_{\mathfrak{S}} &= [\mathbf{0}, \quad \mathbf{0}, \quad \phi(p,j)] \in \mathcal{R}^{6 \times 18}, \\ \phi_{\mathfrak{S}} &= \begin{pmatrix} \mathbf{I} & \mathbf{0} & \mathbf{0} \\ \phi(k,l) & \mathbf{I} & \mathbf{0} \\ \phi(j,l) & \phi(j,k) & \mathbf{I} \end{pmatrix} \in \mathcal{R}^{18 \times 18}, \quad X_{\mathfrak{S}} = \begin{bmatrix} r_l \\ r_k \\ 1 \end{bmatrix} \in \mathcal{R}^{3 \times 1} \end{aligned} \quad (15.14)$$

$$\mathcal{E}_{\phi_{\mathfrak{S}}} = \begin{pmatrix} \mathbf{0} & \mathbf{0} & \mathbf{0} \\ \phi(k,l) & \mathbf{0} & \mathbf{0} \\ \mathbf{0} & \phi(j,k) & \mathbf{0} \end{pmatrix} \in \mathcal{R}^{18 \times 18}, \quad \mathcal{B}_{\mathfrak{S}} = \begin{bmatrix} \mathbf{0} \\ \phi(j,c) \\ \mathbf{0} \end{bmatrix} \in \mathcal{R}^{18 \times 6}$$

In the above, r_l and r_k are configuration dependent parameters that characterize the ratio of the hinge velocities of the j, k, and l hinges within the planar four-bar linkage. Thus, $X_{\mathfrak{S}}$ is configuration dependent and not constant.

15.2.3 Planar Four-Bar Linkage System (Internal Cut)

We once again consider the same four-bar linkage. This time an *internal* cut is made at the hinge joining links k and l. This converts the sub-graph into a tree-topology system, as shown in Fig. 15.7. Hinges j and l connect links j and l to the p parent link. Observe that \mathfrak{S} is now a forest of two sub-trees, unlike the terminal cut-edge



choice in the previous section. One of the trees contains just the body l, while the other contains bodies j and k. The constraint embedding terms for the four-bar linkage with internal cut are as follows:

$$\begin{aligned} \mathcal{E}_{\phi_{\mathfrak{S}}} &= \begin{pmatrix} \mathbf{0} & \mathbf{0} & \mathbf{0} \\ \mathbf{0} & \mathbf{0} & \mathbf{0} \\ \mathbf{0} & \phi(j,k) & \mathbf{0} \end{pmatrix} \in \mathcal{R}^{18 \times 18} \\ \phi_{\mathfrak{S}} &= \begin{pmatrix} \mathbf{I} & \mathbf{0} & \mathbf{0} \\ \mathbf{0} & \mathbf{I} & \mathbf{0} \\ \mathbf{0} & \phi(j,k) & \mathbf{I} \end{pmatrix} \in \mathcal{R}^{18 \times 18}, \quad X_{\mathfrak{S}} = \begin{bmatrix} r_l \\ r_k \\ 1 \end{bmatrix} \in \mathcal{R}^{3 \times 1} \quad (15.15) \\ E_{\mathfrak{S}} &= [\phi(p,l), \mathbf{0}, \phi(p,j)] \in \mathcal{R}^{6 \times 18}, \quad B_{\mathfrak{S}} = \begin{bmatrix} \mathbf{0} \\ \phi(j,c) \\ \mathbf{0} \end{bmatrix} \in \mathcal{R}^{18 \times 6} \end{aligned}$$

In comparison to the earlier terminal cut example, the \mathfrak{S} digraph and the $\mathcal{E}_{\phi_{\mathfrak{S}}}$ and $\phi_{\mathfrak{S}}$ matrices are simpler here. On the other hand, the $E_{\mathfrak{S}}$ matrix is more complex. $E_{\mathfrak{S}}$ contains two non-zero elements, one for each of the base-bodies in the \mathfrak{S} sub-graph.

15.3 Recursive AB Forward Dynamics

Lemma 15.2 shows that the constraint embedding process leads to an SKO model for the closed-chain system. We now derive the Innovations factorization for the system mass matrix and use it to develop the AB forward dynamics algorithms for the closed-chain system.

15.3.1 Articulated Body Inertias for the Aggregated System

First, we describe the articulated body inertia steps from the Riccati equation, (9.33) on page 175, for the aggregated link \mathfrak{S} and its adjacent links:

$$\begin{aligned}
 \mathcal{P}^+(\mathbf{c}) &= \bar{\tau}(\mathbf{c})\mathcal{P}(\mathbf{c}) \\
 \mathcal{P}_{\mathfrak{S}} &= \sum_{\forall c \in \mathcal{C}(\mathfrak{S})} \mathbb{A}(\mathfrak{S}, c)\mathcal{P}^+(\mathbf{c})\mathbb{A}^*(\mathfrak{S}, c) + M_{\mathfrak{S}} \\
 \mathcal{D}_{\mathfrak{S}} &= \underline{H}_{R\mathfrak{S}} \mathcal{P}_{\mathfrak{S}} \underline{H}_{R\mathfrak{S}}^* \\
 \mathcal{G}_{\mathfrak{S}} &= \mathcal{P}_{\mathfrak{S}} \underline{H}_{R\mathfrak{S}}^* \mathcal{D}_{\mathfrak{S}}^{-1} \\
 \boldsymbol{\tau}_{\mathfrak{S}} &= \mathcal{G}_{\mathfrak{S}} \underline{H}_{R\mathfrak{S}} \\
 \mathcal{P}_{\mathfrak{S}}^+ &= \mathcal{P}_{\mathfrak{S}} - \boldsymbol{\tau}_{\mathfrak{S}} \mathcal{P}_{\mathfrak{S}} \\
 \mathcal{P}(p) &= \mathbb{A}(p, \mathfrak{S})\mathcal{P}_{\mathfrak{S}}^+\mathbb{A}^*(p, \mathfrak{S}) + M(p)
 \end{aligned} \tag{15.16}$$

Recall that (14.28) and (14.30) define the following expressions for $\mathbb{A}(p, \mathfrak{S})$ and $\mathbb{A}(\mathfrak{S}, c)$.

$$\mathbb{A}(p, \mathfrak{S}) = E_{\mathfrak{S}} \mathbb{A}_{\mathfrak{S}} \quad \text{and} \quad \mathbb{A}(\mathfrak{S}, c) = B_c$$

$\mathcal{D}_{\mathfrak{S}}$ can be re-expressed as

$$\begin{aligned}
 \mathcal{D}_{\mathfrak{S}} &\stackrel{15.3}{=} X_{\mathfrak{S}}^* (H_{\mathfrak{S}} A_{\mathfrak{S}} P_{\mathfrak{S}} A_{\mathfrak{S}}^* H_{\mathfrak{S}}^*) X_{\mathfrak{S}} = X_{\mathfrak{S}}^* \mathcal{M}_{\mathfrak{S}} X_{\mathfrak{S}} \\
 \text{where } \mathcal{M}_{\mathfrak{S}} &\triangleq H_{\mathfrak{S}} A_{\mathfrak{S}} P_{\mathfrak{S}} A_{\mathfrak{S}}^* H_{\mathfrak{S}}^*
 \end{aligned} \tag{15.17}$$

$\mathcal{M}_{\mathfrak{S}}$ has the structure of a mass matrix for the \mathfrak{S} sub-graph. The primary difference from the true mass matrix of \mathfrak{S} is that the central inertia term is $P_{\mathfrak{S}}$, instead of the usual $M_{\mathfrak{S}}$ spatial inertia term. $P_{\mathfrak{S}}$ includes the articulated body contribution from the descendants of the \mathfrak{S} body. $\mathcal{D}_{\mathfrak{S}}$ is thus the projection of this \mathfrak{S} mass matrix onto its independent degrees of freedom.

15.3.2 Mass Matrix Factorization and Inversion

The Riccati equation solution, and the associated articulated body inertia quantities in (15.16), together with Lemma 9.11 on page 179, lead to the following Innovations factorization and inversion expressions for the mass matrix of the transformed system:

$$\begin{aligned}\mathcal{M}_r &\stackrel{15.8}{=} \mathbf{H}_{Ra} \mathbb{A}_a M \mathbb{A}_a^* \mathbf{H}_{Ra}^* \\ &= [\mathbf{I} + \mathbf{H}_{Ra} \mathbb{A}_a \mathcal{K}] \mathcal{D} [\mathbf{I} + \mathbf{H}_{Ra} \mathbb{A}_a \mathcal{K}]^* \\ [\mathbf{I} + \mathbf{H}_{Ra} \mathbb{A}_a \mathcal{K}]^{-1} &= \mathbf{I} - \mathbf{H}_{Ra} \psi_a \mathcal{K} \\ \mathcal{M}_r^{-1} &= [\mathbf{I} - \mathbf{H}_{Ra} \psi_a \mathcal{K}]^* \mathcal{D}^{-1} [\mathbf{I} - \mathbf{H}_{Ra} \psi_a \mathcal{K}]\end{aligned}\quad (15.18)$$

The ψ_a , \mathcal{D} , and \mathcal{K} operators are those associated with the Riccati equation solution in (15.16). Continuing on, the explicit expression for the reduced generalized expressions from Lemma 9.12 on page 180 takes the form:

$$\ddot{\theta}_R = [\mathbf{I} - \mathbf{H}_{Ra} \psi_a \mathcal{K}]^* \mathcal{D}^{-1} [\mathcal{T}_R - \mathbf{H}_{Ra} \psi_a (\mathcal{K} \mathcal{T}_R + \mathcal{P} \mathfrak{a}' + \mathfrak{b})] - \mathcal{K}^* \psi_a^* \mathfrak{a}' \quad (15.19)$$

Thus, the SKO model for the system has led to an explicit expression for the $\ddot{\theta}_R$ minimal generalized acceleration vector for the closed-chain system.

15.3.3 AB Forward Dynamics Algorithm

Equation (15.19) can be converted into the AB recursive forward dynamics algorithm as described in Algorithm 9.5 on page 182. The overall structure of the AB forward dynamics algorithm remains unchanged, with differences only at the steps involving the aggregated body and its neighbors.

The tip-to-base recursion steps from body c to the aggregated link \mathfrak{S} have the following form:

$$\begin{aligned}\mathfrak{z}^+(c) &= \mathfrak{z}(c) + \mathcal{G}(c) \epsilon(c) \\ \mathfrak{z}_{\mathfrak{S}} &= \sum_{\forall c \in \mathfrak{C}(\mathfrak{S})} \mathbb{A}(\mathfrak{S}, c) \mathfrak{z}^+(c) + \mathfrak{b}_{\mathfrak{S}} + \mathcal{P}_{\mathfrak{S}} \mathfrak{a}'_{\mathfrak{S}} \\ \epsilon_{\mathfrak{S}} &= \mathcal{T}_{R\mathfrak{S}} - \underline{\mathbf{H}}_{R\mathfrak{S}} \mathfrak{z}_{\mathfrak{S}} \\ \mathfrak{v}_{\mathfrak{S}} &= \mathcal{D}_{\mathfrak{S}}^{-1} \epsilon_{\mathfrak{S}}\end{aligned}\quad (15.20)$$

The tip-to-base recursion steps from body \mathfrak{S} to body p are as follows:

$$\begin{aligned}
 \mathfrak{z}_{\mathfrak{S}}^+ &= \mathfrak{z}_{\mathfrak{S}} + \mathcal{G}_{\mathfrak{S}} \epsilon_{\mathfrak{S}} \\
 \mathfrak{z}(p) &= \mathbb{A}(p, \mathfrak{S}) \mathfrak{z}_{\mathfrak{S}}^+ + \mathfrak{b}(p) + \mathcal{P}(p) \mathfrak{a}(p) \\
 \epsilon(p) &= \mathcal{T}(p) - \mathcal{H}(p) \mathfrak{z}(p) \\
 \nu(p) &= \mathcal{D}^{-1}(p) \epsilon(p)
 \end{aligned} \tag{15.21}$$

The base-to-tip accelerations sweep steps are also altered for the aggregated link. The steps from body p to the aggregated body \mathfrak{S} are as follows:

$$\begin{aligned}
 \alpha_{\mathfrak{S}}^+ &= \mathbb{A}^*(p, \mathfrak{S}) \alpha(p) \\
 \ddot{\theta}_{R\mathfrak{S}} &= \nu_{\mathfrak{S}} - \mathcal{G}_{\mathfrak{S}}^* \alpha_{\mathfrak{S}}^+ \\
 \ddot{\theta}_{\mathfrak{S}} &= X_{\mathfrak{S}} \ddot{\theta}_{R\mathfrak{S}} + \dot{X}_{\mathfrak{S}} \dot{\theta}_{R\mathfrak{S}} \\
 \alpha_{\mathfrak{S}} &= \alpha_{\mathfrak{S}}^+ + H_{R\mathfrak{S}}^* \ddot{\theta}_{R\mathfrak{S}} + \mathfrak{a}'_{\mathfrak{S}}
 \end{aligned} \tag{15.22}$$

The steps from the aggregated body \mathfrak{S} to body c are as follows:

$$\begin{aligned}
 \alpha^+(c) &= \mathbb{A}^*(\mathfrak{S}, c) \alpha_{\mathfrak{S}} \\
 \ddot{\theta}(c) &= \nu(c) - \mathcal{G}^*(c) \alpha^+(c) \\
 \alpha(c) &= \alpha^+(c) + H^*(c) \ddot{\theta}(c) + \mathfrak{a}(c)
 \end{aligned} \tag{15.23}$$

The most computationally expensive part of these steps is the evaluation and inversion of the $\mathcal{D}_{\mathfrak{S}}$ symmetric, positive definite matrix in (15.16). Its size is the number of independent degrees of freedom for the aggregated link. Thus, the computational cost of the AB algorithm is no longer linear in the number of independent degrees of freedom for the aggregated links, but, instead, is (in the worst case) quadratic in the *total* degrees of freedom in the \mathfrak{S} aggregation sub-graph, and cubic in the number of *independent* degrees of freedom in the \mathfrak{S} sub-graph. These additional costs, however, are modest when the loops are of moderate size.

15.4 Computing $X_{\mathfrak{S}}$ and $\dot{X}_{\mathfrak{S}}$

$X_{\mathfrak{S}}$ maps the independent generalized velocities to the full generalized velocities of \mathfrak{S} . For the case of direct joint-level constraints, it is straightforward to select the independent coordinates subset, and $X_{\mathfrak{S}}$ is then simply the gradient of the mapping from the independent to the full generalized coordinates. For direct joint-level constraints, $X_{\mathfrak{S}}$ is often constant, and $\dot{X}_{\mathfrak{S}}$ is consequently zero. In the following sections, we look at the less trivial case of loop constraints, and derive expressions for the configuration dependent $X_{\mathfrak{S}}$ and its time-derivative $\dot{X}_{\mathfrak{S}}$ needed in (15.1) and (15.6).

For loop constraints, we have an algebraic constraint on the relative velocities of a pair of physical closure nodes in the sub-graph. Denoting a representative pair of

closure nodes as o and p, such a constraint can be expressed as

$$\begin{aligned} \mathbf{0} &= A(\mathcal{V}_o - \mathcal{V}_p) \stackrel{3.53}{=} A(\mathcal{J}_o - \mathcal{J}_p)\dot{\theta}_{\mathfrak{S}} \\ &= A [\mathcal{J}_{o1} - \mathcal{J}_{p1}, \quad \mathcal{J}_{o2} - \mathcal{J}_{p2}] \begin{bmatrix} \dot{\theta}_{u\mathfrak{S}} \\ \dot{\theta}_{R\mathfrak{S}} \end{bmatrix} = [Y_1, Y_2] \begin{bmatrix} \dot{\theta}_{u\mathfrak{S}} \\ \dot{\theta}_{R\mathfrak{S}} \end{bmatrix} \end{aligned} \quad (15.24)$$

Here, A denotes the constraint on the relative spatial velocities between this pair of closure nodes, and \mathcal{J}_o , \mathcal{J}_p denote sub-graph Jacobians relating the generalized velocities of the sub-graph to the spatial velocities at the o and p closure nodes. $\dot{\theta}_{u\mathfrak{S}}$ is the complement of the $\dot{\theta}_{R\mathfrak{S}}$ sub-vector in $\dot{\theta}_{\mathfrak{S}}$ and represents the dependent generalized velocity coordinates. \mathcal{J}_{o1} , etc., represent sub-blocks within the corresponding partitioned Jacobians. Y_1 and Y_2 are defined as

$$Y_1 \triangleq A(\mathcal{J}_{o1} - \mathcal{J}_{p1}) \quad \text{and} \quad Y_2 \triangleq A(\mathcal{J}_{o2} - \mathcal{J}_{p2}) \quad (15.25)$$

In (15.24), the partitioning is chosen such that Y_1 is square and full rank, and thus invertible. It follows that:

$$\dot{\theta}_{u\mathfrak{S}} = -Y_1^{-1}Y_2\dot{\theta}_{R\mathfrak{S}} \implies X_{\mathfrak{S}} = \begin{bmatrix} -Y_1^{-1}Y_2 \\ \mathbf{I} \end{bmatrix} \quad (15.26)$$

This explicit expression for $X_{\mathfrak{S}}$ for the constraint loop is similar to the one in Exercise 11.4 on page 223. The following exercise derives an expression for $\dot{X}_{\mathfrak{S}}$ for systems with loop constraints.

Exercise 15.1 Expression for $\dot{X}_{\mathfrak{S}}$.

Show that

$$\dot{X}_{\mathfrak{S}} = \begin{bmatrix} -Y_1^{-1}\dot{Y}X_{\mathfrak{S}} \\ \mathbf{0} \end{bmatrix} \quad \text{and} \quad \dot{X}_{\mathfrak{S}}\dot{\theta}_{R\mathfrak{S}} = \begin{bmatrix} -Y_1^{-1}\dot{Y}\dot{\theta}_{\mathfrak{S}} \\ \mathbf{0} \end{bmatrix} \quad (15.27)$$

where $Y \triangleq [Y_1, Y_2]$. ■

Equation (15.27) requires expressions for \dot{Y}_1 and \dot{Y}_2 . From (15.25), these derivatives require \dot{A} and the time derivatives of the \mathcal{J}_{o1} , etc., blocks. The expression for \dot{A} is usually straightforward to obtain from the inter-node constraint expression, and hence, we focus on the time derivative of the Jacobian blocks. The kth column of \mathcal{J}_{o1} is of the form $\phi^*(\mathbb{O}_k, o)H^*(k)$, where \mathbb{O}_k denotes the frame at the kth hinge in $\dot{\theta}_{\mathfrak{S}}$, and $H^*(k)$ is the corresponding joint map matrix for the hinge. This derivative is a simple expression involving the relative linear and angular velocity of the o closure node with respect to the \mathbb{O}_k closure node.

15.5 Generalization to Multiple Branches and Cut-Edges

We summarize extensions for applying the constraint embedding technique to the more general multibody system context.

Multiple cut-edges: Our development of the component-level constraint embedding expression focused on the case of a single aggregation sub-graph during the constraint embedding process. More generally, systems will have multiple aggregation sub-graphs from multiple cut-edge constraints for the system. In this case, the system will contain multiple aggregated links, potentially with multiple constraints embedded within each aggregated link. The structural form of the equations of motion remains the same. The key change to the algorithms is that aggregated link steps need to be executed when an aggregated link is encountered, and regular steps are executed otherwise.

Multiple \mathcal{S} child bodies: Aggregated bodies can also have multiple child bodies. For this case, $\mathcal{B}_{\mathcal{S}}$ is a multi-column matrix, with one column for each child body. Each column has a single non-zero “ $\mathbb{A}(j, c)$ ” entry corresponding to the parent body in the \mathcal{S} sub-graph and the child body. The AB forward dynamics algorithm has the standard gather/scatter structure for tree-topology algorithms. Thus, the tip-to-base sweeps *gather* and accumulate the results from all the branches at the aggregated link. The base-to-tip sweeps *scatter* the results onto the children branches of the aggregated link.

Multiple \mathcal{S} base-bodies: While the (14.26) expression for $E_{\mathcal{S}}$ shows only a single $\mathbb{A}(p, i)$ non-zero entry, more generally, when the sub-graph has multiple base-bodies, $E_{\mathcal{S}}$ will have a non-zero entry for each base-body at locations corresponding to the indices for the base-bodies. This is illustrated in the expressions in (15.15) for the four-bar linkage example.

Closure constraint with the inertial frame: Another situation that we have not explicitly addressed is that of a closure constraint between a body node and the inertial frame. In this case, node p in $\wp(\mathcal{S})$ is the inertial frame. The aggregated link in this case is a base-body attached directly to the inertial frame.

Joint-level constraints involving multiple hinges: It is possible to have the situation where a direct joint-level velocity constraint involves more than two hinges. Instead of a single closure-constraint edge, multiple cut-edges that span all the hinges involved in the constraint must be included in the system digraph before determining the aggregation sub-graph.

Singular constraint maps: Especially in the case of loop constraints, it is possible for the $X_{\mathcal{S}}$ matrix to lose rank at specific *singular* configurations of the sub-graph. The number of independent generalized velocities decreases at such singular configurations. Since the invertibility of $\mathcal{D}_{\mathcal{S}}$ depends on $X_{\mathcal{S}}$ being full-rank, it is important to monitor the rank of $X_{\mathcal{S}}$ and to adjust its size near, and at, singular configurations.

Chapter 16

Under-Actuated Systems

Techniques for the kinematics, dynamics and control of robotic systems largely focus on fully-actuated manipulators. Every degree of freedom is an active degree of freedom for these manipulators. That is, for each degree of freedom, there is an independent generalized force that can be applied by a control actuator. However, important applications involve manipulators with passive degrees of freedom, i.e., degrees of freedom with no corresponding control actuators. A passive degree of freedom can arise by design, due to actuator failure, during manipulation of articulatable objects or due to modes of operation that avoid the use of some actuators [7]. We refer to manipulators with passive degrees of freedom as **under-actuated** manipulators, and for these systems the number of available control actuators (or, more specifically, the number of independent generalized forces) is less than the number of degrees of freedom. Some examples of under-actuated manipulators are described below:

1. Free-flying space manipulators possess six degrees of freedom for the base-body, in addition to the manipulator hinge degrees of freedom. The six base-body degrees of freedom are controlled by an attitude and translation control system, while the manipulator motion is controlled by actuators at the hinges. The manipulator is sometimes operated so as to minimize base-body disturbances and conserve fuel. In this mode of operation, the six base-body degrees of freedom are passive, while the manipulator hinge degrees of freedom are active degrees of freedom.
2. The improved dexterity and maneuverability provided by additional degrees of freedom has motivated the study of hyper-redundant and snake-like robots. It has been proposed that the mass of hyper-redundant manipulators can be reduced by including actuators at only some of the hinges while keeping the remaining hinges passive [18, 39].
3. Flexible-link manipulators are inherently under-actuated. In addition to the hinge degrees of freedom, these manipulators possess deformation degrees of freedom from link flexibility. While careful structural analysis can provide good models for the elastic forces, these generalized forces cannot be directly controlled. As a result, the deformation degrees of freedom represent passive degrees of freedom.

4. Actuator failure can convert an active hinge into a passive one. In the face of actuator failures, some degree of fault-tolerant control is highly desirable for robots in remote or hazardous environments. This requires the control of an under-actuated manipulator.
5. During multi-arm manipulation of task objects, the degrees of freedom associated with loose grasp contacts (e.g. rolling contacts) or internal degrees of freedom of task objects (e.g., shears, plungers) are passive degrees of freedom.
6. Fuel slosh has a significant impact on the dynamics of space vehicles. The complex models for fuel slosh are typically approximated to first order by pendulum models. These pendulum degrees of freedom represent passive degrees of freedom.

Research on these topics has resulted in the development of useful, though largely application-specific, techniques for the analysis and control of these under-actuated systems. The extensibility of these techniques to other types of under-actuated manipulators is not always obvious. For instance, most analysis of free-flying space-robots relies extensively on the non-holonomic constraint arising from the conservation of linear and angular momenta for these manipulators. These techniques cannot be applied to under-actuated systems such as hyper-redundant manipulators or flexible-link manipulators, for whom such momentum constraints do not hold. This chapter develops elements of a general approach for the kinematics and dynamics of under-actuated manipulators [78, 80].

16.1 Modeling of Under-Actuated Manipulators

While the only fundamental requirement is that the under-actuated system have an SKO model, for the sake of exposition, we assume that the system is a canonical rigid-link serial-chain manipulator. There is no loss in generality since the ideas developed here easily extend to general SKO models using the approach from Chap. 9.

In the under-actuated system context, we use the term **active** degree of freedom for a manipulator degree of freedom associated with a control actuator. Conversely, a **passive** degree of freedom is a manipulator degree of freedom with no control actuator. If the active degrees of freedom represent the control inputs and outputs for the system, then the passive degrees of freedom represent the “internal dynamics” of the system. Due to the presence of friction, stiffness, and other such effects, the generalized force associated with a passive degree of freedom can be non-zero.

Typically, the component degrees of freedom of a multiple degree of freedom hinge are either all active or all passive. In the former case the hinge is denoted an **active hinge** and in the latter, a **passive hinge**. It is possible to have hinges with a mix of active and passive component degrees of freedom from events such as actuator failure. However, for modeling purposes, such multiple degree of freedom hinges can be decomposed into equivalent combination of active and passive hinges. In this chapter, without loss in generality, we assume that a manipulator model with

hinges containing a mix of passive and active component degrees of freedom has been replaced by an equivalent manipulator model containing only active and passive hinges.

The number of passive hinges in the manipulator is denoted n_p , and I_p denotes the set of their indices. I_a denotes the corresponding set of indices of the active hinges, and $n_a = (n - n_p)$ represents the number of active hinges in the manipulator. The total number of passive degrees of freedom is denoted N_p , while the total number of active degrees of freedom is denoted N_a . Observe that $N_a + N_p = N$, the total degrees of freedom in the system.

16.1.1 Decomposition into Passive and Active Systems

We use the I_a and I_p sets of hinge indices to decompose the manipulator into a pair of manipulator subsystems: the **active arm** \mathbb{A}_a , and the **passive arm** \mathbb{A}_p . \mathbb{A}_a is the N_a degree of freedom manipulator resulting from freezing all the passive hinges (i.e., all hinges whose index is in I_p), while \mathbb{A}_p is the N_p degree of freedom manipulator resulting from freezing all the active hinges (i.e., all hinges whose index is in the set I_a). This decomposition is illustrated in Fig. 16.1.

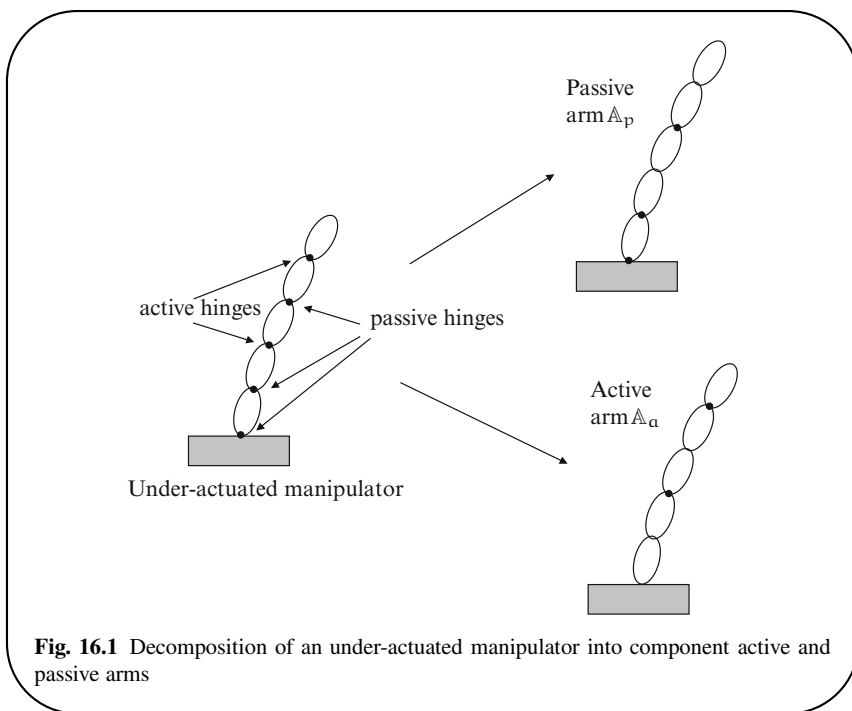


Fig. 16.1 Decomposition of an under-actuated manipulator into component active and passive arms

Let $\dot{\theta}_a \in \mathcal{R}^{N_a}$, $\mathcal{T}_a \in \mathcal{R}^{N_a}$ and $H_a^* \in \mathcal{R}^{6n \times N_a}$ denote the vector of generalized velocities, the vector of generalized forces and the joint map matrix for arm A_a . Similarly, let $\dot{\theta}_p \in \mathcal{R}^{N_p}$, $\mathcal{T}_p \in \mathcal{R}^{N_p}$ and $H_p^* \in \mathcal{R}^{6n \times N_p}$ denote the corresponding quantities for arm A_p . The two vectors $\dot{\theta}_a \in \mathcal{R}^{N_a}$ and $\dot{\theta}_p \in \mathcal{R}^{N_p}$, also represent a decomposition of the vector of generalized velocities $\dot{\theta}$ in a manner consistent with the I_a and I_p sets, respectively. Similarly \mathcal{T}_a and \mathcal{T}_p are decompositions of \mathcal{T} , and H_a^* and H_p^* are decompositions of H^* . The columns of H^* that correspond to the active hinges appear as columns of H_a^* , while those that correspond to the passive hinges appear as columns of H_p^* . Thus, the stacked vector of relative hinge spatial velocities can be expressed as follows:

$$\Delta\gamma \stackrel{3.7}{=} H^* \dot{\theta} = H_a^* \dot{\theta}_a + H_p^* \dot{\theta}_p \quad (16.1)$$

16.1.2 Partitioned Equations of Motion

We use the arm decomposition to partition the equations of motion in (9.2) as follows:

$$\begin{pmatrix} M_{aa} & M_{ap} \\ M_{ap}^* & M_{pp} \end{pmatrix} \begin{bmatrix} \ddot{\theta}_a \\ \ddot{\theta}_p \end{bmatrix} + \begin{bmatrix} C_a \\ C_p \end{bmatrix} = \begin{bmatrix} \mathcal{T}_a \\ \mathcal{T}_p \end{bmatrix} \quad (16.2)$$

where, with $i, j \in \{p, a\}$

$$M_{ij} \triangleq H_i \phi M \phi^* H_j^* \text{ and } C_i \triangleq H_i \phi [\mathbf{b} + M \phi^* \mathbf{a}] \quad (16.3)$$

In (16.2), the sub-matrices M_{aa} and M_{pp} are the mass matrices for the A_a and A_p arms, respectively.

For manipulator control, we need to compute the actuator forces required to obtain a desired motion of the active hinges and the resulting motion induced at the passive hinges. That is, it is necessary to compute the \mathcal{T}_a active hinge forces required to obtain a desired $\ddot{\theta}_a$ active hinge acceleration and the $\ddot{\theta}_p$ acceleration induced at the passive hinges. We assume that the \mathcal{T}_p passive hinge forces vector is known from the $(\theta, \dot{\theta})$ state of the system. These passive hinge forces typically arise from phenomena such as friction, backlash, and stiffness.

Thus, the problem consists of evaluating the required \mathcal{T}_a active hinge forces, and the induced $\ddot{\theta}_p$ passive hinge accelerations for a desired $\ddot{\theta}_a$ generalized acceleration at the active hinges. It is assumed that $(\theta, \dot{\theta})$ system state, and \mathcal{T}_p generalized forces at the passive hinges are known. The form of (16.2) is not convenient, since it contains a mix of the known and unknown quantities on both the left- and right-hand sides of the equation. A transformation of (16.2) that expresses the unknown quantities in terms of the known quantities is as follows:

$$\begin{bmatrix} \mathcal{T}_a \\ \ddot{\theta}_p \end{bmatrix} = \begin{pmatrix} S_{aa} & S_{ap} \\ -S_{ap}^* & S_{pp} \end{pmatrix} \begin{bmatrix} \ddot{\theta}_a \\ \mathcal{T}_p \end{bmatrix} + \begin{bmatrix} C_a - S_{ap} C_p \\ -S_{pp} C_p \end{bmatrix} \quad (16.4)$$

where

$$\begin{aligned}\mathcal{S}_{aa} &\triangleq \mathcal{M}_{aa} - \mathcal{M}_{ap}\mathcal{M}_{pp}^{-1}\mathcal{M}_{ap}^* \\ \mathcal{S}_{ap} &\triangleq \mathcal{M}_{ap}\mathcal{M}_{pp}^{-1} \\ \mathcal{S}_{pp} &\triangleq \mathcal{M}_{pp}^{-1}\end{aligned}\quad (16.5)$$

The expressions in (16.5) require \mathcal{M}_{pp} to be invertible. \mathcal{M}_{pp} is the mass matrix of the passive arm \mathbb{A}_p , and it is easy to verify that since (H, ϕ, M) define an SKO model, so do the (H_p, ϕ, M) operators for the passive arm. Thus, \mathcal{M}_{pp} is invertible.

The direct use of the expression on the right of (16.4) to obtain $\ddot{\theta}_p$ and \mathcal{T}_a requires the computation of \mathcal{M} , the inversion of \mathcal{M}_{pp} and the formation of various matrix/matrix and matrix/vector products. The computational cost of this dynamics algorithm is cubic in N_p and quadratic in N_a . Later, in Sect. 16.2, we describe a simpler $O(N)$ algorithm whose computational complexity is only linear in both N_a and N_p .

16.1.3 Spatial Operator Expression for \mathcal{M}_{pp}^{-1}

Since the \mathcal{M}_{pp} mass matrix of the \mathbb{A}_p passive arm is from an SKO model, the SKO operator factorization and inversion techniques can be used to obtain a closed form spatial operator expression for \mathcal{M}_{pp}^{-1} . Thus, following the development in Sect. 9.5 on page 179, we define the articulated body inertia quantities, $\mathcal{P}(.)$, $\mathcal{D}_p(.)$, $\mathcal{G}_p(.)$, $\mathcal{K}_p(.)$, $\bar{\tau}_p(.)$, $\mathcal{P}^+(.)$ and $\psi(.,.)$ for the \mathbb{A}_p arm. using the recursive Algorithm 16.1.

Algorithm 16.1 Articulated body inertias for the \mathbb{A}_p passive arm

$$\left\{ \begin{array}{l} \mathcal{P}^+(0) = 0 \\ \textbf{for } k = 1 \dots n \\ \quad \mathcal{P}(k) = \phi(k, k-1)\mathcal{P}^+(k-1)\phi^*(k, k-1) + M(k) \\ \quad \left\{ \begin{array}{l} \textbf{if } k \notin I_p \\ \quad \quad \mathcal{P}^+(k) = \mathcal{P}(k) \\ \textbf{else} \\ \quad \quad \mathcal{D}_p(k) = H_p(k)\mathcal{P}(k)H_p^*(k) \\ \quad \quad \mathcal{G}_p(k) = \mathcal{P}(k)H_p^*(k)\mathcal{D}_p^{-1}(k) \\ \quad \quad \mathcal{K}_p\bar{\tau}_p(k) = I - \mathcal{G}_p(k)H_p(k) \\ \quad \quad \mathcal{P}^+(k) = \bar{\tau}_p(k)\mathcal{P}(k) \\ \textbf{end if} \end{array} \right. \\ \textbf{end loop} \end{array} \right. \quad (16.6)$$

Algorithm 16.1 differs from the standard articulated body Riccati equations solution in (9.33). The difference is that the articulated body inertia quantities are being computed for only the \mathbb{A}_p passive arm, and not the full arm. The algorithm skips the articulated body inertia steps for the active bodies, since these hinges are frozen in the \mathbb{A}_p arm. The recursion in (16.6) proceeds from the tip to the base of the manipulator. At each hinge, the active or passive status of the hinge is checked. Depending on the status of the hinge, the appropriate computations are carried out and the recursion proceeds to the next hinge. This continues until the base-body is reached.

Interestingly, the $\mathcal{P}(k)$ steps for the active hinges in (16.6) are exactly the recursion steps for computing composite body inertias seen in (9.20) on page 169. This is because, the freezing of the active hinges is equivalent to converting the neighboring bodies into a composite body. In the extreme case, when all hinges in the system are active hinges, the resulting $\mathcal{P}(k)$ at each hinge is precisely the $\mathcal{R}(k)$ composite body inertia at the hinge. Conversely, when all the hinges are passive, the $\mathcal{P}(k)$ at each hinge is precisely the articulated body inertia of the system at the hinge. In general, though, $\mathcal{P}(k)$ for the \mathbb{A}_p arm is obtained by a hybrid combination of the composite and articulated body inertia steps for the system.

Using the development in Sect. 9.5, the operator $\mathcal{P} \in \mathcal{R}^{6n \times 6n}$ is defined as a block diagonal matrix with its k th diagonal element being $\mathcal{P}(k) \in \mathcal{R}^{6 \times 6}$. The quantities in (16.6) are also used to define the following spatial operators:

$$\begin{aligned}\mathcal{D}_p &\stackrel{\triangle}{=} H_p \mathcal{P} H_p^* \in \mathcal{R}^{N_p \times N_p} \\ \mathcal{G}_p &\stackrel{\triangle}{=} \mathcal{P} H_p^* \mathcal{D}_p^{-1} \in \mathcal{R}^{6n \times N_p} \\ \mathcal{K}_p &\stackrel{\triangle}{=} \mathcal{E}_\phi \mathcal{G}_p \in \mathcal{R}^{6n \times N_p} \\ \bar{\tau}_p &\stackrel{\triangle}{=} \mathbf{I} - \mathcal{G}_p H_p \in \mathcal{R}^{6n \times 6n} \\ \mathcal{E}_\psi &\stackrel{\triangle}{=} \mathcal{E}_\phi \bar{\tau}_p \in \mathcal{R}^{6n \times 6n}\end{aligned}\tag{16.7}$$

The \mathcal{D}_p , \mathcal{G}_p and $\bar{\tau}_p$ operators are all block diagonal. Even though \mathcal{K}_p and \mathcal{E}_ψ are not block diagonal matrices, their only non-zero block elements are the $\mathcal{K}_p(k, k-1)$ and $\psi(k, k-1)$ elements, respectively along the first sub-diagonal. Following (9.36), \mathcal{P} satisfies the Riccati equation

$$\mathbf{M} = \mathcal{P} - \mathcal{E}_\psi \mathcal{P} \mathcal{E}_\psi^* = \mathcal{P} - \mathcal{E}_\phi \mathcal{P} \mathcal{E}_\phi^*\tag{16.8}$$

From Lemma 9.11, it follows that the Innovations Factorization of the mass matrix \mathcal{M}_{pp} is given by

$$\mathcal{M}_{pp} = [\mathbf{I} + H_p \phi \mathcal{K}_p] \mathcal{D}_p [\mathbf{I} + H_p \phi \mathcal{K}_p]^*\tag{16.9}$$

Also, the closed form operator expressions for the inverse of the $[\mathbf{I} + \mathbf{H}_p \phi \mathcal{K}_p]$ factor and \mathcal{M}_{pp}^{-1} are

$$\begin{aligned} [\mathbf{I} + \mathbf{H}_p \phi \mathcal{K}_p]^{-1} &= [\mathbf{I} - \mathbf{H}_p \psi \mathcal{K}_p] \\ \mathcal{M}_{pp}^{-1} &= [\mathbf{I} - \mathbf{H}_p \psi \mathcal{K}_p]^* \mathcal{D}_p^{-1} [\mathbf{I} - \mathbf{H}_p \psi \mathcal{K}_p] \end{aligned} \quad (16.10)$$

16.1.4 Operator Expressions for \mathcal{S} Blocks

Lemma 16.1 below uses the operator expression for the inverse of \mathcal{M}_{pp} to derive new closed form operator expressions for the \mathcal{S}_{ij} matrices from (16.5),

Lemma 16.1 Operator expressions for \mathcal{S} components.

$$\mathcal{S}_{pp} = [\mathbf{I} - \mathbf{H}_p \psi \mathcal{K}_p]^* \mathcal{D}_p^{-1} [\mathbf{I} - \mathbf{H}_p \psi \mathcal{K}_p] \quad (16.11a)$$

$$\begin{aligned} \mathcal{S}_{ap} &= \mathbf{H}_a \{ \psi \mathcal{K}_p + \mathcal{P} \psi^* \mathbf{H}_p^* \mathcal{D}_p^{-1} [\mathbf{I} - \mathbf{H}_p \psi \mathcal{K}_p] \} \\ &= \mathbf{H}_a \{ (\psi - \mathcal{P} \Omega) \mathcal{K}_p + \mathcal{P} \psi^* \mathbf{H}_p^* \mathcal{D}_p^{-1} \} \end{aligned} \quad (16.11b)$$

$$\begin{aligned} \mathcal{S}_{aa} &= \mathbf{H}_a [\psi \mathbf{M} \psi^* - \mathcal{P} \Omega \mathcal{P}] \mathbf{H}_a^* \\ &= \mathbf{H}_a [(\psi - \mathcal{P} \Omega) \mathcal{P} + \mathcal{P} \tilde{\psi}^*] \mathbf{H}_a^* \end{aligned} \quad (16.11c)$$

where

$$\Omega \triangleq \psi^* \mathbf{H}_p^* \mathcal{D}_p^{-1} \mathbf{H}_p \psi \quad (16.12)$$

Ω defined above is the extended operational space compliance matrix for the \mathbb{A}_p passive arm as defined in (10.12) on page 190.

Proof: Equation (16.11a) follows directly from (16.5) and (16.10).

With regards (16.11b):

$$\begin{aligned} \mathcal{S}_{ap} &\stackrel{16.5}{=} \mathcal{M}_{ap} \mathcal{M}_{pp}^{-1} \\ &\stackrel{16.3, 16.11a}{=} \mathbf{H}_a \phi \mathbf{M} \phi^* \mathbf{H}_p^* [\mathbf{I} - \mathbf{H}_p \psi \mathcal{K}_p]^* \mathcal{D}_p^{-1} [\mathbf{I} - \mathbf{H}_p \psi \mathcal{K}_p] \\ &\stackrel{9.45}{=} \mathbf{H}_a \phi \mathbf{M} \psi^* \mathbf{H}_p^* \mathcal{D}_p^{-1} [\mathbf{I} - \mathbf{H}_p \psi \mathcal{K}_p] \\ &\stackrel{9.41}{=} \mathbf{H}_a \{ \phi \mathcal{K}_p + \mathcal{P} \psi^* \mathbf{H}_p^* \mathcal{D}_p^{-1} \} [\mathbf{I} - \mathbf{H}_p \psi \mathcal{K}_p] \\ &\stackrel{9.45}{=} \mathbf{H}_a \{ \psi \mathcal{K}_p + \mathcal{P} \psi^* \mathbf{H}_p^* \mathcal{D}_p^{-1} [\mathbf{I} - \mathbf{H}_p \psi \mathcal{K}_p] \} \\ &\stackrel{16.12}{=} \mathbf{H}_a \{ (\psi - \mathcal{P} \Omega) \mathcal{K}_p + \mathcal{P} \psi^* \mathbf{H}_p^* \mathcal{D}_p^{-1} \} \end{aligned}$$

For (16.11c),

$$\begin{aligned}
S_{aa} &\stackrel{16.5}{=} \mathcal{M}_{aa} - \mathcal{M}_{ap}\mathcal{M}_{pp}^{-1}\mathcal{M}_{ap}^* \stackrel{16.5}{=} \mathcal{M}_{aa} - S_{ap}\mathcal{M}_{ap}^* \\
&\stackrel{16.11b}{=} H_a \left\{ \phi - \psi \mathcal{K}_p H_p \phi - \mathcal{P} \psi^* H^* \mathcal{D}_p^{-1} * \right. \\
&\quad \left. [I - H_p \psi \mathcal{K}_p] H_p \phi \right\} M \phi^* H_a^* \\
&\stackrel{9.43, 9.45}{=} H_a \left\{ \phi - (\phi - \psi) - \mathcal{P} \psi^* H^* \mathcal{D}_p^{-1} H_p \psi \right\} M \phi^* H_a^* \\
&= H_a \left\{ \psi - \mathcal{P} \psi^* H^* \mathcal{D}_p^{-1} H_p \psi \right\} M \phi^* H_a^* \\
&\stackrel{16.12}{=} H_a \{\psi - \mathcal{P}\Omega\} M \phi^* H_a^* \stackrel{10.38c}{=} H_a \{(\psi - \mathcal{P}\Omega)\mathcal{P} + \mathcal{P}\tilde{\psi}^*\} H_a^*
\end{aligned}$$

■

The expressions for the S_{ij} matrices in Lemma 16.1 require only the inverse of the block-diagonal matrix \mathcal{D}_p , an inverse that is relatively easy to obtain.

Exercise 16.1 Alternate expression for S_{aa} .

Show that an explicit operator expression for S_{aa} is as follows:

$$S_{aa} = H_a \phi (\mathfrak{U}_\perp^* M \mathfrak{U}_\perp) \phi^* H_a^* \quad (16.13)$$

where the $\mathfrak{U} = \Omega M$ and $\mathfrak{U}_\perp = I - \mathfrak{U}$ are the projection operators defined in (10.34). ■

Recall that the mass matrix of the full system is $H \phi M \phi^* H^*$, while that of the active arm A_a is $H_a \phi M \phi^* H_a^*$. Thus, from (16.3), the mass matrix of the under-actuated manipulator, S_{aa} , differs from the mass matrix of the active manipulator, \mathcal{M}_{aa} , in the presence of the $\mathfrak{U}_\perp^* M \mathfrak{U}_\perp$ term instead of M . However, unlike M , $\mathfrak{U}_\perp^* M \mathfrak{U}_\perp$ is *not* block-diagonal.

16.2 $O(N)$ Generalized Dynamics Algorithms

One of the primary computations for manipulator control is the computation of the actuator generalized forces \mathcal{T}_a needed to obtain a desired acceleration $\ddot{\theta}_a$ at the active hinges. A secondary need is the computation of the resulting $\ddot{\theta}_p$ acceleration induced at the passive hinges. We derive expressions for $\ddot{\theta}_p$, the active hinge forces vector \mathcal{T}_a , and the link spatial accelerations vector α in Lemma 16.2 below.

Lemma 16.2 Operator expressions for $\ddot{\theta}_p$ and \mathcal{T}_a .

With

$$\begin{aligned}
\underline{a} &\triangleq H_a^* \ddot{\theta}_a + a \\
\underline{z} &\triangleq \psi [\mathcal{K}_p T_p + b + \mathcal{P} \underline{a}] \\
e_p &\triangleq T_p - H_p \underline{z} \\
\nu_p &\triangleq \mathcal{D}_p^{-1} e_p
\end{aligned} \tag{16.14}$$

we have

$$\alpha = \psi^* [H_p^* v_p + \underline{a}] \quad (16.15a)$$

$$\ddot{\theta}_p = [I - H_p \psi K_p]^* v_p - K_p^* \psi^* \underline{a} = v_p - K_p^* \alpha \quad (16.15b)$$

$$\mathcal{T}_a = H_a \{ \underline{z} + \mathcal{P}[\psi^* H_p^* v_p + \tilde{\psi}^* \underline{a}] \} = H_a \mathcal{P}[\alpha - \underline{a} + \underline{z}] \quad (16.15c)$$

Proof: From (16.4) we have that

$$\begin{aligned} \ddot{\theta}_p &= S_{pp} [\mathcal{T}_p - C_p] - S_{ap}^* \ddot{\theta}_a \\ &\stackrel{9.45, 16.11b}{=} [I - H_p \psi K_p]^* \mathcal{D}_p^{-1} \{ \mathcal{T}_p - H_p \psi (K_p \mathcal{T}_p + b + M\phi^* \underline{a}) \} \\ &\quad - \{ K_p^* \psi^* + [I - H_p \psi K_p]^* \mathcal{D}_p^{-1} H_p \psi \mathcal{P} \} H_a^* \ddot{\theta}_a \\ &\stackrel{9.45, 9.41}{=} [I - H_p \psi K_p]^* \mathcal{D}_p^{-1} \{ \mathcal{T}_p - H_p \psi (K_p \mathcal{T}_p + \mathcal{P}\underline{a} + b) \} \\ &\quad - K_p^* \psi^* \underline{a} - \{ K_p^* \psi^* + [I - H_p \psi K_p]^* \mathcal{D}_p^{-1} H_p \psi \mathcal{P} \} H_a^* \ddot{\theta}_a \\ &\stackrel{16.4}{=} [I - H_p \psi K_p]^* \mathcal{D}_p^{-1} \{ \mathcal{T}_p - H_p \psi (K_p \mathcal{T}_p + \mathcal{P}\underline{a} + b) \} - K_p^* \psi^* \underline{a} \\ &\stackrel{16.14}{=} [I - H_p \psi K_p] v_p - K_p^* \psi^* \underline{a} \end{aligned}$$

This establishes the first equality in (16.15b). Also,

$$\begin{aligned} \alpha &\stackrel{9.1}{=} \phi^* [H^* \ddot{\theta} + \underline{a}] \stackrel{16.1, 16.4}{=} \phi^* [H_p^* \ddot{\theta}_p + \underline{a}] \\ &\stackrel{16.15b}{=} \phi^* H_p^* \{ [I - H_p \psi K_p]^* v_p - K_p^* \psi^* \underline{a} \} + \phi^* \underline{a} \stackrel{9.43, 9.45}{=} \psi^* [H_p^* v_p + \underline{a}] \end{aligned}$$

This establishes (16.15a).

Using (16.15a) in the first equality in (16.15b) establishes its second equality. Now

$$\begin{aligned} S_{ap} C_p &\stackrel{16.3, 16.11b}{=} H_a \{ \psi K_p + \mathcal{P} \psi^* H_p^* \mathcal{D}_p^{-1} [I - H_p \psi K_p] \} H_p \phi [b + M\phi^* \underline{a}] \\ &\stackrel{16.15b, 9.45}{=} H_a \{ (\phi - \psi) + \mathcal{P} \psi^* H_p^* \mathcal{D}_p^{-1} H_p \psi \} [b + M\phi^* \underline{a}] \\ &\stackrel{12.2, 16.12}{=} C_a - H_a (\psi - \mathcal{P}\Omega) [M\phi^* \underline{a} + b] \\ &= C_a - H_a (\psi - \mathcal{P}\Omega) M\phi^* \underline{a} - H_a (\psi - \mathcal{P}\Omega) b \\ &\stackrel{9.42, 10.38a}{=} C_a - H_a (\tilde{\psi} \mathcal{P} + \mathcal{P} \phi^* - \mathcal{P}(\phi^* - \psi^* + \Omega \mathcal{P})) \underline{a} - H_a (\psi - \mathcal{P}\Omega) b \\ &= C_a - H_a (\psi - \mathcal{P}\Omega) [\mathcal{P}\underline{a} + b] - H_a \mathcal{P} \tilde{\psi}^* \underline{a} \end{aligned} \quad (16.16)$$

Thus, we have that

$$\begin{aligned}
\mathcal{T}_a &\stackrel{16.4}{=} \mathcal{S}_{aa} \ddot{\theta}_a + \mathcal{S}_{ap} [\mathcal{T}_p - \mathcal{C}_p] + \mathcal{C}_a \\
&\stackrel{16.11c, 16.11b, 16.16}{=} H_a \{ (\psi - \mathcal{P}\Omega) \mathcal{P} + \mathcal{P}\tilde{\Psi}^* \} H_a^* \ddot{\theta}_a \\
&\quad + H_a \{ (\psi - \mathcal{P}\Omega) \mathcal{K}_p + \mathcal{P}\Psi^* H_a^* \mathcal{D}_p^{-1} \} \mathcal{T}_p \\
&\quad + H_a (\psi - \mathcal{P}\Omega) [\mathcal{P}a + b] + H_a \mathcal{P}\tilde{\Psi}^* a \\
&= H_a \left[(\psi - \mathcal{P}\Omega) [\mathcal{P}H_a^* \ddot{\theta}_a + \mathcal{K}_p \mathcal{T}_p + (\mathcal{P}a + b)] \right. \\
&\quad \left. + \mathcal{P} \{ \tilde{\Psi}^* H_a^* \ddot{\theta}_a + \Psi^* H_a^* \mathcal{D}_p^{-1} \mathcal{T}_p + \tilde{\Psi}^* a \} \right] \\
&\stackrel{16.14, 16.12, 16.4}{=} H_a \left[[I - \mathcal{P}\Psi^* H_p^* \mathcal{D}_p^{-1} H_p] \mathfrak{z} + \mathcal{P} \{ \tilde{\Psi}^* a + \Psi^* H_p^* \mathcal{D}_p^{-1} \mathcal{T}_p \} \right] \\
&= H_a [\mathfrak{z} + \mathcal{P}\Psi^* H_p^* \mathcal{D}_p^{-1} (\mathcal{T}_p - H_p \mathfrak{z}) + \mathcal{P}\tilde{\Psi}^* a] \\
&\stackrel{16.14}{=} H_a [\mathfrak{z} + \mathcal{P}\Psi^* H_p^* \mathcal{D}_p^{-1} \epsilon + \mathcal{P}\tilde{\Psi}^* a] \\
&\stackrel{16.14}{=} H_a [\mathfrak{z} + \mathcal{P}(\Psi^* H_p^* \nu + \tilde{\Psi}^* a)] \stackrel{16.15a}{=} H_a [\mathfrak{z} + \mathcal{P}(\alpha - a)]
\end{aligned}$$

This establishes (16.15c). ■

Algorithm 16.2 provides a recursive $O(N)$ procedure for computing the $\ddot{\theta}_p$ and \mathcal{T}_a vectors. It is a conversion of the closed form operator expressions of the vectors in Lemma 16.2, into a recursive tip-to-base sweep followed by a base-to-tip sweep.

The recursion in (16.17a) starts from the tip of the manipulator and proceeds towards the base. At each hinge, the active/passive status of the hinge is checked. If the hinge is active, its acceleration is known, and is used to update the $\mathfrak{z}(\cdot)$ residual force. On the other hand, if the hinge is passive, its generalized force is known, and is used to update the $\mathfrak{z}(\cdot)$ residual force. The recursion continues until the base is reached. Now begins the recursion in (16.17b) from the manipulator base towards the tip. This time, as each new hinge is encountered, its $\ddot{\theta}_p$ hinge acceleration is computed if it is a passive hinge; the unknown \mathcal{T}_a generalized force is computed if it is an active hinge. This continues until the tip is reached and all the hinges have been processed. In summary, this dynamics algorithm requires the following three steps:

1. The recursive computation of all the $\mathcal{V}(k)$ link velocities and the $a(k)$ and $b(k)$ Coriolis terms using a base-to-tip recursion sweep, as in the standard Newton–Euler inverse dynamics Algorithm 9.1 on page 166.
2. Recursive computation of the articulated body quantities using the tip-to-base recursive sweep described in Algorithm 16.1.
3. The inward tip-to-base recursive sweep in (16.17a) to compute the residual forces $\mathfrak{z}(k)$. This is followed by the base-to-tip recursive sweep in (16.17b) to compute the components of $\ddot{\theta}_p$, \mathcal{T}_a and α .

The recursions in Step (2) can be combined and carried out in conjunction with the tip-to-base sweep in Step (3).

An interesting feature of this algorithm is that its structure is a hybrid of known inverse and forward dynamics algorithms for fully-actuated manipulators. When all the hinges are passive, I_a is empty and the steps in the above algorithm reduce to

Algorithm 16.2 Generalized AB dynamics for under-actuated systems
$$\left\{ \begin{array}{l} \mathbf{z}(0) = \mathbf{0} \\ \text{for } k = 1 \cdots n \\ \quad \left\{ \begin{array}{l} \text{if } k \in I_a \\ \quad \mathbf{z}(k) = \phi(k, k-1)\mathbf{z}^+(k-1) + \mathbf{b}(k) + \\ \quad \quad \mathcal{P}(k)[H^*(k)\ddot{\theta}_a(k) + \mathbf{a}(k)] \\ \quad \mathbf{z}^+(k) = \mathbf{z}(k) \\ \text{else} \\ \quad \mathbf{z}(k) = \phi(k, k-1)\mathbf{z}^+(k-1) + \mathbf{b}(k) + \mathcal{P}(k)\mathbf{a}(k) \\ \quad \epsilon_p(k) = \mathcal{T}_p(k) - H(k)\mathbf{z}(k) \\ \quad \mathbf{z}^+(k) = \mathbf{z}(k) + \mathcal{G}_p(k)\epsilon_p(k) \\ \quad \nu_p(k) = \mathcal{D}_p^{-1}\epsilon_p(k) \\ \text{end if} \\ \end{array} \right. \\ \text{end loop} \end{array} \right. \quad (16.17a)$$

$$\left\{ \begin{array}{l} \alpha^+(n+1) = \mathbf{0} \\ \text{for } k = n \cdots 1 \\ \quad \alpha^+(k) = \phi^*(k+1, k)\alpha(k+1) \\ \quad \left\{ \begin{array}{l} \text{if } k \in I_a \\ \quad f(k) = \mathcal{P}(k)\alpha^+(k) + \mathbf{z}(k) \\ \quad \mathcal{T}_a(k) = H(k)f(k) \\ \text{else} \\ \quad \ddot{\theta}_p(k) = \nu_p(k) - \mathcal{G}_p^*(k)\alpha^+(k) \\ \text{end if} \\ \end{array} \right. \\ \quad \alpha(k) = \alpha^+(k) + H^*(k)\ddot{\theta}(k) + \mathbf{a}(k) \\ \text{end loop} \end{array} \right. \quad (16.17b)$$

the AB forward dynamics algorithm. In this case, $\mathcal{P}(k)$ is the articulated body inertia of all the links outboard of the k th link. In the other extreme case, when all the hinges are active, I_p is empty, and the steps in the algorithm reduce to the composite rigid body inertias based inverse dynamics algorithm discussed in Exercise 5.5 on page 91. This algorithm can thus, be regarded as a **generalized dynamics algorithm** which can be used for both the inverse and forward dynamics problems for manipulators.

For a general under-actuated manipulator with both passive and active hinges, $\mathcal{P}(k)$ is formed by a combination of articulated and composite body inertia type

computations for the links outboard of the k th hinge. It is in fact the articulated body inertia for all the links outboard of the k th link for the passive arm \mathbb{A}_p . Similarly, $\mathfrak{z}(k)$ is a hybrid mix of the residual forces in the AB forward dynamics and the composite rigid body inertias based inverse dynamics algorithms.

Since each recursive step in the above algorithm has a fixed computational cost per degree of freedom, the overall computational cost of the algorithm is linear in both N_a and N_p , i.e., it is linear in N . The computational cost per passive degree of freedom is larger than the corresponding cost for an active degree of freedom. Non-zero generalized forces at the passive hinges are accounted for in a very natural manner in the algorithm. Also, the overhead associated with transitions between passive and active status of the hinge is small. When such a transition occurs during run-time, the only change required is to update the I_p and I_a sets.

16.2.1 Application to Prescribed Motion Dynamics

One application of the generalized Algorithm 16.2 dynamics algorithm is to handle **prescribed motion** hinges for the forward dynamics of fully-actuated systems. While the normal forward dynamics problem consists of computing the unknown generalized accelerations of the system given the generalized forces on the system, there are times when some of the generalized accelerations are “prescribed” and known. In reality the problem is to compute the remaining generalized accelerations, and the unknown generalized forces for the prescribed degrees of freedom. Thus, the overall number of unknown and known variables does not change. What does change is that both sets contain a mix of generalized accelerations and forces.

Algorithm 16.2 is the natural generalization of the traditional AB forward dynamics algorithm for handling such prescribed motion hinges. The adaptation associates prescribed motion hinges with the active I_a bodies, and non-prescribed hinges with the passive I_p bodies [51, 82]. This technique is also referred to as *hybrid dynamics* in Featherstone [48].

16.3 Jacobians for Under-Actuated Systems

The end-effector Jacobian matrix, \mathcal{J} , is widely used in motion planning and control of fully-actuated manipulators. For such manipulators, \mathcal{J} describes the velocity domain relationship between the incremental motion of the controlled (i.e., all the hinge) degrees of freedom and the incremental motion of the end-effector frame as follows:

$$\mathcal{V}_{nd} \stackrel{3.53}{=} \mathcal{J}\dot{\theta} = \mathcal{B}^*\phi^*\mathcal{H}^*\dot{\theta} \quad (16.18)$$

\mathcal{V}_{nd} denotes the spatial velocity of the end-effector. \mathcal{B} denotes the pick-off operator for the end-effector node. The \mathcal{J} Jacobian is independent of dynamical quantities such as link masses and inertias, and depends only upon their kinematical properties.

For under-actuated systems, control requires not only the control of the end-effector motion but also of the coupled motion induced in the passive joints. Other than in exceptional cases, relationships such as (16.18) cannot be expressed at the velocity-level, but instead must be expressed at the acceleration-level as follows:

$$\ddot{\alpha}_{nd} = \mathcal{J}_G \ddot{\theta}_a + \text{non-acceleration dependent terms} \quad (16.19)$$

and

$$\ddot{\theta}_p = \mathcal{J}_D \ddot{\theta}_a + \text{non-acceleration dependent terms} \quad (16.20)$$

The non-acceleration dependent terms on the right-hand sides of (16.19) and (16.20) depend on the manipulator state and the passive hinge forces. The coefficient matrices \mathcal{J}_G and \mathcal{J}_D in (16.19) and (16.20) characterize (in the acceleration domain) the effect of the incremental motion of the controlled active hinges on the incremental motion of the end-effector and the passive hinges, respectively. Unlike the fully-actuated Jacobian \mathcal{J} , the \mathcal{J}_G and \mathcal{J}_D Jacobians define acceleration level, and not velocity level, mappings. However, they do define the relationship between the incremental motions of the controlled hinges and the quantities being controlled. We refer to \mathcal{J}_G as the **generalized Jacobian** and \mathcal{J}_D as the **disturbance Jacobian**. \mathcal{J}_D describes the “disturbance” motion induced in the passive degrees of freedom by the motion of the active hinges. The disturbance Jacobian is not meaningful for fully-actuated manipulators, since these manipulators have no passive degrees of freedom. Like \mathcal{J}_G , the disturbance Jacobian \mathcal{J}_D also depends on both the dynamics as well as the kinematical properties of the links.

The properties of these pairs of Jacobian matrices are important for the development of control algorithms for such manipulators. Singularity analysis of \mathcal{J}_G is used to study the desirable and undesirable regions of the workspace.

Exercise 16.2 Expression for the generalized Jacobian.

Show that the \mathcal{J}_G generalized Jacobian has the general form:

$$\mathcal{J}_G = \mathcal{J}_a + \mathcal{J}_p \mathcal{J}_D \quad (16.21)$$

where $\mathcal{J}_a \triangleq \mathcal{B}\phi^* H_a^*$ and $\mathcal{J}_p \triangleq \mathcal{B}\phi^* H_p^*$ are the active and passive sub-blocks, respectively, of the fully-actuated \mathcal{J} Jacobian matrix. ■

16.3.1 The Generalized Jacobian \mathcal{J}_G

The generalized Jacobian $\mathcal{J}_G \in \mathcal{R}^{6 \times n_a}$ in (16.19) defines the relationship between the generalized accelerations of the active hinges and the spatial acceleration of the

end-effector frame. The expression for the generalized Jacobian \mathcal{J}_G is derived in the following lemma.

Lemma 16.3 The generalized Jacobian \mathcal{J}_G .

The generalized Jacobian \mathcal{J}_G is given by

$$\mathcal{J}_G = \mathcal{B}^* [\psi^* - \Omega \mathcal{P}] \mathcal{H}_a^* = \mathcal{B}^* \mathfrak{U}_\perp \phi^* \mathcal{H}_a^* \quad (16.22)$$

Proof: Combining together the expressions in (16.15), it follows that the expression for the link spatial accelerations α is

$$\alpha \stackrel{16.18}{=} [\psi^* - \Omega \mathcal{P}] \mathcal{H}_a^* \ddot{\theta}_a + \psi^* \mathcal{H}_p^* \mathcal{D}^{-1} [\mathbf{I} - \mathcal{H}_p \psi \mathcal{K}_p] \mathcal{T}_p - \Omega [\mathfrak{b} + \mathcal{P}a] + \psi^* a$$

Thus, the spatial acceleration of the end-effector frame, α_{nd} is given by

$$\begin{aligned} \alpha_{nd} &= \mathcal{B}^* \alpha + \dot{\mathcal{B}}^* \mathcal{V}_{nd} \\ &= \mathcal{B}^* [\psi^* - \Omega \mathcal{P}] \mathcal{H}_a^* \ddot{\theta}_a + \mathcal{B}^* \psi^* \mathcal{H}_p^* \mathcal{D}^{-1} [\mathbf{I} - \mathcal{H}_p \psi \mathcal{K}_p] \mathcal{T}_p \\ &\quad - \mathcal{B}^* \Omega [\mathfrak{b} + \mathcal{P}a] + \mathcal{B}^* \psi^* a + \dot{\mathcal{B}}^* \mathcal{V}_{nd} \end{aligned}$$

The first equality in (16.22) follows from comparing this with (16.19), and the second from the further use of (10.39a). ■

Comparing (16.22) with (16.18), we see that the \mathcal{J}_G differs from the \mathcal{J}_a fully-actuated Jacobian sub-block in the additional presence of the \mathfrak{U}_\perp projection operator term. Non-kinematical mass and inertia properties of the links enter into the \mathcal{J}_G generalized Jacobian \mathfrak{U}_\perp . The computation of \mathcal{J}_G can be carried out recursively, as described in Algorithm 16.3. The computational cost of this algorithm is $O(Nn_a)$.

On the other hand, to compute the $\mathcal{J}_G x$ product for a given n_a dimensional vector x , Step (3) of the algorithm should be changed to set $\ddot{\theta}_a = x$. Then a single evaluation of Steps (4) and (5) will result in $\mathcal{J}_G x$.

16.3.2 Computed-Torque for Under-Actuated Systems

The generalized Jacobian can be used to compute the feed-forward active hinge generalized forces $\mathcal{T}_a(t)$ time profile required to achieve a desired end-effector time trajectory. The end-effector trajectory is defined by the time profile of the end-effector spatial acceleration α_{nd} over the time interval of interest. We assume that the state of the manipulator is known at the beginning, i.e., the configuration $\theta(t_0)$ and hinge velocities $\dot{\theta}(t_0)$ are known at the initial time $t = t_0$. A brief sketch of the computational steps at time t is described in Algorithm 16.4.

This iterative procedure results in a time profile for the actuator forces $\mathcal{T}_a(t)$ required to achieve the desired end-effector trajectory. It also computes the trajectory of the passive hinges for the whole time interval. For simplicity, we have assumed

Algorithm 16.3 Computation of the generalized Jacobian, \mathcal{J}_G

The following procedure leads to the computation of the \mathcal{J}_G generalized Jacobian:

1. First, all the hinge velocities are set to zero. This makes the nonlinear velocity dependent terms, $a(k)$ and $b(k)$, zero for all the links. Also, the passive hinge forces, T_p , are set to zero.
2. Next, all the articulated body quantities are computed using the tip-to-base recursion in Algorithm 16.1.
3. Now, set the hinge accelerations as follows:

$$\ddot{\theta}_a(i) = \begin{cases} 1 & \text{for } i = k \\ \mathbf{0} & \text{for } i \neq k \end{cases}$$

Use the tip-to-base and base-to-tip recursions in (16.17) to compute the α_{nd} end-effector spatial accelerations. α_{nd} is the k th column of \mathcal{J}_G .

Repeating Step 3 for each of the n_a columns yields the complete generalized Jacobian matrix \mathcal{J}_G .

Algorithm 16.4 Computed torque for an under-actuated system

1. Compute $\mathcal{J}_G(t)$ using Algorithm 16.3.
2. Assuming that \mathcal{J}_G is invertible, use (16.19) to compute $\ddot{\theta}_a(t)$ via

$$\ddot{\theta}_a(t) = \mathcal{J}_G^{-1}(t)[\alpha_{nd}(t) - \text{velocity and } T_p \text{ dependent terms}]$$

3. For this $\ddot{\theta}_a(t)$, compute $T_a(t)$ and $\ddot{\theta}_p(t)$ using the generalized dynamics algorithm in Sect. 16.2.
 4. Integrate the hinge accelerations (or use measured values) to obtain the hinge velocities $\dot{\theta}(t + \Delta t)$ and configurations $\theta(t + \Delta t)$ at time $t + \Delta t$. Go back to Step 1 and repeat the steps for time $(t + \Delta t)$.
-

above that \mathcal{J}_G is square and non-singular. When \mathcal{J}_G is non-invertible, due to being singular or non-square, this procedure can be modified to use methods such as pseudo-inverses and least-squares solutions in ways similar to those for fully-actuated redundant manipulators.

16.3.3 The Disturbance Jacobian \mathcal{J}_D

The disturbance Jacobian \mathcal{J}_D in (16.20) characterizes the inertial coupling between the active and the passive hinges. It describes the incremental disturbance motion induced in the passive hinges due to the incremental motion of the active hinges. The following lemma provides an operator expression for \mathcal{J}_D .

Lemma 16.4 The disturbance Jacobian \mathcal{J}_D .

The operator expression for the disturbance Jacobian \mathcal{J}_D is given by:

$$\begin{aligned}\mathcal{J}_D &= -\mathcal{S}_{ap}^* \\ &= -[\mathbf{I} - \mathbf{H}_p \boldsymbol{\psi} \mathcal{K}_p]^* \mathcal{D}_p^{-1} \mathbf{H}_p \boldsymbol{\psi} \mathcal{P} \mathbf{H}_a^* - \mathcal{K}_p^* \boldsymbol{\psi}^* \mathbf{H}_a^*\end{aligned}\quad (16.23)$$

Proof: From (16.4), the passive hinge accelerations are given by

$$\ddot{\theta}_p = -\mathcal{S}_{ap}^* \ddot{\theta}_a + \mathcal{S}_{pp} [\mathcal{T}_p - \mathcal{C}_p] \quad (16.24)$$

and the result follows. ■

Using Algorithm 16.3, the computation of \mathcal{J}_D can be carried out simultaneously with the computation of \mathcal{J}_G . The k th column of \mathcal{J}_D is simply the $\ddot{\theta}_p$ vector obtained during the steps for the computation of the k th column of \mathcal{J}_G . The computational cost of this algorithm is also $O(Nn_a)$.

In applications where a larger number of active degrees of freedom are available than are needed to meet the primary objective of end-effector motion control, the redundant active degrees of freedom can be used to meet secondary objectives such as controlling the passive hinge motion to minimize disturbances. In this scenario, at each control sample time, the following steps are executed:

- Algorithm 16.3 is used to recursively compute the generalized and disturbance Jacobians \mathcal{J}_G and \mathcal{J}_D , and to form the composite Jacobian quantity $\begin{bmatrix} \mathcal{J}_G \\ \mathcal{J}_D \end{bmatrix}$.
- The combination of (16.19) and (16.24) characterizes the effect of the active hinge accelerations $\ddot{\theta}_a$ upon the end-effector acceleration α_{nd} and the passive hinge accelerations $\ddot{\theta}_p$ as follows:

$$\begin{bmatrix} \mathcal{J}_G \\ \mathcal{J}_D \end{bmatrix} \ddot{\theta}_a = \begin{bmatrix} \alpha_{nd} \\ \ddot{\theta}_p \end{bmatrix} + \text{velocity and } \mathcal{T}_p \text{ dependent terms} \quad (16.25)$$

Equation (16.25) is solved for the active hinge acceleration $\ddot{\theta}_p$ using the desired value for the end-effector acceleration and a value of zero for the acceleration at the passive hinges. The composite Jacobian matrix might not be square in most cases. When there are only a limited number of degrees of freedom, (16.25) can only be solved approximately, and some performance will be lost. On the other hand, when there are sufficient redundant degrees of freedom, a solution can be chosen to meet additional performance objectives.

- Next, the active hinge accelerations are used in the generalized dynamics Algorithm 16.2 to compute the active hinge forces \mathcal{T}_a .

16.4 Free-Flying Systems as Under-Actuated Systems

Free-flying systems (e.g. space platforms) with inactive base-body control are an important special case of under-actuated systems. We look at some of their properties and discuss the application of the under-actuated formulation and algorithms to these systems. The configuration considered consists of a manipulator mounted on a free-flying space vehicle. The space vehicle is controlled in six degrees of freedom by an attitude and translation control system. The manipulator motion is controlled by actuators acting at the hinges of the manipulator.

Performing manipulation maneuvers with the attitude and translation control system inactive most of the time can help conserve fuel, and is referred to as **reaction-mode control**. The control system turns on when the disturbance motions in the base-body exceed prescribed bounds. One of the desirable goals of space manipulator control is to plan and execute manipulator motions that minimize the activation of the control system to conserve fuel. The internal hinges of the space manipulator represent the active degrees of freedom, while the six base-body degrees of freedom represent passive degrees of freedom. During reaction-mode control, the passive hinge forces are zero, i.e., $\mathcal{T}_p = \mathbf{0}$. These forces are non-zero only when the space vehicle control system is on. The motion planning problem for space manipulators consists of computing active hinge forces to execute a desired end-effector trajectory while minimizing base-body motion. If the manipulator has redundant degrees of freedom, then these can be used to minimize the motion of the base-body [4, 125, 130, 134, 177].

Unlike general under-actuated systems, the linear and angular momentum of free-flying systems possess conservation properties. Also, unlike under-actuated systems, but like fully-actuated systems, the generalized and disturbance Jacobians can define velocity-level maps instead of acceleration-level maps. Due to these special properties, the behavior free-flying system falls between that of fully actuated and general under-actuated systems.

16.4.1 Integrals of Motion for Free-Flying Systems

We describe here an informal derivation of the conservation property of the spatial momentum of free-flying systems. Such conservation properties are referred to as integrals of motion. Noether's theorem from analytical mechanics [11] shows that such invariances arise from symmetries in the kinetic energy Lagrangian of the system. An example of such an integral of motion is the conservation of the system kinetic energy in the absence of external forces. This integral of motion arises because the expression for the kinetic energy does not explicitly depend on time.

A special case of such a symmetry arises when the kinetic energy does not depend upon some of the generalized coordinates of the system. Such generalized coordinates are referred to as **ignorable coordinates** [153], and lead to additional integrals of motion. For free-flying systems, the six base-body degrees of freedom

are ignorable coordinates, because the kinetic energy of the system does not explicitly depend on the orientation, or location, of the system in free-space. With the manipulator kinetic energy given by $\frac{1}{2}\beta^*\mathcal{M}\beta$, the subset of the Lagrangian equations of motion from (4.24) corresponding to the passive degrees of freedom, the lower half of (16.2), can be expressed as:

$$\frac{d[\mathcal{M}_{ap}^* \beta_a + \mathcal{M}_{pp} \beta_p]}{dt} - \frac{1}{2} \nabla_{\theta_p} [\beta^* \mathcal{M} \beta] = \mathcal{T}_p \quad (16.26)$$

Since \mathcal{M} , and consequently the kinetic energy, does not depend on the base-body hinge generalized coordinates θ_p , it follows that

$$\nabla_{\theta_p} [\beta^* \mathcal{M} \beta] = 0$$

The left-hand side of (16.26) is, therefore, an exact differential, and can be rewritten in the form

$$\mathcal{M}_{ap}^* \beta_a + \mathcal{M}_{pp} \beta_p = [\mathcal{M}_{ap}^*, \mathcal{M}_{pp}] \beta = \int_{t_0}^t \mathcal{T}_p dt + \text{constant} \quad (16.27)$$

The left-hand side of (16.27) is precisely the system-level 6-vector spatial momentum of the whole space manipulator at time t . The constant on the right-hand side is the spatial momentum at time t_0 , and the integral term reflects the rate of change of the momentum. During reaction-mode control, $\mathcal{T}_p = 0$, and therefore the left-hand side of (16.27) is constant, i.e., the linear and angular momentum of the manipulator are conserved, and are integrals of motion for the manipulator.

Equation (16.27) is equivalent to a time-varying constraint on the generalized velocities of the system. The conservation of linear momentum is a holonomic constraint and implies that the center of mass of the manipulator remains stationary. On the other hand, the conservation of angular momentum represents a non-holonomic constraint. Methods using these constraints have been developed for analyzing the kinematics, dynamics and control of space manipulators [44, 129, 134, 176]. These methods have primarily focused on the case when the right side of (16.27) is zero, i.e., when the manipulator has zero spatial momentum and is undergoing reaction-mode control. The following exercise derives a simple form of the disturbance Jacobian for free-flying systems.

Exercise 16.3 The disturbance Jacobian for a free-flying system.

Show that the disturbance Jacobian for the free-flying system is given by:

$$\mathcal{J}_D = -\mathcal{R}^{-1}(n) [\phi(n, 1)\mathcal{R}(1)\mathcal{H}^*(1), \dots, \phi(n, n-1)\mathcal{R}(n-1)\mathcal{H}^*(n-1)] \quad (16.28)$$

where $\mathcal{R}(k)$ denotes the composite body inertia at the k th link. ■

Chapter 17

Free-Flying Systems

In addition to the internal hinge degrees of freedom, free-flying manipulators have 6 additional degrees of freedom associated with the overall location and orientation of the manipulator. These additional 6 degrees of freedom are normally assigned to the manipulator base-body. While the base-body link is typically chosen based on design and use considerations, from a more general perspective, any one of the manipulator links can be designated as the base-body with equal validity. This freedom of choice, not available for ground manipulators, is responsible for a **base-invariance symmetry** possessed by free-flying manipulators [83, 148]. In this chapter, we use this symmetry to study free-flying manipulator dynamics.

17.1 Dynamics of Free-Flying Manipulators

While the only fundamental requirement is that the free-flying system have an SKO model, for the sake of exposition, we initially focus on an n rigid-link, free-flying canonical serial-chain manipulator. Once again, there is no loss in generality since the ideas developed here easily extend to general SKO models using the approach from Chap. 9.

17.1.1 Dynamics with Link n as Base-Body

For free-flying manipulators, the n th hinge (between the base-body and the inertial frame) has 6 degrees of freedom, and the components of the generalized velocities vector, $\beta(n)$, for this hinge are the components of the 6-dimensional spatial velocity of the base-body, $V(n)$. The $H(n)$ hinge map matrix for the n th hinge is the 6×6 identity matrix, i.e., $H(n) = I_6$. This model, with the n th link as the base body link, is illustrated in Fig. 17.1, and is referred to as the **regular** model. The SKO operator factorization and inversion result, as well as the $O(N)$ AB forward dynamics

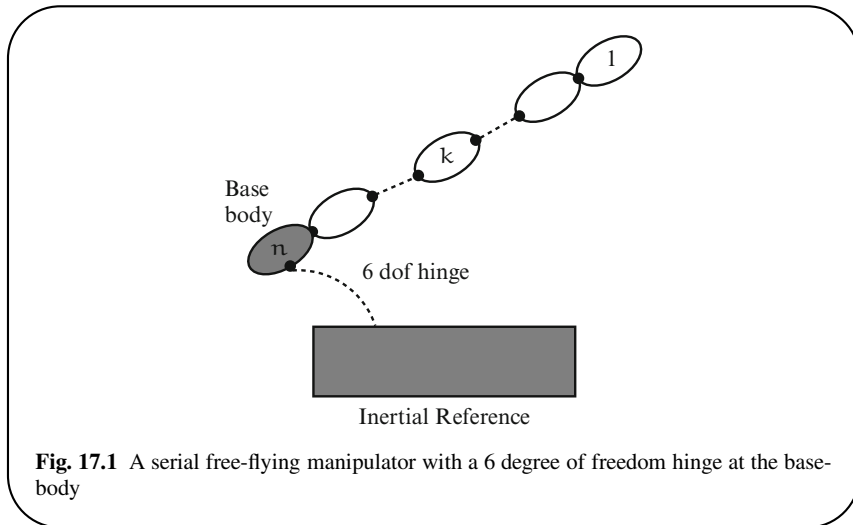


Fig. 17.1 A serial free-flying manipulator with a 6 degree of freedom hinge at the base-body

algorithm for regular manipulators, extend to free-flying manipulators as well. Since $H(n) = I_6$, the n th recursion steps (for the base-body) in (9.33) on page 175 forward dynamics recursion simplify to

$$\mathcal{D}(n) = \mathcal{P}(n), \quad \mathcal{G}(n) = I_6, \quad \tau(n) = I_6, \quad \bar{\tau}(n) = \mathbf{0}_6 \quad (17.1)$$

The residual force computations in Algorithm 9.5 also simplify to

$$\epsilon(n) = \mathcal{T}(n) - \mathfrak{z}(n), \quad \ddot{\theta}(n) = \nu(n) = \mathcal{P}^{-1}(n)\epsilon(n), \quad \alpha(n) = \nu(n) + \alpha(n) \quad (17.2)$$

For a ground manipulator, the choice of the base-body is most conveniently the link attached to the ground. For free-flying manipulators, since none of the links are attached to the ground, the choice of the base-body link is in principle an arbitrary choice.

17.1.2 Dynamics with Link 1 as Base-Body

Now, we examine an alternate model for the serial-chain free-flying manipulator, where link 1 is designated the base-body for the manipulator. We refer to this new model as the **dual** model.

We use the subscript “dl” for quantities associated with the dual model (with link 1 as base-body) to distinguish them from those associated with the regular model. Thus, the vectors β and β_{dl} denote the generalized velocity vectors for the regular and dual manipulator models, respectively.

Figure 17.2 shows the configuration of a serial free-flying manipulator with link 1 chosen as the base-body. As discussed in Sect. 17.3, the six components of the

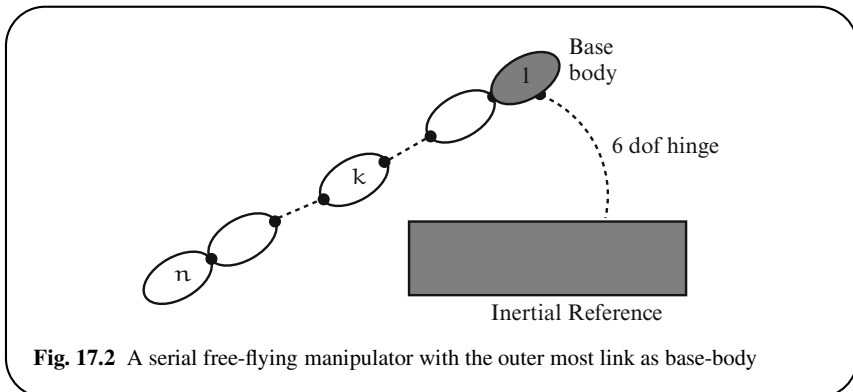


Fig. 17.2 A serial free-flying manipulator with the outer most link as base-body

spatial velocity vector of the base-body form part of the generalized velocity coordinates for the manipulator. Thus, when the base-body is moved from link n to link 1, the components of $\beta(n)$ in β are replaced by the components of $\mathcal{V}(1)$ to obtain the new generalized velocity coordinates vector β_{dl} . The definition of the H_{dl} , ϕ_{dl} etc. operators and the mass matrix M_{dl} all change in the dual formulation. The reversal in direction also reverses the sense of orientation of the internal hinge axes, and, therefore all of the $H(\cdot)$ hinge map matrices reverse sign in the dual model.

Nevertheless, the SKO formulation operator factorization and inversion results for the new mass matrix still apply. Consequently, there is a corresponding version of the AB forward dynamics algorithm (Algorithm 9.5) for this model as well. One important difference between the dual AB algorithm and Algorithm 9.5 is that the since the roles of the base and tip links are reversed, the tip-to-base (base-to-tip) recursions now proceed from link n to 1 (link 1 to n).

Exercise 17.1 Weight matrices for the dual model.

Assuming that the $\phi(k, k-1)$ weight matrices of the regular model SKO operator are invertible, show that the SKO weight matrix elements for the dual model, denoted $\phi(k-1, k)$, are the inverses of $\phi(k, k-1)$, i.e.,

$$\phi(k-1, k) \triangleq \phi^{-1}(k, k-1) = \begin{pmatrix} I_3 & -\tilde{l}(k, k-1) \\ \mathbf{0} & I_3 \end{pmatrix} \quad (17.3)$$

■

We designate the dual articulated body inertia by the symbol $S^+(k)$, and add the subscript “ dl ” to the other quantities, e.g., \mathcal{D}_{dl} , \mathcal{G}_{dl} , τ_{dl} . The quantity corresponding to \mathcal{P}^+ in the dual formulation is designated S , and is given by the expression

$$S \stackrel{\Delta}{=} \bar{\tau}_{dl} S^+$$

The articulated body inertia recursions for the $S(k+1)$ dual articulated body inertias and related quantities are described in Algorithm 17.1. The correspondence between the regular and dual articulated body inertia quantities is illustrated in Fig. 17.3. Observe that the indices for $\mathcal{P}(k)$ and $S(k)$ run from $k = 1 \cdots n$, while those for $\mathcal{P}^+(k)$ and $S^+(k)$ run from $k = 0 \cdots n - 1$.

Algorithm 17.1 Computation of dual articulated body inertias

$$\left\{ \begin{array}{l} S(n) = \mathbf{0} \\ \text{for } k = n-1, \dots, 0 \\ \quad S^+(k) = \phi(k, k+1)[S(k+1) + M(k+1)]\phi^*(k, k+1) \\ \quad \mathcal{D}_{dl}(k) = H(k)S^+(k)H^*(k) \\ \quad \mathcal{G}_{dl}(k) = -S^+(k)H^*(k)\mathcal{D}_{dl}^{-1}(k) \\ \quad \mathcal{K}_{dl}(k-1, k) = \phi(k-1, k)\mathcal{G}_{dl}(k) \\ \quad \tau_{dl}(k) = -\mathcal{G}_{dl}(k)H(k) \\ \quad \bar{\tau}_{dl}(k) = I_6 - \tau_{dl}(k) \\ \quad S(k) = \bar{\tau}_{dl}(k)S^+(k) \\ \quad \psi_{dl}(k-1, k) = \phi(k-1, k)\bar{\tau}_{dl}(k) \\ \text{end loop} \end{array} \right. \quad (17.4)$$

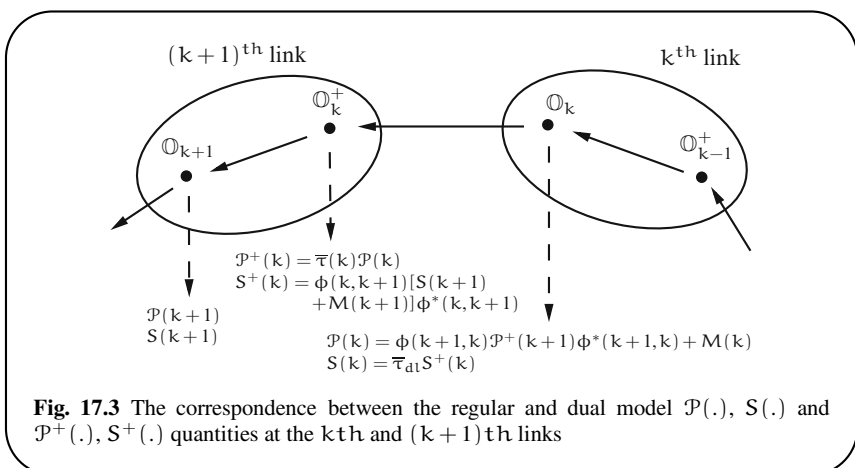


Fig. 17.3 The correspondence between the regular and dual model $\mathcal{P}(.)$, $S(.)$ and $\mathcal{P}^+(.)$, $S^+(.)$ quantities at the k^{th} and $(k+1)^{th}$ links

Exercise 17.2 Dual articulated body inertia properties.

1. Analogous to the $\mathcal{P}^+(k)H^*(k) = \mathbf{0}$ identity, show that

$$S(k)H^*(k) = \mathbf{0} \quad (17.5)$$

2. Show that

$$\tau_{dl}(k)\bar{\tau}(k) = \mathbf{0} \quad \text{and} \quad \tau(k)\bar{\tau}_{dl}(k) = \mathbf{0} \quad (17.6)$$

■

Algorithm 17.2 is the corresponding version of the residual-forces and accelerations sweeps in the dual AB forward dynamics algorithm. Re-expressing (5.8) using the dual $\phi(k, k-1)$ weight matrices shows that the $a_{dl}(k)$ Coriolis acceleration spatial vector in the dual model is related to that of the regular model as follows:

$$a_{dl}(k) \stackrel{\triangle}{=} -\phi^*(k+1, k)a(k+1) \quad (17.7)$$

Algorithm 17.2 Dual AB forward dynamics algorithm

$$\left\{ \begin{array}{l} \mathfrak{z}_{dl}(n) = \mathbf{0} \\ \text{for } k = n-1, \dots, 0 \\ \quad \mathfrak{z}_{dl}^+(k) = \phi(k, k+1)[\mathfrak{z}_{dl}(k+1) + b(k+1) \\ \quad \quad \quad + \{S(k+1) + M(k+1)\}a_{dl}(k+1)] \\ \quad \epsilon_{dl}(k) = T(k) + H(k)\mathfrak{z}_{dl}(k) \\ \quad \mathfrak{z}_{dl}(k) = \mathfrak{z}_{dl}^+(k) + g_{dl}(k)\epsilon_{dl}(k) \\ \quad v_{dl}(k) = D_{dl}^{-1}\epsilon_{dl}(k) \\ \text{end loop} \end{array} \right. \quad (17.8a)$$

$$\left\{ \begin{array}{l} \alpha(0) = \mathbf{0} \\ \text{for } k = 1 \dots n \\ \quad \alpha(k) = \phi^*(k-1, k)\alpha^+(k-1) \\ \quad \ddot{\theta}(k) = v_{dl}(k) - g_{dl}^*(k)\alpha(k) \\ \quad \alpha^+(k) = \alpha(k) - H^*(k)\ddot{\theta}(k) + a_{dl}(k) \\ \text{end loop} \end{array} \right. \quad (17.8b)$$

17.1.3 Direct Computation of Link Spatial Acceleration

The following expression relates the inter-link forces, $f(k)$, the residual forces $\mathfrak{z}(k)$, and the link spatial accelerations $\alpha(k)$ for the regular model:

$$f(k) \stackrel{7.34}{=} P^+(k)\alpha^+(k) + \mathfrak{z}^+(k) = P(k)[\alpha(k) - \mathfrak{a}(k)] + \mathfrak{z}(k) \quad (17.9)$$

The dual version of (17.9) is:

$$-f(k) = S^+(k)[\alpha^+(k) - \mathfrak{a}_{dl}(k)] + \mathfrak{z}_{dl}^+(k) = S(k)\alpha(k) + \mathfrak{z}_{dl}(k) \quad (17.10)$$

The relationships in (17.9) and (17.10) provide alternative ways of expressing the inter-link spatial force f using either the conventional or the dual articulated body inertia quantities. Combining these alternative expressions provides a direct method for computing the spatial accelerations of the links. This is described in the following lemma.

Lemma 17.1 Expression for the link spatial acceleration.

The spatial acceleration, $\alpha(k)$, of the k th link is given by:

$$\begin{aligned} \alpha(k) &= -[P(k) + S(k)]^{-1}[\mathfrak{z}(k) + \mathfrak{z}_{dl}(k) - P(k)\mathfrak{a}(k)] \quad k = 1 \dots n \\ \alpha^+(k) &= -[P^+(k) + S^+(k)]^{-1}[\mathfrak{z}^+(k) + \mathfrak{z}_{dl}^+(k) - S^+(k)\mathfrak{a}_{dl}(k)] \quad k = 0 \dots n-1 \end{aligned} \quad (17.11)$$

Proof: Add together (17.9) and (17.10), to eliminate f . ■

This result implies that the α and α^+ link accelerations can be obtained by combining together the results from the regular and dual articulated body inertia and residual force recursions. Once we have the link accelerations, the hinge generalized accelerations can be obtained by one of the following pair of expressions (see (7.32f)):

$$\ddot{\theta}(k) = v(k) - G^*(k)\alpha^+(k) = v_{dl}(k) - G_{dl}^*(k)\alpha(k) \quad (17.12)$$

17.1.4 Dynamics with Link k as Base-Body

Let us now consider the intermediate link k as the base-body for the manipulator, as shown in Fig. 17.4. For this choice, the components of the $V(k)$ spatial velocity for the k th body provide six of the generalized velocity coordinates for the system. The manipulator now has a tree-topology configuration, with two branches starting at the base. The basic algorithm remains the same as for a serial-chain, except that the recursions now have a scatter/gather structure. The recursions towards the base gather the inputs from the incoming branches, while those proceeding outwards

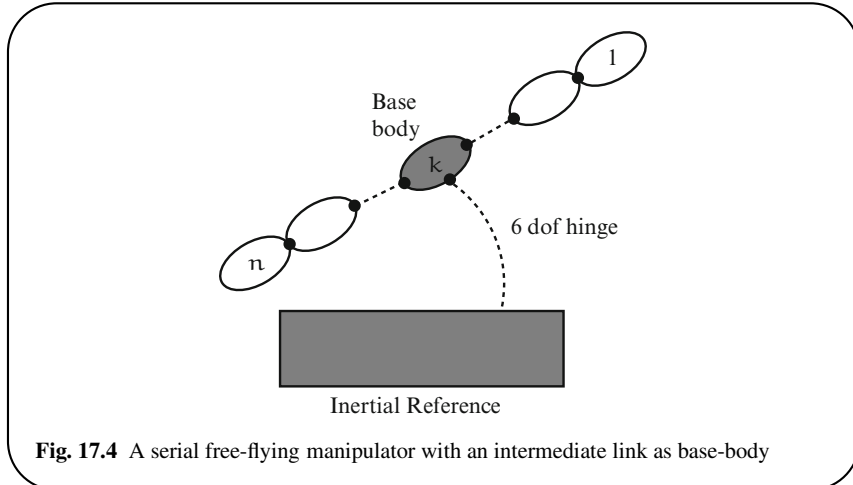


Fig. 17.4 A serial free-flying manipulator with an intermediate link as base-body

scatter their outputs along the outgoing branches. Thus, the articulated body inertia algorithm now involves two separate articulated body inertia recursions starting off at link 1 and link n , respectively, and proceeding independently towards link k . The first recursion, from link 1 to link k , is identical to the recursion in Algorithm 9.5 for computing $\mathcal{P}(.)$ matrices for the regular model. On the other hand, the second recursion from link n to link k is identical to the recursion in Algorithm 17.1 for computing $S(.)$ matrices for the dual model. These recursions end when the k th base-body is reached.

The results from the two recursions are combined at the k th link, to form the quantity $\mathcal{P}(k) + S(k)$. This quantity is precisely the articulated body inertia of the whole manipulator, as seen at frame \mathbb{O}_k , with the k th link serving as the base-body. Similarly $\mathfrak{z}(k) + \mathfrak{z}_{d1}(k)$ is the residual force at frame \mathbb{O}_k with the k th link being the base-body. The corresponding relationships in (17.11) for the “+” quantities have a similar interpretation, but with frame \mathbb{O}_k^+ serving as the reference frame for the k th link. Thus, according to Lemma 17.1, we can compute the spatial accelerations for the k th link by first making it the base-body, computing its articulated body inertia and residual forces and then using Lemma 17.1 to obtain its spatial acceleration. This observation forms the basis for the **base-invariant forward dynamics algorithm** described in the next section.

17.2 The Base-Invariant Forward Dynamics Algorithm

The previous section discussed how any link in a free-flying manipulator can, in principle, be regarded as a base-body. This arbitrariness in the choice of the base-body reflects the inherent base-invariance symmetry of free-flying manipula-

tors. However, the AB forward dynamics algorithms require the designation of a specific link as the base-body for the manipulator, and this specific choice breaks the symmetry. Breaking this symmetry is unnecessary, and the algorithm can be reformulated to preserve, and take advantage of the symmetry. *The key is to simultaneously treat every link in the manipulator as a base-body.* With this in mind, and making use of Lemma 17.1, a new forward dynamics algorithm is described in Algorithm 17.3.

Algorithm 17.3 Base-invariant forward dynamics algorithm

1. Compute the orientations, $\mathcal{V}(k)$ spatial velocities and the α and β Coriolis and gyroscopic terms for all the links recursively.
 2. a. Compute the $\mathcal{P}(k)$ etc. articulated body quantities and the $\mathfrak{z}(k)$ residual forces in a recursion from link 1 to link n using Algorithms 9.5.
b. Simultaneously compute the $S^+(k)$ dual articulated body quantities etc. and the $\mathfrak{z}_{dl}^+(k)$ dual residual forces in a recursion from link n to link 1 using Algorithms 17.1 and 17.2. The recursions in (a) and (b) can be carried out independently.
 3. For the k th link, compute the $\alpha(k)$ link spatial acceleration using Lemma 17.1, and the $\ddot{\theta}(k)$ hinge acceleration using (17.12). These computations can be carried out independently for each link.
 4. For each link, integrate its hinge acceleration and velocity to update its hinge velocity and angle.
-

17.2.1 Parallels with Smoothing Theory

As discussed in Sect. 6.4, the AB forward dynamics tip-to-base recursion is analogous to the recursion for generating optimal *filter* estimates of the state of a discrete-time dynamical system. The subsequent base-to-tip recursion, is analogous to the procedure for updating this estimate, into the optimal *smoothed* estimate of the state.

An alternative formulation of the smoothing algorithm in estimation theory consists of running two independent Kalman filters, one *causal*, and the other *anti-causal*, to generate two sets of filtered estimates of the system state [58, 59]. The optimal smoothed estimate can be obtained by combining the results of this pair of filter estimates.

The structure of the base-invariant algorithm for free-flying systems, is analogous to the structure of this alternative smoothing procedure. It combines, in effect, the results from running the first half of the AB recursion in opposing directions, and dispenses with the latter half of the AB recursion altogether.

17.2.2 Simplifications Using Non-Minimal Coordinates

So far, the hinge angles, together with the six base-body positional and orientation coordinates, have been used as the generalized coordinates for the free-flying manipulator. These coordinates form a minimal set, since their dimension is the same as the number of degrees of freedom for the system. We now examine an alternative and non-minimal choice of coordinates that simplifies the computations in Algorithm 17.3.

Towards this goal, each link is treated as an independent rigid body system. For each link, choose its orientation and positional coordinates as its generalized coordinates and its spatial velocity vector as its 6-dimensional generalized velocity coordinates. Taken together, this results in a system with $6n$ generalized velocity coordinates. These coordinates are clearly non-minimal since only N of them are truly independent. However, with these coordinates, transformations between the hinge and spatial coordinate domains become unnecessary. The modified decoupled dynamics algorithm is described in Algorithm 17.4.

The use of these non-minimal coordinates eliminates the need for the minimal θ and β coordinates and, hence, dispenses with the kinematics computations in Algorithm 17.3 for obtaining the link spatial velocities and orientations. The price paid with the use of redundant coordinates is that the integration method now involves a differential-algebraic equation rather than an ordinary differential equation, since the states being integrated are of non-minimal size. Additional steps are needed to monitor and remove drifts during the integration of the non-minimal coordinates.

Algorithm 17.4 Base-invariant forward dynamics algorithm with non-minimal coordinates

1. Use the generalized velocities (i.e., spatial velocity $\mathcal{V}(k)$) of each link to compute the a and b Coriolis and gyroscopic terms for the link. These can be computed independently for each link.
 2. a. Compute the $\mathcal{P}(k)$ etc. articulated body quantities and the $\mathfrak{z}(k)$ residual forces in a recursion from link 1 to link n using Algorithms 9.5.
b. Simultaneously compute the $S^+(k)$ etc. dual articulated body quantities and the $\mathfrak{z}_{dl}(k)$ dual residual forces in a recursion from link n to link 1 using Algorithms 17.1 and 17.2. The recursions in (a) and (b) can be carried out independently.
 3. For the k th link, compute the $\alpha(k)$ link spatial acceleration using Lemma 17.1.
 4. For each link, integrate its $\alpha(k)$ spatial acceleration and the $\mathcal{V}(k)$ spatial velocity to update its spatial velocity, position and orientation.
-

17.2.3 Computational Issues

As is the case for the AB forward dynamics algorithm (Algorithm 9.5), the decoupled dynamics algorithm described in Algorithm 17.4 is also of $O(N)$ complexity. However, since the latter involves a pair of articulated body recursions, it is computationally more expensive. On the other hand, since some of the computations are decoupled and independent of each other, the algorithm has benefits for parallel implementation. In Algorithm 17.4, the computations in step 1 can be carried out independently and in parallel for all the links. In step 2, the articulated body recursion in one direction is completely independent of the one in the opposite direction. Thus, they can be computed in parallel. Using an architecture in which each link is assigned its own computational node, each link (node) receives the results of the articulated body recursions from its neighbors, updates its own articulated body inertia, and passes the results onto its neighbors. As in step 1, the computations in step 3 are independent from link to link. Thus, each link computes its own spatial acceleration independent of the other nodes. Each node even has its own local integrator to update the state of its link.

17.2.4 Extensions to Tree-Topology Manipulators

The standard AB forward dynamics algorithm for tree-topology systems has been described in Algorithm 9.5. The recursive computations take on a gather/scatter structure. Recursions proceeding from the tips towards the base gather and sum the outputs from the incoming branches as the recursion progresses. On the other hand, the recursions that start from the base and proceed towards the tips scatter their outputs along each of the outgoing branches. Apart from this difference, the algorithm, when extended to tree-topology systems, retains the same sequential recursion steps as for serial-chain systems.

As in the case of serial-chain free-flying manipulators, tree-topology free-flying manipulators also possess the base-invariance symmetry arising from the non-unique choice for the base-body. The structure of the decoupled dynamics algorithm for tree-topology free-flying manipulators is illustrated in Fig. 17.5, and takes into account the fact there are more than two extremal bodies. The overall structure of the decoupled dynamics algorithm remains the same as in Algorithm 17.4. Corresponding to each extremal body, there is a model in which the extremal body is treated as the base-body for the model. Articulated body inertia computations are required for each of these models. At a link with multiple branches, every branch collects the articulated body inertia outputs from all of the other branches at the link. This data is accumulated by each branch to allow its articulated body inertia procedure to proceed. The overlap in the computations among the articulated body inertia recursions for the models is such that there are precisely two recursions proceeding in opposite directions across any serial link segment of the manipulator. Lemma 17.1 is still valid, and is used to compute the spatial accelerations of each of the links.

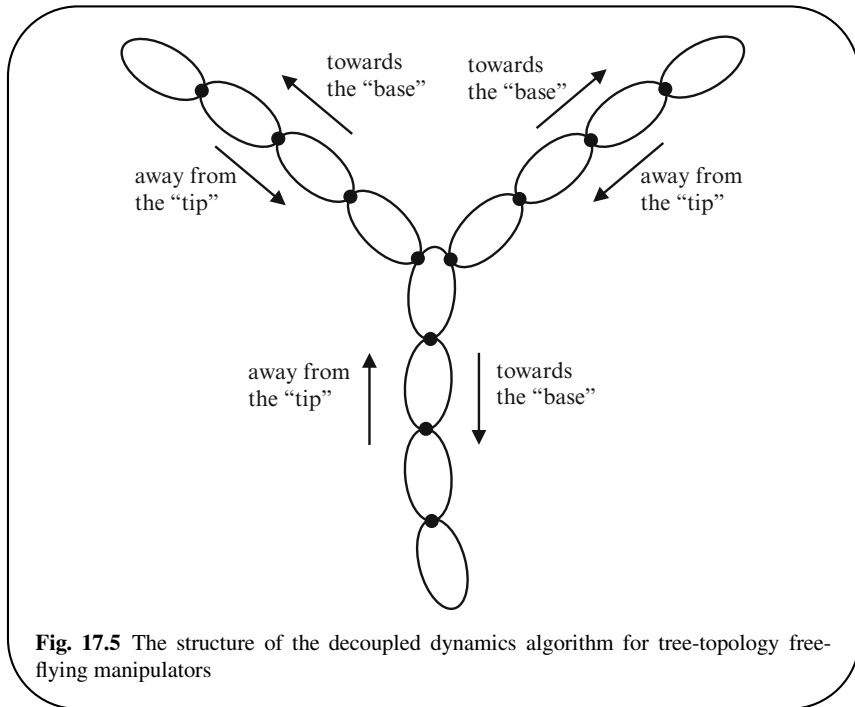


Fig. 17.5 The structure of the decoupled dynamics algorithm for tree-topology free-flying manipulators

17.3 SKO Model with kth Link as Base-Body

We now study the transformations to the SKO and SPO operators as the base-body is changed from the n th link to the k th link.

17.3.1 Generalized Velocities with kth Link as the Base-Body

When link n is the base-body, its spatial velocity, $\mathcal{V}(n)$, defines the velocity generalized coordinates for its 6 degree of freedom hinge, and is a part of the overall generalized velocity vector for the system as follows:

$$\dot{\theta}_n \triangleq \begin{bmatrix} \dot{\theta}(1) \\ \vdots \\ \mathcal{V}(n) \end{bmatrix} \in \mathcal{R}^N \quad (17.13)$$

The base-body switch from the n th link to the k th link, requires that we replace $\mathcal{V}(n)$ with $\mathcal{V}(k)$ in the system's generalized velocity vector. The new generalized

velocity vector, with the k th link as the base-body is denoted, $\dot{\theta}_k$, and is defined as:

$$\dot{\theta}_k \triangleq \begin{bmatrix} \dot{\theta}(1) \\ \vdots \\ \dot{\theta}(k-1) \\ \mathcal{V}(k) \\ \dot{\theta}(k) \\ \vdots \\ \dot{\theta}(n-1) \end{bmatrix} \in \mathcal{R}^N \quad (17.14)$$

17.3.2 Link Velocity Recursions with k th Link as the Base-Body

The switch in base-body link requires us to re-express the link spatial velocities using the new generalized velocities $\dot{\theta}_k$. Recall that the velocity recursions with the n th link as base-body are of the following form

$$\mathcal{V}(j) = \phi^*(j+1, j)\mathcal{V}(j+1) + H^*(j)\dot{\theta}(j) \quad (17.15)$$

for all links. With the k th link as base-body, the spatial velocity of links on the path from link n to link k have the revised form:

$$\mathcal{V}(j) = \phi^*(j-1, j)\mathcal{V}(j-1) + \phi^*(j-1, j)H^*(j-1)\dot{\theta}(j-1) \quad \forall j : n > j > k \quad (17.16)$$

Equation (17.16) is a simple transformation of (17.15) such that the velocity recursions proceed outwards from the new base-body. Though, for simpler exposition, we continue to assume that the $\phi(j+1, j)$ matrices are invertible, more generally this assumption is too strict and is not required. What is required however, is an *inverse* expression of the form in (17.16), that expresses the $\mathcal{V}(j)$ inboard body spatial velocity, in terms of the $\mathcal{V}(j-1)$ outboard body spatial velocity and the $\dot{\theta}(j-1)$ generalized velocity for the hinge connecting the bodies. This inverse expression defines the weights and component joint map matrices for the model with the new base-body.

Observe that the velocity recursions for only the links on the path between the base-body links n and k are affected. The expressions for all other links continue to be defined by (17.15). Thus, in effect, the impact of shifting the base-body is to reverse the direction of the path from the old to the new base-body to obtain the tree graph for the new system. This path reversal is illustrated in Fig. 17.6. It shows that the change in base-body affects only the links on the path joining the old and new base-bodies. With this observation, we denote the links on the path from the old to the new base-body as the \mathfrak{S} serial-chain sub-graph of the original tree graph. Since \mathfrak{S} is a serial-chain, its reversed version, referred to as \mathfrak{S}_r , is a serial-chain as well, albeit a non-canonical one.

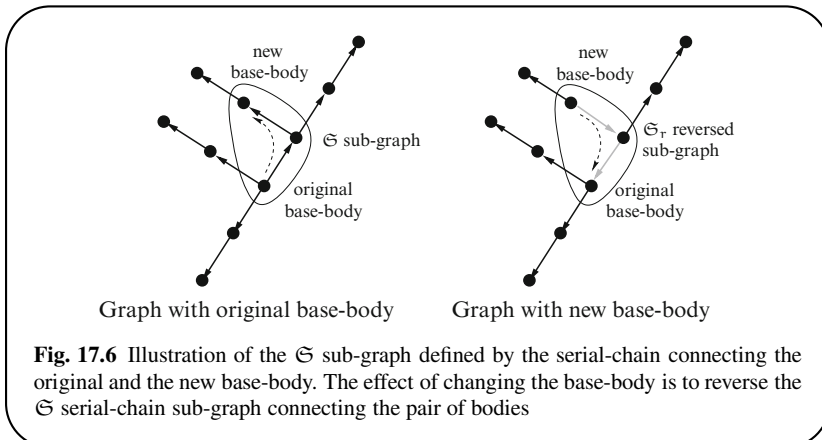


Fig. 17.6 Illustration of the \mathfrak{S} sub-graph defined by the serial-chain connecting the original and the new base-body. The effect of changing the base-body is to reverse the \mathfrak{S} serial-chain sub-graph connecting the pair of bodies

17.3.3 Partitioned System

Since \mathfrak{S} is a serial-chain, it is also a path-induced sub-graph. Using Lemma 14.1, \mathfrak{S} partitions the original graph into child, \mathcal{C} , and parent, \mathcal{P} path-induced forests. Since the link n base-body belongs to \mathfrak{S} , \mathcal{P} is empty, and \mathcal{C} contains all the remaining links in the system. Thus, using (14.2), the \mathcal{E}_ϕ SKO operator and H can be expressed in partitioned form as:

$$\mathcal{E}_\phi = \begin{pmatrix} \mathcal{E}_{\phi_{\mathcal{C}}} & \mathbf{0} \\ \mathcal{B}_{\mathfrak{S}} & \mathcal{E}_{\phi_{\mathfrak{S}}} \end{pmatrix}, \quad H = \begin{pmatrix} H_{\mathcal{C}} & \mathbf{0} \\ \mathbf{0} & H_{\mathfrak{S}} \end{pmatrix}, \quad \dot{\theta} = \begin{bmatrix} \dot{\theta}_{\mathcal{C}} \\ \dot{\theta}_{\mathfrak{S}} \end{bmatrix} \quad (17.17)$$

Since the shift in the base-body only affects the \mathfrak{S} serial-chain, the SKO operator for the transformed system is identical to that in (17.17), with the $\mathcal{E}_{\phi_{\mathfrak{S}}}$ sub-graph SKO operator replaced by a new one. With this observation, we will focus for now on the transformed properties of \mathfrak{S} , since it is the only part that changes. The generalized velocities of the original and reversed serial-chain \mathfrak{S} are:

$$\dot{\theta}_{\mathfrak{S}} \triangleq \begin{bmatrix} \dot{\theta}(k) \\ \vdots \\ \dot{\theta}(n) \end{bmatrix} \in \mathcal{R}^{N_G} \quad \text{and} \quad \dot{\theta}_R \triangleq \begin{bmatrix} \dot{\theta}(k) \\ \dot{\theta}(n-1) \\ \vdots \\ \dot{\theta}(1) \end{bmatrix} \in \mathcal{R}^{N_G} \quad (17.18)$$

N_G denotes the length of the generalized velocities for the \mathfrak{S} serial-chain. Also, define unit vectors e_{Gj} and e_{Rj} that are dimensionally compatible with $\dot{\theta}_{\mathfrak{S}}$ and $\dot{\theta}_R$, respectively. These unit vectors satisfy the following relationships:

$$e_{Gj}^* \dot{\theta}_{\mathfrak{S}} = \dot{\theta}_{\mathfrak{S}}(j) \quad \text{and} \quad e_{Rj}^* \dot{\theta}_R = \dot{\theta}_R(j) \quad \forall k \leq j \leq n \quad (17.19)$$

In particular, e_{Gn} and e_{Rk} are $\mathcal{N}_G \times 6$ matrices such that

$$e_{Gn}^* \dot{\theta}_{\mathfrak{S}} = \mathcal{V}(n) \quad \text{and} \quad e_{Rk}^* \dot{\theta}_R = \mathcal{V}(k) \quad (17.20)$$

17.3.4 Properties of a Serial-Chain SKO Operator

Assuming that \mathfrak{S} is canonical, it follows from (8.30) that

$$\mathcal{E}_{\phi_{\mathfrak{S}}} = \begin{pmatrix} \mathbf{0} & \mathbf{0} & \mathbf{0} & \mathbf{0} & \mathbf{0} \\ \phi(k+1, k) & \mathbf{0} & \dots & \mathbf{0} & \mathbf{0} \\ \mathbf{0} & \phi(k+2, k+1) & \dots & \mathbf{0} & \mathbf{0} \\ \vdots & \vdots & \ddots & \vdots & \vdots \\ \mathbf{0} & \mathbf{0} & \dots & \phi(n, n-1) & \mathbf{0} \end{pmatrix} \quad (17.21)$$

We can re-express $\mathcal{E}_{\phi_{\mathfrak{S}}}$ as

$$\mathcal{E}_{\phi_{\mathfrak{S}}} = \mathbb{S} \Delta_{\phi} \quad (17.22)$$

where

$$\mathbb{S} \triangleq \sum_{j=k}^{n-1} e_{j+1} e_j^* = \begin{pmatrix} \mathbf{0} & \mathbf{0} & \mathbf{0} & \mathbf{0} & \mathbf{0} \\ \mathbf{I} & \mathbf{0} & \dots & \mathbf{0} & \mathbf{0} \\ \mathbf{0} & \mathbf{I} & \dots & \mathbf{0} & \mathbf{0} \\ \vdots & \vdots & \ddots & \vdots & \vdots \\ \mathbf{0} & \mathbf{0} & \dots & \mathbf{I} & \mathbf{0} \end{pmatrix} \in \mathcal{R}^{6n_G \times 6n_G} \quad (17.23)$$

$$\text{and } \Delta_{\phi} \triangleq \begin{pmatrix} \phi(k+1, k) & \dots & \mathbf{0} & \mathbf{0} \\ \mathbf{0} & \ddots & \mathbf{0} & \mathbf{0} \\ \mathbf{0} & \dots & \phi(n, n-1) & \mathbf{0} \\ \mathbf{0} & \dots & \mathbf{0} & \mathbf{I} \end{pmatrix} \mathcal{R}^{6n_G \times 6n_G}$$

In the above, n_G denotes the number of bodies in the \mathfrak{S} serial-chain. Δ_{ϕ} is block-diagonal and invertible, since the component $\phi(j+1, j)$ elements are invertible. Some useful properties of \mathbb{S} are defined in the following remark.

Remark 17.1 Properties of the \mathbb{S} matrix.

Let \mathbb{S} denote the matrix defined in (17.23). Then given compatible, block-diagonal matrices A and B , the following relationships hold:

$$\begin{aligned}
 (\mathbb{S}\mathbb{A}\mathbb{S}^*)\mathbb{S}\mathbb{B} &= \mathbb{S}\mathbb{A}\mathbb{B} \\
 (\mathbb{S}^*\mathbb{A}\mathbb{S})\mathbb{S}^*\mathbb{B} &= \mathbb{S}^*\mathbb{A}\mathbb{B} \\
 \mathbb{A}\mathbb{S}^*(\mathbb{S}\mathbb{B}\mathbb{S}^*) &= \mathbb{A}\mathbb{B}\mathbb{S}^* \\
 (\mathbb{S}\mathbb{A}\mathbb{S}^*)(\mathbb{S}\mathbb{B}\mathbb{S}^*) &= \mathbb{S}\mathbb{A}\mathbb{B}\mathbb{S}^* \\
 (\mathbb{S}^*\mathbb{A}\mathbb{S})(\mathbb{S}^*\mathbb{B}\mathbb{S}) &= \mathbb{S}^*\mathbb{A}\mathbb{B}\mathbb{S}
 \end{aligned} \tag{17.24}$$

$$\begin{aligned}
 (\mathbb{S}\mathbb{S}^*)\mathbb{S}\mathbb{A} &= \mathbb{S}\mathbb{A} & \mathbb{S}\mathbb{A}(\mathbb{S}^*\mathbb{S}) &= \mathbb{S}\mathbb{A} \\
 (\mathbb{S}^*\mathbb{S})\mathbb{S}^*\mathbb{A} &= \mathbb{S}^*\mathbb{A} & \mathbb{A}(\mathbb{S}\mathbb{S}^*)\mathbb{S} &= \mathbb{A}\mathbb{S} \\
 (\mathbb{S}^*\mathbb{S})\mathbb{A}\mathbb{S}^* &= \mathbb{A}\mathbb{S}^* & \mathbb{A}(\mathbb{S}^*\mathbb{S})\mathbb{S}^* &= \mathbb{A}\mathbb{S}^*
 \end{aligned} \tag{17.25}$$

The following additional identities hold:

$$\begin{aligned}
 \mathbb{A}\mathbb{S}(\mathbb{S}^*\mathbb{B}\mathbb{S}) &= \mathbb{A}\mathbb{B}\mathbb{S} \\
 (\mathbb{S}\mathbb{S}^*)\mathbb{A}\mathbb{S} &= \mathbb{A}\mathbb{S} \\
 \mathbb{S}^*\mathbb{A}(\mathbb{S}\mathbb{S}^*) &= \mathbb{S}^*\mathbb{A}
 \end{aligned} \tag{17.26}$$

Also,

$$\mathbb{S}\mathbb{S}^* = \mathbf{I} - \mathbf{e}_k\mathbf{e}_k^*, \quad \mathbb{S}^*\mathbb{S} = \mathbf{I} - \mathbf{e}_n\mathbf{e}_n^*, \quad \mathbf{e}_k^*\mathbb{S} = \mathbf{0}, \quad \mathbb{S}\mathbf{e}_n = \mathbf{0} \tag{17.27}$$

In the above, \mathbf{e}_k denotes a block-vector with only the first block element being non-zero (and the identity matrix), while \mathbf{e}_n has only the last entry being non-zero (and the identity matrix). These expressions can be verified directly using arbitrary block-diagonal A and B matrices. ■

17.3.5 Reversing the SKO Operator

The following lemma defines the SKO properties of the \mathfrak{S}_r reversed sub-graph.

Lemma 17.2 The reversed $\mathcal{E}_{\phi R}$ operator.

The SKO operator $\mathcal{E}_{\phi R}$, together with H_R^* and $\dot{\theta}_R$ for the \mathfrak{S}_r reversed serial-chain are related to the original \mathfrak{S} serial-chain quantities as follows:

$$\mathcal{E}_{\phi R} \triangleq \Delta_{\phi}^{-1} \mathbb{S}^* \tag{17.28a}$$

$$H_R^* \triangleq -\mathcal{E}_{\phi R}^* H_{\mathfrak{S}}^* S_{RG}^* + \mathbf{e}_k e_{Rk}^* \tag{17.28b}$$

$$\dot{\theta}_R = \mathfrak{J}_{RG} \dot{\theta}_{\mathfrak{S}} \quad \text{where} \quad \mathfrak{J}_{RG} \triangleq S_{RG} + e_{Rk} e_k^* \phi_{\mathfrak{S}}^* H_{\mathfrak{S}}^* \tag{17.28c}$$

and

$$\mathbb{S}_{RG} \stackrel{\triangle}{=} \sum_{j=k}^{n-1} e_{Rj+1} \cdot e_G^* \in \mathcal{R}^{\mathcal{N}_G \times \mathcal{N}_G} \quad (17.29)$$

With $\phi_R \stackrel{\triangle}{=} (\mathbf{I} - \mathcal{E}_{\phi_R})^{-1}$ as the SPO operator for the reversed system, the link spatial velocities $\mathcal{V}_{\mathfrak{S}}$ satisfy the following relationships:

$$\mathcal{V}_{\mathfrak{S}} = \mathcal{E}_{\phi_R}^* \mathcal{V}_{\mathfrak{S}} + H_R^* \dot{\theta}_R \quad \text{and} \quad \mathcal{V}_{\mathfrak{S}} = \phi_R^* H_R^* \dot{\theta}_R \quad (17.30)$$

Proof: For \mathfrak{S} , we have

$$\mathcal{V}_{\mathfrak{S}} = \mathcal{E}_{\phi_{\mathfrak{S}}}^* \mathcal{V}_{\mathfrak{S}} + H_{\mathfrak{S}}^* \dot{\theta}_{\mathfrak{S}} \quad \text{and} \quad \mathcal{V}_{\mathfrak{S}} = \phi_{\mathfrak{S}}^* H_{\mathfrak{S}}^* \dot{\theta}_{\mathfrak{S}} \quad (17.31)$$

Thus,

$$\begin{aligned} \mathfrak{J}_{RG} \dot{\theta}_{\mathfrak{S}} &\stackrel{17.28c}{=} (\mathbb{S}_{RG} + e_{Rk} e_k^* \phi_{\mathfrak{S}}^* H_{\mathfrak{S}}^*) \dot{\theta}_{\mathfrak{S}} \stackrel{17.31}{=} \mathbb{S}_{RG} \dot{\theta}_{\mathfrak{S}} + e_{Rk} e_k^* \mathcal{V}_{\mathfrak{S}} \\ &\stackrel{17.19, 17.29}{=} \sum_{j=k}^{n-1} e_{Rj+1} \dot{\theta}_{\mathfrak{S}}(j) + e_{Rk} \mathcal{V}(k) \stackrel{17.18}{=} \dot{\theta}_R \end{aligned}$$

This establishes the last expression for $\dot{\theta}_R$ in (17.28c).

Furthermore,

$$\begin{aligned} H_R^* \mathfrak{J}_{RG} &\stackrel{17.28b, 17.28c}{=} (-\mathcal{E}_{\phi_R}^* H_{\mathfrak{S}}^* \mathbb{S}_{RG}^* + e_k e_k^*) (\mathbb{S}_{RG} + e_{Rk} e_k^* \phi_{\mathfrak{S}}^* H_{\mathfrak{S}}^*) \\ &\stackrel{17.29}{=} -\mathcal{E}_{\phi_R}^* H_{\mathfrak{S}}^* \mathbb{S}_{RG}^* \mathbb{S}_{RG} + e_k e_k^* \phi_{\mathfrak{S}}^* H_{\mathfrak{S}}^* \\ &\stackrel{17.29, 17.27}{=} -\mathcal{E}_{\phi_R}^* H_{\mathfrak{S}}^* + e_k e_k^* \phi_{\mathfrak{S}}^* H_{\mathfrak{S}}^* \\ &= (-\mathcal{E}_{\phi_R}^* + e_k e_k^* \phi_{\mathfrak{S}}^*) H_{\mathfrak{S}}^* \end{aligned} \quad (17.32)$$

In the above we have used the $e_{Rk}^* \mathbb{S}_{RG} = \mathbf{0}$ identity (shown later in (17.37a)). Hence,

$$H_R^* \dot{\theta}_R \stackrel{17.28c}{=} H_R^* \mathfrak{J}_{RG} \dot{\theta}_{\mathfrak{S}} \stackrel{17.32}{=} -\mathcal{E}_{\phi_R}^* H_{\mathfrak{S}}^* \dot{\theta}_{\mathfrak{S}} + e_k e_k^* \mathcal{V}_{\mathfrak{S}} \quad (17.33)$$

We have

$$\begin{aligned} \mathcal{E}_{\phi_R}^* \mathcal{V}_{\mathfrak{S}} + H_R^* \dot{\theta}_R &\stackrel{17.33, 17.31}{=} \mathcal{E}_{\phi_R}^* (\mathcal{E}_{\phi_{\mathfrak{S}}}^* \mathcal{V}_{\mathfrak{S}} + H_{\mathfrak{S}}^* \dot{\theta}_{\mathfrak{S}}) + (-\mathcal{E}_{\phi_R}^* H_{\mathfrak{S}}^* \dot{\theta}_{\mathfrak{S}} + e_k e_k^* \mathcal{V}) \\ &\stackrel{17.22, 17.28a}{=} \mathbb{S} \mathbb{S}^* \mathcal{V}_{\mathfrak{S}} + e_k e_k^* \mathcal{V}_{\mathfrak{S}} \stackrel{17.27}{=} \mathcal{V}_{\mathfrak{S}} \end{aligned}$$

This establishes (17.30). ■

\mathfrak{J}_{RG} in (17.28c) defines the transformation between the original and the new generalized velocities for the system. From (17.28b), $H_R^* = -\mathbb{S} \Delta_{\phi}^{-1} H_{\mathfrak{S}}^* \mathbb{S}^* + e_k e_k^*$, which on closer examination can be seen to be block-diagonal with the 6×6 identity matrix as its first diagonal element. The internal structure of the \mathcal{E}_{ϕ_R} spatial operator is as follows:

$$\mathcal{E}_{\Phi R} = \begin{pmatrix} \mathbf{0} & \phi(k, k+1) & \mathbf{0} & \mathbf{0} & \mathbf{0} \\ \vdots & \vdots & \ddots & \vdots & \vdots \\ \mathbf{0} & \mathbf{0} & \dots & \phi(n-2, n-1) & \mathbf{0} \\ \mathbf{0} & \mathbf{0} & \dots & \mathbf{0} & \phi(n-1, n) \\ \mathbf{0} & \mathbf{0} & \dots & \mathbf{0} & \mathbf{0} \end{pmatrix} \quad (17.34)$$

Exercise 17.3 Relationship between $\phi_{\mathfrak{S}}^*$ and ϕ_R^* .*Show that*

$$\tilde{\phi}_R^* + \phi_{\mathfrak{S}}^* = \phi_R^* e_k e_k^* \phi_{\mathfrak{S}}^* \quad (17.35)$$

In other words,

$$\tilde{\phi}_R^* (\phi_{\mathfrak{S}}^*)^{-1} = \phi_R^* e_k e_k^* - \mathbf{I} \quad (17.36)$$

■

Before moving on, we list a few identities that are easy to verify.

$$\mathbb{S}_{RG}^* e_{Rk} = \mathbf{0} \quad (17.37a)$$

$$\mathbb{S}_{RG}^* \mathbb{S}_{RG} = \mathbf{I} - e_n e_n^* \quad (17.37b)$$

$$\phi_R^* e_n \stackrel{8.21}{=} e_n \quad (17.37c)$$

$$e_n^* H_{\mathfrak{S}}^* = e_n^* \quad (17.37d)$$

$$e_n^* \phi_{\mathfrak{S}}^* \stackrel{8.20}{=} e_n^* \quad (17.37e)$$

Exercise 17.4 The inverse transformation \mathfrak{J}_{GR} .*Show that*

$$\dot{\theta}_{\mathfrak{S}} = \mathfrak{J}_{GR} \dot{\theta}_R \quad \text{where} \quad \mathfrak{J}_{GR} \triangleq \mathbb{S}_{RG}^* + e_{Gn} e_n^* \phi_R^* H_{\mathfrak{R}}^* \quad (17.38)$$

Also, verify that

$$\mathfrak{J}_{GR} * \mathfrak{J}_{RG} = \mathbf{I} \quad (17.39)$$

■

Thus, the \mathfrak{J}_{RG} and \mathfrak{J}_{GR} transformations are the inverses of each other.**17.3.6 Transformed SKO Model**

With the kth link as the base-body, the new system-level SKO operator and joint map matrix partitioned structure in (17.17) have the following form:

$$\underline{\mathcal{E}}_{\Phi} = \begin{pmatrix} \mathcal{E}_{\Phi C} & \mathbf{0} \\ \mathcal{B}_{\mathfrak{S}} & \mathcal{E}_{\Phi R} \end{pmatrix}, \quad \underline{H} = \begin{pmatrix} H_C & \mathbf{0} \\ \mathbf{0} & H_R \end{pmatrix}, \quad \dot{\underline{\theta}} = \begin{bmatrix} \dot{\theta}_C \\ \dot{\theta}_R \end{bmatrix} \quad (17.40)$$

Using (14.4), the corresponding system-level SPO operator $\underline{\phi}$ is

$$\underline{\phi} = \begin{pmatrix} \phi_{\mathcal{C}} & \mathbf{0} \\ \phi_R \mathcal{B}_{\mathfrak{S}} \phi_{\mathcal{C}} & \phi_R \end{pmatrix} \quad (17.41)$$

The new mass matrix of the system is defined by:

$$\underline{\mathcal{M}} = \underline{H} \underline{\phi} \underline{\mathcal{M}} \underline{\phi}^* \underline{H}^* \quad (17.42)$$

Exercise 17.5 Transformed mass matrix.

1. Show that

$$\phi_R^* H_R^* \mathfrak{J}_{RG} = \phi_{\mathfrak{S}}^* H_{\mathfrak{S}}^* \quad (17.43)$$

2. Show that

$$\dot{\underline{\theta}} = \mathfrak{J}_{RG} \dot{\theta} \text{ and } \underline{\phi}^* \underline{H}^* \mathfrak{J}_{RG} = \phi^* H^* \quad \text{where } \mathfrak{J}_{RG} \triangleq \begin{pmatrix} \mathbf{I} & \mathbf{0} \\ \mathbf{0} & \mathfrak{J}_{RG} \end{pmatrix} \quad (17.44)$$

3. Show that the new mass matrix, $\underline{\mathcal{M}}$ is related to the original \mathcal{M} mass matrix by

$$\mathcal{M}_{\mathfrak{S}} = \mathfrak{J}_{RG}^* \underline{\mathcal{M}} \mathfrak{J}_{RG} \quad (17.45)$$

4. Verify that the new mass matrix satisfies the following kinetic energy relationship:

$$\mathfrak{K}_e = \frac{1}{2} \dot{\underline{\theta}}^* \underline{\mathcal{M}} \dot{\underline{\theta}} = \frac{1}{2} \dot{\theta}^* \mathcal{M} \dot{\theta} \quad (17.46)$$

This is consistent with the intuitive expectation that the kinetic energy should be invariant with respect to the choice of the base-body.

5. Verify that $\underline{\mathcal{M}}$ and its operators define an SKO model.



17.4 Base-Invariant Operational Space Inertias

The Ω extended operational space compliance matrix for the system is defined in (10.11) and (10.12) as

$$\Omega = \phi^* H^* \mathcal{M}^{-1} H \phi \quad (17.47)$$

The following lemma shows that the Ω matrix remains independent of the base-body choice for free-flying systems.

Lemma 17.3 Ω is independent of the base-body.

The Ω matrix defined in (17.47) with the n th link as the base-body agrees with that computed when the same definition is used with the k th link as the base-body, i.e.,

$$\Omega = \underline{\Phi}^* \underline{H}^* \underline{\mathcal{M}}^{-1} \underline{H} \underline{\Phi} \quad (17.48)$$

Proof: We have

$$\Omega \stackrel{10.12}{=} \underline{\Phi}^* \underline{H}^* \underline{\mathcal{M}}^{-1} \underline{H} \underline{\Phi} \stackrel{17.45}{=} \underline{\Phi}^* \underline{H}^* (\underline{\mathfrak{J}}_{RG}^* \underline{\mathcal{M}} \underline{\mathfrak{J}}_{RG})^{-1} \underline{H} \underline{\Phi} \stackrel{17.43}{=} \underline{\Phi}^* \underline{H}^* \underline{\mathcal{M}}^{-1} \underline{H} \underline{\Phi}$$

This establishes (17.48). ■

Lemma 10.1 defined the block-diagonal Υ operational space compliance kernel operator as just the block-diagonal elements of the Ω operator. It also defined an $O(N)$ base-to-tips scatter algorithm for computing the elements of Υ in Algorithm 10.3 on page 195. The following lemma shows that the choice of base-body used in this scatter algorithm does not alter the elements of Υ .

Lemma 17.4 Base-invariance of Υ .

The choice of base-body for a free-flying system used in Algorithm 10.3 for computing the Υ block-diagonal matrix does not affect the computed values.

Proof: We have seen in Lemma 17.3 that the value of Ω is independent of the choice of the base-body. Consequently, its block diagonal element values are independent of the choice of the base-body. Since the diagonal elements of Υ are indeed the block-diagonal elements of Ω , this lemma is established. ■

The following remark establishes that $\Upsilon(k)$ is always invertible for a free-flying system.

Remark 17.2 Invertibility of $\Upsilon(k)$.

As discussed in Remark 10.1 on page 196, for ground-based manipulators, $\Upsilon(k)$ is singular for the first set of links connected to the base. This is because there are directions along which spatial forces induce no motion in ground-based manipulators. In contrast, for free-flying systems, Remark 10.2 on page 196 showed that $\Upsilon(\cdot)$ at the base-body is the inverse of the articulated body inertia, i.e., if link n is the base-body, then

$$\Upsilon(n) = \mathcal{P}^{-1}(n) \quad (17.49)$$

Since this relationship holds for any choice of base-body, this implies that $\Upsilon(k)$ is invertible for all k . This invertibility property is consistent with the property that any non-zero spatial force at any body on a free-flying manipulator induces a non-zero acceleration in the body. ■

The following lemma takes us one step further, and establishes the relationship between $\Upsilon(k)$ and the regular and dual articulated body inertia quantities defined earlier in the chapter. It shows that the symmetry of free-flying manipulators allows us to dispense with these algorithms, and express the $\Upsilon(k)$ s directly using the regular and dual articulated body inertias.

Lemma 17.5 Expression for $[\Upsilon(k)]^{-1}$.

$\Upsilon(k)$ and $\Upsilon^+(k)$ can be expressed as follows using the regular and dual articulated body inertia quantities:

$$[\Upsilon^+(k)]^{-1} = \mathcal{P}^+(k) + S^+(k) \quad \forall \quad k = 0 \dots n - 1 \quad (17.50a)$$

$$[\Upsilon(k)]^{-1} = \mathcal{P}(k) + S(k) \quad \forall \quad k = 1 \dots n \quad (17.50b)$$

Proof: We will prove this lemma using induction. From (17.4) we know that $S(n) = \mathbf{0}$. Thus, from (17.49) it follows that

$$[\Upsilon(n)]^{-1} = \mathcal{P}(n) + S(n)$$

Having established (17.50b) for link n , we begin the proof by induction by assuming that (17.50b) is true for link $(k+1)$, i.e.,

$$[\Upsilon(k+1)]^{-1} = \mathcal{P}(k+1) + S(k+1) \quad (17.51)$$

We will show now that both identities in (17.50) then must hold for link k . We have

$$\begin{aligned} [\Upsilon^+(k)]^{-1} &\stackrel{10.22}{=} [\phi^*(k+1, k)\Upsilon(k+1)\phi(k+1, k)]^{-1} \\ &\stackrel{17.3, 17.51}{=} \phi(k, k+1)[\mathcal{P}(k+1) + S(k+1)]\phi^*(k, k+1) \\ &\stackrel{9.33}{=} \mathcal{P}^+(k) + \phi(k, k+1)[M(k+1) + S(k+1)]\phi^*(k, k+1) \\ &\stackrel{17.4}{=} \mathcal{P}^+(k) + S^+(k) \end{aligned}$$

This establishes (17.50a) for the k th link.

Now we proceed to show that (17.50b) also must necessarily hold at the k th link. Now

$$\begin{aligned} &[\mathcal{P}(k) + S(k)]\Upsilon(k) \\ &\stackrel{10.22}{=} [\mathcal{P}(k) + S(k)][\bar{\tau}^*(k)\Upsilon^+(k)\bar{\tau}(k) + H^*(k)\mathcal{D}^{-1}(k)H(k)] \\ &\stackrel{17.5}{=} [\mathcal{P}(k)\bar{\tau}^*(k) + S(k)\bar{\tau}^*(k)]\Upsilon^+(k)\bar{\tau}(k) + \mathcal{P}(k)H^*(k)\mathcal{D}^{-1}(k)H(k) \\ &\stackrel{9.33}{=} [\mathcal{P}^+(k) + S(k)(I - H^*(k)G^*(k))]\Upsilon^+(k)\bar{\tau}(k) + \tau(k) \\ &\stackrel{17.5}{=} [\mathcal{P}^+(k) + S(k)]\Upsilon^+(k)\bar{\tau}(k) + \tau(k) \\ &\stackrel{17.4}{=} [\mathcal{P}^+(k) + \bar{\tau}_{dl}S^+(k)]\Upsilon^+(k)\bar{\tau}(k) + \tau(k) \end{aligned}$$

$$\begin{aligned}
&\stackrel{17.4}{=} [\mathcal{P}^+(k) + S^+(k)] \Upsilon^+(k) \bar{\tau}(k) - \tau_{dl} S^+(k) \Upsilon^+(k) \bar{\tau}(k) + \tau(k) \\
&\stackrel{17.50a}{=} \bar{\tau}(k) - \tau_{dl} S^+(k) \Upsilon^+(k) \bar{\tau}(k) + \tau(k) \\
&\stackrel{9.33}{=} \mathbf{I} - \tau_{dl} S^+(k) \Upsilon^+(k) \bar{\tau}(k) \\
&\stackrel{17.50a}{=} \mathbf{I} - \tau_{dl}(k) [\mathbf{I} - \mathcal{P}^+(k) \Upsilon^+(k)] \bar{\tau}(k) \\
&\stackrel{9.33}{=} \mathbf{I} - \tau_{dl}(k) \bar{\tau}(k) [\mathbf{I} - \mathcal{P}^+(k) \Upsilon^+(k) \bar{\tau}(k)] \stackrel{17.6}{=} \mathbf{I}
\end{aligned}$$

This implies that (17.50b) holds at link k . This concludes the proof by induction. \blacksquare

The positive definiteness of $\mathcal{P}(\cdot)$ and $S^+(\cdot)$ taken together with the above result clearly implies that $\Upsilon(\cdot)$ and $\Upsilon^+(\cdot)$ are also positive definite (and hence invertible).

Lemma 17.5 provides us with the new Algorithm 17.5 to compute the operational space inertias for the links on the free-flying manipulator. Unlike Algorithm 10.3, Algorithm 17.5 has a decoupled structure arising from the base-invariance symmetry of the free-flying manipulators. The two sequential recursions in the earlier algorithms are now replaced by a pair of parallel recursions. This can be used to advantage for a parallel implementation. As is the case for serial-chain manipulators, the operational space inertia at any link of a tree-topology free-flying manipulator is simply obtained by summing up the \mathcal{P} and S articulated body inertias at the link.

Algorithm 17.5 Decoupled computation of operational space inertias

1. a. Compute the articulated body quantities $\mathcal{P}(\cdot)$ recursively from link 1 to link n using Algorithm 9.5.
 - b. Simultaneously compute the dual articulated body quantities $S^+(\cdot)$ recursively from link n to link 1 using Algorithm 17.1.
 2. Compute $\Lambda(k) = [\mathcal{P}(k) + S(k)]$ for the k th link. The computations in this step can be carried out independently for each link.
-

We are also now in a position to restate Lemma 17.1 in a more general form using the $\Upsilon(k)$ terms.

Lemma 17.6 Alternate expression for the link spatial acceleration.

The spatial acceleration $\alpha(k)$ of the k th link is given by:

$$\begin{aligned}
\alpha(k) &= -\Upsilon(k) [\mathfrak{z}(k) + \mathfrak{z}_{dl}(k) - \mathcal{P}(k)\mathfrak{a}(k)] \\
\alpha^+(k) &= -\Upsilon^+(k) [\mathfrak{z}^+(k) + \mathfrak{z}_{dl}^+(k) - S^+(k)\mathfrak{a}_{dl}(k)]
\end{aligned} \tag{17.52}$$

Proof: Combine Lemmas 17.1 and 17.5. \blacksquare

Chapter 18

Spatial Operator Sensitivities for Rigid-Body Systems

In this chapter, we derive analytical operator expressions for the time derivatives and sensitivities of several spatial operator expressions with respect to generalized coordinates for tree-topology rigid-link multibody systems. Such sensitivities have applications such as for diagonalization [84], numerical integration, optimization, Christoffel symbol computations, control [62] and model linearization [81, 85, 116, 117].

18.1 Preliminaries

18.1.1 Notation

For a stacked spatial vector, $X \triangleq \text{col} \left\{ X(k) \right\}_{k=1}^n$, define the notation

$$\begin{aligned} X_S &\triangleq \text{col} \left\{ X(\varphi(k)) \right\}_{k=1}^n \\ \bar{X} &\triangleq \text{diag} \left\{ \overline{X(k)} \right\}_{k=1}^n, \quad \text{and} \quad \widetilde{X} \triangleq \text{diag} \left\{ \widetilde{X(k)} \right\}_{k=1}^n \end{aligned} \quad (18.1)$$

In particular, \bar{X}_S has the following form:

$$\bar{X}_S \triangleq \text{diag} \left\{ \overline{X(\varphi(k))} \right\}_{k=1}^n = \sum_{j=1,n} \sum_{k \in C(j)} e_k \overline{X(j)} e_k^* \quad (18.2)$$

Recall that

$$v^\omega(k) \stackrel{1.21}{=} \begin{bmatrix} \omega(k) \\ \mathbf{0} \end{bmatrix} \Rightarrow \tilde{v}^\omega(k) \stackrel{1.23}{=} \begin{pmatrix} \tilde{\omega}(k) & \mathbf{0} \\ \mathbf{0} & \tilde{\omega}(k) \end{pmatrix}$$

$$\mathcal{V}^v(k) \stackrel{1.21}{=} \begin{bmatrix} \mathbf{0} \\ v(k) \end{bmatrix} \Rightarrow \bar{\mathcal{V}}^v(k) \stackrel{1.25}{=} \begin{pmatrix} \mathbf{0} & \tilde{v}(k) \\ \mathbf{0} & \mathbf{0} \end{pmatrix}$$

Using the notational definitions in (18.1), we have

$$\begin{aligned} \mathcal{V}^\omega &\triangleq \text{col}\left\{\mathcal{V}^\omega(k)\right\}_{k=1}^n, & \mathcal{V}^v &\triangleq \text{col}\left\{\mathcal{V}^v(k)\right\}_{k=1}^n \\ \text{and } \Delta_{\mathcal{V}}^\omega &\triangleq \text{col}\left\{\Delta_{\mathcal{V}}^\omega(k)\right\}_{k=1}^n, & \Delta_{\mathcal{V}}^v &\triangleq \text{col}\left\{\Delta_{\mathcal{V}}^v(k)\right\}_{k=1}^n \end{aligned} \quad (18.3)$$

Furthermore,

$$\begin{aligned} \bar{\mathcal{V}} &\triangleq \text{diag}\left\{\bar{\mathcal{V}}(k)\right\}_{k=1}^n \quad \text{and} \quad \bar{\mathcal{V}}_S \triangleq \text{diag}\left\{\bar{\mathcal{V}}(\varphi(k))\right\}_{k=1}^n \\ \tilde{\mathcal{V}}_S^\omega &\triangleq \text{diag}\left\{\tilde{\mathcal{V}}^\omega(\varphi(k))\right\}_{k=1}^n \stackrel{18.2}{=} \sum_{j=1,n} \sum_{k \in \mathcal{C}(j)} e_k \tilde{\mathcal{V}}^\omega(j) e_k^* \\ \bar{\mathcal{V}}_S^v &\triangleq \text{diag}\left\{\bar{\mathcal{V}}^v(\varphi(k))\right\}_{k=1}^n \stackrel{18.2}{=} \sum_{j=1,n} \sum_{k \in \mathcal{C}(j)} e_k \bar{\mathcal{V}}^v(j) e_k^* \end{aligned} \quad (18.4)$$

Also,

$$\mathcal{V}^\omega = \mathcal{V}_S^\omega + \Delta_{\mathcal{V}}^\omega, \quad [\tilde{\mathcal{V}}^\omega]^* = -\tilde{\mathcal{V}}^\omega, \quad [\tilde{\mathcal{V}}_S^\omega]^* = -\tilde{\mathcal{V}}_S^\omega \quad (18.5)$$

18.1.2 Identities for \mathcal{V}^v

Lemma 18.1 Identities for \mathcal{V}^v .

The following identities hold for \mathcal{V}^v :

$$\bar{\mathcal{V}}^v \mathcal{E}_\phi = \mathcal{E}_\phi \bar{\mathcal{V}}_S^v \quad (18.6a)$$

$$\phi \bar{\mathcal{V}}^v - \bar{\mathcal{V}}_S^v \phi = \phi \left[\bar{\mathcal{V}}^v - \bar{\mathcal{V}}_S^v \right] \phi \quad (18.6b)$$

$$\phi \bar{\mathcal{V}}_S^v - \bar{\mathcal{V}}_S^v \phi = \phi \left[\bar{\mathcal{V}}^v - \bar{\mathcal{V}}_S^v \right] \tilde{\phi} \quad (18.6c)$$

Proof: At the component level we have

$$\begin{aligned} \phi(\varphi(k), k) \bar{\mathcal{V}}^v(k) &\stackrel{1.36e}{=} \bar{\mathcal{V}}^v(k) \\ \bar{\mathcal{V}}^v(\varphi(k)) \phi(\varphi(k), k) &\stackrel{1.36e}{=} \bar{\mathcal{V}}^v(\varphi(k)) \end{aligned} \quad (18.7)$$

For (18.6a),

$$\begin{aligned}
 \mathcal{E}_\phi \bar{\mathcal{V}}_{\mathbb{S}}^v &\stackrel{18.2}{=} \sum_{k=1}^n \sum_{j=1}^n \sum_{i \in \mathcal{C}(j)} e_{\varphi(k)} \phi(\varphi(k), k) e_k^* e_i \bar{\mathcal{V}}^v(j) e_i^* \\
 &= \sum_{k=1}^n e_{\varphi(k)} \phi(\varphi(k), k) \bar{\mathcal{V}}^v(\varphi(k)) e_k^* \\
 &\stackrel{18.7}{=} \sum_{k=1}^n e_{\varphi(k)} \bar{\mathcal{V}}^v(\varphi(k)) e_k^* \\
 &\stackrel{18.7}{=} \sum_{k=1}^n e_{\varphi(k)} \bar{\mathcal{V}}^v(\varphi(k)) \phi(\varphi(k), k) e_k^* \\
 &\stackrel{8.22}{=} \sum_{k=1}^n e_{\varphi(k)} \bar{\mathcal{V}}^v(\varphi(k)) e_{\varphi(k)}^* e_{\varphi(k)} \phi(\varphi(k), k) e_k^* \quad (18.8)
 \end{aligned}$$

Also,

$$\begin{aligned}
 \bar{\mathcal{V}}^v \mathcal{E}_\phi &\stackrel{17.23, 18.2}{=} \sum_{k=1}^n \sum_{i=1, n} e_i \bar{\mathcal{V}}^v(i) e_i^* e_{\varphi(k)} \phi(\varphi(k), k) e_k^* \\
 &= \sum_{k=1}^n e_{\varphi(k)} \bar{\mathcal{V}}^v(\varphi(k)) e_{\varphi(k)}^* e_{\varphi(k)} \phi(\varphi(k), k) e_k^*
 \end{aligned}$$

Comparing this with (18.8) establishes (18.6a).

To establish (18.6b), pre- and post-multiply (18.6a) with ϕ to yield

$$\begin{aligned}
 \mathbf{0} &= \phi \mathcal{E}_\phi \bar{\mathcal{V}}_{\mathbb{S}}^v \phi - \phi \bar{\mathcal{V}}^v \mathcal{E}_\phi \phi = \tilde{\phi} \bar{\mathcal{V}}_{\mathbb{S}}^v \phi - \phi \bar{\mathcal{V}}^v \tilde{\phi} \\
 &= \phi \bar{\mathcal{V}}_{\mathbb{S}}^v \phi - \bar{\mathcal{V}}_{\mathbb{S}}^v \phi - \phi \bar{\mathcal{V}}^v \phi + \phi \bar{\mathcal{V}}^v = \phi \bar{\mathcal{V}}^v - \bar{\mathcal{V}}_{\mathbb{S}}^v \phi - \phi [\bar{\mathcal{V}}^v - \bar{\mathcal{V}}_{\mathbb{S}}^v] \phi
 \end{aligned}$$

For (18.6c), we have

$$\phi \bar{\mathcal{V}}^v - \bar{\mathcal{V}}_{\mathbb{S}}^v \phi \stackrel{18.6b}{=} \phi [\bar{\mathcal{V}}^v - \bar{\mathcal{V}}_{\mathbb{S}}^v] \phi = \phi [\bar{\mathcal{V}}^v - \bar{\mathcal{V}}_{\mathbb{S}}^v] \tilde{\phi} + \phi [\bar{\mathcal{V}}^v - \bar{\mathcal{V}}_{\mathbb{S}}^v]$$

Rearranging terms establishes the result. ■

Exercise 18.1 Identities for $\tilde{\mathcal{V}}$.

Establish the following identities:

$$\mathcal{E}_\phi^* \tilde{\mathcal{V}} = \tilde{\mathcal{V}}^+ \mathcal{E}_\phi^* \quad (18.9a)$$

$$\tilde{\mathcal{V}} \mathcal{E}_\phi^* - \mathcal{E}_\phi^* \tilde{\mathcal{V}} = \tilde{\Delta}_\nu \mathcal{E}_\phi^* \quad (18.9b)$$

$$\tilde{\mathcal{V}} \phi^* - \phi^* \tilde{\mathcal{V}} = \phi^* \tilde{\Delta}_\nu \tilde{\phi}^* \quad (18.9c)$$

$$\phi \tilde{\mathcal{V}} - \tilde{\mathcal{V}} \phi = \tilde{\phi} \tilde{\Delta}_\nu \phi \quad (18.9d)$$

■

18.2 Operator Time Derivatives

We now derive expressions for the inertial frame time derivatives of various spatial operators. For simplicity of exposition, we make the following assumption.

Assumption 18.1 (Operator Time Derivatives).

- *The multibody system is a tree-topology system.*
- *All the bodies in the system are rigid bodies.*
- *All the time derivatives are inertial time derivatives – and, for simplicity, the notation will not state this explicitly.*
- *The kth body frame \mathbb{B}_k coincides with the \mathbb{O}_k hinge frame. Section 18.2.2 discusses the case when this is true, but by default our assumption is that the frames coincide.*
- *The $H^*(k)$ joint map matrix is constant in the body frame of the child body.*

We will make extensive use of (1.28) which relates the time derivatives of spatial vectors in different frames.

18.2.1 Time Derivatives of $\phi(k+1, k)$, $H(k)$ and $M(k)$

Lemma 18.2 Time derivatives of $\phi(k+1, k)$, $H(k)$ and $M(k)$.

We have that

$$\dot{\phi}(\varrho(k), k) = \bar{\mathcal{V}}^v(k) - \bar{\mathcal{V}}^v(\varrho(k)) \quad (18.10a)$$

$$= \tilde{\mathcal{V}}^\omega(\varrho(k)) \phi(\varrho(k), k) \quad (18.10b)$$

$$- \phi(\varrho(k), k) \tilde{\mathcal{V}}^\omega(\varrho(k)) + \bar{\Delta}_\nu^v \quad (18.10c)$$

$$= \bar{\mathcal{V}}(\varrho(k)) \phi(\varrho(k), k) \quad (18.10d)$$

$$- \phi(\varrho(k), k) \bar{\mathcal{V}}(\varrho(k)) + \bar{\Delta}_\nu^v \quad (18.10e)$$

$$\dot{H}^*(k) = \tilde{\mathcal{V}}^\omega(\varrho(k)) H^*(k) \quad (18.10d)$$

$$\dot{M}(k) = \tilde{\mathcal{V}}^\omega(k) M(k) - M(k) \tilde{\mathcal{V}}^\omega(k) \quad (18.10e)$$

Proof: Equation (18.10a) derives directly from Exercise 1.8 on page 13, which established that

$$\frac{d\mathbf{l}(\varphi(k), k)}{dt} = \mathbf{v}(k) - \mathbf{v}(\varphi(k)) \quad (18.11)$$

However, an alternate expression for (18.11) that does not depend upon $\mathbf{v}(\varphi(k))$ is given by:

$$\frac{d\mathbf{l}(\varphi(k), k)}{dt} \stackrel{5.13}{=} \Delta_v(k) + \tilde{\omega}(\varphi(k))\mathbf{l}(\varphi(k), k)$$

Hence,

$$\begin{aligned}\dot{\phi}(\varphi(k), k) &= \begin{pmatrix} \mathbf{0} & [\Delta_v(k) + \tilde{\omega}(\varphi(k))\mathbf{l}(\varphi(k), k)]^\sim \\ \mathbf{0} & \mathbf{0} \end{pmatrix} \\ &= \begin{pmatrix} \mathbf{0} & \widetilde{\Delta}_v(k) + \tilde{\omega}(\varphi(k))\widetilde{\mathbf{l}}(\varphi(k), k) - \widetilde{\mathbf{l}}(\varphi(k), k)\tilde{\omega}(\varphi(k)) \\ \mathbf{0} & \mathbf{0} \end{pmatrix} \\ &= \widetilde{\mathcal{V}}^\omega(\varphi(k))\phi(\varphi(k), k) - \phi(\varphi(k), k)\widetilde{\mathcal{V}}^\omega(\varphi(k)) + \overline{\Delta}_v(k)\end{aligned}$$

This establishes (18.10b).

For (18.10c),

$$\begin{aligned}&\widetilde{\mathcal{V}}^\omega(\varphi(k))\phi(\varphi(k), k) - \phi(\varphi(k), k)\widetilde{\mathcal{V}}^\omega(\varphi(k)) \\ &= (\overline{\mathcal{V}}(\varphi(k)) - \overline{\mathcal{V}}^v(\varphi(k)))\phi(\varphi(k), k) - \phi(\varphi(k), k)(\overline{\mathcal{V}}(\varphi(k)) - \overline{\mathcal{V}}^v(\varphi(k))) \\ &\stackrel{18.7}{=} \overline{\mathcal{V}}(\varphi(k))\phi(\varphi(k), k) - \overline{\mathcal{V}}^v(\varphi(k)) - \phi(\varphi(k), k)\overline{\mathcal{V}}(\varphi(k)) + \overline{\mathcal{V}}^v(\varphi(k)) \\ &= \overline{\mathcal{V}}(\varphi(k))\phi(\varphi(k), k) - \phi(\varphi(k), k)\overline{\mathcal{V}}(\varphi(k))\end{aligned}$$

Equation (18.10d) follows from (1.28), and that $\mathbf{H}^*(k)$ is constant in the body frame of the child body.

Equation (18.10e) is a restatement of (2.22). ■

Lemma 18.3 Time derivatives of spatial operators.

We have

$$\begin{aligned}\dot{\mathcal{E}}_\phi &= \widetilde{\mathcal{V}}^\omega \mathcal{E}_\phi - \mathcal{E}_\phi (\widetilde{\mathcal{V}}^\omega - \overline{\Delta}_v) \\ &= \widetilde{\mathcal{V}}^\omega \mathcal{E}_\phi - \mathcal{E}_\phi \widetilde{\mathcal{V}}^\omega + \mathcal{E}_\phi \overline{\Delta}_v\end{aligned} \quad (18.12a)$$

$$\dot{\mathbf{H}}^* = \widetilde{\mathcal{V}}_S^\omega \mathbf{H}^* \quad (18.12b)$$

$$\dot{\mathbf{M}} = \widetilde{\mathcal{V}}^\omega \mathbf{M} - \mathbf{M} \widetilde{\mathcal{V}}^\omega \quad (18.12c)$$

$$\dot{\phi} = \tilde{\phi} \overline{\Delta}_v \phi + \widetilde{\mathcal{V}}^\omega \phi - \phi \widetilde{\mathcal{V}}^\omega \quad (18.12d)$$

Proof: Using (8.22), the first expression in (18.12a) is an operator level restatement of the component level relationships in (18.10b). The second expression follows by further use of the following relationships:

$$\mathcal{V}^\omega = \mathcal{V}_S^\omega + \Delta_V^\omega \quad \text{and} \quad \Delta_V = \Delta_V^\omega + \Delta_V^v$$

Equations (18.12b) and (18.12c) are simply operator level restatements of (18.10d) and (18.10e), respectively.

For (18.12d),

$$\begin{aligned} \dot{\phi} &\stackrel{\text{A.28}}{=} -\phi \frac{d\phi^{-1}}{dt} \phi = -\phi \frac{d(\mathbf{I} - \mathcal{E}_\phi)}{dt} \phi = \phi \dot{\mathcal{E}}_\phi \phi \\ &\stackrel{18.12a}{=} \phi \left[\tilde{\mathcal{V}}^\omega \mathcal{E}_\phi - \mathcal{E}_\phi \tilde{\mathcal{V}}^\omega + \mathcal{E}_\phi \bar{\Delta}_V^v \right] \phi = \phi \tilde{\mathcal{V}}^\omega \tilde{\phi} - \tilde{\phi} \tilde{\mathcal{V}}^\omega \phi + \tilde{\phi} \bar{\Delta}_V^v \phi \\ &= \tilde{\mathcal{V}}^\omega \phi - \phi \tilde{\mathcal{V}}^\omega + \tilde{\phi} \bar{\Delta}_V^v \phi \end{aligned}$$

■

This lemma shows that the time derivatives of the spatial operators can themselves be analytically expressed in terms of the operators themselves!

Exercise 18.2 Time derivative of $H\phi$.

Show that

$$\frac{dH\phi}{dt} = H\phi \left[\tilde{\Delta}_V^\omega \phi + \mathcal{E}_\phi \bar{\Delta}_V^v \phi - \tilde{\mathcal{V}}^\omega \right] \quad (18.13)$$

■

Exercise 18.3 Operator expression for the α_J Coriolis acceleration.

1. Use (18.13) to derive the following operator expression for the inertial frame derivative Coriolis acceleration α_J defined in Exercise 5.3:

$$\alpha_J = \tilde{\mathcal{V}}_S^\omega \mathcal{V} - \mathcal{E}_\phi^* \tilde{\mathcal{V}}^\omega \mathcal{V} - \tilde{\Delta}_V^v \mathcal{V}^+ \quad (18.14)$$

2. Verify that the $\alpha_J(k)$ component elements in (18.14) agree with the ones in (5.20) on page 81.

■

18.2.2 Time Derivatives with $\mathbb{O}_k \neq \mathbb{B}_k$

While Lemma 18.2 assumes that the body frame coincides with the \mathbb{O}_k frame, Exercise 18.4 addresses the situation when the pair of frames do not coincide for the time derivatives of the link-level component terms. Exercise 18.5 addresses extensions for the time derivatives of the corresponding spatial operators. The expression for the time derivative of $M(k)$ in (18.10e) is valid even in the case where the frames do not coincide.

Exercise 18.4 Time derivative of $\phi(k+1, k)$ with $\mathbb{O}_k \neq \mathbb{B}_k$.

In general, the body frame is not at the hinge location, i.e., $\mathbb{B}_k \neq \mathbb{O}_k$. For this case, we have from (3.23) that

$$\begin{aligned}\phi(k+1, k) &\stackrel{3.23}{=} \phi(\mathbb{B}_{\varphi(k)}, \mathbb{B}_k) \\ &= \phi(\varphi(k), \mathbb{O}_{\varphi(k)}) \phi(\mathbb{O}_{\varphi(k)}, \mathbb{O}_k) \phi(\mathbb{O}_k, k)\end{aligned}\quad (18.15)$$

Define

$$\mathcal{V}_{\mathbb{B}/\mathbb{O}}(k) \triangleq \begin{bmatrix} \mathbf{0} \\ v(\mathbb{O}_k) - v(\mathbb{B}_k) \end{bmatrix} \quad (18.16)$$

1. Show that

$$\frac{d\phi(\mathbb{B}_k, \mathbb{O}_k)}{dt} = \bar{\mathcal{V}}_{\mathbb{B}/\mathbb{O}}(k) \quad (18.17)$$

2. Show that

$$\dot{\phi}(k+1, k) = \bar{\mathcal{V}}^v(k) - \bar{\mathcal{V}}^v(\varphi(k)) \quad (18.18a)$$

$$\begin{aligned}&= \phi(\varphi(k), \mathbb{O}_{\varphi(k)}) \dot{\phi}(\mathbb{O}_{\varphi(k)}, \mathbb{O}_k) \phi(\mathbb{O}_k, k) \\ &\quad + \mathcal{V}_{\mathbb{B}/\mathbb{O}}(\varphi(k)) \phi(\mathbb{O}_{\varphi(k)}, k) \\ &\quad - \phi(\varphi(k), \mathbb{O}_k) \mathcal{V}_{\mathbb{B}/\mathbb{O}}(k)\end{aligned}\quad (18.18b)$$

$$\begin{aligned}&= \tilde{\mathcal{V}}^{\omega}(k+1) \phi(k+1, k) - \phi(k+1, k) \tilde{\mathcal{V}}^{\omega}(k+1) \\ &\quad + \bar{\Delta}_v(k) + \tilde{\Delta}_v(k) \phi(\mathbb{O}_k, k) - \phi(\mathbb{O}_k, k) \tilde{\Delta}_v(k)\end{aligned}\quad (18.18c)$$

$$\begin{aligned}&= \bar{\mathcal{V}}(k+1) \phi(k+1, k) - \phi(k+1, k) \bar{\mathcal{V}}(k+1) \\ &\quad + \bar{\Delta}_v(k) + \bar{\Delta}_v(k) \phi(\mathbb{O}_k, k) - \phi(\mathbb{O}_k, k) \bar{\Delta}_v(k)\end{aligned}\quad (18.18d)$$

■

Equation (18.10) provides the expression for $\dot{\phi}(\mathbb{O}_{\varphi(k)}, \mathbb{O}_k)$ required in (18.18b). It is easy to verify that the expressions for $\dot{\phi}(k+1, k)$ and $\dot{\phi}(\mathbb{O}_{\varphi(k)}, \mathbb{O}_k)$ agree when the k th body frame \mathbb{B}_k coincides with \mathbb{O}_k .

The following exercise generalizes the operator time derivative expressions in Lemma 18.3 to handle the case where \mathbb{B}_k does not coincide with \mathbb{O}_k .

Exercise 18.5 Operator time derivatives with $\mathbb{O}_k \neq \mathbb{B}_k$.

Define

$$\mathcal{V}_{\mathbb{B}/\mathbb{O}} \triangleq \text{col} \left\{ \mathcal{V}_{\mathbb{B}/\mathbb{O}}(k) \right\}_{k=1}^n \quad (18.19)$$

Recall from (5.28) that

$$\Delta_{\mathbb{B}/\mathbb{O}} \triangleq \text{diag} \left\{ \phi(\mathbb{B}_k, \mathbb{O}_k) \right\}_{k=1}^n \quad (18.20)$$

1. Show that

$$\frac{d\Delta_{B/O}}{dt} = \bar{\mathcal{V}}_{B/O} \quad (18.21a)$$

$$\frac{d\Delta_{B/O}^{-1}}{dt} = -\bar{\mathcal{V}}_{B/O} \quad (18.21b)$$

2. Show that

$$\frac{d\mathcal{E}_{\phi_B}}{dt} = \Delta_{B/O} \dot{\mathcal{E}}_{\phi} \Delta_{B/O}^{-1} + \bar{\mathcal{V}}_{B/O} \mathcal{E}_{\phi_B} - \mathcal{E}_{\phi_B} \bar{\mathcal{V}}_{B/O} \quad (18.22a)$$

$$\frac{d\phi_B}{dt} = \Delta_{B/O} \dot{\phi} \Delta_{B/O}^{-1} + \bar{\mathcal{V}}_{B/O} \phi_B - \phi_B \bar{\mathcal{V}}_{B/O} \quad (18.22b)$$

$$\frac{dH_B}{dt} = \dot{H} \Delta_{B/O}^{-1} - H_B \bar{\mathcal{V}}_{B/O} \quad (18.22c)$$

■

18.2.3 Time Derivative of the Mass Matrix

Having developed expressions for the time derivatives of the component spatial operators, an expression for the time derivative of the mass matrix is derived in the following lemma.

Lemma 18.4 Time derivative of the mass matrix.

The expression for the time derivative of the mass matrix is given by

$$\begin{aligned} \dot{\mathcal{M}}(\theta) &= H\phi \left[\left(\tilde{\Delta}_v^\omega + \mathcal{E}_\phi \bar{\Delta}_v^\omega \right) \phi M \right. \\ &\quad \left. - M\phi^* \left(\tilde{\Delta}_v^\omega \mathcal{E}_\phi^* + \tilde{\Delta}_v^\omega \right) \right] \phi^* H^* \end{aligned} \quad (18.23)$$

Proof: The time derivative of the mass matrix is given by

$$\begin{aligned} \dot{\mathcal{M}} &\stackrel{8.45}{=} \frac{dH\phi}{dt} M\phi^* H^* + H\phi \frac{dM}{dt} \phi^* H^* + H\phi M \frac{d\phi^* H^*}{dt} \\ &\stackrel{18.13, 18.12c}{=} H\phi \left[\tilde{\Delta}_v^\omega \phi + \mathcal{E}_\phi \bar{\Delta}_v^\omega \phi - \tilde{\mathcal{V}}^\omega \right] M\phi^* H^* \\ &\quad + H\phi \left[\tilde{\mathcal{V}}^\omega M - M \tilde{\mathcal{V}}^\omega \right] \phi^* H^* \\ &\quad + H\phi M \left[-\phi^* \tilde{\Delta}_v^\omega - \phi^* \tilde{\Delta}_v^\omega \mathcal{E}_\phi^* + \tilde{\mathcal{V}}^\omega \right] \phi^* H^* \\ &= H\phi \left[\left(\tilde{\Delta}_v^\omega + \mathcal{E}_\phi \bar{\Delta}_v^\omega \right) \phi M - M\phi^* \left(\tilde{\Delta}_v^\omega + \tilde{\Delta}_v^\omega \mathcal{E}_\phi^* \right) \right] \phi^* H^* \end{aligned}$$

establishing (18.23). ■

Exercise 18.6 Alternative derivation of $\dot{\mathcal{M}}$ expression.

1. Show that

$$\frac{d\phi \mathbf{M} \phi^*}{dt} = [\tilde{\phi} \bar{\Delta}_V + \tilde{\mathcal{V}}^\omega] \phi \mathbf{M} \phi^* - \phi \mathbf{M} \phi^* [\tilde{\Delta}_V \tilde{\phi}^* + \tilde{\mathcal{V}}^\omega] \quad (18.24)$$

2. Use (18.24) to derive the (18.23) expression for $\dot{\mathcal{M}}$. ■

In the special case that the hinges in the system have no prismatic components, $\tilde{\Delta}_V^\omega = \mathbf{0}$, which further simplifies the various time derivative expressions in this section. From the expression in (18.23), we can see that the composite body inertia based decomposition techniques discussed in Sect. 9.3.2 can be used to develop efficient computational algorithms for computing the time derivative of the mass matrix.

18.3 Operator Sensitivities

Our goal now is to develop analytical expressions for the derivatives of various spatial operator expressions with respect to generalized coordinates. We add the following assumption to the ones at the beginning of Sect. 18.2:

- All hinges in the system are 1 degree of freedom hinges.

This assumption helps simplify the notation for the sensitivity expressions. There is little loss in generality, since multiple degree of freedom hinges can always be expressed as a sequence of 1 degree of freedom hinges.

Our approach will build upon the time derivatives that have already been derived in the earlier sections. To do this, we use the following property of derivatives from (A.23) on page 401, which states that, for an arbitrary function $g(\theta, \dot{\theta})$,

$$\frac{\partial \dot{g}(\theta, \dot{\theta})}{\partial \dot{\theta}} = \frac{d}{dt} \frac{\partial g}{\partial \dot{\theta}} + \frac{\partial g}{\partial \theta} \quad (18.25)$$

For the case where the function is independent of $\dot{\theta}$, i.e., $g(\theta, \dot{\theta}) = g(\theta)$, (18.25) simplifies to

$$\frac{\partial \dot{g}(\theta)}{\partial \dot{\theta}} = \frac{\partial g(\theta)}{\partial \theta} \quad (18.26)$$

Equation (18.26) provides a path for obtaining the sensitivity of operator expressions (since they are functions of θ only) from the partial derivatives of the time derivatives of the spatial operators. The advantage of this approach is that, while the spatial operators are complex, non-linear functions of the generalized coordinates, their time derivatives have simpler linear dependency on the generalized velocities.

Thus, evaluating the left-hand side of (18.26) is much easier compared to directly evaluating the right-hand side. We begin by deriving the partials of various body velocities with respect to generalized velocities, and introducing additional convenient notation in the next section.

18.3.1 The $\tilde{\mathcal{H}}_{\leq i}^\omega$, $\tilde{\mathcal{H}}_{\prec i}^\omega$, and $\tilde{\mathcal{H}}_{=i}^\omega$ Operators

We can use (3.8) to express a joint map matrix in the form:

$$H^*(k) = H_\omega^*(k) + H_v^*(k)$$

where $H_\omega^*(k) \triangleq \begin{bmatrix} h_\omega(k) \\ \mathbf{0} \end{bmatrix}$, $H_v^*(k) \triangleq \begin{bmatrix} \mathbf{0} \\ h_v(k) \end{bmatrix}$

(18.27)

Lemma 18.5 Component-level velocity partials.

The following expressions describe the component-level partial derivatives of body and joint relative spatial velocities:

$$\frac{\partial \mathcal{V}^\omega(k)}{\partial \dot{\theta}_i} = H_\omega^*(i) \cdot \mathbb{1}_{[i \succeq k]}$$
(18.28a)

$$\frac{\partial \mathcal{V}^\omega(\varphi(k))}{\partial \dot{\theta}_i} = H_\omega^*(i) \cdot \mathbb{1}_{[i \succ k]}$$
(18.28b)

$$\frac{\partial \Delta_\mathcal{V}^\omega(k)}{\partial \dot{\theta}_i} = H_\omega^*(i) \cdot \mathbb{1}_{[i=k]}$$
(18.28c)

$$\frac{\partial \Delta_\mathcal{V}^v(k)}{\partial \dot{\theta}_i} = H_v^*(i) \cdot \mathbb{1}_{[i=k]}$$
(18.28d)

$$\frac{\partial \Delta_\mathcal{V}(k)}{\partial \dot{\theta}_i} = H^*(i) \cdot \mathbb{1}_{[i=k]}$$
(18.28e)

$\mathbb{1}_{[<...>]}$ denotes the indicator function introduced in (8.2) on page 138.

Proof: The above expressions follow directly from taking partials of the following basic expressions obtained from (3.8), (18.27) and (3.19b):

$$\Delta_\mathcal{V}^\omega(k) = H_\omega^*(k) \dot{\theta}_k, \quad \Delta_\mathcal{V}^v(k) = H_v^*(k) \dot{\theta}_k, \quad \mathcal{V}^\omega(k) = \sum_{j \succeq k} \Delta_\mathcal{V}^\omega(j)$$

■

The following exercise derives expressions for the partial derivative of the component level quantities such as $\phi(\varphi(k))$ etc., with respect to generalized coordinates. We will use the notational shorthand X_{θ_i} for $\frac{\partial X}{\partial \theta_i}$.

Exercise 18.7 Sensitivities of $\phi(\varphi(k), k)$, $H(k)$ and $M(k)$.

Show that

$$[\phi(\varphi(k), k)]_{\theta_i} = \left[\tilde{H}_\omega^*(i) \phi(\varphi(k), k) - \phi(\varphi(k), k) \tilde{H}_\omega^*(i) \right] \cdot \mathbb{1}_{[k \prec i]} + \bar{H}_v^*(k) \cdot \mathbb{1}_{[k=i]}$$

$$= \begin{cases} \bar{H}_v^*(k) & \text{for } k = i \\ \tilde{H}_\omega^*(i) \phi(\varphi(k), k) - \phi(\varphi(k), k) \tilde{H}_\omega^*(i) & \text{for } k \prec i \\ \mathbf{0} & \text{otherwise} \end{cases} \quad (18.29a)$$

$$[H^*(k)]_{\theta_i} = \tilde{H}_\omega^*(i) H^*(k) \cdot \mathbb{1}_{[k \prec i]}$$

$$= \begin{cases} \begin{bmatrix} \tilde{h}_\omega(i) h_\omega(k) \\ \tilde{h}_\omega(i) h_v(k) \end{bmatrix} & \text{for } k \prec i \\ \mathbf{0} & \text{otherwise} \end{cases} \quad (18.29b)$$

$$[M(k)]_{\theta_i} = [\tilde{H}_\omega^*(i) M(k) - M(k) \tilde{H}_\omega^*(i)] \cdot \mathbb{1}_{[k \leq i]}$$

$$= \begin{cases} \tilde{H}_\omega^*(i) M(k) - M(k) \tilde{H}_\omega^*(i) & \text{for } k \leq i \\ \mathbf{0} & \text{otherwise} \end{cases} \quad (18.29c)$$

■

We use this component-level lemma to derive expressions for the partials of stacked spatial velocities. For a matrix or vector, X , we use the following notation to derive stacked vectors from it:

$$X_{=i} \triangleq \text{col} \left\{ X \cdot \mathbb{1}_{[i=k]} \right\}_{k=1}^n$$

$$X_{\leq i} \triangleq \text{col} \left\{ X \cdot \mathbb{1}_{[k \leq i]} \right\}_{k=1}^n$$

$$X_{\prec i} \triangleq \text{col} \left\{ X \cdot \mathbb{1}_{[k \prec i]} \right\}_{k=1}^n \quad (18.30)$$

Thus, the stacked vector $X_{=i}$ contains only a single non-zero entry, X , at the i th slot. $X_{\prec i}$ contains the non-zero element X at all slots for whom the i th body is a strict ancestor, while $X_{\leq i}$ contains X additionally at the i th slot.

Lemma 18.6 Operator-level velocity partials.

The following expressions describe partial derivatives of stacked spatial velocity vectors:

$$\frac{\partial \mathcal{V}^\omega}{\partial \dot{\theta}_i} = \text{col} \left\{ H_\omega^*(i) \cdot \mathbb{1}_{[k \leq i]} \right\}_{k=1}^n \triangleq \mathcal{H}_{\leq i}^\omega \quad (18.31a)$$

$$\frac{\partial \mathcal{V}^\omega}{\partial \dot{\theta}_i} = \text{col} \left\{ H_\omega^*(i) \cdot \mathbb{1}_{[k < i]} \right\}_{k=1}^n \triangleq \mathcal{H}_{< i}^\omega \quad (18.31b)$$

$$\frac{\partial \Delta_V^\omega}{\partial \dot{\theta}_i} = \text{col} \left\{ H_\omega^*(i) \cdot \mathbb{1}_{[k=i]} \right\}_{k=1}^n \triangleq \mathcal{H}_{=i}^\omega \quad (18.31c)$$

$$\frac{\partial \Delta_V^\nu}{\partial \dot{\theta}_i} = \text{col} \left\{ H_\nu^*(i) \cdot \mathbb{1}_{[k=i]} \right\}_{k=1}^n \triangleq \mathcal{H}_{=i}^\nu \quad (18.31d)$$

$$\frac{\partial \Delta_V}{\partial \dot{\theta}_i} = \text{col} \left\{ H^*(i) \cdot \mathbb{1}_{[k=i]} \right\}_{k=1}^n \triangleq \mathcal{H}_{=i} \quad (18.31e)$$

Proof: The expressions in (18.31) are simply stacked vector, equivalent versions of the component-level expressions in (18.28). ■

For the newly defined $\mathcal{H}_{=i}^\omega$, $\mathcal{H}_{=i}^\nu$ and $\mathcal{H}_{=i}$, block-vectors, it is easy to verify that

$$\tilde{\Delta}_V^\omega \mathcal{H}_{=i}^\omega = \mathbf{0}, \quad \tilde{\Delta}_V^\nu \mathcal{H}_{=i}^\nu = \mathbf{0}, \quad \tilde{\Delta}_V \mathcal{H}_{=i} = \mathbf{0} \quad (18.32)$$

Lemma 18.7 Operator sensitivities of ϕ , H , M .

$$[\mathcal{E}_\phi]_{\theta_i} = \tilde{\mathcal{H}}_{\leq i}^\omega \mathcal{E}_\phi - \mathcal{E}_\phi \tilde{\mathcal{H}}_{< i}^\omega + \mathcal{E}_\phi \overline{\mathcal{H}}_{=i}^\nu \quad (18.33a)$$

$$[\phi]_{\theta_i} = \tilde{\phi} \overline{\mathcal{H}}_{=i} \phi - \phi \tilde{\mathcal{H}}_{\leq i}^\omega + \tilde{\mathcal{H}}_{\leq i}^\omega \phi \quad (18.33b)$$

$$\begin{aligned} [\phi]_{\theta_i}(k,j) = & \phi(k,i) \tilde{H}_\omega^*(i) \phi(i,j) \cdot \mathbb{1}_{[k > i]} - \phi(k,j) \tilde{H}_\omega^*(i) \cdot \mathbb{1}_{[k \geq i]} \\ & + \tilde{H}_\omega^*(i) \phi(k,j) \cdot \mathbb{1}_{[k \leq i]} \end{aligned} \quad (18.33c)$$

$$[H^*]_{\theta_i} = \tilde{\mathcal{H}}_{< i}^\omega H^* \quad (18.33d)$$

$$[M]_{\theta_i} = \tilde{\mathcal{H}}_{\leq i}^\omega M - M \tilde{\mathcal{H}}_{\leq i}^\omega \quad (18.33e)$$

Proof: The expressions in (18.33) follow directly from applying (18.26) to the time derivative expressions in (18.12), together with the expressions in (18.31). ■

Exercise 18.8 Sensitivity of $H\phi$.

Show that

$$[H\phi]_{\theta_i} = H\phi \left[\tilde{\mathcal{H}}_{=i}^\omega \phi + \mathcal{E}_\phi \overline{\mathcal{H}}_{=i}^\nu \phi - \tilde{\mathcal{H}}_{\leq i}^\omega \right] \quad (18.34)$$



18.4 Mass Matrix Related Quantities

18.4.1 Sensitivity of $\phi \mathbf{M} \phi^*$

Lemma 18.8 Sensitivity of $\phi \mathbf{M} \phi^*$.

$$\begin{aligned} [\phi \mathbf{M} \phi^*]_{\theta_i} = & \left[\tilde{\phi} \bar{\mathcal{H}}_{=i} + \tilde{\mathcal{H}}_{\leq i}^\omega \right] \phi \mathbf{M} \phi^* \\ & - \phi \mathbf{M} \phi^* \left[\tilde{\mathcal{H}}_{=i} \tilde{\phi}^* + \tilde{\mathcal{H}}_{\leq i}^\omega \right] \end{aligned} \quad (18.35)$$

Proof: Equation (18.35) follows from applying (18.26) to the time derivative expressions in (18.24). ■

18.4.2 Sensitivity of the Mass Matrix \mathcal{M}_{θ_i}

The sensitivity of the mass matrix with respect to a generalized coordinate is described in the following lemma.

Lemma 18.9 Sensitivity of the mass matrix.

The sensitivity of the mass matrix $\mathcal{M}(\theta)$ is given by the following expression:

$$\begin{aligned} \mathcal{M}_{\theta_i} = & \mathcal{H} \phi \left[\left(\tilde{\mathcal{H}}_{=i}^\omega + \mathcal{E}_\phi \bar{\mathcal{H}}_{=i}^v \right) \phi \mathbf{M} \right. \\ & \left. - \mathbf{M} \phi^* \left(\tilde{\mathcal{H}}_{=i}^\omega + \tilde{\mathcal{H}}_{=i}^v \mathcal{E}_\phi^* \right) \right] \phi^* \mathcal{H}^* \end{aligned} \quad (18.36)$$

Proof: Equation (18.36) follows from applying (18.26) to the time derivative expressions in (18.23). ■

The expression in (18.36) is closed-form, and expresses the mass matrix sensitivity in terms of the operators ϕ , \mathbf{M} , and \mathcal{H} appearing in the mass matrix itself. The analytical form implies that the mass matrix derivatives can be easily computed using operations and spatially recursive algorithms, similar to those used to compute the mass matrix itself. As discussed in Chap. 19, the mass matrix sensitivity expression allows us to develop simple closed-form expressions and recursive algorithms for the Coriolis term in the diagonalized equations of motion.

Remark 18.1 Expression for $\mathcal{M}_D(\theta, \dot{\theta})$.

Equation (4.29) on page 67 defines the mass matrix-related gradient of the generalized momentum as $\mathcal{M}_D(\theta, \dot{\theta})$ as

$$\mathcal{M}_D(\theta, \dot{\theta}) = \nabla_\theta (\mathcal{M} \dot{\theta}) = [\mathcal{M}_{\theta_1} \dot{\theta}, \quad \mathcal{M}_{\theta_2} \dot{\theta}, \quad \dots \quad \mathcal{M}_{\theta_n} \dot{\theta}]$$

The i th column of \mathbf{M}_D is, thus, simply $\mathcal{M}_{\theta_i} \dot{\theta}$, which from (18.36) has the form:

$$\begin{aligned}\mathcal{M}_{\theta_i} \dot{\theta} &\stackrel{18.36}{=} \mathsf{H} \phi \left[\left(\tilde{\mathcal{H}}_{=i}^{\omega} + \mathcal{E}_{\phi} \overline{\mathcal{H}}_{=i}^v \right) \phi \mathbf{M} \right. \\ &\quad \left. - \mathbf{M} \phi^* \left(\tilde{\mathcal{H}}_{=i}^{\omega} + \tilde{\mathcal{H}}_{=i}^v \mathcal{E}_{\phi}^* \right) \right] \phi^* \mathsf{H}^* \dot{\theta} \\ &= \mathsf{H} \phi \left[\left(\tilde{\mathcal{H}}_{=i}^{\omega} + \mathcal{E}_{\phi} \overline{\mathcal{H}}_{=i}^v \right) \phi \mathbf{M} \right. \\ &\quad \left. - \mathbf{M} \phi^* \left(\tilde{\mathcal{H}}_{=i}^{\omega} + \tilde{\mathcal{H}}_{=i}^v \mathcal{E}_{\phi}^* \right) \right] \mathcal{V} \end{aligned} \quad (18.37)$$

■

18.4.3 Sensitivity of the Kinetic Energy

In this section, we derive expressions for the gradient of the system kinetic energy, \mathfrak{K}_e , with respect to the generalized coordinates.

Lemma 18.10 **Operator expression for $\frac{\partial \mathfrak{K}_e}{\partial \theta}$.**

$$\frac{\partial \mathfrak{K}_e}{\partial \theta} = -\mathsf{H} \left[\overline{\mathcal{V}} - \tilde{\Delta}_{\mathcal{V}}^{\omega} \right] \phi \mathbf{M} \mathcal{V} \quad (18.38a)$$

$$= -\mathsf{H} \phi \left\{ \overline{\mathcal{V}} - \left(\mathcal{E}_{\phi} \overline{\Delta}_{\mathcal{V}}^v + \tilde{\Delta}_{\mathcal{V}}^{\omega} \right) \phi \right\} \mathbf{M} \mathcal{V} \quad (18.38b)$$

$$= -\mathsf{H} \phi \left\{ \overline{\mathcal{V}} \mathbf{M} - \left(\mathcal{E}_{\phi} \overline{\Delta}_{\mathcal{V}}^v + \tilde{\Delta}_{\mathcal{V}}^{\omega} \right) [\mathbf{I} + \phi \mathcal{K} \mathsf{H}] \mathcal{P} \right\} \mathcal{V} \quad (18.38c)$$

Proof: We have,

$$\begin{aligned}\frac{\partial \mathfrak{K}_e}{\partial \theta_i} &\stackrel{4.5}{=} \frac{1}{2} \frac{\partial \dot{\theta}^* \mathcal{M} \dot{\theta}}{\partial \theta_i} = \frac{1}{2} \dot{\theta}^* \mathcal{M}_{\theta_i} \dot{\theta} \\ &\stackrel{18.36}{=} \frac{1}{2} \mathcal{V}^* \left[\left(\tilde{\mathcal{H}}_{=i}^{\omega} + \mathcal{E}_{\phi} \overline{\mathcal{H}}_{=i}^v \right) \phi \mathbf{M} - \mathbf{M} \phi^* \left(\tilde{\mathcal{H}}_{=i}^{\omega} + \tilde{\mathcal{H}}_{=i}^v \mathcal{E}_{\phi}^* \right) \right] \mathcal{V} \\ &= \mathcal{V}^* \left(\tilde{\mathcal{H}}_{=i}^{\omega} + \mathcal{E}_{\phi} \overline{\mathcal{H}}_{=i}^v \right) \phi \mathbf{M} \mathcal{V} \\ &\stackrel{8.42}{=} \left(\mathcal{V}^* \tilde{\mathcal{H}}_{=i}^{\omega} + (\mathcal{V} - \Delta_{\mathcal{V}})^* \overline{\mathcal{H}}_{=i}^v \right) \phi \mathbf{M} \mathcal{V} \\ &\stackrel{18.27}{=} \left(\mathcal{V}^* (\tilde{\mathcal{H}}_{=i}^{\omega} + \overline{\mathcal{H}}_{=i}^v) - (\Delta_{\mathcal{V}})^* \overline{\mathcal{H}}_{=i}^v \right) \phi \mathbf{M} \mathcal{V} \\ &\stackrel{18.3}{=} \left(\mathcal{V}^* \overline{\mathcal{H}}_{=i} - (\Delta_{\mathcal{V}}^{\omega} + \Delta_{\mathcal{V}}^v)^* \overline{\mathcal{H}}_{=i}^v \right) \phi \mathbf{M} \mathcal{V} \\ &\stackrel{18.32}{=} \left(\mathcal{V}^* \overline{\mathcal{H}}_{=i} - (\Delta_{\mathcal{V}}^{\omega})^* \overline{\mathcal{H}}_{=i}^v \right) \phi \mathbf{M} \mathcal{V} \end{aligned}$$

$$\begin{aligned}
&\stackrel{18.32}{=} \left(\mathcal{V}^* \bar{\mathcal{H}}_{=i} - (\Delta_{\mathcal{V}}^\omega)^* (\bar{\mathcal{H}}_{=i}^v + \tilde{\mathcal{H}}_{=i}^\omega) \right) \phi \mathbf{M} \mathcal{V} \\
&\stackrel{18.31}{=} (\mathcal{V}^* \bar{\mathcal{H}}_{=i} - (\Delta_{\mathcal{V}}^\omega)^* \bar{\mathcal{H}}_{=i}) \phi \mathbf{M} \mathcal{V} \\
&= (\mathcal{V} - \Delta_{\mathcal{V}}^\omega)^* \bar{\mathcal{H}}_{=i} \phi \mathbf{M} \mathcal{V}
\end{aligned}$$

Hence,

$$\begin{aligned}
\frac{\partial \mathfrak{K}_e}{\partial \theta} &= \text{col} \left\{ \frac{\partial \mathfrak{K}_e}{\partial \theta_i} \right\}_{i=1}^n = \text{diag} \left\{ (\mathcal{V}(i) - \Delta_{\mathcal{V}}^\omega(i))^* \bar{\mathcal{H}}^*(i) \right\}_{i=1}^n \phi \mathbf{M} \mathcal{V} \\
&\stackrel{1.27a}{=} -\text{diag} \left\{ H(i) \left(\bar{\mathcal{V}}(i) - \tilde{\Delta}_{\mathcal{V}}^\omega(i) \right) \right\}_{i=1}^n \phi \mathbf{M} \mathcal{V} \\
&= -H \text{diag} \left\{ \left(\bar{\mathcal{V}}(i) - \tilde{\Delta}_{\mathcal{V}}^\omega(i) \right) \right\}_{i=1}^n \phi \mathbf{M} \mathcal{V} = -H \left(\bar{\mathcal{V}} - \tilde{\Delta}_{\mathcal{V}}^\omega \right) \phi \mathbf{M} \mathcal{V}
\end{aligned}$$

This establishes (18.38a). For (18.38b),

$$\begin{aligned}
H \left[\bar{\mathcal{V}} - \tilde{\Delta}_{\mathcal{V}}^\omega \right] \phi \mathbf{M} \mathcal{V} &= H \left[\bar{\mathcal{V}} \phi - \tilde{\Delta}_{\mathcal{V}}^\omega \phi \right] \mathbf{M} \mathcal{V} \\
&\stackrel{1.29d}{=} H \left[\phi \bar{\mathcal{V}} - \tilde{\Delta}_{\mathcal{V}}^\omega \phi \right] \mathbf{M} \mathcal{V} \\
&= H \phi \left[\bar{\mathcal{V}} - \mathcal{E}_\phi \bar{\Delta}_{\mathcal{V}} \phi - (\mathbf{I} - \mathcal{E}_\phi) \tilde{\Delta}_{\mathcal{V}}^\omega \phi \right] \mathbf{M} \mathcal{V} \\
&= H \phi \left[\bar{\mathcal{V}} - \left(\mathcal{E}_\phi \left(\bar{\Delta}_{\mathcal{V}} - \tilde{\Delta}_{\mathcal{V}}^\omega \right) + \tilde{\Delta}_{\mathcal{V}}^\omega \right) \phi \right] \mathbf{M} \mathcal{V} \\
&= H \phi \left[\bar{\mathcal{V}} - \left(\mathcal{E}_\phi \bar{\Delta}_{\mathcal{V}}^v + \tilde{\Delta}_{\mathcal{V}}^\omega \right) \phi \right] \mathbf{M} \mathcal{V}
\end{aligned}$$

Using this in (18.38a) establishes (18.38b). Equation (18.38c) follows directly from using (9.48) in (18.38b). ■

18.4.4 Equivalence of Lagrangian and Newton–Euler Dynamics

We now prove that the equations of motion obtained using the system-level Lagrangian formulation in Sect. 4.2, and the ones obtained from the Newton–Euler component-level approach in Sect. 5.1.2, are equivalent. There are two parts to establishing the equivalency:

1. First, we need to show that the mass matrices from the two approaches are equivalent. The mass matrix from the Lagrangian approach, as established by (4.5), (4.6), (4.25) (4.26) is $\mathcal{M} = H \phi \mathbf{M} \phi^* H^*$. This is precisely the expression for the mass matrix from the Newton–Euler approach in (5.25). So the mass matrices are indeed equivalent.
2. The second part requires establishing that the Coriolis generalized forces term defined in (4.27) via the Lagrangian approach agrees with the one in (5.25) using the Newton–Euler approach. Proving this is the subject of the following exercise.

Exercise 18.9 Equivalence of Lagrangian and Newton–Euler equations of motion.

In this exercise, we will work with the “inertial derivatives” form of the equations of motion, and make this explicit with the use of the \mathcal{J} subscript.

1. In the Newton–Euler approach, the expression for the Coriolis generalized forces vector, $\mathcal{C}(\theta, \dot{\theta})$, is derived in (5.25) as

$$\mathcal{C}(\theta, \dot{\theta}) \triangleq H\Phi [b_J + M\Phi^* a_J] \quad (18.39)$$

where the stacked vectors b_J and a_J are defined as

$$b_J \triangleq \text{col} \left\{ b_J(k) \right\}_{k=1}^n \quad \text{and} \quad a_J \triangleq \text{col} \left\{ a_J(k) \right\}_{k=1}^n \quad (18.40)$$

The body-level $b_J(k)$ gyroscopic spatial force is defined in Lemma 2.2 on page 27 for the inertial derivative rigid body equations of motion, while the body-level $a_J(k)$ Coriolis spatial acceleration are defined in (5.19) on page 80. Show that $\mathcal{C}(\theta, \dot{\theta})$ in (18.39) can be expressed as:

$$\mathcal{C}(\theta, \dot{\theta}) = H\Phi \left[\bar{v}M - M\Phi^* \left(\tilde{\Delta}_V^v \mathcal{E}_\Phi^* + \tilde{\Delta}_V^\omega \right) \right] v \quad (18.41)$$

2. Equation (4.27) defines the Coriolis generalized forces expression, $\mathcal{C}(\theta, \dot{\theta})$, from the Lagrangian approach as

$$\mathcal{C}(\theta, \dot{\theta}) = \dot{\mathcal{M}}(\theta)\dot{\theta} - \frac{1}{2} \frac{\partial [\dot{\theta}^* \mathcal{M}(\theta) \dot{\theta}]}{\partial \theta} \in \mathcal{R}^N$$

Show that this expression is equivalent to the expression in (18.41). ■

This establishes the equivalency of the Coriolis generalized acceleration obtained via the Lagrangian and the Newton–Euler approaches. Silver [167] studied this equivalency using a component-level approach for serial-chain manipulators.

18.5 Time Derivatives of Articulated Body Quantities

We now turn to the topic of computing the time derivatives of the articulated body inertia operators. The time-derivative of the articulated body inertia quantities are obtained in two steps. First, we develop expressions for the time-derivatives of the articulated body inertia quantities in Lemma 18.11 assuming that $\dot{\mathcal{P}}$ is known. Following this, we address the issue of obtaining analytical expressions for $\dot{\mathcal{P}}$ itself.

Lemma 18.11 Time derivatives of articulated body quantities.

Define the block-diagonal, symmetric operator $\check{\lambda}$ in terms of $\dot{\mathcal{P}}$ as follows:

$$\check{\lambda} \stackrel{\triangle}{=} \dot{\mathcal{P}} - \tilde{\mathcal{V}}_{\mathbb{S}}^{\omega} \mathcal{P} + \mathcal{P} \tilde{\mathcal{V}}_{\mathbb{S}}^{\omega} \quad (18.42)$$

The time derivatives of the articulated body inertia related quantities are given by the following expressions:

$$\dot{\mathcal{D}} = H \check{\lambda} H^* \quad (18.43a)$$

$$\dot{\mathcal{D}}^{-1} = -\mathcal{D}^{-1} H \check{\lambda} H^* \mathcal{D}^{-1} \quad (18.43b)$$

$$\dot{\mathcal{G}} = \bar{\tau} \check{\lambda} H^* \mathcal{D}^{-1} + \tilde{\mathcal{V}}_{\mathbb{S}}^{\omega} \mathcal{G} \quad (18.43c)$$

$$\dot{\tau} = \bar{\tau} \check{\lambda} H^* \mathcal{D}^{-1} H + \tilde{\mathcal{V}}_{\mathbb{S}}^{\omega} \tau - \tau \tilde{\mathcal{V}}_{\mathbb{S}}^{\omega} \quad (18.43d)$$

$$\dot{\bar{\tau}} = -\bar{\tau} \check{\lambda} H^* \mathcal{D}^{-1} H - \tilde{\mathcal{V}}_{\mathbb{S}}^{\omega} \tau + \tau \tilde{\mathcal{V}}_{\mathbb{S}}^{\omega} \quad (18.43e)$$

$$\dot{\mathcal{E}}_{\psi} = \tilde{\mathcal{V}}^{\omega} \mathcal{E}_{\psi} - \mathcal{E}_{\psi} \tilde{\mathcal{V}}_{\mathbb{S}}^{\omega} - \mathcal{E}_{\phi} \left(\bar{\tau} \check{\lambda} H^* \mathcal{D}^{-1} H - \bar{\Delta}_v^v \bar{\tau} \right) \quad (18.43f)$$

$$\dot{\mathcal{P}}^+ = \bar{\tau} \check{\lambda} \bar{\tau}^* + \tilde{\mathcal{V}}_{\mathbb{S}}^{\omega} \mathcal{P}^+ - \mathcal{P}^+ \tilde{\mathcal{V}}_{\mathbb{S}}^{\omega} \quad (18.43g)$$

Proof: Since $\mathcal{D} = H \mathcal{P} H^*$, we have:

$$\begin{aligned} \dot{\mathcal{D}} &= \dot{H} \mathcal{P} H^* + H \dot{\mathcal{P}} H^* + H \mathcal{P} \dot{H}^* \stackrel{18.12b}{=} -H \tilde{\mathcal{V}}_{\mathbb{S}}^{\omega} \mathcal{P} H^* + H \dot{\mathcal{P}} H^* + H \mathcal{P} \tilde{\mathcal{V}}_{\mathbb{S}}^{\omega} H^* \\ &\stackrel{18.42}{=} H \check{\lambda} H^* \end{aligned}$$

This establishes (18.43a).

For (18.43b), we have

$$\dot{\mathcal{D}}^{-1} \stackrel{A.28}{=} -\mathcal{D}^{-1} \dot{\mathcal{D}} \mathcal{D}^{-1} \stackrel{18.43a}{=} -\mathcal{D}^{-1} H \check{\lambda} H^* \mathcal{D}^{-1}$$

For (18.43c),

$$\begin{aligned} \dot{\mathcal{G}} &= \dot{\mathcal{P}} H^* \mathcal{D}^{-1} + \mathcal{P} \dot{H}^* \mathcal{D}^{-1} + \mathcal{P} H^* \dot{\mathcal{D}}^{-1} \\ &\stackrel{18.12b, 18.43b}{=} \dot{\mathcal{P}} H^* \mathcal{D}^{-1} + \mathcal{P} \tilde{\mathcal{V}}_{\mathbb{S}}^{\omega} H^* \mathcal{D}^{-1} - \mathcal{P} H^* \mathcal{D}^{-1} H \check{\lambda} H^* \mathcal{D}^{-1} \\ &= \left(\dot{\mathcal{P}} + \mathcal{P} \tilde{\mathcal{V}}_{\mathbb{S}}^{\omega} \right) H^* \mathcal{D}^{-1} - \tau \check{\lambda} H^* \mathcal{D}^{-1} \stackrel{18.42}{=} \left(\check{\lambda} + \tilde{\mathcal{V}}_{\mathbb{S}}^{\omega} \mathcal{P} \right) H^* \mathcal{D}^{-1} - \tau \check{\lambda} H^* \mathcal{D}^{-1} \\ &= \bar{\tau} \check{\lambda} H^* \mathcal{D}^{-1} + \tilde{\mathcal{V}}_{\mathbb{S}}^{\omega} \mathcal{G} \end{aligned}$$

Furthermore, for (18.43d):

$$\begin{aligned} \dot{\tau} &= \dot{\mathcal{G}} H + \mathcal{G} \dot{H} \stackrel{18.12b, 18.43c}{=} \left(\bar{\tau} \check{\lambda} H^* \mathcal{D}^{-1} + \tilde{\mathcal{V}}_{\mathbb{S}}^{\omega} \mathcal{G} \right) H - \mathcal{G} H \tilde{\mathcal{V}}^{\omega} \\ &= \bar{\tau} \check{\lambda}_{\theta_i} H^* \mathcal{D}^{-1} H + \tilde{\mathcal{V}}_{\mathbb{S}}^{\omega} \tau - \tau \tilde{\mathcal{V}}_{\mathbb{S}}^{\omega} \end{aligned}$$

Equation (18.43e) follows from using $\bar{\tau} = I - \tau$ together with (18.43d).

For (18.43f), we have

$$\begin{aligned}
 \dot{\mathcal{E}}_\Psi &= \dot{\mathcal{E}}_\Phi \bar{\tau} + \mathcal{E}_\Phi \dot{\bar{\tau}} \\
 &\stackrel{18.12a, 18.43e}{=} \left(\tilde{\mathcal{V}}^\omega \mathcal{E}_\Phi - \mathcal{E}_\Phi \tilde{\mathcal{V}}_S^\omega + \mathcal{E}_\Phi \bar{\Delta}_V^\nu \right) \bar{\tau} \\
 &\quad + \mathcal{E}_\Phi \left(-\bar{\tau} \check{\lambda} H^* \mathcal{D}^{-1} H - \tilde{\mathcal{V}}_S^\omega \tau + \tau \tilde{\mathcal{V}}_S^\omega \right) \\
 &= \tilde{\mathcal{V}}^\omega \mathcal{E}_\Psi + (-\mathcal{E}_\Phi \tilde{\mathcal{V}}_S^\omega \bar{\tau} - \mathcal{E}_\Phi \tilde{\mathcal{V}}_S^\omega \tau + \mathcal{E}_\Phi \tau \tilde{\mathcal{V}}_S^\omega) \\
 &\quad + \mathcal{E}_\Phi \bar{\Delta}_V^\nu \bar{\tau} - \mathcal{E}_\Phi \bar{\tau} \check{\lambda} H^* \mathcal{D}^{-1} H \tilde{\mathcal{V}}_S^\omega \\
 &= \tilde{\mathcal{V}}^\omega \mathcal{E}_\Psi (-\mathcal{E}_\Phi \tilde{\mathcal{V}}_S^\omega + \mathcal{E}_\Phi \tau \tilde{\mathcal{V}}_S^\omega) + \mathcal{E}_\Phi \bar{\Delta}_V^\nu \bar{\tau} - \mathcal{E}_\Phi \bar{\tau} \check{\lambda} H^* \mathcal{D}^{-1} H \\
 &= \tilde{\mathcal{V}}^\omega \mathcal{E}_\Psi - \mathcal{E}_\Psi \tilde{\mathcal{V}}_S^\omega + \mathcal{E}_\Phi \bar{\Delta}_V^\nu \bar{\tau} - \mathcal{E}_\Phi \bar{\tau} \check{\lambda} H^* \mathcal{D}^{-1} H
 \end{aligned}$$

This establishes (18.43f).

Since $\mathcal{P}^+ = \bar{\tau} \mathcal{P}$,

$$\begin{aligned}
 \dot{\mathcal{P}}^+ &= \dot{\bar{\tau}} \mathcal{P} + \bar{\tau} \dot{\mathcal{P}} = \left(-\bar{\tau} \check{\lambda} H^* \mathcal{D}^{-1} H - \tilde{\mathcal{V}}_S^\omega \tau + \tau \tilde{\mathcal{V}}_S^\omega \right) \mathcal{P} + \bar{\tau} \dot{\mathcal{P}} \\
 &\stackrel{18.42}{=} -\bar{\tau} \check{\lambda} \tau - \tilde{\mathcal{V}}_S^\omega \tau \mathcal{P} + \tau \tilde{\mathcal{V}}_S^\omega \mathcal{P} + \bar{\tau} \left(\check{\lambda} + \tilde{\mathcal{V}}_S^\omega \mathcal{P} - \mathcal{P} \tilde{\mathcal{V}}_S^\omega \right) \\
 &= \bar{\tau} \check{\lambda} \bar{\tau} - \tilde{\mathcal{V}}_S^\omega \tau \mathcal{P} + \tilde{\mathcal{V}}_S^\omega \mathcal{P} - \bar{\tau} \mathcal{P} \tilde{\mathcal{V}}_S^\omega \\
 &= \bar{\tau} \check{\lambda} \bar{\tau} + \tilde{\mathcal{V}}_S^\omega \bar{\tau} \mathcal{P} - \bar{\tau} \mathcal{P} \tilde{\mathcal{V}}_S^\omega = \bar{\tau} \check{\lambda} \bar{\tau} + \tilde{\mathcal{V}}_S^\omega \mathcal{P}^+ - \mathcal{P}^+ \tilde{\mathcal{V}}_S^\omega
 \end{aligned}$$

This establishes (18.43g). ■

Lemma 18.12 The $\check{\lambda}$ block-diagonal operator.

The block-diagonal operator $\check{\lambda}$ defined in (18.42) satisfies the following forward Lyapunov equation:

$$\begin{aligned}
 \check{\lambda} - \mathcal{E}_\Psi \check{\lambda} \mathcal{E}_\Psi^* &= \left(\tilde{\Delta}_V^\omega \mathcal{P} - \mathcal{P} \tilde{\Delta}_V^\omega \right) \\
 &\quad + \mathcal{E}_\Phi \left(\bar{\Delta}_V^\nu \mathcal{P}^+ - \mathcal{P}^+ \tilde{\Delta}_V^\nu \right) \mathcal{E}_\Phi^*
 \end{aligned} \tag{18.44}$$

Proof: First, let us verify that the forward Lyapunov equation has a well-defined, block-diagonal solution. This follows from Lemma 9.3 on page 166, whose requirements are met since \mathcal{E}_Ψ is an SKO operator, and the expression on the right of (18.44) is block-diagonal. Now, recall the articulated body inertia Riccati equation:

$$\mathbf{0} \stackrel{9.36}{=} \mathcal{P} - \mathbf{M} - \mathcal{E}_\Psi \mathcal{P} \mathcal{E}_\Psi^* \tag{18.45}$$

Differentiating this equation with respect to time leads to

$$\begin{aligned}
\mathbf{0} &= \dot{\mathcal{P}} - \dot{\mathbf{M}} - \dot{\mathcal{E}}_\psi \mathcal{P} \mathcal{E}_\psi^* - \mathcal{E}_\psi \dot{\mathcal{P}} \mathcal{E}_\psi^* - \mathcal{E}_\psi \mathcal{P} \dot{\mathcal{E}}_\psi^* \\
&\stackrel{18.12c, 18.43f}{=} \dot{\mathcal{P}} - \left(\tilde{\mathcal{V}}^\omega \mathbf{M} - \mathbf{M} \tilde{\mathcal{V}}^\omega \right) - \mathcal{E}_\psi \dot{\mathcal{P}} \mathcal{E}_\psi^* \\
&\quad - \left(\tilde{\mathcal{V}}^\omega \mathcal{E}_\psi - \mathcal{E}_\psi \tilde{\mathcal{V}}_S^\omega - \mathcal{E}_\phi \left(\bar{\tau} \check{\lambda} \mathcal{H}^* \mathcal{D}^{-1} \mathcal{H} - \bar{\Delta}_V^\nu \bar{\tau} \right) \right) \mathcal{P} \mathcal{E}_\psi^* \\
&\quad - \mathcal{E}_\psi \mathcal{P} \left(-\mathcal{E}_\psi^* \tilde{\mathcal{V}}^\omega + \tilde{\mathcal{V}}_S^\omega \mathcal{E}_\psi^* - \left(\mathcal{H}^* \mathcal{D}^{-1} \mathcal{H} \check{\lambda} \bar{\tau}^* + \bar{\tau}^* \tilde{\Delta}_V^\nu \right) \mathcal{E}_\phi^* \right) \\
&= \dot{\mathcal{P}} - \tilde{\mathcal{V}}^\omega \mathbf{M} + \mathbf{M} \tilde{\mathcal{V}}^\omega - \tilde{\mathcal{V}}^\omega \mathcal{E}_\psi \mathcal{P} \mathcal{E}_\psi^* + \mathcal{E}_\psi \mathcal{P} \mathcal{E}_\psi^* \tilde{\mathcal{V}}^\omega \\
&\quad - \mathcal{E}_\psi \left(\dot{\mathcal{P}} + \tilde{\mathcal{V}}_S^\omega \mathcal{P} - \mathcal{P} \tilde{\mathcal{V}}_S^\omega \right) \mathcal{E}_\psi^* \\
&\quad + \mathcal{E}_\phi \left(\bar{\tau} \check{\lambda} \mathcal{H}^* \mathcal{D}^{-1} \mathcal{H} - \bar{\Delta}_V^\nu \bar{\tau} \right) \mathcal{P} \mathcal{E}_\psi^* \\
&\quad + \mathcal{E}_\psi \mathcal{P} \left(\mathcal{H}^* \mathcal{D}^{-1} \mathcal{H} \check{\lambda} \bar{\tau}^* + \bar{\tau}^* \tilde{\Delta}_V^\nu \right) \mathcal{E}_\phi^* \\
&\stackrel{18.42, 18.45}{=} \dot{\mathcal{P}} - \tilde{\mathcal{V}}^\omega \mathbf{M} + \mathbf{M} \tilde{\mathcal{V}}^\omega - \tilde{\mathcal{V}}^\omega (\mathcal{P} - \mathbf{M}) + (\mathcal{P} - \mathbf{M}) \tilde{\mathcal{V}}^\omega \\
&\quad - \mathcal{E}_\psi \check{\lambda} \mathcal{E}_\psi^* + \mathcal{E}_\phi \left(\bar{\tau} \check{\lambda} \tau^* \bar{\tau}^* - \bar{\Delta}_V^\nu \mathcal{P}^+ + \bar{\tau} \tau \check{\lambda} \bar{\tau}^* + \mathcal{P}^+ \tilde{\Delta}_V^\nu \right) \mathcal{E}_\phi^* \\
&= \dot{\mathcal{P}} - \tilde{\mathcal{V}}^\omega \mathcal{P} + \mathcal{P} \tilde{\mathcal{V}}^\omega - \mathcal{E}_\psi \check{\lambda} \mathcal{E}_\psi^* + \mathcal{E}_\phi \left(-\bar{\Delta}_V^\nu \mathcal{P}^+ + \mathcal{P}^+ \tilde{\Delta}_V^\nu \right) \mathcal{E}_\phi^* \\
&\stackrel{18.42}{=} \check{\lambda} - \tilde{\Delta}_V^\omega \mathcal{P} + \mathcal{P} \tilde{\Delta}_V^\omega - \mathcal{E}_\psi \check{\lambda} \mathcal{E}_\psi^* + \mathcal{E}_\phi \left(-\bar{\Delta}_V^\nu \mathcal{P}^+ + \mathcal{P}^+ \tilde{\Delta}_V^\nu \right) \mathcal{E}_\phi^*
\end{aligned}$$

This establishes (18.44). ■

We now group sub-expressions in (18.44) to introduce intermediate block-diagonal operators $\dot{\mathcal{P}}^+$ and $\check{\mathcal{P}}^+$ as follows:

$$\check{\lambda} = \underbrace{\left(\tilde{\Delta}_V^\omega \mathcal{P} - \mathcal{P} \tilde{\Delta}_V^\omega \right)}_{\check{\lambda}} + \mathcal{E}_\phi \underbrace{\left(\underbrace{\bar{\tau} \check{\lambda} \bar{\tau}^*}_{\dot{\mathcal{P}}^+} + \bar{\Delta}_V^\nu \mathcal{P}^+ - \mathcal{P}^+ \tilde{\Delta}_V^\nu \right)}_{\check{\mathcal{P}}^+} \mathcal{E}_\phi^* \quad (18.46)$$

Thus, $\check{\lambda}$ can be broken down into the following sequence of sub-expressions:

$$\begin{aligned}
\dot{\mathcal{P}}^+ &\triangleq \bar{\tau} \check{\lambda} \bar{\tau}^* \\
\check{\mathcal{P}}^+ &\triangleq \dot{\mathcal{P}}^+ + \bar{\Delta}_V^\nu \mathcal{P}^+ - \mathcal{P}^+ \tilde{\Delta}_V^\nu \\
\dot{\mathcal{P}} &\triangleq \mathcal{E}_\phi \check{\mathcal{P}}^+ \mathcal{E}_\phi^* \\
\check{\lambda} &= \dot{\mathcal{P}} + \tilde{\Delta}_V^\omega \mathcal{P} - \mathcal{P} \tilde{\Delta}_V^\omega
\end{aligned} \quad (18.47)$$

The expressions in (18.47) can be mapped into the $O(N)$ tips-to-base recursive gather Algorithm 18.1 for computing the elements of the block-diagonal $\check{\lambda}$.

Algorithm 18.1 Computation of $\check{\lambda}$

The diagonal elements of the $\check{\lambda}$ block-diagonal operator can be computed using the following $O(N)$ tips-to-base gather recursive algorithm:

$$\left\{ \begin{array}{l} \check{\mathcal{P}}^+(\text{tips}) = \mathbf{0} \\ \text{for } k = 1 \cdots n \\ \quad \check{\mathcal{P}}(k) = \sum_{j \in \mathcal{C}(k)} \phi(k, j) \check{\mathcal{P}}^+(j) \phi^*(k, j) \\ \quad \check{\lambda}(k) = \check{\mathcal{P}}(k) + \tilde{\Delta}_V^\omega(k) \mathcal{P}(k) - \mathcal{P}(k) \tilde{\Delta}_V^\omega(k) \\ \quad \check{\mathcal{P}}^+(k) = \bar{\tau}(k) \check{\lambda}(k) \bar{\tau}^*(k) \\ \quad \check{\mathcal{P}}^+(k) = \check{\mathcal{P}}^+(k) + \bar{\Delta}_V^\nu(k) \mathcal{P}^+(k) - \mathcal{P}^+(k) \tilde{\Delta}_V^\nu(k) \\ \text{end loop} \end{array} \right. \quad (18.48)$$

Once $\check{\lambda}$ is available, (18.42) leads us to the following expression for $\dot{\mathcal{P}}$:

$$\dot{\mathcal{P}} = \check{\lambda} + \tilde{\mathcal{V}}_S^\omega \mathcal{P} + \mathcal{P} \tilde{\mathcal{V}}_S^\omega \quad (18.49)$$

The following lemma describes the component expressions for the time derivatives of the articulated body inertia quantities.

Lemma 18.13 Component-level time derivatives of articulated body quantities.

$$\begin{aligned} \dot{\mathcal{P}}(k) &= \tilde{\mathcal{V}}^\omega(\varphi(k)) \mathcal{P}(k) - \mathcal{P}(k) \tilde{\mathcal{V}}^\omega(\varphi(k)) + \check{\lambda}(k) \\ \dot{\mathcal{P}}^+(k) &= \tilde{\mathcal{V}}^\omega(\varphi(k)) \mathcal{P}^+(k) - \mathcal{P}^+(k) \tilde{\mathcal{V}}^\omega(\varphi(k)) \\ &\quad + \bar{\tau}(k) \check{\lambda}(k) \bar{\tau}^*(k) \\ \dot{\mathcal{D}}(k) &= \mathcal{H}(k) \check{\lambda}(k) \mathcal{H}^*(k) \\ \dot{\mathcal{G}}(k) &= \tilde{\mathcal{V}}^\omega(\varphi(k)) \mathcal{G}(k) + \bar{\tau}(k) \check{\lambda}(k) \mathcal{H}^*(k) \mathcal{D}^{-1}(k) \\ \dot{\tau}(k) &= \tilde{\mathcal{V}}^\omega(\varphi(k)) \tau(k) - \tau(k) \tilde{\mathcal{V}}^\omega(\varphi(k)) \\ &\quad + \bar{\tau}(k) \check{\lambda}(k) \mathcal{H}^*(k) \mathcal{D}^{-1}(k) \mathcal{H}(k) \\ \dot{\psi}(\varphi(k), k) &= \tilde{\mathcal{V}}^\omega(\varphi(k)) \psi(\varphi(k), k) - \psi(\varphi(k), k) \tilde{\mathcal{V}}^\omega(\varphi(k)) \\ &\quad + \phi(\varphi(k), k) (\bar{\Delta}_V^\nu(k) \bar{\tau}(k) \\ &\quad - \bar{\tau}(k) \check{\lambda}(k) \mathcal{H}^*(k) \mathcal{D}^{-1}(k) \mathcal{H}(k)) \end{aligned} \quad (18.50)$$

Proof: These expressions are the component-level relationships corresponding to the operator level expressions in (18.42) and (18.43). ■

The process for computing the time derivatives of the articulated body inertia operators can be summarized as follows:

1. Compute the articulated body inertia quantities recursively using the tips-to-base gather recursion in (9.33) on page 175.
2. Compute $\check{\lambda}$ using the tips-to-base gather recursion in Algorithm 18.1.
3. Use $\check{\lambda}$ to compute $\dot{\mathcal{P}}$ using (18.49).
4. Use $\check{\lambda}$ in (18.43) to compute the time derivatives of the other articulated body inertia operators.

The above steps can be combined into a single tips-to-base gather recursion to compute all the articulated body inertia time derivatives. This follows from a closer look at the component level time derivative expressions in (18.50). The component-level time-derivative quantities for a body depend only on the articulated body inertia values for the body and those of children bodies, and these are all available when the regular articulated body inertia gather recursion reaches the body. This implies that the regular articulated body inertia gather recursion (Step 1 above) can be extended so that the step at the k th body also computes $\check{\lambda}(k)$ and the articulated body inertia quantity time-derivatives for the k th body using the expressions in (18.50).

Exercise 18.10 Physical interpretation of $\check{\lambda}$.

With

$$\dot{\mathcal{P}}(k) \triangleq \frac{d_{\mathbb{I}} \mathcal{P}(k)}{dt} \quad \text{and} \quad \dot{\mathcal{P}}^+(k) \triangleq \frac{d_{\mathbb{I}} \mathcal{P}^+(k)}{dt}$$

show that the following are true:

$$\check{\lambda}(k) = \frac{d_{\mathbb{O}_k^+} \mathcal{P}(k)}{dt}, \quad \dot{\mathcal{P}}(k) = \frac{d_{\mathbb{O}_k} \mathcal{P}(k)}{dt}, \quad \dot{\mathcal{P}}^+(k) = \frac{d_{\mathbb{O}_k^+} \mathcal{P}^+(k)}{dt} \quad (18.51)$$

■

Thus, while $\dot{\mathcal{P}}(k)$ is the time derivative of $\mathcal{P}(k)$ with respect to the inertial frame \mathbb{I} , $\dot{\mathcal{P}}(k)$ is its time derivative with respect to the \mathbb{O}_k frame, and $\check{\lambda}(k)$ is its time derivative with respect to the \mathbb{O}_k^+ frame. Similarly, while $\dot{\mathcal{P}}^+(k)$ is the time derivative of $\mathcal{P}^+(k)$ with respect to the inertial frame \mathbb{I} , $\dot{\mathcal{P}}^+(k)$ is its time derivative with respect to the \mathbb{O}_k^+ frame.

18.6 Sensitivity of Articulated Body Quantities

Define the block-diagonal, symmetric operator $\check{\lambda}_{\theta_i}$ as the partial derivative of $\check{\lambda}$ with respect to the i th generalized velocity coordinate, i.e.,

$$\check{\lambda}_{\theta_i} \triangleq \frac{\partial \check{\lambda}}{\partial \dot{\theta}_i} \quad (18.52)$$

Lemma 18.14 Sensitivity of articulated body quantities.

$\check{\lambda}_{\theta_i}$ is related to the \mathcal{P}_{θ_i} partial derivative by the following expression:

$$\check{\lambda}_{\theta_i} = \mathcal{P}_{\theta_i} + \mathcal{P} \tilde{\mathcal{H}}_{\prec i}^{\omega} - \tilde{\mathcal{H}}_{\prec i}^{\omega} \mathcal{P} \quad (18.53)$$

Also, the partial derivatives of various articulated body inertia operators are given by the following expressions:

$$\mathcal{D}_{\theta_i} = H \check{\lambda}_{\theta_i} H^* \quad (18.54a)$$

$$[\mathcal{D}^{-1}]_{\theta_i} = -\mathcal{D}^{-1} H \check{\lambda}_{\theta_i} H^* \mathcal{D}^{-1} \quad (18.54b)$$

$$[\mathcal{G}]_{\theta_i} = \bar{\tau} \check{\lambda}_{\theta_i} H^* \mathcal{D}^{-1} + \tilde{\mathcal{H}}_{\prec i}^{\omega} \mathcal{G} \quad (18.54c)$$

$$[\boldsymbol{\tau}]_{\theta_i} = \bar{\tau} \check{\lambda}_{\theta_i} H^* \mathcal{D}^{-1} H + \tilde{\mathcal{H}}_{\prec i}^{\omega} \boldsymbol{\tau} - \boldsymbol{\tau} \tilde{\mathcal{H}}_{\prec i}^{\omega} \quad (18.54d)$$

$$\bar{\tau}_{\theta_i} = -[\boldsymbol{\tau}]_{\theta_i} \quad (18.54e)$$

$$\begin{aligned} [\mathcal{E}_{\psi}]_{\theta_i} &= \tilde{\mathcal{H}}_{\preceq i}^{\omega} \mathcal{E}_{\psi} - \mathcal{E}_{\psi} \tilde{\mathcal{H}}_{\prec i}^{\omega} \\ &\quad - \mathcal{E}_{\phi} \left(\bar{\tau} \check{\lambda}_{\theta_i} H^* \mathcal{D}^{-1} H - \bar{\mathcal{H}}_{=i}^v \bar{\tau} \right) \end{aligned} \quad (18.54f)$$

$$\begin{aligned} \check{\lambda}_{\theta_i} - \mathcal{E}_{\psi} \check{\lambda}_{\theta_i} \mathcal{E}_{\psi}^* &= \left(\tilde{\mathcal{H}}_{=i}^{\omega} \mathcal{P} - \mathcal{P} \tilde{\mathcal{H}}_{=i}^{\omega} \right) \\ &\quad + \mathcal{E}_{\phi} \left(\bar{\mathcal{H}}_{=i}^v \mathcal{P}^+ - \mathcal{P}^+ \tilde{\mathcal{H}}_{=i}^v \right) \mathcal{E}_{\phi}^* \end{aligned} \quad (18.54g)$$

Proof: Equation (18.53) follows from the use of (18.26) and (18.28) in the expression for $\check{\lambda}$ in (18.42). A similar process applied to the time derivative expressions in (18.43) and (18.44) leads to the sensitivity expressions in (18.54). ■

Remark 18.2 Link level sensitivities of articulated body inertias.

Noting that

$$\check{\lambda}_{\theta_i}(k) = \begin{cases} \mathbf{0} & \text{for } k \prec i \\ \tilde{H}_{\omega}^*(i) \mathcal{P}(i) - \mathcal{P}(i) \tilde{H}_{\omega}^*(i) & \text{for } k = i \\ \phi(k, i) \left(\bar{\tau}(i) \check{\lambda}_{\theta_i}(i) \bar{\tau}^*(i) + \bar{H}_v^*(i) \mathcal{P}^+(i) \right. \\ \left. - \mathcal{P}^+(i) \tilde{H}_v^*(i)(i) \right) \phi^*(k, i) & \text{for } k = \wp(i) \\ \psi(k, \wp(i)) \check{\lambda}_{\theta_i}(\wp(i)) \psi^*(k, \wp(i)) & \text{for } k \succ \wp(i) \end{cases} \quad (18.55)$$

it follows that, at the link level, the sensitivity expressions can be expressed as:

$$\mathcal{P}_{\theta_i}(k) = \begin{cases} \tilde{H}_{\omega}^*(i) \mathcal{P}(k) - \mathcal{P}(k) \tilde{H}_{\omega}^*(i) & \text{for } k \preceq i \\ \check{\lambda}_{\theta_i}(k) = \psi(k, i) \mathcal{P}_{\theta_i}(i) \psi^*(k, i) & \text{for } k \succ i \end{cases} \quad (18.56)$$

$$\mathcal{D}_{\theta_i}(k) = H(k) \mathcal{P}_{\theta_i}(k) H^*(k) \cdot \mathbb{1}_{[k \succeq i]} \quad (18.57)$$

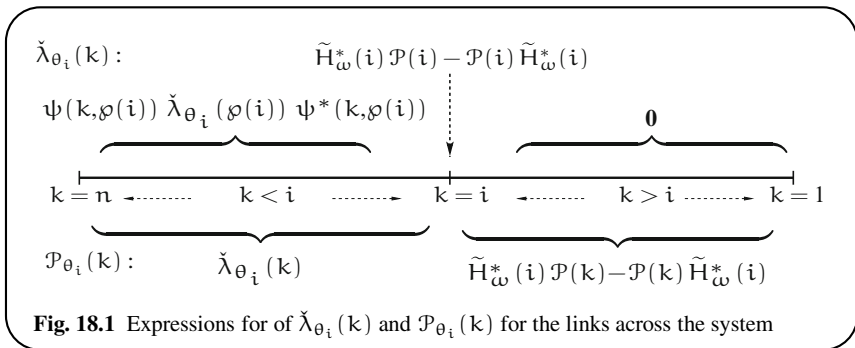
$$\begin{aligned}\mathcal{G}_{\theta_i}(k) &= \tilde{H}_\omega^*(i) \mathcal{G}(k) \mathbb{1}_{[k < i]} \\ &\quad + \bar{\tau}(k) \mathcal{P}_{\theta_i}(k) H^*(k) \mathcal{D}^{-1}(k) \cdot \mathbb{1}_{[k \geq i]}\end{aligned}\quad (18.58)$$

$$\begin{aligned}\tau_{\theta_i}(k) &= [\tilde{H}_\omega^*(i) \tau(k) - \tau(k) \tilde{H}_\omega^*(i)] \cdot \mathbb{1}_{[k < i]} \\ &\quad + \bar{\tau}(k) \mathcal{P}_{\theta_i}(k) H^*(k) \mathcal{D}^{-1}(k) H(k) \cdot \mathbb{1}_{[k \geq i]}\end{aligned}\quad (18.59)$$

$$\begin{aligned}[\psi(k+1, k)]_{\theta_i} &= [\tilde{H}_\omega^*(i) \psi(k+1, k) - \psi(k+1, k) \tilde{H}_\omega^*(i)] \cdot \mathbb{1}_{[k < i]} \\ &\quad + \phi(k+1, k) \left(\bar{H}_v^*(k) \bar{\tau}(k) \cdot \mathbb{1}_{[k=i]} \right. \\ &\quad \left. - \bar{\tau}(k) \mathcal{P}_{\theta_i}(k) H^*(k) \mathcal{D}^{-1}(k) H(k) \cdot \mathbb{1}_{[k \geq i]} \right)\end{aligned}\quad (18.60)$$

■

The values of $\check{\lambda}_{\theta_i}(k)$ and $\mathcal{P}_{\theta_i}(k)$ across the links in the system is illustrated in Fig. 18.1.



18.7 Sensitivity of Innovations Factors

Exercise 18.11 Time derivative of $(I + H\Phi K)$.

Show that

$$\frac{d[I + H\Phi K]}{dt} = H\Phi \left[\tilde{\Delta}_V^\omega \Phi K + \mathcal{E}_\Phi \bar{\Delta}_V^\nu \Phi G + \bar{\tau} \check{\lambda} H^* \mathcal{D}^{-1} \right]\quad (18.61)$$

■

Exercise 18.12 Time derivative of $[I + H\phi K]\mathcal{D}$.*Show that*

$$\frac{d[I + H\phi K]\mathcal{D}}{dt} = H\phi \left[\tilde{\Delta}_v^\omega \tilde{\phi} \mathcal{P} + \mathcal{E}_\phi \bar{\Delta}_v^\nu \phi \mathcal{P} + \check{\lambda} \right] H^* \quad (18.62)$$

■

Exercise 18.13 Time derivative of $[I - H\psi K]$.*Show that*

$$\begin{aligned} \frac{d[I - H\psi K]}{dt} = & -H\psi \left[\tilde{\Delta}_v^\omega \phi \mathcal{K} + \mathcal{E}_\phi \bar{\Delta}_v^\nu \phi \mathcal{G} \right. \\ & \left. + \bar{\tau} \check{\lambda} H^* \mathcal{D}^{-1} \right] [I - H\psi K] \end{aligned} \quad (18.63)$$

■

Exercise 18.14 Sensitivities of $[I + H\phi K]$ and $[I - H\psi K]$.*Show that*

$$[I + H\phi K]_{\theta_i} = H\phi [\tilde{\mathcal{H}}_{=i}^\omega \tilde{\phi} \mathcal{P} + \mathcal{E}_\phi \tilde{\mathcal{H}}_{=i}^\nu \phi \mathcal{P} + \bar{\tau} \check{\lambda}_{\theta_i}] H^* \mathcal{D}^{-1} \quad (18.64)$$

$$\begin{aligned} [I - H\psi K]_{\theta_i} = & -H\psi \left[\tilde{\mathcal{H}}_{=i}^\omega \phi \mathcal{K} + \mathcal{E}_\phi \tilde{\mathcal{H}}_{=i}^\nu \phi \mathcal{G} \right. \\ & \left. + \bar{\tau} \check{\lambda}_{\theta_i} H^* \mathcal{D}^{-1} \right] (I - H\psi K) \end{aligned} \quad (18.65)$$

■

The following exercise develops expressions for $\log\{\det\{\mathcal{M}\}\}$ and its partial derivatives with respect to generalized coordinates. This term appears in expressions for the Fixman potential [57, 72] in the context of internal coordinate molecular dynamics [88]. The Fixman potential is used in internal coordinate molecular dynamics simulations, to correct for systematic biases introduced in the computation of statistical thermodynamic quantities. Its partial derivatives with respect to the generalized coordinates are the generalized forces resulting from the Fixman potential.

Exercise 18.15 Sensitivity of $\log\{\det\{\mathcal{M}\}\}$.1. *Show that*

$$\begin{aligned} \frac{\partial \log\{\det\{\mathcal{M}\}\}}{\partial \theta_i} &= \text{Trace} \{ \mathcal{D}^{-1} H \check{\lambda}_{\theta_i} H^* \} \\ &= \sum_{\forall k: k \succ i} \text{Trace} \{ \mathcal{D}^{-1}(k) H(k) \check{\lambda}_{\theta_i}(k) H^*(k) \} \end{aligned} \quad (18.66)$$

2. *For the case of systems with non-prismatic hinges (i.e., $\bar{\Delta}_v = \mathbf{0}$), Jain [72] uses the (A.29) matrix trace identity to alternatively establish that*

$$\frac{\partial \log\{\det\{\mathcal{M}\}\}}{\partial \theta_i} = 2 \text{Trace}\{\mathcal{P}\Omega \mathcal{H}_{=i}^\omega\} \quad (18.67)$$

Show that (18.67) and (18.66) are equivalent for systems with non-prismatic hinges.

3. Also, show that the generalization of (18.67) for systems with prismatic hinges is:

$$\begin{aligned} \frac{\partial \log\{\det\{\mathcal{M}\}\}}{\partial \theta_i} &= 2 \text{Trace}\left\{ \mathcal{P}\Omega \left(\mathcal{H}_{=i}^\omega + \mathcal{E}_\phi \bar{\mathcal{H}}_{=i}^v \right) \right\} \\ &= 2 \text{Trace}\left\{ \mathcal{P}(i)\Upsilon(i) \tilde{H}_\omega^*(i) \right\} \\ &\quad + 2 \text{Trace}\left\{ \mathcal{P}\Omega \mathcal{E}_\phi \bar{\mathcal{H}}_{=i}^v \right\} \end{aligned} \quad (18.68)$$

■

Chapter 19

Diagonalized Lagrangian Dynamics

The multibody dynamics models we have studied have used hinge coordinates and velocities, for the system-level generalized coordinate and velocity vectors. For a system with N degrees of freedom, (4.26) describes the following Lagrangian form of the equations of motion for the system:

$$\mathcal{M}(\theta)\ddot{\theta} + \mathcal{C}(\theta, \dot{\theta}) = \mathcal{T}, \quad \mathcal{C}(\theta, \dot{\theta}) \stackrel{4.27}{=} \dot{\mathcal{M}}\dot{\theta} - \frac{1}{2} \frac{\partial \dot{\theta}^* \mathcal{M} \dot{\theta}}{\partial \theta} \quad (19.1)$$

The mass matrix \mathcal{M} is a configuration dependent, dense matrix, and the \mathcal{C} term depends non-linearly on both the configuration and velocity coordinates. In this chapter, we study alternative choices of generalized coordinates and velocities that can diagonalize and simplify the equations of motion [1, 2, 63, 84, 90, 168].

19.1 Globally Diagonalized Dynamics

The global diagonalization approach seeks to transform the configuration coordinates θ and their time-derivatives $\dot{\theta}$ into a new set of $(\vartheta, \dot{\vartheta})$ coordinates, in which the equations of motion are decoupled. This approach is based on the requirement that the “square-root” factor of the mass matrix, $\mathbf{m}(\theta)$, is the gradient of a global coordinate transformation.

Assumption 19.1 requires that the mass matrix factor $\mathbf{m}(\theta)$ be the gradient of some function $g(\theta)$. This assumption is very rarely satisfied in practice [25, 105, 171]. Nonetheless, it is of interest to examine the globally diagonalized equations as a step towards the locally diagonalizing transformations discussed later in this chapter.

Assumption 19.1 (Global diagonalization condition). *There exists a smooth and invertible, global generalized coordinate transformation $\vartheta = g(\theta) \in \mathcal{R}^N$ such that*

$$\nabla_\theta \vartheta = \nabla_\theta g = m^*(\theta) \in \mathcal{R}^{N \times N} \quad (19.2)$$

where the matrix function $m(\theta)$ is the “square-root” of the mass matrix, i.e.,

$$m(\theta)m^*(\theta) = M(\theta) \quad (19.3)$$

for all θ .

Assumption 19.1 requires that the mass matrix factor $m(\theta)$ be the gradient of some function $g(\theta)$. This assumption is very rarely satisfied in practice [25, 105, 171]. Nonetheless, it is of interest to examine the globally diagonalized equations as a step towards the locally diagonalizing transformations discussed later in this chapter.

Since $g(\theta)$ does not depend on $\dot{\theta}$, it follows that the new $\dot{\vartheta}$ generalized velocity vector is

$$\dot{\vartheta} = \nabla_\theta g \dot{\theta} \stackrel{19.2}{=} m^*(\theta) \dot{\theta} \quad (19.4)$$

In terms of the velocity vector, $\dot{\vartheta}$, the kinetic energy is

$$\kappa_e(\vartheta, \dot{\vartheta}) \stackrel{4.25}{=} \frac{1}{2} \dot{\vartheta}^* M \dot{\vartheta} \stackrel{19.3}{=} \frac{1}{2} \dot{\vartheta}^* m m^* \dot{\vartheta} \stackrel{19.4}{=} \frac{1}{2} \dot{\vartheta}^* \dot{\vartheta} \quad (19.5)$$

Lemma 19.1 Global diagonalizing coordinate transformations.

When Assumption 19.1 holds, the equations of motion in the new coordinates $(\vartheta, \dot{\vartheta})$ are

$$\ddot{\vartheta} = \zeta \quad \text{where} \quad \zeta \stackrel{\triangle}{=} \ell(\theta) \tau \in \mathcal{R}^N \quad \text{and} \quad \ell(\theta) \stackrel{\triangle}{=} m^{-1}(\theta) \quad (19.6)$$

Proof: Differentiating (19.4),

$$\ddot{\vartheta} = m^* \ddot{\theta} + m^* \dot{\theta} \quad \Rightarrow \quad \ddot{\theta} = \ell^* [\ddot{\vartheta} - m^* \dot{\theta}]$$

Use of this in (19.1) and pre-multiplication by ℓ leads to

$$\ddot{\vartheta} + C(\vartheta, \dot{\vartheta}) = \zeta \quad \text{where} \quad C(\vartheta, \dot{\vartheta}) \stackrel{\triangle}{=} \ell C(\theta, \dot{\theta}) - m^* \dot{\theta} \quad (19.7)$$

However,

$$\frac{\partial \dot{\theta}^* M \dot{\theta}}{\partial \theta} \stackrel{19.5}{=} \frac{\partial \dot{\vartheta}^* \dot{\vartheta}}{\partial \theta} = 2 \frac{\partial \dot{\vartheta}^*}{\partial \theta} \dot{\vartheta} = 2 \frac{d}{dt} \frac{\partial \dot{\vartheta}^*}{\partial \theta} \dot{\vartheta} \stackrel{19.2}{=} 2 \dot{m} \dot{\vartheta} \quad (19.8)$$

Also,

$$\dot{M} \dot{\theta} \stackrel{19.3}{=} (\dot{m} m^* + m \dot{m}^*) \dot{\theta} \stackrel{19.4}{=} \dot{m} \dot{\vartheta} + m \dot{m}^* \dot{\theta} \quad (19.9)$$

Thus,

$$\begin{aligned}\mathcal{C}(\dot{\theta}, \ddot{\theta}) &\stackrel{19.1, 19.7}{=} \ell \left(\dot{\mathcal{M}}\dot{\theta} - \frac{1}{2} \frac{\partial \dot{\theta}^* \mathcal{M} \dot{\theta}}{\partial \theta} \right) - \dot{\mathbf{m}}^* \dot{\theta} \\ &\stackrel{19.8, 19.9}{=} \ell (\dot{\mathbf{m}}\dot{\theta} + \mathbf{m}\dot{\mathbf{m}}^* \dot{\theta} - \dot{\mathbf{m}}\dot{\theta}) - \dot{\mathbf{m}}^* \dot{\theta} \stackrel{19.6}{=} \mathbf{0}\end{aligned}$$

Using this in (19.7) establishes the equations of motion in (19.6). ■

The new equations of motion in (19.6) are very simple. The mass matrix is the configuration independent identity matrix, and there are no Coriolis forces. The component degrees of freedom are completely decoupled and governed by independent second-order linear differential equations. Since \mathbf{T} is the vector of generalized forces corresponding to the generalized velocities vector $\dot{\theta}$, the principle of virtual work implies that ζ is the vector of generalized forces corresponding to the generalized velocities $\dot{\vartheta}$. Equation (19.6) can also be obtained alternatively by deriving the Lagrangian equations of motion in the ϑ coordinate system using the diagonalized expression (19.5) for the kinetic energy in Exercise 4.11 on page 72.

Now that the simplicity resulting from the global coordinate transformation $g(\theta)$ is apparent, we examine conditions under which Assumption 19.1 is satisfied by multibody systems. The answer is based on a result from non-Euclidean geometry. It is known that the mass matrix \mathcal{M} defines a metric tensor [46] on the configuration manifold. Since tensor quantities are invariant under coordinate transformations, a globally diagonalizing transformation exists if and only if the metric tensor is a Euclidean metric tensor, i.e., one with constant coefficients. A manifold with a Euclidean metric is said to be “flat” and the curvature tensor associated with it is identically zero. The precise necessary conditions for the metric tensor associated with \mathcal{M} to be a Euclidean metric are summarized in the following lemma.

Lemma 19.2 Euclidean metrics have zero curvature tensor.

For Assumption 19.1 to hold, it is necessary that the curvature tensor R of \mathcal{M} vanish, that is, each of the $N(N+1)/2$ Riemannian symbols of the first kind R_{hijk} defined below must vanish.

$$\begin{aligned}R_{hijk} &\triangleq \frac{1}{2} \left[\frac{\partial^2 \mathcal{M}_{hk}}{\partial \theta_i \partial \theta_j} + \frac{\partial^2 \mathcal{M}_{ij}}{\partial \theta_h \partial \theta_k} - \frac{\partial^2 \mathcal{M}_{hj}}{\partial \theta_i \partial \theta_k} - \frac{\partial^2 \mathcal{M}_{ik}}{\partial \theta_h \partial \theta_j} \right] \\ &+ \sum_l \left[\left\{ {}^l_{ij} \right\} [hk, l] - \left\{ {}^l_{ik} \right\} [hj, l] \right]\end{aligned} \quad (19.10)$$

The $[ij, k]$ and $\left\{ {}^k_{ij} \right\}$ quantities are the Christoffel symbols of the first and second kind, respectively [119]. While the former are defined by (4.35) on page 68, the second kind are defined as

$$\left\{ {}^k_{ij} \right\} \triangleq \sum_{m=1}^N \mathcal{M}^{-1}(k, m) [ij, m] \quad (19.11)$$

Proof: See [25, 46, 171]. ■

In practice, the conditions in this lemma are very restrictive, and are rarely satisfied by multibody systems. Furthermore, they are extremely difficult to verify, since the first and second derivatives of the mass matrix with respect to the configuration variables θ are required. Also, this condition must hold throughout the configuration space. The next section describes an alternative approach to diagonalizing the equations of motion that is broadly applicable to multibody systems.

19.2 Diagonalization in Velocity Space

Instead of diagonalizing globally in configuration space, we now explore diagonalizing transformations in just velocity space. This transformation replaces the joint-angle velocities $\dot{\theta}$ with a new set of velocities η , while retaining the original θ generalized coordinates. The search for the generalized velocity transformation begins with the following assumption regarding the factorization of the mass matrix.

Assumption 19.2 (Velocity space condition). *There exists a smooth, differentiable and invertible function $\mathbf{m}(\theta)$, with inverse denoted by $\ell(\theta)$, which factors the mass matrix as $\mathcal{M}(\theta) = \mathbf{m}(\theta)\mathbf{m}^*(\theta)$ for all configurations. Unlike Assumption 19.1, $\mathbf{m}^*(\theta)$ is not required to be the gradient of any function.*

Under this assumption, the new generalized velocity coordinates η are defined as

$$\eta \triangleq \mathbf{m}^*(\theta)\dot{\theta} \quad (19.12)$$

The differentiability of \mathbf{m} insures that the η vector is differentiable. Invertibility of $\mathbf{m}(\theta)$ insures that time derivatives $\dot{\theta}$ of the configuration variables can be recovered from η using the relationship:

$$\dot{\theta} \stackrel{19.6, 19.12}{=} \ell^*(\theta)\eta \quad (19.13)$$

Under these conditions, η represents a valid choice for a new generalized velocity vector.

Assumption 19.2 is much weaker than Assumption 19.1. Since \mathbf{m} is no longer the gradient of a function, the transformed velocity vector η is no longer the time derivative of any vector of configuration variables. The $\eta(k)$ components are thus quasi-velocities. Numerical integration of the η vector over time does not lead to the generalized coordinates. The equations of motion using the new generalized velocity coordinates are described in the following lemma.

Lemma 19.3 Diagonalizing velocity transformations.

When Assumption 19.2 holds, the equations of motion using the (θ, η) coordinates are

$$\dot{\eta} + \mathcal{C}(\theta, \eta) = \zeta \quad \text{where} \quad \zeta = \ell(\theta)\mathcal{T} \quad (19.14)$$

with the Coriolis force vector

$$\mathcal{C}(\theta, \eta) \triangleq \ell \left(\dot{\mathbf{m}}\eta - \frac{1}{2} \frac{\partial \dot{\theta}^* \mathcal{M} \dot{\theta}}{\partial \theta} \right) \quad (19.15)$$

Proof: Differentiating (19.12),

$$\dot{\eta} = \mathbf{m}^* \ddot{\theta} + \dot{\mathbf{m}}^* \dot{\theta} \quad \Rightarrow \quad \ddot{\theta} = \ell^* [\dot{\eta} - \dot{\mathbf{m}}^* \dot{\theta}]$$

Use of this in (19.1) and pre-multiplication by ℓ leads to

$$\dot{\eta} + \mathcal{C}(\theta, \eta) = \zeta \quad \text{where} \quad \mathcal{C}(\theta, \eta) = \ell \mathcal{C}(\theta, \dot{\theta}) - \dot{\mathbf{m}}^* \dot{\theta} \quad (19.16)$$

Also,

$$\dot{\mathcal{M}}\dot{\theta} \stackrel{19.3}{=} (\dot{\mathbf{m}}\mathbf{m}^* + \mathbf{m}\dot{\mathbf{m}}^*)\dot{\theta} \stackrel{19.12}{=} \dot{\mathbf{m}}\eta + \mathbf{m}\dot{\mathbf{m}}^*\dot{\theta} \quad (19.17)$$

Thus,

$$\begin{aligned} \mathcal{C}(\theta, \eta) &\stackrel{19.1, 19.16}{=} \ell \left(\dot{\mathcal{M}}\dot{\theta} - \frac{1}{2} \frac{\partial \dot{\theta}^* \mathcal{M} \dot{\theta}}{\partial \theta} \right) - \dot{\mathbf{m}}^* \dot{\theta} \\ &\stackrel{19.17}{=} \ell \left(\dot{\mathbf{m}}\eta + \mathbf{m}\dot{\mathbf{m}}^*\dot{\theta} - \frac{1}{2} \frac{\partial \dot{\theta}^* \mathcal{M} \dot{\theta}}{\partial \theta} \right) - \dot{\mathbf{m}}^* \dot{\theta} \\ &= \ell \left(\dot{\mathbf{m}}\eta - \frac{1}{2} \frac{\partial \dot{\theta}^* \mathcal{M} \dot{\theta}}{\partial \theta} \right) \end{aligned}$$

Using this in (19.16) establishes the result. ■

These equations of motion are simpler than the original ones in (19.1) and are similar to the globally diagonalized equations in (19.6). The mass matrix is once again constant and equal to the identity matrix. The main difference is that the Coriolis force term is no longer zero. However, as we will see in the next section, this Coriolis vector has the special property that it is orthogonal to the generalized velocity vector η , implying that the Coriolis term does no mechanical work.

The diagonal equations of motion in (19.14) occupy a middle ground between the globally decoupled equations of motion in Lemma 19.1 and the standard equations of motion in (19.1). While they are not quite as simple as the globally diagonalized equations of Lemma 19.1, we will see later that they always exist for the broad class of tree-topology systems. This is in stark contrast to the rare existence of globally diagonalizing transformations.

The $\mathbf{m}(\theta)$ mass matrix factor plays a central role in the above diagonalized equations. Numerical (e.g., Cholesky-like) factorization of the mass matrix at each configuration can be used to obtain a candidate factor $\mathbf{m}(\theta)$. The resulting factors however may not smoothly depend on the configuration coordinates and thus, might not be differentiable. Even more problematically, numerical factorization procedures provide no systematic way to compute the Coriolis force term $\mathcal{C}(\theta, \eta)$, since the derivatives of \mathbf{m} are required for this purpose. An alternative path that overcomes

the limitations of the numerical factorization approach uses the SKO operator factorizations of the mass matrix and is discussed in Sect. 19.3.

19.2.1 Coriolis Force Does No Work

The following lemma shows that the Coriolis term $\mathcal{C}(\theta, \eta)$ from the velocity space diagonalization is orthogonal to the generalized velocities η and, therefore, does no mechanical work.

Lemma 19.4 $\mathcal{C}(\theta, \eta)$ **does no work.**

The Coriolis forces vector $\mathcal{C}(\theta, \eta)$ does no work, i.e.,

$$\eta^* \mathcal{C}(\theta, \eta) = 0 \quad (19.18)$$

Proof: Observe that $\mathcal{M} = \mathbf{m}\mathbf{m}^*$ implies that $\dot{\theta}^* \mathcal{M}_\theta \dot{\theta} = 2 \operatorname{col} \left\{ \eta^* \mathbf{m}_{\theta_i}^* \dot{\theta} \right\}$. Consequently,

$$\begin{aligned} \eta^* \mathcal{C}(\theta, \eta) &= \dot{\theta}^* \left(\dot{\mathbf{m}}\eta - \operatorname{col} \left\{ \eta^* \mathbf{m}_{\theta_i}^* \dot{\theta} \right\} \right) = \dot{\theta}^* \dot{\mathbf{m}}\eta - \sum_{i=1}^N \dot{\theta}(i) \eta^* \mathbf{m}_{\theta_i}^* \dot{\theta} \\ &= \dot{\theta}^* \dot{\mathbf{m}}\eta - \eta^* \dot{\mathbf{m}}^* \dot{\theta} = \mathbf{0} \end{aligned}$$

■

The orthogonality of the nonlinear Coriolis forces is similar to the orthogonality condition $\omega^* [\tilde{\omega} \mathcal{J} \omega] = \mathbf{0}$ of the gyroscopic force term in the equations of motion for a single rigid body rotating with angular velocity ω . This property is in contrast to the non-orthogonality of the regular Coriolis forces term $\mathcal{C}(\theta, \dot{\theta})$ in the regular equations of motion in (19.1), for which $\dot{\theta}^* \mathcal{C}(\theta, \dot{\theta}) \neq \mathbf{0}$, as discussed in Exercise 4.4 on page 68.

19.2.2 Rate of Change of the Kinetic Energy

Recall that the kinetic energy of the system is $\mathfrak{K}_e(\theta, \eta) = \frac{1}{2} \eta^* \eta$.

Lemma 19.5 The rate of change of the kinetic energy.

Analogous to the Exercise 4.5 on page 68, the rate of change of the kinetic energy is the dot product of the generalized forces and generalized velocities

$$\frac{d\mathfrak{K}_e(\theta, \eta)}{dt} = \eta^* \zeta \quad (19.19)$$

Proof:

$$\frac{d\mathcal{K}_e(\theta, \eta)}{dt} = \eta^* \dot{\eta} = \eta^* [\zeta - \mathcal{C}(\theta, \eta)] \stackrel{19.18}{=} \eta^* \zeta$$

■

19.3 The Innovations Factors as Diagonalizing Transformations

The Innovations factorization of the mass matrix in (9.49) provides candidate velocity diagonalizing transformations. Define the operators $\mathbf{m}(\theta)$ and $\ell(\theta)$ as:

$$\mathbf{m}(\theta) \triangleq [\mathbf{I} + \mathbf{H}\mathbb{A}\mathcal{K}] \mathcal{D}^{\frac{1}{2}} \quad \ell(\theta) \triangleq \mathbf{m}^{-1}(\theta) \stackrel{9.50}{=} \mathcal{D}^{-\frac{1}{2}} [\mathbf{I} - \mathbf{H}\psi\mathcal{K}] \quad (19.20)$$

so that

$$\mathcal{M}(\theta) \stackrel{9.49}{=} \mathbf{m}(\theta)\mathbf{m}^*(\theta) \quad \text{and} \quad \mathcal{M}^{-1}(\theta) \stackrel{9.51}{=} \ell^*(\theta)\ell(\theta) \quad (19.21)$$

The function $\mathbf{m}(\theta)$ so defined satisfies all of the conditions in Assumption 19.2. Satisfaction of the differentiability property is based on the following rationale. The operators \mathbf{H} and \mathbb{A} are smooth and differentiable functions of the configuration coordinates, so the only potential trouble-spot is in the differentiability of the articulated body quantities in (16.8), particularly the inverse \mathcal{D}^{-1} of the diagonal operator $\mathcal{D} = \mathbf{H}\mathbf{P}\mathbf{H}^*$. The diagonal matrix \mathcal{D} is always positive definite, invertible and a smooth function of the generalized coordinates. Consequently, \mathcal{D}^{-1} is always a smooth and differentiable function of θ .

One issue we have is that \mathbf{m} depends upon $\mathcal{D}^{\frac{1}{2}}$. Since \mathcal{D} is block-diagonal, so is $\mathcal{D}^{\frac{1}{2}}$. In general, the square-root of a matrix is not unique for matrices of dimension greater than one. Thus, $\mathcal{D}^{\frac{1}{2}}$ is unique (modulo sign) only when the block elements are scalar, which occurs when the multibody system has only single degree of freedom hinges. Uniqueness, and in fact smoothness, is required of $\mathcal{D}^{\frac{1}{2}}$ for the smoothness of \mathbf{m} . Due to this constraint, for the rest of this section, we will assume that all the hinges in the system are indeed single degree of freedom hinges. This requirement is not much of a restriction since any multiple degree of freedom hinge can be expressed as a sequence of single degree of freedom hinges.

With the 1 degree of freedom hinge assumption, $\mathbf{m} = [\mathbf{I} + \mathbf{H}\mathbb{A}\mathcal{K}] \mathcal{D}^{\frac{1}{2}}$ is a smooth and differentiable matrix function. $\mathbf{m}(\theta)$, therefore, satisfies all the conditions in Assumption 19.2 and is a valid velocity diagonalizing transformation. This conclusion is summarized in the following lemma.

Lemma 19.6 The SKO velocity diagonalizing transformation.

Systems with an SKO model have velocity diagonalizing transformations satisfying Assumption 19.2, with

$$\mathbf{m} \triangleq [\mathbf{I} + \mathbf{H}\mathbb{A}\mathcal{K}] \mathcal{D}^{\frac{1}{2}} \quad (19.22)$$

and the diagonalized generalized velocity coordinates defined by

$$\eta = \mathcal{D}^{\frac{1}{2}} [\mathbf{I} + H\mathbb{A}\mathcal{K}]^* \dot{\theta} \quad \text{and} \quad \dot{\theta} = [\mathbf{I} - H\psi\mathcal{K}]^* \mathcal{D}^{-\frac{1}{2}} \eta \quad (19.23)$$

Proof: This lemma follows from (19.20) to (19.21) and the above discussion regarding the smoothness of \mathbf{m} . ■

19.3.1 Transformations Between $\dot{\theta}$ and η

The η diagonalizing velocity coordinates are related to the $\dot{\theta}$ generalized velocity coordinates via the transformation $\eta = \mathbf{m}^* \dot{\theta}$. This transformation can be mechanized by an outward recursion from the base of the manipulator to its tip. This outward recursion is specified by the algorithm on the left column of Table 19.1. The inverse transformation $\dot{\theta} = \ell^* \eta$ can also be mechanized by an outward recursion. The right column of Table 19.1 shows this algorithm.

Similarly, the “new” input variables ζ , appearing in the diagonalized equation $\dot{\eta} + \mathcal{C}(\eta, \theta) = \zeta$, are obtained from the “old” inputs \mathcal{T} by the transformation $\zeta = \ell\mathcal{T}$. This is mechanized by the inward, tip-to-base recursion specified on the left column of Table 19.2. The inverse operation $\mathcal{T} = \mathbf{m}\zeta$, from the new variables ζ to the old variables \mathcal{T} , is also performed recursively in an outward direction, as specified by the algorithm in the right column of Table 19.2.

Table 19.1 $\dot{\theta}$ and η can be computed recursively from each other

$\eta = \mathbf{m}^* \dot{\theta} = \mathcal{D}^{\frac{1}{2}} [\mathbf{I} + H\mathbb{A}\mathcal{K}]^* \dot{\theta}$	$\dot{\theta} = \ell^* \eta = [\mathbf{I} - H\psi\mathcal{K}]^* \mathcal{D}^{-\frac{1}{2}} \eta$
$\mathcal{V}(\mathcal{N}+1) = \mathbf{0}$	$\mathcal{V}(\mathcal{N}+1) = \mathbf{0}$
for $k = \mathcal{N} \dots 1$	for $k = \mathcal{N} \dots 1$
$\mathcal{V}^+(k) = \mathbb{A}^*(k+1, k)\mathcal{V}(k+1)$	$\mathcal{V}^+(k) = \mathbb{A}^*(k+1, k)\mathcal{V}(k+1)$
$\eta(k) = \mathcal{D}^{\frac{1}{2}}(k)[\dot{\theta}(k) + \mathcal{G}^*(k)\mathcal{V}^+(k)]$	$\dot{\theta}(k) = \mathcal{D}^{-\frac{1}{2}}(k)\eta(k) - \mathcal{G}^*(k)\mathcal{V}^+(k)$
$\mathcal{V}(k) = \mathcal{V}^+(k) + H^*(k)\dot{\theta}(k)$	$\mathcal{V}(k) = \mathcal{V}^+(k) + H^*(k)\dot{\theta}(k)$
end loop	end loop

It is relatively easy therefore, to go back and forth between the original $\dot{\theta}$ and \mathcal{T} variables in traditional robot dynamics and the η and ζ variables in the diagonalized equations of motion. The two mutually reciprocal outward recursions in Table 19.1 govern the relationships between the new and old velocities. Similarly, the two mutually reciprocal inward recursions in Table 19.2 govern the relationships between the \mathcal{T} and ζ generalized forces. The term “mutually reciprocal” indicates that the corresponding spatial operations are mathematical inverses of each other. Each of the above four recursions represents an $O(\mathcal{N})$ computational algorithm, in

Table 19.2 ζ and \mathcal{T} can be recursively computed from each other

$\zeta = \ell\mathcal{T} = \mathcal{D}^{-\frac{1}{2}}[\mathbf{I} - \mathbf{H}\psi\mathcal{K}]\mathcal{T}$	$\mathcal{T} = \mathbf{m}\zeta = [\mathbf{I} + \mathbf{H}\mathbb{A}\mathcal{K}]\mathcal{D}^{\frac{1}{2}}\zeta$
$\mathfrak{z}(0) = \mathbf{0}$	$\mathfrak{z}(0) = \mathbf{0}$
for $k = 1 \dots N$	for $k = 1 \dots N$
$\mathfrak{z}(k) = \mathbb{A}(k, k-1)\mathfrak{z}^+(k-1)$	$\mathfrak{z}(k) = \mathbb{A}(k, k-1)\mathfrak{z}^+(k-1)$
$\zeta(k) = \mathcal{D}^{-\frac{1}{2}}(k)[\mathcal{T}(k) - \mathbf{H}(k)\mathfrak{z}(k)]$	$\mathcal{T}(k) = \mathcal{D}^{\frac{1}{2}}(k)\zeta(k) + \mathbf{H}(k)\mathfrak{z}(k)$
$\mathfrak{z}^+(k) = \mathfrak{z}(k) + \mathcal{G}(k)\zeta(k)$	$\mathfrak{z}^+(k) = \mathfrak{z}(k) + \mathcal{G}(k)\zeta(k)$
end loop	end loop

the sense that the number of required arithmetical operations increases only linearly with the number of degrees of freedom. Generalization of the serial-chain recursions in Tables 19.1 and 19.2 to tree-topology systems simply requires the replacement of the base-to-tip recursions by base-to-tips scatter recursions, and the tip-to-base recursions by tips-to-base gather recursions.

19.4 Expression for $\mathcal{C}(\theta, \eta)$ for Rigid-Link Systems

The $\mathcal{C}(\theta, \eta) = \ell(\dot{\mathbf{m}}\eta - \frac{1}{2} \frac{\partial \dot{\theta}^* \mathcal{M} \dot{\theta}}{\partial \theta})$ Coriolis term in (19.15) is one of the key parts of the diagonalized equations of motion $\dot{\eta} + \mathcal{C}(\theta, \eta) = \zeta$. The following sections derive analytical operator expressions for the component terms as a step towards obtaining an operator expression for $\mathcal{C}(\theta, \eta)$. The expressions for the time derivatives and sensitivities of the spatial operators are required. These expressions for rigid-link SKO models have been derived in Chap. 18. In order to utilize them, we narrow our attention to rigid-link systems for the remainder of this chapter. We signify this change by switching from the more general $\mathcal{E}_{\mathbb{A}}$ and \mathbb{A} operators to \mathcal{E}_{ϕ} and ϕ rigid-link system operators.

19.4.1 Closed-Form Expression for $\dot{\mathbf{m}}\eta$

In this section, we derive explicit analytical expressions for $\dot{\mathbf{m}}\eta$ needed by $\mathcal{C}(\theta, \eta)$.

Exercise 19.1 Time derivative of $\mathcal{D}^{\frac{1}{2}}$.

Show that for a system with 1 degree of freedom joints,

$$\frac{d\mathcal{D}^{\frac{1}{2}}}{dt} = \frac{1}{2} \mathcal{D}^{-\frac{1}{2}} \mathbf{H} \check{\lambda} \mathbf{H}^* \quad (19.24)$$



Lemma 19.7 Expression for $\dot{\mathbf{m}}$.

For a system with 1 degree of freedom joints, the time derivative of the mass matrix factor \mathbf{m} is given by:

$$\begin{aligned}\dot{\mathbf{m}} &= \mathbf{H}\phi \left[\tilde{\Delta}_V^\omega \phi \mathcal{K} + \mathcal{E}_\phi \bar{\Delta}_V^\nu \phi \mathcal{G} + \frac{1}{2}(\mathbf{I} + \bar{\tau}) \check{\lambda} \mathbf{H}^* \mathcal{D}^{-1} \right] \mathcal{D}^{\frac{1}{2}} \\ &= \mathbf{H}\phi \left[\tilde{\Delta}_V^\omega \tilde{\phi} \mathcal{P} + \mathcal{E}_\phi \bar{\Delta}_V^\nu \phi \mathcal{P} + \frac{1}{2}(\mathbf{I} + \bar{\tau}) \check{\lambda} \right] \mathbf{H}^* \mathcal{D}^{-\frac{1}{2}}\end{aligned}\quad (19.25)$$

where $\check{\lambda}$ is as defined in Section 18.5.

Proof: We have

$$\begin{aligned}\dot{\mathbf{m}} &\stackrel{19.20}{=} \frac{d[\mathbf{I} + \mathbf{H}\phi \mathcal{K}]}{dt} \mathcal{D}^{\frac{1}{2}} + [\mathbf{I} + \mathbf{H}\phi \mathcal{K}] \frac{d\mathcal{D}^{\frac{1}{2}}}{dt} \\ &\stackrel{18.61, 19.24}{=} \mathbf{H}\phi \left[\tilde{\Delta}_V^\omega \phi \mathcal{K} + \mathcal{E}_\phi \bar{\Delta}_V^\nu \phi \mathcal{G} + \bar{\tau} \check{\lambda} \mathbf{H}^* \mathcal{D}^{-1} \right] \mathcal{D}^{\frac{1}{2}} + \frac{1}{2} \mathbf{H}\phi \mathcal{G} \mathcal{D}^{-\frac{1}{2}} \mathbf{H} \check{\lambda} \mathbf{H}^* \\ &= \mathbf{H}\phi \left[\tilde{\Delta}_V^\omega \phi \mathcal{K} + \mathcal{E}_\phi \bar{\Delta}_V^\nu \phi \mathcal{G} + \bar{\tau} \check{\lambda} \mathbf{H}^* \mathcal{D}^{-1} \right] \mathcal{D}^{\frac{1}{2}} + \frac{1}{2} \mathbf{H}\phi \mathcal{G} \mathbf{H} \check{\lambda} \mathbf{H}^* \mathcal{D}^{-\frac{1}{2}} \\ &= \mathbf{H}\phi \left[\tilde{\Delta}_V^\omega \phi \mathcal{K} + \mathcal{E}_\phi \bar{\Delta}_V^\nu \phi \mathcal{G} + \bar{\tau} \check{\lambda} \mathbf{H}^* \mathcal{D}^{-1} \right] \mathcal{D}^{\frac{1}{2}} + \frac{1}{2} \mathbf{H}\phi \tau \check{\lambda} \mathbf{H}^* \mathcal{D}^{-\frac{1}{2}} \\ &= \mathbf{H}\phi \left[\tilde{\Delta}_V^\omega \phi \mathcal{K} + \mathcal{E}_\phi \bar{\Delta}_V^\nu \phi \mathcal{G} + \frac{1}{2}(\mathbf{I} + \bar{\tau}) \check{\lambda} \mathbf{H}^* \mathcal{D}^{-1} \right] \mathcal{D}^{\frac{1}{2}}\end{aligned}$$

This establishes the first equality in (19.25). The latter equality is simply a rearrangement of the first one. We have used the $\mathcal{D}^{-\frac{1}{2}} \mathbf{H} \check{\lambda} \mathbf{H}^* = \mathbf{H} \check{\lambda} \mathbf{H}^* \mathcal{D}^{-\frac{1}{2}}$ identity, which holds for systems with 1 degree of freedom joints, when going from step 2 to 3 in the sequence above. ■

Lemma 19.8 Expression for $\dot{\mathbf{m}}\eta$.

For a system with 1 degree of freedom hinges,

$$\begin{aligned}\dot{\mathbf{m}}\eta &= \mathbf{H}\phi \left[\left(\tilde{\Delta}_V^\omega \mathcal{E}_\phi + \mathcal{E}_\phi \bar{\Delta}_V^\nu \right) \phi \mathcal{P} \tau^* \right. \\ &\quad \left. + \frac{1}{2} \left(\tilde{\Delta}_V^\omega \mathcal{P} - \mathcal{P} \tilde{\Delta}_V^\omega + \mathcal{E}_\psi \check{\lambda} - \check{\lambda} \mathcal{E}_\psi^* + \mathcal{E}_\phi \left\{ \bar{\Delta}_V^\nu \mathcal{P}^+ - \mathcal{P}^+ \tilde{\Delta}_V^\nu \right\} \mathcal{E}_\phi^* \right) \right] \mathcal{V}\end{aligned}\quad (19.26)$$

Proof:

$$\begin{aligned}\dot{\mathbf{m}}\eta &\stackrel{19.25}{=} \mathbf{H}\phi \left[\tilde{\Delta}_V^\omega \tilde{\phi} \mathcal{P} + \mathcal{E}_\phi \bar{\Delta}_V^\nu \phi \mathcal{P} + \frac{1}{2}(\mathbf{I} + \bar{\tau}) \check{\lambda} \right] \mathbf{H}^* \mathcal{D}^{-\frac{1}{2}} \eta \\ &\stackrel{19.23}{=} \mathbf{H}\phi \left[\tilde{\Delta}_V^\omega \tilde{\phi} \mathcal{P} + \mathcal{E}_\phi \bar{\Delta}_V^\nu \phi \mathcal{P} + \frac{1}{2}(\mathbf{I} + \bar{\tau}) \check{\lambda} \right] \mathbf{H}^* [\mathbf{I} + \mathbf{H}\phi \mathcal{K}]^* \hat{\theta}\end{aligned}\quad (19.27)$$

Now

$$[\mathbf{I} + \mathsf{H}\Phi\mathcal{K}]^*\dot{\theta} \stackrel{(9.38)}{=} \mathsf{H}^*(\mathcal{G}^*\phi^*\mathsf{H}^*)\dot{\theta} \stackrel{(9.1)}{=} \mathsf{H}^*\mathcal{G}^*\mathcal{V} = \tau^*\mathcal{V} \quad (19.28)$$

Using (19.28) in (19.27), we have

$$\begin{aligned} \dot{\mathfrak{m}}\eta &\stackrel{19.28}{=} \mathsf{H}\Phi \left[\left(\tilde{\Delta}_V^\omega \mathcal{E}_\phi + \mathcal{E}_\phi \bar{\Delta}_V^\nu \right) \phi \mathcal{P} + \frac{1}{2} (\mathbf{I} + \bar{\tau}) \check{\lambda} \right] \tau^* \mathcal{V} \\ &\stackrel{(13.60)}{=} \mathsf{H}\Phi \left[\left(\tilde{\Delta}_V^\omega \mathcal{E}_\phi + \mathcal{E}_\phi \bar{\Delta}_V^\nu \right) \phi \mathcal{P} \tau^* + \frac{1}{2} (\mathbf{I} + \bar{\tau}) \check{\lambda} \tau^* \right] \mathcal{V} \\ &\stackrel{(9.40)}{=} \mathsf{H}\Phi \left[\left(\tilde{\Delta}_V^\omega \mathcal{E}_\phi + \mathcal{E}_\phi \bar{\Delta}_V^\nu \right) \phi \mathcal{P} \tau^* + \frac{1}{2} (\mathbf{I} + \mathcal{E}_\psi) \check{\lambda} (\mathbf{I} - \mathcal{E}_\psi^*) \right] \mathcal{V} \\ &= \mathsf{H}\Phi \left[\left(\tilde{\Delta}_V^\omega \mathcal{E}_\phi + \mathcal{E}_\phi \bar{\Delta}_V^\nu \right) \phi \mathcal{P} \tau^* + \frac{1}{2} (\check{\lambda} - \mathcal{E}_\psi \check{\lambda} \mathcal{E}_\psi^* + \mathcal{E}_\psi \check{\lambda} - \check{\lambda} \mathcal{E}_\psi^*) \right] \mathcal{V} \\ &\stackrel{(18.44)}{=} \mathsf{H}\Phi \left[\left(\tilde{\Delta}_V^\omega \mathcal{E}_\phi + \mathcal{E}_\phi \bar{\Delta}_V^\nu \right) \phi \mathcal{P} \tau^* \right. \\ &\quad \left. + \frac{1}{2} \left(\tilde{\Delta}_V^\omega \mathcal{P} - \mathcal{P} \tilde{\Delta}_V^\omega + \mathcal{E}_\phi \left(\bar{\Delta}_V^\nu \mathcal{P}^+ - \mathcal{P}^+ \tilde{\Delta}_V^\nu \right) \mathcal{E}_\phi^* + \mathcal{E}_\psi \check{\lambda} - \check{\lambda} \mathcal{E}_\psi^* \right) \right] \mathcal{V} \end{aligned}$$

■

19.4.2 Operator Expression for $\mathcal{C}(\theta, \eta)$

Lemma 19.9 Operator expression for $\mathcal{C}(\theta, \eta)$.

For a system with 1 degree of freedom hinges,

$$\begin{aligned} \mathcal{C}(\theta, \eta) &= \mathcal{D}^{-\frac{1}{2}} \mathsf{H}\Psi \left[\bar{\mathcal{V}} \mathbf{M} - \frac{1}{2} \left(\tilde{\Delta}_V^\omega \mathcal{P} + \mathcal{P} \tilde{\Delta}_V^\omega + \mathcal{E}_\phi \left\{ \bar{\Delta}_V^\nu \mathcal{P}^+ + \mathcal{P}^+ \tilde{\Delta}_V^\nu \right\} \mathcal{E}_\phi^* \right. \right. \\ &\quad \left. \left. + \mathcal{E}_\psi \check{\lambda} - \check{\lambda} \mathcal{E}_\psi^* \right) \right] \mathcal{V} \end{aligned} \quad (19.29)$$

Proof: From (19.15) it follows that:

$$\begin{aligned}
\mathcal{C}(\theta, \eta) &\stackrel{18.38c, 19.26}{=} \ell \mathbb{H} \Phi \left[\bar{\mathbf{v}} \mathbf{M} - \left(\mathcal{E}_\phi \bar{\Delta}_V^\nu + \tilde{\Delta}_V^\omega \right) [\mathbf{I} + \phi \mathcal{K} \mathcal{H}] \mathcal{P} \right. \\
&\quad + \left(\tilde{\Delta}_V^\omega \mathcal{E}_\phi + \mathcal{E}_\phi \bar{\Delta}_V^\nu \right) \phi \mathcal{P} \tau^* + \frac{1}{2} \left(\tilde{\Delta}_V^\omega \mathcal{P} - \mathcal{P} \tilde{\Delta}_V^\omega \right. \\
&\quad \left. \left. + \mathcal{E}_\phi \left\{ \bar{\Delta}_V^\nu \mathcal{P}^+ - \mathcal{P}^+ \tilde{\Delta}_V^\nu \right\} \mathcal{E}_\phi^* + \mathcal{E}_\psi \check{\lambda} - \check{\lambda} \mathcal{E}_\psi^* \right) \right] \mathcal{V} \\
&\stackrel{9.45, 9.38}{=} \mathcal{D}^{-\frac{1}{2}} \mathbb{H} \Psi \left[\bar{\mathbf{v}} \mathbf{M} - \mathcal{E}_\phi \bar{\Delta}_V^\nu [\mathbf{I} + \phi \mathcal{K} \mathcal{H}] \mathcal{P} - \tilde{\Delta}_V^\omega \mathcal{P} \right. \\
&\quad + \mathcal{E}_\phi \bar{\Delta}_V^\nu \phi \mathcal{P} \tau^* + \frac{1}{2} \left(\tilde{\Delta}_V^\omega \mathcal{P} - \mathcal{P} \tilde{\Delta}_V^\omega \right. \\
&\quad \left. \left. + \mathcal{E}_\phi \left\{ \bar{\Delta}_V^\nu \mathcal{P}^+ - \mathcal{P}^+ \tilde{\Delta}_V^\nu \right\} \mathcal{E}_\phi^* + \mathcal{E}_\psi \check{\lambda} - \check{\lambda} \mathcal{E}_\psi^* \right) \right] \mathcal{V} \\
&= \mathcal{D}^{-\frac{1}{2}} \mathbb{H} \Psi \left[\bar{\mathbf{v}} \mathbf{M} + \mathcal{E}_\phi \bar{\Delta}_V^\nu \left\{ \phi \tau - [\mathbf{I} + \phi \mathcal{K} \mathcal{H}] \right\} \mathcal{P} \right. \\
&\quad + \frac{1}{2} \left(- \tilde{\Delta}_V^\omega \mathcal{P} - \mathcal{P} \tilde{\Delta}_V^\omega + \mathcal{E}_\phi \left\{ \bar{\Delta}_V^\nu \mathcal{P}^+ - \mathcal{P}^+ \tilde{\Delta}_V^\nu \right\} \mathcal{E}_\phi^* \right. \\
&\quad \left. \left. + \mathcal{E}_\psi \check{\lambda} - \check{\lambda} \mathcal{E}_\psi^* \right) \right] \mathcal{V} \tag{19.30}
\end{aligned}$$

Now

$$\begin{aligned}
\phi \tau - [\mathbf{I} + \phi \mathcal{K} \mathcal{H}] &\stackrel{9.45}{=} \phi \tau - \phi \psi^{-1} = \phi (\tau - (\mathbf{I} - \mathcal{E}_\psi)) \\
&= \phi (-\bar{\tau} + \mathcal{E}_\phi \bar{\tau}) = -\phi \phi^{-1} \bar{\tau} = -\bar{\tau} \tag{19.31}
\end{aligned}$$

Using (19.31) in (19.30) leads to

$$\begin{aligned}
\mathcal{C}(\theta, \eta) &= \mathcal{D}^{-\frac{1}{2}} \mathbb{H} \Psi \left[\bar{\mathbf{v}} \mathbf{M} - \mathcal{E}_\phi \bar{\Delta}_V^\nu \mathcal{P}^+ + \frac{1}{2} \left(- \tilde{\Delta}_V^\omega \mathcal{P} - \mathcal{P} \tilde{\Delta}_V^\omega \right. \right. \\
&\quad \left. \left. + \mathcal{E}_\phi \left\{ \bar{\Delta}_V^\nu \mathcal{P}^+ - \mathcal{P}^+ \tilde{\Delta}_V^\nu \right\} \mathcal{E}_\phi^* + \mathcal{E}_\psi \check{\lambda} - \check{\lambda} \mathcal{E}_\psi^* \right) \right] \mathcal{V} \\
&= \mathcal{D}^{-\frac{1}{2}} \mathbb{H} \Psi \left[\bar{\mathbf{v}} \mathbf{M} - \frac{1}{2} \left(\tilde{\Delta}_V^\omega \mathcal{P} + \mathcal{P} \tilde{\Delta}_V^\omega \right. \right. \\
&\quad \left. \left. + \mathcal{E}_\phi \left\{ \bar{\Delta}_V^\nu \mathcal{P}^+ + \mathcal{P}^+ \tilde{\Delta}_V^\nu \right\} \mathcal{E}_\phi^* + \mathcal{E}_\psi \check{\lambda} - \check{\lambda} \mathcal{E}_\psi^* \right) \right] \mathcal{V}
\end{aligned}$$

■

Lemma 19.9 explicitly derives, in terms of relatively simple quantities, the very complicated quantity $\mathcal{C}(\theta, \eta) = \ell(\dot{\mathbf{m}} - \frac{1}{2} \dot{\theta}^* \mathcal{M}_\theta \dot{\theta})$, which depends on various derivatives of the system mass matrix. Using this expression, Algorithm 19.1 describes a recursive procedure for computing $\mathcal{C}(\theta, \eta)$. This algorithm is a recursive implementation of (19.29). It proceeds from tip-to-base and is of $O(N)$ computational complexity. It assumes that the spatial velocities \mathcal{V} have already been computed using Table 19.1, for example. Similarly, if the articulated body inertia quantities are not available then they can be computed concurrently.

Algorithm 19.1 Computation of the $\mathcal{C}(\theta, \eta)$ Coriolis forces vector

$\ddot{\lambda}(0) = 0, \mathbf{y}(0) = \mathbf{0}$

for $k = 1 \dots n$

$X(k) = \tilde{\Delta}_{\mathcal{V}}^{\omega}(k)\mathcal{P}(k)$

$Z(k) = \phi(k, k-1)\bar{\Delta}_{\mathcal{V}}^{\nu}(k-1)\mathcal{P}^+(k-1)\phi^*(k, k-1)$

$S(k) = X(k) - Z(k)$

$Y(k, k-1) = \psi(k, k-1)\ddot{\lambda}(k-1)$

$\ddot{\lambda}(k) = Y(k, k-1)\psi^*(k, k-1) + S(k) + S^*(k)$

$y(k) = \sum_{i \in \mathcal{C}(k)} \psi((k), i)y(i) - [-2\bar{\mathcal{V}}(k)\mathbf{M}(k) + X(k) - X^*(k)]\mathcal{V}(k)$

 $+ Y(k, k-1)\mathcal{V}(k-1) - \ddot{\lambda}(k)\bar{\tau}^*(k)\mathcal{V}^+(k)$

$\mathcal{C}(k) = \frac{1}{2}\mathcal{D}^{-\frac{1}{2}}(k)\mathcal{H}(k)y(k)$

end loop

Exercise 19.2 Non-working $\mathcal{C}(\theta, \eta)$ Coriolis Vector.

Derive the orthogonality result $\eta^*\mathcal{C}(\theta, \eta) = 0$ in (19.18) starting with the analytical expression for $\mathcal{C}(\theta, \eta)$ in (19.29). ■

Remark 19.1 Coriolis expressions for systems with revolute hinges.

For systems with only revolute hinges, $\Delta_{\mathcal{V}}^{\nu} = \mathbf{0}$, and, hence, the following simpler versions of (18.38), (19.26), and (19.29) hold for such systems:

$$\begin{aligned} \mathcal{C}(\theta, \eta) &= \frac{1}{2}\mathcal{D}^{-\frac{1}{2}}\mathcal{H}\psi \left[\mathcal{E}_{\psi}\ddot{\lambda} - \dot{\lambda}\mathcal{E}_{\psi}^* - \tilde{\Delta}_{\mathcal{V}}^{\omega}\mathcal{P} - \mathcal{P}\tilde{\Delta}_{\mathcal{V}}^{\omega} + 2\bar{\mathcal{V}}\mathbf{M} \right] \mathcal{V} \\ \frac{\partial \dot{\theta}^* \mathcal{M} \dot{\theta}}{\partial \theta} &= -2\mathcal{H}\phi \left\{ \bar{\mathcal{V}} - \tilde{\Delta}_{\mathcal{V}}^{\omega}\phi \right\} \mathbf{M}\mathcal{V} \quad (19.32) \\ \dot{\mathbf{m}}\eta &= \mathcal{H}\phi \left[\tilde{\Delta}_{\mathcal{V}}^{\omega}\phi \mathcal{K}\mathcal{H}\mathcal{P} + \frac{1}{2} \left(\tilde{\Delta}_{\mathcal{V}}^{\omega}\mathcal{P} - \mathcal{P}\tilde{\Delta}_{\mathcal{V}}^{\omega} + \mathcal{E}_{\psi}\ddot{\lambda} - \dot{\lambda}\mathcal{E}_{\psi}^* \right) \right] \mathcal{V} \end{aligned}$$

Exercise 19.3 Expression for ℓ .

For a system with 1 degree of freedom joints, show that the time derivative of the ℓ mass matrix inverse factor is given by:

$$\dot{\ell} = -\mathcal{D}^{-\frac{1}{2}} \mathcal{H}\psi \left[\tilde{\Delta}_V^\omega \phi \mathcal{K} + \mathcal{E}_\phi \tilde{\Delta}_V^\nu \phi \mathcal{G} + \frac{1}{2}(\mathbf{I} + \bar{\tau}) \check{\lambda} \mathcal{H}^* \mathcal{D}^{-1} \right] [\mathbf{I} - \mathcal{H}\psi \mathcal{K}] \quad (19.33)$$

■

Exercise 19.4 Sensitivity of Innovations factors.

For a system with 1 degree of freedom joints, show that

$$\mathbf{m}_{\theta_i} = \mathcal{H}\phi \left[\tilde{\mathcal{H}}_{=i}^\omega \tilde{\phi} \mathcal{P} + \mathcal{E}_\phi \tilde{\mathcal{H}}_{=i}^\nu \phi \mathcal{P} + \frac{1}{2}(\mathbf{I} + \bar{\tau}) \check{\lambda}_{\theta_i} \right] \mathcal{H}^* \mathcal{D}^{-\frac{1}{2}} \quad (19.34)$$

$$\ell_{\theta_i} = -\mathcal{D}^{-\frac{1}{2}} \mathcal{H}\psi \left[\tilde{\mathcal{H}}_{=i}^\omega \phi \mathcal{K} \mathcal{D} + \mathcal{E}_\phi \tilde{\mathcal{H}}_{=i}^\nu \phi \mathcal{G} + \frac{1}{2}(\mathbf{I} + \bar{\tau}) \check{\lambda}_{\theta_i} \mathcal{H}^* \right] \mathcal{D}^{-\frac{1}{2}} \ell \quad (19.35)$$

■

19.4.3 Decoupled Control

The diagonal equations can also be used to design controllers that are decoupled and non-interacting. The decoupled control approach exploits the dynamical behavior of the η coordinates.

Though control objectives are defined in the physical $(\dot{\theta}, \mathcal{T})$ domain, the control system is designed in the (η, ζ) variables for the diagonalized equations of motion. Stability in the η, ζ coordinates is equivalent to stability in the original $\theta, \dot{\theta}$ coordinates. The control problem consists of finding a feedback relationship for the ζ input in terms of the η velocities. Once ζ is determined, it is possible to go back to physical space to determine the required \mathcal{T} physical inputs by means of the relationship $\mathcal{T} = \mathbf{m}\zeta$, using the inwardly recursive algorithm in Table 19.2.

Lemma 19.10 Rate feedback control using diagonalized dynamics.

The rate feedback control

$$\zeta = -c\eta,$$

in which c is a positive diagonal control gain matrix, renders the system stable in the sense of Lyapunov.

Proof: This result follows by using the kinetic energy as a Lyapunov function and observing that its time derivative, in Lemma 19.5, can be guaranteed to be negative definite, by the choice of the above control law. ■

This control algorithm involves rate feedback only. It can be referred to as a “rate” control algorithm because the feedback quantity is a velocity, in fact, it is a vector of the diagonalizing generalized velocities. It does not guarantee that the manipulator will end up in a prescribed configuration. Additional applications of the diagonalized formulation for manipulator control can be found in [3, 84, 106].

19.5 Un-normalized Diagonalized Equations of Motion

An alternative set of diagonalized equations of motion can be obtained by using a slightly different generalized velocity vector defined as

$$\xi \stackrel{\triangle}{=} [\mathbf{I} + \mathbf{H}\phi\mathcal{K}]^* \dot{\theta} \quad \text{and} \quad \dot{\theta} \stackrel{9.50}{=} [\mathbf{I} - \mathbf{H}\psi\mathcal{K}]^* \xi \quad (19.36)$$

The kinetic energy in these coordinates is

$$\mathfrak{K}_e(\xi, \dot{\xi}) = \frac{1}{2} \dot{\xi}^* \mathcal{D}(\theta) \dot{\xi} \quad (19.37)$$

While no longer the constant identity matrix, the mass matrix for this formulation is the block-diagonal $\mathcal{D}(\theta)$ matrix. While configuration dependent, this mass matrix retains the simpler block-diagonal structure. Also, in this new formulation, the assumption of 1 degree of freedom hinges is no longer required. The equations of motion in the new (θ, ξ) coordinates are described in the following lemma.

Lemma 19.11 Equations of motion with un-normalized diagonalized coordinates.

$$\mathcal{D}\dot{\xi} + \mathcal{C}(\theta, \xi) = \kappa_{in} \quad \text{where} \quad \kappa_{in} \stackrel{\triangle}{=} [\mathbf{I} - \mathbf{H}\psi\mathcal{K}] \mathcal{T} \quad (19.38)$$

$$\begin{aligned} \mathcal{C}(\theta, \xi) &\stackrel{\triangle}{=} \mathbf{H}\psi \left[-\tilde{\Delta}_V^\omega \mathcal{P} - \mathcal{E}_\phi \bar{\Delta}_V^\nu \mathcal{P}^+ + \check{\lambda} \tau^* + \bar{V} \mathbf{M} \right] \nu \\ &\stackrel{19.28}{=} \mathbf{H}\psi \left[\check{\lambda} \mathbf{H}^* \xi - \left(\tilde{\Delta}_V^\omega \mathcal{P} + \mathcal{E}_\phi \bar{\Delta}_V^\nu \mathcal{P}^+ - \bar{V} \mathbf{M} \right) \nu \right] \end{aligned} \quad (19.39)$$

Proof: Using steps paralleling the derivation of (19.15), we have

$$\begin{aligned} \mathcal{C}(\theta, \xi) &= [\mathbf{I} - \mathbf{H}\psi\mathcal{K}] \left(\frac{d[\mathbf{I} + \mathbf{H}\phi\mathcal{K}]\mathcal{D}}{dt} \xi - \frac{1}{2} \frac{\partial \dot{\theta}^* \mathcal{M} \dot{\theta}}{\partial \theta} \right) \\ &\stackrel{18.62, 18.38c, 9.45}{=} \mathbf{H}\psi \left(\left[\tilde{\Delta}_V^\omega \tilde{\phi} \mathcal{P} + \mathcal{E}_\phi \bar{\Delta}_V^\nu \phi \mathcal{P} + \check{\lambda} \right] \mathbf{H}^* \xi \right. \\ &\quad \left. + \left\{ \bar{V} \mathbf{M} - \left(\mathcal{E}_\phi \bar{\Delta}_V^\nu + \tilde{\Delta}_V^\omega \right) [\mathbf{I} + \phi \mathcal{K} \mathbf{H}] \mathcal{P} \right\} \nu \right) \\ &\stackrel{19.28}{=} \mathbf{H}\psi \left(\left[\tilde{\Delta}_V^\omega \tilde{\phi} \mathcal{P} + \mathcal{E}_\phi \bar{\Delta}_V^\nu \phi \mathcal{P} + \check{\lambda} \right] \tau^* \right. \\ &\quad \left. + \left\{ \bar{V} \mathbf{M} - \left(\mathcal{E}_\phi \bar{\Delta}_V^\nu + \tilde{\Delta}_V^\omega \right) [\mathbf{I} + \phi \mathcal{K} \mathbf{H}] \mathcal{P} \right\} \nu \right) \\ &= \mathbf{H}\psi \left(\left\{ \left[\tilde{\Delta}_V^\omega + \mathcal{E}_\phi \bar{\Delta}_V^\nu \right] (\phi \tau - [\mathbf{I} + \phi \mathcal{K} \mathbf{H}]) - \tilde{\Delta}_V^\omega \tau \right\} \mathcal{P} \right. \\ &\quad \left. + \check{\lambda} \tau^* + \bar{V} \mathbf{M} \right) \nu \\ &\stackrel{19.31}{=} \mathbf{H}\psi \left(\left\{ - \left[\tilde{\Delta}_V^\omega + \mathcal{E}_\phi \bar{\Delta}_V^\nu \right] \bar{\tau} - \tilde{\Delta}_V^\omega \tau \right\} \mathcal{P} + \check{\lambda} \tau^* + \bar{V} \mathbf{M} \right) \nu \\ &= \mathbf{H}\psi \left(\left\{ - \tilde{\Delta}_V^\omega - \mathcal{E}_\phi \bar{\Delta}_V^\nu \bar{\tau} \right\} \mathcal{P} + \check{\lambda} \tau^* + \bar{V} \mathbf{M} \right) \nu \end{aligned}$$

■

While these equations of motion are still diagonal, they differ from those in (19.14) in two respects. First, although the mass matrix \mathcal{D} is diagonal, it is configuration dependent. Moreover, while the Coriolis forces term $\mathcal{C}(\theta, \xi)$ is simpler than $\mathcal{C}(\theta, \eta)$, it is no longer orthogonal to the generalized velocities vector. Table 19.3 compares the properties of the regular and the different diagonalizing formulations we have studied so far.

Table 19.3 Comparison of the properties of the regular and different diagonalizing formulations for tree-topology system dynamics

	Regular	Un-normalized	Normalized	Global
Section	8.7	19.5	19.2	19.1
Coordinates	$(\theta, \dot{\theta})$	(θ, ξ)	(θ, η)	$(\vartheta, \dot{\vartheta})$
Diagonal \mathcal{M}		✓	✓	✓
Constant \mathcal{M}			✓	✓
Non-working \mathcal{C}			✓	✓
$\mathcal{C} = \mathbf{0}$				✓

An $O(N)$ computational algorithm for the components of $\mathcal{C}(\theta, \xi)$ is shown in Algorithm 19.2.

Algorithm 19.2 Computation of the $\mathcal{C}(\theta, \xi)$ Coriolis forces vector

$$\left\{ \begin{array}{l} \ddot{\lambda}(0) = 0, \mathbf{y}(0) = \mathbf{0} \\ \textbf{for } k = 1 \dots N \\ \quad X(k) = \tilde{\Delta}_V^\omega(k)\mathcal{P}(k) \\ \quad \ddot{\lambda}(k) = \psi(k, k-1)\ddot{\lambda}(k-1)\psi^*(k, k-1) + X(k) + X^*(k) \\ \quad S(k) = X(k) + \phi(k, k-1)\bar{\Delta}_V^V(k-1)\mathcal{P}^+(k-1) - \bar{V}(k)\mathbf{M}(k) \\ \quad y(k) = \psi(k, k-1)y(k-1) + \ddot{\lambda}(k)\mathcal{H}^*(k)\xi(k) - S(k)V(k) \\ \quad C(k) = H(k)y(k) \\ \textbf{end loop} \end{array} \right.$$

19.5.1 $O(N)$ Forward Dynamics

One important application is that of forward dynamics and numerical integration to predict the motion of the manipulator in response to applied moments. An algorithm based upon the un-normalized diagonalized equations of motion in Lemma 19.11 is described here. The acceleration term is:

$$\begin{aligned}\dot{\xi} &\stackrel{19.38}{=} \mathcal{D}^{-1} [\kappa_{in} - \mathcal{C}(\theta, \xi)] \stackrel{19.38}{=} \mathcal{D}^{-1} \{ [\mathbf{I} - \mathbf{H}\Psi\mathcal{K}] \mathcal{T} - \mathcal{C}(\theta, \xi) \} \\ &= \mathcal{D}^{-1} \{ \mathcal{T} - \mathbf{H}\Psi\mathcal{K}\mathcal{T} - \mathcal{C}(\theta, \xi) \} \stackrel{19.11}{=} \mathcal{D}^{-1} \{ \mathcal{T} - \mathbf{H}\Psi\gamma \}\end{aligned}\quad (19.40)$$

where

$$\gamma \triangleq \mathcal{K}\mathcal{T} + \check{\lambda}\mathbf{H}^*\xi - \left(\tilde{\Delta}_V^\omega \mathcal{P} + \mathcal{E}_\phi \bar{\Delta}_V^\nu \mathcal{P}^+ - \bar{\mathcal{V}}\mathbf{M} \right) \mathcal{V} \quad (19.41)$$

The very first time, \mathcal{V} must be computed explicitly (from $\dot{\theta}$ or ξ) using one of the algorithms in Table 19.1. Algorithm 19.3 is similar to the usual AB forward dynamics algorithm. However, it is a significant improvement because it is only a 2-sweep algorithm involving an inward recursion to compute $\dot{\xi}$, followed by an outward recursion to compute $\dot{\theta}$. The Coriolis effects are completely accounted for in the single inward sweep. The standard $O(N)$ articulated body inertia algorithm typically requires at least one or two preliminary inverse dynamics sweeps, prior to utilization of the forward dynamics algorithm.

Algorithm 19.3 Forward dynamics for un-normalized diagonalized dynamics

1. Compute the articulated body inertia \mathcal{P} and the shifted Kalman gain \mathcal{K} using the Riccati equation in (9.33). Compute also the corresponding time derivative $\check{\lambda}$ using Algorithm 18.1 on page 372.
2. Compute the $\dot{\xi}$ generalized accelerations using the following tip-to-base recursive sweep:

$$\left\{ \begin{array}{l} \mu(0) = \mathbf{0} \\ \textbf{for } k = 1 \dots N \\ \quad \gamma(k) = \mathcal{K}(k, k-1)\mathcal{T}(k-1) + \check{\lambda}(k)\mathbf{H}^*(k)\xi(k) \\ \quad \quad \quad - [\tilde{\Delta}_V^\omega(k)\mathcal{P}(k) - \bar{\mathcal{V}}(k)\mathbf{M}(k)]\mathcal{V}(k) \\ \quad \mu(k) = \psi(k, k-1)\mu(k-1) + \gamma(k) \\ \quad \dot{\xi}(k) = \mathcal{D}^{-1}(k)[\mathcal{T}(k) - \mathbf{H}(k)\mu(k)] \\ \textbf{end loop} \end{array} \right. \quad (19.42)$$

3. Conduct a numerical integration step to obtain the total joint rates ξ at a new time instant.
4. Compute the $\dot{\theta}$ generalized velocities and the \mathcal{V} spatial velocity by the outward recursion in Table 19.1, modified to account for the $\eta = \mathcal{D}^{-\frac{1}{2}}\xi$ relationship.
5. Integrate the $\dot{\theta}$ generalized velocities to obtain the θ generalized coordinates at the new time instant.
6. Go back to the first step and repeat as long as necessary until a prescribed final time has been reached.

Appendix A

Useful Mathematical Identities

A.1 3-Vector Cross-Product Identities

The following useful cross-product identities hold for arbitrary 3-vectors p , q , and r :

$$\begin{aligned}\tilde{p}p &= 0 \\ \tilde{p}^* &= -\tilde{p} \\ \tilde{p}q &= -\tilde{q}p \\ \widetilde{(pq)} &= \tilde{p}\tilde{q} - \tilde{q}\tilde{p} \\ \tilde{p}\tilde{q} &= qp^* - p^*qI \\ \tilde{p}\tilde{q}r + \tilde{r}\tilde{p}q + \tilde{q}\tilde{r}p &= \mathbf{0} \\ \tilde{p}\tilde{q}\tilde{q}p &= -\tilde{q}\tilde{p}\tilde{p}q \\ p^*\tilde{q}r &= r^*\tilde{p}q = q^*\tilde{r}p \\ \widetilde{\mathcal{R}p} &= \mathcal{R}\tilde{p}\mathcal{R}^*\end{aligned}\tag{A.1}$$

\mathcal{R} denotes a rotation matrix.

A.2 Matrix and Vector Norms

The **sup norm** (or 2-norm) of a matrix A is defined as

$$\|A\| \triangleq \sup_x \|Ax\|/\|x\|\tag{A.2}$$

where the norm of a vector x is defined as $\|x\| \triangleq \sqrt{x^*x}$.

Exercise A.1 Norm of \tilde{s} .

Show that $\|\tilde{s}\| = \|s\|$. ■

A.3 Schur Complement and Matrix Inverse Identities

Assume that we have a block-partitioned matrix, $\begin{pmatrix} A & B \\ C & D \end{pmatrix}$, with square A and D sub-matrices. When D is invertible, the **Schur complement** of the matrix is defined as $A - BD^{-1}C$. The following describe factorizations and solutions of equations involving such block partitioned matrices.

1. If D is invertible, then

$$\begin{pmatrix} A & B \\ C & D \end{pmatrix} = \begin{pmatrix} I & BD^{-1} \\ 0 & I \end{pmatrix} \begin{pmatrix} A - BD^{-1}C & 0 \\ 0 & D \end{pmatrix} \begin{pmatrix} I & 0 \\ D^{-1}C & I \end{pmatrix} \quad (\text{A.3})$$

Hence,

$$\begin{pmatrix} A & B \\ C & D \end{pmatrix}^{-1} = \begin{pmatrix} I & 0 \\ -D^{-1}C & I \end{pmatrix} \begin{pmatrix} (A - BD^{-1}C)^{-1} & 0 \\ 0 & D^{-1} \end{pmatrix} \begin{pmatrix} I & -BD^{-1} \\ 0 & I \end{pmatrix} \quad (\text{A.4})$$

Using this factorization, the solution to the following matrix equation

$$\begin{pmatrix} A & B \\ C & D \end{pmatrix} \begin{bmatrix} x_1 \\ x_2 \end{bmatrix} = \begin{bmatrix} b_1 \\ b_2 \end{bmatrix} \quad (\text{A.5})$$

is given by

$$\begin{aligned} y &= D^{-1}b_2 \\ x_1 &= (A - BD^{-1}C)^{-1}(b_1 - By) \\ x_2 &= y - D^{-1}Cx_1 \end{aligned} \quad (\text{A.6})$$

2. If A is invertible, then,

$$\begin{pmatrix} A & B \\ C & D \end{pmatrix} = \begin{pmatrix} I & 0 \\ CA^{-1} & I \end{pmatrix} \begin{pmatrix} A & 0 \\ 0 & D - CA^{-1}B \end{pmatrix} \begin{pmatrix} I & A^{-1}B \\ 0 & I \end{pmatrix} \quad (\text{A.7})$$

Hence,

$$\begin{pmatrix} A & B \\ C & D \end{pmatrix}^{-1} = \begin{pmatrix} I & -A^{-1}B \\ 0 & I \end{pmatrix} \begin{pmatrix} A^{-1} & 0 \\ 0 & (D - CA^{-1}B)^{-1} \end{pmatrix} \begin{pmatrix} I & 0 \\ -CA^{-1} & I \end{pmatrix} \quad (\text{A.8})$$

Using this factorization, the solution to the following matrix equation

$$\begin{pmatrix} A & B \\ C & D \end{pmatrix} \begin{bmatrix} x_1 \\ x_2 \end{bmatrix} = \begin{bmatrix} b_1 \\ b_2 \end{bmatrix} \quad (\text{A.9})$$

is given by

$$\begin{aligned} y &= A^{-1}b_1 \\ x_2 &= (D - CA^{-1}B)^{-1}(b_2 - Cy) \\ x_1 &= y - A^{-1}Bx_2 \end{aligned} \quad (\text{A.10})$$

3. If A , B and C are invertible, and $D = \mathbf{0}$, then (A.8) simplifies to:

$$\begin{pmatrix} A & B \\ C & \mathbf{0} \end{pmatrix}^{-1} = \begin{pmatrix} \mathbf{0} & C^{-1} \\ B^{-1} & -B^{-1}AC^{-1} \end{pmatrix} \quad (\text{A.11})$$

4. Now let us assume that D is invertible, and further that there are constraints $Qb_2 = 0$ and $x_2 = Q^*\lambda$ for some full-rank matrix Q and vector λ . Then (A.9) can be re-expressed as:

$$\begin{pmatrix} I & \mathbf{0} \\ \mathbf{0} & Q \end{pmatrix} \begin{pmatrix} A & B \\ C & D \end{pmatrix} \begin{pmatrix} I & \mathbf{0} \\ \mathbf{0} & Q^* \end{pmatrix} \begin{bmatrix} x_1 \\ \lambda \end{bmatrix} = \begin{bmatrix} b_1 \\ \mathbf{0} \end{bmatrix} \quad (\text{A.12})$$

That is,

$$\begin{aligned} \begin{pmatrix} A & BQ^* \\ QC & QDQ^* \end{pmatrix} \begin{bmatrix} x_1 \\ \lambda \end{bmatrix} &= \begin{bmatrix} b_1 \\ \mathbf{0} \end{bmatrix} \\ \implies (A - BQ^*(QDQ^*)^{-1}QC)x_1 &\stackrel{\text{A.6}}{=} b_1 \end{aligned} \quad (\text{A.13})$$

QDQ^* is invertible because D is invertible and Q is full-rank.

5. Let us assume the same conditions as in (4), except that the original block-matrix has an additional $[c_1, c_2]^*$ term to take the form:

$$\begin{pmatrix} A & B \\ C & D \end{pmatrix} \begin{bmatrix} x_1 \\ x_2 \end{bmatrix} + \begin{bmatrix} c_1 \\ c_2 \end{bmatrix} = \begin{bmatrix} b_1 \\ b_2 \end{bmatrix} \quad (\text{A.14})$$

In this case, (A.13) generalizes to:

$$\begin{aligned} \begin{pmatrix} A & BQ^* \\ QC & QDQ^* \end{pmatrix} \begin{bmatrix} x_1 \\ \lambda \end{bmatrix} &= \begin{bmatrix} b_1 - c_1 \\ -Qc_2 \end{bmatrix} \\ \implies (A - ZC)x_1 + (c_1 - Zc_2) &\stackrel{\text{A.6}}{=} b_1 \quad \text{where } Z \triangleq BQ^*(QDQ^*)^{-1}Q \\ \text{with } \lambda &= -(QDQ^*)^{-1}Q(c_2 + Cx_1) \quad \text{and } x_2 = Q^*\lambda \end{aligned} \quad (\text{A.15})$$

6. Let us assume the same conditions as in (5), except that now the constraint has the form $x_2 = Q^*\lambda + \gamma$. In this case, (A.13) generalizes to:

$$\begin{aligned} \begin{pmatrix} A & BQ^* \\ QC & QDQ^* \end{pmatrix} \begin{bmatrix} x_1 \\ \lambda \end{bmatrix} &= \begin{bmatrix} b_1 - (c_1 + B\gamma) \\ -Q(c_2 + D\gamma) \end{bmatrix} \quad (\text{A.16}) \\ \implies (A - ZC)x_1 + (c_1 + B\gamma - Z(c_2 + D\gamma)) &\stackrel{\text{A.6}}{=} b_1 \\ \text{where } Z &\triangleq BQ^*(QDQ^*)^{-1}Q \\ \text{with } \lambda &= -(QDQ^*)^{-1}Q(c_2 + D\gamma + Cx_1) \quad \text{and} \quad x_2 = Q^*\lambda + \gamma \end{aligned}$$

A.4 Matrix Inversion Identities

1. For any matrix A such that $(I - A)$ is invertible, the following matrix identity holds:

$$A(I - A)^{-1} = (I - A)^{-1}A = (I - A)^{-1} - I \quad (\text{A.17})$$

2. For a pair of matrices A and B such that $(I + AB)$ is invertible, we have

$$(I + AB)^{-1} = I - A(I + BA)^{-1}B \quad (\text{A.18})$$

3. For matrices A , X , R and Y , such that A , R and $[A + XRY^*]$ are invertible, we have

$$[A + XRY^*]^{-1} = A^{-1} - A^{-1}X[R^{-1} + Y^*A^{-1}X]^{-1}Y^*A^{-1} \quad (\text{A.19})$$

Lemma A.1 The 1-resolvent of a nilpotent matrix.

If U is a nilpotent matrix, such that $U^n = \mathbf{0}$, then its 1-resolvent, $W \triangleq (I - U)^{-1}$, is given by

$$W = I + U + U^2 + \dots + U^{n-1} \quad (\text{A.20})$$

Proof: For W as defined in (A.20)

$$UW = WU = U + U^2 + \dots + U^n = U + U^2 + \dots + U^{n-1} = W - I$$

Rearranging terms, we have

$$I = W - UW = (I - U)W \implies (I - U)^{-1} = W$$

■

A.5 Matrix Trace Identities

For a square matrix A

$$\text{Trace}\{A\} = -\text{Trace}\{-A\} \quad (\text{A.21})$$

For matrices A and B such that AB is square, we have

$$\text{Trace}\{AB\} = \text{Trace}\{BA\} \quad (\text{A.22})$$

A.6 Derivative and Gradient Identities

A.6.1 Function Derivatives

The following identities hold for function derivatives of a smooth function $g(\theta, \dot{\theta})$:

$$\begin{aligned} \frac{\partial \dot{g}}{\partial \ddot{\theta}} &= \frac{\partial g}{\partial \dot{\theta}} \\ \frac{\partial \dot{g}}{\partial \dot{\theta}} &= \frac{d}{dt} \frac{\partial g}{\partial \dot{\theta}} + \frac{\partial g}{\partial \theta} \\ \frac{\partial \dot{g}}{\partial \theta} &= \frac{d}{dt} \frac{\partial g}{\partial \theta} \end{aligned} \quad (\text{A.23})$$

A.6.2 Vector Gradients

We now define the notation for gradients and derivatives of vector functions with respect to a vector. Let $f(\theta) \in \mathcal{R}^m$ be a smooth function of a vector, $\theta \in \mathcal{R}^n$. Then the gradient, $\nabla_\theta f(\theta)$, is an $m \times n$ matrix defined as follows:

$$\nabla_\theta f(\theta) \triangleq \begin{pmatrix} \frac{\partial f_1}{\partial \theta_1} & \cdots & \frac{\partial f_1}{\partial \theta_n} \\ \vdots & \ddots & \vdots \\ \frac{\partial f_m}{\partial \theta_1} & \cdots & \frac{\partial f_m}{\partial \theta_n} \end{pmatrix} \in \mathcal{R}^{m \times n} \quad (\text{A.24})$$

Exercise A.2 Product gradient and chain rules.

- Given a vector $x \in \mathcal{R}^p$, a smooth, vector-valued function $f(x) \in \mathcal{R}^m$, and a smooth, scalar valued function $g(x)$, show that the following product rule holds:

$$\nabla_x [f(x)g(x)] = \nabla_x f(x) \cdot g(x) + f(x) \cdot \nabla_x g(x) \quad (\text{A.25})$$

- Given a smooth vector-valued function $f(y) \in \mathcal{R}^m$ of another vector-valued function $y(x) \in \mathcal{R}^n$, which in turn is a smooth function of a vector $x \in \mathcal{R}^p$, show that the following chain rule holds:

$$\nabla_x f(x) = \nabla_y f(y) \cdot \nabla_x y(x) \quad (\text{A.26})$$



At times, we need to differentiate a row-vector valued functions $f(\theta)$ with respect to the variables vector $\theta \in \mathcal{R}^m$. We use the following notation for this purpose:

$$\frac{df(\theta)}{d\theta} \triangleq [\nabla_{\theta}(f^*)]^* = \begin{bmatrix} \frac{\partial f}{\partial \theta_1} \\ \vdots \\ \frac{\partial f}{\partial \theta_m} \end{bmatrix} \quad (\text{A.27})$$

The notational convention in (A.27) also applies to partial derivatives such as $\frac{\partial f}{\partial \theta}$.

A.6.3 Matrix Derivatives

Let $A(t)$ be a differentiable and invertible matrix. We derive an expression for the time derivative of the inverse of $A(t)$ in terms of the time derivative of $A(t)$. Since $A(t)A^{-1}(t) = I$, differentiating both sides with respect to t yields

$$\frac{dA(t)}{dt}A^{-1}(t) + A(t)\frac{dA^{-1}(t)}{dt} = \mathbf{0}$$

Rearranging terms, we obtain

$$\frac{dA^{-1}(t)}{dt} = -A^{-1}(t)\frac{dA(t)}{dt}A^{-1}(t) \quad (\text{A.28})$$

Moreover, we have the following identity from Graham [61]:

$$\frac{d \log \{\det\{A(t)\}\}}{dt} = \text{Trace} \left\{ A^{-*} \frac{dA(t)}{dt} \right\} \quad (\text{A.29})$$

Appendix B

Attitude Representations

This appendix summarizes some attitude representation schemes that are alternatives to the direction-cosine matrix attitude representation scheme. References [43, 165] contains a detailed discussion on this topic. Since different conventions exist, a key to working with attitude representations is a clear definition of how they compose with each other, and how they transform vector representations. The $\mathbb{R}_{\mathbb{B}}$ direction-cosine matrix representations for attitude is the least ambiguous, because its composition operation is simply the normal matrix/vector multiplication operation, i.e.,

$$\mathbb{I}p = \mathbb{R}_{\mathbb{B}} \mathbb{B}p$$

for a 3-vector p . We refer to direction-cosine matrices as rotation matrices.

Exercise B.1 Time derivative of a rotation matrix.

Let $\mathfrak{R}(t)$ denote a rotation matrix that is a smooth function of time. Show that

$$\frac{d\mathbb{R}_{\mathbb{B}}}{dt} = \tilde{\omega} \mathbb{R}_{\mathbb{B}}$$

for some 3-vector w . As discussed in (1.8) on page 5, $w = \mathbb{I}\omega(\mathbb{I}, \mathbb{B})$, the angular velocity of the \mathbb{B} frame with respect to the \mathbb{I} frame expressed in the \mathbb{I} frame. ■

In this appendix, we work exclusively with the \mathbb{I} and \mathbb{B} pair of frames while studying the properties of attitude representations. With this in mind, we use the more compact ω notation for $\omega(\mathbb{I}, \mathbb{B})$ to simplify the expressions.

B.1 Euler Angles

Euler angles, $\theta = (\psi, \gamma, \phi)$ are an example of a minimal, 3-parameter attitude representation. This representation is based on expressing rotations as consisting of a sequence of three principal axis rotations. There are several possible options for Euler

angle representations based on the specific choice of the principal axes [43, 69]. For instance, the ZXZ Euler angles representation is defined as a sequence of principal axis rotations about the z axis, the x axis, and, once again, the z axis. The expression for ${}^{\mathbb{I}}\mathfrak{R}_{\mathbb{B}}(\theta)$ for the ZXZ Euler angle representation is as follows:

$$\begin{aligned} {}^{\mathbb{I}}\mathfrak{R}_{\mathbb{B}}(\theta) &= \begin{pmatrix} c_{\psi} & -s_{\psi} & 0 \\ s_{\psi} & c_{\psi} & 0 \\ 0 & 0 & 1 \end{pmatrix} \begin{pmatrix} 1 & 0 & 0 \\ 0 & c_{\gamma} & -s_{\gamma} \\ 0 & s_{\gamma} & c_{\gamma} \end{pmatrix} \begin{pmatrix} c_{\phi} & -s_{\phi} & 0 \\ s_{\phi} & c_{\phi} & 0 \\ 0 & 0 & 1 \end{pmatrix} \\ &= \begin{pmatrix} c_{\psi}c_{\phi} - s_{\psi}c_{\gamma}s_{\phi} & -c_{\psi}s_{\phi} - s_{\psi}c_{\gamma}c_{\phi} & s_{\psi}s_{\gamma} \\ s_{\psi}c_{\phi}c_{\psi}c_{\gamma}s_{\phi} & -s_{\psi}s_{\phi} + c_{\psi}c_{\gamma}c_{\phi} & -c_{\psi}s_{\gamma} \\ s_{\gamma}s_{\phi} & s_{\gamma}c_{\phi} & 1 \end{pmatrix} \quad (\text{B.1}) \end{aligned}$$

The orientation of frame \mathbb{B} is obtained through a sequence of rotations. We begin with \mathbb{B} aligned with frame \mathbb{I} . Then, we rotate \mathbb{B} about its z axis through the angle ψ . Next, we rotate it about its x axis by the angle γ , and, finally, about its z axis by the angle ϕ , to obtain the final orientation of frame \mathbb{B} .

For the ZXZ Euler angle representation, the ${}^{\mathbb{B}}\omega$ angular velocity is related to the time derivatives of the Euler angles, $\dot{\theta}$, as follows:

$${}^{\mathbb{B}}\omega = \begin{pmatrix} s_{\gamma}s_{\phi} & c_{\phi} & 0 \\ s_{\gamma}c_{\phi} & -s_{\phi} & 0 \\ c_{\gamma} & 0 & 1 \end{pmatrix} \dot{\theta} \quad (\text{B.2})$$

When $\sin(\gamma) \neq 0$, the matrix in (B.2) is invertible, and the inverse relationship is given by

$$\dot{\theta} = \frac{1}{s_{\gamma}} \begin{pmatrix} s_{\phi} & c_{\phi} & 0 \\ s_{\gamma}c_{\phi} & -s_{\gamma}s_{\phi} & 0 \\ -c_{\gamma}s_{\phi} & -c_{\gamma}c_{\phi} & s_{\gamma} \end{pmatrix} {}^{\mathbb{B}}\omega \quad (\text{B.3})$$

The relationship in (B.3) is undefined when $\sin(\gamma) = 0$. All 3-parameter attitude representations have such singularities. A representation of size 4 or more is required to avoid singularities.

B.2 Angle/Axis Parameters

Euler's theorem states that every rotation is equivalent to a rotation about a fixed vector. With \mathbf{n} denoting the axis of rotation unit vector, and θ the angle of rotation, the following exponential formula defines the expression for the rotation matrix:

$${}^{\mathbb{I}}\mathfrak{R}_{\mathbb{B}}(\mathbf{n}, \theta) = \exp[\tilde{\mathbf{n}}\theta] \quad (\text{B.4})$$

Thus, the four parameters, $\mathbb{I}\rho_{\mathbb{B}} \triangleq (\mathbf{n}, \theta)$, can be used to represent the relative attitude of the two frames. This representation is known as the **angle/axis representation** of attitude.

Exercise B.2 Derivation of the Euler–Rodrigues formula.

1. Verify that the characteristic polynomial¹ of a 3×3 skew-symmetric matrix \tilde{s} is

$$\lambda^3 + \sigma^2\lambda \quad (\text{B.5})$$

where $\sigma \triangleq \|s\|$ is the vector norm of s .

2. Use this to derive the following **Euler–Rodrigues formula** for a rotation matrix in terms of its angle/axis representation coordinates:

$$\begin{aligned} \mathbb{R}_{\mathbb{B}}(\mathbb{I}\rho_{\mathbb{B}}) &= \cos(\theta)\mathbf{I}_3 + [1 - \cos(\theta)]\mathbf{n}\mathbf{n}^* + \sin(\theta)\tilde{\mathbf{n}} \\ &= \mathbf{I}_3 + [1 - \cos(\theta)]\tilde{\mathbf{n}}\tilde{\mathbf{n}} + \sin(\theta)\tilde{\mathbf{n}} \end{aligned} \quad (\text{B.6})$$

■

Exercise B.3 Trace and characteristic polynomial of a rotation matrix.

Let $\mathfrak{R}(\mathbf{n}, \theta)$ denote a rotation matrix.

1. Show that

$$\gamma \triangleq \text{Trace}\{\mathfrak{R}(\mathbf{n}, \theta)\} = 1 + 2\cos(\theta) \quad (\text{B.7})$$

2. Show that the characteristic polynomial of $\mathfrak{R}(\mathbf{n}, \theta)$ is

$$\lambda^3 - \gamma\lambda^2 + \gamma\lambda - 1 \quad (\text{B.8})$$

3. Verify that \mathbf{n} is the eigen-vector of $\mathfrak{R}(\mathbf{n}, \theta)$ with eigen-value of 1.

4. Show that when $\sin(\theta) \neq 0$, \mathbf{n} can be obtained from the $\mathfrak{R}(\mathbf{n}, \theta)$ rotation matrix using the following relationship:

$$\tilde{\mathbf{n}} = (\mathfrak{R} - \mathfrak{R}^*) / (2\sin(\theta)) \quad (\text{B.9})$$

■

Remark B.1 Eigen-values of a rotation matrix.

The axis of rotation \mathbf{n} for a rotation matrix $\mathbb{R}_{\mathbb{B}}$ is its eigen-vector corresponding to the eigenvalue 1. The angle of rotation, θ , appears in the other complex eigen-values of the matrix, which, using (B.8) can be shown to be of the form $\exp[j\theta]$ and

¹ The characteristic polynomial of a matrix, A , is defined as the polynomial of λ , defined by the matrix determinant, $\det(\lambda\mathbf{I} - A)$.

$\exp[-\mathbf{j}\theta]$. Given a rotation matrix \mathfrak{R} instead of these relationships, it is simpler to obtain θ by using the (B.7) expression for the trace of a \mathfrak{R} and \mathbf{n} from the expression in (B.9). ■

Exercise B.4 Angular velocity from the angle/axis rates.

Derive the following expression for the ${}^{\mathbb{B}}\omega$ angular velocity in terms of $\dot{\mathbf{n}}$ and $\dot{\theta}$ angle/axis rates:

$$\begin{aligned} {}^{\mathbb{B}}\omega &= \dot{\theta}\mathbf{n} - (1 - \cos\theta)\tilde{\mathbf{n}}\dot{\mathbf{n}} + \sin(\theta)\dot{\mathbf{n}} \\ &= [\sin(\theta) - (1 - \cos\theta)\tilde{\mathbf{n}}, \quad \mathbf{n}] \begin{bmatrix} \dot{\mathbf{n}} \\ \dot{\theta} \end{bmatrix} \end{aligned} \quad (\text{B.10})$$

■

Exercise B.5 Angle/axis rates from the angular velocity.

Show that the expression for the $\dot{\mathbf{n}}$ and $\dot{\theta}$ time derivatives in terms of the ${}^{\mathbb{B}}\omega$ angular velocity is:

$$\begin{bmatrix} \dot{\mathbf{n}} \\ \dot{\theta} \end{bmatrix} = \begin{bmatrix} \frac{1}{2}[\tilde{\mathbf{n}} - \cot(\theta/2)\tilde{\mathbf{n}}\tilde{\mathbf{n}}] \\ \mathbf{n}^* \end{bmatrix} {}^{\mathbb{B}}\omega \quad (\text{B.11})$$

■

B.3 Unit Quaternions/Euler Parameters

Unit quaternions (also known as **Euler parameters**) are closely related to the angle/axis parameters and also consist of four scalar parameters. Given an angle/axis representation of the attitude ${}^{\mathbb{I}}\rho_{\mathbb{B}} = (\mathbf{n}, \theta)$, the corresponding quaternion representation, denoted ${}^{\mathbb{I}}\underline{\mathbf{q}}_{\mathbb{B}} \triangleq \begin{bmatrix} \mathbf{q} \\ q_0 \end{bmatrix} \in \mathcal{R}^4$, is defined as:

$$q_0 \triangleq \cos(\theta/2); \quad \mathbf{q} \triangleq \begin{bmatrix} q_1 \\ q_2 \\ q_3 \end{bmatrix} = \sin(\theta/2)\mathbf{n} \quad (\text{B.12})$$

It is easy to verify that quaternions have unit magnitude, that is,

$$\underline{\mathbf{q}}^* \underline{\mathbf{q}} = q_0^2 + \mathbf{q}^* \mathbf{q} = 1 \quad (\text{B.13})$$

A description of quaternions and their transformations can be found in [30, 43, 69].

Exercise B.6 Quaternion expression for a rotation matrix.

Show that the ${}^{\mathbb{I}}\mathfrak{R}_{\mathbb{B}}$ rotation matrix can be obtained from the corresponding ${}^{\mathbb{I}}\underline{\mathbf{q}}_{\mathbb{B}} = (\mathbf{q}, q_0)$ quaternion representation by any of the following expressions:

$$\begin{aligned}
{}^{\mathbb{I}}\mathfrak{R}_{\mathbb{B}}\left({}^{\mathbb{I}}\underline{\mathbf{q}}_{\mathbb{B}}\right) &= (q_0^2 - q^* q) \mathbf{I}_3 + 2qq^* + 2q_0 \tilde{q} \\
&= (2q_0^2 - 1)\mathbf{I}_3 + 2qq^* + 2q_0 \tilde{q} \\
&= \mathbf{I}_3 + 2\tilde{q}\tilde{q} + 2q_0 \tilde{q} \\
&= \mathbf{I}_3 + 2(q_0\mathbf{I}_3 + \tilde{q})\tilde{q} \\
&= (q_0\mathbf{I}_3 + \tilde{q})^2 + qq^* \\
&= \begin{pmatrix} 2[q_0^2 + q_1^2] - 1 & 2[q_1q_2 - q_0q_3] & 2[q_1q_3 + q_0q_2] \\ 2[q_1q_2 + q_0q_3] & 2[q_0^2 + q_2^2] - 1 & 2[q_2q_3 - q_0q_1] \\ 2[q_1q_3 - q_0q_2] & 2[q_2q_3 + q_0q_1] & 2[q_0^2 + q_3^2] - 1 \end{pmatrix}
\end{aligned} \tag{B.14}$$

■

Observe that, in contrast to (B.6), the (B.14) expression for ${}^{\mathbb{I}}\mathfrak{R}_{\mathbb{B}}({}^{\mathbb{I}}\underline{\mathbf{q}}_{\mathbb{B}})$ does not involve trigonometric quantities. Indeed, one of the key advantages of quaternions is that quaternion transformations typically involve algebraic expressions instead of the computationally expensive trigonometric functions typically encountered for other types of attitude representations.

Exercise B.7 Basic properties of unit quaternions.

Let $\underline{\mathbf{q}} = (q, q_0)$ denote a unit quaternion:

1. Show that the orthogonality of the matrix $\mathfrak{R}(\underline{\mathbf{q}})$ in (B.14) follows from the unit magnitude of $\underline{\mathbf{q}}$.
2. Verify that the unit quaternions $\underline{\mathbf{q}}$ and $-\underline{\mathbf{q}}$ are equivalent, in the sense that they both map to the same rotation matrix, i.e. $\mathfrak{R}(\underline{\mathbf{q}}) = \mathfrak{R}(-\underline{\mathbf{q}})$.
3. Show that the inverse of a quaternion $\underline{\mathbf{q}}$, denoted $\underline{\mathbf{q}}^{-1}$, is the unit quaternion given by

$$\underline{\mathbf{q}}^{-1} = \begin{bmatrix} -q \\ q_0 \end{bmatrix} \tag{B.15}$$

An equivalent representation for $\underline{\mathbf{q}}^{-1}$ is $(q, -q_0)$.

4. Show that the trace of the $\mathfrak{R}(\underline{\mathbf{q}})$ rotation matrix is given by

$$\text{Trace}\{\mathfrak{R}(\underline{\mathbf{q}})\} = 4q_0^2 - 1 \tag{B.16}$$

5. Show that $\underline{\mathbf{q}}$ is the eigen-vector of $\mathfrak{R}(\underline{\mathbf{q}})$ with eigenvalue of 1, i.e.,

$$\mathfrak{R}\underline{\mathbf{q}} = \underline{\mathbf{q}} \tag{B.17}$$

6. Show that when $q_0 \neq 0$, $\underline{\mathbf{q}}$ can be obtained from the \mathfrak{R} rotation matrix using the following relationship:

$$\tilde{q} = (\mathfrak{R} - \mathfrak{R}^*) / (4q_0) \tag{B.18}$$

■

B.3.1 The $E_+(\underline{q})$ and $E_-(\underline{q})$ Matrices

For a unit quaternion $\underline{q} = (q, q_0)$, define the 4×4 matrices, $E_+(\underline{q})$ and $E_-(\underline{q})$, as [30, 69, 97]

$$E_+(\underline{q}) \triangleq \begin{pmatrix} q_0 \mathbf{I}_3 + \tilde{\underline{q}} & \underline{q} \\ -\underline{q}^* & q_0 \end{pmatrix} \quad \text{and} \quad E_-(\underline{q}) \triangleq \begin{pmatrix} q_0 \mathbf{I}_3 - \tilde{\underline{q}} & \underline{q} \\ -\underline{q}^* & q_0 \end{pmatrix} \quad (\text{B.19})$$

Exercise B.8 Properties of E_- and E_+ matrices.

Let $\underline{q} = (q, q_0)$ denote a unit quaternion:

1. Show that $E_+(\underline{q})$ and $E_-(\underline{q})$ are orthogonal matrices, i.e.,

$$\begin{aligned} E_-^*(\underline{q})E_-(\underline{q}) &= E_-(\underline{q})E_-^*(\underline{q}) = \mathbf{I} \\ E_+^*(\underline{q})E_+(\underline{q}) &= E_+(\underline{q})E_+^*(\underline{q}) = \mathbf{I} \end{aligned} \quad (\text{B.20})$$

2. Show that

$$\begin{aligned} E_-^*(\underline{q})E_+(\underline{q}) &= E_+(\underline{q})E_-^*(\underline{q}) = \begin{pmatrix} \Re(\underline{q}) & \mathbf{0} \\ \mathbf{0} & 1 \end{pmatrix} \triangleq \mathbb{T}(\underline{q}) \\ E_+^*(\underline{q})E_-(\underline{q}) &= E_-(\underline{q})E_+^*(\underline{q}) = \begin{pmatrix} \Re^*(\underline{q}) & \mathbf{0} \\ \mathbf{0} & 1 \end{pmatrix} = \mathbb{T}(\underline{q}^{-1}) \end{aligned} \quad (\text{B.21})$$

The $\mathbb{T}(.)$ homogeneous transforms defined above have zero translation vectors and only rotational components.

3. Verify that

$$E_+(\underline{q}^{-1}) = E_+^*(\underline{q}) \quad \text{and} \quad E_-(\underline{q}^{-1}) = E_-^*(\underline{q}) \quad (\text{B.22})$$

4. With \underline{p} denoting another unit quaternion, show that

$$E_+(\underline{p})\underline{q} = E_-(\underline{q})\underline{p} \quad (\text{B.23})$$

5. With \underline{p} denoting another unit quaternion, show that each of the $E_-(\underline{q})$ and $E_-^*(\underline{q})$ pair of matrices commutes with each of the $E_+(\underline{p})$ and $E_+^*(\underline{p})$ matrix pair, i.e.,

$$E_-(\underline{q})E_+(\underline{p}) = E_+(\underline{p})E_-(\underline{q}) \quad (\text{B.24a})$$

$$E_-(\underline{q})E_+^*(\underline{p}) = E_+^*(\underline{p})E_-(\underline{q}) \quad (\text{B.24b})$$

$$E_-^*(\underline{q})E_+(\underline{p}) = E_+(\underline{p})E_-^*(\underline{q}) \quad (\text{B.24c})$$

$$E_-^*(\underline{q})E_+^*(\underline{p}) = E_+^*(\underline{p})E_-^*(\underline{q}) \quad (\text{B.24d})$$

6. Show that $\underline{\mathbf{q}}$ is an eigen-vector of $\mathbb{T}(\underline{\mathbf{q}})$ with eigenvalue 1, i.e.,

$$\mathbb{T}(\underline{\mathbf{q}})\underline{\mathbf{q}} = \underline{\mathbf{q}} \quad (\text{B.25})$$

■

B.3.2 Quaternion Transformations

We denote the composition operation between two quaternions by the symbol “ \otimes ”. The composition of two quaternions $\underline{\mathbf{p}}$ and $\underline{\mathbf{q}}$ is defined as

$$\underline{\mathbf{p}} \otimes \underline{\mathbf{q}} \triangleq \mathbb{E}_+(\underline{\mathbf{p}})\underline{\mathbf{q}} \stackrel{\text{B.23}}{=} \mathbb{E}_-(\underline{\mathbf{q}})\underline{\mathbf{p}} \quad (\text{B.26})$$

Exercise B.9 Composition of unit quaternions.

Let $\underline{\mathbf{q}} = (q, q_0)$ and $\underline{\mathbf{p}} = (p, p_0)$ denote unit quaternions:

1. Verify that,

$$\underline{\mathbf{p}} \otimes \underline{\mathbf{q}} = \begin{bmatrix} p_0 q + p q_0 + \tilde{p} q \\ p_0 q_0 - p^* q \end{bmatrix} \quad (\text{B.27})$$

Verify that $\underline{\mathbf{p}} \otimes \underline{\mathbf{q}}$ is of unit norm and is hence also a unit quaternion. Thus, the composition of two quaternions yields another quaternion.

2. For quaternion composition to be consistent with the composition of rotation matrices, we must have

$$\Re(\underline{\mathbf{p}} \otimes \underline{\mathbf{q}}) = \Re(\underline{\mathbf{p}}) \Re(\underline{\mathbf{q}}) \quad (\text{B.28})$$

Show that this identity holds.

3. Show that the composition of quaternions is an associative operation. That is, with $\underline{\mathbf{r}}$ denoting another quaternion, we have,

$$\underline{\mathbf{p}} \otimes (\underline{\mathbf{q}} \otimes \underline{\mathbf{r}}) = (\underline{\mathbf{p}} \otimes \underline{\mathbf{q}}) \otimes \underline{\mathbf{r}} \quad (\text{B.29})$$

4. Show that

$$\underline{\mathbf{p}}^{-1} \otimes \underline{\mathbf{q}} = \mathbb{E}_+^*(\underline{\mathbf{p}})\underline{\mathbf{q}} \quad \text{and} \quad \underline{\mathbf{p}} \otimes \underline{\mathbf{q}}^{-1} = \mathbb{E}_-^*(\underline{\mathbf{q}})\underline{\mathbf{p}} \quad (\text{B.30})$$

■

Exercise B.10 The quaternion identity element.

Show that the $\mathbf{e}_{\underline{\mathbf{q}}} = (0, 0, 0, 1)^*$ unit quaternion is the identity element for unit quaternions by establishing the following identities for an arbitrary quaternion $\underline{\mathbf{q}}$:

$$\underline{\mathbf{q}} \otimes \mathbf{e}_{\underline{\mathbf{q}}} = \underline{\mathbf{q}} \quad \text{and} \quad \underline{\mathbf{q}} \otimes \underline{\mathbf{q}}^{-1} = \mathbf{e}_{\underline{\mathbf{q}}} \quad (\text{B.31})$$

■

Exercise B.11 Unit quaternion products and inverses.

For a pair of quaternions $\underline{\mathbf{p}}$ and $\underline{\mathbf{q}}$, show that:

1. $(\underline{\mathbf{p}} \otimes \underline{\mathbf{q}})^{-1} = \underline{\mathbf{q}}^{-1} \otimes \underline{\mathbf{p}}^{-1}$
2. With $\underline{\mathbf{r}} \triangleq \underline{\mathbf{p}} \otimes \underline{\mathbf{q}}$, show that,

$$\underline{\mathbf{q}} = \underline{\mathbf{p}}^{-1} \otimes \underline{\mathbf{r}} \quad \text{and} \quad \underline{\mathbf{p}} = \underline{\mathbf{r}} \otimes \underline{\mathbf{q}}^{-1} \quad (\text{B.32})$$

■

Exercise B.12 Transforming vectors with unit quaternions.

Given a vector $\mathbf{x} \in \mathcal{R}^3$, and a quaternion $\underline{\mathbf{q}} = \underline{\mathbf{q}}_{\mathbb{B}}$ defining the attitude of frame \mathbb{B} with respect to frame \mathbb{I} , show that

$$\begin{bmatrix} \mathbb{I}\mathbf{x} \\ 0 \end{bmatrix} = \underline{\mathbf{q}} \otimes \begin{bmatrix} \mathbb{B}\mathbf{x} \\ 0 \end{bmatrix} \otimes \underline{\mathbf{q}}^{-1} \quad (\text{B.33})$$

■

B.3.3 Quaternion Differential Kinematics**Exercise B.13 Quaternion rates from the angular velocity.**

With $\underline{\mathbf{q}}_{\mathbb{B}} = \underline{\mathbf{q}} = (\mathbf{q}, q_0)$, Show that the time derivative of the quaternion is related to the $\mathbb{B}\omega$ angular velocity as follows:

$$\begin{aligned} \dot{\underline{\mathbf{q}}}_{\mathbb{B}} &= \frac{1}{2} \begin{bmatrix} (\mathbf{q}_0 \mathbf{I}_3 + \tilde{\mathbf{q}}) \mathbb{B}\omega \\ -\mathbf{q}^* \mathbb{B}\omega \end{bmatrix} = \frac{1}{2} \begin{pmatrix} -\mathbb{B}\tilde{\omega} & \mathbb{B}\omega \\ -\mathbb{B}\omega^* & 0 \end{pmatrix} \underline{\mathbf{q}} \\ &= \frac{1}{2} \mathbf{E}_+(\underline{\mathbf{q}}) \begin{bmatrix} \mathbb{B}\omega \\ 0 \end{bmatrix} = \frac{1}{2} \underline{\mathbf{q}} \otimes \begin{bmatrix} \mathbb{B}\omega \\ 0 \end{bmatrix} \end{aligned} \quad (\text{B.34})$$

■

Exercise B.14 Constant unit quaternion norms.

1. Show that the solution to the (B.34) ordinary differential equation has unit norm for all time t .
2. Show that when $\mathbf{q}_0 \neq 0$,

$$\dot{\mathbf{q}}_0 = -\mathbf{q}^* \dot{\mathbf{q}} / q_0 \quad (\text{B.35})$$

■

Exercise B.15 Unit quaternion rate to angular velocity.

Let $\mathbb{I}\underline{\mathbf{q}}_{\mathbb{B}} = \underline{\mathbf{q}} = (\mathbf{q}, q_0)$ denote a unit quaternion:

1. Show that the mapping from quaternion rates to the ${}^{\mathbb{B}}\omega$ angular velocity representation is given by the following expression:

$$\begin{bmatrix} {}^{\mathbb{B}}\omega \\ 0 \end{bmatrix} = 2E_+^*(\underline{\mathbf{q}}) \dot{\underline{\mathbf{q}}} = 2\underline{\mathbf{q}}^{-1} \otimes \dot{\underline{\mathbf{q}}} \quad (\text{B.36})$$

Alternatively,

$${}^{\mathbb{B}}\omega = 2[q_0 \mathbf{I}_3 - \tilde{\mathbf{q}}] \dot{\mathbf{q}} - \mathbf{q} \dot{\mathbf{q}}_0 \quad (\text{B.37})$$

When $q_0 \neq 0$,

$${}^{\mathbb{B}}\omega = 2[q_0 \mathbf{I}_3 - \tilde{\mathbf{q}} + \mathbf{q} \mathbf{q}^*/q_0] \dot{\mathbf{q}} \quad (\text{B.38})$$

2. Show that the mapping from quaternion rates to the ${}^{\mathbb{I}}\omega$ angular velocity representation is as follows:

$$\begin{bmatrix} {}^{\mathbb{I}}\omega \\ 0 \end{bmatrix} = 2E_-^*(\underline{\mathbf{q}}) \dot{\underline{\mathbf{q}}} = 2\dot{\underline{\mathbf{q}}} \otimes \underline{\mathbf{q}}^{-1} \quad (\text{B.39})$$

Alternatively,

$${}^{\mathbb{I}}\omega = 2[q_0 \mathbf{I}_3 + \tilde{\mathbf{q}}] \dot{\mathbf{q}} - \mathbf{q} \dot{\mathbf{q}}_0 \quad (\text{B.40})$$

When $q_0 \neq 0$,

$${}^{\mathbb{I}}\omega = 2[q_0 \mathbf{I}_3 + \tilde{\mathbf{q}} + \mathbf{q} \mathbf{q}^*/q_0] \dot{\mathbf{q}} \quad (\text{B.41})$$

■

Exercise B.16 Quaternion double time derivatives.

Let $\mathbb{I}\underline{\mathbf{q}}_{\mathbb{B}} = \underline{\mathbf{q}} = (\mathbf{q}, q_0)$ denote a unit quaternion. Show that

$$\ddot{\underline{\mathbf{q}}} = \frac{1}{2} \underline{\mathbf{q}} \otimes \begin{bmatrix} {}^{\mathbb{B}}\dot{\omega} \\ 0 \end{bmatrix} + \frac{1}{4} \|{}^{\mathbb{B}}\omega\|^2 \underline{\mathbf{q}} \quad (\text{B.42})$$

Establish the converse relationship

$$\begin{bmatrix} {}^{\mathbb{B}}\dot{\omega} \\ 0 \end{bmatrix} = 2\underline{\mathbf{q}}^{-1} \otimes \ddot{\underline{\mathbf{q}}} - \frac{1}{2} \|{}^{\mathbb{B}}\omega\|^2 \mathbf{e}_{\underline{\mathbf{q}}} \quad (\text{B.43})$$

■

B.4 Gibbs Vector Attitude Representations

Now we use the connection between rotation matrices and skew-symmetric matrices to define the **Gibbs vector** attitude representation [172].

Exercise B.17 Gibbs vector attitude representation.

Let s denote a 3-vector with magnitude σ :

1. Use the characteristic polynomial for skew-symmetric matrices in Exercise B.2 to show that

$$\begin{aligned} [\mathbf{I} - \tilde{s}]^{-1} &= \mathbf{I} + (\tilde{s}^2 + \tilde{s})/(1 + \sigma^2) \\ &= \mathbf{I} + \tilde{s}(\mathbf{I} + \tilde{s})/(1 + \sigma^2) \end{aligned} \quad (\text{B.44})$$

2. Use this identity to show that

$$[\mathbf{I} - \tilde{s}]^{-1}[\mathbf{I} + \tilde{s}] = \mathbf{I} + 2(\tilde{s}^2 + \tilde{s})/(1 + \sigma^2) \quad (\text{B.45})$$

Verify that $\mathfrak{R}(s) \triangleq [\mathbf{I} - \tilde{s}]^{-1}[\mathbf{I} + \tilde{s}]$ is a rotation matrix. Such a representation of attitude matrices using a 3-vector, s , is also known as the **Rodrigues or Gibbs vector representation** for attitude matrices.

3. Establish the converse relationship

$$\begin{aligned} \tilde{s} &= -[\mathbf{I} - \mathfrak{R}(s)] [\mathbf{I} + \mathfrak{R}(s)]^{-1} \\ &= -[\gamma \mathbf{I} - (1 + \gamma)\mathfrak{R}(s) + \mathfrak{R}^2(s)]/(1 + \gamma) \end{aligned} \quad (\text{B.46})$$

where $\gamma \triangleq \text{Trace}\{\mathfrak{R}(s)\}$.

4. Show that the Gibb's vector, s , is the axis of rotation for the $\mathfrak{R}(s)$ rotation matrix.
5. Show that the Gibb's vector, s , for a quaternion $\underline{\mathbf{q}} = (\mathbf{q}, q_0)$, with $q_0 \neq 0$, is given by

$$s = \mathbf{q}/q_0 = \tan(\theta/2)\mathbf{n} \quad (\text{B.47})$$

so that $\mathfrak{R}(s) = \mathfrak{R}(\underline{\mathbf{q}}) = \mathfrak{R}(\mathbf{n}, \theta)$. ■

We now look at the problem of finding the family of rotation matrices that will transform one vector into another [15]. Let a and b denote two vectors of identical norm, i.e., $\|a\| = \|b\|$. The goal is to find a parametrization of all rotation matrices \mathfrak{R} such that $\mathfrak{R}a = b$.

Exercise B.18 Rotation of vectors.

For a pair of 3-vectors a and b of the same norm, let s denote a Gibb's vector attitude representation such that $\mathfrak{R}(s)a = b$:

1. Show that s must satisfy the following relationship:

$$\widetilde{(a + b)}s = (a - b) \quad (\text{B.48})$$

2. Now show that the general solution for s satisfying $\mathfrak{R}(s)\mathbf{a} = \mathbf{b}$ is given by

$$\mathbf{s} = \lambda \widetilde{(\mathbf{a} - \mathbf{b})(\mathbf{a} + \mathbf{b})} + \alpha(\mathbf{a} + \mathbf{b}) \quad (\text{B.49})$$

where $\lambda = 1/\|(\mathbf{a} + \mathbf{b})\|^2$, and α is an arbitrary constant.

■

This exercise shows how to compute a rotation matrix that transforms a given vector, \mathbf{a} , into another given vector, \mathbf{b} . This rotation matrix is not unique, as reflected by the arbitrary parameter α in (B.49). After being rotated to coincide with \mathbf{b} , any additional rotation of \mathbf{a} about the axis \mathbf{b} leaves the vector unchanged, leading to the non-uniqueness of the rotation. A similar circumstance holds if vector \mathbf{a} is rotated about itself prior to rotating it to coincide with \mathbf{b} .

Appendix C

Solutions

Solutions for Chapter 1

Solution 1.1 (pp. 8): Position and velocity vector derivatives

1.

$$\frac{d_{\mathbb{B}} \omega(\mathbb{B})}{dt} \stackrel{1.12}{=} \alpha(\mathbb{B}) + \tilde{\omega}(\mathbb{B})\omega(\mathbb{B}) = \alpha(\mathbb{B})$$

This proves the first part of (1.17). The second expression follows since the angular velocity of \mathbb{I} with respect to \mathbb{B} is $-\omega(\mathbb{B})$ in (1.12).

2. Equation (1.18) follows by differentiating (1.15) with respect to the inertial frame and using (1.12) for the inertial derivative of $\mathbf{l}(x, y)$.
3. Equation (1.19a) follows from noting that $\delta_v = \frac{d_{\mathbb{B}} \mathbf{l}(y, P)}{dt}$ and thus,

$$v(P) = v(y) + \frac{d_{\mathbb{I}} \mathbf{l}(y, P)}{dt} \stackrel{1.12}{=} v(y) + \delta_v + \tilde{\omega}(\mathbb{B})\mathbf{l}(y, P) \quad (C.1)$$

The last term in (1.19a) vanishes because $\mathbf{l}(y, P)$ is instantaneously zero.

Equation (1.19b) follows by differentiating (C.1) with respect to the inertial frame.

Solution 1.2 (pp. 9): Spatial vector cross-product identities

The identities can be established by direct verification using the 3-vector components of the A and B spatial vectors.

Solution 1.3 (pp. 10): Relationship between the $\widetilde{(\)}$, $\overline{(\)}$ and $\widehat{(\)}$ operators

These (1.27) equations can be established by direct verification for arbitrary spatial vectors A, B and C.

Solution 1.4 (pp. 10): Time derivative relationship for spatial vectors

With $X = \begin{bmatrix} x \\ y \end{bmatrix}$, we have

$$\frac{d_F X}{dt} = \begin{bmatrix} \frac{d_F x}{dt} \\ \frac{d_F y}{dt} \end{bmatrix} \stackrel{1.12}{=} \begin{bmatrix} \frac{d_G x}{dt} + \tilde{\omega} x \\ \frac{d_G y}{dt} + \tilde{\omega} y \end{bmatrix} \stackrel{1.21, 1.23}{=} \frac{d_G X}{dt} + \tilde{\mathcal{V}}^\omega(F, G) X$$

Solution 1.5 (pp. 12): Identities involving $\tilde{(\cdot)}$, $\widehat{(\cdot)}$ and $\phi(\cdot, \cdot)$

The first two identities can be established by direct verification using arbitrary 3-vectors $l(x, y)$ and X . The last one is a simple rearrangement of the second identity.

Solution 1.6 (pp. 12): Rigid body transformation of $\tilde{\mathcal{V}}(x)$

From (1.33) on page 12 we know that $\mathcal{V}(y) = \phi^*(x, y)\mathcal{V}(x)$. Thus,

$$\tilde{\mathcal{V}}(y) \stackrel{1.34}{=} \phi^*(x, y)\tilde{\mathcal{V}}(x)\phi^{-*}(x, y)$$

and the first equation follows. The latter equation is merely a transposed version of the first equation, followed by the use of (1.26).

Solution 1.7 (pp. 13): Relationships involving X^ω and X^ν

The first pair of identities can be verified directly by expanding out X and Y into their component 3-vectors and evaluating them.

Equation (1.36b) follows directly from (1.36a).

Equation (1.36c) follows by direct verification.

Equation (1.36d) follows from (1.36c).

Equation (1.36e) can be verified directly by additionally using $\phi(x, y)$ for an arbitrary $l(x, y)$ 3-vector.

Solution 1.8 (pp. 13): The inertial frame derivative of $\phi(x, y)$

For the inertial frame derivative, we use the inertial frame representation of $\phi(x, y)$ from (1.30). Now,

$$\frac{d_I l(x, y)}{dt} = v(y) - v(x)$$

Hence,

$$\frac{d_I \phi(x, y)}{dt} = \begin{bmatrix} \mathbf{0} & \tilde{\mathcal{V}}(y) - \tilde{\mathcal{V}}(x) \\ \mathbf{0} & \mathbf{0} \end{bmatrix} \stackrel{1.25, 1.21}{=} \bar{\mathcal{V}}^\nu(y) - \bar{\mathcal{V}}^\nu(x)$$

Solution 1.9 (pp. 14): Local time derivative of $\phi^*(x, y)$

1. We have

$$v_{\mathbb{F}}(\mathbb{F}, \mathbb{G}) \stackrel{1.11}{=} v_{\mathbb{G}}(\mathbb{F}, \mathbb{G}) + \tilde{\omega}(\mathbb{F}, \mathbb{G})l(\mathbb{F}, \mathbb{G}) \quad (C.2)$$

Equation (1.39) follows from using the above in (1.40).

2. The latter equality in (1.42) is a direct application of the last identity in (1.34) to (1.39).

For the first equality, differentiate (1.41) and use the chain rule to get

$$\begin{aligned} \frac{d\phi^*(\mathbb{F}, \mathbb{G})}{dt} &\stackrel{1.41, 1.12}{=} \left(\begin{array}{cc} \tilde{\omega}(\mathbb{G}, \mathbb{F})^{\mathbb{G}\mathfrak{R}_{\mathbb{F}}} & \mathbf{0}_3 \\ \mathbf{0}_3 & \tilde{\omega}(\mathbb{G}, \mathbb{F})^{\mathbb{G}\mathfrak{R}_{\mathbb{F}}} \end{array} \right) \left(\begin{array}{cc} \mathbf{I}_3 & \mathbf{0}_3 \\ -\mathbb{F}\tilde{l}(\mathbb{F}, \mathbb{G}) & \mathbf{I}_3 \end{array} \right) \\ &\quad + \left(\begin{array}{cc} \mathbb{G}\mathfrak{R}_{\mathbb{F}} & \mathbf{0}_3 \\ \mathbf{0}_3 & \mathbb{G}\mathfrak{R}_{\mathbb{F}} \end{array} \right) \left(\begin{array}{cc} \mathbf{0}_3 & \mathbf{0}_3 \\ -\tilde{v}_{\mathbb{F}}(\mathbb{F}, \mathbb{G}) & \mathbf{0}_3 \end{array} \right) \\ &\stackrel{1.41}{=} \left(\begin{array}{cc} \tilde{\omega}(\mathbb{G}, \mathbb{F}) & \mathbf{0}_3 \\ \mathbf{0}_3 & \tilde{\omega}(\mathbb{G}, \mathbb{F}) \end{array} \right) \phi^*(\mathbb{F}, \mathbb{G}) \\ &\quad + \left(\begin{array}{cc} \mathbb{G}\mathfrak{R}_{\mathbb{F}} & \mathbf{0}_3 \\ \mathbf{0}_3 & \mathbb{G}\mathfrak{R}_{\mathbb{F}} \end{array} \right) \left(\begin{array}{cc} \mathbf{0}_3 & \mathbf{0}_3 \\ -\tilde{v}_{\mathbb{F}}(\mathbb{F}, \mathbb{G}) & \mathbf{0}_3 \end{array} \right) \left(\begin{array}{cc} \mathbf{I}_3 & \mathbf{0}_3 \\ -\mathbb{F}\tilde{l}(\mathbb{F}, \mathbb{G}) & \mathbf{I}_3 \end{array} \right) \\ &= \left(\begin{array}{cc} \tilde{\omega}(\mathbb{G}, \mathbb{F}) & \mathbf{0}_3 \\ \mathbf{0}_3 & \tilde{\omega}(\mathbb{G}, \mathbb{F}) \end{array} \right) \phi^*(\mathbb{F}, \mathbb{G}) \\ &\quad + \left(\begin{array}{cc} \mathbf{0}_3 & \mathbf{0}_3 \\ -\tilde{v}_{\mathbb{F}}(\mathbb{F}, \mathbb{G}) & \mathbf{0}_3 \end{array} \right) \left(\begin{array}{cc} \mathbb{G}\mathfrak{R}_{\mathbb{F}} & \mathbf{0}_3 \\ \mathbf{0}_3 & \mathbb{G}\mathfrak{R}_{\mathbb{F}} \end{array} \right) \left(\begin{array}{cc} \mathbf{I}_3 & \mathbf{0}_3 \\ -\mathbb{F}\tilde{l}(\mathbb{F}, \mathbb{G}) & \mathbf{I}_3 \end{array} \right) \\ &\stackrel{1.41}{=} \left(\begin{array}{cc} \tilde{\omega}(\mathbb{G}, \mathbb{F}) & \mathbf{0}_3 \\ \mathbf{0}_3 & \tilde{\omega}(\mathbb{G}, \mathbb{F}) \end{array} \right) \phi^*(\mathbb{F}, \mathbb{G}) + \left(\begin{array}{cc} \mathbf{0}_3 & \mathbf{0}_3 \\ \tilde{v}_{\mathbb{F}}(\mathbb{G}, \mathbb{F}) & \mathbf{0}_3 \end{array} \right) \phi^*(\mathbb{F}, \mathbb{G}) \\ &= \left(\begin{array}{cc} \tilde{\omega}(\mathbb{G}, \mathbb{F}) & \mathbf{0}_3 \\ \tilde{v}_{\mathbb{F}}(\mathbb{G}, \mathbb{F}) & \tilde{\omega}(\mathbb{G}, \mathbb{F}) \end{array} \right) \phi^*(\mathbb{F}, \mathbb{G}) = \tilde{V}_{\mathbb{F}}(\mathbb{G}, \mathbb{F})\phi^*(\mathbb{F}, \mathbb{G}) \end{aligned}$$

3. We have

$$\begin{aligned} \phi^*(\mathbb{G}, \mathbb{F}) \frac{d\phi^*(\mathbb{F}, \mathbb{G})}{dt} \phi^*(\mathbb{G}, \mathbb{F}) &\stackrel{1.42}{=} \phi^*(\mathbb{G}, \mathbb{F}) \tilde{V}_{\mathbb{F}}(\mathbb{G}, \mathbb{F}) \phi^*(\mathbb{F}, \mathbb{G}) \phi^*(\mathbb{G}, \mathbb{F}) \\ &= \phi^*(\mathbb{G}, \mathbb{F}) \tilde{V}_{\mathbb{F}}(\mathbb{G}, \mathbb{F}) = -\phi^*(\mathbb{G}, \mathbb{F}) \tilde{V}_{\mathbb{F}}(\mathbb{F}, \mathbb{G}) \end{aligned}$$

This expression agrees with the one in (1.43) and establishes the result.

4. We have that

$$\begin{aligned}
 & \frac{d\phi^*(G, H)}{dt} \phi^*(F, G) + \phi^*(G, H) \frac{d\phi^*(F, G)}{dt} \\
 & \stackrel{1.42}{=} \tilde{\mathcal{V}}_G(H, G) \phi^*(G, H) \phi^*(F, G) + \phi^*(G, H) \phi^*(F, G) \tilde{\mathcal{V}}_G(G, F) \\
 & = \tilde{\mathcal{V}}_G(H, G) \phi^*(F, H) + \phi^*(F, H) \tilde{\mathcal{V}}_G(G, F) \\
 & = \begin{pmatrix} \tilde{\omega}(H, F) & \mathbf{0}_3 \\ \tilde{v}_G(H, G) - \tilde{\omega}(H, G) \tilde{l}(F, H) + \tilde{v}_G(G, F) - \tilde{l}(F, H) \tilde{\omega}(G, F) & \tilde{\omega}(H, F) \end{pmatrix} \\
 & = \begin{pmatrix} \tilde{\omega}(H, F) & \mathbf{0}_3 \\ \tilde{v}_G(H, F) - \tilde{\omega}(H, G) \tilde{l}(F, H) - \tilde{v}_G(G, F) - \tilde{l}(F, H) \tilde{\omega}(G, F) & \tilde{\omega}(H, F) \end{pmatrix}
 \end{aligned}$$

Using (C.2) in the lower left expression, for $v_G(H, F)$ and simplifying we obtain

$$\begin{aligned}
 & \frac{d\phi^*(G, H)}{dt} \phi^*(F, G) + \phi^*(G, H) \frac{d\phi^*(F, G)}{dt} \\
 & = \begin{pmatrix} \tilde{\omega}(H, F) & \mathbf{0}_3 \\ \tilde{v}_F(H, F) - \tilde{\omega}(H, F) \tilde{l}(F, H) & \tilde{\omega}(H, F) \end{pmatrix} \\
 & = \tilde{\mathcal{V}}_F(H, F) \phi^*(F, H) \stackrel{1.42}{=} \frac{d\phi^*(F, H)}{dt}
 \end{aligned}$$

establishing the result.

Solutions for Chapter 2

Solution 2.1 (pp. 19): Rigid body center of mass

We have $I(x, a) = I(x, y) + I(y, a)$. Therefore,

$$\begin{aligned}
 p(x) & \stackrel{2.8}{=} \frac{1}{m} \int_{\Omega} I(x, a) \rho(a) d\vartheta(a) \\
 & = \frac{1}{m} \int_{\Omega} I(x, y) \rho(a) d\vartheta(a) + \frac{1}{m} \int_{\Omega} I(y, a) \rho(a) d\vartheta(a) \stackrel{2.8}{=} I(x, y) + p(y)
 \end{aligned}$$

Solution 2.2 (pp. 19): Parallel-axis theorem for rotational inertias

1. We have

$$\begin{aligned}
 \mathcal{J}(x) &\stackrel{2.8}{=} -\int_{\Omega} \tilde{l}(x, a) \tilde{l}(x, a) \rho(a) d\vartheta(a) \\
 &= -\int_{\Omega} \tilde{l}(x, \mathbb{C}) \tilde{l}(x, \mathbb{C}) \rho(a) d\vartheta(a) - \int_{\Omega} \tilde{l}(\mathbb{C}, a) \tilde{l}(\mathbb{C}, a) \rho(a) d\vartheta(a) \\
 &\quad - \int_{\Omega} \tilde{l}(x, \mathbb{C}) \tilde{l}(\mathbb{C}, a) \rho(a) d\vartheta(a) - \int_{\Omega} \tilde{l}(\mathbb{C}, a) \tilde{l}(x, \mathbb{C}) \rho(a) d\vartheta(a) \\
 &\stackrel{2.8}{=} \mathcal{J}(\mathbb{C}) - m \tilde{p}(x) \tilde{p}(x) - m \tilde{l}(x, \mathbb{C}) \tilde{p}(\mathbb{C}) - m \tilde{p}(\mathbb{C}) \tilde{l}(x, \mathbb{C}) \\
 &= \mathcal{J}(\mathbb{C}) - m \tilde{p}(x) \tilde{p}(x)
 \end{aligned}$$

The last step used the fact that $p(\mathbb{C}) = \mathbf{0}$.

2. The symmetry of $\mathcal{J}(x)$ is easy to verify from its definition. Its positive semi-definiteness follows from the positive semi-definiteness of the integrand $-\tilde{l}(x, k) \tilde{l}(x, k) \rho(k)$. Since $-m \tilde{p}(x) \tilde{p}(x) = m[\tilde{p}(x)]^* \tilde{p}(x)$ is always positive semi-definite implies that $\mathcal{J}(x) \geq \mathcal{J}(\mathbb{C})$ for all points x .
3. For $\mathcal{J}(x)$ to fail to be positive definite, there must exist a non-zero vector y such that $y^* \mathcal{J}(x) y = 0$. That is,

$$\begin{aligned}
 0 = y^* \mathcal{J}(x) y &\stackrel{2.8}{=} -\int_{\Omega} y^* \tilde{l}(x, a) \tilde{l}(x, a) y \rho(a) d\vartheta(a) \\
 &= \int_{\Omega} z^*(a) z(a) \rho(a) d\vartheta(a) \quad \text{where } z(a) \triangleq \tilde{l}(x, a) y
 \end{aligned}$$

The above integral can vanish in the following cases:

Point mass: Here $\rho(a) = 0$ for all $l(x, a) \neq 0$ and $\mathcal{J}(x) \equiv 0$.

Infinitely thin rod along y : Here $\rho(a) = 0$ for all $l(x, a) \neq ky$ for some scalar $k \neq 0$.

Solution 2.3 (pp. 20): Positive semi-definiteness of spatial inertias

$\mathcal{J}(\mathbb{C})$ being positive definite or positive semi-definite implies the same property for $M(\mathbb{C})$. The same property also applies to $M(x) = \phi(x, \mathbb{C}) M(\mathbb{C}) \phi^*(x, \mathbb{C})$ in (2.12) since $\phi(x, y)$ is always non-singular.

Solution 2.4 (pp. 21): Invariance of the kinetic energy

From (2.12), we have

$$\begin{aligned}\mathfrak{K}_e &= \frac{1}{2} \mathcal{V}^*(x) M(x) \mathcal{V}(x) \stackrel{2.12}{=} \frac{1}{2} \mathcal{V}^*(x) \phi(x, y) M(y) \phi^*(x, y) \mathcal{V}(x) \\ &\stackrel{1.33}{=} \frac{1}{2} \mathcal{V}^*(y) M(y) \mathcal{V}(y)\end{aligned}$$

Since the points x and y are arbitrary, this establishes the invariance of the kinetic energy.

Solution 2.5 (pp. 22): Relationship of spatial momenta about points x and y

$$\begin{aligned}\mathfrak{h}(x) &\stackrel{2.16}{=} M(x) \mathcal{V}(x) \stackrel{2.12}{=} \phi(x, y) M(y) \phi^*(x, y) \mathcal{V}(x) \\ &\stackrel{1.33}{=} \phi(x, y) M(y) \mathcal{V}(y) \stackrel{2.16}{=} \phi(x, y) \mathfrak{h}(y)\end{aligned}$$

Solution 2.6 (pp. 25): Time derivative of rigid body spatial inertia

We have

$$\mathbb{I}M(z) = \begin{pmatrix} \mathbb{I}\mathfrak{R}_{\mathbb{B}} & \mathbf{0} \\ \mathbf{0} & \mathbb{I}\mathfrak{R}_{\mathbb{B}} \end{pmatrix} \mathbb{B}M(z) \begin{pmatrix} \mathbb{B}\mathfrak{R}_{\mathbb{I}} & \mathbf{0} \\ \mathbf{0} & \mathbb{B}\mathfrak{R}_{\mathbb{I}} \end{pmatrix}$$

Differentiating this equation while noting that $\mathbb{B}M$ is constant leads to:

$$\begin{aligned}\dot{M}(z) &= \begin{pmatrix} \tilde{\omega} & \mathbf{0} \\ \mathbf{0} & \tilde{\omega} \end{pmatrix} \mathbb{B}M(z) - M(z) \begin{pmatrix} \tilde{\omega} & \mathbf{0} \\ \mathbf{0} & \tilde{\omega} \end{pmatrix} \\ &= \tilde{\mathcal{V}}^{\omega}(z) M(z) - M(z) \tilde{\mathcal{V}}^{\omega}(z)\end{aligned}$$

Solution 2.7 (pp. 26): $b_J(\mathbb{C})$ gyroscopic spatial force does no work

We can verify that $b_J(z)$ does no work by taking its dot product with the spatial velocity vector to obtain:

$$\mathcal{V}^*(\mathbb{C}) b_J(\mathbb{C}) \stackrel{2.23}{=} \begin{bmatrix} \omega^*(\tilde{\omega} \mathscr{J}(\mathbb{C}) \omega) \\ \mathbf{0} \end{bmatrix} = \mathbf{0}$$

Solution 2.8 (pp. 27): Inertial generalized accelerations at two points

$$\begin{aligned}
\dot{\beta}_J(y) &\triangleq \frac{d_{\mathbb{I}} \mathcal{V}(y)}{dt} = \frac{d_{\mathbb{I}}[\phi^*(x, y)\mathcal{V}(x)]}{dt} \\
&= \phi^*(x, y)\dot{\beta}_J(x) + \frac{d_{\mathbb{I}}[\phi^*(x, y)]}{dt}\beta_J(x) \\
&\stackrel{1.37}{=} \phi^*(x, y)\dot{\beta}_J(x) + \left[-\tilde{\mathcal{V}}(y) + \tilde{\mathcal{V}}(x) \right] \mathcal{V}(x) \\
&= \phi^*(x, y)\dot{\beta}_J(x) - \tilde{\mathcal{V}}(y)\mathcal{V}(x) = \phi^*(x, y)\dot{\beta}_J(x) + \begin{bmatrix} \mathbf{0} \\ \tilde{\omega}[v(y) - v(x)] \end{bmatrix} \\
&\stackrel{1.15}{=} \phi^*(x, y)\dot{\beta}_J(x) + \begin{bmatrix} \mathbf{0} \\ \tilde{\omega}\tilde{\omega} I(x, y) \end{bmatrix}
\end{aligned}$$

Solution 2.9 (pp. 28): $b_J(z)$ gyroscopic spatial force does work

We can verify that $b_J(z)$ does work by taking its dot product with the spatial velocity vector as follows:

$$\mathcal{V}^*(z)b_J(z) \stackrel{2.26}{=} \mathcal{V}^*(z)\tilde{\mathcal{V}}^\omega(z)\mathcal{M}(z)\mathcal{V}^\omega(z)$$

This expression is non-zero in general and hence, the gyroscopic force does work. Assuming that the spatial force is zero, i.e., $f(z) \equiv 0$, the time derivative of the kinetic energy of the body is:

$$\begin{aligned}
\frac{d\mathfrak{K}_e}{dt} &= \frac{1}{2} \frac{d\beta_J^*(z)\mathcal{M}(z)\beta_J(z)}{dt} = \beta_J^*(z)\mathcal{M}(z)\dot{\beta}_J(z) + \frac{1}{2}\beta_J^*(z)\dot{\mathcal{M}}(z)\beta_J(z) \\
&\stackrel{2.26, 2.22}{=} \beta_J^*(z)[f(z) - b_J(z)] - \beta_J^*(z)\mathcal{M}(z)\tilde{\mathcal{V}}^\omega(z)\beta_J(z) \\
&\stackrel{2.26}{=} -mv^*(z)\tilde{\omega}\tilde{\omega}p(z) - m\omega^*\tilde{p}(z)\tilde{\omega}v(z) = 0
\end{aligned}$$

This proves that the kinetic energy is conserved in the absence of external forces.

Solution 2.10 (pp. 28): Non-conservation of spatial momentum

For any point x on the rigid body, from (2.17), $\mathfrak{h}(x) = \phi(x, \mathbb{C})\mathfrak{h}(\mathbb{C})$. Differentiating this equation with respect to time in the inertial frame leads to

$$\begin{aligned}
\frac{d_{\mathbb{I}}\mathfrak{h}(x)}{dt} &= \frac{d_{\mathbb{I}}\phi(x, \mathbb{C})}{dt}\mathfrak{h}(\mathbb{C}) + \phi(x, \mathbb{C})\frac{d_{\mathbb{I}}\mathfrak{h}(\mathbb{C})}{dt} \stackrel{2.21}{=} \frac{d_{\mathbb{I}}\phi(x, \mathbb{C})}{dt}\mathfrak{h}(\mathbb{C}) + \phi(x, \mathbb{C})f(\mathbb{C}) \\
&\stackrel{1.15, 1.37}{=} \begin{bmatrix} m[\tilde{v}(\mathbb{C}) - \tilde{v}(x)]v(\mathbb{C}) \\ \mathbf{0} \end{bmatrix} + f(x) = \begin{bmatrix} m\tilde{v}(\mathbb{C})v(x) \\ \mathbf{0} \end{bmatrix} + f(x) \\
&= -\bar{\mathcal{V}}^v(x)\mathfrak{h}(\mathbb{C}) + f(x)
\end{aligned} \tag{C.3}$$

The $\bar{\mathcal{V}}^v(x)\mathfrak{h}(\mathbb{C})$ quantity vanishes if and only if either: (a) the point x coincides with \mathbb{C} ; (b) $v(\mathbb{C})$ or $v(x)$ is zero, i.e., the body is spinning about the $\mathbf{l}(x, \mathbb{C})$ vector. This establishes (2.27).

Solution 2.11 (pp. 30): Equations of motion using spatial momentum

We have

$$\begin{aligned}\frac{d_{\mathbb{B}}\mathfrak{h}(x)}{dt} &\stackrel{1.28}{=} \bar{\mathcal{V}}^{\omega}(x)\mathfrak{h}(x) + \frac{d_{\mathbb{B}}\mathfrak{h}(x)}{dt} = \bar{\mathcal{V}}^{\omega}(x)\mathfrak{h}(x) + \frac{d_{\mathbb{B}}M(x)\beta_{\mathbb{B}}(x)}{dt} \\ &= \bar{\mathcal{V}}^{\omega}(x)\mathfrak{h}(x) + M(x)\dot{\beta}_{\mathbb{B}}(x)\end{aligned}$$

Combining this with (C.3) leads to

$$\mathfrak{f}(x) = M(x)\dot{\beta}_{\mathbb{B}}(x) + \left[\bar{\mathcal{V}}^{\omega}(x) + \bar{\mathcal{V}}^v(x) \right] \mathfrak{h}(x) \stackrel{1.22}{=} M(x)\dot{\beta}_{\mathbb{B}}(x) + \bar{\mathcal{V}}(x)\mathfrak{h}(x)$$

This agrees with (2.28) and establishes the result.

Solution 2.12 (pp. 32): Invariance of $\mathcal{V}_{\mathbb{I}}$ to velocity reference point

Now

$$\phi^*(x, \mathbb{I})\mathcal{V}(x) \stackrel{1.33}{=} \phi^*(x, \mathbb{I})\phi^*(\mathbb{C}, x)\mathcal{V}(\mathbb{C}) \stackrel{1.32}{=} \phi^*(\mathbb{C}, \mathbb{I})\mathcal{V}(\mathbb{C}) \stackrel{2.30}{=} \mathcal{V}_{\mathbb{I}}$$

establishing (2.31).

Solution 2.13 (pp. 32): Time derivative of $M_{\mathbb{I}}$

Differentiating (2.32) we have

$$\begin{aligned}\frac{d_{\mathbb{I}}M_{\mathbb{I}}}{dt} &\stackrel{2.32}{=} \phi(\mathbb{I}, \mathbb{C})\frac{d_{\mathbb{I}}M(\mathbb{C})}{dt}\phi^*(\mathbb{I}, \mathbb{C}) + \frac{d_{\mathbb{I}}\phi(\mathbb{I}, \mathbb{C})}{dt}M(\mathbb{C})\phi^*(\mathbb{I}, \mathbb{C}) \\ &\quad + \phi(\mathbb{I}, \mathbb{C})M_{\mathbb{I}}\frac{d_{\mathbb{I}}\phi^*(\mathbb{I}, \mathbb{C})}{dt} \\ &\stackrel{2.22, 1.37}{=} \phi(\mathbb{I}, \mathbb{C})\left[\bar{\mathcal{V}}^{\omega}M(\mathbb{C}) - M(\mathbb{C})\tilde{\mathcal{V}}^{\omega}\right]\phi^*(\mathbb{I}, \mathbb{C}) \\ &\quad + \bar{\mathcal{V}}^v(\mathbb{C})M(\mathbb{C})\phi^*(\mathbb{I}, \mathbb{C}) - \phi(\mathbb{I}, \mathbb{C})M(\mathbb{C})\tilde{\mathcal{V}}^v(\mathbb{C})\end{aligned}\tag{C.4}$$

However, from (1.36) we have

$$\bar{\mathcal{V}}^v(\mathbb{C}) = \phi(\mathbb{I}, \mathbb{C})\bar{\mathcal{V}}^v(\mathbb{C})$$

and obtain

$$\begin{aligned}
 \frac{d_{\mathbb{I}} M_{\mathbb{I}}}{dt} &\stackrel{\text{C.4}}{=} \phi(\mathbb{I}, \mathbb{C}) \left[\bar{\mathcal{V}}^v(\mathbb{C}) + \bar{\mathcal{V}}^\omega(\mathbb{C}) \right] M(\mathbb{C}) \phi^*(\mathbb{I}, \mathbb{C}) \\
 &\quad - \phi(\mathbb{I}, \mathbb{C}) M(\mathbb{C}) \left[\tilde{\mathcal{V}}^v(\mathbb{C}) + \tilde{\mathcal{V}}^\omega(\mathbb{C}) \right] \phi^*(\mathbb{I}, \mathbb{C}) \\
 &\stackrel{1.25}{=} \phi(\mathbb{I}, \mathbb{C}) \bar{\mathcal{V}}(\mathbb{C}) M(\mathbb{C}) \phi^*(\mathbb{I}, \mathbb{C}) - \phi(\mathbb{I}, \mathbb{C}) M(\mathbb{C}) \tilde{\mathcal{V}}(\mathbb{C}) \phi^*(\mathbb{I}, \mathbb{C}) \\
 &\stackrel{1.35, 2.30}{=} \bar{\mathcal{V}}_{\mathbb{I}} \phi(\mathbb{I}, \mathbb{C}) M(\mathbb{C}) \phi^*(\mathbb{I}, \mathbb{C}) - \phi(\mathbb{I}, \mathbb{C}) M(\mathbb{C}) \phi^*(\mathbb{I}, \mathbb{C}) \tilde{\mathcal{V}}_{\mathbb{I}} \\
 &\stackrel{2.32}{=} \bar{\mathcal{V}}_{\mathbb{I}} M_{\mathbb{I}} - M_{\mathbb{I}} \tilde{\mathcal{V}}_{\mathbb{I}}
 \end{aligned}$$

Solution 2.14 (pp. 33): Equations of motion about a fixed velocity reference point

1. We have

$$\begin{aligned}
 \frac{d_{\mathbb{I}} \mathfrak{h}_{\mathbb{I}}}{dt} &\stackrel{2.34}{=} \frac{d_{\mathbb{I}} \phi(\mathbb{I}, \mathbb{C})}{dt} \mathfrak{h}(\mathbb{C}) + \phi(\mathbb{I}, \mathbb{C}) \frac{d_{\mathbb{I}} \mathfrak{h}(\mathbb{C})}{dt} \\
 &\stackrel{2.21, 1.37}{=} \bar{\mathcal{V}}^v(\mathbb{C}) \mathfrak{h}(\mathbb{C}) + \phi(\mathbb{I}, \mathbb{C}) \mathfrak{f}(\mathbb{C}) \stackrel{2.35}{=} \mathbf{0} + \mathfrak{f}_{\mathbb{I}} = \mathfrak{f}_{\mathbb{I}}
 \end{aligned}$$

The last equality above used the $\bar{\mathcal{V}}^v(\mathbb{C}) \mathfrak{h}(\mathbb{C}) = \mathbf{0}$ identity.

2. From (2.36) we have

$$\mathfrak{f}_{\mathbb{I}} \stackrel{2.36}{=} \frac{d_{\mathbb{I}} \mathfrak{h}_{\mathbb{I}}}{dt} \stackrel{2.34}{=} M_{\mathbb{I}} \dot{\beta}_{\mathbb{I}} + \frac{d_{\mathbb{I}} M_{\mathbb{I}}}{dt} \mathcal{V}_{\mathbb{I}} \stackrel{2.33}{=} M_{\mathbb{I}} \dot{\beta}_{\mathbb{I}} - \bar{\mathcal{V}}_{\mathbb{I}} M_{\mathbb{I}} \mathcal{V}_{\mathbb{I}}$$

3. We can verify that $\mathfrak{b}_{\mathbb{I}}$ is non-working by taking its dot product with $\mathcal{V}_{\mathbb{I}}$ and noting that $\mathcal{V}_{\mathbb{I}}^* \bar{\mathcal{V}}_{\mathbb{I}} = \mathbf{0}$. Recognizing that the kinetic energy can also be written as $\frac{1}{2} \beta_{\mathbb{I}}^* M_{\mathbb{I}} \beta_{\mathbb{I}}$ and differentiating it with respect to time leads to the conclusion that it is conserved in the absence of external forces.

Solutions for Chapter 3

Solution 3.1 (pp. 41): Hinge map matrix for a universal joint

The orientation of the second axis in a universal joint depends on the general coordinate of the first axis. The hinge map matrix for the universal joint is

$$H^* = \begin{pmatrix} 1 & 0 \\ 0 & \cos \theta_1 \\ 0 & \sin \theta_1 \\ 0 & 0 \\ 0 & 0 \\ 0 & 0 \end{pmatrix}$$

Solution 3.2 (pp. 41): Hinge map matrix for a sphere rolling on a surface

Let Δ_v denote the spatial velocity of the frame fixed to the center of the sphere. Also, let \tilde{l} denote the vector from the center of the sphere to the instantaneous point of contact. The orientation of this vector is constant in the inertial frame but is changing in the body frame. The zero linear velocity of the contact point translates to the following constraint expression:

$$\Delta_v + \widetilde{\Delta_\omega}l = \mathbf{0} \Rightarrow \begin{bmatrix} -\tilde{l}, & I_3 \end{bmatrix} \Delta_v = \mathbf{0}_3 \quad \text{where} \quad \Delta_v \triangleq \begin{bmatrix} \Delta_\omega \\ \Delta_v \end{bmatrix}$$

where Δ_ω and Δ_v are the angular and linear velocity components of Δ_v at the center of the sphere. This implicit 3-dimensional constraint implies that Δ_v must be of the following form:

$$\Delta_v = \begin{bmatrix} I_3 \\ \tilde{l} \end{bmatrix} \beta$$

where $\beta \in \mathcal{R}^3$ is the vector of generalized velocities for this contact hinge. Thus, with $\beta = \Delta_\omega$ as the generalized velocity coordinates, the hinge map matrix for the rolling contact is given by

$$H^* = \begin{bmatrix} I_3 \\ \tilde{l} \end{bmatrix} \in \mathcal{R}^{6 \times 3}$$

Solution 3.3 (pp. 46): Velocity recursion with $B_k \neq O_k$

In this context, the recursion in (3.19b) can be more precisely expressed as:

$$V(O_k) = \phi^*(O_{k+1}, O_k)V(O_{k+1}) + H^*(k)\dot{\theta}(k)$$

Now use the following versions of (3.20) and (3.23) in the equation above to establish the result:

$$V(k) \triangleq V(B_k) = \phi^*(O_k, B_k)V(O_k)$$

$$\text{and } V(k+1) \triangleq V(B_{k+1}) = \phi^*(O_{k+1}, B_{k+1})V(O_{k+1})$$

Solution 3.4 (pp. 47): Velocity recursion with inertially fixed reference point

We have

$$\begin{aligned} V_I(k) &\stackrel{3.24}{=} \phi^*(O_k, I)V(O_k) \\ &\stackrel{3.19b}{=} \phi^*(O_k, I)\{\phi^*(O_{k+1}, O_k)V(O_{k+1}) + H^*(k)\beta(k)\} \end{aligned}$$

$$\begin{aligned} &\stackrel{3.24}{=} \phi^*(\mathcal{O}_k, \mathbb{I}) \{ \phi^*(\mathcal{O}_{k+1}, \mathcal{O}_k) \phi^*(\mathcal{O}_{k+1}, \mathbb{I}) \mathcal{V}_{\mathbb{I}}((k+1)) + H^*(k) \beta(k) \} \\ &\stackrel{3.25}{=} \mathcal{V}_{\mathbb{I}}(k+1) + H_{\mathbb{I}}^*(k) \beta(k) \stackrel{3.25}{=} \mathcal{V}_{\mathbb{I}}(k+1) + \Delta_{\mathcal{V}}^{\mathbb{I}}(k) \beta(k) \end{aligned}$$

establishing (3.26).

Solution 3.5 (pp. 50): Internal structure of the ϕ operator

Since $(\mathbf{I} - \mathcal{E}_{\phi})$ is lower-triangular, and has identity matrices along the diagonal, the same holds true for its inverse, ϕ , as well establishing (3.37). Now, let us examine the lower-triangular component elements of the matrices on both sides of the operator identity:

$$\phi - \mathcal{E}_{\phi} \phi = \mathbf{I}$$

This identity implies that for $i > j$,

$$\phi(i, j) - \phi(i, i-1)\phi(i-1, j) = \mathbf{0} \Rightarrow \phi(i, j) = \phi(i, i-1)\phi(i-1, j)$$

Applying this next to $\phi(i-1, j)$, and continuing on in this vein, leads to the first half of (3.38). Since the product of a sequence of rigid body transformation matrices is also a rigid body transformation matrix, the latter equality in (3.38) follows as well.

Solution 3.6 (pp. 51): The $\tilde{\phi}$ spatial operator

- For a matrix A such that $(\mathbf{I} - A)$ is invertible, (A.17) on page 400 states that:

$$A(\mathbf{I} - A)^{-1} = (\mathbf{I} - A)^{-1}A = (\mathbf{I} - A)^{-1} - \mathbf{I}$$

(3.41) is a consequence of this identity with $A = \mathcal{E}_{\phi}$ and $\phi = (\mathbf{I} - \mathcal{E}_{\phi})^{-1}$.

- From (3.15) it follows that

$$\mathcal{V}^+ \stackrel{3.15}{=} \mathcal{E}_{\phi}^* \mathcal{V} \stackrel{3.39}{=} \mathcal{E}_{\phi}^* \phi^* H^* \dot{\theta} \stackrel{3.41}{=} \tilde{\phi}^* H^* \dot{\theta}$$

Solution 3.7 (pp. 53): Recursive evaluation of $\tilde{\phi}x$ and $\tilde{\phi}^*x$

With $y = \phi x$, we have $\bar{y} \stackrel{\triangle}{=} \tilde{\phi}x = \mathcal{E}_{\phi}y$. This implies that $\bar{y}(k) = \phi(k, k-1)y(k)$. Thus, the computational algorithm for \bar{y} is the one in (3.43) except that the computational step in the loop is now given by

$$\bar{y}(k) = \phi(k, k-1)[\bar{y}(k-1) + x(k-1)]$$

with initial condition $\bar{y}(0) = 0$.

Similarly, with $y = \phi^*x$, we have $\bar{y} \stackrel{\triangle}{=} \tilde{\phi}^*x = \mathcal{E}_{\phi}^*y$. Thus,

$$\bar{y}(k) = \phi^*(k+1, k)y(k+1)$$

Thus, the computational algorithm for \bar{y} is the same as in (3.45) except that the computational step within the loop has the form:

$$\bar{y}(k) = \phi^*(k+1, k)[\bar{y}(k+1) + x(k+1)]$$

with initial condition $\bar{y}(n+1) = 0$.

Solutions for Chapter 4

Solution 4.1 (pp. 63): System center of mass

1. The overall spatial inertia of the system referenced to the base-body frame is obtained by using the parallel axis theorem for spatial inertias to reference all the link spatial inertias to \mathbb{B}_n and summing them up. That is,

$$\begin{aligned} M_S &= \sum_{k=1}^n \phi(n, k) M(k) \phi^*(n, k) \stackrel{4.4}{=} [\phi(n, 1), \dots, \phi(n, n)] \mathbf{M} \begin{bmatrix} \phi^*(n, 1) \\ \vdots \\ \phi^*(n, n) \end{bmatrix} \\ &\stackrel{3.37}{=} E \phi \mathbf{M} \phi^* E^* \stackrel{4.10}{=} E [\mathcal{R} + \tilde{\phi} \mathcal{R} + \mathcal{R} \tilde{\phi}^*] E^* = E \mathcal{R} E^* = \mathcal{R}(n) \end{aligned}$$

establishing the result. We have used the following facts in the above derivation:

$$E \phi \stackrel{3.37}{=} [\phi(n, 1), \dots, \phi(n, n)] \quad \text{and} \quad \tilde{\phi} \mathcal{R} E^* = \mathbf{0} \quad (\text{C.5})$$

2. The base-body frame referenced spatial momentum of the system is obtained by referencing the spatial momentum for each of the bodies to the \mathbb{B}_n frame and summing them up. This leads to:

$$\begin{aligned} h_S &\stackrel{2.17}{=} \sum_{k=1}^n \phi(n, k) h(k) \stackrel{2.16}{=} \sum_{k=1}^n \phi(n, k) M(k) \mathcal{V}(k) \stackrel{C.5}{=} E \phi \mathbf{M} \mathcal{V} \\ &\stackrel{3.39}{=} E \phi \mathbf{M} \phi^* H^* \dot{\theta} \stackrel{4.10}{=} E [\mathcal{R} + \tilde{\phi} \mathcal{R} + \mathcal{R} \tilde{\phi}^*] H^* \dot{\theta} \stackrel{C.5}{=} E \phi \mathcal{R} H^* \dot{\theta} \end{aligned}$$

For a free flying system, $H^*(n) = I$ and $\dot{\theta}(n) = \mathcal{V}(n)$, and hence h_S can be re-expressed as

$$h_S = \mathcal{R}(n) \mathcal{V}(n) + \sum_{k=1}^{n-1} \phi(n, k) \mathcal{R}(k) H^*(k) \dot{\theta}(k)$$

3. The system level spatial momentum h_S , the system level spatial inertia M_S and the center of mass velocity \mathcal{V}_C (referenced about \mathbb{B}_n) are related together by

$$\mathfrak{h}_S = M_S \mathcal{V}_{\mathbb{C}} \stackrel{4.13}{=} \mathcal{R}(n) \mathcal{V}_{\mathbb{C}} \quad (C.6)$$

4. For a free-flying system, we have,

$$\begin{aligned} \mathcal{V}_{\mathbb{C}} &\stackrel{4.16}{=} \mathcal{R}^{-1}(n) \left[\mathcal{R}(n) \mathcal{V}(n) + \sum_{k=1}^{n-1} \phi(n, k) \mathcal{R}(k) H^*(k) \dot{\theta}(k) \right] \\ &= \mathcal{V}(n) + \mathcal{R}^{-1}(n) \sum_{k=1}^{n-1} \phi(n, k) \mathcal{R}(k) H^*(k) \dot{\theta}(k) \end{aligned}$$

establishing (4.18).

From (4.16) it follows directly that adding δ_V to the $\mathcal{V}(n)$ base-body spatial velocity will result in an additional $\mathcal{R}(n)\delta_V$ of spatial momentum system to the system. Now for the spatial momentum to be zero, we must have

$$0 = \mathfrak{h}_S + \mathcal{R}(n)\delta_V \implies \delta_V = -\mathcal{R}^{-1}(n)\mathfrak{h}_S \stackrel{C.6}{=} -\mathcal{V}_{\mathbb{C}}$$

Solution 4.2 (pp. 65): Trace of the mass matrix

From the decomposition of the mass matrix in (4.19), and noting that the trace of strictly lower- and upper-triangular matrices is zero, we have

$$\begin{aligned} \text{Trace}\{\mathcal{M}(\theta)\} &\stackrel{4.19}{=} \text{Trace}\{H\mathcal{R}H^* + H\tilde{\phi}\mathcal{R}H^* + H\mathcal{R}\tilde{\phi}^*H^*\} \\ &= \text{Trace}\{H\mathcal{R}H^*\} = \sum_{i=1}^n \text{Trace}\{H(k)\mathcal{R}(k)H^*(k)\} \end{aligned}$$

In the above we have used the zero trace property of $H\tilde{\phi}\mathcal{R}H^*$ which is a consequence of its strictly lower-triangular structure.

Solution 4.3 (pp. 68): The $M_D(\theta, \dot{\theta})$ matrix

1. We have

$$\begin{aligned} M_D^* \dot{\theta} &\stackrel{4.29}{=} [\nabla_{\theta}(\mathcal{M}\dot{\theta})]^* \dot{\theta} \stackrel{A.24}{=} \left[\frac{\partial \mathcal{M}\dot{\theta}}{\partial \theta(1)}, \dots, \frac{\partial \mathcal{M}\dot{\theta}}{\partial \theta(n)} \right]^* \dot{\theta} \\ &= \begin{bmatrix} \frac{\partial \dot{\theta}^* \mathcal{M}}{\partial \theta(1)} \\ \vdots \\ \frac{\partial \dot{\theta}^* \mathcal{M}}{\partial \theta(n)} \end{bmatrix} \dot{\theta} = \begin{bmatrix} \frac{\partial \dot{\theta}^* \mathcal{M}\dot{\theta}}{\partial \theta(1)} \\ \vdots \\ \frac{\partial \dot{\theta}^* \mathcal{M}\dot{\theta}}{\partial \theta(n)} \end{bmatrix} \stackrel{A.27}{=} \frac{\partial}{\partial \theta} (\dot{\theta}^* \mathcal{M}\dot{\theta}) \end{aligned}$$

2.

$$\begin{aligned} M_D(\theta, \dot{\theta})\dot{\theta} &\stackrel{4.29}{=} \left[\frac{\partial M_D}{\partial \theta(1)}, \dots, \frac{\partial M_D}{\partial \theta(N)} \right]^* \dot{\theta} = \sum_{k=1}^N \frac{\partial M_D}{\partial \theta(k)} \dot{\theta}(k) \\ &= \left[\sum_{k=1}^N \frac{\partial M_D}{\partial \theta(k)} \dot{\theta}(k) \right] \dot{\theta} = \dot{M}(\theta)\dot{\theta} \end{aligned}$$

Solution 4.4 (pp. 68): $\dot{M}\dot{\theta} - 2\mathcal{C}$ is a non-working force

1. Equation (4.33) follows from combining (4.31) and (4.32).
2. The work done by a generalized force is given by its dot product with the $\dot{\theta}$ generalized velocities vector. Thus, the work done by $\dot{M}\dot{\theta} - 2\mathcal{C}$ is given by

$$\dot{\theta}^* [\dot{M}\dot{\theta} - 2\mathcal{C}] \stackrel{4.33}{=} \dot{\theta}^* (M_D^* - M_D)\dot{\theta} = \mathbf{0}$$

The last equality follows since $(M_D^* - M_D)$ is skew-symmetric.

3. The work done by the \mathcal{C} Coriolis generalized forces vector is given by

$$\dot{\theta}^* \mathcal{C}(\theta, \dot{\theta}) \stackrel{4.32}{=} \dot{\theta}^* \left[M_D - \frac{1}{2} M_D^* \right] \dot{\theta} = \frac{1}{2} \dot{\theta}^* M_D \dot{\theta}$$

Since M_D is not skew-symmetric, the work done by \mathcal{C} is non-zero in general.

Solution 4.5 (pp. 68): Rate of change of the kinetic energy

$$\begin{aligned} \frac{dK_e}{dt} &\stackrel{4.25}{=} \dot{\theta}^* M \dot{\theta} + \frac{1}{2} \dot{\theta}^* \dot{M} \dot{\theta} \stackrel{4.26, 4.31}{=} \dot{\theta}^* \left[(\mathcal{T} - \mathcal{C}) + \frac{1}{2} M_D \dot{\theta} \right] \\ &\stackrel{4.32}{=} \dot{\theta}^* \left[\mathcal{T} - (M_D - \frac{1}{2} M_D^*) \dot{\theta} + \frac{1}{2} M_D \dot{\theta} \right] \stackrel{4.32}{=} \dot{\theta}^* \left[\mathcal{T} - \frac{1}{2} (M_D - M_D^*) \dot{\theta} \right] = \dot{\theta}^* \mathcal{T} \end{aligned}$$

The last step follows since $(M_D - M_D^*)$ is skew-symmetric.

Solution 4.6 (pp. 69): Christoffel symbols of the first kind

1. The identities in (4.36) follow from simply comparing the definitions of $\mathfrak{C}_i(j, k)$, $\mathfrak{C}_i(k, j)$ and $\mathfrak{C}_i(i, k)$.
For (4.37),

$$\mathfrak{C}_j(i, k) + \mathfrak{C}_k(j, i) \stackrel{4.35}{=} \frac{1}{2} \left[\frac{\partial \mathcal{M}(i, j)}{\partial \theta(k)} + \frac{\partial \mathcal{M}(j, k)}{\partial \theta(i)} - \frac{\partial \mathcal{M}(i, k)}{\partial \theta(j)} \right] \\ + \frac{1}{2} \left[\frac{\partial \mathcal{M}(k, j)}{\partial \theta(i)} + \frac{\partial \mathcal{M}(k, i)}{\partial \theta(j)} - \frac{\partial \mathcal{M}(j, i)}{\partial \theta(k)} \right]$$

When the mass matrix is symmetric, the above expression simplifies to $\frac{\partial \mathcal{M}(k, j)}{\partial \theta(i)}$.

2. For multibody systems, the mass matrix is symmetric, and also $\frac{\partial \mathcal{M}(i, k)}{\partial \theta(j)} = 0$ for $j \geq i, k$ as discussed in Remark 4.1. Using these properties in the definition of the left- and right-hand sides of the identities in (4.38) establishes the identities. Moreover, since $\mathfrak{C}_i(j, k)$ depends only upon $\mathcal{M}(i, j)$, $\mathcal{M}(i, k)$ and $\mathcal{M}(j, k)$, and these terms depend only upon $\theta(l)$ for $l < \max(i, j, k)$, this implies that $\mathfrak{C}_i(j, k)$ depends only upon $\theta(l)$ for $l < \max(i, j, k)$.

3. We have

$$\begin{aligned} \mathfrak{C}(i) \stackrel{4.27}{=} & \left\{ \dot{\mathcal{M}}(\theta) \dot{\theta} - \frac{1}{2} \frac{\partial}{\partial \theta} [\dot{\theta}^* \mathcal{M}(\theta) \dot{\theta}] \right\} (i) = \sum_{k=1}^N \dot{\mathcal{M}}(i, k) \dot{\theta}(k) - \frac{1}{2} \dot{\theta} \frac{\partial \mathcal{M}}{\partial \theta(i)} \dot{\theta} \\ = & \sum_{j, k=1}^N \frac{\partial \mathcal{M}(i, k)}{\partial \theta(j)} \dot{\theta}(j) \dot{\theta}(k) - \frac{1}{2} \sum_{j, k=1}^N \frac{\partial \mathcal{M}(j, k)}{\partial \theta(i)} \dot{\theta}(j) \dot{\theta}(k) \\ = & \sum_{j, k=1}^N \left[\frac{\partial \mathcal{M}(i, k)}{\partial \theta(j)} - \frac{1}{2} \frac{\partial \mathcal{M}(j, k)}{\partial \theta(i)} \right] \dot{\theta}(j) \dot{\theta}(k) \\ = & \sum_{j, k=1}^N \frac{1}{2} \left[\frac{\partial \mathcal{M}(i, k)}{\partial \theta(j)} + \frac{\partial \mathcal{M}(i, j)}{\partial \theta(k)} - \frac{1}{2} \frac{\partial \mathcal{M}(j, k)}{\partial \theta(i)} \right] \dot{\theta}(j) \dot{\theta}(k) \\ \stackrel{4.35}{=} & \sum_{j, k=1}^N \mathfrak{C}_i(j, k) \dot{\theta}(j) \dot{\theta}(k) = \dot{\theta}^* \mathfrak{C}_i \dot{\theta} \end{aligned}$$

4. We have

$$M_D(i, j) \stackrel{4.29}{=} \frac{\partial [\mathcal{M} \dot{\theta}](i)}{\partial \theta(j)} = \sum_{k=1}^N \frac{\partial \mathcal{M}(i, k)}{\partial \theta(j)} \dot{\theta}(k) \stackrel{4.37}{=} \sum_{k=1}^N [\mathfrak{C}_i(j, k) + \mathfrak{C}_k(j, i)] \dot{\theta}(k)$$

Solution 4.7 (pp. 70): Hamiltonian form of the equations of motion

We have

$$\frac{\partial \mathcal{H}}{\partial p} \stackrel{4.42}{=} \mathcal{M}^{-1} p \stackrel{4.28}{=} \dot{\theta}$$

This establishes the first expression in (4.43). Also,

$$\begin{aligned}\frac{\partial \mathcal{H}}{\partial \theta} &\stackrel{4.42}{=} \frac{1}{2} \text{col} \left\{ \mathfrak{p}^* \frac{\partial \mathcal{M}^{-1}}{\partial \theta(k)} \mathfrak{p} \right\}_{k=1}^N \stackrel{4.42, A.28}{=} -\frac{1}{2} \text{col} \left\{ \mathfrak{p}^* \mathcal{M}^{-1} \frac{\partial \mathcal{M}}{\partial \theta(k)} \mathcal{M}^{-1} \mathfrak{p} \right\}_{k=1}^N \\ &\stackrel{4.28}{=} -\frac{1}{2} \text{col} \left\{ \frac{\partial \dot{\theta}^* \mathcal{M} \dot{\theta}}{\partial \theta(k)} \right\}_{k=1}^N \stackrel{4.28}{=} -\frac{1}{2} \frac{\partial \dot{\theta}^* \mathcal{M} \dot{\theta}}{\partial \theta} \stackrel{4.27}{=} -\dot{\mathcal{M}} \dot{\theta} + \mathcal{C} \\ &\stackrel{4.28}{=} -\dot{\mathfrak{p}} + \mathcal{M} \ddot{\theta} + \mathcal{C} \stackrel{4.24}{=} -\dot{\mathfrak{p}} + \mathcal{T}\end{aligned}$$

This establishes the latter expression in (4.43).

Solution 4.8 (pp. 71): Lagrangian equations of motion using quasi-velocities

We have

$$\frac{\partial \mathcal{L}}{\partial \dot{\theta}} \stackrel{A.27}{=} [\nabla_{\dot{\theta}} \mathcal{L}]^* \stackrel{A.26}{=} [\nabla_{\beta} \dot{\mathcal{L}} \cdot \nabla_{\dot{\theta}} \beta]^* = [\nabla_{\beta} \dot{\mathcal{L}} \cdot \mathbf{A}]^* \stackrel{A.27}{=} \mathbf{A}^*(\theta) \frac{\partial \dot{\mathcal{L}}}{\partial \beta} \quad (\text{C.7})$$

Therefore, differentiating this with respect to t we have

$$\frac{d}{dt} \frac{\partial \mathcal{L}}{\partial \dot{\theta}} \stackrel{C.7}{=} \mathbf{A}^* \left[\frac{d}{dt} \frac{\partial \dot{\mathcal{L}}}{\partial \beta} \right] + \dot{\mathbf{A}}^* \frac{\partial \dot{\mathcal{L}}}{\partial \beta} \quad (\text{C.8})$$

Similarly,

$$\frac{\partial \mathcal{L}}{\partial \theta} \stackrel{A.27}{=} [\nabla_{\theta} \mathcal{L}]^* \stackrel{A.26}{=} [\nabla_{\beta} \dot{\mathcal{L}} \cdot \nabla_{\theta} \beta + \nabla_{\theta} \dot{\mathcal{L}}]^* \stackrel{A.27}{=} \frac{\partial \beta}{\partial \theta} \frac{\partial \dot{\mathcal{L}}}{\partial \beta} + \frac{\partial \dot{\mathcal{L}}}{\partial \theta} \quad (\text{C.9})$$

Combining (C.8) and (C.9) it follows that

$$\begin{aligned}\mathcal{T} &\stackrel{4.24}{=} \frac{d}{dt} \frac{\partial \mathcal{L}}{\partial \dot{\theta}} - \frac{\partial \mathcal{L}}{\partial \theta} = \mathbf{A}^* \left[\frac{d}{dt} \frac{\partial \dot{\mathcal{L}}}{\partial \beta} \right] - \frac{\partial \dot{\mathcal{L}}}{\partial \theta} + \left[\dot{\mathbf{A}}^* - \frac{\partial \beta}{\partial \theta} \right] \frac{\partial \dot{\mathcal{L}}}{\partial \beta} \\ &= \mathbf{A}^* \left[\frac{d}{dt} \frac{\partial \dot{\mathcal{L}}}{\partial \beta} \right] - \frac{\partial \dot{\mathcal{L}}}{\partial \theta} + \gamma^* \frac{\partial \dot{\mathcal{L}}}{\partial \beta}\end{aligned}$$

and therefore

$$\mathbf{A}^{-*} \mathcal{T} = \left[\frac{d}{dt} \frac{\partial \dot{\mathcal{L}}}{\partial \beta} \right] - \mathbf{A}^{-*} \frac{\partial \dot{\mathcal{L}}}{\partial \theta} + \mathbf{A}^{-*} \gamma^* \frac{\partial \dot{\mathcal{L}}}{\partial \beta}$$

establishing (4.44). Now observe that

$$\dot{\mathbf{A}}(\theta) = \sum_{i=1}^n \frac{\partial \mathbf{A}}{\partial \theta(k)} \dot{\theta}(k) \quad \text{and} \quad \frac{\partial \beta}{\partial \theta} = \frac{\partial \mathbf{A} \dot{\theta}}{\partial \theta} \quad (\text{C.10})$$

Thus,

$$\begin{aligned}\gamma(i,j) &= \dot{A}(i,j) - \frac{\partial \beta(i)}{\partial \theta(j)} = \sum_{k=1}^n \frac{\partial A(i,j)}{\partial \theta(k)} \dot{\theta}(k) - \frac{\partial \sum_{k=1}^n A(i,k) \dot{\theta}(k)}{\partial \theta(j)} \\ &= \sum_{k=1}^n \left(\frac{\partial A(i,j)}{\partial \theta(k)} - \frac{\partial A(i,k)}{\partial \theta(j)} \right) \dot{\theta}(k)\end{aligned}$$

This establishes (4.46).

Solution 4.9 (pp. 72): Lagrangian equations of motion under coordinate transformations

Since $\eta = h(\theta)$, therefore

$$\dot{\eta} = A(\theta) \dot{\theta}$$

Thus, $A(i,j) = \frac{\partial h(i)}{\partial \theta(j)}$ and

$$\frac{\partial A(i,j)}{\partial \theta(k)} = \frac{\partial A(i,k)}{\partial \theta(j)} = \frac{\partial^2 h(i)}{\partial \theta(j) \partial \theta(k)}$$

Therefore, the (4.46) expression for the $\gamma(i,j)$ elements are zero. Hence, $\gamma = \mathbf{0}$.

Solution 4.10 (pp. 72): Non-working $\dot{\underline{M}}\beta - 2\underline{C}$ generalized force

We have

$$\begin{aligned}\beta^* A^{-*} \frac{\partial \dot{\mathcal{L}}}{\partial \theta} &= \dot{\theta}^* \frac{\partial \dot{\mathcal{L}}}{\partial \theta} = \frac{1}{2} \dot{\theta}^* [\nabla_\theta \beta^* \underline{M}(\theta) \beta]^* = \frac{1}{2} [\nabla_\theta \beta^* \underline{M}(\theta) \beta] \dot{\theta} \\ &= \frac{1}{2} \beta^* \dot{\underline{M}}(\theta) \beta\end{aligned}\tag{C.11}$$

Also,

$$\gamma A^{-1} \beta = \gamma \dot{\theta} \stackrel{4.48}{=} \mathbf{0}\tag{C.12}$$

Therefore

$$\begin{aligned}\beta^* (\dot{\underline{M}}\beta - 2\underline{C}) &\stackrel{4.50}{=} \beta^* \left(-\dot{\underline{M}}\beta + 2A^{-*} \frac{\partial \dot{\mathcal{L}}}{\partial \theta} - 2A^{-*} \gamma^* \frac{\partial \dot{\mathcal{L}}}{\partial \beta} \right) \\ &\stackrel{C.11,C.12}{=} -\beta^* \dot{\underline{M}}\beta + \beta^* \dot{\underline{M}}\beta - 0 = 0\end{aligned}$$

Solution 4.11 (pp. 73): Nonlinear diagonalizing coordinate transformations

- (4.49) on page 72 describes the effect of a coordinate transformation upon the Lagrangian equations of motion which in the $(\eta, \dot{\eta})$ coordinates are given by

$$\frac{d}{dt} \frac{\partial \tilde{\mathcal{L}}}{\partial \dot{\eta}} - \frac{\partial \tilde{\mathcal{L}}}{\partial \eta} = A^{-*} \mathcal{T} \quad (\text{C.13})$$

Since $\mathcal{M}(\theta) = A^*(\theta)A(\theta)$, this means that

$$\kappa_e = \mathcal{L}(\theta, \dot{\theta}) = \tilde{\mathcal{L}}(\eta, \dot{\eta}) = \frac{1}{2} \dot{\eta}^* \dot{\eta} \quad \text{and} \quad \frac{\partial \tilde{\mathcal{L}}}{\partial \eta} = \mathbf{0} \quad (\text{C.14})$$

Using these in (C.13) leads to

$$\ddot{\eta} = A^{-*} \mathcal{T} = \zeta$$

establishing (4.51).

- This time

$$\kappa_e = \tilde{\mathcal{L}}(\theta, \beta) = \frac{1}{2} \beta^* \beta \quad \text{and} \quad \frac{\partial \tilde{\mathcal{L}}}{\partial \theta} = \mathbf{0} \quad (\text{C.15})$$

Since β are now quasi-velocities, the appropriate Lagrangian equations of motion are those in (4.44) and using (C.15) take the form:

$$\dot{\beta} - A^{-*} \gamma^* \beta = \zeta$$

and the result follows.

- From Exercise 4.10 we have

$$0 = \beta^* (\dot{\mathcal{M}}\beta - 2\mathcal{C}) = -2\beta^* \mathcal{C}$$

The above uses the fact that \mathcal{M} is the constant identity matrix. This implies that the $\mathcal{C}(\theta, \beta)$ Coriolis forces vector do no work.

Solutions for Chapter 5

Solution 5.1 (pp. 79): $\alpha(k)$ for helical & cylindrical hinges

The hinge map matrix for a helical hinge with axis $h_\omega(k)$ and pitch p has the form

$$H^*(k) = \begin{bmatrix} h_\omega(k) \\ ph_\omega(k) \end{bmatrix} \implies \Delta_V(k) = \begin{bmatrix} \Delta_\omega(k) \\ p\Delta_\omega(k) \end{bmatrix}$$

Thus,

$$\alpha(k) \stackrel{5.12}{=} - \begin{bmatrix} \tilde{\Delta}_\omega(k)\omega(k) \\ \tilde{\Delta}_\omega(k)\{v(k) + p\omega(k)\} \end{bmatrix}$$

For a cylindrical hinge with axis $h_\omega(k)$, the axis of rotation and translation are the same. For this case

$$H^*(k) = \begin{pmatrix} h_\omega(k) & \mathbf{0} \\ \mathbf{0} & h_\omega(k) \end{pmatrix} \implies \Delta_v(k) = \begin{bmatrix} \Delta_\omega(k) \\ \Delta_v(k) \end{bmatrix} = \begin{bmatrix} h_\omega(k)\dot{\theta}_1(k) \\ h_\omega(k)\dot{\theta}_2(k) \end{bmatrix}$$

Thus,

$$\alpha(k) \stackrel{5.15}{=} - \begin{bmatrix} \tilde{\Delta}_\omega(k)\omega(k) \\ \tilde{\Delta}_\omega(k)v(k) + \tilde{\Delta}_v(k)\omega(k) \end{bmatrix}$$

Solution 5.2 (pp. 80): $\alpha_B(k)$ with body frame derivatives but $B_k \neq \mathbb{O}_k$

Since the reference for the k th body does not coincide with \mathbb{O}_k , we have from (3.20) that

$$V(k) \stackrel{\triangle}{=} V(B_k) = \phi^*(\mathbb{O}_k, B_k)V(\mathbb{O}_k) \quad (C.16)$$

and the spatial acceleration $\alpha_B(k)$ is defined as

$$\alpha_B(k) \stackrel{\triangle}{=} \frac{d_k V(k)}{dt}$$

Differentiating (C.16) with respect to the k th body frame and noting that $\phi^*(\mathbb{O}_k, B_k)$ is constant in the k th body frame, we have

$$\begin{aligned} \alpha_B(k) &\stackrel{C.16}{=} \phi^*(\mathbb{O}_k, B_k) \frac{d_k V(\mathbb{O}_k)}{dt} = \phi^*(\mathbb{O}_k, B_k)\alpha(k) \\ &\stackrel{5.8}{=} \phi^*(\mathbb{O}_k, B_k) \{ \phi^*(\mathbb{O}_{k+1}, \mathbb{O}_k)\phi^*(B_{k+1}, \mathbb{O}_{k+1})\alpha_B(k+1) \\ &\quad + H^*(k)\ddot{\theta}(k) + \alpha(k) \} \\ &= \phi^*(B_{k+1}, B_k)\alpha_B(k+1) + \phi^*(\mathbb{O}_k, B_k)H^*(k)\ddot{\theta}(k) + \phi^*(\mathbb{O}_k, B_k)\alpha(k) \\ &\stackrel{3.22}{=} \phi^*(B_{k+1}, B_k)\alpha_B(k+1) + H_B^*(k)\ddot{\theta}(k) + \phi^*(\mathbb{O}_k, B_k)\alpha_B(k) \end{aligned}$$

This establishes (5.18). Note further that

$$\phi^*(\mathbb{O}_k, B_k)\tilde{V}(\mathbb{O}_k)\Delta_v(k) \stackrel{1.35, C.16}{=} \tilde{V}(k)\phi^*(\mathbb{O}_k, B_k)\Delta_v(k) \quad (C.17)$$

and that

$$\begin{aligned} \phi^*(\mathbb{O}_k, k)\bar{\Delta}_v(k)\Delta_v(k) &= \phi^*(\mathbb{O}_k, k) \begin{bmatrix} \mathbf{0} \\ \tilde{\Delta}_\omega(k)\Delta_v(k) \end{bmatrix} \\ &= \begin{bmatrix} \mathbf{0} \\ \tilde{\Delta}_\omega(k)\Delta_v(k) \end{bmatrix} = \bar{\Delta}_v(k)\Delta_v(k) \end{aligned} \quad (C.18)$$

Thus (5.18) can be re-expressed as:

$$\alpha_B(k) \stackrel{C.17, C.18, 3.22}{=} \tilde{\mathcal{V}}(k)\Delta_{\mathcal{V}}^B(k) - \bar{\Delta}_{\mathcal{V}}(k)\Delta_{\mathcal{V}}k + \phi^*(\mathcal{O}_k, k) \frac{d_{k+1}H^*(k)}{dt} \dot{\theta}(k)$$

This establishes (5.18).

Solution 5.3 (pp. 81): $\alpha_J(k)$ with inertial frame derivatives

Differentiating (5.6) with respect to the inertial frame \mathbb{I} , we obtain

$$\alpha_J(k) \triangleq \frac{d_{\mathbb{I}}\mathcal{V}(k)}{dt} \stackrel{1.28}{=} \alpha(k) + \tilde{\mathcal{V}}^\omega(k)\mathcal{V}(k) \stackrel{1.36}{=} \alpha(k) + \bar{\mathcal{V}}(k)\mathcal{V}(k) \quad (C.19)$$

Using (C.19) in (5.8) we have

$$\alpha_J(k) = \phi^*(k+1, k)\alpha_J(k+1) + H^*(k)\ddot{\theta}(k) + \alpha_J(k) \quad (C.20)$$

where the velocity dependent Coriolis acceleration term, $\alpha_J(k)$, is given by

$$\alpha_J(k) \triangleq \alpha(k) + \bar{\mathcal{V}}(k)\mathcal{V}(k) - \bar{\mathcal{V}}(k+1)\mathcal{V}(k+1)$$

This establishes the first equality in (5.19).

For the latter equality in (5.19), we have

$$\begin{aligned} & \alpha(k) + \bar{\mathcal{V}}(k)\mathcal{V}(k) - \bar{\mathcal{V}}(k+1)\bar{\mathcal{V}}(k+1) \\ & \stackrel{5.11}{=} \tilde{\mathcal{V}}(k)\Delta_{\mathcal{V}}(k) - \bar{\Delta}_{\mathcal{V}}(k)\Delta_{\mathcal{V}}(k) + \frac{d_{k+1}H^*(k)}{dt} \dot{\theta}(k) \\ & \quad + \bar{\mathcal{V}}(k)\mathcal{V}(k) - \bar{\mathcal{V}}(k+1)\mathcal{V}(k+1) \end{aligned} \quad (C.21)$$

The individual terms in (C.21) can be re-expressed as follows:

$$\begin{aligned} \tilde{\mathcal{V}}(k)\Delta_{\mathcal{V}}(k) &= [\tilde{\mathcal{V}}^\omega(k) + \tilde{\mathcal{V}}^v(k)]\Delta_{\mathcal{V}}(k) \stackrel{1.36}{=} \tilde{\mathcal{V}}^\omega(k)\Delta_{\mathcal{V}}(k) + \tilde{\mathcal{V}}^v(k)\Delta_{\mathcal{V}}^\omega(k) \\ &\stackrel{1.36}{=} [\tilde{\mathcal{V}}^\omega(k+1) + \tilde{\Delta}_{\mathcal{V}}^\omega(k)]\Delta_{\mathcal{V}}(k) + \tilde{\mathcal{V}}^v(k)\Delta_{\mathcal{V}}^\omega(k) \\ &= \tilde{\mathcal{V}}^\omega(k+1)\Delta_{\mathcal{V}}(k) + \tilde{\Delta}_{\mathcal{V}}^\omega(k)\Delta_{\mathcal{V}}^\omega(k) - \tilde{\Delta}_{\mathcal{V}}^\omega(k)\mathcal{V}^v(k) \\ \bar{\Delta}_{\mathcal{V}}(k)\Delta_{\mathcal{V}}(k) &\stackrel{1.36}{=} \tilde{\Delta}_{\mathcal{V}}^\omega(k)\Delta_{\mathcal{V}}^\omega(k) \\ \bar{\mathcal{V}}(k)\mathcal{V}(k) &\stackrel{1.36}{=} \tilde{\mathcal{V}}^\omega(k)\mathcal{V}^v(k) = [\tilde{\mathcal{V}}^\omega(k+1) + \tilde{\Delta}_{\mathcal{V}}^\omega(k)]\mathcal{V}^v(k) \\ \bar{\mathcal{V}}(k+1)\mathcal{V}(k+1) &\stackrel{1.36}{=} \tilde{\mathcal{V}}^\omega(k+1)\mathcal{V}^v(k+1) \end{aligned}$$

Substituting the above expressions into (C.21) and simplifying we obtain the latter equality in (5.19).

Equation (5.20a) is a component-level expansion of the first equality in (5.19).

The top angular half of (5.20b) is a simple carryover from $\alpha(k)$. For the lower linear half, observe from (5.12) and (5.20a) that

$$\begin{aligned} -\tilde{\Delta}_v(k)\omega(k+1) - \tilde{\Delta}_\omega(k)v(k) + \tilde{\omega}(k)v(k) - \tilde{\omega}(k+1)v(k+1) \\ = \tilde{\omega}(k+1)[v(k) - v(k+1) + \Delta_v(k)] \end{aligned}$$

Solution 5.4 (pp. 88): Inclusion of gravitational forces

1. The application of a pseudo-acceleration \mathbf{g} at the base-body results in the following altered version of the expression for α in (5.22):

$$\bar{\alpha} = \mathcal{E}_\phi^* \bar{\alpha} + H^* \ddot{\theta} + \alpha + E^* \mathbf{g}$$

Using (3.36), we then obtain

$$\bar{\alpha} = \phi^* [H^* \ddot{\theta} + \alpha + E^* \mathbf{g}]$$

Thus, the effect of the pseudo-acceleration can be handled by replacing α by $\alpha + E^* \mathbf{g}$. This leads to the Coriolis forces vector expression in (5.39).

2. Adding the additional gravitational force leads to the following body level equations of motion:

$$\begin{aligned} f(k) &\stackrel{5.1}{=} \phi(k, k-1)f(k-1) + M(k)\alpha(k) + b(k) + M(k)\mathbf{g} \\ &= \phi(k, k-1)f(k-1) + M(k)[\alpha(k) + \mathbf{g}] + b(k) \end{aligned}$$

This in turn leads to the following altered expression for f in (5.22):

$$f = \mathcal{E}_\phi f + M[\alpha + E^* \mathbf{g}] + b \Rightarrow f = \phi[M[\alpha + E^* \mathbf{g}] + b]$$

Using this expression for f with the rest of the expressions in (5.23) leads to (5.40).

3. We have that

$$\phi^* E^* \mathbf{g} = \text{col} \left\{ \phi^*(n, k) \mathbf{g} \right\}_{k=1}^n$$

However, since \mathbf{g} is a purely linear acceleration, $\phi^*(n, k)\mathbf{g} = \mathbf{g}$. Hence, the above equation simplifies to $E^* \mathbf{g}$ and establishes (5.41).

Solution 5.5 (pp. 92): Inverse dynamics using composite body inertias

1.

$$\begin{aligned} \mathfrak{f} &\stackrel{5.23}{=} \phi[\mathbf{M}\phi^*(\mathbf{H}^*\dot{\theta} + \mathbf{a}) + \mathbf{b}] \stackrel{4.10}{=} (\tilde{\phi}\mathcal{R} + \mathcal{R}\phi)(\mathbf{H}^*\ddot{\theta} + \mathbf{a}) + \phi\mathbf{b} \\ &\stackrel{5.23}{=} \mathcal{R}\mathbf{a} + \phi[\mathbf{b} + \mathcal{E}_\phi\mathcal{R}(\mathbf{H}\ddot{\theta} + \mathbf{a})] \end{aligned}$$

establishing (5.44).

2. Define

$$\begin{aligned} \mathbf{y}^+ &\stackrel{\triangle}{=} \mathbf{y} + \mathcal{R}(\mathbf{H}^*\ddot{\theta} + \mathbf{a}) \stackrel{5.44}{=} \phi[\mathbf{b} + \mathcal{E}_\phi\mathcal{R}(\mathbf{H}^*\ddot{\theta} + \mathbf{a})] + \mathcal{R}(\mathbf{H}^*\ddot{\theta} + \mathbf{a}) \\ &= \phi\mathbf{b} + \tilde{\phi}\mathcal{R}(\mathbf{H}^*\ddot{\theta} + \mathbf{a}) + \mathcal{R}(\mathbf{H}^*\ddot{\theta} + \mathbf{a}) = \phi[\mathbf{b} + \mathcal{R}(\mathbf{H}^*\ddot{\theta} + \mathbf{a})] \end{aligned} \quad (\text{C.22})$$

Thus

$$\mathcal{E}_\phi\mathbf{y}^+ \stackrel{\text{C.22}}{=} \tilde{\phi}[\mathbf{b} + \mathcal{R}(\mathbf{H}^*\ddot{\theta} + \mathbf{a})] \stackrel{5.44}{=} \mathbf{y} - \mathbf{b} \Rightarrow \mathbf{y} = \mathcal{E}_\phi\mathbf{y}^+ + \mathbf{b}$$

The first expression in the (5.45) recursion is a component level expression of the above. The second expression follows from the $\mathbf{y}^+ = \mathbf{y} + \mathcal{R}(\mathbf{H}^*\ddot{\theta} + \mathbf{a})$ definition of \mathbf{y}^+ .

Solution 5.6 (pp. 94): Expression for $\dot{\mathbf{H}}_{\mathbb{I}}^*(k)$

$$\begin{aligned} \frac{d_{\mathbb{I}}\mathbf{H}_{\mathbb{I}}^*(k)}{dt} &\stackrel{3.25}{=} \frac{d_{\mathbb{I}}\phi^*(\mathcal{O}_k, \mathbb{I})}{dt}\mathbf{H}^*(k) + \phi^*(\mathcal{O}_k, \mathbb{I})\frac{d_{\mathbb{I}}\mathbf{H}^*(k)}{dt} \\ &\stackrel{1.28, 1.37}{=} \tilde{\mathcal{V}}^v(k)\mathbf{H}^*(k) + \phi^*(\mathcal{O}_k, \mathbb{I})\left[\tilde{\mathcal{V}}^\omega(k)\mathbf{H}^*(k) + \frac{d_{k+1}\mathbf{H}^*(k)}{dt}\right] \\ &\stackrel{1.36}{=} \phi^*(\mathcal{O}_k, \mathbb{I})\left[\left\{\tilde{\mathcal{V}}^v(k) + \tilde{\mathcal{V}}^\omega(k)\right\}\mathbf{H}^*(k) + \frac{d_{k+1}\mathbf{H}^*(k)}{dt}\right] \\ &\stackrel{1.22}{=} \phi^*(\mathcal{O}_k, \mathbb{I})\left[\tilde{\mathcal{V}}(k)\mathbf{H}^*(k) + \frac{d_{k+1}\mathbf{H}^*(k)}{dt}\right] \\ &\stackrel{5.48, 1.35}{=} \tilde{\mathcal{V}}_{\mathbb{I}}(k)\phi^*(\mathcal{O}_k, \mathbb{I})\mathbf{H}^*(k) + \phi^*(\mathcal{O}_k, \mathbb{I})\frac{d_{k+1}\mathbf{H}^*(k)}{dt} \\ &\stackrel{3.25}{=} \tilde{\mathcal{V}}_{\mathbb{I}}(k)\mathbf{H}_{\mathbb{I}}^*(k) + \phi^*(\mathcal{O}_k, \mathbb{I})\frac{d_{k+1}\mathbf{H}^*(k)}{dt} \end{aligned}$$

Solutions for Chapter 6

Solution 6.1 (pp. 102): Properties of the $\tau(k)$ and $\bar{\tau}(k)$ projection matrices

1. We have

$$\tau(k) \cdot \tau(k) \stackrel{6.16}{=} \mathcal{G}(k)\mathcal{H}(k)\mathcal{G}(k)\mathcal{H}(k) \stackrel{6.14}{=} \mathcal{G}(k)\mathcal{H}(k) = \tau(k)$$

This implies that $\tau(k)$ is a projection operator. Since $\tau(k)$ is a projection operator, it follows directly that so are $\bar{\tau}(k) = \mathbf{I} - \tau(k)$ and their transposes.

2. These identities follow by using (6.14) and the definitions in (6.16).

Solution 6.2 (pp. 104): The $\mathcal{G}(k)$ Kalman gain and the link spatial acceleration

We have $\mathcal{G}^*(k)\alpha(k) \stackrel{6.15}{=} \mathcal{G}^*\bar{\tau}^*(k)\alpha^+(k) \stackrel{6.18}{=} \mathbf{0}$.

Solution 6.3 (pp. 105): Properties of $\mathcal{P}^+(k)$

1. We have

$$\begin{aligned} \mathcal{P}^+(k) &\stackrel{6.24}{=} \mathcal{P}(k)\bar{\tau}^*(k) \stackrel{6.16}{=} \mathcal{P}(k)[\mathbf{I} - \mathcal{H}^*(k)\mathcal{G}^*(k)] \\ &\stackrel{6.13}{=} \mathcal{P}(k) - \mathcal{P}(k)\mathcal{H}^*(k)\mathcal{D}^{-1}(k)\mathcal{H}(k)\mathcal{P}(k) \\ &= [\mathbf{I} - \mathcal{P}(k)\mathcal{H}^*(k)\mathcal{D}^{-1}(k)\mathcal{H}(k)]\mathcal{P}(k) \\ &\stackrel{6.13}{=} [\mathbf{I} - \mathcal{G}(k)\mathcal{H}(k)]\mathcal{P}(k) \stackrel{6.16}{=} \bar{\tau}(k)\mathcal{P}(k) \end{aligned}$$

That is,

$$\mathcal{P}^+(k) = \mathcal{P}(k)\bar{\tau}^*(k) = \bar{\tau}(k)\mathcal{P}(k) \quad (\text{C.23})$$

Thus

$$\bar{\tau}(k)\mathcal{P}(k)\bar{\tau}^*(k) \stackrel{\text{C.23}}{=} \mathcal{P}(k)[\bar{\tau}^*(k)]^2 = \mathcal{P}(k)\bar{\tau}^*(k)$$

2. We have $\mathcal{H}(k)\mathcal{P}^+(k) \stackrel{6.25}{=} \mathcal{H}(k)\bar{\tau}(k)\mathcal{P}(k) \stackrel{6.18}{=} \mathbf{0}$. The latter equality is obtained by transposing this equality and using the symmetry of $\mathcal{P}^+(k)$.

Solution 6.4 (pp. 107): Ordering of $\mathcal{R}(k)$, $\mathcal{P}(k)$ and $\mathcal{M}(k)$

We have

$$\mathcal{P}^+(k) \stackrel{6.25}{=} \mathcal{P}(k) - \tau(k)\mathcal{P}(k)\tau^*(k)$$

Since $\tau(k)\mathcal{P}(k)\tau^*(k) \geq 0$ this implies that $\mathcal{P}(k) \geq \mathcal{P}^+(k)$.

$\mathcal{P}(k) \geq \mathcal{M}(k)$ follows from (6.28).

For link 1, $\mathcal{R}(1) = \mathcal{P}(1) = \mathcal{M}(1)$, and hence $\mathcal{R}(1) \geq \mathcal{P}(1)$. Now we prove that if $\mathcal{R}(k) \geq \mathcal{P}(k)$ then necessarily $\mathcal{R}(k+1) \geq \mathcal{P}(k+1)$. For this, observe that $\mathcal{R}(k) \geq \mathcal{P}(k)$ implies that $\mathcal{R}(k) \geq \mathcal{P}^+(k)$. Then comparing (4.8) on page 60 with (6.28) implies that $\mathcal{R}(k+1) \geq \mathcal{P}(k+1)$.

Solution 6.5 (pp. 111): Relationship of $\nu(k)$ to $\alpha(k)$

$$\begin{aligned} \mathcal{G}^*(k)\alpha(k) &\stackrel{6.43}{=} \mathcal{G}^*(k)[\psi^*(k+1, k)\alpha(k+1) + \mathcal{H}^*(k)\nu(k)] \\ &= \mathcal{G}^*(k)\bar{\tau}^*(k)\phi^*(k+1, k)\alpha(k+1) + \mathcal{G}^*(k)\mathcal{H}^*(k)\nu(k) \stackrel{6.18, 6.14}{=} \nu(k) \end{aligned}$$

Solutions for Chapter 7

Solution 7.1 (pp. 121): Decomposition of $\phi\mathbf{M}\phi^*$ using \mathcal{P}

1. Equation (7.7) on page 117 states that $\mathbf{M} = \mathcal{P} - \mathcal{E}_\phi \mathcal{P} \mathcal{E}_\psi^*$. Pre and post multiplying this equation by ϕ and ψ^* , respectively leads to

$$\begin{aligned} \phi\mathbf{M}\psi^* &\stackrel{3.41, 7.8}{=} \phi\mathcal{P}\psi^* - \tilde{\phi}\mathcal{P}\tilde{\psi}^* = (\tilde{\phi} + \mathbf{I})\mathcal{P}(\tilde{\psi}^* + \mathbf{I}) - \tilde{\phi}\mathcal{P}\tilde{\psi}^* \\ &= \tilde{\phi}\mathcal{P}\tilde{\psi}^* + \mathcal{P} + \tilde{\phi}\mathcal{P} + \mathcal{P}\tilde{\psi}^* - \tilde{\phi}\mathcal{P}\tilde{\psi}^* = \mathcal{P} + \tilde{\phi}\mathcal{P} + \mathcal{P}\tilde{\psi}^* \end{aligned}$$

and the result follows.

2. We have

$$\begin{aligned} \phi\mathbf{M}\phi^* &= (\phi\psi^{-1})\psi\mathbf{M}\phi^* \stackrel{7.15}{=} (\phi\psi^{-1})[\psi\mathcal{P} + \mathcal{P}\tilde{\phi}^*] \\ &\stackrel{7.11}{=} \phi\mathcal{P} + [\mathbf{I} + \phi\mathcal{K}\mathcal{H}]\mathcal{P}\tilde{\phi}^* = \mathcal{P} + \tilde{\phi}\mathcal{P} + \mathcal{P}\tilde{\phi}^* + \phi\mathcal{K}\mathcal{H}\mathcal{P}\mathcal{E}_\phi^*\phi^* \\ &\stackrel{6.13}{=} \mathcal{P} + \tilde{\phi}\mathcal{P} + \mathcal{P}\tilde{\phi}^* + \phi\mathcal{K}\mathcal{D}\mathcal{G}^*\mathcal{E}_\phi^*\phi^* \stackrel{6.36}{=} \mathcal{P} + \tilde{\phi}\mathcal{P} + \mathcal{P}\tilde{\phi}^* + \phi\mathcal{K}\mathcal{D}\mathcal{K}^*\phi^* \end{aligned}$$

3. From (4.10) on page 61 it follows that \mathcal{R} forms the diagonal part of $\phi\mathbf{M}\phi^*$, while (7.16) shows that its diagonal part is given by \mathcal{P} plus the positive semi-definite diagonal part of $\phi\mathcal{K}\mathcal{D}\mathcal{K}^*\phi^*$. This establishes that $\mathcal{R} \geq \mathcal{P}$.
-

Solution 7.2 (pp. 125): Expression relating \mathfrak{z} and \mathfrak{z}^+

1. We have

$$\epsilon \stackrel{7.25b}{=} [\mathbf{I} - \mathsf{H}\psi\mathcal{K}]\mathcal{T} - \mathsf{H}\psi[\mathcal{P}\mathfrak{a} + \mathfrak{b}] \quad (\text{C.24})$$

Therefore

$$\begin{aligned} \mathcal{T} &\stackrel{\text{C.24}}{=} [\mathbf{I} - \mathsf{H}\psi\mathcal{K}]^{-1} \{ \epsilon + \mathsf{H}\psi[\mathcal{P}\mathfrak{a} + \mathfrak{b}] \} \\ &\stackrel{7.17, 7.12}{=} [\mathbf{I} + \mathsf{H}\phi\mathcal{K}]\epsilon + \mathsf{H}\phi[\mathcal{P}\mathfrak{a} + \mathfrak{b}] \end{aligned} \quad (\text{C.25})$$

Therefore

$$\begin{aligned} \mathfrak{z} &\stackrel{7.25a}{=} \psi[\mathcal{K}\mathcal{T} + \mathcal{P}\mathfrak{a} + \mathfrak{b}] \stackrel{\text{C.25}}{=} \psi\mathcal{K}[\mathbf{I} + \mathsf{H}\phi\mathcal{K}]\epsilon + \{\psi\mathcal{K}\mathsf{H}\phi + \psi\}[\mathcal{P}\mathfrak{a} + \mathfrak{b}] \\ &\stackrel{7.10, 7.12}{=} \phi\mathcal{K}\epsilon + \{\phi - \psi + \psi\}[\mathcal{P}\mathfrak{a} + \mathfrak{b}] \end{aligned}$$

from which (7.26) follows.

2. Pre-multiplying (7.26) by $\phi^{-1} = (\mathbf{I} - \mathcal{E}_\phi)$ and rearranging terms, we have

$$\mathfrak{z} = \mathcal{E}_\phi\mathfrak{z} + [\mathcal{K}\epsilon + \mathcal{P}\mathfrak{a} + \mathfrak{b}] \stackrel{7.3}{=} \mathcal{E}_\phi(\mathfrak{z} + \mathcal{G}\epsilon) + \mathcal{P}\mathfrak{a} + \mathfrak{b} \stackrel{7.27}{=} \mathcal{E}_\phi\mathfrak{z}^+ + \mathcal{P}\mathfrak{a} + \mathfrak{b}$$

3. Now

$$\begin{aligned} \mathfrak{z}^+ &\stackrel{7.27}{=} \mathfrak{z} + \mathcal{G}\epsilon \stackrel{7.26}{=} \phi[\mathcal{K}\epsilon + \mathcal{P}\mathfrak{a} + \mathfrak{b}] + \mathcal{G}\epsilon \\ &\stackrel{7.3}{=} \tilde{\phi}\mathcal{G}\epsilon + \phi[\mathcal{P}\mathfrak{a} + \mathfrak{b}] + \mathcal{G}\epsilon = \phi[\mathcal{G}\epsilon + \mathcal{P}\mathfrak{a} + \mathfrak{b}] \end{aligned}$$

Solution 7.3 (pp. 125): Expression for α in terms of ν

From (7.25d) we have $\ddot{\theta} = [\mathbf{I} - \mathsf{H}\psi\mathcal{K}]^*\nu - \mathcal{K}^*\psi^*\mathfrak{a}$. Thus, it follows that

$$\begin{aligned} \alpha &\stackrel{5.23}{=} \phi^*[\mathsf{H}^*\ddot{\theta} + \mathfrak{a}] \stackrel{7.25d}{=} \phi^*\mathsf{H}^* \{ [\mathbf{I} - \mathsf{H}\psi\mathcal{K}]^*\nu - \mathcal{K}^*\psi^*\mathfrak{a} \} + \phi^*\mathfrak{a} \\ &\stackrel{7.12}{=} \psi^*\mathsf{H}^*\nu - \phi^*\mathsf{H}^*\mathcal{K}^*\psi^*\mathfrak{a} + \phi^*\mathfrak{a} \stackrel{7.10}{=} \psi^*\mathsf{H}^*\nu + \psi^*\mathfrak{a} = \psi^*[\mathsf{H}^*\nu + \mathfrak{a}] \end{aligned}$$

This establishes (7.30).

The first equality in (7.31) results from combining (7.25d) and (7.30) as follows:

$$\ddot{\theta} \stackrel{7.25d}{=} [\mathbf{I} - \mathsf{H}\psi\mathcal{K}]^*\nu - \mathcal{K}^*\psi^*\mathfrak{a} = \nu - \mathcal{K}^*\psi^*\mathsf{H}^*\nu - \mathcal{K}^*\psi^*\mathfrak{a} \stackrel{7.30}{=} \nu - \mathcal{K}^*\alpha$$

The second equality follows from the additional use of (7.3) in the first equality.

Solution 7.4 (pp. 127): Relationship between ν , α and a

The first identity in (7.33) follows from

$$\begin{aligned}\alpha &\stackrel{7.30}{=} \psi^*[\mathbf{H}^*\nu + a] \stackrel{7.8}{=} \tilde{\psi}^*[\mathbf{H}^*\nu + a] + [\mathbf{H}^*\nu + a] \\ &\stackrel{7.8}{=} \mathcal{E}_\psi^* \psi^*[\mathbf{H}^*\nu + a] + [\mathbf{H}^*\nu + a] \stackrel{7.25d}{=} \mathcal{E}_\psi^* \alpha + \mathbf{H}^*\nu + a \\ &\stackrel{7.32e}{=} \bar{\tau}^* \alpha^+ + \mathbf{H}^*\nu + a\end{aligned}$$

The second identity in (7.33) follows by multiplying both sides of the first identity by \mathcal{G}^* and noting that $\mathcal{G}^* \bar{\tau}^* = \mathbf{0}$ and $\mathcal{G}^* \mathbf{H}^* = \mathbf{I}$.

Solution 7.5 (pp. 128): Computing inter-link spatial force $f(k)$

We have

$$\begin{aligned}f &\stackrel{5.23}{=} \phi[\mathbf{M}\alpha + b] \stackrel{7.30}{=} \phi[\mathbf{M}\psi^*(\mathbf{H}^*\nu + a) + b] \\ &\stackrel{7.15}{=} [\tilde{\phi}\mathcal{P} + \mathcal{P}\psi](\mathbf{H}^*\nu + a) + \phi b \stackrel{7.30}{=} \tilde{\phi}\mathcal{P}\mathbf{H}^*\nu + \tilde{\phi}\mathcal{P}a + \mathcal{P}\alpha + \phi b \\ &\stackrel{7.3}{=} \phi\mathcal{K}\epsilon + \phi\mathcal{P}a - \mathcal{P}a + \mathcal{P}\alpha + \phi b \stackrel{7.26}{=} \mathcal{P}[\alpha - a] + z\end{aligned}$$

This establishes the first half of (7.34).

From (7.33) we have that $\alpha = \bar{\tau}^* \alpha^+ + \mathbf{H}^*\nu + a$. It thus, follows that

$$\begin{aligned}f &\stackrel{7.34}{=} \mathcal{P}(\alpha - a) + z \stackrel{7.33}{=} \mathcal{P}[\bar{\tau}^* \alpha^+ + \mathbf{H}^*\nu + a] - \mathcal{P}a + z \\ &\stackrel{6.25, 7.32b}{=} \mathcal{P}^+ \alpha^+ + \mathcal{P}\mathbf{H}^*\nu + z^+ - \mathcal{G}\epsilon \stackrel{7.25c}{=} \mathcal{P}^+ \alpha^+ + z^+\end{aligned}$$

Solution 7.6 (pp. 129): Including gravitational accelerations

1. The proof here is an extension of the proof of Lemma 7.6 on page 123 to include in the additional gravitational term. The Coriolis term expression with gravity included in is defined by (5.39), and consists of replacing a with a' where $a' \triangleq a + E^*g$. The new version of (7.23) with the gravitational term requires a similar change to obtain

$$\begin{aligned}[\mathbf{I} - \mathbf{H}\psi\mathcal{K}]\mathbf{H}\phi(\mathbf{M}\phi^*a' + b) \\ &= (\mathbf{H}\psi\mathcal{P} + \mathcal{D}\mathcal{K}^*\phi^*)a' + \mathbf{H}\psi b \\ &= (\mathbf{H}\psi\mathcal{P} + \mathcal{D}\mathcal{K}^*\phi^*)/1a + (\mathbf{H}\mathcal{P} + \mathcal{D}\mathcal{K}^*\phi^*)E^*g + \mathbf{H}\psi b \\ &\stackrel{7.3}{=} (\mathbf{H}\psi\mathcal{P} + \mathcal{D}\mathcal{K}^*\phi^*)a + \mathcal{D}(\mathcal{G}^* + \mathcal{K}^*\phi^*)E^*g + \mathbf{H}\psi b \\ &\stackrel{7.3, 3.41}{=} (\mathbf{H}\psi\mathcal{P} + \mathcal{D}\mathcal{K}^*\phi^*)a + \mathcal{D}\mathcal{G}^*(\mathbf{I} + \tilde{\phi}^*)E^*g + \mathbf{H}\psi b \quad (C.26) \\ &\stackrel{3.40}{=} (\mathbf{H}\psi\mathcal{P} + \mathcal{D}\mathcal{K}^*\phi^*)a + \mathcal{D}\mathcal{G}^*\phi^*E^*g + \mathbf{H}\psi b \\ &\stackrel{5.41}{=} (\mathbf{H}\psi\mathcal{P} + \mathcal{D}\mathcal{K}^*\phi^*)a + \mathcal{D}\mathcal{G}^*\bar{E}^*g + \mathbf{H}\psi b\end{aligned}$$

When compared with (7.23), (C.26) contains the additional $\mathcal{D}\mathcal{G}^*\bar{\mathcal{E}}^*\mathfrak{g}$ gravitational term. Updating (7.24) to include this additional term results in the following altered expression:

$$\begin{aligned} & [\mathbf{I} - \mathsf{H}\psi\mathcal{K}]^*\mathcal{D}^{-1}[\mathbf{I} - \mathsf{H}\psi\mathcal{K}]\mathsf{H}\phi(\mathbf{M}\phi^*\mathfrak{a} + \mathfrak{b}) \\ &= [\mathbf{I} - \mathsf{H}\psi\mathcal{K}]^*\mathcal{D}^{-1}[\mathsf{H}\psi(\mathcal{P}\mathfrak{a} + \mathfrak{b})] + \mathcal{K}^*\psi^*\mathfrak{a} + [\mathbf{I} - \mathsf{H}\psi\mathcal{K}]^*\mathcal{G}^*\bar{\mathcal{E}}^*\mathfrak{g} \end{aligned}$$

The additional $[\mathbf{I} - \mathsf{H}\psi\mathcal{K}]^*\mathcal{G}^*\bar{\mathcal{E}}^*\mathfrak{g}$ term also needs to be included in (7.21) resulting in the desired (7.36) expression.

2. We repeat the steps in the proof of Exercise 7.3, but this time using the expression for $\tilde{\theta}$ from (7.36) instead of from (7.21). We obtain:

$$\begin{aligned} \alpha &\stackrel{5.23}{=} \phi^*[\mathsf{H}^*\tilde{\theta} + \mathfrak{a}] \stackrel{7.30,7.36}{=} \psi^*[\mathsf{H}^*\nu + \mathfrak{a}] - \phi^*\mathsf{H}^*[\mathbf{I} - \mathsf{H}\psi\mathcal{K}]^*\mathcal{G}^*\bar{\mathcal{E}}^*\mathfrak{g} \\ &\stackrel{7.12}{=} \psi^*[\mathsf{H}^*\nu + \mathfrak{a}] - \psi^*\mathsf{H}^*\mathcal{G}^*\bar{\mathcal{E}}^*\mathfrak{g} = \psi^*[\mathsf{H}^*(\nu - \mathcal{G}^*\bar{\mathcal{E}}^*\mathfrak{g}) + \mathfrak{a}] \\ &\stackrel{7.37}{=} \psi^*[\mathsf{H}^*\tilde{\nu} + \mathfrak{a}] \end{aligned}$$

establishing (7.38a).

Equation (7.38b) is obtained by simply using (7.25c) in (7.36).

For (7.38c) repeat the steps in the proof of (7.31).

3. The proof of (7.39) exactly parallels the proof of Exercise 7.4 on page 127 except for using the expression for α in (7.38a) as a starting point.
4. The proof of (7.40) is similar to that of Exercise 7.5. We have

$$\begin{aligned} \mathfrak{f} &\stackrel{5.23}{=} \phi[\mathbf{M}(\alpha + \bar{\mathcal{E}}^*\mathfrak{g}) + \mathfrak{b}] \stackrel{7.38a}{=} \phi[\mathbf{M}[\psi^*(\mathsf{H}^*\tilde{\nu} + \mathfrak{a}) + \bar{\mathcal{E}}^*\mathfrak{g}] + \mathfrak{b}] \\ &\stackrel{7.15}{=} [\tilde{\phi}\mathcal{P} + \mathcal{P}\psi](\mathsf{H}^*\tilde{\nu} + \mathfrak{a}) + \phi\mathfrak{b} + \phi\mathbf{M}\bar{\mathcal{E}}^*\mathfrak{g} \\ &\stackrel{7.38a,7.37}{=} \tilde{\phi}\mathcal{P}\mathsf{H}^*\nu + \tilde{\phi}\mathcal{P}\mathfrak{a} + \mathcal{P}\alpha + \phi\mathfrak{b} + [\phi\mathbf{M} - \tilde{\phi}\mathcal{P}\mathsf{H}^*\mathcal{G}^*]\bar{\mathcal{E}}^*\mathfrak{g} \\ &\stackrel{5.41,7.25c}{=} \phi\mathcal{K}\epsilon + \phi\mathcal{P}\mathfrak{a} - \mathcal{P}\mathfrak{a} + \mathcal{P}\alpha + \phi\mathfrak{b} + [\phi\mathbf{M}\phi^* - \tilde{\phi}\mathcal{P}\mathsf{H}^*\mathcal{G}^*\phi^*]\mathsf{E}^*\mathfrak{g} \\ &\stackrel{7.26,7.16}{=} \mathcal{P}[\alpha - \mathfrak{a}] + \mathfrak{z} + [\tilde{\phi}\mathcal{P} + \mathcal{P}\phi^* - \tilde{\phi}\mathcal{P}\mathsf{H}^*\mathcal{G}^*]\mathsf{E}^*\mathfrak{g} \\ &\stackrel{5.41,7.3}{=} \mathcal{P}[\alpha + \bar{\mathcal{E}}^*\mathfrak{g} - \mathfrak{a}] + \mathfrak{z} + [\tilde{\phi}\mathcal{P} - \tilde{\phi}\mathcal{P}\mathsf{H}^*\mathcal{G}^*]\mathsf{E}^*\mathfrak{g} \\ &= \mathcal{P}[\alpha + \bar{\mathcal{E}}^*\mathfrak{g} - \mathfrak{a}] + \mathfrak{z} + \tilde{\phi}\mathcal{P}\bar{\tau}^*\mathsf{E}^*\mathfrak{g} = \mathcal{P}[\alpha + \bar{\mathcal{E}}^*\mathfrak{g} - \mathfrak{a}] + \mathfrak{z} \end{aligned}$$

The last step follows from the $\tilde{\phi}\mathcal{P}\bar{\tau}^*\mathsf{E}^*\mathfrak{g} = \mathbf{0}$ identity which is a consequence of the strictly lower-triangular nature of $\tilde{\phi}$. This establishes the first half of (7.40). Now using (7.39) in the above we have

$$\begin{aligned} \mathfrak{f} &\stackrel{7.40}{=} \mathcal{P}(\alpha + \bar{\mathcal{E}}^*\mathfrak{g} - \mathfrak{a}) + \mathfrak{z} \stackrel{7.39}{=} \mathcal{P}[\bar{\tau}^*\alpha^+ + \mathsf{H}^*(\nu - \mathcal{G}^*\bar{\mathcal{E}}^*\mathfrak{g}) + \mathfrak{a} + \bar{\mathcal{E}}^*\mathfrak{g} - \mathfrak{a}] + \mathfrak{z} \\ &\stackrel{6.25,7.32b}{=} \mathcal{P}^+(\alpha^+ + \bar{\mathcal{E}}^*\mathfrak{g}) + \mathcal{P}\mathsf{H}^*\nu + \mathfrak{z}^+ - \mathcal{G}\epsilon \stackrel{7.25c}{=} \mathcal{P}^+(\alpha^+ + \bar{\mathcal{E}}^*\mathfrak{g}) + \mathfrak{z}^+ \end{aligned}$$

5. (7.41) follows directly from the operator expression in (7.38c) for $\tilde{\theta}$.

Solutions for Chapter 8

Solution 8.1 (pp. 147): Root/tip nodes and BWA matrices

1. The first part of (8.20) is a generalized restatement of (8.4) for BWA matrices. The latter half follows from the following:

$$\mathbb{A}^{-1} \cdot \mathbf{e}_r \stackrel{8.15}{=} (\mathbf{I} - \mathcal{E}_{\mathbb{A}}) \mathbf{e}_r \stackrel{8.20}{=} \mathbf{e}_r$$

2. The proof here is completely analogous to that of the first part with the use of (8.5).
-
-

Solutions for Chapter 9

Solution 9.1 (pp. 165): Recursive evaluation of $\tilde{\mathbb{A}}x$ and $\tilde{\mathbb{A}}^*x$

We have that $y \stackrel{\triangle}{=} \tilde{\mathbb{A}}x = \mathbb{A}\bar{y} - x$ where $\bar{y} = \mathbb{A}x$. This implies that

$$y(k) = \bar{y}(k) - x(k) = \stackrel{9.5}{=} \sum_{\forall i \in \mathcal{C}(k)} \mathbb{A}(k, i)\bar{y}(i) = \sum_{\forall i \in \mathcal{C}(k)} \mathbb{A}(k, i)[y(i) + x(i)]$$

Thus, the computational algorithm for y is the one in (9.5) except that the computational step in the loop is now given by the above expression with initial condition $y(0) = 0$.

Similarly $y \stackrel{\triangle}{=} \tilde{\mathbb{A}}^*x = \bar{y} - x$ where $\bar{y} = \mathbb{A}^*x$. It thus follows that the computational algorithm for $\tilde{\mathbb{A}}^*x$ is the same as in (9.8) except that the computational step in the loop is now given by

$$y(k) = \mathbb{A}^*(\varphi(k), k)[y(\varphi(k)) + x(\varphi(k))]$$

with initial condition $y(n+1) = 0$.

Solution 9.2 (pp. 180): Determinant of the mass matrix

1. We have

$$\mathbf{I} - H\mathbb{A}\mathcal{K} \stackrel{9.37}{=} \mathbf{I} - H\mathbb{A}\mathcal{E}_{\mathbb{A}}\mathcal{G} \stackrel{8.19}{=} \mathbf{I} - H\tilde{\mathbb{A}}\mathcal{G}$$

For a canonical tree, $\tilde{\mathbb{A}}$ is strictly lower triangular, while H and \mathcal{G} are block-diagonal. Hence, $[\mathbf{I} + H\mathbb{A}\mathcal{K}]$ is lower triangular with identity blocks along the diagonal. Moreover, from (9.50) we know that $[\mathbf{I} - H\psi\mathcal{K}]$ is its inverse. From

matrix theory, we know that the inverse of a lower-triangular matrix is also lower-triangular, and that the diagonal elements are inverses of each other. It thus, follows that for a canonical tree, $[\mathbf{I} - \mathbf{H}\Psi\mathcal{K}]$ is also lower-triangular with identity blocks along its diagonal.

2. For canonical trees, the above part established that $[\mathbf{I} + \mathbf{H}\mathcal{A}\mathcal{K}]$ is a lower-triangular matrix with identity matrices along the diagonal. Since, the determinant of a lower-triangular matrix is the product of the determinants of the block elements along its diagonal, it follows that (9.52) holds for canonical trees. Since all tree can be converted into canonical trees by a simple renumbering of the bodies, there exists a permutation matrix which transforms the Newton–Euler factors for a tree into the corresponding factors for a canonical version of the tree. Since permutation matrices are orthogonal, their determinants are 1, and hence, the determinant of the canonical and non-canonical versions of the Newton–Euler factors are equal to each other and are both 1. This establishes (9.52).

3. For (9.53), we have

$$\begin{aligned}\det\{\mathcal{M}\} &\stackrel{9.49}{=} \det\{[\mathbf{I} + \mathbf{H}\mathcal{A}\mathcal{K}] \mathcal{D} [\mathbf{I} + \mathbf{H}\mathcal{A}\mathcal{K}]^*\} \\ &= \det\{[\mathbf{I} + \mathbf{H}\mathcal{A}\mathcal{K}]\} \det\{\mathcal{D}\} \det\{[\mathbf{I} + \mathbf{H}\mathcal{A}\mathcal{K}]^*\} \\ &\stackrel{9.52}{=} \det\{\mathcal{D}\} = \prod_{k=1,n} \det\{\mathcal{D}(k)\}\end{aligned}$$

Solutions for Chapter 10

Solution 10.1 (pp. 197): $\Upsilon(k)$ for a micro/macro manipulator system

From (10.16) we have the following general expression for $\Upsilon(k)$:

$$\Upsilon(k) = \sum_{\forall i: i \succeq k} \psi^*(i, k) H^*(i) D^{-1}(i) H(i) \psi(i, k) \quad (C.27)$$

Thus,

$$\begin{aligned}\Upsilon(1) &= \sum_{\forall i: i \succeq 1} \psi^*(i, 1) H^*(i) D^{-1}(i) H(i) \psi(i, 1) \\ &= \sum_{\forall i: \wp(\mathfrak{S}) \succ i \succeq 1} \psi^*(i, 1) H^*(i) D^{-1}(i) H(i) \psi(i, 1) \\ &\quad + \sum_{\forall i: i \succeq \wp(\mathfrak{S})} \psi^*(i, 1) H^*(i) D^{-1}(i) H(i) \psi(i, 1)\end{aligned}$$

$$\begin{aligned}
&\stackrel{\text{8.17, C.27}}{=} \Upsilon_{\mathcal{S}}(1) + \psi^*(\varphi(\mathcal{S}), 1) \left\{ \sum_{\forall i: i \succ \varphi(\mathcal{S})} \psi^*(i, \varphi(\mathcal{S})) H^*(i)* \right. \\
&\quad \left. \mathcal{D}^{-1}(i) H(i) \psi(i, \varphi(\mathcal{S})) \right\} \psi^*(\varphi(\mathcal{S}), 1) \\
&\stackrel{\text{C.27}}{=} \Upsilon_{\mathcal{S}}(1) + \psi^*(\varphi(\mathcal{S}), 1) \Upsilon(\varphi(\mathcal{S})) \psi^*(\varphi(\mathcal{S}), 1)
\end{aligned}$$

The above steps have used the fact that $\mathcal{D}(i)$ does not depend on the generalized coordinates and other properties of the bodies inboard of the i th body in including $\Upsilon_{\mathcal{S}}(1)$ in the above expressions. This establishes (10.23). (10.24) is a direct consequence of (10.23) and the positive semi-definite nature of $\psi^*(\mathcal{P}(\varphi(\mathcal{S}), 1) \Upsilon(\varphi(\mathcal{S})) \psi(\mathcal{P}(\varphi(\mathcal{S}), 1))$.

Solution 10.2 (pp. 199): Computation of the mass matrix inverse

1. Expanding out the factorized form of the mass matrix inverse, it follows that

$$\begin{aligned}
\mathcal{M}^{-1} &\stackrel{\text{9.51}}{=} \mathcal{D}^{-1} - \mathcal{K}^* \psi^* H^* \mathcal{D}^{-1} - \mathcal{D}^{-1} H \psi \mathcal{K} + \mathcal{K}^* \Omega \mathcal{K} \\
&\stackrel{\text{10.13}}{=} \mathcal{D}^{-1} - \mathcal{K}^* \psi^* H^* \mathcal{D}^{-1} - \mathcal{D}^{-1} H \psi \mathcal{K} + \mathcal{K}^* [\Upsilon + \tilde{\psi}^* \Upsilon + \Upsilon \tilde{\psi} + \mathcal{R}] \mathcal{K}
\end{aligned}$$

Therefore,

$$\begin{aligned}
\mathcal{M}^{-1} &\stackrel{\text{9.51}}{=} \mathcal{D}^{-1} - \mathcal{K}^* \psi^* H^* \mathcal{D}^{-1} - \mathcal{D}^{-1} H \psi \mathcal{K} \\
&\quad + \mathcal{K}^* [\Upsilon + \psi^* \mathcal{E}_{\psi}^* \Upsilon + \Upsilon \mathcal{E}_{\psi} \psi + \mathcal{R}] \mathcal{K} \\
&= (\mathcal{D}^{-1} + \mathcal{G}^* \underline{\Upsilon} \mathcal{G}) - \mathcal{K}^* \psi^* (H^* \mathcal{D}^{-1} - \bar{\tau}^* \underline{\Upsilon} \mathcal{G}) \\
&\quad - (\mathcal{D}^{-1} H - \mathcal{G}^* \underline{\Upsilon} \bar{\tau}) \psi \mathcal{K} + \mathcal{K}^* \mathcal{R} \mathcal{K} \\
&\stackrel{\text{10.30}}{=} L - \mathcal{K}^* \psi^* U - U \psi \mathcal{K} + \mathcal{K}^* \mathcal{R} \mathcal{K}
\end{aligned}$$

The last equality used the following

$$\begin{aligned}
\mathcal{D}^{-1} H - \mathcal{G}^* \underline{\Upsilon} \bar{\tau} &= \mathcal{D}^{-1} H - \mathcal{G}^* \underline{\Upsilon} + \mathcal{G}^* \underline{\Upsilon} \bar{\tau} = \mathcal{D}^{-1} H - \mathcal{G}^* \underline{\Upsilon} + \mathcal{G}^* \underline{\Upsilon} \mathcal{G} H \\
&= L H - \mathcal{G}^* \underline{\Upsilon} \stackrel{\text{10.30}}{=} U
\end{aligned}$$

This establishes the decomposition of \mathcal{M}^{-1} .

2. For a serial-chain system, $\mathcal{R} = \mathbf{0}$, and hence (10.29) reduces to (10.31). Also, for a serial-chain system $\mathcal{E}_{\phi}^* \Upsilon \mathcal{E}_{\phi}$ is block-diagonal, and hence, $\underline{\Upsilon} = \Upsilon^+$ follows from (10.20). Since the component terms of L in (10.30) are block-diagonal, so is L . Similarly, U is block-diagonal as well. The product $\psi \mathcal{K}$ is strictly lower-triangular, establishing that (10.31) is a decomposition into block-diagonal, strictly upper-triangular and strictly lower-triangular terms.

Algorithm 10.4 is a recursive implementation of the above expressions for the elements of \mathcal{M}^{-1} .

Solution 10.3 (pp. 207): Ground connected equations of motion

In Lemma 10.6, assume that system B is the inertial frame. Since the inertial frame is immovable, we have

$$\underline{\Lambda}^B = \mathbf{0} \quad \text{and} \quad \bar{\mathcal{C}}_{os}^B = \mathbf{0}$$

Substituting these into (10.48) and keeping just the upper part results in (10.53).

Solutions for Chapter 11

Solution 11.1 (pp. 214): Mapping between \mathcal{T} and $\ddot{\theta}$ for closed-chain systems

This result is obtained by setting combining together (11.9a)-(11.9c) and (11.8).

Solution 11.2 (pp. 215): Torque minimization using squeeze forces

The squeeze force has the parametric form $\mathcal{T}_{sq} = G_c^* \lambda$ for some λ . The norm of the overall generalized force is given by

$$\|\mathcal{T}\|_W^2 = \|\mathcal{T}_{mv} + \mathcal{T}_{sq}\|_W^2 = \|\mathcal{T}_{mv} + G_c^* \lambda\|_W^2 = (\mathcal{T}_{mv} + G_c^* \lambda)^* W (\mathcal{T}_{mv} + G_c^* \lambda)$$

The gradient of the above with respect to λ must be zero for the minimum norm solution. Taking the gradient and setting it to zero yields,

$$\mathbf{0} = G_c W (\mathcal{T}_{mv} + G_c^* \lambda) \quad \Rightarrow \quad \lambda = -(G_c W G_c^*)^{-1} G_c W \mathcal{T}_{mv} \quad (\text{C.28})$$

Thus $X = G_c W$ minimizes the norm. Since the squeeze force is $\mathcal{T}_{sq} = G_c^* \lambda$, the minimum norm \mathcal{T} value is

$$\mathcal{T}_{mv} + G_c^* \lambda \stackrel{11.14, \text{C.28}}{=} \mathcal{T}_{mv} - \mathcal{P}_{ms} \mathcal{T}_{mv} \stackrel{11.15}{=} (\mathbf{I} - \mathcal{P}_{ms})(\mathbf{I} - \mathcal{P}_{ms})\mathcal{T} = (\mathbf{I} - \mathcal{P}_{ms})\mathcal{T}$$

The last step used the projection matrix property of $(\mathbf{I} - \mathcal{P}_{ms})$.

Solution 11.3 (pp. 218): Expression for \mathcal{Y}_C with loop constraints

This result is obtained by combining the expressions in and (11.20) and (11.21).

Solution 11.4 (pp. 223): Explicit expression for \underline{P}

The result follows by directly using the expression for \underline{P} in (11.37).

Solution 11.5 (pp. 224): Transformed and partitioned augmented dynamics

Substituting $\ddot{\theta} = \underline{P}\ddot{\theta}$ into (11.31) transforms it as follows:

$$\begin{pmatrix} \mathcal{M} & G_c^* \\ G_c & \mathbf{0} \end{pmatrix} \begin{bmatrix} \underline{P}\ddot{\theta} \\ -\lambda \end{bmatrix} = \begin{bmatrix} \mathcal{T} - \mathcal{C} \\ \dot{\mathcal{U}} \end{bmatrix} \quad (\text{C.29})$$

Pre-multiplying the top half of both sides of (C.29) with \underline{P}^* leads to

$$\begin{pmatrix} \underline{\mathcal{M}} & \underline{G}_r^* \\ \underline{G}_r & \mathbf{0} \end{pmatrix} \begin{bmatrix} \ddot{\theta} \\ -\lambda \end{bmatrix} \stackrel{11.37, 11.41}{=} \begin{bmatrix} \underline{P}^*(\mathcal{T} - \mathcal{C}) \\ \dot{\mathcal{U}} \end{bmatrix} \stackrel{11.41}{=} \begin{bmatrix} \underline{\mathcal{T}} \\ \dot{\mathcal{U}} \end{bmatrix} \quad (\text{C.30})$$

Applying the partitioned structure in $\underline{G} = [G_r, \mathbf{0}]$ from (11.37) to (C.30) leads to the partitioned equations in (11.42).

Solution 11.6 (pp. 224): Reduction of augmented dynamics

We begin by rearranging the blocks in the transformed equations of motion in (11.42) to obtain:

$$\begin{pmatrix} \underline{\mathcal{M}}_{11} & G_r^* & \underline{\mathcal{M}}_{12} \\ G_r & \mathbf{0} & \mathbf{0} \\ \underline{\mathcal{M}}_{21} & \mathbf{0} & \underline{\mathcal{M}}_{22} \end{pmatrix} \begin{bmatrix} \ddot{\theta}_1 \\ -\lambda \\ \ddot{\theta}_2 \end{bmatrix} = \begin{bmatrix} \underline{\mathcal{T}}_1 \\ \dot{\mathcal{U}} \\ \underline{\mathcal{T}}_2 \end{bmatrix} \quad (\text{C.31})$$

Using (A.10) to solve the above equation, we obtain

$$\ddot{\theta}_2 = \left\{ \underline{\mathcal{M}}_{22} - [\underline{\mathcal{M}}_{21}, \mathbf{0}] \left(\begin{pmatrix} \underline{\mathcal{M}}_{11} & G_r^* \\ G_r & \mathbf{0} \end{pmatrix}^{-1} \begin{bmatrix} \underline{\mathcal{M}}_{12} \\ \mathbf{0} \end{bmatrix} \right)^{-1} \cdot \left(\begin{bmatrix} \underline{\mathcal{T}}_2 - [\underline{\mathcal{M}}_{21}, \mathbf{0}] \left(\begin{pmatrix} \underline{\mathcal{M}}_{11} & G_r^* \\ G_r & \mathbf{0} \end{pmatrix}^{-1} \begin{bmatrix} \underline{\mathcal{T}}_1 \\ \dot{\mathcal{U}} \end{bmatrix} \right)^{-1} \right) \right\}^{-1} \quad (\text{C.32})$$

Additionally, from (A.11) we have

$$\begin{pmatrix} \underline{\mathcal{M}}_{11} & G_r^* \\ G_r & \mathbf{0} \end{pmatrix}^{-1} = \begin{pmatrix} \mathbf{0} & G_r^{-1} \\ G_r^{-*} & -G_r^{-*} \underline{\mathcal{M}}_{11}^{-1} G_r^{-1} \end{pmatrix} \quad (\text{C.33})$$

Substituting this into (C.32) and expanding out the matrix products we see that the equation simplifies to

$$\ddot{\theta}_2 = \underline{\mathcal{M}}_{22}^{-1} \left(\underline{\mathcal{T}}_2 - \underline{\mathcal{M}}_{21} G_r^{-1} \dot{\mathcal{U}} \right) \quad \text{or} \quad \underline{\mathcal{M}}_{22} \ddot{\theta}_2 = \underline{\mathcal{T}}_2 - \underline{\mathcal{M}}_{21} G_r^{-1} \dot{\mathcal{U}} \quad (\text{C.34})$$

Solution 11.7 (pp. 224): Transformed projected dynamics

Using (11.39) in (11.36) we see that

$$\underline{\mathcal{M}}_r \stackrel{11.39, 11.36}{=} \underline{X}_c^* \underline{P}^* \underline{\mathcal{M}} \underline{P} \underline{X}_c \stackrel{11.41}{=} \underline{X}_c^* \underline{\mathcal{M}} \underline{X}_c \stackrel{11.38}{=} \underline{\mathcal{M}}_{22} \quad (\text{C.35})$$

Thus, the projected dynamics equations of motion in (11.36) becomes

$$\underline{\mathcal{M}}_{22} \ddot{\underline{\theta}}_r \stackrel{11.43}{=} \underline{X}_c^* (\underline{\mathcal{T}} - \underline{\mathcal{C}} - \underline{\mathcal{M}} \ddot{\underline{\theta}}_p) \stackrel{11.39, \text{C.30}, 11.42}{=} (\underline{\mathcal{T}}_2 - \underline{X}_c^* \underline{\mathcal{M}} \underline{P}^{-1} \ddot{\underline{\theta}}_p) \quad (\text{C.36})$$

Note however, that $\ddot{\underline{\theta}}_p$ defined by

$$\ddot{\underline{\theta}}_p \triangleq \underline{P} \begin{bmatrix} G_r^{-1} \dot{\underline{\mathcal{U}}} \\ \mathbf{0} \end{bmatrix} \in \mathcal{R}^N \quad (\text{C.37})$$

satisfies the particular solution condition, (11.35), since

$$G_c \ddot{\underline{\theta}}_p \stackrel{\text{C.37}}{=} G_c \underline{P} \begin{bmatrix} G_r^{-1} \dot{\underline{\mathcal{U}}} \\ \mathbf{0} \end{bmatrix} \stackrel{11.37}{=} [G_r, \mathbf{0}] \begin{bmatrix} G_r^{-1} \dot{\underline{\mathcal{U}}} \\ \mathbf{0} \end{bmatrix} = \dot{\underline{\mathcal{U}}}$$

Substituting (C.37) in (C.36) leads to

$$\underline{\mathcal{M}}_{22} \ddot{\underline{\theta}}_r = \left(\underline{\mathcal{T}}_2 - \underline{X}_c^* \underline{\mathcal{M}} \begin{bmatrix} G_r^{-1} \dot{\underline{\mathcal{U}}} \\ \mathbf{0} \end{bmatrix} \right) \stackrel{11.38}{=} \left(\underline{\mathcal{T}}_2 - \underline{\mathcal{M}}_{21} G_r^{-1} \dot{\underline{\mathcal{U}}} \right) \quad (\text{C.38})$$

With $\ddot{\underline{\theta}}_r \equiv \ddot{\underline{\theta}}_2$, this last expression agrees with (11.43) and establishes the result.

Solutions for Chapter 12

Solution 12.1 (pp. 238): Simplification of $\mathcal{R}_G(k)$

The expression for $\mathcal{R}_G(k)$ in (12.18) and the recursion in (12.19) for $\mathcal{R}_{G1}(k)$ follows from substituting the expression for $\Phi_G(k+1, k)$ from (12.4) into (12.14) and expanding out the partitioned products.

A similar process leads the expressions for $X_l(k+1)$, $X_l(j+1)$ and $\mathcal{M}_G(k, k)$.

Solution 12.2 (pp. 242): Structure of $\mathcal{P}_G(k)$ and related quantities

The partitioned structure and related recursive algorithms follow by starting with the expressions in (12.21) and (12.25) and using the partitioned structure of $\Phi_G(k+1, k)$ to explicitly compute the products.

Solutions for Chapter 13

Solution 13.1 (pp. 269): Additional forward dynamics simplifications

From (13.69), $\mathcal{D}_m(k) = H_{MfL}(k) [A_{fL}(k)\Gamma_{fL}(k)A_{fL}^*(k) + M_{fL}(k)] H_{MfL}^*(k)$. Applying the (A.19) matrix identity,

$$[A + BCB^*]^{-1} = A^{-1} - A^{-1}B[C^{-1} + B^*A^{-1}B]^{-1}B^*A^{-1}$$

to the expression for $\mathcal{D}_m(k)$ with

$$A = H_{MfL}(k)M_{fL}(k)H_{MfL}^*(k), \quad B = H_{MfL}(k)A_{fL}(k), \quad C = \Gamma_{fL}(k)$$

establishes (13.70).

Solutions for Chapter 14

Solution 14.1 (pp. 274): Non-tree path-induced sub-graphs

1. Since a directed cycle containing an edge, represents a directed path connecting the node pair for the edge, the path (and the cycle) must belong to \mathfrak{S} since it is path-induced.
 2. Similarly, all paths connecting a pair of nodes in \mathfrak{S} must be in the sub-graph since it is path-induced, and the result follows.
-
-

Solution 14.2 (pp. 278): Mass matrix invariance of the outer sub-system

The expressions in (14.6) and (14.7) are obtained by directly evaluating $\mathcal{M} = H\mathbb{A}\mathbb{M}\mathbb{A}^*\mathbb{H}^*$ using the following component partitioned expressions from (14.4) and (14.5):

$$H = \begin{pmatrix} H_{\mathfrak{S}} & \mathbf{0} \\ \mathbf{0} & H_{\mathcal{P}} \end{pmatrix}, \quad \mathbb{A} = \begin{pmatrix} \mathbb{A}_{\mathfrak{S}} & \mathbf{0} \\ \mathbb{A}_{\mathcal{P}} E_{\mathfrak{S}} \mathbb{A}_{\mathfrak{S}} & \mathbb{A}_{\mathcal{P}} \end{pmatrix}, \quad \mathbb{M} = \begin{pmatrix} \mathbb{M}_{\mathfrak{S}} & \mathbf{0} \\ \mathbf{0} & \mathbb{M}_{\mathcal{P}} \end{pmatrix}$$

Solution 14.3 (pp. 292): Mass matrix invariance with aggregation

First, we have

$$H\mathbb{A} \stackrel{14.18, 14.20}{=} (H_a \mathfrak{J}_a^{-1})(\mathfrak{J}_a \mathbb{A}_a) = H_a \mathbb{A}_a \quad (\text{C.39})$$

Using this directly establishes the \mathcal{M} equalities in (14.24).

Moreover

$$\begin{aligned} H\mathbb{A}(\mathbf{M}\mathbb{A}^*\mathfrak{a} + \mathfrak{b}) &\stackrel{\text{C.39}}{=} H_a\mathbb{A}_a(\mathbf{M}\mathbb{A}^*\mathfrak{a} + \mathfrak{b}) \stackrel{\text{14.18}}{=} H_a\mathbb{A}_a(\mathbf{M}\mathbb{A}_a^*\mathfrak{J}_a^{-*}\mathfrak{a} + \mathfrak{b}) \\ &\stackrel{\text{14.21}}{=} H_a\mathbb{A}_a(\mathbf{M}\mathbb{A}_a^*\underline{\mathfrak{a}} + \mathfrak{b}) \end{aligned}$$

This establishes the \mathcal{C} equalities in (14.24).

Solutions for Chapter 15

Solution 15.1 (pp. 310): Expression for $\dot{X}_{\mathfrak{S}}$

With $Z \triangleq Y_1^{-1}Y_2$,

$$\begin{aligned} \frac{dZ}{dt} &= \frac{dY_1^{-1}}{dt}Y_2 + Y_1^{-1}\frac{dY_2}{dt} \stackrel{\text{A.28}}{=} -Y_1^{-1}\frac{dY_1}{dt}Y_1^{-1}Y_2 + Y_1^{-1}\frac{dY_2}{dt} \\ &= Y_1^{-1}\left[\frac{dY_2}{dt} - \frac{dY_1}{dt}Z\right] \end{aligned}$$

Thus,

$$\dot{X}_{\mathfrak{S}} = \begin{bmatrix} -\dot{Z} \\ \mathbf{0} \end{bmatrix} = \begin{bmatrix} Y_1^{-1} [\dot{Y}_1 Z - \dot{Y}_2] \\ \mathbf{0} \end{bmatrix} = \begin{bmatrix} -Y_1^{-1} \dot{Y} X_{\mathfrak{S}} \\ \mathbf{0} \end{bmatrix}$$

This establishes the first half of (15.27).

Using this, we have

$$\dot{X}_{\mathfrak{S}} \dot{\theta}_{R\mathfrak{S}} = \begin{bmatrix} -Y_1^{-1} \dot{Y} X_{\mathfrak{S}} \dot{\theta}_{R\mathfrak{S}} \\ \mathbf{0} \end{bmatrix} = \begin{bmatrix} -Y_1^{-1} \dot{Y} \dot{\theta}_{\mathfrak{S}} \\ \mathbf{0} \end{bmatrix}$$

This establishes the second half of (15.27).

Solutions for Chapter 16

Solution 16.1 (pp. 320): Alternate expression for \mathcal{S}_{aa}

We have

$$\begin{aligned} \phi \mathfrak{U}_{\perp}^* \mathbf{M} \mathfrak{U}_{\perp} \phi^* &\stackrel{\text{10.36}}{=} \phi \mathbf{M} \mathfrak{U}_{\perp} \phi^* \stackrel{\text{10.39a}}{=} \phi \mathbf{M} (\psi^* - \Omega \mathcal{P}) = \phi \mathbf{M} \psi^* - \phi \mathfrak{U}^* \mathcal{P} \\ &\stackrel{\text{9.41, 10.38a}}{=} \phi \mathcal{P} + \mathcal{P} \tilde{\psi}^* - (\phi - \psi + \mathcal{P} \Omega) \mathcal{P} = (\psi - \mathcal{P} \Omega) \mathcal{P} + \mathcal{P} \tilde{\psi}^* \end{aligned}$$

Pre- and post-multiplying the above with H_a and H_a^* and comparing with the expression for \mathcal{S}_{aa} in (16.11c) establishes the lemma.

Solution 16.2 (pp. 325): Expression for the generalized Jacobian

Ignoring all the velocity dependent terms, we have

$$\alpha_{nd} \stackrel{16.18}{=} \partial \ddot{\theta} = \partial_a \ddot{\theta}_a + \partial_p \ddot{\theta}_p \stackrel{16.20}{=} \partial_a \ddot{\theta}_a + \partial_p \partial_D \ddot{\theta}_a = (\partial_a + \partial_p \partial_D) \ddot{\theta}_a$$

Solution 16.3 (pp. 330): The disturbance Jacobian for a free-flying system

Equation (4.18) on page 63 showed that the center of mass spatial velocity, \mathcal{V}_C is given by the following relationship when the base-body generalized forces are zero:

$$\mathcal{V}_C = \mathcal{V}(n) + \mathcal{R}^{-1}(n) \sum_{k=1}^{n-1} \phi(n, k) \mathcal{R}(k) H^*(k) \dot{\theta}(k) \quad (C.40)$$

For the case when the system has zero spatial momentum, $\mathcal{V}_C = \mathbf{0}$ and so we can re-express (C.40) as:

$$\mathcal{V}(n) = -\mathcal{R}^{-1}(n) \sum_{k=1}^{n-1} \phi(n, k) \mathcal{R}(k) H^*(k) \dot{\theta}(k)$$

The expression for the ∂_D disturbance Jacobian is obtained by converting (16.28) into a matrix form.

Solutions for Chapter 17

Solution 17.1 (pp. 333): Weight matrices for the dual model

In the dual model, the k th link is the parent of the $(k+1)$ th link. Thus the velocity recursion in (3.19b) can be re-expressed as:

$$\mathcal{V}(k) = \phi^*(k-1, k) \mathcal{V}(k-1) - \phi^*(k-1, k) H^*(k-1) \dot{\theta}(k-1)$$

Thus $\phi^*(k-1, k)$ matrices are the weight matrices in the dual model.

Solution 17.2 (pp. 335): Dual articulated body inertia properties

1. Using (17.4) we have

$$\begin{aligned} S(k) H^*(k) &= S^+(k) [I + H^*(k) G_{dl}^*(k)] H^*(k) \\ &= S^+(k) [I - H^*(k) D_{dl}^{-1}(k) H(k) S^+(k)] H^*(k) = \mathbf{0} \end{aligned}$$

This establishes (17.5).

2. Again using (17.4) we have

$$\tau_{d1}(k)\bar{\tau}(k) = \tau_{d1}(k) + g_{d1}(k)H(k)g(k)H(k) = \tau_{d1}(k) + g_{d1}(k)H(k) = \mathbf{0}$$

This establishes the first expression in (17.6).

The latter expression has an analogous proof.

Solution 17.3 (pp. 347): Relationship between $\phi_{\mathfrak{S}}^*$ and ϕ_R^*

$$\begin{aligned} \tilde{\phi}_R^*(\phi_{\mathfrak{S}}^*)^{-1} &= \tilde{\phi}_R^*(I - \mathcal{E}_{\phi_{\mathfrak{S}}}^*) = (\phi_R^* - I) - \phi_R^* \mathcal{E}_{\phi_R}^* \mathcal{E}_{\phi_{\mathfrak{S}}}^* \\ &\stackrel{17.22, 17.28a}{=} (\phi_R^* - I) - \phi_R^* \mathbb{S} \mathbb{S}^* \stackrel{17.27}{=} \phi_R^* e_k e_k^* - I \end{aligned}$$

Post-multiplying the above with $\phi_{\mathfrak{S}}^*$ establishes (17.36).

Solution 17.4 (pp. 347): The inverse transformation \mathfrak{J}_{GR}

Observe that

$$\begin{aligned} \mathfrak{J}_{GR} \dot{\theta}_R &\stackrel{17.38}{=} (\mathbb{S}_{RG}^* + e_{Gn} e_n^* \phi_R^* H_R^*) \dot{\theta}_R \stackrel{17.29, 17.30}{=} \sum_{j=k}^{n-1} e_{Gj} \dot{\theta}_R(j+1) + e_{Gn} e_n^* \mathcal{V}_{\mathfrak{S}} \\ &= \sum_{j=k}^{n-1} e_{Gj} \dot{\theta}_R(j+1) + e_{Gn} \mathcal{V}_{\mathfrak{S}}(n) \stackrel{17.18}{=} \dot{\theta}_{\mathfrak{S}} \end{aligned}$$

This establishes (17.38).

Now,

$$\begin{aligned} \mathfrak{J}_{GR} * \mathfrak{J}_{RG} &\stackrel{17.28c, 17.38}{=} (\mathbb{S}_{RG}^* + e_{Gn} e_n^* \phi_R^* H_R^*) (\mathbb{S}_{RG} + e_{Rk} e_k^* \phi_{\mathfrak{S}}^* H_{\mathfrak{S}}^*) \\ &\stackrel{17.37a}{=} \mathbb{S}_{RG}^* \mathbb{S}_{RG} + e_{Gn} e_n^* \phi_R^* H_R^* (\mathbb{S}_{RG} + e_{Rk} e_k^* \phi_{\mathfrak{S}}^* H_{\mathfrak{S}}^*) \end{aligned} \quad (C.41)$$

However,

$$\begin{aligned} \phi_R^* H_R^* &\stackrel{17.28b}{=} \phi_R^* (-\mathcal{E}_{\phi_R}^* H_{\mathfrak{S}}^* \mathbb{S}_{RG}^* + e_k e_{Rk}^*) \\ \Rightarrow \phi_R^* H_R^* \mathbb{S}_{RG} &\stackrel{17.37a}{=} \phi_R^* (-\mathcal{E}_{\phi_R}^* H_{\mathfrak{S}}^* \mathbb{S}_{RG}^* \mathbb{S}_{RG}) \stackrel{17.37b, 17.37c}{=} -\tilde{\phi}_R^* H_{\mathfrak{S}}^* \end{aligned} \quad (C.42)$$

Also,

$$\phi_R^* H_R^* e_{Rk} e_k^* \stackrel{17.28b}{=} \phi_R^* (-\mathcal{E}_{\phi_R}^* H_{\mathfrak{S}}^* \mathbb{S}_{RG}^* + e_k e_{Rk}^*) e_{Rk} e_k^* \stackrel{17.37a}{=} \phi_R^* e_k e_k^* \quad (C.43)$$

Therefore

$$\begin{aligned}
 \mathfrak{J}_{RG} * \mathfrak{J}_{RG} &\stackrel{C.41,C.42,C.43}{=} S_{RG}^* S_{RG} + e_{Gn} e_n^* (-\tilde{\phi}_R^* H_S^* + \phi_R^* e_k e_k^* \phi_S^* H_S^*) \\
 &\stackrel{17.35}{=} S_{RG}^* S_{RG} + e_{Gn} e_n^* (-\tilde{\phi}_R^* + \tilde{\phi}_R^* + \phi_S^*) H_S^* \\
 &= S_{RG}^* S_{RG} + e_{Gn} e_n^* \phi_S^* H_S^* \stackrel{17.37e}{=} S_{RG}^* S_{RG} + e_{Gn} e_n^* H_S^* \\
 &\stackrel{17.37d}{=} S_{RG}^* S_{RG} + e_{Gn} e_{Gn}^* \stackrel{17.37e}{=} I
 \end{aligned}$$

This establishes (17.39).

Solution 17.5 (pp. 348): Transformed mass matrix

1. We have

$$\begin{aligned}
 \phi_R^* H_R^* \mathfrak{J}_{RG} &\stackrel{17.32}{=} \phi_R^* (-\mathcal{E}_{\phi_R}^* + e_k e_k^* \phi_S^*) H_S^* \\
 &\stackrel{17.35}{=} (-\tilde{\phi}_R^* + \tilde{\phi}_R^* + \phi_S^*) H_S^* = \phi_S^* H_S^*
 \end{aligned}$$

establishing (17.43).

2. The $\dot{\theta} = \underline{\mathfrak{J}}_{RG} \dot{\theta}$ directly from the use of (17.28c) and the definition of $\dot{\theta}$ in (17.40). For the latter equality, we have

$$\begin{aligned}
 \underline{\phi}^* \underline{H}^* \underline{\mathfrak{J}}_{RG} &\stackrel{17.40,17.41,17.44}{=} \begin{pmatrix} \phi_C^* H_C^* & \phi_C^* \mathcal{B}_S^* \phi_R^* H_R^* \mathfrak{J}_{RG} \\ \mathbf{0} & \phi_R^* H_R^* \mathfrak{J}_{RG} \end{pmatrix} \\
 &\stackrel{17.43}{=} \begin{pmatrix} \phi_C^* H_C^* & \phi_C^* \mathcal{B}_S^* \phi_S^* H_S^* \\ \mathbf{0} & \phi_S^* H_S^* \end{pmatrix} \stackrel{14.4,17.17}{=} \underline{\phi}^* \underline{H}^*
 \end{aligned}$$

This establishes (17.44).

3. We have

$$\mathcal{M} = H \phi M \phi^* H^* \stackrel{17.44}{=} \underline{\mathfrak{J}}_{RG}^* \underline{H} \underline{\phi} \underline{M} \underline{\phi}^* \underline{H}^* \underline{\mathfrak{J}}_{RG} \stackrel{17.42}{=} \underline{\mathfrak{J}}_{RG}^* \underline{\mathcal{M}} \underline{\mathfrak{J}}_{RG}$$

This establishes (17.45).

4. Now,

$$\mathcal{K}_e = \frac{1}{2} \dot{\theta}^* \mathcal{M} \dot{\theta} \stackrel{17.45}{=} \frac{1}{2} \dot{\theta}^* \underline{\mathfrak{J}}_{RG}^* \underline{\mathcal{M}} \underline{\mathfrak{J}}_{RG} \dot{\theta} \stackrel{17.44}{=} \frac{1}{2} \dot{\theta}^* \underline{\mathcal{M}} \dot{\theta}$$

establishing (17.46)

5. $\underline{\phi}$ is an SPO operator and \underline{H} and \underline{M} are both block-diagonal. Also, \underline{H} is full rank because H and H_R are both full rank. Thus, the SKO model requirements are satisfied.

Solutions for Chapter 18

Solution 18.1 (pp. 356): Identities for $\tilde{\mathcal{V}}$

At the component level,

$$\mathcal{V}^+(k) \stackrel{3.15}{=} \phi^*(\varphi(k), k) \mathcal{V}(\varphi(k)) \Rightarrow \tilde{\mathcal{V}}^+(k) \phi^*(\varphi(k), k) \stackrel{1.35}{=} \phi^*(\varphi(k), k) \tilde{\mathcal{V}}(\varphi(k))$$

The above relationship establishes the component level equivalence of the elements of the operator expressions on the left and right of (18.9a).

Equation (18.9b) then follows from using the fact that $\mathcal{V} = \mathcal{V}^+ + \Delta_{\mathcal{V}}$ in (18.9a).

Equation (18.9c) follows from pre- and post-multiplying (18.9b) by ϕ^* and simplifying.

Equation (18.9d) is simply a transposed version of (18.9c).

Solution 18.2 (pp. 358): Time derivative of $H\phi$

$$\begin{aligned} \frac{dH\phi}{dt} &= \dot{H}\phi + H\dot{\phi} \stackrel{18.12, 18.5}{=} -H\tilde{\mathcal{V}}_S^\omega \phi + H \left[\tilde{\phi} \bar{\Delta}_{\mathcal{V}} \phi + \tilde{\mathcal{V}}^\omega \phi - \phi \tilde{\mathcal{V}}^\omega \right] \\ &\stackrel{18.5}{=} H\tilde{\Delta}_{\mathcal{V}}^\omega \phi + H\tilde{\phi} \bar{\Delta}_{\mathcal{V}} \phi - H\phi \tilde{\mathcal{V}}^\omega \\ &= H\tilde{\Delta}_{\mathcal{V}}^\omega \phi + H\tilde{\phi} \left[\tilde{\Delta}_{\mathcal{V}}^\omega + \bar{\Delta}_{\mathcal{V}}^\nu \right] \phi - H\phi \tilde{\mathcal{V}}^\omega \\ &= H\phi \tilde{\Delta}_{\mathcal{V}}^\omega \phi + H\tilde{\phi} \bar{\Delta}_{\mathcal{V}}^\nu \phi - H\phi \tilde{\mathcal{V}}^\omega = H\phi \left[\tilde{\Delta}_{\mathcal{V}}^\omega \phi + \mathcal{E}_\phi \bar{\Delta}_{\mathcal{V}}^\nu \phi - \tilde{\mathcal{V}}^\omega \right] \end{aligned}$$

This establishes the result.

Solution 18.3 (pp. 358): Operator expression for the a_J Coriolis acceleration

1.

$$\begin{aligned} \phi^* a_J &\stackrel{8.43}{=} \frac{d_I \phi^* H^*}{dt} \dot{\theta} \stackrel{18.13}{=} [\tilde{\mathcal{V}}^\omega - \phi^* \tilde{\Delta}_{\mathcal{V}}^\omega - \phi^* \tilde{\Delta}_{\mathcal{V}}^\nu \mathcal{E}_\phi^*] \phi^* H^* \dot{\theta} \\ &\stackrel{18.13}{=} [\tilde{\mathcal{V}}^\omega - \phi^* \tilde{\Delta}_{\mathcal{V}}^\omega - \phi^* \tilde{\Delta}_{\mathcal{V}}^\nu \mathcal{E}_\phi^*] \mathcal{V} \end{aligned} \quad (\text{C.44})$$

Hence,

$$\begin{aligned} a_J &\stackrel{\text{C.44}}{=} \phi^{-*} [\tilde{\mathcal{V}}^\omega - \phi^* \tilde{\Delta}_{\mathcal{V}}^\omega - \phi^* \tilde{\Delta}_{\mathcal{V}}^\nu \mathcal{E}_\phi^*] \mathcal{V} \\ &= [\phi^{-*} \tilde{\mathcal{V}}^\omega - \tilde{\Delta}_{\mathcal{V}}^\omega - \tilde{\Delta}_{\mathcal{V}}^\nu \mathcal{E}_\phi^*] \mathcal{V} \\ &= -\tilde{\Delta}_{\mathcal{V}}^\omega \mathcal{V} + [I - \mathcal{E}_\phi^{**}] \tilde{\mathcal{V}}^\omega \mathcal{V} - \tilde{\Delta}_{\mathcal{V}}^\nu \mathcal{V}^+ \\ &= -\tilde{\Delta}_{\mathcal{V}}^\omega \mathcal{V} + \tilde{\mathcal{V}}^\omega \mathcal{V} - \mathcal{E}_\phi^* \tilde{\mathcal{V}}^\omega \mathcal{V} - \tilde{\Delta}_{\mathcal{V}}^\nu \mathcal{V}^+ \\ &\stackrel{18.5}{=} \tilde{\mathcal{V}}_S^\omega \mathcal{V} - \mathcal{E}_\phi^* \tilde{\mathcal{V}}^\omega \mathcal{V} - \tilde{\Delta}_{\mathcal{V}}^\nu \mathcal{V}^+ \end{aligned} \quad (\text{C.45})$$

This establishes (18.14).

2. The k th element of α_J from (C.45) is given by:

$$\begin{aligned}\alpha_J(k) &= \begin{bmatrix} \tilde{\omega}(\varphi(k))\omega(k) \\ \tilde{\omega}(\varphi(k))v(k) \end{bmatrix} - \phi^*(\varphi(k), k) \begin{bmatrix} \mathbf{0} \\ \tilde{\omega}(\varphi(k))v(\varphi(k)) \end{bmatrix} - \begin{bmatrix} \mathbf{0} \\ \tilde{\Delta}_v(k)\omega(\varphi(k)) \end{bmatrix} \\ &= \begin{bmatrix} -\tilde{\omega}(k)\omega(\varphi(k)) \\ \tilde{\omega}(\varphi(k))[v(k) - v(\varphi(k)) + \Delta_v(k)] \end{bmatrix} \\ &= \begin{bmatrix} -\tilde{\omega}(k)[\omega(k) - \Delta_\omega(k)] \\ \tilde{\omega}(\varphi(k))[v(k) - v(\varphi(k)) + \Delta_v(k)] \end{bmatrix}\end{aligned}$$

The further use of $\varphi(k) = k + 1$ establishes the result

Solution 18.4 (pp. 359): Time derivative of $\phi(k+1, k)$ with $\mathbb{O}_k \neq \mathbb{B}_k$

1. Equation (18.17) follows from (1.37) when applied to the \mathbb{B}_k and \mathbb{O}_k frame pair on the k th rigid link.
2. Equation (18.18a) follows directly from Exercise 1.8 on page 13.
Equation (18.18b) follows from differentiating (18.15).
Equation (18.18c) and (18.18d) follow from further manipulation and rearrangement of the earlier expressions.

Solution 18.5 (pp. 360): Operator time derivatives with $\mathbb{O}_k \neq \mathbb{B}_k$

1. (18.21a) follows from the use of (18.17) in its operator definition in (18.20).
For (18.21b), we have

$$\begin{aligned}\frac{d\Delta_{\mathbb{B}/\mathbb{O}}^{-1}}{dt} &\stackrel{18.21a, A.28}{=} -\Delta_{\mathbb{B}/\mathbb{O}}^{-1} \frac{d\Delta_{\mathbb{B}/\mathbb{O}}}{dt} \Delta_{\mathbb{B}/\mathbb{O}}^{-1} \stackrel{18.21a}{=} -\Delta_{\mathbb{B}/\mathbb{O}}^{-1} \bar{\nabla}_{\mathbb{B}/\mathbb{O}} \Delta_{\mathbb{B}/\mathbb{O}}^{-1} \\ &\stackrel{1.36}{=} -\bar{\nabla}_{\mathbb{B}/\mathbb{O}}\end{aligned}$$

In the last equality we have used the fact that $\bar{\nabla}_{\mathbb{B}/\mathbb{O}}$ only contains non-zero linear velocity values together with (1.36) in:

$$\bar{\nabla}_{\mathbb{B}/\mathbb{O}} = \bar{\nabla}_{\mathbb{B}/\mathbb{O}} \Delta_{\mathbb{B}/\mathbb{O}}^{-1} = \Delta_{\mathbb{B}/\mathbb{O}} \bar{\nabla}_{\mathbb{B}/\mathbb{O}} \quad (C.46)$$

2. We have

$$\begin{aligned} \frac{d\mathcal{E}_{\phi_B}}{dt} &\stackrel{5.29}{=} \frac{d\Delta_{B/O}\mathcal{E}_\phi\Delta_{B/O}^{-1}}{dt} \\ &\stackrel{18.21a, 18.21b}{=} \Delta_{B/O}\frac{d\mathcal{E}_\phi}{dt}\Delta_{B/O}^{-1} + \bar{\mathcal{V}}_{B/O}\mathcal{E}_\phi\Delta_{B/O}^{-1} - \Delta_{B/O}\mathcal{E}_\phi\bar{\mathcal{V}}_{B/O} \\ &\stackrel{C.46}{=} \Delta_{B/O}\frac{d\mathcal{E}_\phi}{dt}\Delta_{B/O}^{-1} + \bar{\mathcal{V}}_{B/O}\Delta_{B/O}\mathcal{E}_\phi\Delta_{B/O}^{-1} - \Delta_{B/O}\mathcal{E}_\phi\Delta_{B/O}^{-1}\bar{\mathcal{V}}_{B/O} \\ &\stackrel{5.29}{=} \Delta_{B/O}\frac{d\mathcal{E}_\phi}{dt}\Delta_{B/O}^{-1} + \bar{\mathcal{V}}_{B/O}\mathcal{E}_{\phi_B} - \mathcal{E}_{\phi_B}\bar{\mathcal{V}}_{B/O} \end{aligned}$$

This establishes (18.22a).

For (18.22b),

$$\begin{aligned} \frac{d\phi_B}{dt} &\stackrel{A.28}{=} \phi_B \frac{d(\mathbf{I} - \mathcal{E}_{\phi_B})}{dt} \phi_B \\ &\stackrel{18.22a}{=} \phi_B \left(\Delta_{B/O} \frac{d\mathcal{E}_\phi}{dt} \Delta_{B/O}^{-1} + \bar{\mathcal{V}}_{B/O}\mathcal{E}_{\phi_B} - \mathcal{E}_{\phi_B}\bar{\mathcal{V}}_{B/O} \right) \phi_B \\ &\stackrel{5.30}{=} \Delta_{B/O}\phi \frac{d\mathcal{E}_\phi}{dt} \phi \Delta_{B/O}^{-1} + \phi_B \bar{\mathcal{V}}_{B/O}\tilde{\phi}_B - \tilde{\phi}_B \bar{\mathcal{V}}_{B/O}\phi_B \\ &\stackrel{5.30}{=} -\Delta_{B/O}\phi \frac{d(\mathbf{I} - \mathcal{E}_\phi)}{dt} \phi \Delta_{B/O}^{-1} - \phi_B \bar{\mathcal{V}}_{B/O} + \bar{\mathcal{V}}_{B/O}\phi_B \\ &\stackrel{A.28}{=} -\Delta_{B/O} \frac{d\phi}{dt} \Delta_{B/O}^{-1} - \phi_B \bar{\mathcal{V}}_{B/O} + \bar{\mathcal{V}}_{B/O}\phi_B \end{aligned}$$

For (18.22c), we have

$$\begin{aligned} \frac{dH_B}{dt} &\stackrel{5.31}{=} \frac{dH\Delta_{B/O}^{-1}}{dt} \stackrel{18.21b}{=} \dot{H}\Delta_{B/O}^{-1} - H\bar{\mathcal{V}}_{B/O} \\ &\stackrel{C.46}{=} \dot{H}\Delta_{B/O}^{-1} - H\Delta_{B/O}^{-1}\bar{\mathcal{V}}_{B/O} \stackrel{5.31}{=} \dot{H}\Delta_{B/O}^{-1} - H_B\bar{\mathcal{V}}_{B/O} \end{aligned}$$

Solution 18.6 (pp. 361): Alternative derivation of $\dot{\mathcal{M}}$ expression

1. We have

$$\begin{aligned} \frac{d\phi\mathbf{M}\phi^*}{dt} &= \dot{\phi}\mathbf{M}\phi^* + \phi\dot{\mathbf{M}}\phi^* + \phi\mathbf{M}\dot{\phi}^* \\ &\stackrel{18.12}{=} \left[\tilde{\phi}\bar{\Delta}_V\phi + \tilde{\mathcal{V}}^\omega\phi - \phi\tilde{\mathcal{V}}^\omega \right] \mathbf{M}\phi^* + \phi \left[\tilde{\mathcal{V}}^\omega\mathbf{M} - \mathbf{M}\tilde{\mathcal{V}}^\omega \right] \phi^* \\ &\quad + \phi\mathbf{M} \left[-\phi^*\tilde{\Delta}_V\tilde{\phi}^* - \phi^*\tilde{\mathcal{V}}^\omega + \tilde{\mathcal{V}}^\omega\phi^* \right] \\ &= \left[\tilde{\phi}\bar{\Delta}_V + \tilde{\mathcal{V}}^\omega \right] \phi\mathbf{M}\phi^* - \phi\mathbf{M}\phi^* \left[\tilde{\Delta}_V\tilde{\phi}^* + \tilde{\mathcal{V}}^\omega \right] \end{aligned}$$

This establishes (18.24).

2. For $\dot{\mathcal{M}}$, we have

$$\begin{aligned}
 \dot{\mathcal{M}} &= \dot{\mathbf{H}}\phi\mathbf{M}\phi^*\mathbf{H}^* + \mathbf{H}\frac{d\phi\mathbf{M}\phi^*}{dt}\mathbf{H}^* + \mathbf{H}\phi\mathbf{M}\phi^*\dot{\mathbf{H}}^* \\
 &\stackrel{18.12,18.24}{=} -\mathbf{H}\tilde{\mathcal{V}}_{\mathcal{S}}^\omega\phi\mathbf{M}\phi^*\mathbf{H}^* + \mathbf{H}\phi\mathbf{M}\phi^*\tilde{\mathcal{V}}_{\mathcal{S}}^\omega\mathbf{H}^* \\
 &\quad + \mathbf{H}\left\{\left[\tilde{\phi}\bar{\Delta}_{\mathcal{V}} + \tilde{\mathcal{V}}^\omega\right]\phi\mathbf{M}\phi^* - \phi\mathbf{M}\phi^*\left[\tilde{\Delta}_{\mathcal{V}}\tilde{\phi}^* + \tilde{\mathcal{V}}^\omega\right]\right\}\mathbf{H}^* \\
 &\stackrel{18.5}{=} \mathbf{H}\left\{\left[\tilde{\phi}\bar{\Delta}_{\mathcal{V}} + \tilde{\Delta}_{\mathcal{V}}^\omega\right]\phi\mathbf{M}\phi^* - \phi\mathbf{M}\phi^*\left[\tilde{\Delta}_{\mathcal{V}}\tilde{\phi}^* + \tilde{\Delta}_{\mathcal{V}}^\omega\right]\right\}\mathbf{H}^* \\
 &= \mathbf{H}\phi\left\{\left[\mathcal{E}_\phi\bar{\Delta}_{\mathcal{V}} + (\mathbf{I} - \mathcal{E}_\phi)\tilde{\Delta}_{\mathcal{V}}^\omega\right]\phi\mathbf{M}\right. \\
 &\quad \left.- \mathbf{M}\phi^*\left[\tilde{\Delta}_{\mathcal{V}}\mathcal{E}_\phi^* + \tilde{\Delta}_{\mathcal{V}}^\omega(\mathbf{I} - \mathcal{E}_\phi^*)\right]\right\}\phi^*\mathbf{H}^* \\
 &\stackrel{1.22}{=} \mathbf{H}\phi\left\{\left[\mathcal{E}_\phi\bar{\Delta}_{\mathcal{V}} + \tilde{\Delta}_{\mathcal{V}}^\omega\right]\phi\mathbf{M} - \mathbf{M}\phi^*\left[\tilde{\Delta}_{\mathcal{V}}\mathcal{E}_\phi^* + \tilde{\Delta}_{\mathcal{V}}^\omega\right]\right\}\phi^*\mathbf{H}^*
 \end{aligned}$$

This establishes (18.23).

Solution 18.7 (pp. 363): Sensitivities of $\phi(\varphi(k), k)$, $H(k)$ and $M(k)$

The expressions in (18.29) follow directly from applying (18.26) and (18.28) to the time derivative expressions in (18.10), together with the expressions in (18.28).

Solution 18.8 (pp. 364): Sensitivity of $H\phi$

Equation (18.34) follows from applying (18.26) and (18.31) to the time derivative expressions in (18.13).

Solution 18.9 (pp. 368): Equivalence of Lagrangian and Newton–Euler equations of motion

1. From (2.2) we see that the $\mathfrak{b}_{\mathcal{J}}$ stacked vector can be expressed as

$$\mathfrak{b}_{\mathcal{J}} = [\bar{\mathcal{V}}\mathbf{M} - \mathbf{M}\bar{\mathcal{V}}] \mathcal{V}$$

Also, we have seen in (C.44) that

$$\phi^*\mathfrak{a}_{\mathcal{J}} = [\tilde{\mathcal{V}}^\omega - \phi^*\tilde{\Delta}_{\mathcal{V}}^\omega - \phi^*\tilde{\Delta}_{\mathcal{V}}^v\mathcal{E}_\phi^*] \mathcal{V}$$

Using these in (18.39) leads to

$$\begin{aligned}
 \mathcal{C}(\theta, \dot{\theta}) &= \mathbf{H}\phi\left[\bar{\mathcal{V}}\mathbf{M} - \mathbf{M}\bar{\mathcal{V}} + \mathbf{M}\left(\tilde{\mathcal{V}}^\omega - \phi^*\tilde{\Delta}_{\mathcal{V}}^\omega - \phi^*\tilde{\Delta}_{\mathcal{V}}^v\mathcal{E}_\phi^*\right)\right]\mathcal{V} \\
 &\stackrel{1.22}{=} \mathbf{H}\phi\left[\bar{\mathcal{V}}\mathbf{M} - \mathbf{M}\bar{\mathcal{V}}^v - \mathbf{M}\phi^*\left(\tilde{\Delta}_{\mathcal{V}}^\omega + \tilde{\Delta}_{\mathcal{V}}^v\mathcal{E}_\phi^*\right)\right]\mathcal{V}
 \end{aligned}$$

Noting that $\bar{\mathcal{V}}^T \mathcal{V} = \mathbf{0}$ helps simplify the above expression and leads to the expression in (18.41). This establishes the first part of this exercise.

2. We have

$$\begin{aligned}\dot{\mathcal{M}}(\theta)\dot{\theta} &= \frac{1}{2} \frac{\partial[\dot{\theta}^* \mathcal{M}(\theta) \dot{\theta}]}{\partial \theta} \\ &\stackrel{18.23, 18.38b}{=} \mathsf{H}\phi \left[\bar{\mathcal{V}} - \left(\mathcal{E}_\phi \bar{\Delta}_{\mathcal{V}}^\omega + \tilde{\Delta}_{\mathcal{V}}^\omega \right) \phi \right] \mathbf{M} \mathcal{V} \\ &\quad + \mathsf{H}\phi \left[\left(\tilde{\Delta}_{\mathcal{V}}^\omega + \mathcal{E}_\phi \bar{\Delta}_{\mathcal{V}}^\omega \right) \phi \mathbf{M} - \mathbf{M} \phi^* \left(\tilde{\Delta}_{\mathcal{V}}^\omega \mathcal{E}_\phi^* + \tilde{\Delta}_{\mathcal{V}}^\omega \right) \right] \mathcal{V} \\ &= \mathsf{H}\phi \left[\bar{\mathcal{V}} \mathbf{M} - \mathbf{M} \phi^* \left(\tilde{\Delta}_{\mathcal{V}}^\omega \mathcal{E}_\phi^* + \tilde{\Delta}_{\mathcal{V}}^\omega \right) \right] \mathcal{V}\end{aligned}$$

This is indeed the expression in (18.41) and establishes the second part of this exercise.

Solution 18.10 (pp. 373): Physical interpretation of $\check{\lambda}$

In general

$$\dot{\mathcal{P}}(k) = \frac{d_{\mathbb{I}} \mathcal{P}(k)}{dt} = \frac{d_{\mathbb{O}_k^+} \mathcal{P}(k)}{dt} + \tilde{\mathcal{V}}^\omega(\varphi(k)) \mathcal{P}(k) - \mathcal{P}(k) \tilde{\mathcal{V}}^\omega(\varphi(k))$$

Comparing this expression with that of $\dot{\mathcal{P}}(k)$ in (18.50) establishes the equality for $\check{\lambda}(k)$ in (18.51). Also,

$$\check{\lambda}(k) \stackrel{18.51}{=} \frac{d_{\mathbb{O}_k^+} \mathcal{P}(k)}{dt} = \frac{d_{\mathbb{O}_k} \mathcal{P}(k)}{dt} + \tilde{\Delta}_{\mathcal{V}}^\omega(k) \mathcal{P}(k) - \mathcal{P}(k) \tilde{\Delta}_{\mathcal{V}}^\omega(k)$$

Comparing this expression with that for $\check{\lambda}(k)$ in (18.48) establishes the equality for $\check{\mathcal{P}}(k)$ in (18.51). On a similar note,

$$\dot{\mathcal{P}}^+(k) = \frac{d_{\mathbb{I}} \mathcal{P}^+(k)}{dt} = \frac{d_{\mathbb{O}_k^+} \mathcal{P}^+(k)}{dt} + \tilde{\mathcal{V}}^\omega(\varphi(k)) \mathcal{P}^+(k) - \mathcal{P}^+(k) \tilde{\mathcal{V}}^\omega(\varphi(k))$$

Comparing this expression with that for $\dot{\mathcal{P}}^+(k)$ in (18.50) establishes the equality for $\check{\mathcal{P}}^+(k)$ in (18.51).

Solution 18.11 (pp. 375): Time derivative of $(\mathbf{I} + \mathsf{H}\phi \mathcal{K})$

We have

$$[\mathbf{I} + \mathsf{H}\phi \mathcal{K}] = [\mathbf{I} + \mathsf{H}\tilde{\phi} \mathcal{G}] = [\mathbf{I} - \mathsf{H}\mathcal{G} + \mathsf{H}\phi \mathcal{G}] = \mathsf{H}\phi \mathcal{G} \quad (\text{C.47})$$

Thus,

$$\begin{aligned}
 \frac{d[I + H\phi K]}{dt} &= \frac{dH\phi}{dt} G + H\phi \dot{G} \\
 &\stackrel{18.13, 18.43c}{=} H\phi \left[\left(\tilde{\Delta}_V^\omega \phi - \tilde{V}^\omega + \mathcal{E}_\phi \bar{\Delta}_V^\nu \phi \right) G + \bar{\tau} \check{\lambda} H^* \mathcal{D}^{-1} + \tilde{V}_S^\omega G \right] \\
 &\stackrel{18.5}{=} H\phi \left[\left(\tilde{\Delta}_V^\omega \phi - \tilde{\Delta}_V^\omega + \mathcal{E}_\phi \bar{\Delta}_V^\nu \phi \right) G + \bar{\tau} \check{\lambda} H^* \mathcal{D}^{-1} \right] \\
 &= H\phi \left[\left(\tilde{\Delta}_V^\omega \tilde{\phi} + \mathcal{E}_\phi \bar{\Delta}_V^\nu \phi \right) G + \bar{\tau} \check{\lambda} H^* \mathcal{D}^{-1} \right] \\
 &= H\phi \left[\tilde{\Delta}_V^\omega \phi K + \mathcal{E}_\phi \bar{\Delta}_V^\nu \phi G + \bar{\tau} \check{\lambda} H^* \mathcal{D}^{-1} \right]
 \end{aligned}$$

Solution 18.12 (pp. 376): Time derivative of $[I + H\phi K]\mathcal{D}$

We have

$$\begin{aligned}
 \frac{d[I + H\phi K]\mathcal{D}}{dt} &= \frac{d[I + H\phi K]}{dt} \mathcal{D} + [I + H\phi K] \frac{d\mathcal{D}}{dt} \\
 &\stackrel{18.61, 18.43a, C.47}{=} H\phi \left[\tilde{\Delta}_V^\omega \phi K + \mathcal{E}_\phi \bar{\Delta}_V^\nu \phi G + \bar{\tau} \check{\lambda} H^* \mathcal{D}^{-1} \right] \mathcal{D} + H\phi G H \check{\lambda} H^* \\
 &= H\phi \left[\tilde{\Delta}_V^\omega \phi K + \mathcal{E}_\phi \bar{\Delta}_V^\nu \phi G + \bar{\tau} \check{\lambda} H^* \mathcal{D}^{-1} \right] \mathcal{D} + H\phi \tau \check{\lambda} H^* \\
 &= H\phi \left[\tilde{\Delta}_V^\omega \phi K + \mathcal{E}_\phi \bar{\Delta}_V^\nu \phi G + \check{\lambda} H^* \mathcal{D}^{-1} \right] \mathcal{D} \\
 &= H\phi \left[\tilde{\Delta}_V^\omega \tilde{\phi} \mathcal{P} + \mathcal{E}_\phi \bar{\Delta}_V^\nu \phi \mathcal{P} + \check{\lambda} \right] H^*
 \end{aligned}$$

Solution 18.13 (pp. 376): Time derivative of $[I - H\psi K]$

Since $[I - H\psi K]^{-1} = [I + H\phi K]$ it follows from (A.28) on page 402 that

$$\begin{aligned}
 \frac{d[I - H\psi K]}{dt} &= -[I + H\phi K] \frac{d[I - H\psi K]}{dt} [I - H\psi K] \\
 &\stackrel{18.61}{=} -[I + H\phi K] H\phi \left[\tilde{\Delta}_V^\omega \phi K + \mathcal{E}_\phi \bar{\Delta}_V^\nu \phi G + \bar{\tau} \check{\lambda} H^* \mathcal{D}^{-1} \right] [I - H\psi K] \\
 &\stackrel{9.45}{=} -H\psi \left[\tilde{\Delta}_V^\omega \phi K + \mathcal{E}_\phi \bar{\Delta}_V^\nu \phi G + \bar{\tau} \check{\lambda} H^* \mathcal{D}^{-1} \right] [I - H\psi K]
 \end{aligned}$$

This establishes the result.

Solution 18.14 (pp. 376): Sensitivities of $[I + H\phi K]$ and $[I - H\psi K]$

The expressions are obtained by starting with the time derivative expressions in (18.61) and (18.63) and using the standard process for converting them into sensitivity expressions.

Solution 18.15 (pp. 377): Sensitivity of $\log\{\det\{\mathcal{M}\}\}$

- From (9.53) on page 180, we have

$$\det\{\mathcal{M}\} = \prod_{k=1}^n \det\{\mathcal{D}(k)\}$$

Hence,

$$\log\{\det\{\mathcal{M}\}\} = \sum_{k=1}^n \log\{\det\{\mathcal{D}(k)\}\} \quad (\text{C.48})$$

Differentiating with respect to t we have

$$\begin{aligned} \frac{d \log\{\det\{\mathcal{M}\}\}}{dt} &\stackrel{\text{C.48}}{=} \sum_{k=1}^n \frac{d \log\{\det\{\mathcal{D}(k)\}\}}{dt} \stackrel{\text{A.29}}{=} \sum_{k=1}^n \mathcal{D}^{-1}(k) \dot{\mathcal{D}}(k) \\ &= \text{Trace}\{\mathcal{D}^{-1} \dot{\mathcal{D}}\} \stackrel{\text{18.43a}}{=} \text{Trace}\{\mathcal{D}^{-1} H \check{\lambda} H^*\} \end{aligned}$$

To establish the first expression in (18.66), differentiate both sides by $\dot{\theta}_i$ and use (18.53). Use the component level expressions in (18.55) to establish the latter half of (18.66).

- For (18.68), we have

$$\begin{aligned} 2 \text{Trace}\{\mathcal{P}\Omega \mathcal{H}_{=i}^\omega\} &\stackrel{\text{A.22}}{=} 2 \text{Trace}\{\mathcal{H}_{=i}^\omega \mathcal{P}\Omega\} \\ &\stackrel{\text{A.22}}{=} \text{Trace}\{\mathcal{H}_{=i}^\omega \mathcal{P}\Omega\} + \text{Trace}\{[\mathcal{H}_{=i}^\omega \mathcal{P}\Omega]^*\} \\ &\stackrel{\text{A.22,A.21}}{=} \text{Trace}\{\mathcal{H}_{=i}^\omega \mathcal{P}\Omega\} - \text{Trace}\{\Omega \mathcal{P} \mathcal{H}_{=i}^\omega\} \\ &= \text{Trace}\{\mathcal{H}_{=i}^\omega \mathcal{P}\Omega\} - \text{Trace}\{\mathcal{P} \mathcal{H}_{=i}^\omega \Omega\} \\ &= \text{Trace}\{[\mathcal{H}_{=i}^\omega \mathcal{P} - \mathcal{P} \mathcal{H}_{=i}^\omega] \Omega\} \\ &= \text{Trace}\{[\mathcal{H}_{=i}^\omega \mathcal{P} - \mathcal{P} \mathcal{H}_{=i}^\omega] \Omega\} \\ &\stackrel{\text{18.54g}}{=} \text{Trace}\{[\check{\lambda}_{\theta_i} - \mathcal{E}_\psi \check{\lambda}_{\theta_i} \mathcal{E}_\psi^*] \Omega\} \\ &\stackrel{\text{10.12}}{=} \text{Trace}\{[\check{\lambda}_{\theta_i} - \mathcal{E}_\psi \check{\lambda}_{\theta_i} \mathcal{E}_\psi^*] \psi^* H^* \mathcal{D}^{-1} H \psi\} \\ &= \text{Trace}\{\mathcal{D}^{-1} H \psi [\check{\lambda}_{\theta_i} - \mathcal{E}_\psi \check{\lambda}_{\theta_i} \mathcal{E}_\psi^*] \psi^* H^*\} \\ &= \text{Trace}\{\mathcal{D}^{-1} H [\psi \check{\lambda}_{\theta_i} \psi^* - \tilde{\psi} \check{\lambda}_{\theta_i} \tilde{\psi}^*] H^*\} \\ &= \text{Trace}\{\mathcal{D}^{-1} H [(I + \tilde{\psi}) \check{\lambda}_{\theta_i} (I + \tilde{\psi}^*) - \tilde{\psi} \check{\lambda}_{\theta_i} \tilde{\psi}^*] H^*\} \\ &= \text{Trace}\{\mathcal{D}^{-1} H [\check{\lambda}_{\theta_i} + \tilde{\psi} \check{\lambda}_{\theta_i} + \check{\lambda}_{\theta_i} \tilde{\psi}^*] H^*\} \\ &= \text{Trace}\{\mathcal{D}^{-1} H \check{\lambda}_{\theta_i} H^*\} \end{aligned}$$

The last equality above uses the zero block-diagonal elements property of $\tilde{\psi}$. The last expression is the same as (18.66), and establishes the equivalency of (18.66) and (18.67).

3. For (18.68), we have

$$\begin{aligned}
 \frac{d \log \{\det \{\mathcal{M}\}\}}{dt} &\stackrel{A.29}{=} \text{Trace} \{\mathcal{M}^{-1} \dot{\mathcal{M}}\} \\
 &\stackrel{9.51, 18.23}{=} \text{Trace} \left\{ [\mathbf{I} - \mathbf{H} \psi \mathcal{K}]^* \mathcal{D}^{-1} [\mathbf{I} - \mathbf{H} \psi \mathcal{K}] \mathbf{H} \phi \cdot \right. \\
 &\quad \left. \left[(\tilde{\Delta}_v^\omega + \mathcal{E}_\phi \bar{\Delta}_v^\nu) \phi \mathbf{M} - \mathbf{M} \phi^* (\tilde{\Delta}_v^\nu \mathcal{E}_\phi^* + \tilde{\Delta}_v^\omega) \right] \phi^* \mathbf{H}^* \right\} \\
 &\stackrel{9.45}{=} \text{Trace} \{ \mathcal{D}^{-1} \mathbf{H} \psi \left[(\tilde{\Delta}_v^\omega + \mathcal{E}_\phi \bar{\Delta}_v^\nu) \phi \mathbf{M} \right. \\
 &\quad \left. - \mathbf{M} \phi^* (\tilde{\Delta}_v^\nu \mathcal{E}_\phi^* + \tilde{\Delta}_v^\omega) \right] \psi^* \mathbf{H}^* \} \\
 &\stackrel{10.12}{=} \text{Trace} \left\{ \left[(\tilde{\Delta}_v^\omega + \mathcal{E}_\phi \bar{\Delta}_v^\nu) \phi \mathbf{M} - \mathbf{M} \phi^* (\tilde{\Delta}_v^\nu \mathcal{E}_\phi^* + \tilde{\Delta}_v^\omega) \right] \Omega \right\} \\
 &= 2 \text{Trace} \left\{ \left[(\tilde{\Delta}_v^\omega + \mathcal{E}_\phi \bar{\Delta}_v^\nu) \phi \mathbf{M} \Omega \right] \right\} \\
 &= 2 \text{Trace} \left\{ \tilde{\Delta}_v^\omega \phi \mathbf{M} \Omega \right\} + 2 \text{Trace} \left\{ \mathcal{E}_\phi \bar{\Delta}_v^\nu \phi \mathbf{M} \Omega \right\} \\
 &\stackrel{10.38a}{=} 2 \text{Trace} \left\{ \tilde{\Delta}_v^\omega [\phi - \psi + \mathcal{P} \Omega] \right\} + 2 \text{Trace} \left\{ \mathcal{E}_\phi \bar{\Delta}_v^\nu \phi \mathbf{M} \Omega \right\} \\
 &\stackrel{10.38a}{=} 2 \text{Trace} \left\{ \tilde{\Delta}_v^\omega \mathcal{P} \Omega \right\} + 2 \text{Trace} \left\{ \mathcal{E}_\phi \bar{\Delta}_v^\nu \phi \mathbf{M} \Omega \right\}
 \end{aligned}$$

The last equality uses the zero diagonal elements property of $\phi - \psi$.

Solutions for Chapter 19

Solution 19.1 (pp. 387): Time derivative of $\mathcal{D}^{\frac{1}{2}}$

We have

$$\dot{\mathcal{D}} = \frac{d \mathcal{D}^{\frac{1}{2}} \cdot \mathcal{D}^{\frac{1}{2}}}{dt} = \frac{d \mathcal{D}^{\frac{1}{2}}}{dt} \mathcal{D}^{\frac{1}{2}} + \mathcal{D}^{\frac{1}{2}} \frac{d \mathcal{D}^{\frac{1}{2}}}{dt}$$

For a system with 1 degree of freedom joints, the diagonal block elements of $\mathcal{D}^{\frac{1}{2}}$ are in fact scalar values, so that $\mathcal{D}^{1/2}$ and $\frac{d \mathcal{D}^{1/2}}{dt}$ commute. Thus, the above can be transformed into

$$\frac{d \mathcal{D}^{\frac{1}{2}}}{dt} = \frac{1}{2} \mathcal{D}^{-\frac{1}{2}} \dot{\mathcal{D}} \stackrel{18.43a}{=} \frac{1}{2} \mathcal{D}^{-\frac{1}{2}} \mathbf{H} \check{\lambda} \mathbf{H}^*$$

Solution 19.2 (pp. 391): Non-working $\mathcal{C}(\theta, \eta)$ Coriolis Vector

$$\begin{aligned}
 \eta^* \mathcal{C}(\theta, \eta) &\stackrel{19.29}{=} \eta^* \mathcal{D}^{-\frac{1}{2}} \mathbf{H} \psi \left[\bar{\mathbf{V}} \mathbf{M} - \frac{1}{2} \left(\tilde{\Delta}_v^\omega \mathcal{P} + \mathcal{P} \tilde{\Delta}_v^\omega \right) \right. \\
 &\quad \left. + \mathcal{E}_\phi \left\{ \bar{\Delta}_v^\nu \mathcal{P}^+ + \mathcal{P}^+ \tilde{\Delta}_v^\nu \right\} \mathcal{E}_\phi^* + \mathcal{E}_\psi \check{\lambda} - \check{\lambda} \mathcal{E}_\psi^* \right] \nu
 \end{aligned}$$

Observe that

$$\eta^* \mathcal{D}^{-\frac{1}{2}} H \Psi \stackrel{19.23}{=} \dot{\theta}^* [\mathbf{I} + H \phi K] H \Psi \stackrel{9.45}{=} \dot{\theta}^* H \phi$$

Thus,

$$\begin{aligned} \eta^* \mathcal{C}(\theta, \eta) &= \dot{\theta}^* H \phi \left[\bar{V} M - \frac{1}{2} \left(\tilde{\Delta}_V^\omega P + P \tilde{\Delta}_V^\omega \right. \right. \\ &\quad \left. \left. + \mathcal{E}_\phi \left\{ \bar{\Delta}_V^\nu P^+ + P^+ \tilde{\Delta}_V^\nu \right\} \mathcal{E}_\phi^* + \mathcal{E}_\psi \check{\lambda} - \check{\lambda} \mathcal{E}_\psi^* \right) \right] V \\ &\stackrel{9.1}{=} V^* \left[\bar{V} M - \frac{1}{2} \left(\tilde{\Delta}_V^\omega P + P \tilde{\Delta}_V^\omega \right. \right. \\ &\quad \left. \left. + \mathcal{E}_\phi \left\{ \bar{\Delta}_V^\nu P^+ + P^+ \tilde{\Delta}_V^\nu \right\} \mathcal{E}_\phi^* + \mathcal{E}_\psi \check{\lambda} - \check{\lambda} \mathcal{E}_\psi^* \right) \right] V \\ &\stackrel{1.26}{=} -\frac{1}{2} V^* \left[\tilde{\Delta}_V^\omega P + P \tilde{\Delta}_V^\omega \right. \\ &\quad \left. + \mathcal{E}_\phi \left\{ \bar{\Delta}_V^\nu P^+ + P^+ \tilde{\Delta}_V^\nu \right\} \mathcal{E}_\phi^* + \mathcal{E}_\psi \check{\lambda} - \check{\lambda} \mathcal{E}_\psi^* \right] V \end{aligned}$$

Since the matrix expression in the middle is skew-symmetric, the expression evaluates to zero.

Solution 19.3 (pp. 392): Expression for $\dot{\ell}$

It follows from $\ell^{-1} = m$ and (A.28) on page 402 that

$$\begin{aligned} \dot{\ell} &\stackrel{A.28}{=} -\ell m \ell \\ &\stackrel{19.25}{=} -\mathcal{D}^{-\frac{1}{2}} [\mathbf{I} - H \Psi K] H \Psi \left[\tilde{\Delta}_V^\omega \phi K \right. \\ &\quad \left. + \mathcal{E}_\phi \bar{\Delta}_V^\nu \phi G + \frac{1}{2} (\mathbf{I} + \bar{\tau}) \check{\lambda} H^* \mathcal{D}^{-1} \right] \mathcal{D}^{\frac{1}{2}} \mathcal{D}^{-\frac{1}{2}} [\mathbf{I} - H \Psi K] \\ &\stackrel{9.45}{=} -\mathcal{D}^{-\frac{1}{2}} H \Psi \left[\tilde{\Delta}_V^\omega \phi K + \mathcal{E}_\phi \bar{\Delta}_V^\nu \phi G + \frac{1}{2} (\mathbf{I} + \bar{\tau}) \check{\lambda} H^* \mathcal{D}^{-1} \right] [\mathbf{I} - H \Psi K] \end{aligned}$$

Solution 19.4 (pp. 392): Sensitivity of Innovations factors

The expressions are obtained by starting with the time derivative expressions in (19.25) and (19.33) and using the standard process for converting them into sensitivity expressions.

Solutions for Appendix A

Solution A.1 (pp. 397): Norm of \tilde{s}

We have

$$\|\tilde{s}\|^2 = -x^* \tilde{s} s x \stackrel{A.1}{=} -x^* [ss^* - \|s\|^2 \mathbf{I}] x = \|s\|^2 \|x\|^2 - (x^* s)^2$$

Clearly the above achieves a maximum of $\|s\|^2 \|x\|^2$ when $x^* s = 0$. Hence, using (A.2) it follows that $\|\tilde{s}\| = \|s\|$.

Solution A.2 (pp. 401): Product gradient and chain rules

1. The (k, j) element of $\nabla_x [f(x)g(x)]$ is

$$\nabla_x [f(x)g(x)](k, j) = \frac{\partial f_k \cdot g}{\partial x_j} = \frac{\partial f_k}{\partial x_j} \cdot g + f_k \cdot \frac{\partial g}{\partial x_j} \quad (C.49)$$

On the other hand, the (k, j) element of $\nabla_x f(x) \cdot g(x) + f(x) \cdot \nabla_x g(x)$, the right-hand side of (A.25), is given by:

$$[\nabla_x f(x) \cdot g(x) + f(x) \cdot \nabla_x g(x)](k, j) = \frac{\partial f_k}{\partial x_j} \cdot g + f_k \frac{\partial g}{\partial x_j}$$

This is identical to the expression in (C.49). Thus, the component-level values on both sides of (A.25) agree and establish (A.25).

2. The (k, j) element of $\nabla_x f(x)$ is

$$[\nabla_x f(x)](k, j) = \frac{\partial f_k}{\partial x_j} = \sum_{i=1}^n \frac{\partial f_k}{\partial y_i} \cdot \frac{\partial y_i}{\partial x_j} \quad (C.50)$$

On the other hand, the (k, j) element of $\nabla_y f(y) \cdot \nabla_x y(x)$, the right-hand side of (A.26), is given by:

$$[\nabla_y f(y) \cdot \nabla_x y(x)](k, j) = \sum_{i=1}^n [\nabla_y f(y)](k, i) \cdot [\nabla_x y(x)](i, j) = \sum_{i=1}^n \frac{\partial f_k}{\partial y_i} \cdot \frac{\partial y_i}{\partial x_j}$$

This is identical to the expression in (C.50). Thus, the component-level values on both sides of (A.26) agree and establish (A.26).

Solutions for Appendix B

Solution B.1 (pp. 403): Time derivative of a rotation matrix

Since rotation matrices are orthogonal, $\mathfrak{R}\mathfrak{R}^* = \mathbf{I}$. Differentiating this with respect to time yields

$$\dot{\mathfrak{R}}\mathfrak{R}^* + \mathfrak{R}\dot{\mathfrak{R}}^* = \mathbf{0} \Rightarrow \dot{\mathfrak{R}}\mathfrak{R}^* = -[\mathfrak{R}\dot{\mathfrak{R}}^*]^*$$

This implies that $\dot{\mathfrak{R}}\mathfrak{R}^*$ is skew-symmetric, i.e., there exists a 3-vector w , such that, $\dot{\mathfrak{R}}\mathfrak{R}^* = \tilde{w}$. This establishes the result.

Solution B.2 (pp. 405): Derivation of the Euler–Rodrigues formula

1. While this can be established by direct verification using an arbitrary vector s we use alternative derivation. Thus

$$\tilde{s}^3 \stackrel{\text{A.1}}{=} \tilde{s}(ss^* - \|s\|^2\mathbf{I}) = -\sigma^2\tilde{s} \quad (\text{C.51})$$

We know that the characteristic polynomial of \tilde{s} is a polynomial of order 3 and, that it is the unique polynomial of order 3 that \tilde{s} satisfies as well. It follows therefore, from (C.51) that the characteristic polynomial of \tilde{s} is $(\lambda^3 + \sigma^2\lambda)$.

2. We have that

$$\begin{aligned} \mathfrak{R}_{\mathbb{B}}(\mathbf{n}, \theta) &\stackrel{\text{B.4}}{=} \exp[\tilde{\mathbf{n}}\theta] = \mathbf{I} + \tilde{\mathbf{n}}\theta + \frac{\tilde{\mathbf{n}}^2\theta^2}{2!} + \frac{\tilde{\mathbf{n}}^3\theta^3}{3!} + \dots \\ &\stackrel{\text{C.51}}{=} \mathbf{I} + \sum_{k=0}^{\infty} \frac{(-1)^k\theta^{2k+1}}{(2k+1)!} \tilde{\mathbf{n}} + \sum_{k=0}^{\infty} \frac{(-1)^k\theta^{2k+2}}{(2k+2)!} \tilde{\mathbf{n}}^2 \\ &= \mathbf{I} + \sin(\theta)\tilde{\mathbf{n}} + [1 - \cos(\theta)]\tilde{\mathbf{n}}^2 \\ &\stackrel{\text{A.1}}{=} \cos(\theta)\mathbf{I}_3 + [1 - \cos(\theta)]\mathbf{n}\mathbf{n}^* + \sin(\theta)\tilde{\mathbf{n}} \end{aligned}$$

Solution B.3 (pp. 405): Trace and characteristic polynomial of a rotation matrix

1. The result follows by applying the trace operation to (B.6) on page 405 and noting that $\text{Trace}\{\mathbf{I}\} = 3$, $\text{Trace}\{\mathbf{n}\mathbf{n}^*\} = 1$, and $\text{Trace}\{\tilde{\mathbf{n}}\} = 0$.
2. Since \mathfrak{R} is a 3×3 matrix, its characteristic polynomial is of the form $\lambda^3 + a\lambda^2 + b\lambda + c$ for some constants a , b and c . From matrix theory we know that $-a$ is equal to the trace γ , and $-c$ is the determinant 1 of the matrix. That is the polynomial is of the form $\lambda^3 - \gamma\lambda^2 + b\lambda - 1$. Furthermore, we know that 1 is an eigen-value of \mathfrak{R} and hence, must satisfy the characteristic polynomial. Using this fact implies that $b = \gamma$, establishing the result.

3. Use the second expression from (B.6) to verify that

$$\mathfrak{R}\mathbf{n} = \mathbf{n}$$

This establishes that \mathbf{n} is an eigen-vector with eigen-value 1.

4. Since $\tilde{\mathbf{n}}\tilde{\mathbf{n}}$ is a symmetric matrix, from (B.6) we obtain

$$\mathfrak{R} - \mathfrak{R}^* = 2 \sin(\theta) \tilde{\mathbf{n}}$$

from which (B.9) follows.

Solution B.4 (pp. 406): Angular velocity from the angle/axis rates

Differentiating $\mathbf{n}^*\mathbf{n} = 1$, we obtain $\mathbf{n}^*\dot{\mathbf{n}} = 0$. Thus

$$\tilde{\mathbf{n}}\tilde{\mathbf{n}}\tilde{\mathbf{n}} = \tilde{\mathbf{n}}[\mathbf{n}\dot{\mathbf{n}}^* - \mathbf{n}^*\dot{\mathbf{n}}\mathbf{I}] = \mathbf{0} \quad (\text{C.52})$$

Also, it is easy to verify that

$$\tilde{\mathbf{n}}\tilde{\mathbf{n}}\tilde{\mathbf{n}} = -\tilde{\mathbf{n}} \quad (\text{C.53})$$

Using these cross product identities, we have,

$$\begin{aligned} {}^{\mathbb{B}}\tilde{\omega} &= {}^{\mathbb{B}}\mathfrak{R}_{\mathbb{I}}{}^{\mathbb{I}}\dot{\mathfrak{R}}_{\mathbb{B}} = [\mathbf{I}_3 + (1 - \cos(\theta))\tilde{\mathbf{n}}\tilde{\mathbf{n}} - \sin(\theta)\tilde{\mathbf{n}}] \times \\ &\quad \left[(\sin(\theta)\tilde{\mathbf{n}}\tilde{\mathbf{n}} + \cos(\theta)\tilde{\mathbf{n}})\dot{\theta} + (\sin(\theta) + (1 - \cos(\theta))\tilde{\mathbf{n}})\tilde{\mathbf{n}} \right. \\ &\quad \left. + (1 - \cos(\theta))\tilde{\mathbf{n}}\tilde{\mathbf{n}} \right] \\ &= \left[\sin(\theta)\tilde{\mathbf{n}}\tilde{\mathbf{n}} + \cos(\theta)\tilde{\mathbf{n}} - \sin^2(\theta)\tilde{\mathbf{n}}\tilde{\mathbf{n}}\tilde{\mathbf{n}} - \sin(\theta)\cos(\theta)\tilde{\mathbf{n}}\tilde{\mathbf{n}} \right. \\ &\quad \left. + \sin(\theta)(1 - \cos(\theta))\tilde{\mathbf{n}}\tilde{\mathbf{n}}\tilde{\mathbf{n}}\tilde{\mathbf{n}} + \cos(\theta)(1 - \cos(\theta))\tilde{\mathbf{n}}\tilde{\mathbf{n}}\tilde{\mathbf{n}} \right]\dot{\theta} \\ &\quad + \sin(\theta)\tilde{\mathbf{n}} + (1 - \cos(\theta))\tilde{\mathbf{n}}\tilde{\mathbf{n}} - \sin^2(\theta)\tilde{\mathbf{n}}\tilde{\mathbf{n}} - \sin(\theta)(1 - \cos(\theta))\tilde{\mathbf{n}}\tilde{\mathbf{n}}\tilde{\mathbf{n}} \\ &\quad + \sin(\theta)(1 - \cos(\theta))\tilde{\mathbf{n}}\tilde{\mathbf{n}}\tilde{\mathbf{n}} + (1 - \cos(\theta))^2\tilde{\mathbf{n}}\tilde{\mathbf{n}}\tilde{\mathbf{n}}\tilde{\mathbf{n}} + (1 - \cos(\theta))\tilde{\mathbf{n}}\tilde{\mathbf{n}} \\ &\quad - \sin(\theta)(1 - \cos(\theta))\tilde{\mathbf{n}}\tilde{\mathbf{n}}\tilde{\mathbf{n}} + (1 - \cos(\theta))^2\tilde{\mathbf{n}}\tilde{\mathbf{n}}\tilde{\mathbf{n}}\tilde{\mathbf{n}} \\ &\stackrel{\text{C.52,C.53}}{=} \tilde{\mathbf{n}}\dot{\theta} + \sin(\theta)\tilde{\mathbf{n}} + (1 - \cos(\theta))\tilde{\mathbf{n}}\tilde{\mathbf{n}} - \sin^2(\theta)\tilde{\mathbf{n}}\tilde{\mathbf{n}} \\ &\quad - (1 - \cos(\theta))^2\tilde{\mathbf{n}}\tilde{\mathbf{n}} + (1 - \cos(\theta))\tilde{\mathbf{n}}\tilde{\mathbf{n}} \\ &= \tilde{\mathbf{n}}\dot{\theta} + \sin(\theta)\tilde{\mathbf{n}} - (1 - \cos(\theta))\tilde{\mathbf{n}}\tilde{\mathbf{n}} + (1 - \cos(\theta))\tilde{\mathbf{n}}\tilde{\mathbf{n}} \\ &= \tilde{\mathbf{n}}\dot{\theta} + \sin(\theta)\tilde{\mathbf{n}} - (1 - \cos(\theta))\widetilde{\mathbf{n}}\tilde{\mathbf{n}} \end{aligned}$$

Hence

$${}^{\mathbb{B}}\omega = \mathbf{n}\dot{\theta} + \sin(\theta)\dot{\mathbf{n}} - (1 - \cos(\theta))\widetilde{\mathbf{n}}\tilde{\mathbf{n}} \quad (\text{C.54})$$

This establishes (B.10).

Solution B.5 (pp. 406): Angle/axis rates from the angular velocity

We have

$$\begin{aligned} & [\sin(\theta) - (1 - \cos\theta)\tilde{\mathbf{n}}, \quad \mathbf{n}] \begin{bmatrix} \frac{1}{2}[\tilde{\mathbf{n}} - \cot(\theta/2)\tilde{\mathbf{n}}\tilde{\mathbf{n}}\tilde{\mathbf{n}}] \\ \mathbf{n}^* \end{bmatrix} \\ &= \frac{1}{2} \left[-(1 - \cos\theta)\tilde{\mathbf{n}}\tilde{\mathbf{n}} + (1 - \cos\theta)\cot(\theta/2)\tilde{\mathbf{n}}\tilde{\mathbf{n}} \right. \\ &\quad \left. + \sin(\theta)\tilde{\mathbf{n}} - \sin(\theta)\cot(\theta/2)\tilde{\mathbf{n}}\tilde{\mathbf{n}} \right] + \mathbf{n}\mathbf{n}^* \end{aligned} \quad (\text{C.55})$$

However,

$$\begin{aligned} \tilde{\mathbf{n}}\tilde{\mathbf{n}} &= \mathbf{n}\mathbf{n}^* - \mathbf{I}, \quad \tilde{\mathbf{n}}\tilde{\mathbf{n}}\tilde{\mathbf{n}} = -\tilde{\mathbf{n}} \\ \sin(\theta)\cot(\theta/2) &= 2\cos^2(\theta/2), \quad (1 - \cos\theta)\cot(\theta/2) = \sin(\theta/2) \end{aligned}$$

Using these in (C.55) leads to

$$\begin{aligned} & [\sin(\theta) - (1 - \cos\theta)\tilde{\mathbf{n}}, \quad \mathbf{n}] \begin{bmatrix} \frac{1}{2}[\tilde{\mathbf{n}} - \cot(\theta/2)\tilde{\mathbf{n}}\tilde{\mathbf{n}}] \\ \mathbf{n}^* \end{bmatrix} \\ &= \frac{1}{2} \left[-(1 - \cos\theta)\tilde{\mathbf{n}}\tilde{\mathbf{n}} - \sin\theta\tilde{\mathbf{n}} + \sin(\theta)\tilde{\mathbf{n}} - (1 + \cos(\theta/2))\tilde{\mathbf{n}}\tilde{\mathbf{n}} \right] + \mathbf{n}\mathbf{n}^* \\ &= -\tilde{\mathbf{n}}\tilde{\mathbf{n}} + \mathbf{n}\mathbf{n}^* = \mathbf{I} \end{aligned}$$

This implies that expressions in (B.11) and (B.10) are indeed inverses of each other, establishing the result.

Solution B.6 (pp. 407): Quaternion expression for a rotation matrix

Using $\cos(\theta) = 2\cos^2(\theta/2) - 1 = 1 - 2\sin^2(\theta/2)$, $\sin(\theta) = 2\sin(\theta/2)\cos(\theta/2)$, and (B.12) in (B.6), we obtain

$$\begin{aligned} {}^{\mathbb{R}}\mathfrak{R}_{\mathbb{B}}(\mathbf{n}, \theta) &= \cos(\theta)\mathbf{I}_3 + [1 - \cos(\theta)]\mathbf{n}\mathbf{n}^* + \sin(\theta)\tilde{\mathbf{n}} \\ &\stackrel{\text{B.12}}{=} (2q_0^2 - 1)\mathbf{I}_3 - \mathbf{q}\mathbf{q}^* + 2q_0\tilde{\mathbf{q}} \stackrel{\text{B.12}}{=} (q_0^2 - q^*q)\mathbf{I}_3 - \mathbf{q}\mathbf{q}^* + 2q_0\tilde{\mathbf{q}} \end{aligned}$$

This establishes the first equality in (B.14). The remaining equalities follow from using, and manipulating, 3-vector cross-product identities.

Solution B.7 (pp. 407): Basic properties of unit quaternions

1. We have

$$\begin{aligned}\Re(\underline{\mathbf{q}})\Re^*(\underline{\mathbf{q}}) &\stackrel{\text{B.14}}{=} [\mathbf{I} + 2\tilde{\mathbf{q}}^2]^2 - 4q_0^2\tilde{\mathbf{q}}^2 \\ &= \mathbf{I} + 4\tilde{\mathbf{q}}^2 + 4\tilde{\mathbf{q}}^4 - 4q_0^2\tilde{\mathbf{q}}^2 \\ &= \mathbf{I} + 4\tilde{\mathbf{q}}^2(\mathbf{I} + \tilde{\mathbf{q}}^2 - q_0^2\mathbf{I}) \\ &\stackrel{\text{A.1}}{=} \mathbf{I} + 4\tilde{\mathbf{q}}^2(q^*q\mathbf{I} + qq^* - q^*q\mathbf{I}) = \mathbf{I}\end{aligned}$$

2. It is easy to verify using (B.14) that $\Re(\underline{\mathbf{q}}) = \Re(-\underline{\mathbf{q}})$.
 3. Once again it is easy to check from (B.14) that $\Re(q_0, -\mathbf{q}) = \Re^*(q_0, \mathbf{q})$. Since the inverse of a rotation matrix is its transpose, the result follows.
 4. We have

$$\text{Trace}\{\Re(\underline{\mathbf{q}})\} \stackrel{\text{B.7}}{=} 1 + 2\cos(\theta) = 1 + 4\cos^2(\theta/2) - 2 \stackrel{\text{B.12}}{=} 4q_0^2 - 1$$

establishing (B.16).

5. Exercise B.3 established that \mathbf{n} is an eigen-vector of \Re with eigen-value 1. Since $\mathbf{q} = \sin(\theta/2)\mathbf{n}$, \mathbf{q} is also an eigen-vector of \Re with eigen-value 1.
 6. From (B.9) we obtain

$$\begin{aligned}\tilde{\mathbf{q}} &\stackrel{\text{B.12}}{=} \sin(\theta/2)(\Re - \Re^*)/(2\sin(\theta)) = (\Re - \Re^*)/(4\cos(\theta/2)) \\ &\stackrel{\text{B.12}}{=} (\Re - \Re^*)/(4q_0)\end{aligned}$$

This establishes (B.18).

Solution B.8 (pp. 409): Properties of E_- and E_+ matrices

1. The identities in (B.20) are established by evaluating and simplifying the various products.
 2. Similarly, the identities in (B.21) are established by evaluating and simplifying the various products.
 3. These identities are easily established by examining (B.19).
 4. We have

$$E_+(\underline{\mathbf{p}})\underline{\mathbf{q}} = \begin{bmatrix} p_0\mathbf{q} + \mathbf{p}q_0 + \tilde{\mathbf{p}}\mathbf{q} \\ p_0q_0 - \mathbf{p}^*\mathbf{q} \end{bmatrix} = \begin{pmatrix} q_0\mathbf{I} - \tilde{\mathbf{q}} & \mathbf{q} \\ -\mathbf{q}^* & q_0 \end{pmatrix} \begin{bmatrix} \mathbf{p} \\ p_0 \end{bmatrix} = E_-(\underline{\mathbf{q}})\underline{\mathbf{p}}$$

establishing (B.23).

5. We have

$$\begin{aligned}
 & E_-(\underline{\mathbf{q}})E_+(\underline{\mathbf{p}}) \\
 &= \begin{pmatrix} q_0 \mathbf{I}_3 - \tilde{\mathbf{q}} & \mathbf{q} \\ -\mathbf{q}^* & q_0 \end{pmatrix} \begin{pmatrix} p_0 \mathbf{I}_3 + \tilde{\mathbf{p}} & \mathbf{p} \\ -\mathbf{p}^* & p_0 \end{pmatrix} \\
 &= \begin{pmatrix} (q_0 \mathbf{I}_3 - \tilde{\mathbf{q}})(p_0 \mathbf{I}_3 + \tilde{\mathbf{p}}) - \mathbf{q}\mathbf{p}^* & (q_0 \mathbf{I}_3 - \tilde{\mathbf{q}})\mathbf{p} + \mathbf{q}\mathbf{p}_0 \\ -\mathbf{q}^*(p_0 \mathbf{I}_3 + \tilde{\mathbf{p}}) - \mathbf{q}_0\mathbf{p}^* & -\mathbf{q}^*\mathbf{p} + q_0\mathbf{p}_0 \end{pmatrix} \quad (\text{C.56}) \\
 &= \begin{pmatrix} q_0 p_0 \mathbf{I}_3 - \tilde{\mathbf{q}}\mathbf{p}_0 + q_0 \tilde{\mathbf{p}} - \tilde{\mathbf{q}}\tilde{\mathbf{p}} - \mathbf{q}\mathbf{p}^* & (q_0 \mathbf{p} - \tilde{\mathbf{q}}\mathbf{p} + \mathbf{q}\mathbf{p}_0) \\ -\mathbf{q}^*\mathbf{p}_0 - \mathbf{q}^*\tilde{\mathbf{p}} - \mathbf{q}_0\mathbf{p}^* & -\mathbf{q}^*\mathbf{p} + q_0\mathbf{p}_0 \end{pmatrix}
 \end{aligned}$$

Similarly,

$$\begin{aligned}
 & E_+(\underline{\mathbf{p}})E_-(\underline{\mathbf{q}}) \\
 &= \begin{pmatrix} p_0 \mathbf{I}_3 + \tilde{\mathbf{p}} & \mathbf{p} \\ -\mathbf{p}^* & p_0 \end{pmatrix} \begin{pmatrix} q_0 \mathbf{I}_3 - \tilde{\mathbf{q}} & \mathbf{q} \\ -\mathbf{q}^* & q_0 \end{pmatrix} \\
 &= \begin{pmatrix} q_0 p_0 \mathbf{I}_3 - \tilde{\mathbf{q}}\mathbf{p}_0 + q_0 \tilde{\mathbf{p}} - \tilde{\mathbf{p}}\tilde{\mathbf{q}} - \mathbf{p}\mathbf{q}^* & (q_0 \mathbf{p} + \tilde{\mathbf{p}}\mathbf{q} + \mathbf{q}\mathbf{p}_0) \\ -\mathbf{q}^*\mathbf{p}_0 + \mathbf{p}^*\tilde{\mathbf{q}} - \mathbf{q}_0\mathbf{p}^* & -\mathbf{q}^*\mathbf{p} + q_0\mathbf{p}_0 \end{pmatrix}
 \end{aligned}$$

Comparing the matrix terms in this expression with those in (C.56) shows that they are the same. This establishes (B.24a).

A similar explicit evaluation process establishes (B.24b).

(B.24c) is simply the transpose of (B.24b), while (B.24d) is the transpose of (B.24a).

6. Since \mathbf{q} is an eigen-vector of $\mathfrak{R}(\mathbf{q}, q_0)$ from (B.17), (B.25) follows directly from the expression for $\mathbb{T}(\underline{\mathbf{q}})$ in (B.20).

Solution B.9 (pp. 409): Composition of unit quaternions

- The (B.27) follows from direct evaluation of the product in (B.26).
The unit norm property of $\underline{\mathbf{r}} = \underline{\mathbf{p}} \otimes \underline{\mathbf{q}}$ follows from

$$\|\underline{\mathbf{r}}\|^2 = \underline{\mathbf{r}}^* \underline{\mathbf{r}} \stackrel{\text{B.27}}{=} \underline{\mathbf{q}}^* E_+^*(\underline{\mathbf{p}}) E_+(\underline{\mathbf{p}}) \underline{\mathbf{q}} \stackrel{\text{B.20}}{=} \underline{\mathbf{q}}^* \underline{\mathbf{q}} = 1$$

- Define $\underline{\mathbf{r}} \stackrel{\triangle}{=} \underline{\mathbf{p}} \otimes \underline{\mathbf{q}} = (r, r_0)$. The (B.28) identity can be established by the brute force use of (B.14) on both sides of the equation and a series of algebraic manipulations. We however, use a simpler approach, and show that $\underline{\mathbf{r}}$ defined by (B.27) is an eigen-vector of $\mathbb{T}(\underline{\mathbf{p}})\mathbb{T}(\underline{\mathbf{q}})$ with eigenvalue 1 as required by (B.25). have

$$\mathbb{T}(\underline{\mathbf{p}})\mathbb{T}(\underline{\mathbf{q}}) = \begin{pmatrix} \Re(\underline{\mathbf{p}})\Re(\underline{\mathbf{q}}) & 0 \\ 0 & 1 \end{pmatrix} \stackrel{\text{B.21}}{=} E_+(\underline{\mathbf{p}})E_-^*(\underline{\mathbf{p}})E_+(\underline{\mathbf{q}})E_-^*(\underline{\mathbf{q}})$$

Thus,

$$\begin{aligned} \mathbb{T}(\underline{\mathbf{p}})\mathbb{T}(\underline{\mathbf{q}})\underline{\mathbf{r}} &\stackrel{\text{B.26}}{=} E_+(\underline{\mathbf{p}})E_-^*(\underline{\mathbf{p}})E_+(\underline{\mathbf{q}})E_-^*(\underline{\mathbf{q}})E_-(\underline{\mathbf{q}})\underline{\mathbf{p}} \\ &\stackrel{\text{B.14}}{=} E_+(\underline{\mathbf{p}})E_-^*(\underline{\mathbf{p}})E_+(\underline{\mathbf{q}})\underline{\mathbf{p}} \\ &\stackrel{\text{B.26}}{=} E_+(\underline{\mathbf{p}})E_-^*(\underline{\mathbf{p}})E_-(\underline{\mathbf{p}})\underline{\mathbf{q}} \\ &\stackrel{\text{B.14}}{=} E_+(\underline{\mathbf{p}})\underline{\mathbf{q}} \\ &\stackrel{\text{B.26}}{=} \underline{\mathbf{r}} \end{aligned}$$

This establishes that $\underline{\mathbf{r}}$ is an eigen-vector corresponding to the eigen-value of 1, and hence it is the quaternion corresponding to the $\mathbb{T}(\underline{\mathbf{p}})\mathbb{T}(\underline{\mathbf{q}})$ rotational transformation and verifies (B.28).

3. Now

$$\begin{aligned} \underline{\mathbf{p}} \otimes (\underline{\mathbf{q}} \otimes \underline{\mathbf{r}}) &\stackrel{\text{B.26}}{=} E_+(\underline{\mathbf{p}})E_-(\underline{\mathbf{r}})\underline{\mathbf{q}} \stackrel{\text{B.24a}}{=} E_-(\underline{\mathbf{r}})E_+(\underline{\mathbf{p}})\underline{\mathbf{q}} \\ &\stackrel{\text{B.26}}{=} E_-(\underline{\mathbf{r}})(\underline{\mathbf{p}} \otimes \underline{\mathbf{q}}) \stackrel{\text{B.26}}{=} (\underline{\mathbf{p}} \otimes \underline{\mathbf{q}}) \otimes \underline{\mathbf{r}} \end{aligned}$$

4. We have

$$\underline{\mathbf{p}}^{-1} \otimes \underline{\mathbf{q}} \stackrel{\text{B.26}}{=} E_+(\underline{\mathbf{p}}^{-1})\underline{\mathbf{q}} \stackrel{\text{B.22}}{=} E_+^*(\underline{\mathbf{p}})\underline{\mathbf{q}}$$

establishing the first half of (B.30). For the latter half,

$$\underline{\mathbf{p}} \otimes \underline{\mathbf{q}}^{-1} \stackrel{\text{B.26}}{=} E_-(\underline{\mathbf{q}}^{-1})\underline{\mathbf{p}} \stackrel{\text{B.22}}{=} E_-^*(\underline{\mathbf{q}})\underline{\mathbf{p}}$$

Solution B.10 (pp. 409): The quaternion identity element

It is easy to verify that $E_+(\mathbf{e}_{\underline{\mathbf{q}}}) = E_-(\mathbf{e}_{\underline{\mathbf{q}}}) = \mathbf{I}_4$. Thus

$$\underline{\mathbf{q}} \otimes \mathbf{e}_{\underline{\mathbf{q}}} \stackrel{\text{B.26}}{=} E_-(\mathbf{e}_{\underline{\mathbf{q}}})\underline{\mathbf{q}} = \underline{\mathbf{q}}$$

The latter identity in (B.31) can be established by explicitly evaluating $E_+(\underline{\mathbf{q}})\underline{\mathbf{q}}^{-1}$ and verifying that it is simply $\mathbf{e}_{\underline{\mathbf{q}}}$.

Solution B.11 (pp. 410): Unit quaternion products and inverses

1. Now

$$(\underline{\mathbf{p}} \otimes \underline{\mathbf{q}}) \otimes (\underline{\mathbf{q}}^{-1} \otimes \underline{\mathbf{p}}^{-1}) \stackrel{\text{B.29}}{=} \underline{\mathbf{p}} \otimes (\underline{\mathbf{q}} \otimes \underline{\mathbf{q}}^{-1}) \otimes \underline{\mathbf{p}}^{-1} \stackrel{\text{B.31}}{=} \underline{\mathbf{p}} \otimes \underline{\mathbf{p}}^{-1} = \mathbf{e}_{\underline{\mathbf{q}}}$$

This establishes that $(\underline{\mathbf{q}}^{-1} \otimes \underline{\mathbf{p}}^{-1})$ is the inverse of $\underline{\mathbf{p}} \otimes \underline{\mathbf{q}}$.

2. Now $\underline{r} \stackrel{\text{B.26}}{=} E_+(\underline{p})\underline{q}$. Thus

$$\underline{q} \stackrel{\text{B.20}}{=} E_+^*(\underline{p})\underline{r} \stackrel{\text{B.22}}{=} E_+(\underline{p}^{-1})\underline{r} \stackrel{\text{B.26}}{=} \underline{p}^{-1} \otimes \underline{r}$$

A similar derivation leads to $\underline{p} = \underline{r} \otimes \underline{q}^{-1}$.

Solution B.12 (pp. 410): Transforming vectors with unit quaternions

We have

$$\begin{aligned} \begin{bmatrix} \mathbb{I}_x \\ 0 \end{bmatrix} &= \begin{pmatrix} \mathbb{I}\Re_{\mathbb{B}}(\underline{q}) & 0 \\ 0 & 1 \end{pmatrix} \begin{bmatrix} \mathbb{B}_x \\ 0 \end{bmatrix} \\ &\stackrel{\text{B.21}}{=} E_+(\underline{q})E_-^*(\underline{q}) \begin{bmatrix} \mathbb{B}_x \\ 0 \end{bmatrix} \stackrel{\text{B.22}}{=} E_+(\underline{q})E_-(\underline{q}^{-1}) \begin{bmatrix} \mathbb{B}_x \\ 0 \end{bmatrix} \stackrel{\text{B.26}}{=} \underline{q} \otimes \begin{bmatrix} \mathbb{B}_x \\ 0 \end{bmatrix} \otimes \underline{q}^{-1} \end{aligned}$$

Solution B.13 (pp. 410): Quaternion rates from the angular velocity

With $q_0 = \cos(\theta/2)$,

$$\dot{q}_0 = -\frac{1}{2} \sin(\theta/2) \hat{\theta} \stackrel{\text{B.11}}{=} -\frac{1}{2} \sin(\theta/2) \mathbf{n}^* \mathbb{B} \boldsymbol{\omega} = -\frac{1}{2} q^* \mathbb{B} \boldsymbol{\omega}$$

This establishes the lower half of the first equality in (B.34).

Also, with $q = \sin(\theta/2)\mathbf{n}$,

$$\begin{aligned} \dot{q} &= \frac{1}{2} \cos(\theta/2) \hat{\theta} \mathbf{n} + \sin(\theta/2) \dot{\mathbf{n}} \\ &\stackrel{\text{B.11}}{=} \frac{1}{2} q_0 \mathbf{n} \mathbf{n}^* \mathbb{B} \boldsymbol{\omega} + \frac{\sin(\theta/2)}{2} [\tilde{\mathbf{n}} - \cot(\theta/2) \tilde{\mathbf{n}} \tilde{\mathbf{n}}] \mathbb{B} \boldsymbol{\omega} \\ &= \frac{1}{2} [q_0 \mathbf{n} \mathbf{n}^* + \tilde{q} - \cos(\theta/2) \tilde{\mathbf{n}} \tilde{\mathbf{n}}] \mathbb{B} \boldsymbol{\omega} \\ &= \frac{1}{2} [q_0 \mathbf{n} \mathbf{n}^* + \tilde{q} - q_0 \tilde{\mathbf{n}} \tilde{\mathbf{n}}] \mathbb{B} \boldsymbol{\omega} \\ &= \frac{1}{2} [q_0 (\mathbf{n} \mathbf{n}^* - \tilde{\mathbf{n}} \tilde{\mathbf{n}}) + \tilde{q}] \mathbb{B} \boldsymbol{\omega} = \frac{1}{2} [q_0 \mathbf{I} + \tilde{q}] \mathbb{B} \boldsymbol{\omega} \end{aligned}$$

This establishes the upper half of the first equality in (B.34).

The second equality in (B.34) is a rearrangement of the first one.

The third equality follows by using the definition of $E_+(\underline{q})$ from (B.19).

The last equality follows from (B.26).

Solution B.14 (pp. 410): Constant unit quaternion norms

1. The rate of change of the norm of $\underline{q}(t)$ is given by

$$\frac{d\|\underline{q}(t)\|^2}{dt} = \frac{1}{2} \frac{d\underline{q}^*\underline{q}}{dt} = \underline{q}^* \dot{\underline{q}} \stackrel{B.34}{=} \frac{1}{2} \underline{q}^* E_+(\underline{q}) \begin{bmatrix} \mathbb{B}\omega \\ 0 \end{bmatrix} \stackrel{B.22, B.26}{=} \frac{1}{2} \underline{e}_{\underline{q}}^* \begin{bmatrix} \mathbb{B}\omega \\ 0 \end{bmatrix} = 0$$

2. From the above we have that

$$0 = \underline{q}^* \dot{\underline{q}} = \underline{q}^* \dot{\underline{q}} + q_0 \dot{q}_0$$

from which (B.35) follows.

Solution B.15 (pp. 411): Unit quaternion rate to angular velocity

1. (B.36) follows by using (B.32) in (B.34). From this it follows that

$$\mathbb{B}\omega \stackrel{B.19}{=} 2[q_0 \mathbf{I}_3 - \tilde{\underline{q}}] \dot{\underline{q}} - \underline{q} \dot{q}_0 \stackrel{B.35}{=} 2[q_0 \mathbf{I}_3 - \tilde{\underline{q}}] \dot{\underline{q}} + \underline{q}(\underline{q}^* \dot{\underline{q}} / q_0)$$

from which (B.37) follows.

2. We have

$$\begin{bmatrix} \mathbb{I}\omega \\ 0 \end{bmatrix} \stackrel{B.33}{=} \underline{q} \otimes \begin{bmatrix} \mathbb{B}\omega \\ 0 \end{bmatrix} \otimes \underline{q}^{-1} \stackrel{B.36}{=} 2 \dot{\underline{q}} \otimes \underline{q}^{-1} \stackrel{B.30}{=} 2 E_-^* \dot{\underline{q}}$$

establishing (B.39). From this it follows that

$$\mathbb{I}\omega \stackrel{B.19}{=} 2[q_0 \mathbf{I}_3 + \tilde{\underline{q}}] \dot{\underline{q}} - \underline{q} \dot{q}_0 \stackrel{B.35}{=} 2[q_0 \mathbf{I}_3 + \tilde{\underline{q}}] \dot{\underline{q}} + \underline{q}(\underline{q}^* \dot{\underline{q}} / q_0)$$

establishing (B.41).

Solution B.16 (pp. 411): Quaternion double time derivatives

Differentiating (B.34) we have

$$\begin{aligned} \ddot{\underline{q}} &= \frac{1}{2} \underline{q} \otimes \begin{bmatrix} \mathbb{B}\dot{\omega} \\ 0 \end{bmatrix} + \frac{1}{2} \dot{\underline{q}} \otimes \begin{bmatrix} \mathbb{B}\omega \\ 0 \end{bmatrix} \stackrel{B.34}{=} \frac{1}{2} \underline{q} \otimes \begin{bmatrix} \mathbb{B}\dot{\omega} \\ 0 \end{bmatrix} + \frac{1}{2} \left\{ \frac{1}{2} \underline{q} \otimes \begin{bmatrix} \mathbb{B}\omega \\ 0 \end{bmatrix} \right\} \otimes \begin{bmatrix} \mathbb{B}\omega \\ 0 \end{bmatrix} \\ &\stackrel{B.27}{=} \frac{1}{2} \underline{q} \otimes \begin{bmatrix} \mathbb{B}\dot{\omega} \\ 0 \end{bmatrix} + \frac{1}{4} \underline{q} \otimes (\|\mathbb{B}\omega\|^2 \underline{e}_{\underline{q}}) \end{aligned}$$

establishing (B.42).

(B.43) follows by composing both sides of (B.42) with \underline{q}^{-1} and rearranging terms.

Solution B.17 (pp. 412): Gibbs vector attitude representation

1. From Exercise (B.2) on page 405 it follows that

$$\tilde{s}^3 = -\sigma^2 \tilde{s}, \quad \tilde{s}^5 = \sigma^4 \tilde{s}, \quad \dots \quad \tilde{s}^{2k+1} = (-1)^k \sigma^{2k} \tilde{s}$$

Thus,

$$\tilde{s}^4 = -\sigma^2 \tilde{s}^2, \quad \tilde{s}^6 = \sigma^4 \tilde{s}^2, \quad \dots \quad \tilde{s}^{2k+2} = (-1)^k \sigma^{2k} \tilde{s}^2$$

Using these expressions for the powers of \tilde{s} , we have

$$\begin{aligned} [\mathbf{I} - \tilde{s}]^{-1} &= \mathbf{I} + \tilde{s} + \tilde{s}^2 + \dots = \mathbf{I} + \sum_{k=0}^{\infty} (-1)^k \sigma^{2k} (\tilde{s} + \tilde{s}^2) \\ &= \mathbf{I} + (\tilde{s} + \tilde{s}^2) \sum_{k=0}^{\infty} (-1)^k \sigma^{2k} = \mathbf{I} + (\tilde{s}^2 + \tilde{s}) / (1 + \sigma^2) \end{aligned}$$

2.

$$\begin{aligned} \mathfrak{R}(s) &\stackrel{\text{B.44}}{=} (\mathbf{I} + \tilde{s}) + \tilde{s}(\mathbf{I} + \tilde{s})^2 / (1 + \sigma^2) = \mathbf{I} + (\tilde{s}^3 + 2\tilde{s}^2 + (2 + \sigma^2)\tilde{s}) / (1 + \sigma^2) \\ &\stackrel{\text{B.5}}{=} \mathbf{I} + 2(\tilde{s}^2 + \tilde{s}) / (1 + \sigma^2) \end{aligned}$$

To establish that $\mathfrak{R}(s)$ is a rotation matrix it suffices to verify that $\mathfrak{R}(s)\mathfrak{R}^*(s) = \mathbf{I}$ and that $\det \mathfrak{R}(s) = 1$. Since

$$\mathbf{I} - \tilde{s}^2 = [\mathbf{I} - \tilde{s}][\mathbf{I} + \tilde{s}] = [\mathbf{I} + \tilde{s}][\mathbf{I} - \tilde{s}]$$

it follows that

$$\mathfrak{R}(s) \stackrel{\text{B.45}}{=} [\mathbf{I} - \tilde{s}]^{-1} [\mathbf{I} + \tilde{s}] = [\mathbf{I} + \tilde{s}] [\mathbf{I} - \tilde{s}]^{-1}$$

and that

$$\mathfrak{R}^*(s) \stackrel{\text{B.45}}{=} [\mathbf{I} + \tilde{s}]^{-1} [\mathbf{I} - \tilde{s}]$$

Thus,

$$\mathfrak{R}(s)\mathfrak{R}^*(s) = [\mathbf{I} - \tilde{s}]^{-1} [\mathbf{I} + \tilde{s}] [\mathbf{I} + \tilde{s}]^{-1} [\mathbf{I} - \tilde{s}] = \mathbf{I}$$

establishing the orthogonality of $\mathfrak{R}(s)$. Furthermore,

$$d \triangleq \det[\mathbf{I} - \tilde{s}] = \det[\mathbf{I} - \tilde{s}]^* = \det[\mathbf{I} + \tilde{s}]$$

Hence, $\det[\mathbf{I} - \tilde{s}]^{-1} = 1/d$. Putting these together we have

$$\det \mathfrak{R}(s) = \det[\mathbf{I} - \tilde{s}]^{-1} \det[\mathbf{I} + \tilde{s}] = (1/d)d = 1$$

This establishes that $\mathfrak{R}(s)$ is a rotation matrix since it is orthogonal and has determinant 1.

3. From (B.45) it follows that $\mathfrak{R} - \mathfrak{R}\tilde{s} = \mathbf{I} + \tilde{s}$ from which the first half of (B.46) follows. Now let us assume that for some constants a, b and c to be determined, we have

$$-[\mathbf{I} - \mathfrak{R}][\mathbf{I} + \mathfrak{R}]^{-1} = a\mathfrak{R}^2 + b\mathfrak{R} + c\mathbf{I}$$

Then it follows that

$$\begin{aligned} -\mathbf{I} + \mathfrak{R} &= [\mathbf{I} + \mathfrak{R}][a\mathfrak{R}^2 + b\mathfrak{R} + c\mathbf{I}] \\ &= a\mathfrak{R}^3 + (a+b)\mathfrak{R}^2 + (b+c)\mathfrak{R} + c\mathbf{I} \\ &\stackrel{\text{B.8}}{=} ((1+\gamma)a+b)\mathfrak{R}^2 + (-a\gamma+b+c)\mathfrak{R} + (a+c)\mathbf{I} \end{aligned}$$

For this to hold, the coefficients must satisfy the following linear equations:

$$(1+\gamma)a + b = 0, \quad -a\gamma + b + c = 1, \quad a + c = -1$$

The solution to these equations is

$$a = -1/(1+\gamma), \quad b = 1, \quad c = -\gamma/(1+\gamma)$$

which establishes the result.

4. For s to the axis of rotation, we need to show that it an eigen-vector of $\mathfrak{R}(s)$ with eigen-value 1. We have

$$\mathfrak{R}(s)s \stackrel{\text{B.45}}{=} [\mathbf{I} + 2(\tilde{s}^2 + \tilde{s})/(1+\sigma^2)] = s$$

This establishes the result.

5. With s defined by (B.47), we have $\sigma = \tan(\theta/2)$. Thus,

$$\begin{aligned} \mathfrak{R}(s) &\stackrel{\text{B.45}}{=} \mathbf{I} + 2(\sigma^2 \tilde{\mathbf{n}}^2 + \sigma \tilde{\mathbf{n}})/(1+\sigma^2) \\ &= \mathbf{I} + 2\cos^2(\theta/2)(\tan^2(\theta/2)\tilde{\mathbf{n}}^2 + \tan(\theta/2)\tilde{\mathbf{n}}) \\ &= \mathbf{I} + (1 - \cos(\theta))\tilde{\mathbf{n}}^2 + \sin(\theta)\tilde{\mathbf{n}} \end{aligned}$$

The last expression agrees with the expression for a rotation matrix in (B.6) establishing the result.

Solution B.18 (pp. 413): Rotation of vectors

1. Since $\mathfrak{R}(s)a = b$,

$$b \stackrel{\text{B.45}}{=} [\mathbf{I} - \tilde{s}]^{-1}[\mathbf{I} + \tilde{s}]a \implies [\mathbf{I} - \tilde{s}]b = [\mathbf{I} + \tilde{s}]a$$

from which (B.48) follows.

2. Since any vector s satisfying (B.48) will generate a rotation matrix $\mathfrak{R}(s)$ with the desired properties, we look for the general solution to the linear matrix equation

in (B.48). We now verify that $s_p \stackrel{\triangle}{=} \lambda(\widetilde{a+b})(\widetilde{a-b})$ is a *particular* solution to the linear equations. Since a and b have the same norm, the $(a+b)$ and $(a-b)$ vectors are mutually orthogonal because

$$(a+b)^*(a-b) = a^*a - a^*b + b^*a - b^*b = 0$$

Now

$$\begin{aligned} \widetilde{(a+b)}s_p &= -\lambda \widetilde{(a+b)} \widetilde{(a+b)}(a-b) \\ &\stackrel{A.1}{=} -\lambda [(a+b)(a+b)^* - \|a+b\|^2 I] (a-b) = (a-b) \end{aligned}$$

Thus, s_p is indeed a particular solution for (B.48). To determine all the remaining solutions observe that the class of homogeneous solutions for (B.48) is simply $s = \alpha(a+b)$ for an arbitrary scalar α . Combining the particular and homogeneous solution leads to the general solution in (B.49).

References

- [1] Aghili, F.: Simplified Lagrangian mechanical systems with constraints using square-root factorization. In: Multibody Dynamics 2007, ECCOMAS Thematic Conference (2007)
- [2] Aghili, F.: A gauge-invariant formulation for constrained robotic systems using square-root factorization and unitary transformation. In: IEEE/RSJ International Conference on Intelligent Robots and Systems, pp. 2814–2821 (2008)
- [3] Aghili, F.: Dynamics and control of constrained mechanical systems in terms of reduced quasi-velocities. In: IEEE International Conference on Robotics and Automation, pp. 1225–1232 (2008)
- [4] Alexander, H., Cannon, R.: Experiments on the control of a satellite Manipulator. In: Proceedings of American Control Conference (1987)
- [5] Anderson, B.D.O., Moore J.B.: Optimal Filtering. Prentice-Hall, Englewood Cliffs, NJ (1979)
- [6] Anderson, K.: An order-n formulation for the motion simulation of general multi-rigid-body tree systems. *Comput. Struct.* **46**(3), 547–559 (1993)
- [7] Arai, H., Tachi, S.: Position control of manipulator with passive joints using dynamic coupling. *IEEE Trans. Robot. Autom.* **7**, 528–534 (1991)
- [8] Arimoto, S., Miyazaki, F.: Stability and Robustness of PID Feedback Control for Robot Manipulators of Sensory Capability. MIT Press, Cambridge, MA (1983)
- [9] Armstrong, B., Khatib, O., Burdick, J.: The explicit model and inertial parameters of the PUMA 560 Arm. In: IEEE International Conference on Robotics and Automation, San Francisco, CA (1986)
- [10] Armstrong, W.: Recursive solution to the equations of motion of an N-link Manipulator. In: 5th World Congress on Theory of Machines and Mechanisms, Montreal, Canada, vol. 2, pp. 1343–1346 (1979)
- [11] Arnold, V.I.: Mathematical Methods of Classical Mechanics. Springer, Heidelberg (1984)
- [12] Asada, H., Slotine, J.J.E.: Robot Analysis and Control. Wiley, New York (1986)
- [13] Ascher, U.M., Pai, D., Cloutier, B.: Forward dynamics, elimination methods, and formulation stiffness in robotic simulation. *Int. J. Robot. Res.* **16**(6), 749–758 (1997)
- [14] Ascher, U.M., Petzold, L.R.: Computer methods for ordinary differential equations and differential-algebraic equations. SIAM (1998)
- [15] Austin, M., Krishnaprasad, P., Wang, L.S.: Almost Poisson integration of rigid body systems. Technical Report TR 91-45r1, Systems Research Center, University of Maryland, MD (1991)
- [16] Bae, D., Haug, E.: A recursive formulation for constrained mechanical system dynamics: Part I. Open loop systems. *Mech. Struct. Mach.* **15**(3), 359–382 (1987)
- [17] Bae, D., Haug, E.: A recursive formulation for constrained mechanical system dynamics: Part II. Closed loop systems. *Mech. Struct. Mach.* **15**(4), 481–506 (1987–1988)

- [18] Baillieul, J.: The nonlinear control theory of super-articulated mechanisms. In: Proceedings of American Control Conference, San Diego, CA, pp. 2448–2451 (1990)
- [19] Balafoutis, C., Misra, P., Patel, R.: Recursive evaluation of dynamic robot models. *IEEE J. Robot. Autom.* **2**(3), 146–155 (1986)
- [20] Balakrishnan, A.: Applied Functional Analysis. Springer, New York (1976)
- [21] Banerjee, A.K.: Contributions of Multibody Dynamics to Space Flight: A Brief Review. *J. Guid. Control Dynam.* **26**(3), 385–394 (2003)
- [22] Banerjee, A.K., Dickens, J.: Dynamics of an arbitrary flexible body in large rotation and translation. *J. Guid. Control Dynam.* **13**(2), 221–227 (1990)
- [23] Baraff, D.: Linear-time dynamics using Lagrange multipliers. In: Proceedings of ACM SIGGRAPH '96, New Orleans, pp. 137–146 (1996)
- [24] Baumgarte, J.: Stabilization of constraints and integrals of motion in dynamical systems. *Comput. Method. Appl. Mech. Eng.* **1**, 1–16 (1972)
- [25] Bedrossian, N.: Linearizing coordinate transformations and euclidean systems. In: Workshop on Nonlinear Control of Articulated Flexible Structures, Santa Barbara, CA (1991)
- [26] Bodley, C.S., Devers, A.D., Park, A.C., Frisch, H.P.: A digital computer program for the dynamic interaction simulation of controls and structure (DISCOS). NASA Technical Paper 1219, NASA (1978)
- [27] Bowling, A., Khatib, O.: Design of macro/mini manipulators for optimal dynamic performance. In: IEEE International Conference on Robotics and Automation, pp. 449–454 (1997)
- [28] Brandl, H., Johann, R., Otter, M.: A very efficient algorithm for the simulation of robots and similar multibody systems without inversion of the mass matrix. In: IFAC/IFIP/IMACS Symposium (1st), Vienna, Austria, pp. 95–100 (1986)
- [29] Brandl, H., Johann, R., Otter, M.: An algorithm for the simulation of multibody systems with kinematic loops. In: World Congress on the Theory of Machines and Mechanisms (7th), Seville, Spain (1987)
- [30] Breckenridge, W.: Quaternions – proposed standard conventions. IOM 343-79-1199, Jet Propulsion Laboratory (1979)
- [31] Brogliato, B.: Nonsmooth Mechanics. Springer, London (1999)
- [32] Burdick, J.: An algorithm for generation of efficient manipulator dynamic equations. In: IEEE International Conference on Robotics and Automation, San Francisco, CA (1986)
- [33] Chang, C., Nikravesh, P.: Optimal design of mechanical systems with constraint violation stabilization method. *J. Mech. Transm. Autom. Des.* **107**, 493–498 (1985)
- [34] Chang, K.S., Khatib, O.: Efficient recursive algorithm for the operational space inertia matrix of branching mechanisms. *Adv. Robot.* **4**(8), 703–715 (2001)
- [35] Changizi, K., Shabana, A.: A recursive formulation for the dynamic analysis of open loop deformable multibody systems. *ASME J. Appl. Mech.* **55**(3), 687–693 (1988)
- [36] Chen, J.: The effects of gear reduction on robot dynamics. In: Rodriguez, G., Seraji, H. (eds.) NASA Conference on Space Telerobotics, Pasadena, CA (Submitted to ASME J. Dyn. Meas. Contr.) (1989)
- [37] Chen, J., Ou, J.: Development of efficient computer program for dynamic simulation of telerobotic manipulation. In: Proceedings of the 3rd Annual Conference on Aerospace Computational Control, Oxnard, CA, vol. 1, pp. 248–262, (JPL Publication 89–45, 1989) (1989)
- [38] Cherowitzo, W.: Graph and Digraph Glossary. <http://www-math.cudenver.edu/~wcherowi/courses/m4408/glossary.htm/> (2009)
- [39] Chirikjian, G., Burdick, J.: Kinematics of hyper-redundant locomotion with applications to grasping. In: IEEE International Conference on Robotics and Automation, Sacramento, CA, pp. 720–725 (1991)
- [40] Cottle, R., Pang, J., Stone, R.: The Linear Complementarity Problem. Academic, New York (1992)
- [41] Craig, J.J.: Introduction to Robotics. Addison-Wesley, Reading, MA (1986)
- [42] Critchley, R., Anderson, K.: A generalized recursive coordinate reduction method for multi-body dynamic systems. *Int. J. Multiscale Comput. Eng.* **12**(2), 181–200 (2003)
- [43] Diebel, J.: Representing attitude: Euler angles, unit quaternions, and rotation vectors. <http://citeseerx.ist.psu.edu/viewdoc/summary?doi=?doi=10.1.1.110.5134> (2006)

- [44] Dubowsky, S., Vafa, Z.: A virtual manipulator model for space robotic systems. In: Rodriguez, G. (ed.) *Proceedings of the Workshop on Space Telerobotics*, Pasadena, CA (1987)
- [45] Duindam, V., Stramigioli, S.: Singularity-free dynamic equations of open-chain mechanisms with general holonomic and nonholonomic joints. *IEEE Trans. Robot. Autom.* **24**(3), 517–526 (2008)
- [46] Eisenhart, L.: *Riemannian Geometry*. Princeton University Press, Princeton (1960)
- [47] Featherstone, R.: The calculation of robot dynamics using articulated-body inertias. *Int. J. Robot. Res.* **2**(1), 13–30 (1983)
- [48] Featherstone, R.: *Robot Dynamics Algorithms*. Kluwer, Boston, MA (1987)
- [49] Featherstone, R.: A divide-and-conquer articulated-body algorithm for parallel $O(\log(n))$ calculation of rigid-body dynamics. Part 1: Basic algorithm. *Int. J. Robot. Res.* **18**(9), 867–875 (1999)
- [50] Featherstone, R.: A divide-and-conquer articulated-body algorithm for parallel $O(\log(n))$ calculation of rigid-body dynamics. Part 2: Trees, loops, and accuracy. *Int. J. Robot. Res.* **18**(9), 876–892 (1999)
- [51] Featherstone, R.: *Rigid Body Dynamics Algorithms*. Springer, New York (2008)
- [52] Featherstone, R.: Exploiting sparsity in operational-space dynamics. *Int. J. Robot. Res.* **29**, 1353–1368 (2010)
- [53] Featherstone, R., Orin, D.: Robot dynamics: equations and algorithms. In: *IEEE International Conference on Robotics and Automation*, San Francisco, CA, pp. 826–834 (2000)
- [54] Fijany, A.: Parallel algorithms and architectures in robotics. PhD thesis, University of Orsay (Paris XI) (1988)
- [55] Fijany, A., Bejczy, A.: Parallel algorithms and architectures for manipulator inverse dynamics. In: OSU Conference, Columbus, OH (1989)
- [56] Fijany, A., Scheid, R.: Efficient conjugate gradient algorithms for computation of the manipulator forward dynamics. In: Rodriguez, G., Seraji, H. (eds.) *NASA Conference on Space Telerobotics*, Pasadena, CA (1989)
- [57] Fixman, M.: Simulation of polymer dynamics. I. General theory. *J. Chem. Phys.* **69**(4), 1527–1537 (1978)
- [58] Fraser, D., Potter, J.: The optimum linear smoother as a combination of two optimum linear filters. *IEEE Trans. Autom. Contr.* 387–390 (1969)
- [59] Gelb, A.: *Applied Optimal Estimation*. MIT Press, Cambridge, MA (1974)
- [60] Goldstein, H.: *Classical Mechanics*. Addison-Wesley, Reading, MA (1980)
- [61] Graham, A.: *Kronecker Products and Matrix Calculus: With Applications*. Horwood Halsted Press, New York (1981)
- [62] Hardt, M.W.: Multibody dynamical algorithms, numerical optimal control, with detailed studies in the control of jet engine compressors and biped walking. PhD thesis, University of California, San Diego (1999)
- [63] Herman, P., Kozlowski, K.: A survey of equations of motion in terms of inertial quasi-velocities for serial manipulators. *Arch. Appl. Mech.* **76**, 579–614 (2006)
- [64] Ho, J.: Direct path method for flexible multibody spacecraft dynamics. *J. Spacecraft Rockets (AIAA)* **14**(2), 102–110 (1977)
- [65] Ho, J., Herber, D.: Development of dynamics and control simulation of large flexible space systems. *J. Guid. Control Dyn.* **8**(3), 374–383 (1985)
- [66] Hollerbach, J.: A recursive Lagrangian formulation of manipulator dynamics and a comparative study of dynamics formulation complexity. *IEEE Trans. Syst. Man Cybern.* **10**(11), 730–736 (1980)
- [67] Hsu, Y., Anderson, K.: Low operational order analytic sensitivity analysis for tree-type multibody dynamics systems. *J. Guid. Control Dyn.* **24**(6), 1133–1143 (2001)
- [68] Hu, W., Marhefka, D.W., Orin, D.E.: Hybrid kinematic and dynamic simulation of running machines. *IEEE Trans. Robot. Autom.* **21**(3), 490–497 (2010)
- [69] Hughes, P.: *Spacecraft Attitude Dynamics*. Wiley, New York (1986)
- [70] Huston, R.: *Multibody Dynamics*. Butterworth-Heinemann, Stoneham, MA (1990)

- [71] Jain, A.: Unified formulation of dynamics for serial rigid multibody systems. *J. Guid. Control Dyn.* **14**(3), 531–542 (1991)
- [72] Jain, A.: Compensating mass matrix potential for constrained molecular dynamics. *J. Comput. Phys.* **136**, 289–297 (1997)
- [73] Jain, A.: Correction to ‘spatial operator algebra for multibody system dynamics’. <http://dartslab.jpl.nasa.gov/References/pdf/gen-mbody-correction.pdf> (2009)
- [74] Jain, A.: Recursive algorithms using local constraint embedding for multibody system dynamics. In: ASME 2009 International Design Engineering Technical Conferences & Computers and Information in Engineering Conference, San Diego, CA (2009)
- [75] Jain, A.: Graph theoretic structure of multibody system spatial operators. In: The 1st Joint International Conference on Multibody System Dynamics, Lappeenranta, Finland (2010)
- [76] Jain, A.: Graph theory roots of spatial operators for kinematics and dynamics. In: IEEE International Conference on Robotics and Automation, Anchorage, Alaska (2010)
- [77] Jain, A., Rodriguez, G.: Recursive dynamics for geared robotic manipulators. In: IEEE Conference on Decision and Control, Honolulu, Hawaii (1990)
- [78] Jain, A., Rodriguez, G.: Kinematics and dynamics of under-actuated manipulators. In: IEEE International Conference on Robotics and Automation, Sacramento, CA, pp. 1754–1759 (1991)
- [79] Jain, A., Rodriguez, G.: Recursive flexible multibody system dynamics using spatial operators. *J. Guid. Control Dyn.* **15**(6), 1453–1466 (1992)
- [80] Jain, A., Rodriguez, G.: An analysis of the kinematics and dynamics of underactuated manipulators. *IEEE Trans. Robot. Autom.* **9**(4), 411–422 (1993)
- [81] Jain, A., Rodriguez, G.: Linearization of manipulator dynamics using spatial operators. *IEEE Trans. Syst. Man Cybern.* **23**(1), 239–248 (1993)
- [82] Jain, A., Rodriguez, G.: Recursive dynamics algorithm for multibody systems with prescribed motion. *J. Guid. Control Dyn.* **16**(5), 830–837 (1993)
- [83] Jain, A., Rodriguez, G.: Base-invariant symmetric dynamics of free-flying space manipulators. *IEEE Trans. Robot. Autom.* **11**(4), 585–597 (1995)
- [84] Jain, A., Rodriguez, G.: Diagonalized Lagrangian robot dynamics. *IEEE Trans. Robot. Autom.* **11**(4), 571–584 (1995)
- [85] Jain, A., Rodriguez, G.: Multibody mass matrix sensitivity analysis using spatial operators. *Int. J. Multiscale Comput. Eng.* **1**(2–3) (2003)
- [86] Jain, A., Kreutz, K., Rodriguez, G.: Multi-Arm grasp and manipulation of objects with internal degrees of freedom. In: IEEE Conference on Decision and Control, Honolulu, Hawaii (1990)
- [87] Jain, A., Kreutz, K., Rodriguez, G.: Recursive dynamics of multiarm robotic systems in loose grasp of articulated task objects. In: 3rd International Symposium on Robotics and Manufacturing, Vancouver, Canada (1990)
- [88] Jain, A., Vaidehi, N., Rodriguez, G.: A fast recursive algorithm for molecular dynamics simulations. *J. Comput. Phys.* **106**(2), 258–268 (1993)
- [89] de Jalon, J.G., Alvarez, E., de Ribera, F.A., Rodriguez, I., Funes, F.J.: A fast and simple semi-recursive dynamic formulation for multi-rigid-body systems. *Adv. Comput. Multibody Syst.*, 1–24 (2005)
- [90] Junkins, J.L., Schaub, H.: An instantaneous eigenstructure quasivelocity formulation for nonlinear multibody dynamics. *J. Astronaut. Sci.* **45**(3), 279–295 (1997)
- [91] Kailath, T.: An innovations approach to least-squares estimation. *IEEE Trans. Inform. Theory* **IT-14** (1968)
- [92] Kailath, T.: Fredholm resolvents, Wiener-Hopf equations, and Riccati differential equations. *IEEE Trans. Inform. Theory* **15**, 665–672 (1969)
- [93] Kailath, T.: A view of three decades of linear filtering theory. *IEEE Trans. Inform. Theory* **20**, 147–181 (1974)
- [94] Kamman, J., Huston, R.: Dynamics of constrained multibody systems. *ASME J. Appl. Mech.* **51**, 889–903 (1984)
- [95] Kane, T., Levinson, D.: The use of Kane’s dynamical equations in robotics. *Int. J. Robot. Res.* **2**(3), 3–21 (1983)

- [96] Kane, T., Levinson, D.: Dynamics: Theory and Applications. McGraw-Hill, New York (1985)
- [97] Kane, T., Likins, P., Levinson, D.: Spacecraft Dynamics. McGraw-Hill, New York (1983)
- [98] Kane, T., Ryan, R., Banerjee, A.: Dynamics of a cantilevered beam attached to a moving base. *J. Guid. Control Dyn.* **10**(2), 139–151 (1987)
- [99] Keat, J.: Multibody system order n dynamics formulation based in velocity transform method. *J. Guid. Control Dyn.* **13**(2), 201–212 (1990)
- [100] Khatib, O.: Dynamic control of manipulators in operational space. In: 6th CISM-IFTOMM Congress on Theory of Machines and Mechanisms, New Delhi, India (1983)
- [101] Khatib, O.: The operational space formulation in the analysis, design, and control of manipulators. In: 3rd International Symposium Robotics Research, Paris (1985)
- [102] Khatib, O.: A unified approach for motion and force control of robot manipulators: The operational space formulation. *IEEE J. Robot. Autom.* **3**(1), 43–53 (1987)
- [103] Khatib, O.: Object manipulation in a multi-effector system. In: 4th International Symposium on Robotics Research, Santa Cruz, CA, pp. 137–144 (1988)
- [104] Kim, S., Haug, E.: A recursive formulation for flexible multibody dynamics, Part I: open-loop systems. *Comput. Meth. Appl. Mech. Eng.* **71**(3), 293–314 (1988)
- [105] Koditschek, D.: Robot kinematics and coordinate transformations. In: IEEE Conference on Decision and Control, Ft. Lauderdale, FL, pp. 1–4 (1985)
- [106] Kozlowski, K., Herman, P.: Control of robot manipulators in terms of quasi-velocities. *J. Intell. Robot. Syst.* **53**(3), 205–221 (2008)
- [107] Kreutz, K.: On manipulator control by exact linearization. *IEEE Trans. Autom. Contr.* **34**, 763–767 (1989)
- [108] Kreutz, K., Lokshin, A.: Load balancing and closed-chain multiple arm control. In: American Control Conference, Atlanta, GA (1988)
- [109] Kreutz, K., Wen, J.: Attitude control of an object commonly held by multiple robot arms: a Lyapunov approach. In: American Control Conference, Atlanta, GA (1988)
- [110] Kreutz-Delgado, K., Jain, A., Rodriguez, G.: Recursive formulation of operational space control. *Int. J. Robot. Res.* **11**(4), 320–328 (1992)
- [111] Kwatny, H.G., Blankenship, G.: Nonlinear Control and Analytical Mechanics: A Computational Approach. Birkhäuser, Boston (2000)
- [112] Lanczos, C.: The Variational Principles of Mechanics. University of Toronto Press, Toronto (1949)
- [113] Lathrop, R.: Constrained (closed-loop) robot simulation by local constraint propagation. In: IEEE International Conference on Robotics and Automation, San Francisco, CA, pp. 689–694 (1986)
- [114] Lee, C.S.G., Chang, P.R.: Efficient parallel algorithms for robot inverse dynamics computations. *IEEE Trans. Syst. Man Cybern.* **16**, 532–542 (1986)
- [115] Lee, C.S.G., Chang, P.R.: Efficient algorithms for robot forward dynamics computations. In: IEEE International Conference on Robotics and Automation, Raleigh, NC, pp. 654–699 (1987)
- [116] Li, C.J.: An efficient method for linearization of dynamic models of robot manipulators. *IEEE Trans. Robot. Autom.* **5**(4), 397–408 (1989)
- [117] Li, C.J., Hemami, A., Sankar, T.: A new computational method for linearized dynamic models for robot manipulators. *Int. J. Robot. Res.* **9**(1), 134–144 (1990)
- [118] Likins, P.: Modal method for analysis of free rotations of spacecraft. *AIAA J.* **5**, 1304–1308 (1967)
- [119] Lovelock, D., Rund, H.: Tensors, Differential Forms, and Variational Principles. Dover, New York (1989)
- [120] Luh, J., Walker, M., Paul, R.: On-line computational scheme for mechanical manipulators. *ASME J. Dyn. Syst. Meas. Contr.* **102**(2), 69–76 (1980)
- [121] Mani, N., Haug, E., Atkinson, K.: Application of singular value decomposition for analysis of mechanical system dynamics. *J. Mech. Trans. Automat. Des.* **107**, 82–87 (1985)

- [122] Mariti, L., Pennestri, E., Valentini, P.P., Belfiore, N.P.: Review and comparison of solution strategies for multibody dynamics equations. In: The 1st Joint International Conference on Multibody System Dynamics, Lappeenranta, Finland (2010)
- [123] McPhee, J.J., Ishac, M.G., Andrews, G.C.: Wittenburg's formulation of multibody dynamics equations from a graph-theoretic perspective. *Mech. Mach. Theory* **31**(2), 201–213 (1996)
- [124] Meirovitch, L.: Methods of Analytical Dynamics. McGraw-Hill, New York (1970)
- [125] Mukherjee, R., Nakamura, Y.: Formulation and efficient computation of inverse dynamics of space robots. In: *IEEE Trans. Robot. Autom.* **8**, 400–406 (1992)
- [126] Murphy, S.H.: Modeling and simulation of multiple manipulators on a mobile platform. PhD thesis, R.P.I., Troy, NY (1990)
- [127] Murphy, S.H., Wen, J., Saridis, G.: Recursive calculation of geared robot manipulator dynamics. In: *IEEE International Conference on Robotics and Automation*, Cincinnati, OH, pp. 839–844 (1990)
- [128] Murray, R., Li, Z., Sastry, S.: A Mathematical Introduction to Robotic Manipulation. CRC Press, Boca Raton, FL (1994)
- [129] Nakamura, Y., Mukherjee, R.: Nonholonomic path planning for space robots. In: *IEEE International Conference on Robotics and Automation*, Scottsdale, AZ (1989)
- [130] Nakamura, Y., Mukherjee, R.: Nonholonomic path planning for space robot via bi-directional approach. In: *IEEE International Conference on Robotics and Automation*, Cincinnati, OH (1990)
- [131] Nguyen, B., Trinkle, J.C.: dvc3D: a three dimensional physical simulation tool for rigid bodies with contacts and Coulomb friction. In: The 1st Joint International Conference on Multibody System Dynamics, Lappeenranta, Finland (2010)
- [132] Orlandea, N., Chace, M., Calahan, D.: A sparsity-oriented approach to the dynamic analysis and design of mechanical systems – Part 1. *ASME J. Eng. Ind.* **99**(2), 773–779 (1977)
- [133] Padilla, C.E., von Flotow, A.H.: Nonlinear strain-displacement relations and flexible multi-body dynamics. In: Proceedings of the 3rd Annual Conference on Aerospace Computational Control, vol. 1, Oxnard, CA, pp. 230–245, (JPL Publication 89–45, Jet Propulsion Laboratory, Pasadena, CA, 1989) (1989)
- [134] Papadopoulos, E., Dubowsky, S.: On the nature of control algorithms for space manipulators. In: *IEEE International Conference on Robotics and Automation*, Cincinnati, OH (1990)
- [135] Paul, R.P.: Robot Manipulators: Mathematics, Programming, and Control. MIT Press, Cambridge, MA (1982)
- [136] Pfeiffer, F.: Mechanical System Dynamics. Springer, Berlin (2005)
- [137] Ramoni, M.F.: Bayesian Networks Representation and Reasoning. <http://ocw.mit.edu/NR/rdonlyres/Health-Sciences-and-Technology/HST-951JMedical-Decision-SupportSpring2003/695229E8-B5C8-4F33-A5B9-C4079AFAF967/0/lecture5.pdf> (2009)
- [138] Roberson, R., Schwertassek, R.: Dynamics of Multibody Systems. Springer, Berlin (1988)
- [139] Rodriguez, G.: Recursive forward dynamics for two robot arms in a closed chain based on Kalman filtering and Bryson-Frazier smoothing. In: Jamshidi, M. (ed.) *Robotics*, North-Holland, Amsterdam (1986)
- [140] Rodriguez, G.: Kalman filtering, smoothing and recursive robot arm forward and inverse dynamics. *IEEE J. Robot. Autom.* **3**(6), 624–639 (1987)
- [141] Rodriguez, G.: Kalman filtering, smoothing, and topological tree dynamics. In: VPI/SU Symposium on Control of Large Structures, Blacksburg, VA (1987)
- [142] Rodriguez, G.: Recursive multirigid body topological tree dynamics via Kalman filtering and Bryson-Frazier smoothing. In: VPI/SU Symposium on Control of Large Structures, Blacksburg, VA (1987)
- [143] Rodriguez, G.: Spatially random models, estimation theory, and robot arm dynamics. In: Rodriguez G. (ed.) *Proceedings of the Workshop on Space Telerobotics*, Jet Propulsion Laboratory, Pasadena, CA (JPL Publication 87–13, 1987) (1987)
- [144] Rodriguez, G.: Recursive forward dynamics for multiple robot arms moving a common task object. *IEEE Trans. Robot. Autom.* **5**(4), 510–521 (1989)
- [145] Rodriguez, G.: Random field estimation approach to robot dynamics. *IEEE Trans. Syst. Man Cybern.* **20**(5), 1081–1093 (1990)

- [146] Rodriguez, G.: Spatial operator approach to flexible multibody manipulator inverse and forward dynamics. In: IEEE International Conference on Robotics and Automation, Cincinnati, OH (1990)
- [147] Rodriguez, G.: Spatial operator approach to flexible multibody system dynamics and control. In: 4th Annual Conference on Computational Control, Williamsburg, VA (1990)
- [148] Rodriguez, G., Jain, A.: 2-Way recursive decomposition of the free-flying robot mass matrix. *J. Appl. Math. Comput.* **7**(2), 101–119 (1997)
- [149] Rodriguez, G., Kreutz-Delgado, K.: Spatial operator factorization and inversion of the manipulator mass matrix. *IEEE Trans. Robot. Autom.* **8**(1), 65–76 (1992)
- [150] Rodriguez, G., Scheid, R.: Recursive inverse kinematics for robot arms via Kalman filtering and Bryson-Frazier smoothing. In: AIAA Guidance, Navigation, and Control Conference, Monterey, CA (1987)
- [151] Rodriguez, G., Kreutz-Delgado, K., Jain, A.: A spatial operator algebra for manipulator modeling and control. *Int. J. Robot. Res.* **10**(4), 371–381 (1991)
- [152] Rodriguez, G., Jain, A., Kreutz-Delgado, K.: Spatial operator algebra for multibody system dynamics. *J. Astronaut. Sci.* **40**(1), 27–50 (1992)
- [153] Rosenberg, R.: Analytical Dynamics of Discrete Systems. Plenum, New York (1977)
- [154] Rosenthal, D.: Order N formulation for equations of motion of multibody systems. In: SDIO/NASA Workshop on Multibody Simulations, Arcadia, CA (1987)
- [155] Rosenthal, D.: Triangularization of equations of motion for robotic systems. *J. Guid. Control Dyn.* **11**(3), 278–281 (1988)
- [156] Rosenthal, D.: An order n formulation for robotic systems. *J. Astronaut. Sci.* **38**(4), 511–530 (1990)
- [157] Saha, S.K.: A decomposition of the manipulator inertia matrix. *IEEE Trans. Robot. Autom.* **13**(2), 301–304 (1997)
- [158] Schwerin, R.V.: Multibody System Simulation: Numerical Methods, Algorithms, and Software. Springer, Berlin (1999)
- [159] Schwertassek, R.: Recursive generation of multibody system equations. In: SDIO/NASA Workshop on Multibody Simulations, Arcadia, CA (1987)
- [160] Schwertassek, R.: Multibody kinematical equations in terms of relative variables. *Z. Angew. Math. Mech.* **68**(6), 207–211 (1988)
- [161] Schwertassek, R., Senger, K.: Representation of joints in multibody systems. *Z. Angew. Math. Mech.* **68**(2), 111–119 (1988)
- [162] Selig, J.: Geometrical Fundamentals of Robotics. Springer, New York (2004)
- [163] Shabana, A.A.: Dynamics of Multibody Systems. Cambridge University Press, Cambridge (1998)
- [164] Shi, P., McPhee, J.J.: Dynamics of flexible multibody systems using virtual work and linear graph theory. *Multibody Syst. Dyn.* **4**, 355–381 (2000)
- [165] Shuster, M.: A survey of attitude representations. *J. Astronaut. Sci.* **41**(4), 439–517 (1993)
- [166] Siciliano, B., Khatib, O.: Springer Handbook of Robotics. Springer, Heidelberg (2008)
- [167] Silver, W.: On the equivalence of Lagrangian and Newton–Euler dynamics for manipulators. *Int. J. Robot. Res.* **1**(2), 118–128 (1982)
- [168] Sinclair, A.J., Hurtado, J.E., Junkins, J.L.: Linear feedback control using quasi velocities. *J. Guid. Control Dyn.* **29**(6), 1309–1314 (2006)
- [169] Singh, R., VanderVoort, R., Likins, P.: Dynamics of flexible bodies in tree topology – a computer-oriented approach. *J. Guid. Control Dyn.* **8**(5), 584–590 (1985)
- [170] Spong, M.: Modeling and control of elastic joint robots. *ASME J. Dyn. Syst. Meas. Contr.* **109**, 310–319 (1989)
- [171] Spong, M.: Remarks on robot dynamics: canonical transformations and Riemannian geometry. In: IEEE International Conference on Robotics and Automation, Nice, France, pp. 554–559 (1992)
- [172] Stueelpnagel, J.: On the parametrization of the three-dimensional rotation group. *SIAM Rev.* **6**(4), 422–430 (1964)
- [173] Sundials: Initial Value Problems. Website, <http://sundials.wikidot.com/ivp-problems> (2010)

- [174] Tasora, A., Negrut, D., Anitescu, M.: Large-scale parallel multibody dynamics with frictional contact on the graphical processing unit. *J. Multibody Syst. Dyn.* **222**(K4), 315–326 (2008)
- [175] Trinkle, J.: Formulation of multibody dynamics as complementarity problems. In: ASME International Design Engineering Technical Conference, Chicago, IL (2003)
- [176] Umetani, Y., Yoshida, K.: Resolved motion rate control of space manipulators with generalized Jacobian matrix. *IEEE Trans. Robot. Autom.* **5**(3), 303–314 (1989)
- [177] Vafa, Z.: Space manipulator motions with no satellite attitude disturbances. In: IEEE International Conference on Robotics and Automation, Cincinnati, OH (1990)
- [178] Vereshchagin, A.: Computer simulation of the dynamics of complicated mechanisms of robot-manipulators. *Eng. Cybern.* **6**, 65–70 (1974)
- [179] Walker, M., Orin, D.: Efficient dynamic computer simulation of robotic mechanisms. *ASME J. Dyn. Syst. Meas. Contr.* **104**(3), 205–211 (1982)
- [180] Wen, J., Bayard, D.: A new class of control laws for robotic manipulators. *Int. J. Contr.* **47**, 1361–1385 (1988)
- [181] Wen, J., Kreutz, K.: A control perspective for multiple arm systems. In: 2nd International Symposium on Robotics and Manufacturing, Albuquerque, NM (1988)
- [182] Wen, J., Kreutz, K., Bayard, D.: A new class of energy based control laws for revolute arms. In: American Control Conference, Atlanta, GA (1988)
- [183] West, D.B.: Introduction to Graph Theory. Prentice-Hall, Englewood Cliffs, NJ (2001)
- [184] Wikipedia: Tree (graph theory). [http://en.wikipedia.org/w/index.php?title=Tree_\(graph_theory\)&oldid=327865637](http://en.wikipedia.org/w/index.php?title=Tree_(graph_theory)&oldid=327865637) (2009)
- [185] Wittenburg, J.: Dynamics of Systems of Rigid Bodies. BG Teubner, Stuttgart (1977)
- [186] Yamane, K., Nakamura, Y.: Dynamics computation of structure-varying kinematic chains and its application to human figures. *IEEE Trans. Robot. Autom.* **16**(2), 124–134 (2000)
- [187] Yamane, K., Nakamura, Y.: Dynamics simulation of humanoid robots: Forward dynamics, contact, and experiments. In: CISM-IFToMM Symposium on Robot Design, Dynamics, and Control (ROMANSY2008), Tokyo, Japan, pp. 301–308 (2008)
- [188] Yamane, K., Nakamura, Y.: Robotic Science and Systems IV, The MIT Press, chap A numerically robust LCP solver for simulating articulated rigid bodies in contact, pp. 89–104 (2009)
- [189] Zanganeh, K., Angeles, J.: A formalism for the analysis and design of modular kinematic structures. *Int. J. Robot. Res.* **17**(7), 720–730 (1998)

List of Notation

Symbols	
X^ω	the spatial vector with just the angular component of the X spatial vector 9
X^ν	the spatial vector with just the linear component of the X spatial vector 9
X_S	$= \text{col} \left\{ X(\varphi(k)) \right\}_{k=1}^n$ – a shifted version of a X stacked vector with the kth slot being occupied by the $X(\varphi(k))$ element 353
$[ij, k]$	Christoffel symbols of the first kind 381
$\begin{Bmatrix} k \\ ij \end{Bmatrix}$	Christoffel symbols of the second kind 381
$\text{col} \left\{ x(i) \right\}_{i=m}^p$	the stacked vector consisting of the $x(i)$ elements for bodies m through p in the multibody system 48
\mathbb{F}_x	representation of vector x in frame \mathbb{F} 4
\mathbf{I}	the identity matrix of appropriate dimension 12
$\mathbb{1}_{[\text{set}]}$	indicator function that returns a 1 if the element belongs to the set, and 0 otherwise 138
$\nabla_\theta f(\theta)$	the gradient of a the vector-valued function f with respect to the θ vector 401
\hat{z}	an operator related to the cross-product operator for spatial vectors 10
\tilde{l}	cross product operator $l \otimes (\cdot)$ 6
\widetilde{X}	$= \text{diag} \left\{ \widetilde{X}(k) \right\}_{k=1}^n$ – a block-diagonal matrix with $\widetilde{X}(k)$ diagonal elements from the X stacked vector 353
$\{l\}^\sim$	same as \tilde{l} 6
\overline{X}	$= \text{diag} \left\{ \overline{X}(k) \right\}_{k=1}^n$ – block-diagonal matrix with $\overline{X}(k)$ diagonal elements from the X stacked vector 353
\tilde{x}	$= -\{\tilde{x}\}^*$ – cross-product related operator for spatial vectors 10

0	the zero matrix of appropriate dimension	9
$i \not\prec j$	node j is not the ancestor of node i in a digraph	136
$i \prec j$	node j is the ancestor of node i in a digraph	136
$j \not\succ i$	node j is not the ancestor of node i in a digraph	136
$j \succ i$	node j is the ancestor of node i in a digraph	136
A		
$\alpha(k)$	the Coriolis spatial acceleration for the k th link	77
$\alpha_B(k)$	the Coriolis acceleration for the k th body in the serial-chain equations of motion with body spatial acceleration, defined as the body frame derivative of the spatial velocity of the body frame.	80
$\alpha_J(k)$	the Coriolis acceleration for the k th body in the serial-chain equations of motion with body spatial accelerations defined as the inertial frame derivative of the spatial velocity of the body frame	81
α_S	the stacked sub-vector of Coriolis spatial acceleration vectors for the S sub-graph bodies	294
$\alpha_{\mathbb{I}}(k)$	the Coriolis spatial acceleration for the k th body with inertially referenced spatial accelerations	94
$\alpha^+(k)$	$= \phi^*(k+1, k)\alpha(k+1) \in \mathcal{R}^6$ - the rigidly propagated $\alpha(k+1)$ (body-frame derivative) spatial acceleration from the \mathbb{O}_{k+1} frame to the \mathbb{O}_k^+ frame	101
$\alpha_{\mathbb{I}}(k)$	$\in \mathcal{R}^6$, spatial acceleration of the k th link referred to frame \mathbb{I}	94
\mathbb{A}	$= (\mathbf{I} - \mathcal{E}_{\mathbb{A}})^{-1}$ – a generic SPO operator	144
\mathbb{A}_a	the SPO operator for the aggregated tree	289
\mathbb{A}_c	the SPO operator for the C child sub-graph	276
\mathbb{A}_p	the SPO operator for the P parent sub-graph	276
\mathbb{A}_S	the SPO operator for a S sub-graph	276
$\tilde{\mathbb{A}}$	$= \mathbb{A} - \mathbf{I}$ – a spatial operator derived from a generic \mathbb{A} SPO operator	146
B		
$b(k)$	the gyroscopic spatial force for the k th link	76
$b_J(z)$	the gyroscopic spatial force for the equations of motion of a rigid body using inertial frame derivatives	26
b_S	the stacked sub-vector corresponding to the bodies in the S sub-graph	295
$\beta(k)$	the vector of generalized velocity coordinates for the k th hinge	39
β_B	$= \mathbb{B}\mathcal{V}$ – the rigid body generalized velocity coordinates defined as the body frame representation of the body's spatial velocity	24

β_J	$= \mathbb{V}$ – the rigid body generalized velocity coordinates defined as the inertial frame representation of the body's spatial velocity	24
β_I	\mathbb{V}_I – the rigid body generalized velocity coordinates defined as the inertially referenced spatial velocity of the body	33
b_I	b_I the gyroscopic spatial force associated with the equations of motion about an inertially fixed velocity reference point	33
\mathbb{B}	\mathbb{B} a body-fixed coordinate frame	23
\mathbb{B}_k	\mathbb{B}_k the reference frame for the k th link	36
\mathcal{B}	$\mathcal{B} \in \mathcal{R}^{6n \times 6n_{nd}}$ – the pick-off operator for body nodes	55
$\mathcal{B}_{\mathfrak{S}}$	$\mathcal{B}_{\mathfrak{S}}$ the connector block whose non-zero elements define the parent/child connectivity between links in the \mathfrak{S} sub-graph and their children in the \mathcal{C} child sub-graph	276
C		
$\mathcal{C}(k)$	$\mathcal{C}(k)$ the set of immediate child nodes of the k th node in a digraph	136
\mathcal{C}	\mathcal{C} the induced sub-graph consisting of the descendant nodes of the \mathfrak{S} sub-graph	274
$\mathcal{C}(\theta, \dot{\theta})$	$\mathcal{C}(\theta, \dot{\theta})$ the system-level Coriolis and gyroscopic forces vector	67
$\mathcal{C}_i(j, k)$	$\mathcal{C}_i(j, k)$ Christoffel symbol of the first kind	68
\mathbb{C}	\mathbb{C} the location of the center of mass for a rigid body	19
D		
$\frac{d_F x}{ds}$	$\frac{d_F x}{ds}$ derivative of vector $x(s)$ with respect to s in frame F	5
$\mathcal{D}(k)$	$\mathcal{D}(k) \mathcal{P}(k) \mathcal{H}^*(k)$ – the articulated body hinge inertia for the k th body	101
$\Delta_{B/O}$	$\Delta_{B/O} = \text{diag}\{\phi(\mathbb{B}_k, \mathbb{O}_k)\}$ – the \mathbb{B}_k body frame to the \mathbb{O}_k transformation operator	83
$\mathcal{V}_{B/O}(k)$	$\mathcal{V}_{B/O}(k)$ the relative spatial velocity of the \mathbb{O}_k frame with respect to the \mathbb{B}_k frame on the k th body	359
$\Delta_{\mathcal{V}}^\omega$	$\Delta_{\mathcal{V}}^\omega = \text{col}\{\Delta_{\mathcal{V}}^\omega(k)\}_{k=1}^n$ – the stacked vector of angular relative hinge spatial velocities for all the links	354
$\Delta_{\mathcal{V}}^v$	$\Delta_{\mathcal{V}}^v = \text{col}\{\Delta_{\mathcal{V}}^v(k)\}_{k=1}^n$ – the stacked vector of linear relative hinge spatial velocities for all the links	354
$\Delta_v(k)$	$\Delta_v(k)$ the relative linear velocity across the k th hinge	38
$\Delta_{\mathcal{V}}(k)$	$\Delta_{\mathcal{V}}(k)$ relative spatial velocity across the k th hinge	39
$\Delta_\omega(k)$	$\Delta_\omega(k)$ the relative angular velocity across the k th hinge	38
$\Delta_{\mathcal{V}}^B(k)$	$\Delta_{\mathcal{V}}^B(k)$ the hinge relative spatial velocity $\Delta_{\mathcal{V}}(k)$ referenced to the k th link body frame \mathbb{B}_k	80
$\Delta_{\mathcal{V}}^I(k)$	$\Delta_{\mathcal{V}}^I(k)$ the spatial velocity across the k th hinge in the inertially referenced formulation of the equations of motion	47

E

$\epsilon(k)$	the articulated body inertia innovations generalized force	111
e_k	$\in \mathcal{R}^{N \times m_k}$ – a n elements block-vector with all zero elements except for the k th element which is the identity matrix	138
\mathcal{E}_ϕ	the SKO operator for rigid-link multibody systems	48
\mathcal{E}_{Φ_B}	$= \Delta_{B/\mathbb{O}} \mathcal{E}_\phi \Delta_{B/\mathbb{O}}^{-1}$ – the SKO operator for rigid-link multi-body systems for the case when $B_k \neq \mathbb{O}_k$	83
\mathcal{E}_{A_C}	the SKO operator for the C child sub-graph	275
\mathcal{E}_{A_P}	the SKO operator for the P parent sub-graph	275
\mathcal{E}_{A_S}	the SKO operator for the S sub-graph	275
\mathcal{E}_{A_a}	the SKO operator for the aggregated tree	288
\mathcal{E}_A	a generic SKO operator	144
$\tilde{\mathcal{E}}$	a transformed version of the E base pick-off operator	87
E	the base pick-off operator	62
E_S	the connector block whose non-zero elements define the parent/child connectivity between links in S and their parents in the P sub-graph	276
\mathcal{E}_ψ	$= \mathcal{E}_\phi \bar{\tau}$ – the articulated body SKO operator	116

F

$f(\mathbb{F})$	spatial force at the \mathbb{F} frame	15
$f(k)$	the spatial force of interaction between the $(k+1)$ th and the k th links	75
f_c	the constraint spatial forces being applied at nodes on the multibody system	131
$f_c^i(k)$	the constraint spatial force at the i th node on the k th body	131
f_{ext}	the stacked vector of external spatial forces on the system .	85
$f_{ext}^i(k)$	the external spatial forces on the i th node on the k th body	85
$f_{\mathbb{I}}$	the equivalent spatial force on a rigid body associated with an inertially fixed velocity reference point	32
$f_{\mathbb{I}}(k)$	$\in \mathcal{R}^6$ – the spatial force of interaction between the $(k+1)$ th and the k th link referred to frame \mathbb{I}	94

G

g	the gravity spatial acceleration vector	87
g_l	the gravity linear acceleration vector	87
$\mathcal{G}(k)$	$\mathcal{P}(k)H^*(k)\mathcal{D}^{-1}(k)$ – the articulated body Kalman gain operator for the k th body	101

H

$h_\omega(k)$	the angular sub-block of the joint map matrix $H^*(k)$ for the k th body	40
---------------	--	----

$h_v(k)$	the linear sub-block of the joint map matrix $H^*(k)$ for the kth body	40
$H^*(k)$	the hinge map matrix for the kth hinge	39
H	the block-diagonal spatial operator of hinge map matrices ..	49
$H_B = H \Delta_{B/\mathbb{O}}^{-1}$	- the block-diagonal spatial operator of hinge map matrices when $B_k \neq \mathbb{O}_k$	84
$H_{\mathbb{I}}$	the block-diagonal spatial operator of hinge map matrices for inertially referenced formulation of the equations of motion	47
H_C	the H operator for the C child sub-graph	291
H_P	the H operator for the P parent sub-graph	291
H_S	the H operator for the S sub-graph	291
H_a	the H operator for the aggregated tree	291
$\mathcal{H}_{=i}$	$= \text{col} \left\{ H^*(i) \cdot \mathbb{1}_{[k=i]} \right\}_{k=1}^n$ - the derivative of Δ_V with respect to $\dot{\theta}_i$	363
$\mathcal{H}_{=i}^\omega$	$= \text{col} \left\{ H_\omega^*(i) \cdot \mathbb{1}_{[k=i]} \right\}_{k=1}^n$ - the derivative of Δ_V^ω with respect to $\dot{\theta}_i$	363
$\mathcal{H}_{\leq i}^\omega$	$= \text{col} \left\{ H_\omega^*(i) \cdot \mathbb{1}_{[k \leq i]} \right\}_{k=1}^n$ - the derivative of V^ω with respect to $\dot{\theta}_i$	363
$\mathcal{H}_{\prec i}^\omega$	$= \text{col} \left\{ H_\omega^*(i) \cdot \mathbb{1}_{[k \prec i]} \right\}_{k=1}^n$ - the derivative of V_S^ω with respect to $\dot{\theta}_i$	363
$\mathcal{H}_{=i}^v$	$= \text{col} \left\{ H_v^*(i) \cdot \mathbb{1}_{[k=i]} \right\}_{k=1}^n$ - the derivative of V^v with respect to $\dot{\theta}_i$	363
$\mathfrak{h}(z)$	spatial momentum of a rigid body	21
I		
\mathbb{I}	an inertially-fixed coordinate frame	23
J		
\mathcal{J}	$\in \mathcal{R}^{6n_{nd} \times \mathcal{N}}$ - the Jacobian matrix	55
$\mathcal{J}(k)$	rotational inertia of a rigid body	18
K		
\mathcal{K}	$= \mathcal{E}_\phi \mathcal{G}$ - the spatial operator formed from the shifted Kalman gain elements	116
$\mathcal{K}(k+1, k)$	$= \phi(k+1, k) \mathcal{G}(k)$ - the shifted Kalman gain operator ..	108
\mathfrak{K}_e	the system kinetic energy	17
L		
$\check{\mathcal{P}}^+$	$= \dot{\mathcal{P}}^+ + \bar{\Delta}_V^V \mathcal{P}^+ - \mathcal{P}^+ \tilde{\Delta}_V^V$ - an operator associated with the time derivative of the articulated body inertia, $\dot{\mathcal{P}}$	371

$\check{\lambda}$	the forward Lyapunov equation solution associated with the time derivative of the \mathcal{P} articulated body inertia	368
$\check{\lambda}_{\theta_i}$	$= \frac{\partial \check{\lambda}}{\partial \dot{\theta}_i}$ – an intermediate spatial operator used for the computation of the sensitivity of the \mathcal{P} articulated body inertia spatial operator	373
$\iota(\mathbb{F}, \mathbb{G})$	vector from frame \mathbb{F} to frame \mathbb{G}	3
Λ	operational space inertia matrix	188
$\underline{\Lambda}$	the operational space compliance matrix	188
\mathcal{L}	the Lagrangian function	67
M		
m	mass of a rigid body	18
$M_D(\theta, \dot{\theta})$	the gradient of the generalized momentum	67
\mathcal{M}	the mass matrix of a multibody system	67
$\mathbf{M}_{\mathbb{B}}$	$= \Delta_{\mathbb{B}/\mathbb{O}} \mathbf{M} \Delta_{\mathbb{B}/\mathbb{O}}^*$ – the block-diagonal spatial operator of body spatial inertias about the body frame when $\mathbb{B}_k \neq \mathbb{O}_k$	84
$M(k)$	the spatial inertia of the k th link	57
$M(x)$	spatial inertia of a rigid body referenced to point x	18
$\mathbf{M}_{\mathbb{I}}$	the block-diagonal spatial operator with inertially referenced body spatial inertias along the diagonal	95
$M_{\mathbb{I}}$	$\triangleq \phi(\mathbb{I}, \mathbb{C}) M \phi^*(\mathbb{I}, \mathbb{C}) \in \mathcal{R}^{6 \times 6}$, the inertially referenced spatial inertia of a body	32
$M_{\mathfrak{S}}$	rigid body spatial inertia matrix for the \mathfrak{S} sub-graph	295
N		
n	the number of bodies in the multibody system	35
n_G	the number of bodies in the \mathfrak{S} sub-graph	344
$n_{nd}(k)$	number of nodes on the k th body	54
n_{nd}	the number of nodes on the system	54
$v(k)$	the articulated body inertia innovations generalized acceleration	111
\bar{v}	$= v - g^* \bar{E}^* g$ – the articulated body innovations acceleration with gravity contribution included	129
N	the total number of velocity degrees of freedom for the system	47
O		
\mathbb{O}_k^i	the i th node on the k th links	54
$\omega(x)$	the angular velocity of the x frame	6
$\omega(\mathbb{F}, \mathbb{G})$	the angular velocity of the \mathbb{G} frame with respect to the \mathbb{F} frame	13
Ω	the extended operational space compliance matrix	190
\mathbb{O}_k	outboard hinge reference frame for the k th link	35
\mathbb{O}_k^+	inboard hinge reference frame for the k th link	35

P	
$\wp(k)$	the set of parent nodes of the k th node in a digraph
\mathcal{P}	\mathcal{P} the induced sub-graph for the nodes not in, or descendant of, the \mathfrak{S} sub-graph
$p(k)$	$p(k)$ the 3-vector from the point k to the center of mass of a rigid body
ϕ	$\phi = (\mathbf{I} - \mathcal{E}_\phi)^{-1}$ – the SPO operator for rigid-link multibody systems
$\phi(x, y)$	$\phi(x, y)$ rigid body transformation matrix for the x and y frames ..
$\phi_{\mathbb{B}}$	$\phi_{\mathbb{B}} = \Delta_{\mathbb{B}/\mathbb{O}} \phi \Delta_{\mathbb{B}/\mathbb{O}}^{-1}$ – the SPO operator for the case when $\mathbb{B}_k \neq \mathbb{O}_k$
$\phi(k, k-1)$	$\phi(k, k-1)$ the rigid body transformation matrix from frame \mathbb{B}_k to frame \mathbb{B}_{k-1}
$\tilde{\phi}$	$\tilde{\phi} = \phi - \mathbf{I}$ – the strictly lower-triangular spatial operator de- rived from the ϕ SPO operator
ψ	$\psi = (\mathbf{I} - \mathcal{E}_\psi)^{-1}$ – the articulated body SPO operator
$\psi(k+1, k)$	$\psi(k+1, k) = \phi(k+1, k)\bar{\tau}(k)$ – the articulated body transforma- tion matrix for the k th body
$\tilde{\psi}$	$\tilde{\psi} = \psi - \mathbf{I}$ – the articulated body spatial operator derived from the ψ SPO operator
$\mathcal{P}(k)$	$\mathcal{P}(k)$ the articulated body inertia of the k th link
$\dot{\mathcal{P}}$	$\dot{\mathcal{P}} = \mathcal{E}_\phi \check{\mathcal{P}}^+ \mathcal{E}_\phi^*$ – an operator associated with the time deriva- tive of the articulated body inertia, $\dot{\mathcal{P}}$
$\mathcal{P}^+(k)$	$\mathcal{P}^+(k) \triangleq \mathcal{P}(k)\bar{\tau}^*(k)$ the articulated body inertia $\mathcal{P}(k)$ trans- formed across the joint from \mathbb{O}_k to \mathbb{O}_{k+1} for the k th body
$\dot{\mathcal{P}}^+$	$\dot{\mathcal{P}}^+ = \bar{\tau}\check{\lambda}\bar{\tau}^*$ – an operator associated with the time derivative of the articulated body inertia, $\dot{\mathcal{P}}$
R	
$r_p(k)$	$r_p(k)$ number of hinge generalized coordinates for the k th hinge ..
$r_v(k)$	$r_v(k)$ the number of generalized velocity coordinates for the k th hinge
$\mathcal{R}(k)$	$\mathcal{R}(k)$ the composite rigid body inertia associated with the k th hinge
\mathcal{R}	\mathcal{R} the block-diagonal spatial operator consisting of compos- ite body inertia of the links
$\mathbb{F}\mathfrak{R}_{\mathbb{G}}$	$\mathbb{F}\mathfrak{R}_{\mathbb{G}} \in \mathbb{R}^{3 \times 3}$ – a rotation matrix that transforms vector repre- sentations from the \mathbb{G} frame to the \mathbb{F} frame
S	
\mathbb{S}	\mathbb{S} the adjacency matrix for digraphs
\mathbb{S}_W	\mathbb{S}_W a BWA matrix for a tree digraph

T	
θ	the vector of generalized coordinates for the system 48
$\tau(k)$	the articulated body projection operator for the k th hinge . 102
$\bar{\tau}(k)$	$= \mathbf{I} - \tau(k)$ – the complement of projection operator $\tau(k)$
	for the k th hinge 102
$\mathcal{T}(k)$	the generalized force vector for the k th hinge 77
${}^F\mathbb{T}_{\mathbb{G}}$	homogeneous transform 4
\mathfrak{T}	a rooted directed tree of nodes and edges 137
U	
\mathfrak{U}	the projection operator for operational space dynamics ... 199
\mathfrak{U}_\perp	$= \mathbf{I} - \mathfrak{U}$ – the complement of the \mathfrak{U} projection operators
	for operational space dynamics 199
γ^+	matrix associated with γ 194
γ	kernel matrix associated with operational space inertias... 191
V	
$v_{\mathbb{F}}(\mathbb{F}, \mathbb{G})$	the linear velocity of the \mathbb{G} frame with respect to the \mathbb{F} frame..... 14
$v(x)$	linear velocity vector for point x 7
$v_{\mathbb{I}}$	the linear velocity of the inertially fixed velocity reference frame \mathbb{I} for a rigid body 31
$v_{\mathbb{I}}(k)$	the linear velocity of the inertially fixed velocity reference frame \mathbb{I} for the k th body 93
v^ω	$= \text{col} \left\{ v^\omega(k) \right\}_{k=1}^n$ – the stacked vector of angular spatial velocities for all the links 354
$v^\omega(\mathbb{F})$	the angular spatial velocity component of the $\mathcal{V}(\mathbb{F})$ spatial velocity of \mathbb{F} frame 9
v_{nd}	$= \in \mathcal{R}^{6n_d}$ – the stacked vector of spatial velocities of the task space nodes (also used as generalized velocities for Operational Space dynamics)..... 54
$v_{\mathbb{F}}(\mathbb{F}, \mathbb{G})$	the spatial velocity of the \mathbb{G} frame with respect to the \mathbb{F} frame..... 14
v^v	$= \text{col} \left\{ v^v(k) \right\}_{k=1}^n$ d – the stacked vector of linear spatial velocities for all the links 354
$v^v(\mathbb{F})$	the linear spatial velocity component of the $\mathcal{V}(\mathbb{F})$ spatial velocity of \mathbb{F} frame 9
$v(\mathbb{O}_k^i)$	$\in \mathcal{R}^6$ – the spatial velocity of the i th node on the k th links 54
v	the stacked vector of link spatial velocities 48
$v(\mathbb{F})$	spatial velocity of the \mathbb{F} frame 9
$v(k)$	spatial velocity of the \mathbb{B}_k frame 43
$v^+(k)$	spatial velocity of \mathbb{O}_k^+ frame 43

$\tilde{\mathcal{V}}^\omega(z)$	$a \in \mathcal{R}^{6 \times 6}$ cross-product matrix associated with the $\mathcal{V}^\omega(z)$	
	angular spatial velocity	25
$\tilde{\mathcal{V}}_\mathfrak{S}^\omega$	$= \text{diag} \left\{ \tilde{\mathcal{V}}^\omega(\varphi(k)) \right\}_{k=1}^n$ – the block-diagonal matrix with $\tilde{\mathcal{V}}^\omega(\varphi(k))$ elements	354
$\bar{\mathcal{V}}_\mathfrak{S}^v$	$= \text{diag} \left\{ \bar{\mathcal{V}}^v(\varphi(k)) \right\}_{k=1}^n$ – the block-diagonal matrix with $\bar{\mathcal{V}}^v(\varphi(k))$ elements	354
$\bar{\mathcal{V}}$	$= \text{diag} \left\{ \bar{\mathcal{V}}(k) \right\}$ – the block-diagonal spatial operator with $\bar{\mathcal{V}}(k)$ diagonal elements	354
$\bar{\mathcal{V}}_\mathfrak{S}$	$= \text{diag} \left\{ \bar{\mathcal{V}}(\varphi(k)) \right\}$ – the block-diagonal, shifted up version of the $\bar{\mathcal{V}}$ spatial operator	354
$\mathcal{V}_\mathfrak{S}$	the stacked sub-vector corresponding to the \mathfrak{S} sub-graph bodies	290
$\mathcal{V}_\mathbb{I}$	the inertially referenced spatial velocity of a point on a body, with ω and $v_\mathbb{I}$ denoting the angular and linear velocity components, respectively	31
$\mathcal{V}_\mathbb{I}(k)$	the spatial velocity of the kth link referred to frame \mathbb{I} , with $\omega(k)$ and $u(k)$ denoting the angular and linear velocity components, respectively	93
Z		
$\mathfrak{z}(k)$	the residual spatial force for the kth link	107
$\mathfrak{z}^+(k)$	the $\mathfrak{z}(k)$ articulated body inertia residual force propagated across the kth hinge	108
\mathfrak{z}_δ	the correction residual spatial force due to a non-zero tip force	131

Index

Symbols

- $\phi(\cdot, \cdot)$, 11
 - group property, 11
- E_+ matrix, 408
- E_- matrix, 408
- $\hat{\cdot}$ operator, 10
 - identities, 12
- $\tilde{\cdot}$ cross-product operator
 - for 3-vectors, 6
 - for spatial vectors, 9
- kth articulated body system, 100
- 1-resolvent
 - BWA matrix, 143
 - SKO operator, 159
 - SPO operator, 159
 - elements, 144
 - of a nilpotent matrix, 400

A

- AB forward dynamics
 - SKO models, 182
 - flexible-link systems, 264, 267
 - for free-flying dual model, 335
 - free-flying systems, 338, 339
 - geared systems, 243
 - optimized algorithm for geared systems, 242
 - serial-chain systems, 126, 130
 - standard algorithm for geared systems, 241
 - tree-topology systems, 182
 - under-actuated systems, 322
 - with constraint embedding, 308
- absolute coordinates, 38
- acatastatic constraint, 39, 210
- active
 - degree of freedom, 314
 - arm, 315
 - hinge, 314

- active contact, 225
- acyclic digraph (DAG), 137
- adjacency matrix, 138
 - BWA, see BWA matrix
 - block-weighted, see BWA matrix
 - canonical tree, 140
 - digraph, 138
 - lower-triangular, 140
 - properties, 138
 - serial-chain, 140
 - strictly canonical tree, 140
 - tree, 140
- adjacent node, 135
- aggregation
 - SPO operator, 289
 - at the component level, 292
 - condition, see aggregation condition
 - for sub-structuring SKO models, 290
 - mass matrix, 291
 - of a sub-graph, 283
 - of an induced sub-graph, 283
 - preservation of tree structure, 285
 - sub-graph, 287
- aggregation condition, 284, 299
 - path-induced sub-graphs, 285
 - preservation of tree property, 287
 - transformed SKO model, 291
- algorithm for computing
 - ϕx recursively, 51
 - $\phi^* x$ recursively, 52
 - θ^δ correction accelerations, 131
 - Δx recursively, 162
 - $\Delta^* x$ recursively, 163
 - Υ operational space compliance kernel, 195
- extended operational space compliance matrix, 192

- operational space compliance
 - kernel, 195
- articulated body inertia, *see*
 - articulated body inertia
- composite body inertia, *see*
 - composite body inertia
- diagonalizing generalized forces, 386
- diagonalizing velocity
 - coordinates, 386
- disturbance Jacobian, 328
- dual
 - articulated body inertias, 334
 - residual forces, 335
- elements of $\mathbb{A}X\mathbb{B}^*$, 168
- elements of $\mathbb{A}^*X\mathbb{B}$, 173
- forward dynamics, *see* forward dynamics
- generalized dynamics, 322
- generalized forces for external forces, 86
- generalized Jacobian, 326
- inverse dynamics, *see* inverse dynamics
- link spatial velocities, 45
- link transformations, 43
- mass matrix
 - inverse, 198
 - using composite body inertias, 64, 169, 238, 261
 - using inverse dynamics, 90
- operational space
 - Coriolis vector, 203
 - inertia, 194, 351
- under-actuated computed-torque, 326
- velocity diagonalization Coriolis vector, 391
- algorithm for computing
 - mass matrix inverse, 200
- ancestor node, 135
- angle/axis representation, 405
- angular velocity, 5
 - based quasi-velocities, 71
- from angle/axis parameter rates, 406
- from Euler angle rates, 404
- from quaternion rates, 411
- to quaternion rates, 410
- anti-causal filter, 112, 338
- arborescence digraph, 137
- articulated body
 - kth system, 100
 - dual type, 333
 - forward dynamics, *see* AB forward dynamics
 - hinge inertia, 101
 - inertia, *see* articulated body inertia
 - model, *see* articulated body model
 - time-derivative, 368–373
 - transformation matrix, 105
- articulated body inertia, 99, 117
 - relationship to spatial inertias, 107
 - for SKO models, 175
 - for flexible-link systems, 262
 - for geared systems, 239, 240
 - for under-actuated systems, 317
 - force decompositions based on, 99
 - positive semi-definiteness of, 104
 - relationship to composite body inertias, 107, 121
 - serial-chain systems, 106
 - with constraint embedding, 307
- articulated body model, 97, 99–111, 115
 - based force decompositions, 128
 - comparison with the composite body model, 117
 - projection operators for, 102
- assumed modes, 250
- attitude representation, 23
 - angle/axis parameters, 404
 - Euler angles, 403
 - Gibbs vector, 412
 - Rodrigues vector, 412
 - unit quaternions, *see* quaternions
- augmented dynamics, 212
 - equivalence to projected dynamics, 222

- augmented forward dynamics,
212–221
algorithm, 213, 219
loop constraints, 215
- B**
- backward Lyapunov equation, 170,
191
base-body, 35
base-invariant
computation of operational space
inertia, 351
forward dynamics, 338, 339
operational space inertia, 348
symmetry, 338
- base-to-tip recursion, 52
base-to-tips scatter recursion, 163
bilateral constraint, 209
block-weighted adjacency matrix,
see BWA matrix
- body reference frame, 36
at hinge frame, 45, 77
at non-hinge frame, 46, 80, 358
- BWA matrix, 141–149
SKO operator, 159
SPO operator, 159
1-resolvent, 143
for multibody systems, 150–159
nilpotency, 143
permutation transformation, 148
powers of, 142
similarity-shift transformation,
149
transforming, 147
tree digraph, 142
- C**
- canonical tree digraph, 137
adjacency matrix, 140
cantilever modes, 250
catastatic constraint, 39, 210, 301
causal filter, 112, 338
center of mass, 19
equations of motion about, 25
of a multibody system, 62
- of a rigid body, 18
spatial velocity, 63
- centeroid, 19
- characteristic polynomial
of a rotation matrix, 405
of a skew-symmetric matrix, 405
- child node, 135
child nodes of a sub-graph, 284
child sub-graph, 274
- Christoffel symbols
for multibody systems, 69
of the first kind, 68, 381
of the second kind, 381
relationship to $M_D(i,j)$, 69
relationship to Coriolis terms, 69
- closed differential form, 71
closed-chain dynamics, 150,
209–227, 297
SKO model, 185, 299
augmented approach, see
augmented dynamics
bilateral constraints, 209
constraint embedding approach,
see constraint embedding
dynamics
direct approach, see direct
dynamics
projected approach, see projected
dynamics
SKO model, 302
unilateral constraints, 224
- compatible operators, 162
compatible operators and vectors,
162
- complementarity
approach, 224
condition, 226
problem
LCP, 226
NCP, 226
- composite body inertia, 59–66, 98,
107
based computation of the mass
matrix, 238, 261
for flexible-link systems, 261

- for geared systems, 237
- for inverse dynamics, 91
- Lyapunov equation for, 61, 168
- recursive computation of
 - for SKO models, 169
 - for flexible-link systems, 261
 - for geared systems, 237
 - for serial-chain systems, 60
- relationship to articulated body
 - inertias, 121
 - serial-chain systems, 59
- composite body method, 65
- composite body model, 92, 97, 98, 115
 - comparison with the articulated body model, 117
- computed-torque for under-actuated systems, 326
- configuration kinematics, 42
- connected digraph, 136
- conservation of
 - kinetic energy, 28, 30, 329
 - spatial momentum, 25, 28, 33, 329
- constrained dynamics, *see*
 - closed-chain dynamics
- constraint
 - acatastatic, 39, 210
 - bilateral, 209
 - catastatic, 39, 210
 - force, 222
 - squeeze, 214
 - holonomic, *see* holonomic constraint
 - loop, 215
 - non-holonomic, *see*
 - non-holonomic constraint
 - rheonomic, 210
 - scleronomic, 210
 - unilateral, *see* unilateral constraint
- constraint embedding, 212, 297–311
 - AB forward dynamics, 308
 - direct joint-level constraints, 303
 - four-bar linkage example, 305, 306
 - geared example, 304
- generalizations, 311
- loop constraints, 303
- SKO model, 302
- strategy, 297
- constraint forces, 131
 - closed-chain, 218
 - inter-link, *see* inter-link spatial forces
- contact
 - active, 225
 - inactive, 225
 - separation, 225
- contact hinge, 41
- control
 - computed-torque, 326
 - decoupled, 392
 - operational space, 189
 - rate-feedback, 392
- coordinate transformations, 72
 - diagonalizing, 72, 379–382
 - with kth link as base-body, 341
- coordinate-frame representations, 4
- coordinate-free representations, 4
- coordinates
 - generalized, *see* generalized coordinates
 - generalized velocity, *see* generalized velocity coordinates
- Coriolis acceleration, 77, 358, 434
 - dual, 335
 - for a cylindrical hinge, 80
 - for a helical hinge, 80
 - for a prismatic hinge, 79
 - for a rotary pin hinge, 79
 - for simple hinges, 79
 - with hinge frame as body frame, 77
 - with inertial frame derivatives, 80
 - with non-hinge frame as body frame, 80
- Coriolis forces vector, 67
 - for SKO models, 160
 - for diagonalized dynamics, 382, 387, 393

- for flexible-link systems, 257
- for geared systems, 236
- for serial-chain rigid-link system, 82
- Lagrangian form, 67
- non-working, 384, 391
- operational space, 202
- with velocity diagonalization, 389
 - algorithm for computing, 391
- correction generalized accelerations, 212
- cross product
 - for 3-vectors, 6
 - for spatial vectors, 9–10
 - identities, 10, 397
- curvature tensor, 381
- cut-edge, 138, 209
 - multibody, 151
- cyclic digraph, 137
- cylindrical hinge, 40, 41
 - Coriolis acceleration, 80
- D**
- DAG, 137
- DCA algorithm, 218
- decomposition of the mass matrix
 - using composite body inertias, 63, 168
- decoupled control, 392
- decoupled forward dynamics, 338, 339
- derivative
 - with respect to a vector, 401
 - with respect to generalized coordinates, *see* sensitivity
 - with respect to time, *see* time derivative
- of a vector
 - with respect to a frame, 5
 - with respect to the body frame, 7
 - with respect to the inertial frame, 7
- of spatial inertias, 25, 32
- of spatial operators, 353
- of vectors, 5–8
- time, *see* time derivative
- descendant node, 135
- determinant
 - of the mass matrix, 180
 - of the Newton-Euler factor, 180
- diagonalized dynamics
 - condition, 379, 382
 - Coriolis forces vector, 382, 387, 393
- diagonalizing coordinate transformations, 72
 - algorithm for computing, 386
 - global, 379–382
 - velocity, 382–392
- diagonalizing generalized forces
 - algorithm for computing, 386
- differential equation
 - differential-algebraic, *see* differential-algebraic equation
 - ordinary, *see* ordinary differential equation
- differential kinematics, 43
 - hinge, 37
 - with $\mathbb{B}_k \neq \mathbb{O}_k$, 45
- differential-algebraic equation, 213, 222, 339
- digraph
 - acyclic graph (DAG), 137
 - adjacency matrix, *see* adjacency matrix
 - adjacent nodes, 135
 - aggregation condition, 284
 - aggregation of a sub-graph, 283
 - arborescence, 137
 - connected, 136
 - cut-edge, 138, 209
 - cyclic, 137, 209
 - disconnected, 136
 - edge, 135
 - edge-contraction, 283
 - for a multibody system, *see* multibody digraph
 - forest, 137
 - homeomorphic, 279
 - multiply-connected, 137, 209

- node, 135
 - node-contraction, 283
 - partitioning, 273–275
 - polytree, 137
 - properties, 141
 - related nodes, *see* related nodes
 - root node, 135
 - rooted, 136
 - serial-chain, 137
 - simple tree, 137
 - simply-connected, 137
 - spanning tree, 138
 - standard, 150
 - tree, 137
 - unrelated nodes, *see* unrelated nodes
 - direct dynamics, 212
 - directed acyclic graph, 137
 - directed cycle, 209
 - in path-induced sub-graph, 274
 - directed graph, *see* digraph
 - direction cosine matrix, *see* rotation matrix
 - disconnected digraph, 136
 - distance function, 225
 - disturbance Jacobian, 325
 - computation of, 328
 - of free-flying systems, 328, 330
 - divide and conquer algorithm, 208
 - dual
 - articulated body inertia, 334
 - Coriolis acceleration, 335
 - force decomposition, 336
 - model, 332
 - residual force, 335
 - weight matrices, 333
 - dynamics
 - augmented dynamics, 212
 - closed-chain systems, 209
 - constraint embedding dynamics, 212
 - diagonalized, 379
 - direct dynamics, 212
 - flexible-link systems, 245
 - for SKO models, 160
 - free-flying systems, 331
 - geared systems, 229
 - hybrid, 324
 - invariance across Newtonian frames, 30, 82
 - operational space, 189
 - prescribed motion, 322
 - projected dynamics, 212
 - rigid body systems, 17
 - serial-chain systems, 75
 - tree-topology systems, 155
 - under-actuated systems, 313
- E**
- edge, 135
 - multibody, 150
 - edge-contraction, 283
 - equations of motion
 - for SKO models, 160
 - for flexible-link systems, 245–255
 - for geared systems, 230–234
 - for tree-topology systems, 155
 - for under-actuated systems, 316
 - Hamilton form, 70
 - Lagrangian form of, *see* Lagrangian dynamics
 - operational space, 187, 189
 - rigid body, 25
 - Euclidean metric tensor, 381
 - Euler angles, 41, 403
 - Euler equation for rotational motion, 71
 - Euler parameters, *see* quaternions
 - Euler–Rodrigues formula, 405
 - explicit hinge constraints, 36
 - extended operational space
 - compliance matrix, 190
 - algorithm for computing, 192
 - operator decomposition, 191
 - for serial-chains, 197
 - external force
 - compensating for, 86
 - equivalent generalized forces, 85
 - inclusion of, 85, 129

- F**
- feedback linearization, 189
 - Fixman potential, 376
 - flexible joints, 233
 - flexible-link system
 - SKO models, 255–257
 - articulated body inertia, 262
 - as under-actuated systems, 261
 - composite body inertias, 261
 - Coriolis forces vector, 257
 - equations of motion, 245–255
 - forward dynamics, 264, 267
 - Innovations operator factorization, 263
 - inverse dynamics for, 259
 - lumped mass model, 245–249
 - mass matrix, 257
 - decomposition, 261
 - recursive computation of, 261
 - modal model, 249–255
 - force
 - constraint, 222
 - move, 214
 - squeeze, 214
 - force decomposition
 - dual model, 336
 - using articulated body model, 99, 128
 - using composite body model, 98
 - using terminal body model, 98
 - force recursion
 - for aggregated bodies, 295
 - for serial-chains, 76
 - for tree systems, 156
 - forest digraph, 137, 147
 - forward dynamics, 88
 - AB algorithm, *see* AB forward dynamics
 - $O(N)$ algorithm, *see* AB forward dynamics
 - $O(N^3)$ algorithm, 122
 - $O(N^2)$ algorithm, 122
 - articulated body model, 97
 - augmented dynamics algorithm, 213
 - base-invariant, 338
 - DCA algorithm, 208
 - decoupled form, 338, 339
 - diagonalized dynamics, 394
 - divide and conquer algorithm, 208
 - flexible-link systems, 264
 - for SKO models, 182
 - free-flying systems, 337
 - geared systems, 239, 243
 - of under-actuated systems, 322
 - projected dynamics algorithm, 223
 - un-normalized diagonalized dynamics, 395
 - with bilateral constraints, 211
 - with loop constraints, 215, 219
 - with unilateral constraints, 227
 - forward kinematics, 42
 - forward Lyapunov equation, 370
 - for SPO operators, 166
 - frame
 - body reference, 36
 - hinge, 37
 - Newtonian, 30, 82
 - of interest, *see* node
 - frame of interest, 54
 - free generalized accelerations, 212
 - free-flying system, 331
 - as under-actuated system, 329–330
 - base-invariant symmetry, 338
 - disturbance Jacobian, 328, 330
 - dual articulated body inertias, 333
 - dual model, 332
 - forward dynamics, 337–339
 - generalized Jacobian, 325, 328
 - regular model, 332
 - with tree topology, 340
 - free-free modes, 250
 - friction, 227
- G**
- gap function, 225
 - gather recursion, 162
 - geared system, 229
 - articulated body inertia, 239

- articulated body inertias, 240
- composite body inertia, 237
- Coriolis forces vector, 236
- equations of motion, 230–234
- forward dynamics, 239, 243
- Innovations operator factorization, 240
- mass matrix, 236
 - decomposition, 237
 - recursive computation of, 238
- optimized AB forward dynamics, 242
- standard AB forward dynamics, 241
- generalized accelerations, 24
 - correction, 212
 - free, 212
 - inertial, 27
 - innovations, 111
- generalized coordinates, 23, 37
 - absolute, 38
 - diagonalizing transformation, 379
 - for flexible-links, 251
 - for geared systems, 233
 - hinge, 37
 - minimal, 212
 - non-minimal, 212
 - relative, 38
 - transformation, 72
- generalized dynamics algorithm, 322
- generalized forces, 24
 - for external forces, 85
- generalized inverse, 214
- generalized Jacobian, 325
 - computation of, 326
 - of free-flying systems, 325, 328
- generalized momentum, 67
 - gradient of, 67, 365
- generalized speeds, see generalized velocity coordinates
- generalized velocity coordinates, 23, 39
 - diagonalizing transformation, 382
 - for flexible-links, 251
 - for geared systems, 233, 234
- hinge, 39
 - quasi-velocities, 23
 - transformation, 70
- Gibbs vector attitude representation, 412
- global diagonalization condition, 379
- gradient
 - with respect to a vector, 401
 - of the generalized momentum, 67, 365
- graph
 - directed, see digraph
 - undirected, 135
- gravitational force, 87, 128, 202
- group
 - of homogeneous transforms, 4
 - of rigid body transformation matrices, 11
- gyroscopic force, 75
 - using β_B , 30
 - using β_J , 26, 28
- H**
- Hamilton form of equations of motion, 70
- helical hinge, 40, 41
 - Coriolis acceleration, 80
- hinge, 35
 - articulated body inertia, 101
 - contact, 41
 - cylindrical, 40, 41, 80
 - explicit constraints, 36
 - frame, 37
 - helical, 41, 80
 - implicit constraints, 36
 - kinematics, 37
 - prismatic, 40
 - rotary pin, 40
 - spherical, 40, 41
 - universal, 41
- hinge map matrix, 39
 - configuration dependent, 41
 - cylindrical hinge, 40
 - prismatic hinge, 40

rotary pin hinge, 40
 spherical hinge, 40
 holonomic constraint, 210
 homeomorphic digraphs, 279
 homogeneous transform, 4, 37, 42
 homogenous transform
 time derivative, 38
 hybrid dynamics, 324

I

ignorable coordinates, 329
 implicit hinge constraints, 36
 inactive contact, 225
 inboard link, 35
 indicator function, 138, 362
 induced sub-graph, 273
 inertia
 articulated body, 99
 composite body, 59
 moments of, 18
 rotational, 18
 spatial, 18
 inertial generalized accelerations, 27
 inertially fixed reference point, 47
 based velocity recursion, 47
 for a rigid body, 31–33
 for serial-chains, 93
 innovations generalized acceleration,
 111
 innovations generalized force, 111
 Innovations operator factorization,
 58, 120
 after constraint embedding, 308
 for SKO models, 179
 for flexible-link systems, 263
 for geared systems, 240
 for serial-chain systems, 115, 120,
 122
 for tree-topology systems, 179
 for under-actuated systems, 319
 of the mass matrix, 115, 120
 sensitivity, 375
 time derivative, 375
 innovations process, 113
 integrals of motion, 34, 329

inter-link spatial forces, 75
 articulated-body model
 decomposition, 99
 composite-body model
 decomposition, 98
 computation, 128
 operator decomposition, 128
 terminal-body model
 decomposition, 97
 inverse dynamics, 88
 for computing the mass matrix, 90
 for flexible-link systems, 260
 for serial-chains, 88–93
 for under-actuated systems, 322
 Newton–Euler algorithm, 89
 Newton-Euler algorithm, 166
 of flexible-link systems, 259
 of under-actuated systems, 322
 using composite rigid body
 inertias, 91
 inverse kinematics, 42

J

Jacobi cross-product identity, 10
 Jacobian
 disturbance, 325
 for under-actuated systems,
 324–328
 generalized, 325
 in operational space dynamics,
 188
 mapping for external forces, 86
 operator, 55
 joint, see hinge

K

Kalman gain, 101, 113
 shifted, 108
 Kane’s method, 161
 kinematics
 differential, 43
 forward, 42
 hinge, 37
 inverse, 42
 kinetic energy, 18
 as Lagrangian, 67

- conservation, 28, 30, 329
 flexible body, 251
 integral of motion, 329
 rate of change of, 384
 sensitivity of, 366
 serial-chain, 57
 using diagonalizing coordinates, 380
- L**
- Lagrange multipliers, 211, 222
 Lagrangian dynamics
 Coriolis forces vector, 67
 equations of motion, 66–70
 equivalence with Newton–Euler
 dynamics, 367
 symmetries of, 34, 329
 LCP, 226
 linear complementarity
 problem, 226
 linear velocity constraints, 36
 link, 35
 base-body, 35
 flexible, 245
 inboard, 35
 outboard, 35
 tip-body, 35
 link transformations, 43
 load balancing, 215
 loop constraints, 215, 303
 lower-triangular
 SKO matrix, 146
 SPO matrix, 145, 146
 lower-triangular adjacency matrix, 140
 lumped mass model for flexible
 systems, 245–249
 Lyapunov equation
 backward, see backward
 Lyapunov equation
 discrete, 61
 for composite body inertias
 SKO model, 168
 flexible-link systems, 261
 geared systems, 237
- serial-chain, 61
 forward, see forward Lyapunov
 equation
 in estimation theory, 112
 Lyapunov recursion, 60
- M**
- mass matrix, 58, 67
 after aggregation, 291
 Christoffel symbols, 68, 381
 computation of the inverse, 198
 computation using inverse
 dynamics, 90
 constant, 380, 382
 decomposition, 63, 168, 237, 261
 decomposition of the inverse, 198
 determinant, 180
 diagonal, 380, 382, 393
 Fixman potential, 376
 for SKO models, 160
 for flexible-link systems, 257
 for geared systems, 236
 for serial-chain rigid-link system, 82
 generalized momentum, 67
 identity matrix, 380, 382
 Innovations operator factorization,
 see Innovations operator
 factorization
 invariance to aggregation, 292
 inverse, v, 198
 operator decomposition, 198
 kinetic energy, 58
 metric tensor, 381
 Newton-Euler operator
 factorization, see
 Newton-Euler operator
 factorization
 operator expression, 58
 operator inverse, 121
 partitioned, 278
 for under-actuated systems, 316
 recursive computation of, 64, 169,
 238, 261
 Riemannian symbols, 73, 381

- sensitivity, 365
 - sparsity structure, 282
 - time derivative, 360
 - trace, 65
 - mass matrix inverse
 - algorithm for computing, 200
 - operator factorization
 - after constraint embedding, 308
 - for SKO models, 179
 - for flexible-link systems, 263
 - for geared systems, 240
 - for rigid-link serial-chains, 121
 - for under-actuated systems, 319
 - matrix
 - block partitioned, 398
 - inverse identities, 398
 - norm, 397
 - Schur complement, 398
 - metric tensor, 381
 - micro/macro manipulators, 196
 - mixed dynamics, 322
 - modal
 - integrals, 252
 - joint map matrix, 253
 - mass matrix, 252
 - model for flexible systems, 249–255
 - spatial acceleration, 253
 - spatial displacement, 250
 - spatial displacement influence vector, 250
 - spatial force, 254
 - spatial velocity, 251, 253
 - stiffness matrix, 254
 - modal matrix, 250
 - mode shape, 251
 - modes
 - assumed, 250
 - cantilever, 250
 - free-free, 250
 - molecular dynamics, 376
 - moments of inertia, 18
 - momentum
 - generalized, 67
 - spatial, 21
 - move force, 214
 - move/squeeze decomposition, 214
 - projection matrix, 214
 - multibody digraph, 150
 - multibody system
 - BWA matrix, 150–159
 - SKO operator, 159
 - SKO-forest, 151
 - SKO model, 160
 - SPO operator, 159
 - articulated body model, 97
 - closed-chain, see closed-chain dynamics, 209, 297
 - composite body model, 97
 - constrained, see closed-chain dynamics, 209, 297
 - cut-edge, 151
 - digraph, 150
 - edge, 150
 - node, 150
 - standard, 150
 - free-flying, 331
 - geared hinge, 229
 - model
 - articulated body, 97
 - composite body, 97
 - terminal body, 97
 - serial-chain, 35
 - spanning tree, 151
 - standard digraph, 150
 - terminal body model, 97
 - topological classification, 150
 - tree-topology, see tree-topology system, 150
 - under-actuated, 313
 - multiply-connected
 - digraph, 137, 209
 - path-induced sub-graph, 274
- N
- NCP, 226
 - Newton–Euler dynamics, 82
 - equivalence with Lagrangian dynamics, 367

- Newton–Euler inverse dynamics, 88
 Newton–Euler operator factorization
 determinant, 180
 diagonalizing transformation, 385
 flexible-link systems, 257
 for SKO models, 156
 for SKO models, 160
 geared link systems, 236
 of the mass matrix, 58
 sensitivity, 375
 serial-chain systems, 58, 82, 115
 time derivative, 375
 tree-topology systems, 291, 302
 Newtonian frame, 30, 82
 nilpotent matrix, 400
 ϕ spatial operator, 49
 BWA matrix, 143
 1-resolvent, 400
 tree adjacency matrix, 140
 node, 54
 adjacent, 135
 ancestor, 135
 child, 135
 descendant, 135
 multibody, 150
 parent, 135
 related, 135
 unrelated, 135
 weight dimension, *see* weight dimension
 node-contraction, 283
 Noether’s theorem, 34, 329
 non-Euclidean geometry, 381
 non-holonomic constraint, 210
 non-integrable velocity coordinates, 23
 nonlinear complementarity problem, 226
 norm
 of a matrix, 397
 of a vector, 397
- O**
- operational space
 algorithm for computing Υ , 195
 compliance kernel, *see* operational space compliance kernel
 compliance matrix, 189, 217
 computation of Coriolis vector, 203
 control, 189
 Coriolis generalized forces, 202
 dynamics, 189
 equations of motion, 187
 extended compliance matrix, *see* extended operational space compliance matrix, 217
 inertia, *see* operational space inertia
 operational space compliance kernel, 191
 algorithm for computing, 195
 base-invariance, 349
 for free-flying systems, 196, 349
 for micro/macro systems, 197
 singularity, 196, 349
 operational space inertia
 algorithm for computing, 194
 base-invariant, 348
 base-invariant computation of, 351
 inverse, 189
 operator, 48
 SKO, *see* SKO operator
 SPO, *see* SPO operator
 articulated body, 116
 backward Lyapunov equation, 170
 compatibility, 162
 derivatives, 353
 expressions with $\mathbb{B}_k \neq \mathbb{O}_k$, 83
 for serial-chain systems, 47
 forward Lyapunov equation, 166
 identities, 117, 176
 Innovations factorization, *see* Innovations operator factorization
 Jacobian, 55
 mass matrix expression, 58, 120
 mass matrix inverse expression, 121

- Newton-Euler factorization, [see](#)
 Newton-Euler operator
 factorization
 pick-off, [see](#) pick-off operator
 Riccati equation, 174
 sensitivity, 361–368
 spatial inertias, 58
 spatial kernel, [see](#) SKO operator
 spatial propagation, [see](#) SPO
 operator
 time derivatives, 356–361
- operator decomposition
 of Ω , 191
 for serial-chains, 197
 of \mathcal{M}^{-1} , 198
 for serial-chains, 199
 of $\phi \mathbf{M} \phi^*$, 61, 121
 of $\phi \mathbf{M} \psi^*$, 121
 of $\mathbf{A} \mathbf{X} \mathbf{B}^*$, 166
 of $\mathbf{A}^* \mathbf{X} \mathbf{B}$, 170
 for serial-chains, 172
 of inter-link spatial forces f , 128
 of the mass matrix \mathcal{M} , 63, 168
- optimal
 estimation theory, 111
 filter, 112, 338
 smoother, 113, 338
 smoothing, 112
- ordinary differential equation, 70, 213, 222, 339
- outboard link, 35
- P**
- parallel-axis theorem
 for rotational inertias, 19
 for spatial inertias, 20
- parent node, 135
- parent nodes of a sub-graph, 284
- parent sub-graph, 274
- partial velocities, 161
- partitioning
 induced by sub-graphs, 274
 of a mass matrix, 278
 of an SKO operator, 276
- of an SKO model, 277
 of an SPO operator, 277
 of free-flying system, 343
 of multibody systems, 277
 using serial-chain segments, 282
- passive
 degree of freedom, 314
 arm, 315
 hinge, 314
- path-induced sub-graph, 273, 343
 aggregation condition, 285
 induced partitions, 274
 multiply-connected, 274
 partition of SKO and SPO
 operators, 275
 with directed cycle, 274
- permutation
 re-indexing of nodes, 140
 transformation of a BWA matrix, 148
- Pfaffian form, 210
- pick-off operator
 constraint force, 131
 external forces, 85
 gravitational acceleration, 87, 128, 202
 nodes, 55
 operational space, 188
- polytree digraph, 137
- positive semi-definiteness
 of articulated body inertia, 104
 of rotational inertias, 19
 of spatial inertias, 20
 of the mass matrix, 58
- prescribed motion dynamics, 324
- prismatic hinge, 40
 Coriolis acceleration, 79
- projected dynamics, 212, 221–222
 equivalence to augmented
 dynamics, 222
 forward dynamics, 223
- projection matrix, 104
 articulated body, 102
 operational space, 199

Q

quasi-velocities, 23, 382
 angular velocity as, 71
 diagonalizing velocity
 coordinates, 382
 Lagrangian equations of motion,
 70
 quaternions, 41, 406–411
 E_+ matrix, 408
 E_- matrix, 408
 acceleration, 411
 attitude representation, 406
 based transformation of vectors,
 410
 composition of, 409
 identity element, 409
 rate from angular velocity, 410
 rates to angular velocity, 411

R

rate-feedback control, 392
 reaction-mode control, 329
 recursion
 backward Lyapunov, 171
 base-to-tip, 52
 base-to-tips, 163
 forward Lyapunov, 167
 gather, 162
 Lyapunov, 60
 Riccati equation, 174
 scatter, 163
 tip-to-base, 51
 tips-to-base, 162
 regular free-flying system model,
 332
 related nodes, 135
 Ω simplification, 197
 SPO operator sparsity, 146, 278
 backward Lyapunov equation, 174
 elements in $\mathbb{A}X\mathbb{B}^*$, 167
 elements in $\mathbb{A}^*X\mathbb{B}$, 172
 in a serial-chain digraph, 137
 mass matrix sparsity, 169
 relative coordinates, 38
 residual spatial forces vector, 107

reversing

 a serial-chain digraph, 141
 a tree digraph, 140
 an SKO operator, 345

rheonomic constraint, 210

Riccati equation, 105
 discrete-time systems, 113
 for SPO operators, 174
 operator form, 117

Riemannian symbols of the first
 kind, 73, 381

rigid body

 center of mass, 18
 conservation of
 kinetic energy, 30
 spatial momentum, 33
 dynamics, 25
 rotational, 71
 equations of motion, 25
 rotational, 71
 first moment of inertia, 18
 gyroscopic force, 26, 30
 kinetic energy, 18
 mass, 18
 moments of inertia, 18
 second moment of inertia, 18
 spatial inertia, 18
 spatial momentum, 21
 transformation, see rigid body
 transformation

rigid body dynamics, 17

 about arbitrary point, 29–31
 about center of mass, 25–27
 about inertially fixed velocity
 reference point, 31–33

based on spatial momentum, 30

using body frame spatial
 velocities, 29–31
 using inertial spatial velocities,
 27–29

rigid body transformation

 matrix, 11–12
 of $\tilde{V}(x)$, 13
 of spatial forces, 15
 of spatial inertias, 20

- of spatial momentum, 22
- of spatial velocities, 12
- operator, 43
- properties, 22
- time derivative, 13
- Rodrigues vector attitude
 - representation, 412
- root node, 135
- rooted digraph, 136
 - for multibody systems, 150
- rotary pin hinge, 40
- Coriolis acceleration, 79
- rotation matrix, 4
 - characteristic polynomial, 405
 - direction-cosine matrix, 403
 - eigen-values, 406
 - eigen-vectors, 404, 405
 - exponential form, 404
 - from angle/axis parameters, 405
 - from Euler angles, 404
 - from quaternions, 406
 - time-derivative, 5, 403
 - trace, 405
- rotation of vectors, 412
- rotational inertia, 18

- S**
- scatter recursion, 163
- Schur complement, 398
- scleronomic constraint, 210
- semi-group
 - property of $\phi(i,j)$, 50
 - property of $\psi(i,j)$, 117
 - property of $\Lambda(i,j)$, 146
- sensitivity
 - of \mathcal{D} , 374
 - of \mathcal{D}^{-1} , 374
 - of \mathcal{G} , 374
 - of \mathcal{P} , 374
 - of \mathcal{P}^+ , 374
 - of τ , 374
 - of \mathcal{E}_ψ , 374
 - of H , 364
 - of $H(k)$, 363
 - of ϕ , 364
- of $\phi(\varphi(k), k)$, 363
- of $\phi M \phi^*$, 365
- of M , 364
- of $M(k)$, 363
- of $\bar{\tau}$, 374
- of articulated body quantities, 373–377
- of Innovations factors, 375
- of Newton–Euler factors, 375
- of spatial operators, 361–368
- of the kinetic energy, 366
- of the mass matrix M , 365
- of vector quantities, 353
- separating contact, 225
- serial-chain digraph, 137
 - adjacency matrix properties, 140
 - reversal, 141
- serial-chain equations of motion, 81
 - inclusion of external forces, 85
 - inclusion of gravitational forces, 87
 - operator form of, 82
 - using inertially fixed reference point, 93
- serial-chain system
 - Coriolis acceleration, 77, 80, 434
 - equations of motion, *see* serial-chain equations of motion
 - inverse dynamics, 88–93
 - kinematics, 35
 - kinetic energy, 57
 - model, 35–42
 - reversal, 345
 - rigid multibody system, 35
 - simple hinge Coriolis acceleration, 79
 - spatial operators, 47
 - velocity recursion, 46
- similarity transformation, 83, 96
- similarity-shift transformation, 147, 149
- simple tree digraph, *see* tree
- simply-connected digraph, 137
- skew-symmetric matrix

- associated with cross-products, 6
- characteristic polynomial, 405
- property of $(M_D^* - M_D)$, 68
- SKO formulation
 - issues for non-tree systems, 185
 - procedure, 182
 - SKO model, 160
- SKO model, 159–185
 - AB forward dynamics, 182
 - aggregation condition, 288
 - backward Lyapunov equation, 170
 - definition, 160
 - development procedure, 183
 - existence, 161
 - for aggregated tree, 290
 - for closed-chain systems, 302
 - for flexible systems, 255–257
 - for geared systems, 234
 - for passive system, 317
 - forward dynamics, 180
 - forward Lyapunov equation, 166
 - generalizations, 161
 - identities, 176
 - Innovations operator factorization, 179
 - inverse dynamics, 166
 - mass matrix, 168
 - non-tree generalization, 185
 - partitioning, 275–278
 - Riccati equation, 174
 - with kth link as base-body, 341
 - with constraint embedding, 302
 - with new base-body, 347
- SKO operator
 - BWA matrix, 159
 - after aggregation, 288
 - of reversed serial-chains, 345
 - partitioned, 276
- SKO-forest, 151
- spanning tree, 138
 - multibody, 151
- sparsity structure
 - SPO operator, 278
 - mass matrix, 169, 282
 - of serial-chain \mathcal{E}_A , 145
- of serial-chain \mathbb{A} , 145
- of tree \mathcal{E}_A , 145
- of tree \mathbb{A} , 145
- of tree SKO, 280
- of tree SPO, 281
- spatial acceleration, 76
 - from innovations accelerations, 125
 - modal, 253
- spatial deformation, 246
- spatial force, 15
 - inter-link, 75
 - residual, 107
 - rigid body transformation, 15
- spatial inertia, 17–21
 - of full system, 62
 - rigid body transformation, 18
 - spatial operator, 58
- spatial inertias
 - composition of, 21
- spatial kernel operator (SKO), *see* SKO operator
- spatial momentum, 21
 - of full system, 63
 - rigid body transformation, 22
- spatial operator, *see* operator
- spatial propagation operator (SPO), *see* SPO operator
- spatial vector, 8–14
 - cross product for, 9–10
 - spatial force, *see* spatial force
 - spatial momentum, *see* spatial momentum
 - spatial velocity, *see* spatial velocity
- spatial velocity, 9
 - modal, 251
 - recursive algorithm for, 45
 - relative, 39
 - rigid body transformation, 12
- spherical hinge, 40, 41
- SPO operator
 - 1-resolvent matrix, 159
 - after aggregation, 289
 - backward Lyapunov equation, 170

- forward Lyapunov equation, 166
 identities, 176
 partitioned, 277
 product with vectors, 162
 Riccati equation, 174
 sparsity structure, 278
 squeeze force, 214
 stacked vectors, 48
 standard digraph, 150
 strictly canonical tree digraph, 137
 adjacency matrix, 140
 structural
 mass matrix, 248
 stiffness matrix, 248
 sub-graph, 273
 path-induced, 273
 aggregation, 283
 child nodes, 284
 child sub-graph, 274
 induced, 273
 induced partitions, 274
 parent nodes, 284
 parent sub-graph, 274
 sub-structured SKO models, 290
 symmetries of the Lagrangian, 34
- T**
- terminal-body model, 76, 97
 time derivative
 of $H_I^*(k)$, 94
 of \mathcal{D} , 368
 of \mathcal{D}^{-1} , 368
 of \mathcal{G} , 368
 of \mathcal{P} , 368
 of \mathcal{P}^+ , 368
 of τ , 368
 of \mathcal{E}_ψ , 368
 of H , 357
 of $H(k)$, 356
 of ϕ , 357
 of $\phi(k+1, k)$, 356, 359
 of M , 357
 of $M(k)$, 356
 of $\bar{\tau}$, 368
- U**
- under-actuated system, 313
 articulated body inertia, 317
 decomposition, 315
 disturbance Jacobian, 325
 equations of motion, 316

- flexible-link systems, 261
- forward dynamics, 322
- free-flying system, 329–330
- generalized Jacobian, 325
- Innovations operator factorization, 319
- inverse dynamics, 322
- mixed dynamics, 322
- modeling, 314–320
 - relation to prescribed motion systems, 322
- undirected graph, 135
- unilateral constraint
 - complementarity approach, 224
 - distance function, 225
 - forward dynamics, 227
 - gap function, 225
 - penalty method, 224
- unit quaternions, see quaternions, 41
- universal joint, 41
- unrelated nodes, 135
- SPO operator sparsity, 146, 278
 - elements in $\mathbb{A}X\mathbb{B}^*$, 167
 - elements in $\mathbb{A}^*X\mathbb{B}$, 172
 - in tree digraphs, 137
 - mass matrix sparsity, 169
- V**
- vector
 - derivative, 5–8
- norm, 397
- rotation of, 412
- velocity
 - degrees of freedom, 39
 - diagonalization condition, 382
 - diagonalizing coordinate transformations, 382–392
 - generalized, see generalized velocity coordinates
 - hinge coordinates, 39
 - reference frame, 31
- velocity recursion
 - for aggregated body, 294
 - for serial-chains, 44
 - for tree systems, 154
 - with $\mathbb{B}_k \neq \mathbb{O}_k$, 46
 - with kth link as base-body, 342
- W**
- weight dimension, 141
 - determination, 184
 - for rigid-link systems, 153
- weight matrices, 141
 - determination, 184
 - for dual model, 333
 - for rigid-link systems, 153
 - general properties, 161